The Dissertation Committee for Robert Murchison Forkner Certifies that this is the approved version of the following dissertation:

Depositional periodicity and the hierarchy of stratigraphic forcing in the Triassic carbonates of the Dolomite Alps, N. Italy

Committee:

Mark Cloos, Supervisor

Robert L. Folk

Linda A. Hinnov

Ursula Hammes

Randall Marrett

Depositional periodicity and the hierarchy of stratigraphic forcing in the Triassic carbonates of the Dolomite Alps, N. Italy

by

Robert Murchison Forkner B.S.; M.S.

Dissertation

Presented to the Faculty of the Graduate School of

The University of Texas at Austin

in Partial Fulfillment

of the Requirements

for the Degree of

Doctor of Philosophy

The University of Texas at Austin

May 2007

Dedication

This dissertation is dedicated to the memory of

Dr. Robert K. Goldhammer

Acknowledgements

The list of people I would like to thank is quite long and involves more than just those involved in the science. However, it would be remiss of me to not thank Bob Goldhammer first and foremost. To be honest, I didn't come to the University of Texas to study carbonates, to get a PhD, or to get into the Austin music scene. I came to UT to work with a guy who was larger than himself and inspired everyone around him to work the problem and be huge. Bob's infectious interest in carbonate rocks and cycles and depositional systems made those things seem like the most important thing in the world to us students, even when it meant staying late on Friday nights arguing about the heartbreak of diagenesis. Bob's outgoing nature, wit, and continuous support for his students inspired me to work hard and pursue this work on these rocks called "carbonates" in a place called "the Dolomites", and I'll always be thankful for that, whether I end up being a grazer or not!

The next person (and group of people) that I have to thank are Mark Cloos, my committee members (Bob Folk, Linda Hinnov, Ursula Hammes, and Randy Marrett), and several exemplary scientists from Italy (Carlo Doglioni, Andrea Cozzi, and Nereo Preto) and the US (Lawrie Hardie, Stacy Atchley, Dan Lehrmann, and Steve Bachtel). After the accident that took Bob's life, I was sure that I wanted to continue my work in the Dolomites, even though I had only visited the area once with Bob and had yet to spend a single working field season there. All of the people listed above worked with me to make sure that if I

wanted to continue that I would be able to do so. Mark took great pains to learn a few things about carbonate sedimentology and come onboard as my advisor, and everyone else offered their time, advice, constructive criticism, and help with funding to make sure that I would finish with a decent piece of work having been completed. There can be no doubt that I would not have finished without the help of the people mentioned above. Thanks to you all.

There are also a number of UT grad students who helped out along the way, including Matt Davis, Younis Altobi, Beatriz Garcia-Fresca, Brook C.D. Riley, Ted Playton, Ned Frost, Esti Ucar, Alka Tripathy, John Hooker, Jesse Kimball, Barbara Tillotson, Matt Campbell, Tina Foster, and Jose Delgado. Thanks to all you felons and chicas!

Outside of science, there are many people who helped my keep things together over the past few years. More than anyone else, my wife Stefanie, who climbed up mountains even though she hates heights and could have taken the chairlift and put up with my ramblings and odd decision making for the past few years. Vielen dank für alles liebchen! Also my parents Emma and Larry, Grandparents Tommye and Lee, brother John, and sister Lauren.

Ich möchte mich auch bei all den wunderbaren Leuten in ganz Europe bedanken, die mir geholfen und mich bei diesem Projekt unterstützt haben. Denn zweifelslos ohne deren Hilfe hätte dieser dumme Amerikaner keinen Platz zum Schlafen, keine Kruste zu essen, und keinen Berg zu erklimmen, gehabt. Vielen Dank an Elfi und Jo, Jenny und Carlo, Doris und Jochen, Gisela und

Franz, Inge und Bernd, Roger, Jenni und Frederic, Natascha und Guido, Monique und Bernd, Nathalie und Achim, und Petra und Yvonne in Eupen und Umgebung! Alaaf!

Ein großer Dank geht auch an die wohl beste ladinische Familie in den Dolomiten, die Familie Delmonego, die meine Socken gestopft, meine Hosen gewaschen, und den Rosenkranz gebetet haben als ich den Sella (zweimal!) während eines Gewitters erklummen habe. Vielen herzlichen Dank dafür, dass Sie auf den verrückten, zu viel Kaese essenden Amerikaner aufgepasst haben.

Playing music also helped to keep my head screwed on straight and there is no better town than Austin to play music in! Many thanks to my bandmates Chris Buckley and Charles Branch, as well as Donnelle McKaskle and the Celtic Cultural Center, all of the Austin session musicians, pubs, and folks who came out to hear us play. Thanks much also to all the other bodhrán players and musicians out there who made the off-hours fun: Mark Stone, Albert Alfonso, Darius Bartlett, Paul Marshall, Máirtín de Cógáin, Steve and Alie Twigger, and Rich Brotherton. Go raibh maith agaibh!

Depositional periodicity and the hierarchy of stratigraphic forcing in the Triassic Carbonates of the Dolomite Alps, N. Italy

Publication No._____

Robert Murchison Forkner, PhD

The University of Texas at Austin, 2007

Supervisor: Mark Cloos

The Dolomite Alps of northern Italy are a classic field locality in the development carbonate stratigraphic theory. Included in the many discoveries rooted in the geology of the Dolomites is the concept of a hierarchy of stratigraphic forcing in the Alpine Triassic. The hierarchy states that carbonate sedimentation is dominantly a record of eustasy, resulting in organized stacking patterns, and that these stacking patterns reflect the interplay between low frequency (1-10 my) eustatic cycles and their component bundled high-frequency (100 & 20 kyr) eustatic cycles.

The overall aim of this study is to further investigate the validity of the hierarchical model after recent dating of Anisian and Ladinian successions called the Milankovitchian periodicity and/or allocyclicity of the cyclic series into question. The study was completed using four sub-studies, 3 based on data

collected in the field and a fourth based in cycle theory and computer modeling. First, it can be shown that allocyclic forcing exists in the Anisian/Ladinian platforms of the Dolomites by comparing the stratigraphic sections measured from 2 time-equivalent, independent carbonate platforms, the Latemar and Mendola Pass. Second, computer modeling of Anisian/Ladinian carbonate platform stratigraphy using Milankovitchain solar insolation as a proxy for high-frequency eustasy shows that both pure Milankovitch forcing and mixed Milankovitch/sub-Milankovitch forcing will produce synthetic carbonate platforms with stratigraphic successions comparable to those of the Anisian/Ladinian platforms of the Dolomites. Third, it can be shown that the while the Norian Dolomia Principale (a regional carbonate shelf) was affected by differential subsidence, megacycles systematically increase in their number of component cycles from 2-3:1 in the eastern Dolomites (updip) to 5-6:1 in the western Dolomites (seaward). In conclusion, the concept that carbonate platform stratigraphy is a record of an interplay between eustasy, subsidence, and sedimentation is upheld, while the validity of Milankovitchian forcing acting on all Alpine carbonate cycles is questioned. Instead, cyclic carbonates with sub-Milankovitch periodicities were common in the early and mid-Triassic, while cycles with Milankovitchian periodicities were common in the late Triassic.

Table of Contents

List of Tables

List of Figures

List of Illustrations

Introduction: The Cyclic Carbonates of the Dolomite Alps, Northern Italy

INTRODUCTION TO THE STUDY

Prior to my beginning graduate work at UT Austin, an invitation was made by Dr. R.K. Goldhammer to accompany him on a trip to the Dolomite Alps in the late summer of 2002 (instead of attending Master of Science commencement at Baylor University). This trip was made primarily for Dr. Goldhammer to re-familiarize himself with the area and to begin the process of "resurrecting" his Milankovitchian interpretation of Latemar cyclicity. For myself, it served as introduction not only to the wit and wisdom of Dr. Goldhammer, but also to the Dolomites. Several days were spent at both the Latemar platform and the coeval Mendola Pass section near Bolzano. During that time I became familiar with Dr. Goldhammer's ideas surrounding carbonate cyclicity, and we both agreed that I would pursue a project that had cyclostratigraphic analysis as a major portion of the study. The work on the Latemar and Mendola Pass in this study came from interest generated after this introduction to the "Latemar controversy", and serves as a sort of "eustatic benchmark" from which to view the cyclostratigraphy of Norian deposits.

The impetus behind pursuing work on the Norian Dolomia Principale was provided through insightful and enlightening classwork assigned by Dr. Goldhammer during his 383M graduate carbonate stratigraphy class in early

2003. During that time, a major question that had been asked was what "role" carbonates played in the development of Mesozoic passive margin systems. A central question within that scope of investigation was what role synsedimentary extension played in the development of carbonate platforms. While one might consider differential subsidence within a carbonate-producing environment to produce either thicker/thinner or more/fewer cycles from one place to the next (depending on subsidence and sedimentation rates), an attempt at quantifying this behavior in a stratigraphic sense has received very little attention within the literature. As a result, students under Dr. Goldhammer undertook a variety of research projects, most of which were directed at investigating the relationship between passive margin development and carbonate sedimentation. In this case, the Tethyan passive margin system preserved in the Dolomites of Northern Italy was chosen as a field area (partially due to the ongoing “resurrection” of the Latemar controversy), with the hypothesis being that if synsedimentary extensional features were looked for, they would likely be found. The reasoning behind this assumption had to do with analysis of subsurface data (mostly reflection seismic) from other passive margins (e.g., Angola, offshore Gulf of Mexico) that developed as a result of the rifting of Pangaea- nearly all of which showed growth faulting, block faulting, halokenesis, etc., contemporaneous to carbonate sedimentation. By comparison, we hypothesized that the sedimentary succession of the Dolomites would bear similar evidences of extensional tectonic activity (i.e., differential section thickness, synsedimentary faults, etc.). The rare

opportunity to view a relatively undeformed succession of seismic scale outcrop from the Pangaean breakup allows for investigation of the stratigraphic packaging of platform carbonate successions in the Dolomites and allows for analysis of cyclic signals preserved within these outcrops.

This dissertation combines 5 separate, but related chapters related to the central topic of high-frequency carbonate depositional cyclicity in the Alpine Triassic of Northern Italy. These chapters include: 1) A study of fundamental high-frequency allocyclicity in the Anisian/Ladinian Latemar platform and coeval Mendola buildup; 2) forward modeling of high-frequency carbonate cyclicity using Milankovitchian solar insolation as a proxy for high-frequency eustatic oscillations; 3) analysis of faults and kinematic indicators in late Triassic sediments identified in the Passo Falzarego area; 4) investigation into the cycle stacking within the lower portion Norian Dolomia Principale; and 5) an attempt to reconcile mid Triassic platform carbonate cyclicity with late Triassic platform carbonate cylicity.

PROBLEM

The fundamental issue examined in this dissertation is our ability to extract information related to the temporal and/or periodic framework of stratigraphic forcing mechanisms in middle and late-Triassic platform carbonate successions. Central to this investigation is recognition of the timing, or frequency of repetitive

occurrence of shallowing-upward carbonate successions (also known as depositional cycles) and how they compare within the context of the Triassic (Anisian/Ladinian compared to Norian) and the Pleistocene / Holocene. The problem that this investigation addresses is the apparent discrepancy in sub-Milankovitchian cycle periods from the Anisian/Ladinian Latemar platform to the Milankovitchian cycle periods of the Norian Dolomia Principale and Pleistocene / Holocene platform carbonate successions. If cycle periods can be identified and determined to be markedly different (e.g., order of magnitude difference in cycle periodicities) among these periods of geologic time, we must attempt to determine a reason for the discrepancy.

PURPOSE

The purpose of this dissertation is to examine the stratigraphies of the Anisian/Ladinian Latemar platform (and time-equivalent stratigraphy at Mendola Pass) and the lower Norian Dolomia Principale in the Dolomites and identify key similarities and differences in facies and cycle stacking patterns with the hope of extracting allogenic forcing signals from both. The original comparison between mid-Triassic platform carbonates and late Triassic shelf carbonates of the Dolomite alps was done by Goldhammer et al. (1987, 1990) as a model for the nesting of cycles and “hierarchy of stratigraphic forcing”. This publication helped to formally define the expected framework of cyclic forcing for high-frequency, meter-scale carbonate depositional cycles within lower-frequency km-scale

sequences. Goldhammer et al. (1987, 1990) concluded that the thinning-upward grouping of 5 shallowing-upwards facies successions (also called depositional cycles) into one “megacycle” formed as the result of astroclimatic forcing of eustatic sea level oscillations within the Milankovitch (20 kyr precession modulated by 100 kyr eccentricity) band. In addition, Goldhammer et al. (1990) concluded that depositional cycles within the Dolomia Principale formed as the result of eustatic oscillations at the same periodicity along with a strong (if not dominant) influence of local subsidence driven by block faulting (Bosellini and Hardie, 1985; Goldhammer et al., 1990).

Since 1990, however, biostratigraphic studies and the dating of single zircons extracted from ashfall tuffs preserved within the cyclic interior of the Latemar platform has cast doubt on the timing of the periodicity of the Latemar cycles as originally proposed by Goldhammer et al. (1987), and the periodicity of composite cycle bundling as a whole (Brack et al., 1990). This study aims to re-examine the idea that deterministic, nested cyclic forcing mechanisms with Milankovitchian periodicities are recorded in the depositional cycles of the Alpine Triassic of the Dolomites, particularly in light of the new zircon ages at the Latemar and middle and late Triassic as a whole.

Recognition of a systematic allogenic control on carbonate stratigraphy in the mid-Triassic of the Alps has major implications for the study of other cyclic

carbonate successions in the area and in other localities from different geologic ages. In this case, a comparison is being drawn between the 'model' eustatic signature derived from the Latemar and that extracted from the Dolomia Principale. In theory, if the sea level oscillations that formed the cyclic stratigraphy of the Latemar and Mendola pass were mainly under the control of Milankovitchian astronomical forcing, and if the response of Mid-Triassic (Anisian 245-237 Ma, Ladinian 237-228 Ma) carbonates to that forcing was to form bundled depositional cycles, then it is also possible that the same cyclic forcing of carbonate deposition persisted into the Norian (216.5-203.6 Ma). If this theory proves true, it can serve as a benchmark from which to test the cyclostratigraphy of the Dolomia Principale. In the same way, if it can be proven that Anisian/Ladinian cycle periodicities are sub-Milankovitchain, those sets of periodicities can be tested against the sedimentary record of the Norian. This is important as the Dolomia Principale is a broad carbonate shelf, ca. 100 kilometers wide, and is thought to have undergone synsedimentary faulting as the result of rift-related extension and/or differential compaction. If the eustatic mechanisms active in the Anisian/Ladinian were also active in the Norian, we should see similar stacking trends through both successions. Excursions from predicted stacking may be a record of autocyclicity driven by any number of processes, including differential subsidence and/or lateral sediment transport (e.g., channel migration, storm events, etc.).

A second, more intriguing set of implications surrounding the development of cyclic successions in the Alpine Triassic is related to the dating of Anisian and Ladinian carbonates via ash-fall tuffs intercalated with the cyclic stratigraphy at the Latemar. Recent work has concluded that the Anisian/Ladinian Latemar platform formed in less than 1 million years (Emmerich et al., 2004; Kent et al., 2005) and, that the bounding dates of the Norian stage are 216.5 Ma-203.6 Ma (12.9 m.y. total) instead of 227.5 Ma-208 Ma (19.5 m.y. total) Ma. This adds 6.6 million years to the Norian at the expense of the Anisian and Ladinian stages (Gradstein et al., 2004; Muttoni et al., 2004; Furin et al., 2005). If correct, these dates significantly change the timing of cyclic successions of like-facies in the Dolomites, moving their periodicity into separate octaves. This raises the question of how peritidal carbonate systems create identical sedimentary successions at timescales differing by more than an order of magnitude. Of interest, then, is a re-examination of the claim of allocyclicity at the Latemar, a re-examination of the nature of all proposed forcing mechanisms from the standpoint of sedimentary modeling, analysis of the cyclic stratigraphy of the Dolomia Principale in light of the possibility of the platform having undergone synsedimentary extension, and comparison of these individual studies in the context of the “hierarchy of stratigraphic forcing” elegantly put forth by Goldhammer et al. (1990).

In order to fully investigate this problem, this dissertation has been divided into 6 chapters. While each chapter can be read independently of the others, they function together as portions of a larger image: the nature of cyclic platform carbonates from the mid to late Triassic of the Southern Alps. The chapters are titled as follows:

Chapter 1. Cycles, mountains, outcrops, and Ladin farm life- an introduction to the cyclic carbonates of the Dolomite Alps.

Chapter 2. On the allocyclic interpretation of the 'Latemar cycles' (M. Triassic, the Dolomites, Italy) and implications for high-frequency cyclostratigraphic forcing.

Chapter 3. Forward modeling of high-frequency platform-interior carbonate cyclic stratigraphy using Milankovitchian solar insolation as a proxy for high-frequency composite eustasy.

Chapter 4. Structural evidence for synsedimentary deformation of the Dolomia Principale.

Chapter 5. Stratigraphic analysis of the Lower Dolomia Principale, the Dolomites, N. Italy.

Chapter 6. The current state of the hierarchy of stratigraphic forcing in the alpine Triassic.

Chapter 1: Cycles, Mountains, Outcrops, and Ladin farm life- an introduction to the Dolomite Alps

CARBONATE DEPOSITIONAL CYCLES

Brief Background

Recognition of repetitive facies successions in carbonate strata has received considerable attention throughout the history of geological investigation (Smith, 1816; Seuss, 1888; Grabau, 1913; Fischer, 1964; Schwarzacher, 1975; Goldhammer et al., 1987, 2003; Walker and James, 1990; Einsele et al., 1991; Read 1995; Kerans, 1995, and many others). Much of the content in these investigations addresses the mechanisms by which repetitive strata develop, whether through global, predictable (deterministic) mechanisms, or through random mechanisms, including local sediment dispersion, facies migration, etc. Deciphering the link between the sedimentary record and sedimentary process is not straightforward, but hopes of eventually cracking this natural code have inspired the work behind many studies, including this one.

Introduction to Carbonate Depositional Cycles

In studies of modern tidal flats on Andros Island, Bahamas, workers have noticed that cores of Holocene sediments typically “shallow upwards”, i.e., the facies succession within a ca. 2 meter thick core of Holocene sediment indicate an increasingly shallow depositional environment upwards through the profile

(**Figure 1. 1** *see* Hardie and Ginsburg, 1977, p.122). This is thought to record "normal depositional processes" which can include the following: tidal flat progradation, vertical aggradation of subtidal carbonate sediments, migration of subaqueous carbonate sand dunes, or accretionary processes related to distributary tidal flooding and drainage (Tucker and Wright, 1990). These depositional processes lead to the building up of carbonate sediments to, or slightly above, sea level (Tucker and Wright, 1990). In ancient successions containing like facies (e.g., peritidal cycles at Tre Cime di Lavaredo, discussed in chapter 5) it becomes apparent that the pattern of shallowing-upwards facies successions repeats, with each profile beginning with comparably deeper-water facies (e.g., bioturbated wackestone interpreted as an offshore subtidal environment) and ending with the shallowest-water facies (e.g., microbial laminite) (Tucker and Wright, 1990; Demicco and Hardie, 1994). Shallow-water deposits are overlain by deeper-water facies that subsequently shallow upwards, thus repeating the process. These shallowing-upward facies successions may repeat hundreds of times within a single formation (**Figure 1. 2;** Fischer, 1964; Grotzinger, 1986; Goldhammer et al., 1987; Koerschner and Read, 1989). The repetitive nature of these meter-scale facies successions has led to their being known as "shallowing-upward depositional cycles". Excellent treatment of the topic of shallow water carbonate cycles, their origins, and rates of deposition is given in Tucker and Wright (1990); Demicco and Hardie (1994); and

Goldhammer (2003). Much of the background information on depositional cycles within this dissertation is a synthesis of these publications.

The first task in cyclostratigraphic analysis is to define depositional cyclicity. A "cycle" refers to a series of connected events that proceed forward, returning to a starting point before repeating. Cyclic sedimentation is defined as the "succession of related depositional processes and/or environmental processes that generate a succession of repetitive, orderly arranged facies in the rock record" (Goldhammer, 2003). When applied to a sedimentary sequence, cycles are a distinctive series of lithologies that are arranged vertically in a predictable way (Goldhammer, 2003). This is in distinction to rhythmic stratigraphy, which assumes a temporal periodicity for the cyclic framework. In other words, the phrase "depositional cycle" refers to repetitive lithologies, not necessarily time-periodicity. Only when periodic behavior can be proven are depositional cycles said to be "periodic"

Perhaps the most objective, all-inclusive definition of a depositional cycle within the shallow marine carbonate realm comes from Goldhammer et al. (1991, *in* Franseen et al., 1991), which is based on Wilson (1975) James (1984) and Hardie and Shinn (1986):

> "A relatively conformable succession of genetically related subtidal subfacies bounded by peritidal subfacies, subaerial exposure surfaces, and/or marine flooding surfaces (very thin intervals characterized by slow rates of deposition). Cycles are the thinnest recognizable allocyclic or

> autocyclic depositional unit and they may be progradational and/or aggradational and thus subfacies within cycles [shallow] upwards. Individual cycles typically contain both a "transgressive" and a "regressive" component, and the relative proportion of these components within any given cycle is a function of the cycle's position in a lower frequency cycle or sequence." (Goldhammer, 2003).

This definition illustrates the variable nature of individual cycles, but does not imply any interpretation regarding a cyclic driver or causal mechanism. Indeed, two main categories of cycles have been defined, those that are autocycles and those that are allocycles (**Figure 1. 3**). Autocycles form internally within a sedimentary system and operate in complete independence from external or extrabasinal forcing (Goldhammer, 2003). Examples of autocyclic deposition may include repetitive channel avulsion and lateral accretion of fluvial deposits, lobe switching in river deltas, sedimentary infill of locally faulted or downdropped areas, and progradation of carbonate sediments across a platform without the influence of sea level change (Ginsburg, 1971; Tucker and Wright, 1990; Goldhammer, 2003). Allocyclic deposition, in contrast, is driven by forces external to the depositional system and includes processes such as climate change, global tectonism, and eustatic oscillations (Goldhammer, 2003). Both allocycles and autocycles undoubtedly exist in the sedimentary record. The challenge for the sedimentologist is to decipher the signals that each process leaves encoded within the stratigraphy.

In carbonate depositional environments, cyclic sedimentation is the most common type of platform-interior stratigraphic theme. Depositional cycles are the

norm for most shallow-marine carbonate platforms (ancient and modern), mainly because carbonate platform sedimentation rates (up to 100 cm/1000 yr) can outpace the rates of subsidence of a passive margin (commonly 3-6 cm/1000 yr), allowing carbonates to “keep up” with accommodation changes simply by forming sediment (Schlager, 1981; Goldhammer, 2003). The addition of sediment to accommodation space in carbonate forming environments, then, produces depositional cycles via lateral progadation of near-shore tidal-flat facies over downdip, deeper-water subtidal facies and/or vertical aggradation of offshore subtidal environments to sea level.

Cyclic events versus cyclic stratigraphy- where’s the match?

The “shallowing-upward” nature of repetitive carbonate stratigraphy requires oscillatory behavior of depositional environments though time. This is because of the observational link between facies and depositional environment, and by extension the requirement that laterally-adjacent sub-environments must have shifted though the geologic time to create vertical facies successions in the rock record (Hardie and Shinn, 1986; Demicco and Hardie, 1994). There are three plausible causes for the formation of carbonate shallowing-upward cycles: eustatic oscillations, intrabasinal autocyclicity, and variable local subsidence (Walker and James, 1990, Demicco and Hardie, 1994; Goldhammer, 2003). These processes are summarized as follows:

Eustatic Oscillations

A popular interpretation for the presence of depositional sequences in the rock record involves eustatic (global sea level) oscillations as a mechanism by which successions are generated (*see* Figure 1. 1). Some eustatic oscillations are periodic (e.g., astroclimatic cycles) while others are not (e.g., tectonic processes). Currently recognized eustatic drivers with (at least) meter-scale amplitudes compiled by Allen and Allen (1990) and Goldhammer (2003) include:

1. Continuing differentiation of the mantle as a result of plate tectonic processes, whereby water is added to the ocean/atmospheric system by volcanic processes and removed via subduction, leading to long term (myr scale) changes in sea level.
2. Changes in ocean basin volume as a result of sediment accumulation or removal. Sediment may be added through clastic or carbonate depositional processes and may be removed through subduction.
3. Changes in ocean basin volume as a result of ocean ridge volume expansion and contraction. Rapid rates of spreading result in the extrusion of more oceanic crust leading to a more voluminous spreading ridge. More rock at the ridges lessens ocean basin volume leading to long-term sea level rise. Slower rates of spreading produce the opposite effect.

4. Changes in the amount of seawater in the oceans due to removal and trapping of water on the continents, primarily in the form of land-locked glacial ice, but also lakes, or groundwater (meter-to-10s of meters of sea level change). Climatic perturbations related to Milankovitchian orbital forcing are commonly implied as the cause for these oscillations.
5. Trapping and partial evaporation of restricted basins formerly connected to ocean basins (e.g., Mediterranean Sea).
6. Periodic perturbations in solar insolation may heat and therefore expand ocean water volume (Schulz and Schafer-Neth, 1997). This was proposed by Zühlke et al. (2003) as a driver for high-frequency cycles in the Latemar platform of the Dolomites (m-scale sea level oscillations).

The processes described above can change sea level on a global scale, and increase or decrease the volume of ocean that sediment can fill. What is far less understood is how changes in sea level actually relate to the generation of depositional cycles. Indeed, the lack of temporal constraint of depositional cycles, and the force-fitting of many depositional sequences (justifiably or not) into a temporal framework is one of the main reasons that cyclostratigraphic problems are still the subject of sedimentologic debate. As an example, Goldhammer et al. (1987) and Hinnov and Goldhammer (1991) concluded that

the shallowing-upward cycles exposed at the Latemar platform formed as the result of sea level change driven by Milankovitchian eustasy. This conclusion was based on the observation that fundamental cycles at the Latemar are grouped (on average) into thinning-upward bundles of 5 (Goldhammer et al., 1987; Hinnov and Goldhammer, 1991; Preto et al., 2001, 2004). In addition, these depositional cycles were interpreted to not only be lithologically repetitive, but also temporally periodic, with each cycle forming as a result of 20 kyr precessional cycle and each grouping of 5 cycles modulated by the 100 kyr eccentricity cycle.

Intrabasinal Autocyclicity

Perhaps the most oft-cited abstract in the science of stratigraphy is that of Ginsburg (1971), in which the author explains a scheme by which shallowing-upward tidal-flat cycles may form through progradation without a eustatic change in sea level, but rather variable sedimentation rates and constant subsidence (**Figure 1. 4**). This scheme relies on the observation that modern sediment in tidal flat cycles is generated in the subtidal "carbonate factory" and transported to the supratidal zone where it accumulates. In the model, carbonate sedimentation begins once the substrate has subsided to a water depth (lag depth) consistent with sedimentation in the subtidal factory (ca. 1 m). Once sedimentation begins, processes such as high tides and storms move sediments shoreward, depositing them in the supratidal zone. As this process continues, sediment transport leads

to the progradation of the supratidal environment over the subtidal, creating a shallowing-upward facies succession. At some point, all of the available accommodation space is filled and the entirety of the subtidal factory is covered by tidal flat sediments, effectively shutting down carbonate sedimentation and allowing background subsidence to resume. Upon subsiding to the proper lag depth, sedimentation resumes and a new facies succession is deposited, with the process reoccurring ad infinitum. A similar idea was presented by James (1984), but rather than arguing for shoreline progradation, James argued for the existence of a varied number of tidal flat islands and banks prograding and accreting across the subtidal zone until accommodation is filled (James, 1984; Walker and James, 1990).

Autocyclicity is an attractive explanation for randomly stacked carbonate cycles occurring in modern and ancient settings. However, the known existence of periodic drivers that may lead to the formation of depositional cycles (e.g., composite eustatic forcing) make it difficult to argue that carbonate sedimentation is always a function of autocyclic processes.

Tectonic Cyclicity

A third driver thought to generate sedimentary successions is synsedimentary tectonism, particularly that involving variable subsidence (**Figure 1. 5**). In a study of the Norian Dolomia Principale (DP), Bosellini and Hardie

(1985) suggested that shallowing-upward cycles developed independent of each other (from locality to locality) as a result of being on separate fault blocks with individual, unique subsidence histories. Hardie and Shinn (1986) conclude that the overprint of differential subsidence on DP depositional cycles led to the development of depositional successions that differ so greatly from locality to locality that they cannot be correlated using stacking pattern analysis. The difficulty in correlating the vertical thickness series of cycles within the DP suggests that even if a eustatic driver had been acting, subsidence was far stronger a driver for the development of sedimentary successions in a vertical sense, likely resulting in differential thickness of individual sedimentary successions and/or different numbers of shallowing-upward successions from locality to locality. As a result, individual fault blocks likely record a unique mixture of tectonic autocycles and eustatic allocycles, possibly making correlation by comparative cycle stacking impossible.

The Cyclic Hierarchy

Workers investigating cyclic stratigraphy have long recognized that sedimentary cycles are deposited at different orders of magnitude (both in time/frequency and thickness/amplitude), and can sometimes be correlated over wide geographic areas (**Table 1**, Fischer, 1964; Schwarzacher, 1975; Vail et al., 1977; Goldhammer et al., 1990). In most cases, the development of sedimentary cycles is affected by multiple inputs (both eustatic and autogenic), generating

unique characteristic stacking patterns for a given locality or period of geologic time (Goldhammer, 2003). Therefore correlating cycles and stacking patterns generates a relativistic relationship between the sections in question, as current dating techniques have not yet been able to date individual carbonate depositional cycles empirically (Preto et al., 2001; Goldhammer, 2003). In rare cases, age-bracketing of sections constrains cycle periodicities, but this level of data control is atypical.

1st-, 2nd-, and 3rd- Order Cycles

Sloss (1963) introduced the theory that continental sediments in North America were bounded by regional unconformities, and that 6 such unconformities had occurred in the Phanerozoic. While Sloss (1963) recognized that these stratigraphic packages represented groupings larger than formations (e.g., member, formation, group, supergroup), he did not identify a global driver for his cratonic sequences. The concept of a global allocycle was first proposed by J. Tuzo Wilson (1966) in his writings on the opening and closing of ocean basins through sea-floor spreading and subsequent destruction by subduction. This “Wilson cycle”, as it came to be known, is a 200+ million year series of tectonic events beginning with the rifting of a continent, the development of an ocean, and destruction with the collision of the two continental masses.

The construction curves showing sea level change through time led geologists at Exxon, spearheaded by Vail et al. (1977), to identify 3 groups of cycles with a unique hierarchical temporal bracketing (*see* Vail et al., 1977, fig, 1). These groups were termed “orders”: first-order cycles have durations of 200-400 myr, second-order cycles have durations of 10-100 myr, and third-order cycles have durations of 1-10 myr (Vail et al., 1977; Goldhammer, 2003). These orders of cyclicity were based on regional stratigraphic frameworks constructed from a global dataset of reflection seismic data supplemented by well control (Vail et al., 1977). The global sea level chart used by Vail et al. (1977) based on globally correlatable depositional sequences identified in reflection seismic data.

Vail et al. (1977) speculated as to the drivers behind each order of cyclicity. 1st-order cycles (200-400 myr duration) are thought to be driven by the breakup of continents and the closings of oceans. Eustatic sea level falls when supercontinents are assembled and rises during times of rifting and seafloor spreading. Two 1st-order, or J.Tuzo Wilson cycles have occurred during Phanerozoic time (Goldhammer, 2003). 2nd-order cycles (10-100 myr duration) are attributed to volume changes of spreading ridges driven by variable rates of seafloor spreading (described above) (Goldhammer, 2003). In short, 1st- and 2nd-order cycles are driven by tectonic mechanisms.

The origin of 3rd-order cycles is problematic. According to a summary of studies compiled by Goldhammer (2003), two main causes for third-order cycles predominate: A) the waxing and waning of polar or land-locked ice fields (glacio-eustatic driver), and B) changes in ocean basin volume related to tectonism. Glacio-eustasy can readily account for the volumes and timing required for 3rd-order cycles (1-10 cm/kyr with amplitudes as great as 50-300 m) (Kendall and Schlager, 1981; Goldhammer, 2003). However, cycles with frequencies of 1-10 myr (3rd-order cycles) have been documented during periods of geologic time when no evidence for glaciation has been found. In these cases, tectono-eustatic oscillations of sea level are hypothesized, implying either changes in seafloor spreading rates or thermal subsidence as a direct driver for sea level change- though neither of these drivers are periodic (Goldhammer, 2003). It is also possible that 3rd-order cycles occur as the result of multiple processes (both cyclic and non-cyclic) acting together (e.g., thermal subsidence, climatic change brought on by volcanism, etc.). In addition, Lourens and Hilgen (1997) write that over the past 15 m.y. a correlation exists between 3rd-order sea level change, ocean cooling (recorded from $\delta^{18}O$ measurements) and long-term modulations of obliquity and eccentricity (operating at 1.2 m.y., and 2.4 m.y., respectively). Sea level oscillations with million-year frequencies were also conceptually linked to seismic-scale depositional sequences of the Tertiary by Matthews and Frohlich (1994), although a causative mechanism was not identified. The cause of 3rd-order depositional drivers is ever more problematic.

4th- and 5th-Order Cycles

Following in the paradigm set forth by Vail et al. (1977), workers identified and defined higher-frequency orders of periodic depositional cyclicity. According to Goldhammer (2003), Miall (1984) was the first to describe "4th-order" cycles, with durations between 0.2 and 0.5 myr. 5th-order cycles, with durations between 0.01 and 0.1 myr, were defined by Goldhammer et al. (1987, 1990) and Koerschner and Read (1989). These are the highest-frequency eustatic cyclicities recorded as depositional cycles in the rock record (Goldhammer, 2003). 4th and 5th-order cycles are thought to be the product of Milankovitchian astroclimatic forcing. Eccentricity (ca. 100 – ca. 400 kyr) drives 4th-order cycles, and precession (ca. 20 kyr) and obliquity (ca. 40 kyr) drive 5th-order cycles. However, many researchers use the order hierarchy regardless of any absolute age constraints on the stratigraphy in question (Goldhammer, 2003). Much of this stems from work done in the late 1980s and early 1990s, in which cyclic successions were considered to exhibit stacking patterns and cycle bundling frequencies consistent with predicted Milankovitchian glacio-eustasy (Grotzinger, 1986; Goldhammer et al., 1987; Hinnov and Goldhammer, 1991). Of course, even in sections that appear stratigraphically deterministic, normal sedimentary processes such as lateral sediment transport, storm activity and associated erosion can locally alter the cyclicity of the stratigraphy such that it may not be perfectly match the proposed forcing mechanism in a all locations (**Figure 1. 6**).

According to a treatise on cyclic sedimentation by Goldhammer (2003), 4th and 5th-order cycles are driven by any of the following 4 processes: 1. High-frequency glacio-eustatic oscillations generated by Milankovitch climatic rhythms; 2. Autocyclic mechanisms internal to the depositional system, and 3. Differential subsidence **(Figure 1. 7)**. Studies from modern environments (Barbados, New Guinea) have confirmed the existence of Milankovitch-band sea level oscillations and their effects on the growth of platform carbonates (Imbrie and Imbrie, 1980) (**Figure 1. 8**). Because of the close match between the stacking in cycle thickness series with that expected for Milankovitchian forcing, many stratigraphers have assigned relative periodicities to fundamental shallowing-upward cycles (many times assumed to be 5th-order) and megacycle bundles (4th-order) to the Milankovitch band. This assumption is the main issue of contention in the Latemar controversy (discussed in Chapter 2)

Millennial cycles

A millennial-frequency allocyclic driver has been proposed to account for governing carbonate depositional cycles at the Latemar cyclic succession in the Dolomites of Northern Italy. Several authors have recently concluded, based on U-Pb zircon dating, biostratigraphy and magnetostratigraphy, that the high-frequency, shallowing-upward Latemar cycles formed at rates of 4.2 kyr/cycle (Mundil et al., 2003; Zühlke et al., 2003; Zühlke, 2004) or 0.9-1.97 kyr/cycle (Kent et al., 2004; Emmerich et al., 2005). Drivers for these cycles are as of yet

undetermined, but hypotheses include Bond cycles or Heinrich events (rapid warming events leading to catastrophic shedding of glacial ice), millennial tides, and/or thermal expansion and contraction of ocean waters via millennial-scale variations in solar insolation. These mechanisms are hypothetical and not based on observational evidence. None of these periodic behaviors are recognized as drivers for carbonate depositional cycles in the Holocene or Pleistocene. A more in-depth treatment of this subject will be discussed in Chapter 2 in the context of the Latemar debate.

Depositional Cycles and their timing – A summary of the Holocene and Pleistocene

Comparative sedimentology has always been a first-order approach to understanding facies and their place within a depositional framework (Hardie, 1977; Hardie and Ginsburg, 1977; Demicco and Hardie, 1994). In many cases, the identification of facies in Holocene environments has been used as a template for the identification and/ or depth ranking of facies in order to determine cycle tops (**Figure 1. 9**) (e.g., Goldhammer et al., 1990; Preto et al., 2001, 2004). In addition, derivation of recent sea level history from dated depositional cycles suggests that high-frequency sea level oscillations in tune with the formation of carbonate depositional cycles operate at frequencies consistent with ca. 20 kyr and ca. 100 kyr Milankovitchian eustasy (Vecsei, 2004; Gischler, 2003; Strasser and Samankassou, 2003; Parkinson, 1989; Taft, 1968).

Zühlke et al. (2003; 2004), by Kent et al. (2004), and Emmerich et al. (2005) question the rates at which on-platform fundamental allogenic depositional cycles can accumulate. These authors conclude that cycles and megacycles may form at much more rapid periodicities, and therefore must be driven by "sub-Milankovitch-scale mechanisms". Proposed drivers for sub-20 kyr eustatic change include millennial-scale tidal forcing (*see* Munk et al., 2002) and various types of ice-breakout events related to solar insolation (*see* Bond et al., 1992). These sub-Milankovitchian processes were cross-applied to the Triassic, but are the direct result of modern icehouse climatic conditions, plate arrangement and ocean circulation patterns that may not be directly applicable to the greenhouse of the mid-Triassic (Zühlke, 2004).

As with comparative sedimentology, periodic cyclic behaviors and their frequencies have been identified in speleothems, tree rings, ice cores, and ice-rafted debris cycles (IRD). However no relationship between these cyclic processes, meter-scale sea level oscillations, and the formation of shallowing-upward sedimentary successions has been established (Kent et al., 2004 and responses). Comparatively little has been accomplished with regard to dating and identifying the time scales of cyclic drivers responsible for the formation of the shallowing-upward platform carbonate facies succession in the Holocene. Indeed, there are only 10 to 20 publications that include any dates on Holocene

successions at all. Ten of these publications are reviewed here in order to better understand the current state of knowledge surrounding modern depositional cycles and the processes interpreted to create them. This is important because if millennial-scale cyclic processes described above cannot be correlated to modern carbonate depositional cycles, it becomes increasingly difficult to believe that these processes formed depositional cycles in the geologic past.

Taft, 1968

The study by Taft (1968) of modern carbonate sediments on the New Providence platform, Bahamas was cited by Goldhammer (1987) for comparative purposes in his study of mid-Triassic carbonates at the Latemar. The main reason for this was the similarity in facies succession between Latemar coarsening-upward cycles and the dated facies succession studied by Taft (1968). Both successions coarsen up from mudstone/wackestones at their bases, through packstones and grainstones in their midsections, to composite-grain grainstones or gravelstones near their tops. Latemar cycles are distinguished from the New Providence succession by the presence of mm to cm-scale oncoids near cycle tops as well as dolomitized pisolitic caliche and tepee exposure caps, both of which are absent in the New Providence succession. The facies successions are otherwise very similar.

Radiocarbon dating of the 2.5 meter-thick succession indicates that Holocene sediments began accumulating on 20.8 kyr-old Pleistocene bedrock at 6.7 kyr BP. Additionally, the succession was dated at regular (sub-meter) intervals to determine relative rates of deposition. Basal mud and wackestone facies were found to have accumulated at ca. 30 cm/kyr, mid-sequence skeletal sands at ca. 225 cm/kyr, and the upper-most composite grain sands and cemented layers have been accumulating at ca. 30 cm/kyr. The sediment-water interface atop the Holocene succession is 4-8 meters below sea level at present, which explains the lack of exposure cap atop the succession.

The importance of the Taft (1968) study was explained by Goldhammer (1987). The central argument put forth was that while the facies succession at New Providence platform was generated by a sea level rise beginning from ca. 20 kyr BP, with the succession itself accumulating for only 6 kyr when the platform was last flooded. An additional detail noted by Goldhammer was that rates of deposition of facies types vary through the succession, with both basal and top sediments accumulating at the lower rates, such that portions of a single succession (e.g. the basal muds and upper composite grain gravels) may be condensed in terms of time-thickness relative to other portions of the succession (e.g. mid-cycle skeletal sands). These realizations are of critical importance when attempting to relate cycle thickness and sedimentation rates to a temporal

driver, and highlight the importance of considering variable rates of sedimentation per facies within a single depositional cycle.

Logan et al., 1969

In a seminal study of Quaternary through Holocene carbonate deposits in Shark Bay, Western Australia, Logan et al. (1969) identify three transgressive events, each with an associated depositional facies succession. The transgressions are (from oldest to youngest) the Dampier marine phase (mid Pleistocene), the Bibra marine Phase (late Pleistocene, ca. 39.1-28.8 kyr BP), and the recent Late Holocene transgressive phase (5 kyr BP to present). Each transgressive phase deposited a shallowing-upward facies succession with a vadose diagenetic cap. However, there is evidence (modern sediments and fossils found over 5 m above modern sea level) that these successions became emergent as the result of tectonic uplift, and therefore a pure eustatic driver cannot be absolutely identified as the causal mechanism for the formation of these deposits (p. 79). However, eustatic rise during the Pleistocene and Holocene has been described subsequent to Logan et al. (1969) (see summaries below), and is likely a component of the relative sea level drivers at work in Shark Bay.

The three marine transgressions studied by Logan et al. (1969) include the Dampier, Bibra, and Late Holocene marine phases. The Dampier marine

phase in Shark Bay occurred in mid-Pleistocene time (starting 90.5 kyr BP) and is composed of two formations - the Dampier Formation, composed of a pelecypod coquina and a mixed skeletal grainstone with minor coral reefs, and the Carbala Oolite, composed of a lower pelecypod coquina and mixed-skeletal grainstone, and an upper ooid grainstone. The Bibra formation overlies the Dampier formation. The contact is separated from it by an erosion surface showing evidence of incipient soil and calcrete formation. The Bibra formation itself consists of coral biostromes, and mixed skeletal and lithoclastic grainstones with a thickness of 0.3-1 meter. Dating of skeletal fragments from Bibra beds place the age of the skeletal material at between 39.1 kyr +/- 0.6 kyr and 28.8 kyr +/- 0.4 kyr. While the spread of dates within the Bibra is broad, it does place the formation within the late Pleistocene. The final sequence of rocks present in Shark Bay are the Late-Holocene to recent rocks is thought to have been the result of a sea level rise of 100-150 meters over the past 15 kyr. The actual flooding of Shark Bay, however, is thought to have occurred ca. 5 kyr BP (from radiocarbon dates on shell material). Sediments deposited since this transgression include mixed lithoclastic and skeletal grainstones and calcareous silts and muds, and include laminite-capped tidal flat facies within the shallow peritidal reaches of Shark Bay.

Again, as with other published studies, shallowing-upward facies successions in Shark Bay formed as a result of eustatic rise with periods on the

order of 10s of kyr. Repetitious, stacked shallowing-upward facies successions with millennial scale age have not been recognized.

Tudhope, 1989

Tudhope (1989) focused on the shallowing-upward lagoon-fill sedimentation, as recorded behind the Great Barrier Reef of Australia. Tudhope (1989) describes sediments within the 5-25 m deep lagoon behind the Davies reef, described as a "typical mid-shelf reef in the Central Great Barrier Reef" complex. These sediments are organized into a shallowing-upward facies succession that include a basal member of coralline gravel (reef-derived) that fines upward into a bioturbated muddy sand. In certain areas of the lagoon, the succession also contains in-situ patch reef framework overlying the bioturbated sand. The succession is typically capped by crossbedded coralline beach sands, muddy horizons with mangrove rhizoliths, or simply karstified/caliche caps. However, Tudhope notes that the Holocene succession has not yet filled available accommodation and so the current succession is not complete.

Radiocarbon (^{14}C) dating of the muddy sand member of the Holocene cycle suggests that the accumulation of muddy sand in the lagoon interior did not begin until 2.5 – 3 kyr BP. Tudhope suggests that the record of modern sediments in the lagoonal interior of Davies reef reflects a multi-millennial sea level rise that has been ongoing for at least 4 kyr. Tudhope hypothesizes that

Holocene sea level rise led to the growth of a coralline rim around the reef, which shed the coralline gravel forming the basal bed of the Holocene succession. Once sea level rise slowed, coral growth caught up to sea level (at ca. 3 – 4 kyr BP) and consequently the reef acted as an increasingly effective energy barrier, leading to the deposition of increasingly muddy sediments in the interior lagoon. Reef stabilization at sea level also led to the lateral growth of the reef complex, and consequently a greater supply of reef-derived debris for the platform interior lagoon and greater sedimentation rate. Tudhope hypothesizes that eventually the lagoon at Davies reef will fill in with sediment and become a flat-topped island.

As with other studies of Holocene shallow marine carbonates, Tudhope shows that the modern platform interior carbonate shallowing-upward succession formed since approximately 6 kyr BP. The lagoonal-interior example from Davies reef described here is at least 4 kyr in age, but has not yet filled the available accommodation space (6 to 24 meters). It is possible that a complete shallowing-upward facies succession will eventually be present at Davies reef. Although projected dates for the cycle's completion are not given, the current sedimentation rate of 3.4 mm/yr (3.4 m/kyr) suggests that sediment will infill the lagoon within 2-7 kyr. In order for vadose features to form, additional time is required, suggesting that a complete depositional cycle at Davies reef may represent ca. 10 kyr of actual depositional time.

Parkinson, 1989

Parkinson (1989) described and dated Holocene carbonate deposits in the southwest coast of Florida an attempt to identify a sedimentary record of sea level change. Parkinson postulated that a study of the southwest Florida coastline would be ideal for determining the effects of sea level rise because "the extremely low relief allows for the detection of minor sea level oscillations and the low-energy setting should favor sequence preservation." (p. 960).

Parkinson (1989) concludes that one retrogradational/progradational succession accumulated during the Holocene sea level rise. Flooding of the Southwestern Florida margin led to the deposition of (in ascending order) organic rich quartz packstones, organic rich peats and skeletal packstones. Parkinson shows that initial flooding over Pleistocene deposits led to the development of marginal swamps whose aggradation rates could not keep up with sea level rise. Their drowning resulted in burial by subsequent deposits of skeletal packstones. These deposits are then overlain by one of two types of progradational successions. The first (seaward islands) is an oyster rudstone or vermetid reef talus rudstone that grades up into in-place reefal material that is sometimes capped by red mangrove peat. The other progradational succession (interior islands) consists of oyster rudstone capped by red mangrove peat. Holocene sediments adjacent to the shoreline consist entirely of red mangrove peat.

Dating of the Holocene retrogradational/progradational package forming the Holocene sedimentary successions described in southwest Florida is based on ^{14}C measurements made from organic buildups within the progradational members of the successions. Sediments dated by Parkinson (1989) formed in association with Holocene transgression are greater than 3.5 kyr in age. Parkinson suggests that this date is consistent with hypotheses made by previous workers that the rate of Holocene sea level rise slowed somewhat ca. 3.5 kyr BP and that sediments were then able to "catch up" with eustatic rise. Furthermore, the Holocene depositional succession of southwest Florida formed at the end of 120 m of sea level rise that had been ongoing for 15+ kyr, but has been slowing since 3.5 kyr BP. Parkinson (1989) interprets 3 phases of sea level rise. The first phase occurred from 15 to 7 kyr BP (rate of rise of ca. 10 m/ kyr) and was responsible for the flooding of the western margin of peninsular Florida. The second occurred during the mid Holocene, 7 to 3.5 kyr BP (rate of rise of ca. 2.6 m/kyr) and resulted in the deposition of a transgressive/ retrogradational succession in Southwest Florida. The final phase of sea level rise (ca. 3.5 kyr BP to present) has the lowest rate of the three, ca. 0.4 m/kyr. Sedimentation to caught up with sea level rise and prograded seaward. Parkinson (1989) concludes that the entire Holocene shallowing-upward succession of carbonates along the coast of southwest Florida was deposited over the past 3.5 kyr **(Figure 1. 10)**.

Ramsay, 1995

One of the first publications to conclude that millennial-scale sea level oscillations are recorded in the carbonate rock record was published by Ramsay (1995). By dating cemented aeolianite and littoral sand bodies at several levels relative to present sea level in South Africa, Ramsay concluded that two oscillations in sea level with meter-scale amplitudes occurred over the past 9 kyr. Specifically, Ramsay analyzed sands cemented by blocky, equant calcite spar cements interpreted to have formed in a mixed marine-phreatic diagenetic environment. However, the texture and composition of the cemented sands is not described. Ramsay only assumes that the indurated layers of sand were formed along beaches and that the cements are analogous to Holocene beachrock, such as those described by Strasser et al. (1989). These measurements are not of shallowing-upward depositional cycles, but of paragenesis within an inherently autocyclic (aeolian) system. Additionally, Ramsay warns that "there has been no isostatic response study in southern Africa" and that models of relative uplift and emergence of the area were used in the construction of his Holocene sea level curve. However, if Ramsay is correct regarding the beach origin of indurated sands, then it stands to reason that sea level oscillations may be associated with their formation.

The beachrock sea level curve for South Africa generated by Ramsay (1995) is shown in **Figure 1. 11**). It was generated by dating cements in beachrocks and measuring their position relative to present day sea level. Ramsay proposes that sea level reached present level in South Africa at 6.4 kyr BP, and continued to rise for 2 kyr before reaching a highstand 3.5 m above present day sea level at 4.5 kyr BP. Sea level then fell to -2 m (relative to present) at 3 kyr BP. Sea level then rose and fell again, peaking 1.5 m above present day sea level at 1.61 kyr BP, and returning to modern levels at 0.9 kyr BP. Ramsay suggests that these sea level changes are the result of a combination of isostatic emergence and thermal expansion of seawater during mid-Holocene times. These oscillations are not correlated to any other locality. In addition, it must be noted that Ramsay (1995) dated beachrock cements, not shallowing-upward facies successions.

Chappell, 2002

Precision U-series dating of coral terraces exposed at Huon Peninsula, Papua, New Guinea have yielded the only evidence linking carbonate depositional successions to sub-20 kyr Milankovitchian drivers. The set of coral terraces investigated date from 30 to 65 kyr BP and are all raised well above current sea level due to tectonic uplift. Dating of terraces and wave-cut notches leads Chappell to conclude that tectonic uplift events are meter-scale and occur with a frequency of approximately one per kyr. By dating coral terraces and

assuming that uplift was steady at 3m/kyr, Chappell concluded that sea level oscillations occurred at 33, 38, 44.5, 52, and 58-60 kyr. Chappell's analysis invokes a process that involves 6-7 kyr of relative stillstand in sea level followed by a 10-15 m sea level rise over 1-2 kyr. Chappell interprets these rises in sea level as related to Heinrich events, which are episodes of ice breakout evidenced by layers of rafted debris littered cyclically on the seafloor of the North Atlantic. It should to be noted, however, that Chappell's analysis applies to one tectonically active locality. He does not correlate time-equivalent carbonate platformal deposits (e.g. filled lagoonal or tidal flat successions) with the coral terraces in New Guinea. Therefore, while it is clear that carbonate reefs specifically can accumulate rapidly enough to keep up with relative sea level rise at the rate of ca. 10mm/yr, a corresponding relationship has not been observed in lagoonal or tidal flat deposits.

Alsharhan and Kendall, 2003

Alsharhan and Kendall (2003) reviewed Holocene coastal carbonates and evaporites in the Arabian Gulf. Facies descriptions and depositional framework are presented in the context of Holocene sea level rise. Alsharhan and Kendall (2003) observe that maximum sea level low of -120 m during the Pleistocene (ca. 18 kyr BP) left the Arabian Gulf entirely exposed. Subsequent sea level rise to modern times left five notches cut into the bathymetry of the gulf (*see* Alsharhan and Kendall, 2003, Fig. 2, p. 194, reproduced here in **Figure 1. 12**). The notches

record episodes of sea level stillstand or reworking by shoreface ravinement. These 3-4 kyr pulses in sea level rise (as they are interpreted) would fit into the sub-Milankovitch framework for the Triassic Latemar succession as proposed by Zühlke et al. (2001), except that instead of producing depositional cycles, these pulses in sea level rise are substrate-subtractive, as they record an episode of erosion. This may be because longer-term "ice-house" sea level rise was too rapid for shallow water carbonates to colonize the substrate and generate sediment. Alsharhan and Kendall (2003) is fundamentally important because it shows (per this author's interpretation), in a modern environment, that a record of sub-Milankovitch sea level change exists. However, it remains unclear whether the record of notches in the Arabian Gulf represent true oscillations or stillstands in sea level during longer-term rise, or high energy events that do not relate to sea level oscillations at all.

Strasser and Samankassou, 2003

While studies dating Holocene sediments for facies-based accumulation rates are common, comparatively few have made the attempt at dating entire shallowing-upwards facies successions. Strasser and Samakassou (2003) conclude that carbonate sedimentation in the Holocene of Florida Bay, the Bahamas, and Bermuda are a product of the 20 kyr precessional cycle. They used ^{14}C dating of organic material within subtidal deposits and found that Holocene carbonate successions formed over the past 6 kyr at rates of 0.3 to 3

mm/yr. Average sea level rise in the region over the past 6 kyr has been ca. 5 m, with the turnaround from transgressive sedimentation to progradation occurring approximately 3.5 kyr BP. Additionally, Strasser and Samakassou (2003) note that while sedimentation rates for individual facies could be quite rapid (highest rate of 1.3 m/kyr from a single coral surrounded by muddy sediment) that sediment accumulation did not begin upon initial flooding but instead was initiated only after a lag depth (ca. 1 m) was attained and carbonate-producing organisms colonized the Pleistocene substrate. Gischler (2003) made a similar observation for isolated platform carbonates off Belize. Strasser and Samankassou do not report any stacked or repetitive shallowing-upward facies successions within the Holocene succession. This study found relatively young (0.6-1 kyr age) facies successions in landward positions on various platforms, but does not identify millennial-scale, repetitious phenomenon in any localities investigated.

Strasser and Samakassou (2003) also report that none of the successions that they investigated filled all the accommodation produced over the past 6 kyr, nor have indicators of subaerial exposure formed on the tops of shallowing-upward facies successions. This is a key observation, as no evidence of millennial scale sea level oscillations in the Holocene successions of the Holocene of Florida Bay, the Bahamas, or Bermuda is presented (**Figures 1. 13 and 1. 14**).

Gischler, 2003

Gischler (2003) analyzes a suite of 31 vibracores taken from the interior lagoons of Glovers Reef, Lighthouse Reef, and Turneffe Island in a study of the Holocene carbonate record of isolated carbonate platforms off Belize. Gischler identifies four main facies types through his coring project. The lowermost deposit is Pleistocene bedrock with abundant blocky calcite cements and recrystallized skeletal fragments indicative of exposure and alteration via meteoric diagenesis. Overlying the bedrock is a cm-thick soil composed of rooted carbonate mudstone with admixed quartz and clay particles (likely of aeolian origin). The soil is in turn overlain by mangrove peat, with recognizable roots from red and black mangrove plants identifiable in the core. Gischler also identifies modern carbonate lagoonal sediments consisting of mixed skeletal packstones at Lighthouse Reef and mixed skeletal packstones to wackestones at both Glovers Reef and the Turneffe Islands.

Gischler (2003) interprets the Holocene record of the Belize isolated platforms as follows. Soils formed on top of subaerially exposed Pleistocene bedrock while sea level was below platform tops. Mangrove peats developed during transgressive flooding of the platform tops (Glovers Reef at 8.5 kyr BP; Lighthouse Reef at 7 kyr BP; and the Turneffe Islands at 6 kyr BP). As sea level rise progressed, reefs colonized platform margins and lagoonal sedimentation

occurred in platform interiors, as it remains to the present. The Glovers lagoon is presently an average of 18 meters deep and Lighthouse and Turneffe lagoons are an average of 8 meters deep. The modern platform-top sediments have not yet aggraded to sea level. These platforms record only one Holocene-aged shallowing-upward succession of facies.

Vecsei, 2004

Vecsei (2004) uses a database of low-latitude carbonate banks to assess their production since 20 kyr BP. Vecsei is able to identify three main phases of carbonate production worldwide. Banks investigated include localities in the Caribbean, the southwestern Indian Ocean, northern Indian Ocean, southeastern Asia, the Caroline Islands, the Coral Sea, the Melanesian Borderland, and the Hawaiian chain. Phase 1 of carbonate production, as identified by Vecsei, occurred from 20 to 14 kyr BP. Global and local sea level records indicate a rise in sea level from approximately -120 m to -70 m during this time (ca. 9 m/kyr avg). This rise in sea level is identified through recognition of shallow biotic communities on the summits of carbonate platforms. From 14-6 kyr BP, Vecsei recognizes a second phase of production from -70 m to -20 m, when sea level rise slowed to ca. 5 m/kyr. Bank summits within 20 m of present sea level were flooded during this phase of the Holocene transgression. While banks were initially able to keep up with this second phase, most eventually drowned, as the rate of sea level rise was too rapid for substantial reef growth. Where reefs were

able to keep up, lagoonal interiors of some banks reach ca. 50 m deep. Phase 3 of carbonate production has been ongoing since 6 kyr BP, with the rate of sea level rise slowing to ca. 2 m/kyr. The Bahama bank platform tops were flooded during this phase of the Holocene transgression and carbonate production has kept up with sea level rise. This is the best modern example of a "carbonate factory", with abundant carbonate production ongoing in submerged settings ca. 10 m deep and shallower.

Vecsei (2004) also presents a composite sea level record derived from measurements of recent dated shallow water carbonate deposits (mostly shallow water corals) from around the globe (six total records from Barbados, Mayotte, Tahiti, the Great Barrier Reef, and the Caribbean and the Pacific). This composite curve (*see* Figure 3 in Vecsei, 2004) shows steadily decelerating sea level rise over the past 10 kyr, without any indicators of millennial-scale perturbations.

Summary and Implications of Holocene and Pleistocene Studies

By examining carbonate successions from various Holocene environments it is clear that a shallowing-upward carbonate facies successions has formed over the past 5-7 kyr as a result of a final stage of platform flooding, related to the 20 kyr, precession-driven rise in sea level. A key point within this framework is that although precession operates at approximately 20 kyr, the

actual resulting depositional succession generated represents roughly 30 percent or less of that time. It is important to realize that the majority of the time represented by a shallowing-upward facies succession per oscillation of cyclic mechanism (e.g., precession) is comprised of non-deposition (e.g. subaerial exposure, erosion, dissolution, flooding, attainment of lag depth, etc). This point was made quite clear by Goldhammer (1987, p. 225-233) by comparing the Holocene sea level curve to sediments accumulating on the New Providence platform, Bahamas (Taft , 1968) (**Figure 1. 15**).

The realization that the record of allogenic cyclicity would not be perfect was introduced by Schwarzacher (1975) and termed the “faulty recording mechanism” of the rock record. This is due the complexity of sedimentary processes rising from variable environmental inputs, biotic activity, antecedent topography, etc., that may or may not hinder the translation of a faithful record of environmental change through time to preserved rock. Schwarzacher’s view was a refinement of the view held by his former instructor Bruno Sander, who first recognized the potential of carbonates to record rhythmic sedimentary drivers through his studies in the Alpine Dachstein Limestone (Sander, 1951). To paraphrase, Sander suggested that a record of rhythmic forcing within the sedimentary record suggests (if not validates) a connection between cyclic driver and sedimentary product. However, the absence of that same rhythmic record within any stratigraphic succession does not necessarily indicate the absence of

time-cylicity, but rather the inability of the sediment to record the behavior of the cyclic driver (Sander, 1951; Goldhammer et al., 1990).

A solid understanding of Sander's Rule may be the key to approaching the topic of the relationship between carbonate depositional cyclicity and their forcing mechanisms. As an example, while millennial scale climate processes are now documented for the late Pleistocene, cyclic stacks of shallowing-upwards marine carbonate facies successions with millennial periodicities are not recognized in Pleistocene or Holocene environments (*see* chapter 3, Tables 1 & 2). Indeed, one might expect that millennial-scale sea level drivers would provide a means by which to form a series of like-timed, stacked sedimentary successions within the Holocene carbonate stratigraphic record. Investigation into the presence or absence of a temporal linkage of cyclic process to depositional cycle remains a central problem in cyclostratigraphy.

REGIONAL TECTONICS: AN OVERVIEW OF THE DEVELOPMENT OF THE TETHYS

Introduction

When approaching the carbonate massifs preserved in the Triassic of the Dolomites, one is immediately awestruck at the realization that these edifices, many which are nearly a kilometer in vertical relief, were formerly below sea level. That same notion piqued the curiosity of early scientists, prompting

seminal geologic studies of the area (Neumayr, 1885; Suess, 1893) and culminated in the realization that the Dolomite Alps were once part of the Mesozoic Tethys ocean system (Bernoulli and Lemoine, 1980). This ocean system was originally thought to have existed in the equatorial latitudes and to have stretched from what is now the Alps to the Himalayas. This idea was based on regional observations made by Suess (1875), who noticed close affinities between Alpine and Himalayan oceanic fauna of Triassic age. It was further recognized that Alpine-type mountain ranges formed as the result of the deformation and destruction of former ocean basins and uplift of continental margins during orogenic processes (Hsü and Bernoulli, 1978).

The Tethyan ocean system and uplifted Alpine carbonate belts developed in three main phases: the initial continental rifting during the Permian and Triassic, passive margin development during the Jurassic and Cretaceous, and post-Cretaceous orogeny. Each phase is recorded in the geologic record with distinct lithological and structural elements, summarized as follows:

Permian through mid-Triassic: Early Rifting

After the Hercynian orogeny the areas now occupied by the central Atlantic and Mediterranean were part of one land mass known collectively as Pangaea (Laubscher and Bernoulli, 1978) (**Figure 1. 16**). No remnants of Pre-Jurassic oceanic crust are known from these areas, and most sedimentary

deposits are continental or shallow-marine (Laubscher and Bernoulli, 1978; Bernoulli, 1980). Plate reconstructions by Smith et al. (1973) indicate that the Panthallasic Ocean had a wedge-shaped embayment along the eastern margin of Pangaea, between present-day Asia and Arabia (**Figure 1. 17**). This wedge-shaped re-entrant is known as the Paleotethys (Laubscher and Bernoulli, 1978). A belt of Permo-Triassic pelagic deposits and andesitic volcanics extending from the Caucases through Afghanistan and to the North of the Tibetan plateau testify to its existence and subsequent closure (Dewey et al., 1973; Hsü and Bernoulli, 1978). This zone, known as the Cimmerian-Indosinian suture, is the line of closure of the Paleotethys via north-directed subduction beneath Asia during Triassic times (**Figure 1. 18**) (Hsü and Bernoulli, 1978; Bernoulli, 1980). North-directed subduction of the Paleotethyan system during the Permo-Triassic, however, is discordant with the structural and stratigraphic development of the Alpine Triassic, which records ocean basin development and the evolution of a passive margin system (discussed in Chapter 4) (Bernoulli and Lemoine, 1980). As a result, workers recognize two Tethyan oceans- the Paleotethys, which closed via north-directed subduction during the Triassic, and the Tethys, which opened in the Triassic and closed in the late Cretaceous (Laubscher and Bernoulli, 1978).

During the Permian and Triassic, shallow seas extended from the Paelotethys onto the eastern margin of Pangaea (**Figure 1. 19**) (Laubscher and

Bernoulli, 1978). In the Dolomites, evidence for this includes marginal marine clastic and evaporite deposits (e.g. Upper Permian Gardena Sandstone and Bellerophon Evaporites) as well as shallow water carbonates. Transgression of seawater from the east continued throughout the Early Triassic, recording an increasing marine influence over eastern Pangaea and leading to the development of marginal marine evaporites stratigraphically above terrestrial fluvio-clastics in the South Alpine area (**Figure 1. 20**) (Bellerophon Evaporites, the Dolomites; Muschelkalk evaporites, Germany) (Laubscher and Bernoulli, 1978). It is possible that the facies record of encroachment of marine waters from the east was related to incipient rifting of Pangaea and westward development of the Tethyan system. Additional evidence supporting this interpretation includes a thickening of the Permian and Early Triassic sedimentary successions from west to east in the Dolomites (from 10's of meters to several hundred meters over ca. 100 km) (*see* Chapter5, Figures 5. 3, 5. 58).

Early rifting related to the breakup of Pangaea began to affect the Southern Alpine region in the Early to Mid Triassic, with encroaching marine sediments and faults generally becoming younger from east to west as rifting propagated across the area (Bernoulli and Lemoine, 1978). No oceanic crust was generated during this phase of rifting (e.g. Bernoulli and Lemoine, 1978, Bosellini, 1991). However, in the southern Alps, strike-slip flower structures with both normal and thrust faults indicates that early Triassic rifting was concurrent

with sinistral strike-slip. Left-lateral movement between Africa and Eurasia was likely a predecessor to actual sea floor spreading (Bernoulli and Lemoine, 1980; Hsü and Bernoulli, 1978; Doglioni, 1987; Bertotti, 1993). Both flower structures and NS-striking normal faults and grabens linked by EW-trending strike-slip faults, are observed in the Dolomites (Doglioni, 1987). The Mid-Triassic (Anisian/Ladinian) was also a time of increased subsidence in the region of the present day Dolomites, and was embodied by the development of pelagic basins and thick (hundreds of m) carbonate platforms, e.g., the Ladinian platforms of the Dolomites and Lombard basin (Bertotti et al., 1993). Many of these platforms are cut by depositionally overlapped normal faults (10s and 100s of meter-scale) and are crosscut by Ladinian volcanics (Lemoine and Trumpy, 1987; Bertotti et al., 1993). Volcanism in the Southern Alps during the Anisian and Ladinian filled much of the basinal areas with volcaniclastic material (e.g. Marmolada conglomerate) and pillow basalts (Bertotti et al., 1993). It is hypothesized that the partial infill of the mid-Triassic basins by volcanics allowed for rapid progradation of the Carnian platforms (e.g. Cassian Dolomite), further leveling bathymetry preceding the development of the wide carbonate shelves of the late Triassic of the Alps (e.g., Norian Dolomia Principale, Rhaetian Dachstein Limestone) (Bertotti et al., 1993).

Late Triassic through Jurassic: Rifting

Carbonate platforms developed in the late Triassic over a relatively flat antecedent topography (Carnian platforms and basins infilled with lowstand carbonates and clastics) throughout the Southern Alps (Bertotti et al., 1993). This carbonate shelf developed over the entire Southern Alpine region, and is known by different names in different areas (Dolomia Principale, Hauptdolomit). Early in the history of the Norian, evidence of substantial (100's of meters of offset) normal faulting can be found within the shelf, including the formation of kilometer-scale fault-bounded "mini" basins in the Lombard basin, directly west of the Dolomites (Jadoul et al., 1992). This period of extension is the onset of rifting of the Ligurian ocean system and the beginning of the formation of the South Alpine passive margin proper (*see* Figure 1. 5) (Laubscher and Bernoulli, 1978; Doglioni, 1987; Bertotti et al., 1993). This is thought mainly because the trend of synsedimentary extension continues throughout the Alpine succession from the early Norian through the drowning of Alpine carbonates in the Jurassic, including normal faulting, tilting of tectonic blocks (both 100s of m-scale) producing angular unconformities (e.g. Trento-Atesina high relative to Carnico-Bellunese basin), and differential thickness of Jurassic platform carbonates (e.g. Calcari Grigi near Val Badia, Dolomites) (Doglioni, 1987; Bertotti et al., 1993).

During the Jurassic, the Southern Alpine region developed from the geometries shown in Figure 5. 5 to those shown in **Figure 1. 21**. Jurassic

oceanic crust can be found on the margins of the Central Atlantic, as well as in the Ligurian-Piemonte and Eastern Mediterranean ophiolite zones, implying sinistral movements between Africa and Eurasia at the time (Laubscher and Bernoulli, 1978). Late Triassic and early Jurassic sinistral movements led to the formation of en echelon extensional troughs oriented roughly NS, linked by EW-oriented left-lateral strike-slip faults (Laubscher and Bernoulli, 1978; Doglioni, 1987). A similar pattern of deformation can be observed in the late Carnian and early Norian of the Dolomites, suggesting a structural linkage between the Southern Alps and the greater rift system (Doglioni, 1987). Rhaetian deposits of platform carbonates (e.g. Dachstein Limestone, Calcari Grigi) reach thicknesses of 2.5 km in areas of the Lombard basin, for instance, due the high sedimentation rates near the fault-bounded blocks. In the Dolomites, these deposits are overlain by a submarine hardground, followed by the deep-water marly/nodular Ammonitico Rosso (mid-Jurassic) and Cretaceous Puez Marls (Bosellini, 1991). The facies change from shallow-water shelf carbonates to deep-water marls in the mid-Jurassic signals a progressive foundering and drowning of portions of the Southern Alps associated with rifting, and a climate change from arid to comparably more humid, both affecting carbonates' ability to keep up with subsidence (Bosellini, 1991; Bertotti et al., 1993)

Alpine Inversion

The Southern Alps, and in particular the Dolomites, are thought to have undergone two separate periods of inversion via convergence (**Figure 1. 22**). The first, Paleogene in age, is thought to be related to the formation of the Dinarides (present day region of the former Yugoslavia). The second and more significant, and is Neogene in age. Both episodes are thought to be related to changing directions of relative motion (e.g., EW sinistral to dextral to NS convergence) between Africa and Eurasia. Excellent treatment of the Alpine inversion of the Dolomite Alps can be found in Doglioni (1987).

Dinaric Convergence

A phase of convergence is thought to be related to the formation of the Dinaric foreland (Upper Cretaceous-Paleogene?). This stems from the dating and orientation of structures (E-W and ENE-WSW) that were later overprinted by NNW-SSE Neogene reverse faults (**Figure 1. 23**) (Doglioni, 1987, 1992). This phase includes N-S and NNW-SSE trending thrusts and fold axes, W and WSW slickensides on fault surfaces (**Figure 1. 24**) (Doglioni, 1987, 1992). Relative dating of deformation can be surmised from the deformation of Lower Cretaceous (Neocomian) Marls and Lower Miocene conglomerates with detachment horizons in the upper Permian Bellerophon formation and Carnian Raibl formation in the Eastern Dolomites (Doglioni, 1987). Again, this deformation is thought to be the related to the Paleogene formation of the Dinaric

Alps, and perhaps represents the westernmost external deformation of the chain (Doglioni, 1987).

Neogene Convergence

Neogene deformation formed the majority of the present topography of the Dolomites, causing 3-5 km of uplift via the formation of a 60 km-wide south-vergent “pop-up” synclinorium (**Figure 1. 25**) (Doglioni, 1987, 1992). This synclinorium is bounded by the Valsugana thrust to the south (which cuts Miocene sediments) and the northward-verging Funes and Pso. Delle Erbe back thrusts (Doglioni, 1987) (**Figure 1. 26**). Neogene deformation shortened the sedimentary cover in the synclinorium, with areal balances by Doglioni (1987) of folds and faults in both basement and sedimentary cover totaling no more than 10% (ca 5 km) shortening from north to south. As a result, the uplift of the synclinorium did not significantly deform the sedimentary units of the Dolomites, and left synsedimentary deformations intact. Neogene orogenic processes in the Alps are related to NS shortening between the African and European plates (Doglioni, 1987).

TECTONICS OF THE DOLOMITES – AN OVERVIEW

Excellent treatment of the broad tectonic history of the Dolomites has been given in several publications by Bernoulli (1977) and Doglioni (1985, 1990,

1992). A brief summary of the tectonic history of the Dolomites and Southern Alps follows.

The post-Hercynian history of the Alpine depocenter begins in the Permian. According to Bernoulli and Lemoine (1980), the Southern Alps were located slightly to the southeast of a major fault line marking the future breakup of Pangaea and expansion of the Tethys (**Figure 1. 27**) Bernoulli and Lemoine, 1980, Figure 2). The general history of the tectonics of the Dolomites can be broken into four phases: 1. Lower Permian Rifting; 2. Mid-Triassic Rifting; Liassic (lower Jurassic) rifting, and 4. Alpine inversion.

Lower Permian Rifting

The rifting history recorded in the Dolomites begins in the Lower Permian after a period of erosion of former Hercynian mountains (Winterer and Bosellini, 1981). Initial rifting (possibly controlled and/or linked by EW sinistral strike-slip faulting) left the crust broken into NS-striking blocks, which subsequently acted to influence the structural grain of the sedimentary cover. (**Figures 1. 28 and 1. 29**) (Doglioni, 1985). These rifts were filled with felsic volcanics (mostly ignimbrites) known as the Bozner porphyry (Winterer and Bosellini, 1981). These bodies of volcanic rock greatly influenced subsequent stratigraphic development of the region, with thicker masses of felsic volcanics forming positive structural elements. In the Italian Alps, Permo-Triassic sedimentary fill in the central Trento

platform (also known as the Atesina platform) reached a thickness of ca. 2 km, while Permo-Triassic sedimentary fill in the Lombard basin (to the west) and in the Carnico-Bellunese basin (to the east) reached ca 5 km in thickness (**Figure 1. 30**). Abrupt differences in sedimentary thickness is thought to be due to synsedimentary faulting. However, the faults themselves are poorly exposed. The Dolomites are located in the eastern portion of the Trento/Atesina platform, with sedimentary cover thickening to the east, towards the Carnico-Bellunese Basin. Permian sediments consist of alluvial clastics in the western Dolomites, and restricted marine sediments in the east that uncomformably overlie either the Bozner porphyry or Hercynian basement where Permian volcanics are absent (Winterer and Bosselini, 1981; Bosellini, 1991).

Middle Triassic Rifting

The tectonics of Middle Triassic rifting recorded in the Dolomites is dominated by sinistral strike-slip tectonics. Doglioni (1985) suggests that this period of tectonic activity included the creation of flower structures concentrated along the Stava line/Cima Bocche anticline that are a reflection of a narrow but elongate EW-striking basement high (**Figure 1. 31**) (Doglioni, 1985). These features generally follow the prior structural grain striking roughly EW at N 70^{o} E and are cut by Late Ladinian-age volcanic dykes (Doglioni, 1985). Thick carbonate buildups (500m+) grew atop topographic highs and were flanked by starved, deep-water basinal areas with depths on the order of 800-1000 m

(Goldhammer, 1987; Bosellini, 1991). The Latemar platform grew on structural highs, as platform margins are very thin (only be a few meters wide) and reflect fault control (Goldhammer, 1987). Basinal areas were rather small (see Figure 1. 6), interspersed with platforms, and were short-lived due to infill by rift-related volcanics and volcaniclastics (Bernoulli and Lemoine, 1980; Winterer and Bosellini, 1981; Doglioni, 1985; Goldhammer, 1987).

There are several competing interpretations of the tectonic history of the Ladinian of the Dolomites (Bosellini, 1991). The large amount of stratigraphic, volcanic, and tectonic data accumulated by workers analyzing the Ladinian has led to four main interpretations regarding the origins of these structures and deposits: 1. the Ladinian of the Dolomites is an “aborted” continental rift, based on the existence of extensional structures and mafic volcanics (Bechstädt et al., 1978, Bosellini, 1991), 2. the Ladinian tectonics of the Dolomites reflects northward directed subduction of a lithospheric slab under the Southern Alps, based on the generation of calkalkaline volcanics (Castellarin et al., 1988); 3. the Ladinian tectonics of the Dolomites was dominated by a sinistral strike-slip system, generating both extensional (pull apart basins) and compressional (flower structures) structures (Doglioni, 1985; 1988); and 4. the Ladinian tectonics of the Dolomites were the result of local volcanism, based on the observation that structures are limited aerially to localities adjacent to volcanic and plutonic rocks of late-Ladinian age (Bosellini, 1984, 1991).

Late Triassic/Jurassic Rifting

The late Triassic and Jurassic period of rifting is separated from prior episodes of rifting in the Dolomites because oceanic crust began to form in the central Atlantic region and in the Ligurian ocean during this phase of rifting (Western Tethys) to the west of the southern Alps (Doglioni, 1985). These areas of oceanic crust formation then became the locus of sea floor spreading (Bernoulli and Lemoine, 1980; Winterer and Bosellini, 1981; Doglioni, 1985). The Dolomites then became part of a passive margin system, which is marked stratigraphically by a regional carbonate shelf many hundreds of km in aerial extent (Norian Dolomia Principale, Rhaetian Dachstein, and Liassic Calcari Grigi) (Winterer and Bosellini, 1981; Doglioni, 1985; Bosellini, 1991). These regional carbonate shelves were broken into 10+km-scale NS-trending blocks that underwent locally-unique subsidence histories, which can be recognized by differential thickness (100s of meters) of the formations (over 10s of km) as well as stacking pattern analysis of time-equivalent cyclic depositional successions that are uncorrelatable (Bosellini and Hardie, 1985; Jadoul et al., 1992; Carulli et al., 1998; Cozzi and Podda, 1998; Cozzi, 2000, this study).

Jurassic rifting in the Dolomites generated differential sediment thickness across the region. Late Triassic and Jurassic carbonates are ca 1 km thick in the eastern portion of the Trento/Atesina Platform and are over 2.5 km thick in the adjacent the Lombard and Carnico-Bellunese Basins directly to the east and

west (Winterer and Bosellini, 1981; Doglioni, 1985; Cozzi, pers. commun) (*see* Figure 1. 30).

The middle to upper Liassic marked a sedimentary turning point in the Southern Alps, with sedimentation rates abruptly slowing from 100s of m/myr to less than 10 m/myr (Winterer and Bosellini, 1981). This is accompanied by a shutdown in production of shallow-water carbonates and the deposition of red/green nodular limestone (Ammonitico Rosso) (Winterer and Bosellini, 1981). This is thought to have been the result of rapid subsidence of the Dolomites area as the result of renewed extensional tectonism that took the carbonate factory out of the photic zone.

REGIONAL STRATIGRAPHY OF THE DOLOMITES

An excellent overview of the regional stratigraphy of the Dolomites is given by Bosellini (1989, 1991) and is summarized below.

Basement and Early Permian

The stratigraphy of the Dolomite Alps contains a record of Permian through Cretaceous volcanism and sedimentation (**Figure 1. 32**). Most of the sedimentation took place in shallow marine settings (platform carbonates only a few meters deep; basins no more than 1000 meters deep). The basement of the Dolomites is made up of metamorphic and meta-sedimentary Paleozoic rocks

deformed by the Hercynian orogeny. These metamorphic rocks are capped in certain areas by Permian volcanics, known as the Bozner Porphyry (**Figure 1. 33**). The majority of the volcanics filled in NS-striking rift-related lows in the paleotopography, and subsequently acted as topographic highs during the Triassic (**Figure 1. 34**). The Bozner porphyry covers nearly 2000 km^2 and has local thicknesses exceeding 2 km (Bosellini, 1991). It has also been subdivided into two groups, a lower third made up of andesitic lava domes, and an upper two-thirds made up of rhyodacitic and rhyolitic ash flow tuffs (D'Amico, 1986; Bosellini, 1991). The radiometric ages for the volcanics range from 267 to 270 Ma for both members (D'Amico, 1986).

The sedimentary record of the Dolomite Alps begins uncomformably above the Bozner Porphyry (or above the Hercynian metamorphics where the Porphyry is not present) and consists of the mixed fluvial and paleosol beds of the Gardena Sandstone (Bosellini, 1991). The Gardena was deposited in a semi-arid setting, which is evidenced by gypsic and carbonitic rhizoliths in the numerous red paleosol profiles within the formation (**Figure 1. 35**) (Massari et al., 1988). Marine transgressions eventually overtook the depositional record, encroaching from the east (Bernoulli and Lemoine, 1980; Bosellini, 1991). Marine incursion is marked by a change from terrestrial sedimentation to proximal and shallow marine sedimentation and the deposition of the Bellerophon formation. The Bellerophon formation is a succession of mixed

peritidal dolomites and gypsic evaporites, recording a range of environments from coastal sabkha to shallow carbonate shelf/ramp (**Figure 1. 36**) (Bosellini and Hardie, 1973). Dolomite-evaporite cycles are easily observable in outcrops of the Bellerophon.

Lower to Mid-Triassic

Transitional terrestrial-to-marine deposits continue after Bellerophon time, with deposition of the Scythian (lowermost Triassic) Werfen formation unconformably atop the Bellerophon (Assereto et al., 1973; Bosellini, 1991). The Werfen is made up of a mixture of very shallow water carbonate and terrestrial clastic deposits. An excellent discussion of the Werfen and its occurrences throughout the Southern Alps can be found in Neri (1991).

Middle Triassic strike-slip tectonic activity resumed after the deposition of the Werfen, leading to localized subaerial exposure and erosion at various localities (Doglioni, 1985; Bosellini, 1991). As a result, there are complex facies associations in deposits formed during this period. The Western Dolomites (near the towns of Corvara and Colfosco) were affected by uplift and erosion such that the Werfen formation was entirely eroded (Bosellini, 1991). As a result, fluvial conglomerates (known as the Richtofen formation) lie uncomformably on the Bellerophon. Later, in the Anisian, renewed transgression (or relative sea level rise, whether eustatic or as the result of subsidence) revitalized carbonate

production on structural highs (Contrin Formation) in the western Dolomites, while basinal deposits (Braies Group) accumulated further to the east, off the margins of the uplifted localities (**Figure 1. 37**) (Doglioni, 1985; Bosellini, 1991).

Early Ladinian buildups in the Dolomites are some of the best known for their well-preserved records of platform-interior cyclic carbonate deposition (e.g. Latemar, Mendola Pass). While these deposits are arguably the most famous in the Dolomites (from a stratigraphic perspective), they are also at the center of a heated scientific debate, namely, the "Latemar controversy" (described in Chapter 2). Early to mid- Ladinian carbonate buildups grew on locally block-faulted structures (Bosellini, 1984, 1991; Doglioni, 1985) (**Figure 1. 38**). These are the buildups known for km-scale thicknesses of cyclic platform interior stratigraphy made famous by the studies of Goldhammer and others at Johns Hopkins in the mid-1980s and early 1990s, and include the Latemar platform, Mendola pass, the Rosengarten, and the Cernera massif (known collectively as the Schlern Dolomite) (**Figure 1. 39**). The end of the Ladinian was marked by extensive volcanism, such that many of the carbonate platforms (including the Latemar) were buried and entombed, only to be crosscut by late Ladinian volcanic intrusions (Bosellini, 1991).

The latest Ladinian and early Carnian of the Dolomites are characterized by progressive infilling of basinal areas by volcanics (including pillow lavas) and

later by volcaniclastics (Marmolada conglomerate; La Valle / Wengen volcaniclastic turbidites) (**Figure 1. 40**) (Bosellini, 1991). Once sedimentary input from volcanic sources slowed, formation of carbonates resumed on topographic highs. Locally, the platform carbonates that developed in the early Carnian are known as either the lower Cassian Dolomite or upper Schlern Dolomite, with the basinal equivalent known as the San Cassian (or San Cassiano) Formation (Bosellini, 1991). Cassian sedimentation was multi-stage, and at least two sequences of Cassian Dolomite development can be inferred from the deposits at the Sella Massif (informally called the lower and upper Cassian Dolomite) (Bosellini, 1991). Progradation of carbonate slope deposits during this time dominated the sedimentary record of Carnian platforms, and may represent some of the highest known carbonate accumulation rates in geologic history (30-50 cm/kyr sustained accumulation) (**Figure 1. 41**).

Towards the late Carnian, the Southern Alps were either uplifted, or sea level dropped considerably. Stillstand-to falling sea level is evidenced by toplap of Carnian Cassian platform carbonates at the Sella massif, as well as the deposition of the Dürrenstein shallow-water carbonates first in the former Cassian basins, and then on the former slopes of Carnian buildups (**Figure 1. 42**) (Bosellini, 1991). The stratigraphy of the Dürrenstein is also clearly cyclic, and has been investigated by Preto and Hinnov (2003).

The end of Dürrenstein deposition marked an important shift in the depositional regime of the Dolomites in that most of the basinal areas had been filled with volcaniclastics, turbidites and carbonates. As a result, by the end of the Carnian, there was minimal topographic relief throughout the Southern Alps such that subsequent deposits were regional, blanketing the entire area in sediment (Bosellini, 1991). Sea level drop at the end of Dürrenstein deposition allowed for the deposition of terrestrial and shallow-marine clastics (the Raibl Formation) that lie uncomformably over the Dürrenstein. The Raibl shows various types of depositional sub-environments at different localities, from fluvial to near shore marsh/lagoon to foreshore in the western Dolomites to marly limestones and evaporites further to the east (**Figure 1. 43**).

Late Triassic and Jurassic

Following the deposition of the Raibl, a different mode of carbonate sedimentation began in the Dolomites- that of a broad (hundreds of km-across), shallow (peritidal) carbonate shelf, the Norian Dolomia Principale (DP) (**Figure 1. 44**). The DP in the Dolomites can be observed in most localities in the central and eastern Dolomites, and may be volumetrically the largest carbonate formation in the region (hence its name). While the DP appears in the field as flat, monotonous, cyclic stratigraphy, abrupt changes in formational thickness (hundreds of meters) over relatively short distances (10s of km) suggest that the DP may also have experienced the effects of synsedimentary tectonism, perhaps

from continued rifting on the regional scale (see chapter 4 on the DP) (Bosellini and Hardie, 1985, Doglioni, 1992, Cozzi, 2002). Several orders of depositional cyclicity exist within the DP and are discussed in Chapter 5.

Latest Triassic and Jurassic deposits in the Dolomites have received comparably less attention than other deposits, likely because of the extreme difficulty and danger in getting access to the rocks themselves (these deposits all lie at the tops of cliffs that may be nearly a kilometer high). What can be said is that after the deposition of the DP came the Rhaetian Dachstein limestone, which is far better exposed in the Bavarian Alps to the north and the Julian Alps to the east (Cozzi et al., 2005; Schwarzacher, 2005). The Dachstein, of course, is the famous formation measured by Fischer that led to his seminal publication on Milankovitch cyclicity in platform carbonates (Fischer, 1964). After the Dachstein comes the cyclic Calcari Grigi peritidal limestone, which is followed by the Jurassic and Cretaceous “drowning succession” of deep water carbonates (Ammonitico Rosso) and marls (Puez marls). It is thought that the drowning succession is a record of the foundering of the Dolomites region as the result of regional subsidence related to the opening of the Atlantic and associated seaways to the east (Tethys) and west (Ligurian ocean) (Winterer and Bosellini, 1981).

This investigation centers on examination of platform-interior depositional cycles of the Anisian/Ladinian Latemar platform as well as the Norian Dolomia Principale.

REFERENCES

Alsharhan, A.S., and Kendall, C.G.St.C., 2003, Holocene coastal carbonates and evaporites of the southern Arabian Gulf and their ancient analogues: Earth-Science Reviews, v. 61, p. 191-243.

Assereto, R., 1973, The Permian-Triassic boundary in the Southern Alps (Italy): Memoir of the Canadian Society of Petroleum Geologists, is. 2, The Permian and Triassic systems and their mutual boundary, p.176-199

Bernoulli, D., 1980, Ancient continantal margins of the Tethyan ocean: Notes from the Geological Institute, The University of Basel, Switzerland, p. 1-19

Bernoulli, D., and Lemoine, M., 1980, Birth and early evolution of the Tethys: the overall situation: Memorie Bureau de Recherches Geologiques et Minieres, no. 115, p. 168-179.

Bertotti, G., Picotti, V., Bernoulli, D., and Castellarin, A., 1993, From rifting to drifting: tectonic evolution of the South-Alpine upper crust from the Triassic to the Early Cretaceous: Sedimentary Geology, Vol. 86, pp. 53-76.

Bloom, A.L., Broecker, W.S., Chappell, J.M.A., Matthews, R.K., and Mesolella, K.J., 1974, Quaternary sea level fluctuations on a tectonic coast: Quaternary Research, v. 4, p. 185-205.

Bond, G., Kromer, B., Beer, J., Muscheler, R., Evans, M.N., Showers, W., Hoffman, S., Lotti-Bond, R., Hajdas, I., and Bonani, G., 2001, Persistent solar influence on North Atlantic climate during the Holocene: Science, v. 294, p. 2130-2136.

Bond, G., Showers, W., Cheseby, M., Lotti, R., Almasi, P., deMenocal, P., Priore, P., Cullen, H., Hajdas, I., and Bonani, G., 1997, A Pervasive millennial-scale cycle in North Atlantic Holocene and glacial climates: Science, v. 278, p. 1257-1266.

Bosellini, A., 1984, Progradation geometries of carbonate platforms: examples from the Triassic of the Dolomites (Northern Italy): Sedimentology, vol. 31, p. 1-24.

Bosellini, A., 1991, Geology of the Dolomites: An introduction: Dolomieu Conference on carbonate platforms and dolomitization. Ortisei, 43 p.

Bosellini, A., and Hsü, K.J., 1973, Mediterranean plate tectonics and Triassic paleogeography: Nature, v. 244, p. 144-146.

Bosellini, A., and Hardie, L.A., 1988, Facies e cicli della Dolomia Principale delle Alpi Venete: Memorie della Societa Geologica Italiana, v. 30, p. 245-266.

Chappell, J., 2002, Sea level changes forced ice breakouts in the last glacial cycle: new results from coral terraces: Quaternary Science Reviews, v. 21, p. 1229-1240.

Cozzi, A., Hinnov, L.A., and Hardie, L.A., 2005, Orbitally forced Lofer cycles in the Dachstein Limestone of the Julian Alps (northeastern Italy): Geology, v. 33, is. 10, p.789-792.

Cozzi, A., 2002, Facies Patterns of a Tectonically-Controlled Upper Triassic Platform-Slope Carbonate Depositional System (Carnian Prealpls, Northeastern Italy): Facies, v. 47, p. 151-178.

Demicco R.V., and Hardie, L.A., 1994, Sedimentary structures and early diagenetic features of shallow marine carbonate deposits: SEPM Atlas Series No. 1, 265 p.

Dewey, J.F., Pitman, W.C., Ryan, W.B., Bonnin, J., 1973, Plate tectonics and the evolution of the Alpine System: Geological Society of America Bulletin, v. 84, p. 3137-3180.

Doglioni, C., 1992, Relationships between Mesozoic extensional tectonics, stratigraphy, and Alpine inversion in the Southern Alps: Eclogae Geolgica Helvetica, v. 85, no. 1, p. 105-126.

Doglioni C., 1988, Examples of strike-slip tectonics on platform-basin margins: Tectonophysics, v. 156, p. 293-302.

Doglioni C., 1987, Tectonics of the Dolomites (Southern Alps, Northern Italy): Journal of Structural Geology, v. 9, no. 2, p.181-193.

Einsele, G., Ricken, W., and Seilacher, A. (eds.), 1991, Cycle and Events in Stratigraphy: New York: Springer-Verlag

Emmerich, A., Glasmacher, U.A., Bauer, F., Bechstädt, T., and Zühlke, R., 2005, Meso-/Cenozoic basin and carbonate platform development in the SW-Dolomites unraveled by basin modeling and apatite FT analysis: Rosengarten and Latemar (Northern Italy): Sedimentary Geology, vol. 175, is. 1-4, p.415-438.

Favre, P., and Stampfli, G.M., 1992, From rifting to passive margin: The examples of the Red Sea, Central Atlantic, and Alpine Tethys: Tectonophysics, v. 215, p. 69-97.

Fischer, A.G., 1964, The Lofer Cyclothems of the Alpine Triassic: Kansas Geological Society Bulletin, v. 169, p.107-149.

Ginsburg, R.N., 1971, Landward movement of carbonate mud: New model for regressive cycles in carbonates (abs.): American Association of Petroleum Geologists Bulletin, v. 55, p. 340.

Ginsburg, R.N., Hardie, L.A., Bricker, O.P., Garrett, P., Wanless, H.R., 1977, Exposure Index: A quantitative approach to defining position within the tidal zone. *in* Hardie, L.A., *ed*., Sedimentation on the Modern Carbonate Tidal Flats of Northwest Andros Island, Bahamas. The Johns Hopkins University Studies in Geology, no. 22., p. 7-11.

Gischler, E., 2003, Holocene lagoonal development in the isolated carbonate platforms off Belize: Sedimentary Geology, v. 159, p. 113-132.

Goldhammer, R.K., 2003, Cyclic Sedimentation, *in* Middleton, G.V., ed., Encyclopedia of Sediments and Sedimentary Rocks, Springer-Verlag, Netherlands p. 173-185.

Goldhammer, R.K., Dunn, P.A., and Hardie, L.A., 1990, Depositional cycles, composite sea level changes, cycle stacking patterns, and the hierarchy of stratigraphic forcing: Examples from the Alpine Triassic platform carbonates: Geological Society of America Bulletin, v. 102 p. 535-562.

Goldhammer, R.K., Dunn, P.A., and Hardie, L.A., 1987, High-frequency glacio-eustatic sea level oscillations with Milankovitch characteristics recorded in Middle Triassic platform carbonates in Northern Italy: American Journal of Science, v. 287, p. 853-892.

Grabau, A.W., 1913, Principles of Stratigraphy: New York: Seiler and Co.

Grotzinger, J.P., 1986 Cyclicity and paleoenvironmental dynamics, Rocknest platform, northwest Canada: Geological Society of America Bulletin, v. 97, p. 1208-1231.

Hardie, L.A., and Ginsburg., R.N., 1977, Layering: The origin and environmental significance of lamination and thin bedding. *In* Hardie, L.A., *ed*., Sedimentation on the Modern Carbonate Tidal Flats of Northwest Andros Island, Bahamas. The Johns Hopkins University Studies in Geology, no. 22. p. 50-123.

Hardie, L.A., and Shinn, E.A., 1986, Carbonate depositional environments, modern and ancient, 3, Tidal Flats: Colorado School of Mines Quarterly, v. 81, p. 1-74.

Hinnov, L.A., 2000, New perspectives on orbitally forced stratigraphy: Annual Review of Earth and Planetary Sciences, v. 28, p. 419-475.

Hinnov, L.A. and Goldhammer, R.K., 1991, Spectral analysis of the Middle Triassic Latemar Limestone: Journal of Sedimentary Petrology, v. 61, p. 1173-1193.

Hinnov, L.A. and Preto, N., 2003, Analyzing the depositional signal of the Latemar Limestone (Dolomites, Italy): a multiple working hypothesis approach. in Brack, P., Schlager, W. and Stefani., M., eds., Abstract Volume, Triassic Geochronology and Cyclostratigraphy - a Field Symposium, St.Christina/Italy, September 11-13, p. 10.

Hsü, K.J., and Bernoulli, D., 1978, Genesis of the Tethys and the Mediterranean: DSDP, Vol. 42, pp. 943-949.

Jadoul, F.; Berra, F.; and Frisia, S., 1992, Stratigraphic and paleogeographic evolution of a carbonate platform in an extensional tectonic regime: the example of the Dolomia Principale in Lombardy (Italy): Ri. It. Paleont. Strat., Vol. 98, No.1, pp. 29-44.

James, N.P., 1984, Shallowing-upward sequences in carbonates: *In* Walker, R.G., (ed.), Facies Models. Geoscience Canada Reprint Series 1, p. 213-228.

Kendall, G. St.C. and Schlager, W.,1981, Carbonates and relative changes in sea level: Marine Geology, v. 44, p 181-212.

Kent, D.V., Muttoni, G., and Brack, P., 2004, Magnetostratigraphic conformation of a much faster tempo for sea level change for the Middle Triassic Latemar platform carbonates: Earth and Planetary Science Letters, v. 228, p. 369-377.

Kerans, C.,1995, Use of one- and two-dimensional cycle analysis in establishing high-frequency sequence frameworks. *In* Read, J.F., Kerans, C., and Weber, L.J., (eds.), Milankovitch sea level changes, cycles, and reservoirs on carbonate platforms in greenhouse and icehouse worlds. SEPM Short Course Notes, no. 35, p. 1-20.

Koerschner III, W.F., and Read, J.F., 1989, Field and modeling studies of Cambrian carbonate cycles, Virginia Appalachians: Journal of Sedimentary Petrology, Vol. 59, p. 654-687.

Laubscher, H., and Bernoulli, D., 1978, Mediterranean and Tethys, *in* Nainn, A.E.M., Kanes, W.H., and Stehli, F.G., (eds.), The ocean basins and margins, 4A: New York, Plenum Press, p. 1-28.

Lemoine, M., and Trumpy, R., 1987, Pre-oceanic rifting in the Alps: Tectonophysics, v. 133, p. 305-320.

Logan, B.W., Read, J.F., and Davies, G.R., 1969, History of carbonate sedimentation, Quaternary epoch, Shark Bay, Western Australia: *in* American Association of Petroleum Geologists – Memoir 13, p. 38-84.

Lourens, L.J, and Hilgen, F.J., 1997, Long-periodic variations in the Earth's obliquity and their relation to third-order eustatic cycles and late Neogene glaciation: Quaternary International, v. 40, p. 43-52.

Matthews, R.K., and Frohlich, C., 1994, Orbital forcing of glacioeustasy and its implications for petroleum exploration and production: AAPG Annual meeting abstracts, v. 4, p. 61-62.

Miall, A.D., 1984, Principles of Sedimentart Basin Analysis, 2nd edition, New York: Springer-Verlag, 1990.

Mundil, R., Zühlke, R., Bechstadt, T., Brack, P., Egenhoff, S., Meier, M., Oberli, F., Peterhänsel, A., and Rieber, H., 2003, Cyclicities in Triassic Platform Carbonates: synchronizing radio-isotopic and orbital clock: Terra Nova, v. 15/2, p. 81-87.

Munk, W., Dzieciuch, M., and Jayne, S., 2002, Millennial climate variability: Is there a tidal connection?: Journal of Climate, v. 15. p.370-385.

Parkinson, R.W., 1989, Decelerating Holocene sea level rise and its influence on southwest Florida coastal evolution: A transgressive/regressive stratigraphy: Journal of Sedimentary Petrology, v. 59, no. 6, p. 960-972.

Preto, N., Hinnov, L.A., Hardie, L.A., and De Zanche, V., 2001, Middle Triassic orbital signature recorded in the shallow-marine Latemar carbonate buildup (Dolomites, Italy): Geology, v. 29, no. 12, p. 1123-1126.

Preto, N., Hinnov, L A., De Zanche, V., Mietto, P.,, and Hardie, L.A., 2004, The Milankovitch interpretation of the Latemar platform cycles (Dolomites, Italy): implications for geochronology, biostratigraphy, and middle Triassic carbonate accumulation: SEPM Special Publication No. 81, p. 167-182.

Read, J.F., 1995 Overview of carbonate platform sequences, cycle stratigraphy, and reservoirs in greenhouse and icehouse worlds. *In* Read, J.F., Kerans, C., and Weber, L.J., (eds.), Milankovitch sea level changes, cycles, and reservoirs on carbonate platforms in greenhouse and icehouse worlds: SEPM Short Course Notes, no. 35, p. 1-102.

Read, J.F., and Goldhammer, R.K., 1988, Use of Fischer plots to determine third-order sea level curves in Ordivician peritidal carbonates, Appalachians: Geology, v. 16, no. 10, p.895-899.

Sander, B., 1951, Contributions to the study of depositional fabrics; rhythmically deposited Triassic limestones and dolomites. *English translation by Eleanora Bliss* Knopf, 160 p.

Scandone, P., 1975, Triassic seaways and the Jurassic Tethys ocean in the central Mediterranean area: Nature, v. 256, p. 117-118.

Schlager, W., 1999, Scaling of sedimentation rates and drowning of reefs and carbonate platforms: Geology, v. 27, no. 2, p. 183-186.

Schulz, M., and Schaefer-Neth, C., 1997, Translating Milankovitch climate forcing into eustatic fluctuations via thermal deep water expansion: a conceptual link.: Terra Nova, v. 9, no. 5, p. 228-232.

Schwarzacher, W., 1975, Sedimentation Models and Quantitative Stratigraphy: New York, Elsevier, 382 p.

Schwarzacher, W., 2005, The stratification and cyclicity of the Dachstein Limestone in Lofer, Leogang and Steinernes Meer (Northern Calcareous Alps, Austria): Sedimentary Geology v. 181, is. 1-2, p. 93-106

Shinn, E.A., 1986, Modern Carbonate Tidal Flats: Their Diagnostic Features., in Hardie, L.A., and Shinn, E.A., Carbonate Depositional Environments, Modern and Ancient: Colorado School of Mines Quarterly, v. 81, No. 1, p. 7-33.

Sloss, L.L., 1963, Sequences in the cratonic interior of North America: Geological Society of America Bulletin, v. 74, is. 2, p. 93-113.

Strasser, A., and Samankassou, E., 2003, Carbonate sedimentation rates today and in the past: Holocene of Florida Bay, Bahamas, and Bermuda vs. Upper Jurassic and Lower Cretaceous of the Jura Mountains (Switzerland and France): Geologica Croatica, v. 56, no. 1, p. 1-18.

Suess, E., 1888 Das Anilitz der Erder, Volume 2. *English translation by Sollas*, 1906 Oxford: Clarendon

Press, p. 1-254.

Taft, W.H., 1968, Lithification of modern marine carbonate sediments at Yellow Bank, Bahamas, Bulletin of Marine Science, v. 18, is. 4, p.762-828

Tudhope, A.W., 1989, Shallowing-upwards sedimentation in a coral reef lagoon, Great Barrier Reef of Australia: Journal of Sedimentary Petrology, v. 59, no. 6, p. 1036-1051.

Vail, P.R., Mitchum jr., R.M., Thompson III, S., 1977, Seismic stratigraphy and global changes of sea level, part 4: Global cycles of relative changes of sea level: *in* Payton, C.E., ed., Seismic Stratigraphy – Applications to Hydrocarbon Exploration: American Association of Petroleum Geologists Memoir 36, p.83-97.

Vecsei, A, 2004, Carbonate production on isolated banks since 20 k.a. BP, climatic implications: Palaeogeography, Palaeoclimatology, Palaeoecology, V. 214, Is. 1-2, p. 3-10

Walker, R.G., and James, N.P., (eds.), 1990, Facies Models: Response to sea level change: Geological Association of Canada, 317 p.

Wilson, J.T., 1966, Did the Atlantic close and then re-open?: Nature, v. 211, is. 5050, p. 676-681.

Wilson, J.L., 1975, Carbonate facies in geologic history, New York: Springer-Verlag.

Winterer, E.L., and Bosellini, 1981, Subsidence and sedimentation on Jurassic passive continental margin, Southern Alps, Italy: AAPG Bulletin, v. 65, is. 3, p. 394-421

Zühlke, R., 2004, Integrated cyclostratigraphy of a model Mesozoic carbonate platform - the Latemar (Middle Triassic, Italy). in D´Argenio, B., Fischer, A., Premoli Silva, I. and Weissert, H., eds., Multidisciplinary Approach to Cyclostratigraphy: Society for Sedimentary Geology, Special Publication.

Zühlke, R., Bechstädt, T., and Mundil, R., 2003, Sub-Milankovitch and Milankovitch forcing on a model Mesozoic carbonate platform – the Latemar (Middle Triassic, Italy): Terra Nova, v. 15, no. 2, p. 69-80.

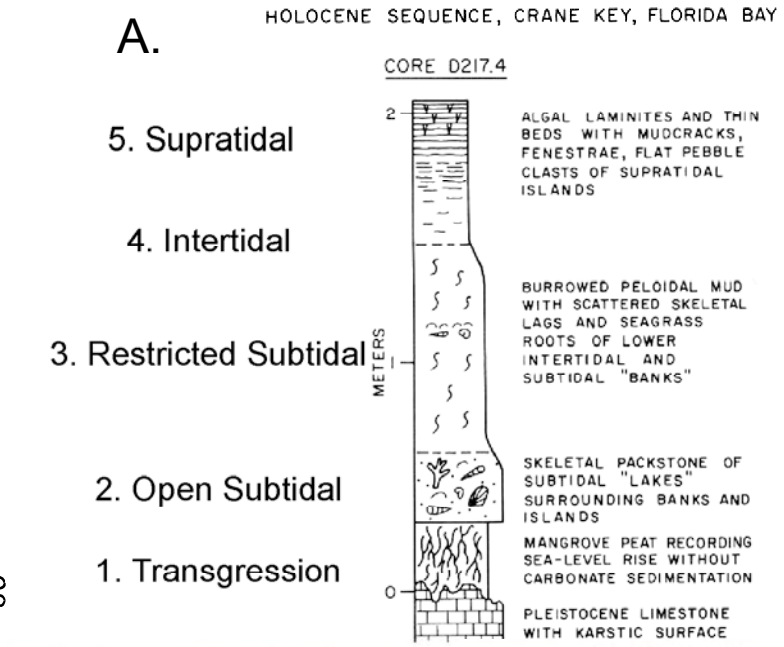

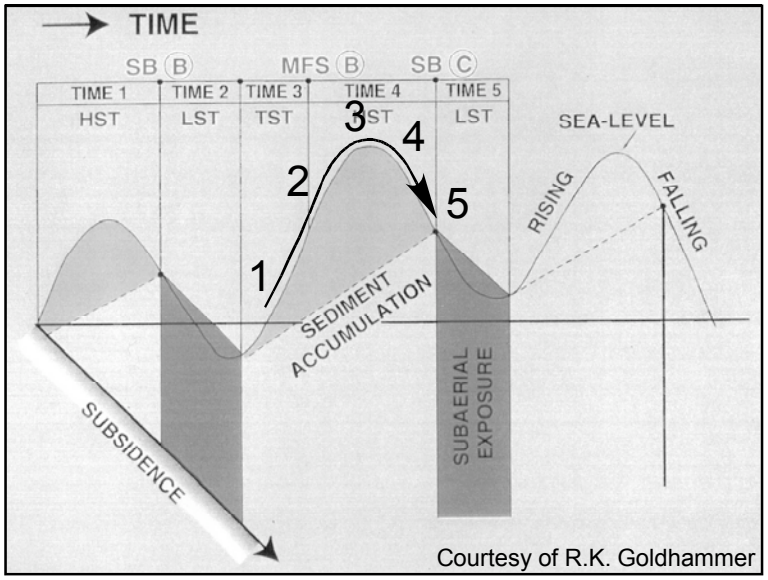

Photos courtesy of R.K. Goldhammer

Figure 1.1. A. Holocene shallowing-upward depositional cycle from Crane Key, Florida Bay, with like-facies keyed to B. diagram depicting relative sea level rise and fall and photographs of representative facies keyed to shallowing-upward succession in modern environments (with equivalent descriptions) are also shown.

Figure 1.2. Cima Ovest, Tre Cime di Lavaredo, the Dolomites, N. Italy. Cima Ovest is an outcrop of over 700 m high made up of several hundred stacked, meter-scale peritidal carbonate depositional cycles. It is hypothesized that these cycles formed as the result of relative sea level oscillations driven by a combination of eustasy and steady, long-term subsidence. This outcrop has never been fully measured for stratigraphic analysis, but was partially measured in this study.

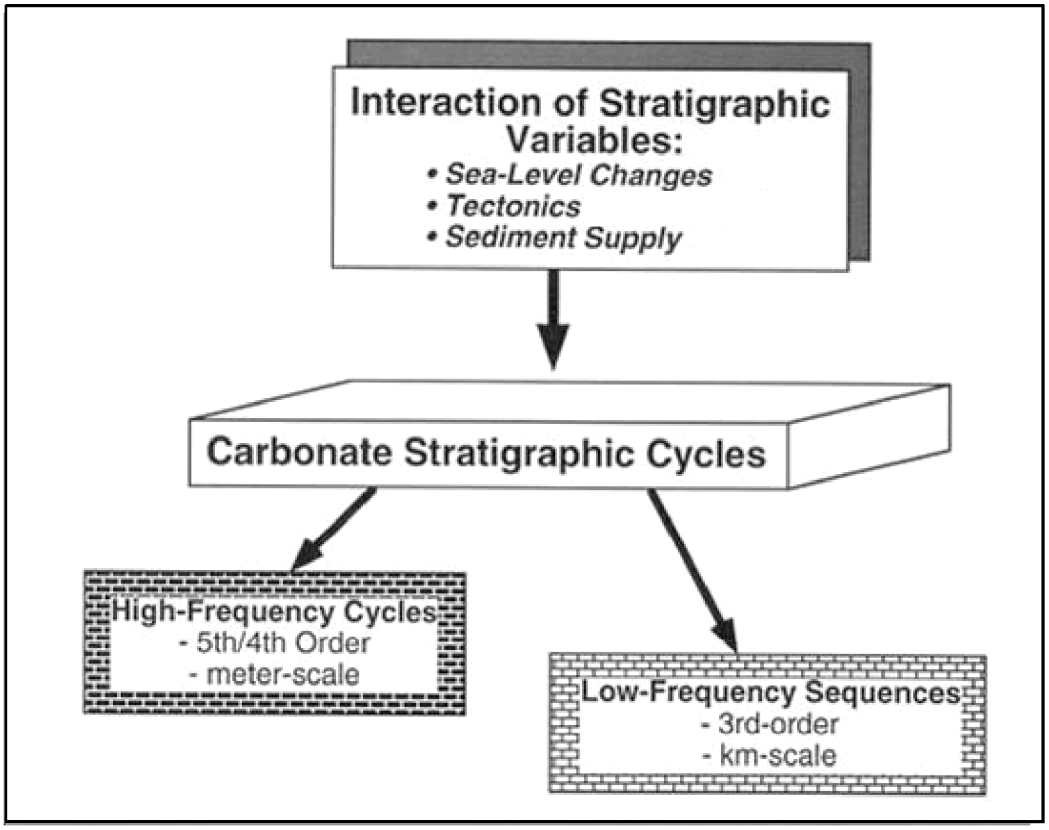

Courtesy of R.K. Goldhammer

Figure 1.3. The interaction of sea level changes, tectonics, subsidence, and sediment supply through time act to form depositional cycles in carbonate producing environments.

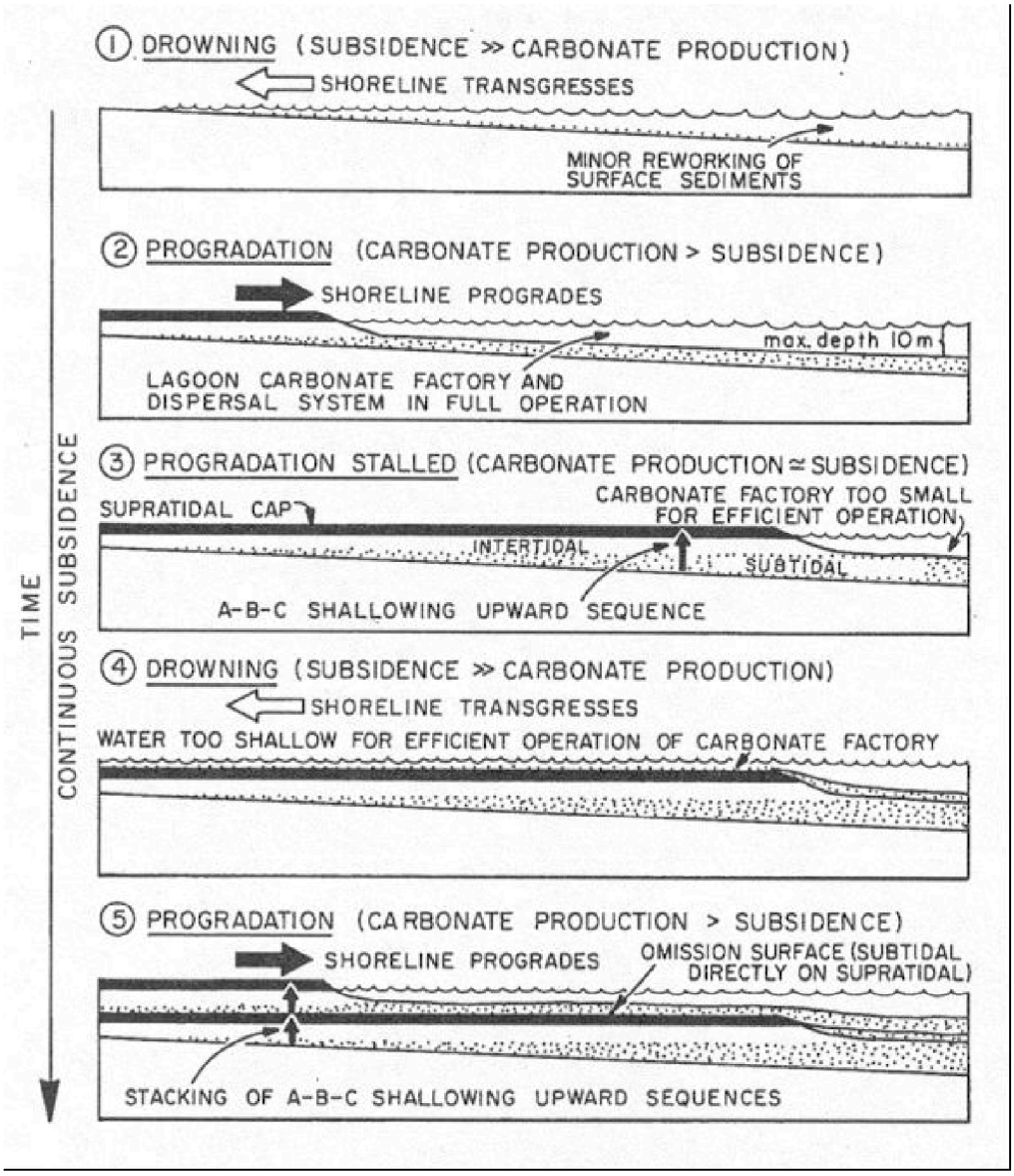

Figure 1.4. Schematic representation of autocyclicity after Ginsburg (1971). Diagram from Hardie (1986). The model postulates that carbonate cycles can form as a result of carbonate sedimentation and long-term subsidence alone. Sediment is produced in subtidal lagoonal environments when appropriate depth exists in the lagoon for healthy circulation across the platform. Accommodation is then filled via shoreline/tidal flat progradation over the lagoon, which eventually limits the amount of sediment feeding the tidal flats by progressively limiting the area represented by the lagoonal carbonate factory. After sedimentary shutdown, subsidence continues until appropriate lagoonal depth is re-attained and the sedimentary process resumes.

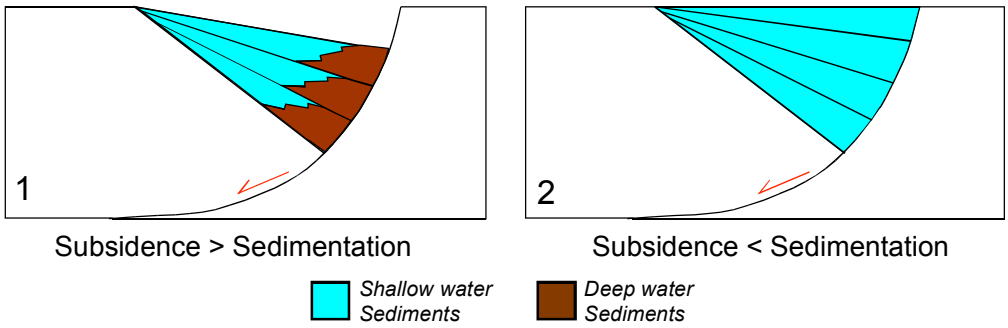

Figure 1.5. Diagram of the effect of synsedimentary extension on stratigraphy, in this case related to listric normal faulting (after Doglioni, 1992). In example 1, subsidence outpaces sedimentation, leading to depth dependent facies variability and the formation of a growth fault. In example 2, sedimentation keeps up with subsidence. In this case, beds thicken towards the hanging wall of faults without extreme depth-dependent facies variability occurring. In either case, sediment infill of accommodation space generated by faults can occur in repetitive facies successions that, while lithologically repetitive, are not temporally periodic.

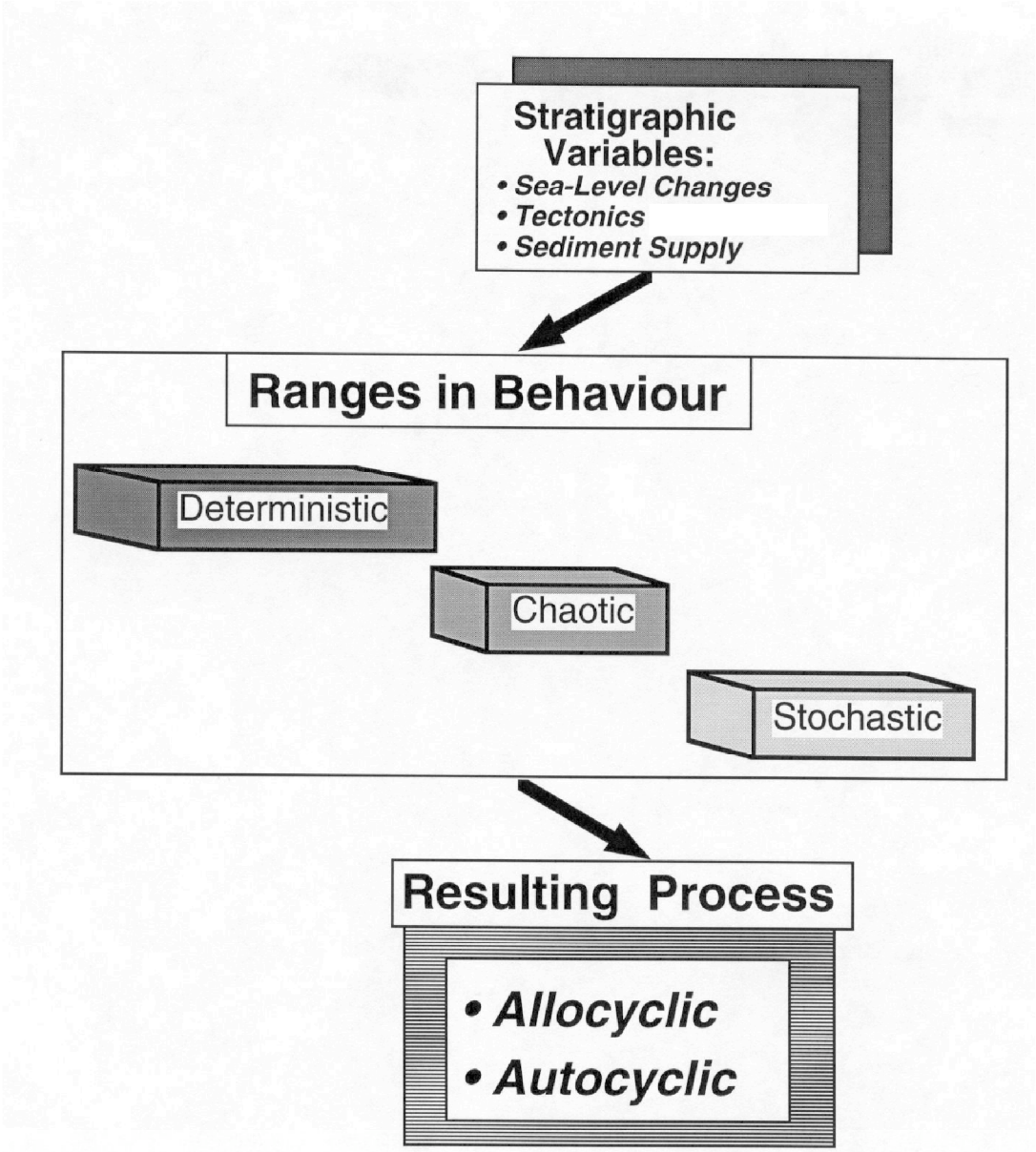

Figure 1.6. Flow chart depicting stratigraphic variables acting upon sediment and how the nature of these behaviors determines the type of cyclicity (autocyclic/intrabasinal or allocyclic/extrabasinal) that are produced. Even if the actors upon the sediment are deterministic (predictable, e.g., Milankovitchian orbital forcing acting to produce sea level changes) and produce allocycles the majority of the time, normal sedimentary processes (e.g. current action and sediment transport; storms, etc.) will add a measure of “chaos” (unpredictability) to the final arrangement of depositional cycles in the rock record such that even the most deterministic signal will have some degree of chaotic overprint due to normal sedimentary processes.

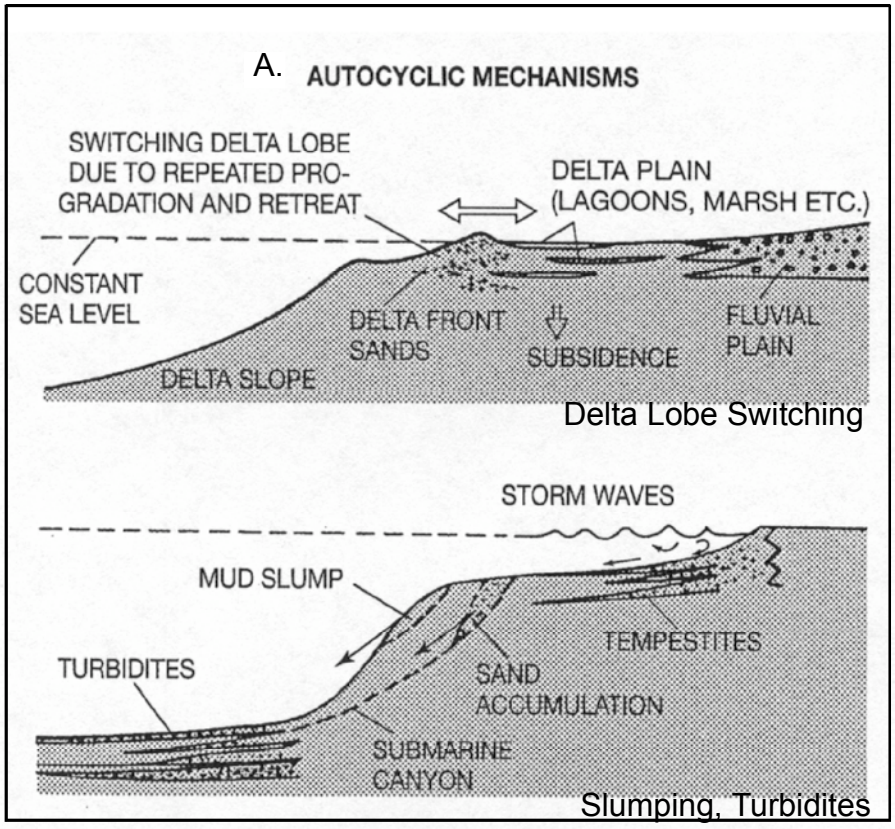

Figure 1.7. Representations of geologic behaviors and resulting depositional processes. A. Autocyclic processes are intrabasinal and may exhibit purely random (non-predictable) organization. B. Allocyclic processes are extra-basinal in their influence, but may exhibit some degree of chaotic organization when recorded as sedimentary depositional cycles. Figure from Goldhammer (2003).

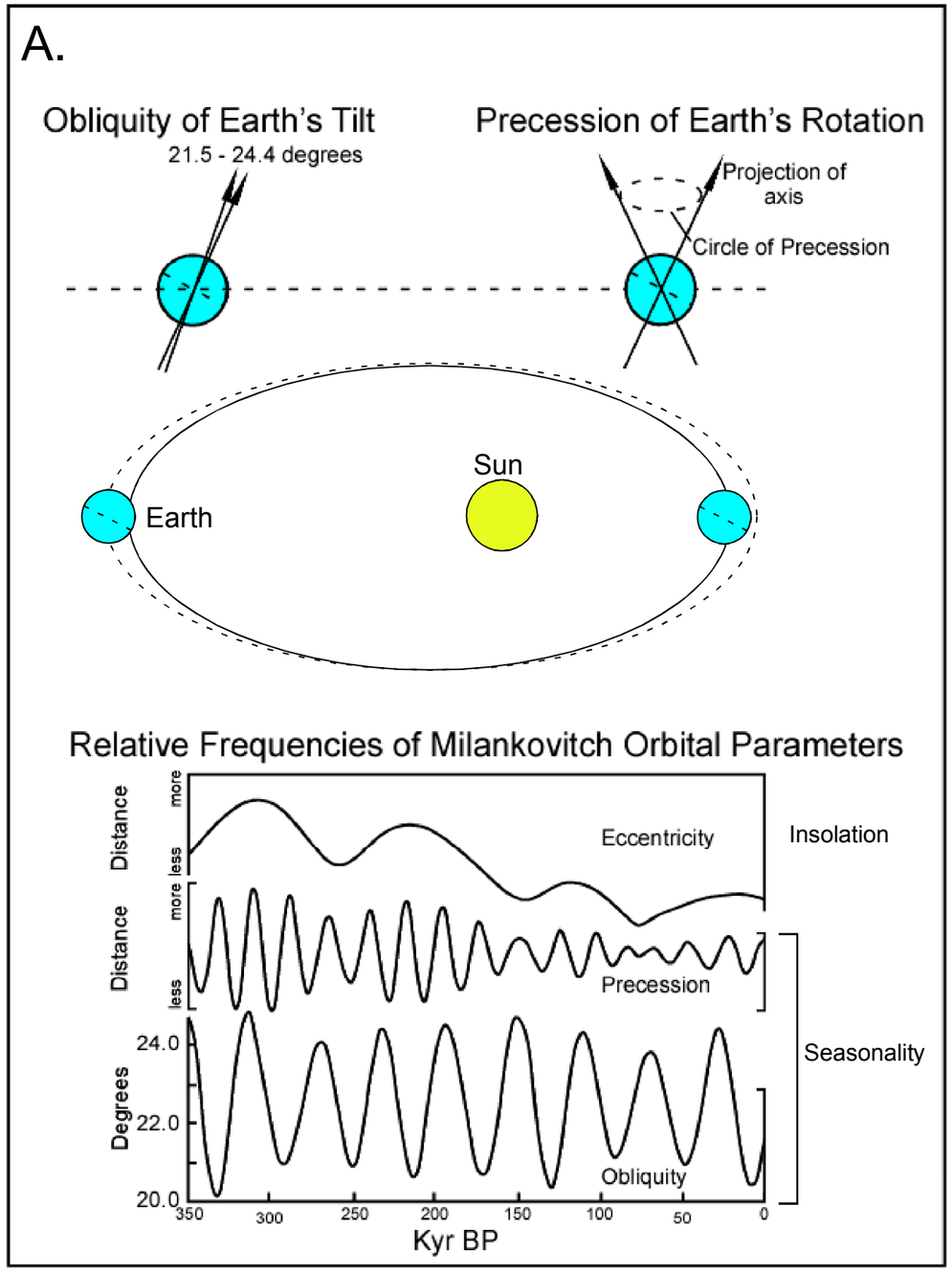

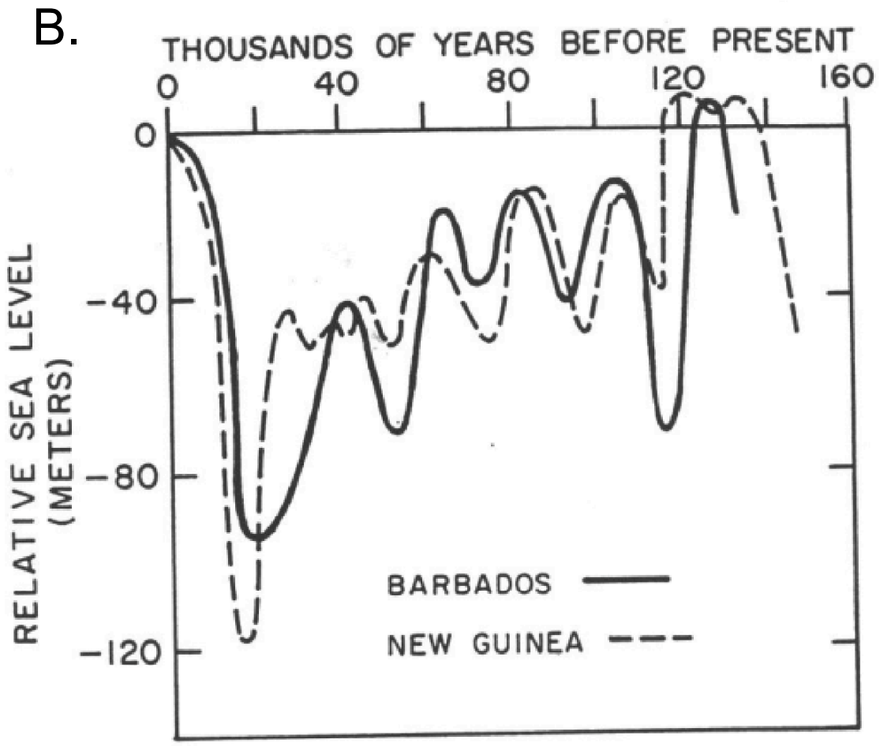

Figure 1.8. A. Milankovitchian orbital parameters and their periodicities (right) (from Imbrie and Imbrie 1980) and B. Holocene/Pleistocene sea level curve (above) from Goldhammer 1987. A. Variations in orbital geometry (right) are quasi-periodic and affect climate via changing the distribution of solar radiation to the atmosphere through time. B. There have been 5 major rises and falls in sea level over the past 120 kyr (above), all of which are asymmetrically modulated into a ca. 100-kyr package. This is likely a function of the combined eustatic response to both the Precession (ca. 20 kyr) and the Eccentricity (ca. 100 kyr).

After Imbrie and Imbrie (1980)

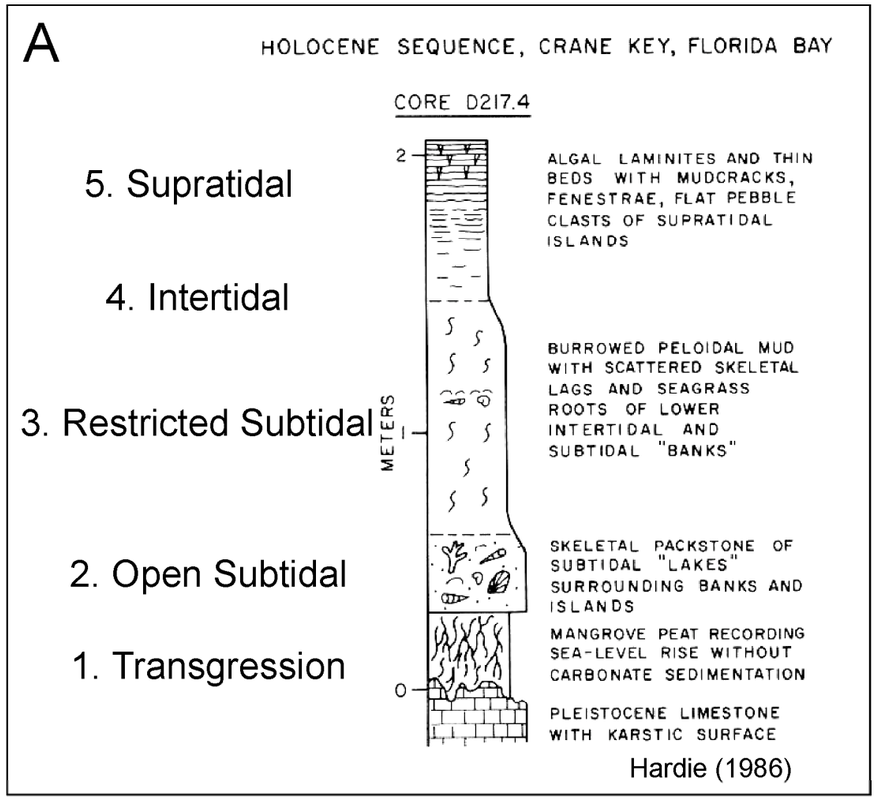

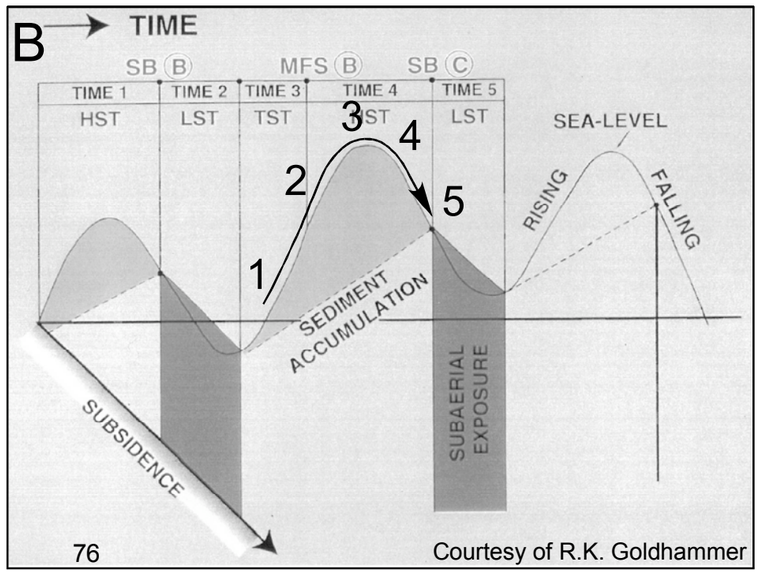

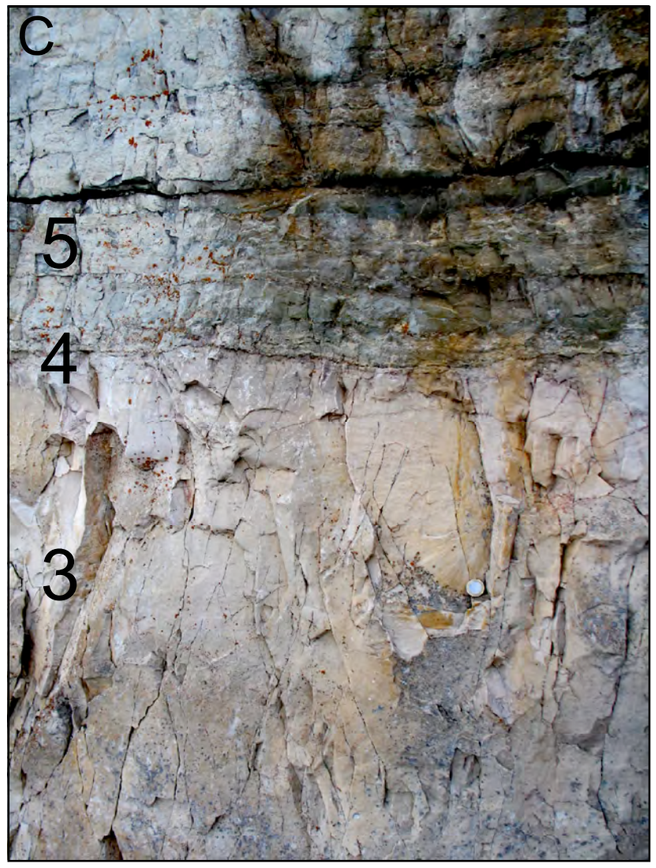

Figure 1.9. A. Holocene shallowing-upward depositional successio from Crane Key, Florida Bay, with facies keyed to B. diagram depicting relative sea level rise and fall. These diagrams are compared to C. a very similar laminite-capped depositional cycle from the Norian Dolomia Principale, Cima Ovest Tre Cime di Lavaredo, the Dolomites, N. Italy (1 Euro coin for scale, image appx. 1 meter in the vertical dimension). The similarity in facies succession between the Holocene and Triassic examples is the basis for the interpretation for facies-specific depositional environments in the ancient.

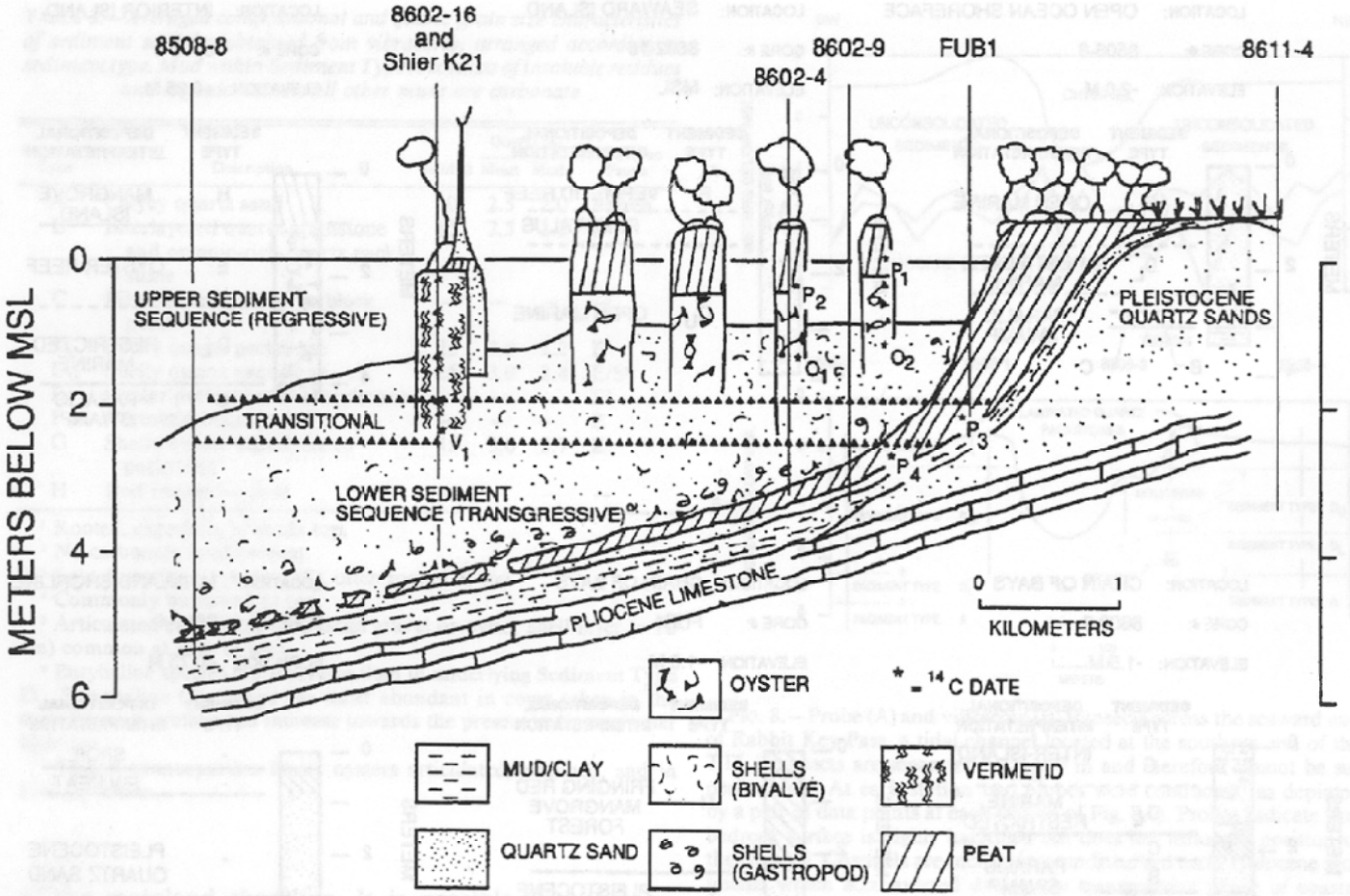

Figure 1.10. Sketch from Parkinson (1989) illustrating the stratigraphic relationships of Pleistocene and Holocene sediments along the Southwest coast of Florida. Note that only one shallowing-upward facies succession has developed in Holocene time, traceable over several kilometers.

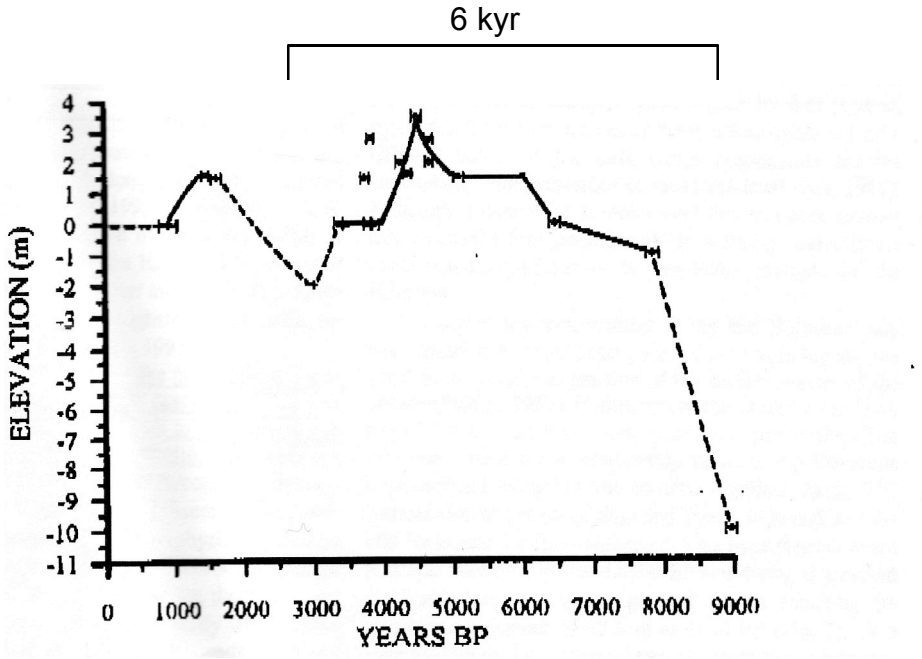

Figure 1.11. Holocene sea-level fluctuations derived from the dating of carbonate cemented aeolian sandstones in South Africa, from Ramsay (1995). The figure shows a single clear oscillation with a wavelength of ca. 6 kyr.

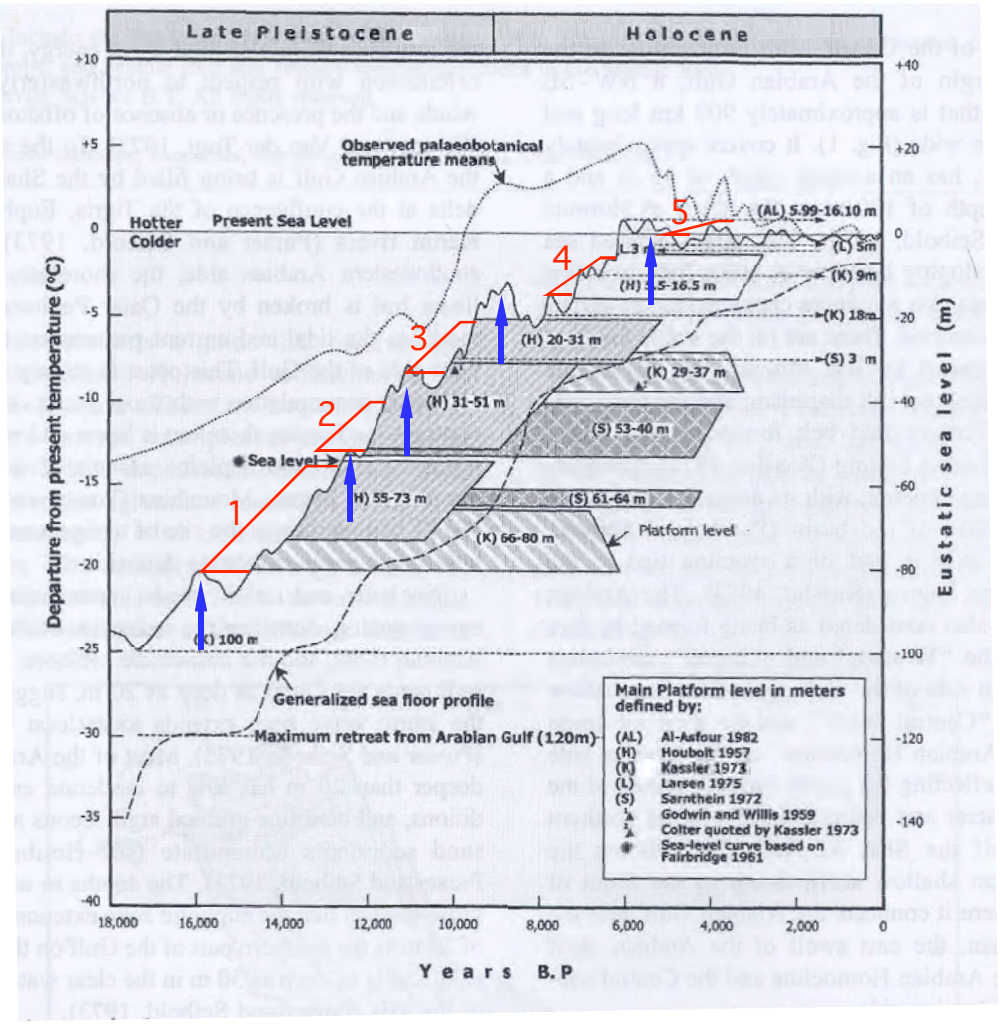

Figure 1.12. Figure 2 from Alshahan and Kendall (2003). Figure shows departure from mean present temperature, sea level, and terrace heights for the Arabian Gulf area over the last 18 kyr. Red brackets show transgressive (ravinement?) terraces created during ca. 20 kyr transgression. Note that there are 5 terraces, each following a pulse in sea level rise, as marked by blue arrows. Note 5 sea level pulses (ca. 4 kyr cyclicity) superimposed on the 18 kyr Pleistocene sea level rise.

A.

Locality, sample number (lab number)	Material dated	C^{14} age (a BP)	Depth below sea floor (not compacted) (cm)	Major facies in core	Average accumulation rate (mm/a)
Crane Key (Florida)					
CK-1B (B-5407)	peat	1040±60	90	peat, mud, some sand	0.9
CK-2B (B-5408)	peat	1070±40	85	peat, mud, some sand	0.8
CK-3B (B-5409)	peat	1360±60	50	peat, mud, sand	0.4 (erosion)
Cotton Key (Florida)					
Flo-4 (B-7792)	bivalve shells	1040±100	115	mud, shells	1.1
Flo-6 (B-7793)	corals	680±110	90	mud, roots	1.3
Pigeon Key (Florida)					
Flo-19 (B-7807)	roots	2320±90	85	peat, mud	3.0 (up to Flo-22)
Flo-22 (B-7794)	peat	2140±30	30	peat, mud	0.1 (erosion)
Little Crawl Key (Florida)					
Flo-23a (B-7795)	corals	1210±30	75	sand, coral gravel	0.6 (winnowing)
Flo-23c (B-7797)	corals	1210±40			
Three Creeks (Bahamas)					
Bah-6 (B-7801)	corals	3720±70	140	mud, roots	0.4
Lee Stocking (Bahamas)					
LSC-1 (B-5411)	peat	3440±90	120	peat, sand, mud	0.3
LSC-2 (B-5412)	peat	2530±120	85	peat, sand, mud	0.3
The Lagoon (Bermuda)					
Ber-9 (B-7427)	shell debris	2490±30	105	mud, some sand	0.4
Ber-19 (B-7429)	shell debris	5630±40	65	sand, mud	0.1 (lag deposit)
Tucker's Town (Bermuda)					
Ber-27 (B-7433)	shell debris	2840±30	130	sand	0.5

B.

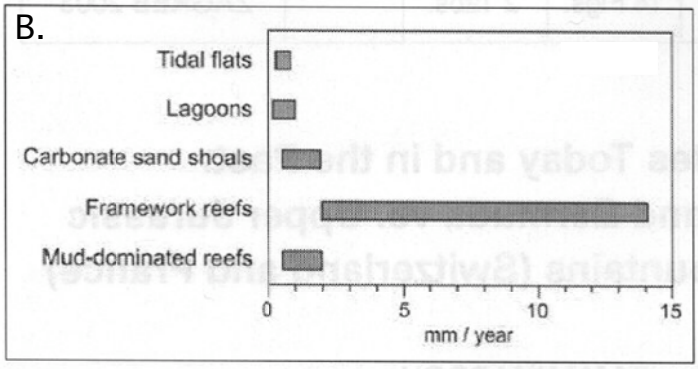

Figure 1.13. A. Table of dated material from Holocene depositional cycles and B. compilation histogram of 352 measured Holocene sedimentation rates for carbonate systems (Strasser and Samankassou, 2003). Note that rates of deposition for tidal flats and lagoons are the lowest of all measured rates, from 0-1 mm/yr (0-1 m/kyr). This chart does not include any information regarding lag depth or rates for the progression of vadose diagenesis. These rates would have to be added to sedimentation rates in order to generate an comparative framework for ancient cycles.

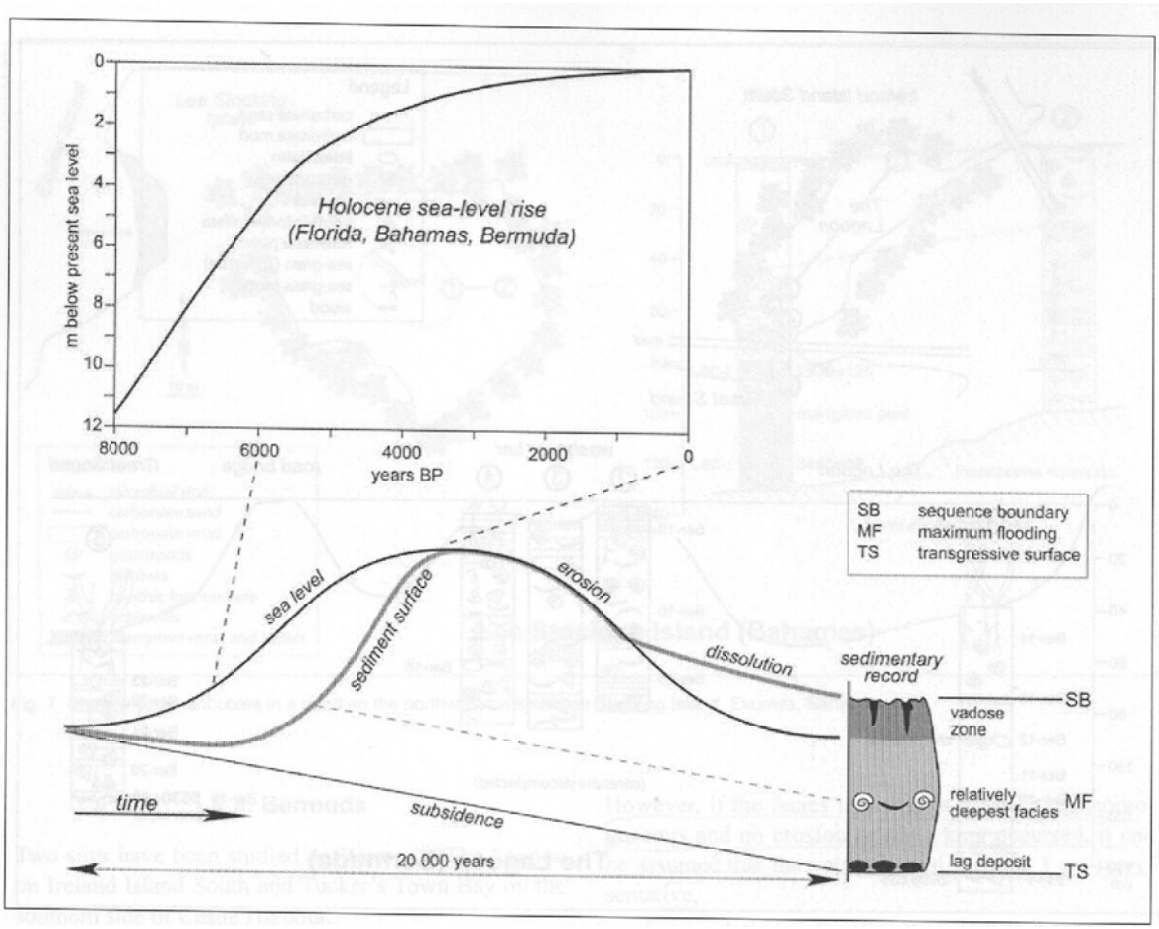

Figure 1.14. Figure 10 from Strasser and Samakassou (2003). This figure is quite similar to that from Goldhammer et al. (1987) depicting how a shallowing-upward facies succession forms in response to sea level rise. Of fundamental importance is the realization that although the sea level oscillation that generates the cycle operates at a 20 kyr frequency, the cycle itself represents less than 20 kyr of sustained deposition. This is because of two factors: a. flooding the platform to lag depth amenable to colonization of the substrate by carbonate-producing organisms, and b. much of the history of the succession is spent exposed in the vadose zone.

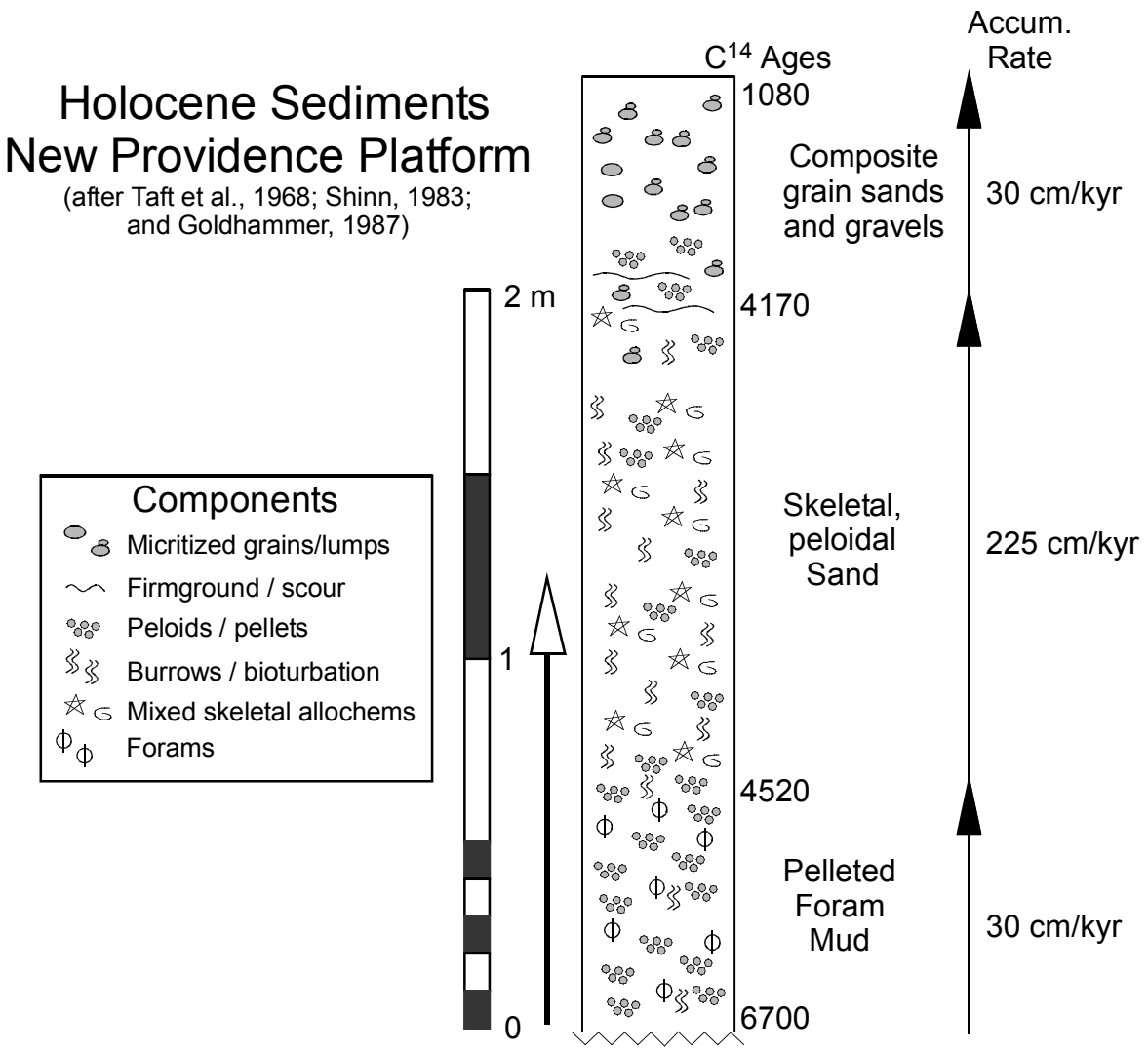

Figure 1.15. Dated Holocene sediments from the New Providence Platform, (after Taft, 1968; Shinn, 1983; and Goldhammer, 1987). Figure shows that the highest accumulation rates are in the middle of the succession, when open marine conditions were likely at their peak in the area. As accommodation began to fill, accumulation rates dropped, and composite cemented grains began to form. This figure serves to illustrate the point that accumulation rates for carbonates fluctuate such that the sedimentary period and the cyclic period may not be the same.

Type	Other terms	Duration, m.y.	Probable cause
First-order	—	200–400	Major eustatic cycles caused by formation and breakup of supercontinents
Second-order	Super cycle (Vail, Mitchum, and Thompson, 1977b); sequence (Sloss, 1963)	10–100	Eustatic cycles induced by volume changes in global mid-ocean spreading ridge system
Third-order	Mesothem (Ramsbottom, 1979); megacyclothem (Heckel, 1986)	1–10	Possibly produced by ridge changes and continental ice growth and decay
Fourth-order	Cyclothem (Wanless and Weller, 1932); major cycle (Heckel, 1986)	0.2–0.5	Milankovich glacioeustatic cycles, astronomical forcing
Fifth-order	Minor cycle (Heckel, 1986)	0.01–0.2	Milankovich glacioeustatic cycles, astronomical forcing

Source: Vail, P. R., R. M. Mitchum, Jr., and S. Thompson, III (1977b); Miall (1990, p. 447).

Table 1.1. Stratigraphic cycles, their durations, and their postulated causes. From Goldhammer, 2003

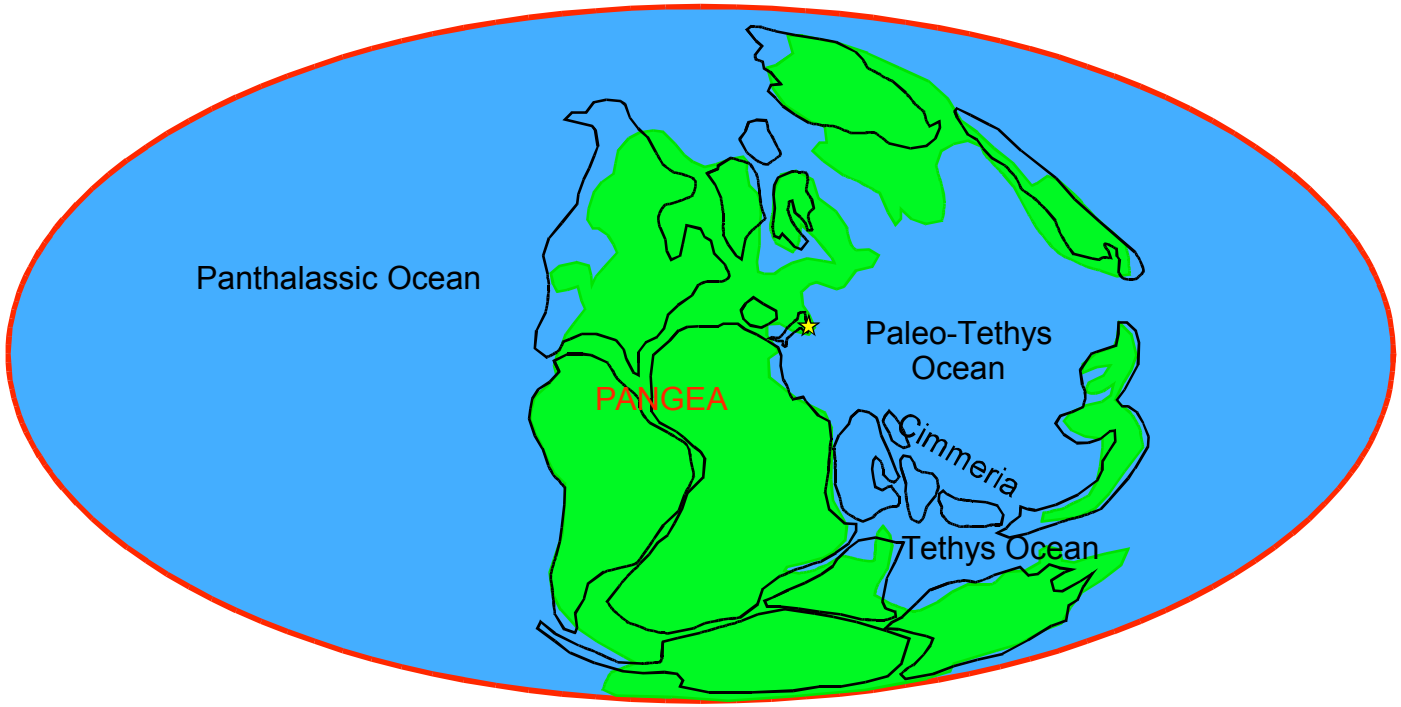

Figure 1.16. Position of land masses during the Permian, ca. 255 mya. Land masses in green, ocean in blue, modern continental areas outlined in black. Location of the Dolomites is marked with a yellow star. Reconstruction by Scotese, (2002)

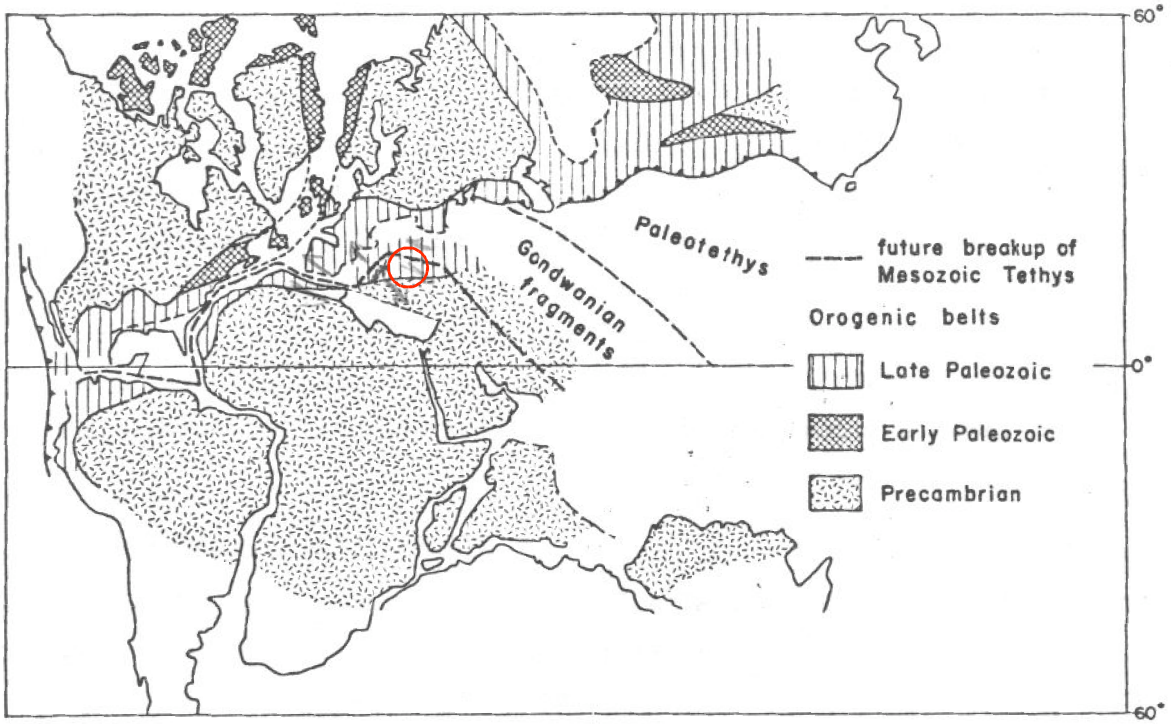

Figure 1.17. Restoration of the continents in Triassic times, from Bernoulli and Lemoine (1980). General location of the Dolomites in red circle.

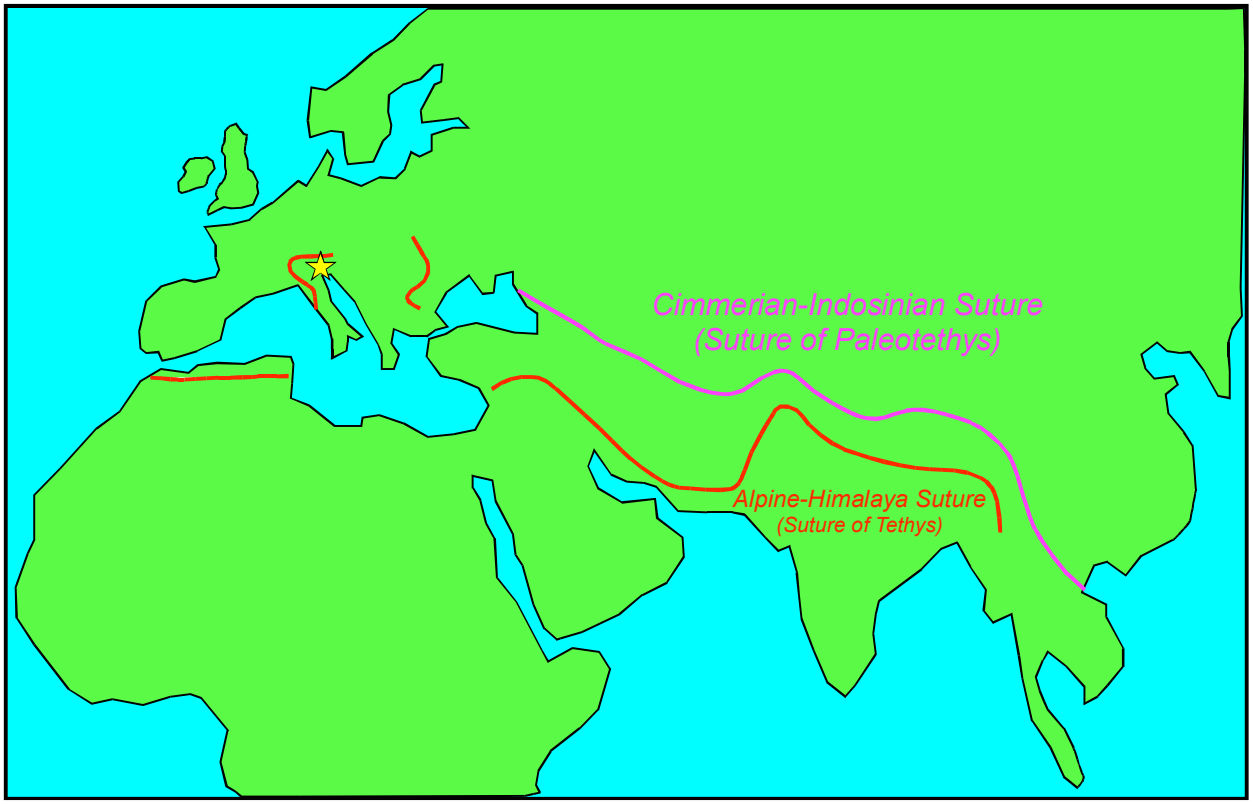

Figure 1.18. Modern position of the continental land masses, showing suture lines of the Paleotethys and Tethys oceans, after Hsu and Bernoulli (1978). During the latest Jurassic, sinistral movement related to the opening of the central Atlantic became dextral as the north and south Atlantic began to open (Winterer and Bosellini, 1981). As a result, the Tethys began to close via subduction to the north, with the closing of the Piemonte-Ligurian ocean following during the Cretaceous (Hsu and Bernoulli, 1978, Winterer and Bosellini, 1981). Convergence during the Cenozoic led to the development of the Alps (Bosellini, 1991).

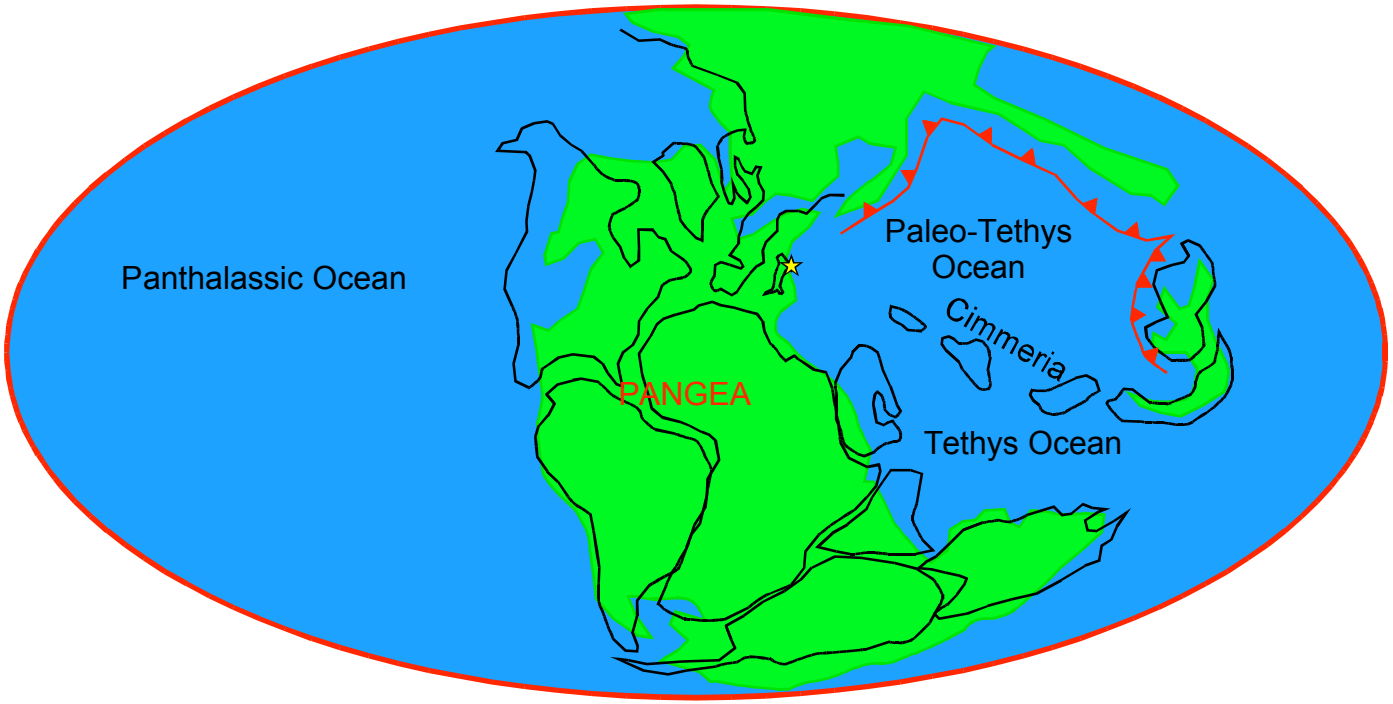

Figure 1.19. Early Triassic (237 Ma) plate reconstruction by Scotese (2003). Plate reconstruction shows the Pangaean supercontinent as well as the wedge-shaped Paleotethys ocean undergoing north-directed subduction. The location of the Dolomites is marked with a star.

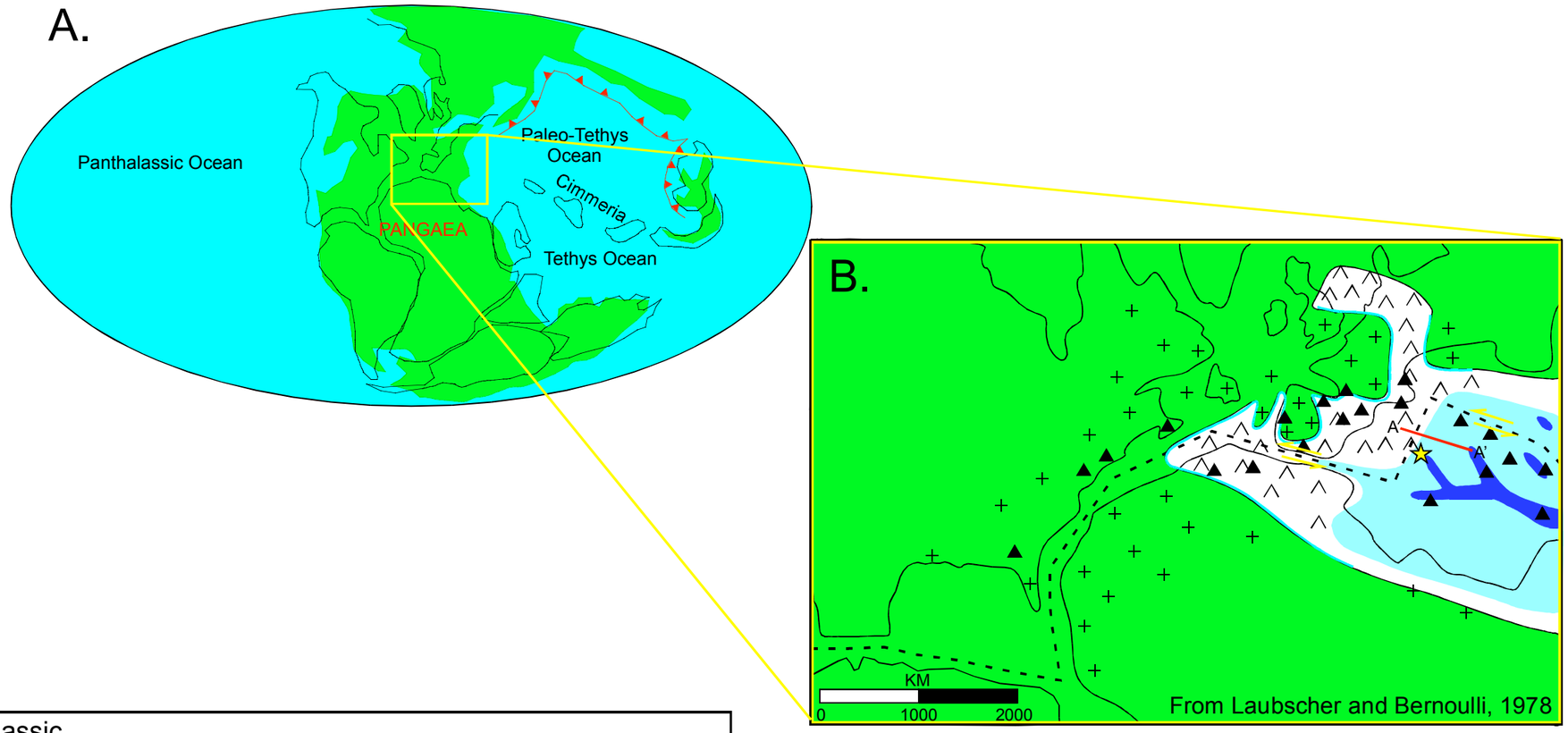

Figure 1.20. A. Late Triassic paleogeography of the earth after Scotese (2002), and B. of the area comprising the present southern Alpine region after Laubscher and Bernoulli (1978). C. A cross-section through the late Triassic carbonate shelf is also shown, including the Dolomia Principale.

A.

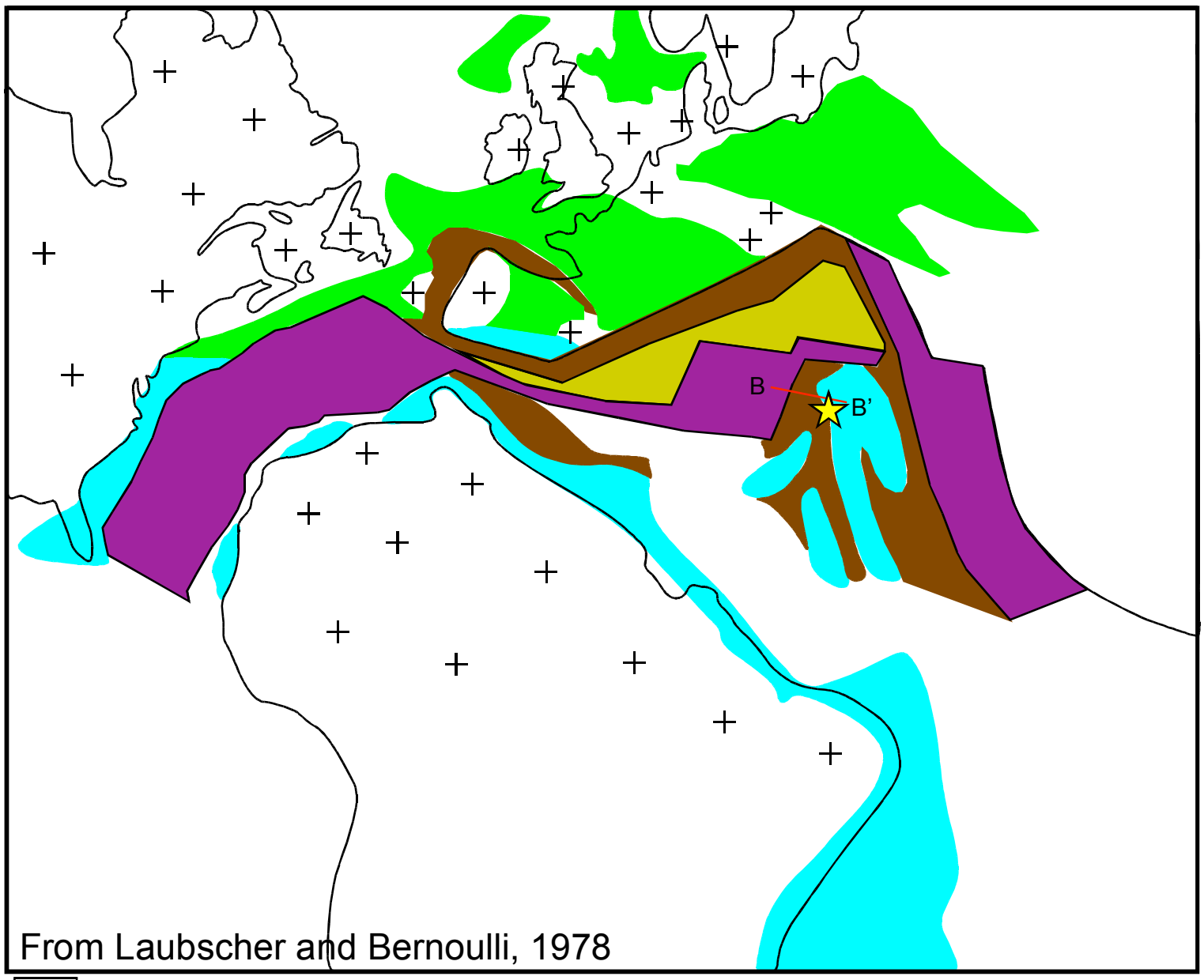

B.

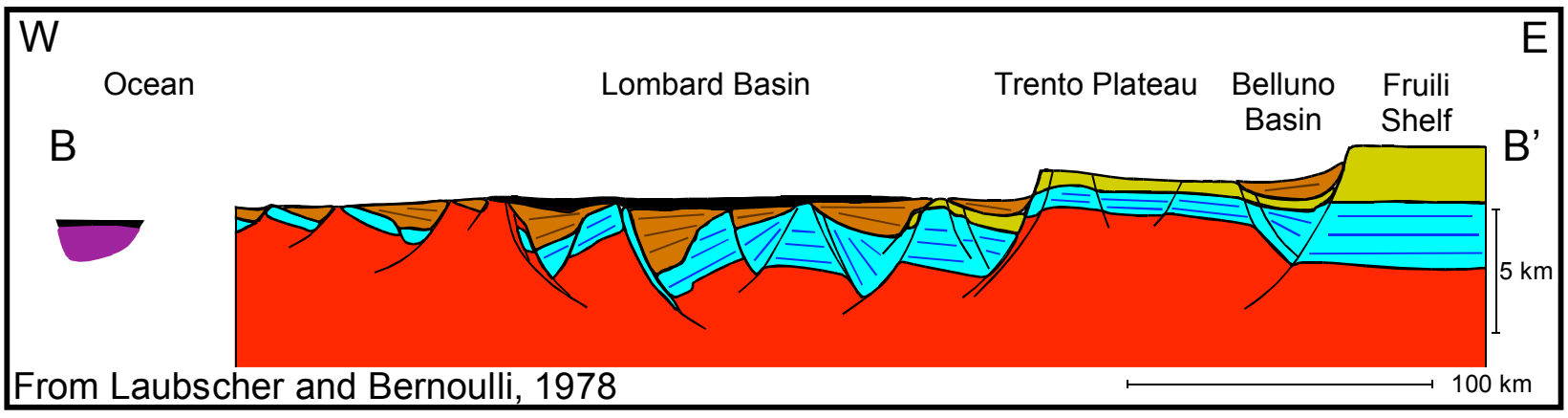

Figure 1.21. A. Early Jurassic paleogeography of the southern Alps with B. cross section depicting the results of rifting and differential subsidence on the stratigraphic development of the region.

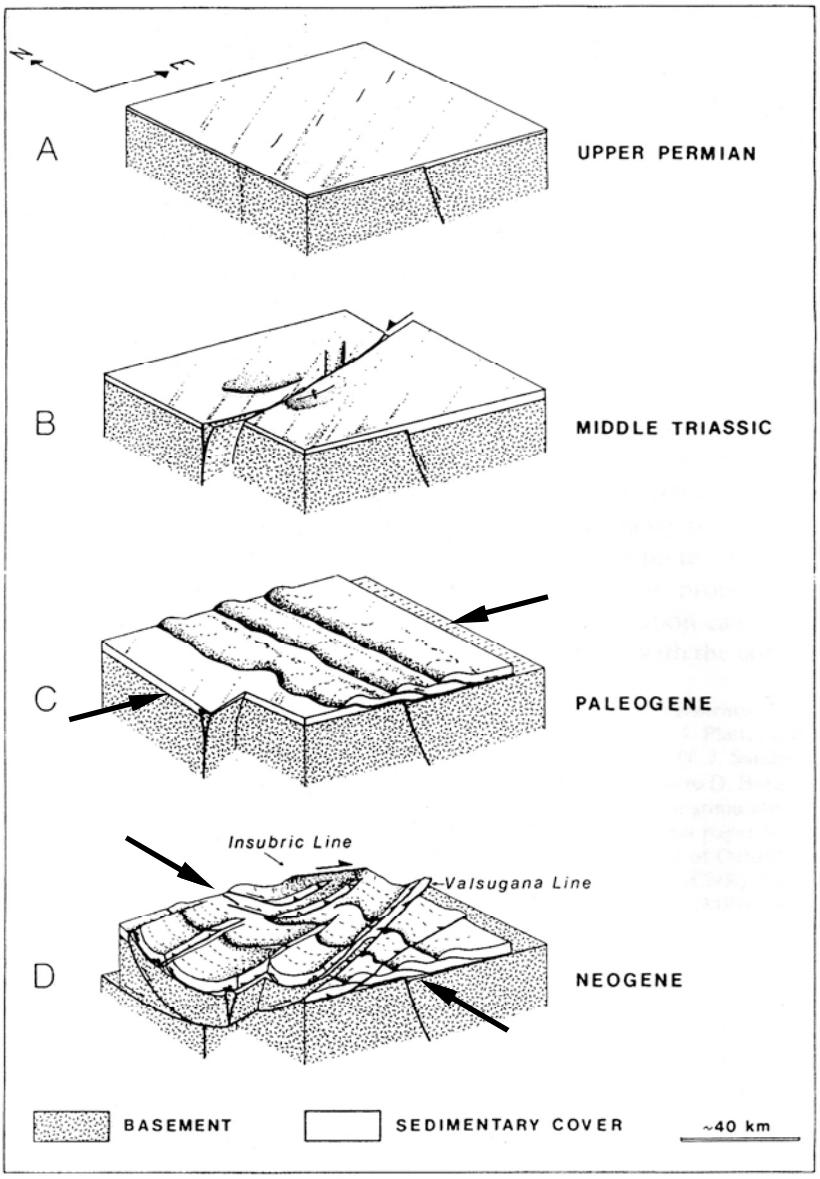

Figure 1.22. Diagram depicting the main tectonic phases in the history of the Dolomite Alps, from Doglioni, 1986. A. Permo-Triassic Rifting; B. Mid-Triassic sinistral strike-slip; C. Paleogene (?) EW shortening; D. Neogene NS shortening.

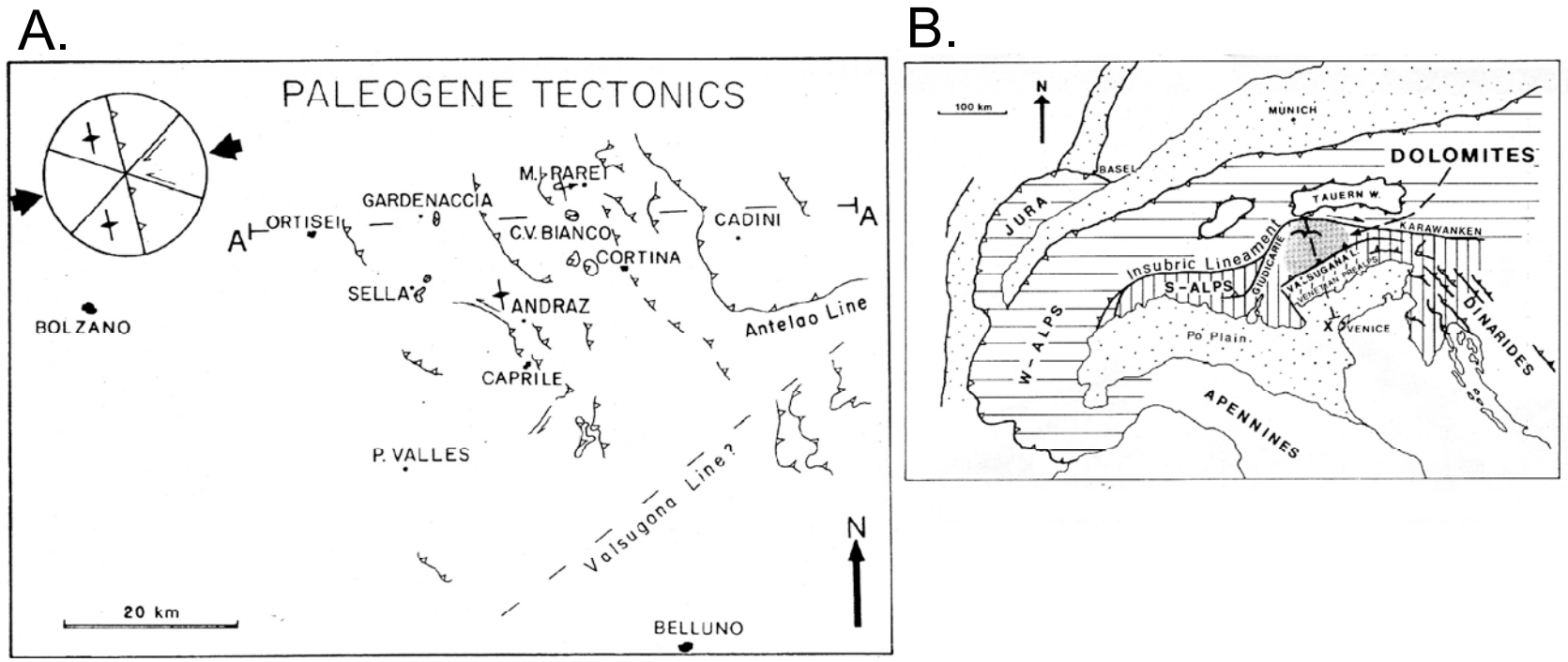

Figure 1.23. Reconstruction of Paleogene (Upper Cretaceous-Paleogene?) tectonics in the Dolomites as compared to the orientation of thrust belts in the Dinarides (both from Doglioni, 1986). A. Paleogene tectonics of the Dolomites; B. Map depicting locations of both the Dolomites and Dinarides.

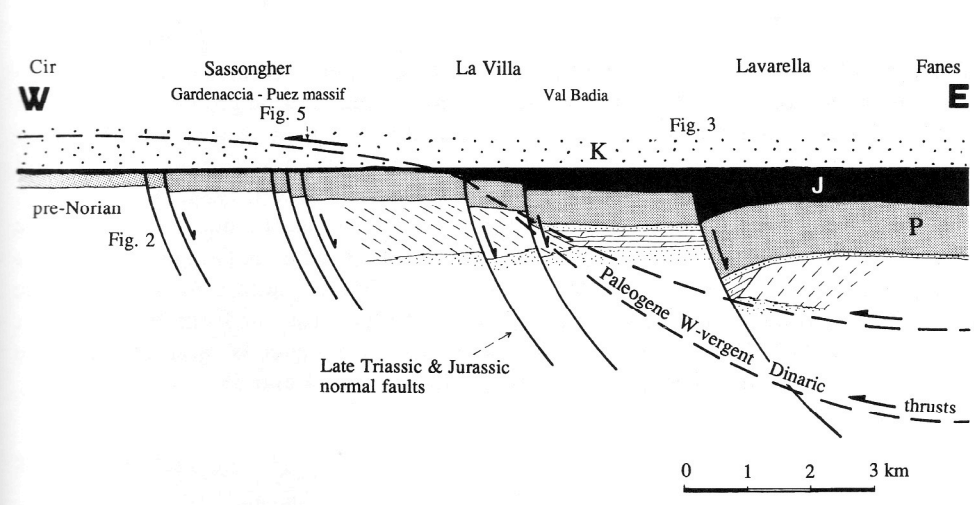

Figure 1.24. Diagram depicting pre-inversion structural and stratigraphic relationships between the Sella Massif (adjacent to the Puez massif) and the Fanes group to the east (from Doglioni, 1992). NS-trending, E-dipping normal faults characterize the late Triassic structure of the area. “Dinaric” faulting then affected the area sometime in the Paleogene, generating roughly NS-striking, W-vergent thrusts through the Mesozoic strata. P - Norian Dolomia Principale; J - Jurassic Calcari Grigi; K - Cretaceous Puez marls.

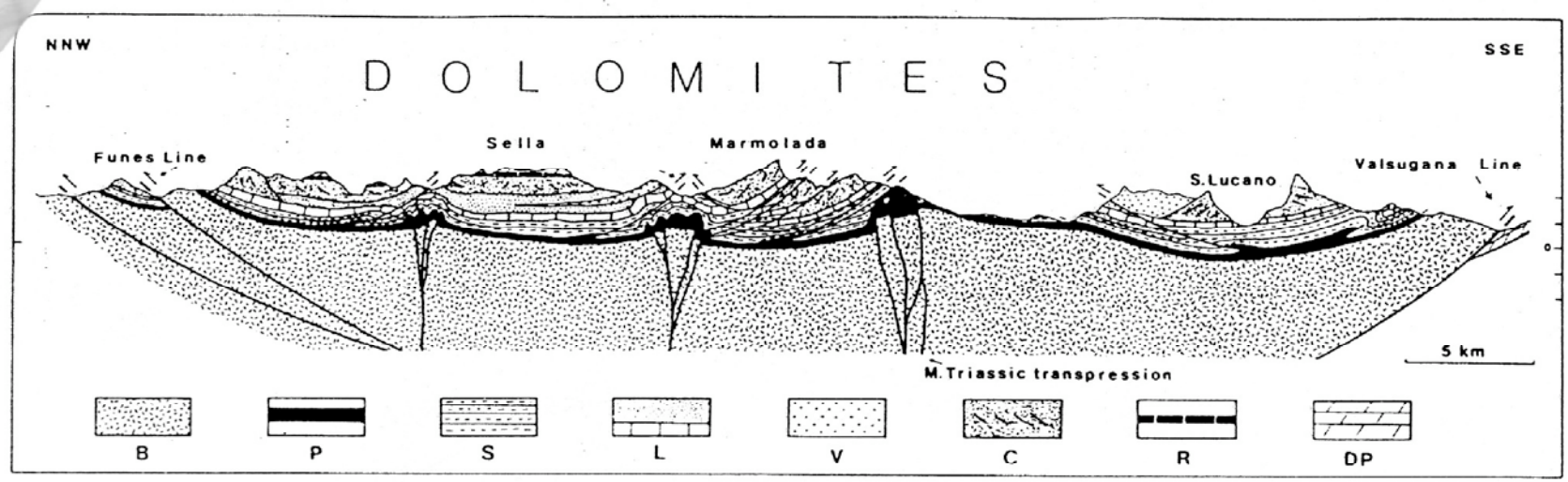

Figure 1.25. NS cross section of the central Dolomites (from Doglioni, 1986). The bowl-shaped synclinorium is bound by the Valsugana line to the south and Funes line (backthrusts) to the north. Flower structures involving the basement are thought to be mid-Triassic in age. B - Pre-Upper Permian Basement; P- Upper Permian sediments (Gardena sandstone and Bellerophon evaporites); S - Scythian Werfen formation; L - Anisian Contrin formation and Ladinian-Carnian basinal deposits; C - Ladinian and Carnian Carbonate platforms; R - Upper Carnian Raibl formation; DP - Norian Dolomia Principale.

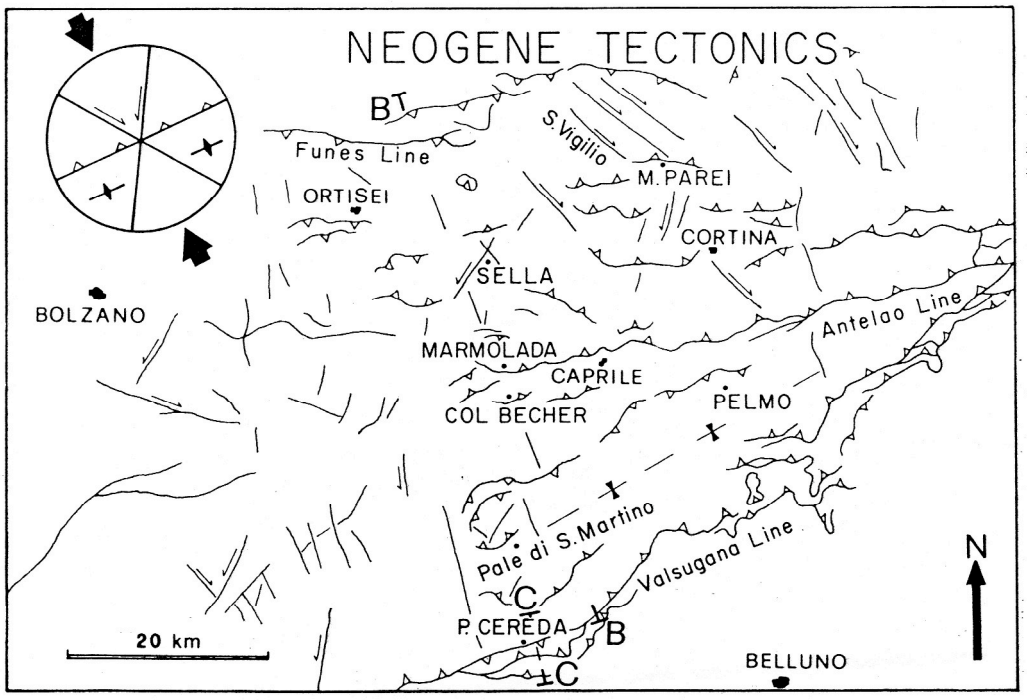

Figure 1.26. Neogene tectonics of the Dolomites, from Doglioni (1986). Neogene tectonics of the Dolomites were generated by north-south collision of the African continent into Europe.

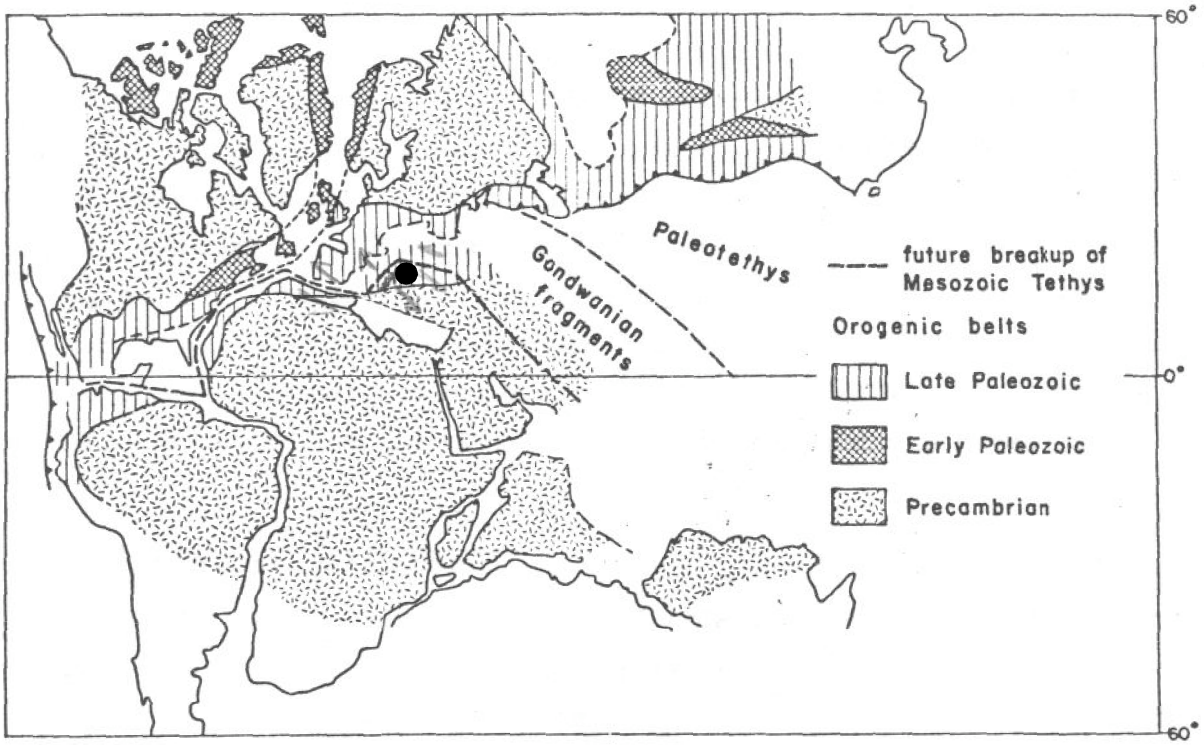

Figure 1.27. Palinspastic restoration of the continents in Triassic times. Approximate position of the Dolomite Alps marked by a black circle. Note the proximal position of the Dolomites to the zone of continental rifting. Figure from Bernoulli and Lemoine (1980).

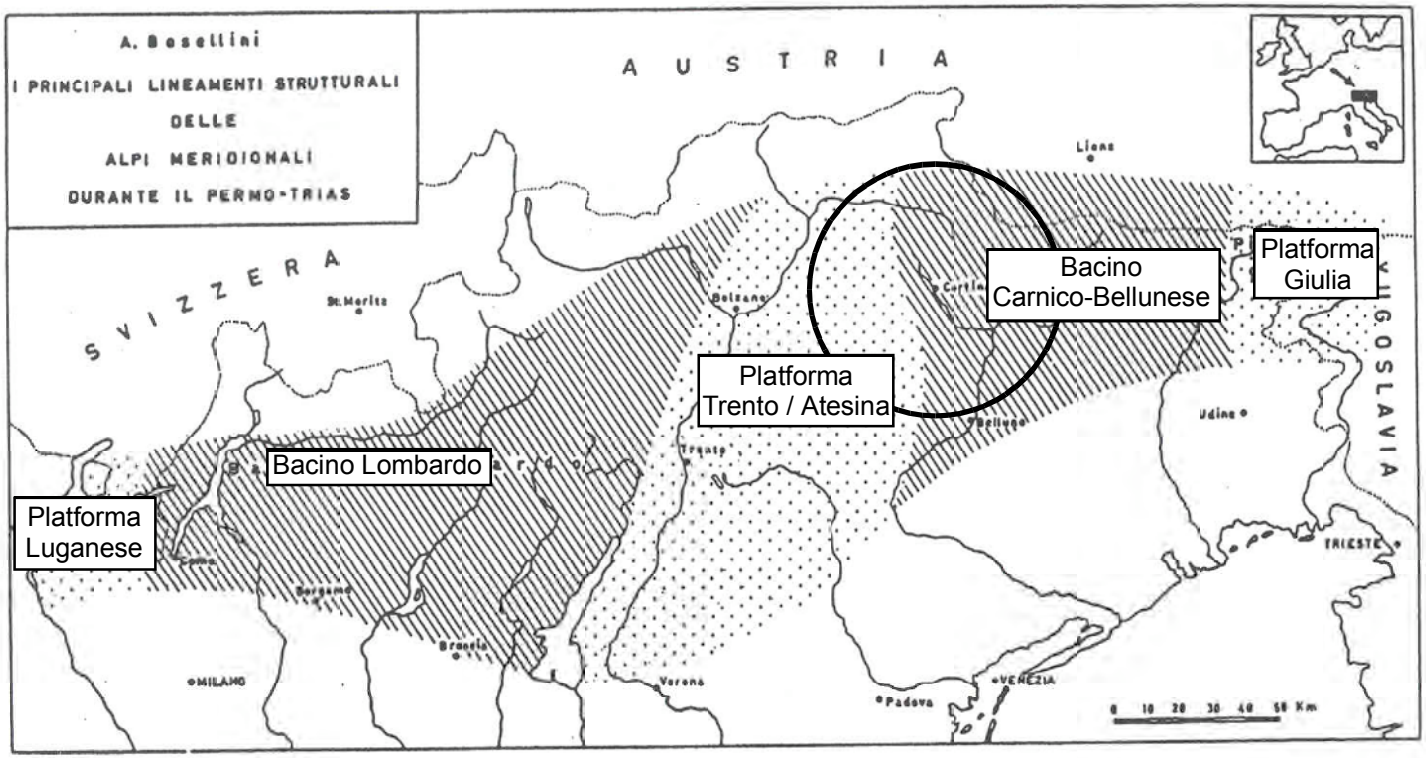

Figure 1.28. Distribution of Permian structural elements in the Southern Alps. Note NS trend to basin and platform margins, the effect of Permian rifting in the area. Dolomites area circled in black. Figure from Bosellini (1965).

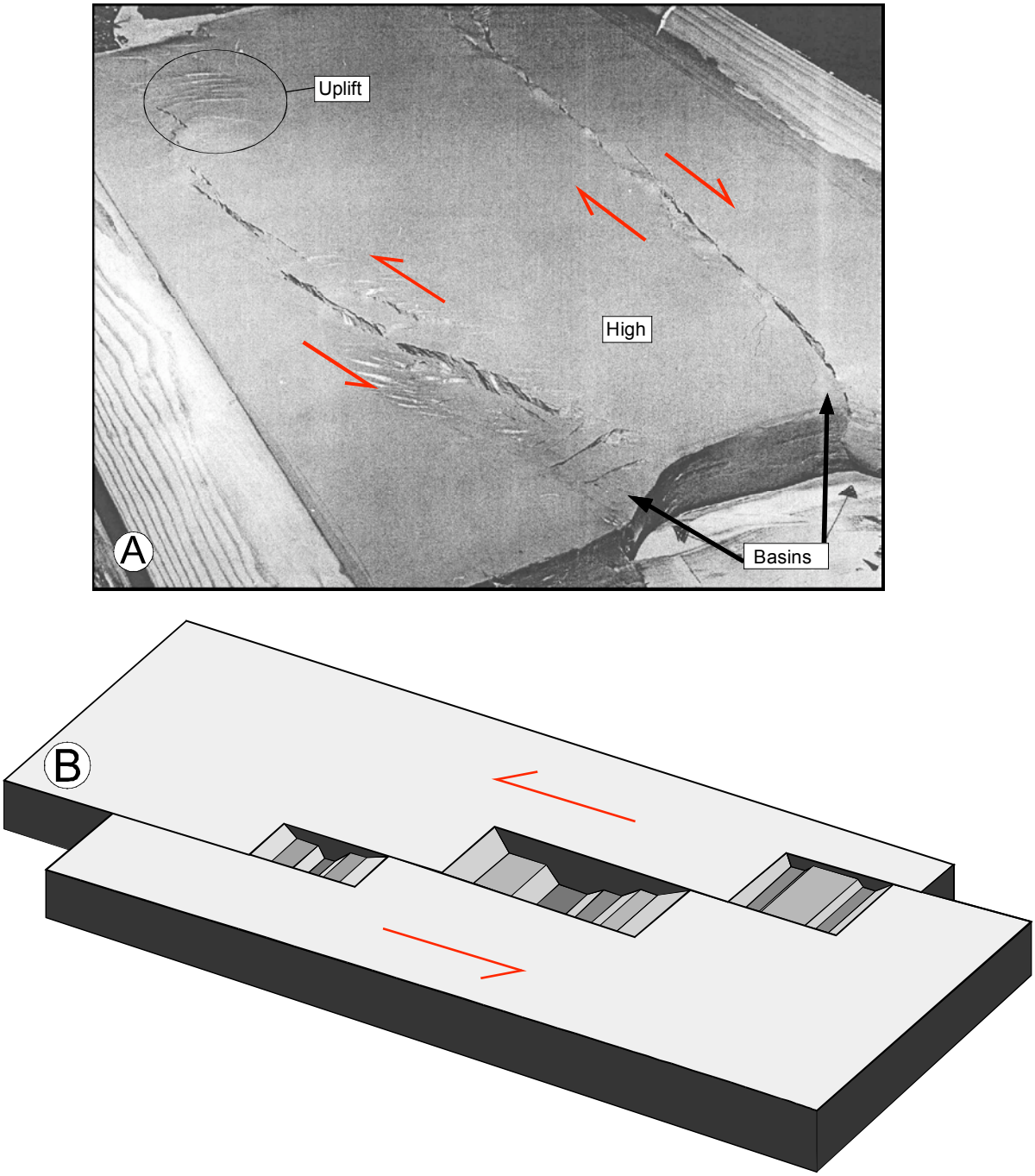

Figure 1.29. Modeled development of basins via subsidence along releasing bends of strike-slip faults. A. Clay cake model demonstrating basin development along releasing bends and uplift along restraining bends. Model shows that differential subsidence from locality to locality is a characteristic of strike-slip basin systems. Photgraph of clay cake model was taken at Johns Hopkins laboratories and and is thought to have been an experiment by Prof. Ernst Cloos. B) Drawing depicting basin development along releasing bends in a strike-slip fault system.

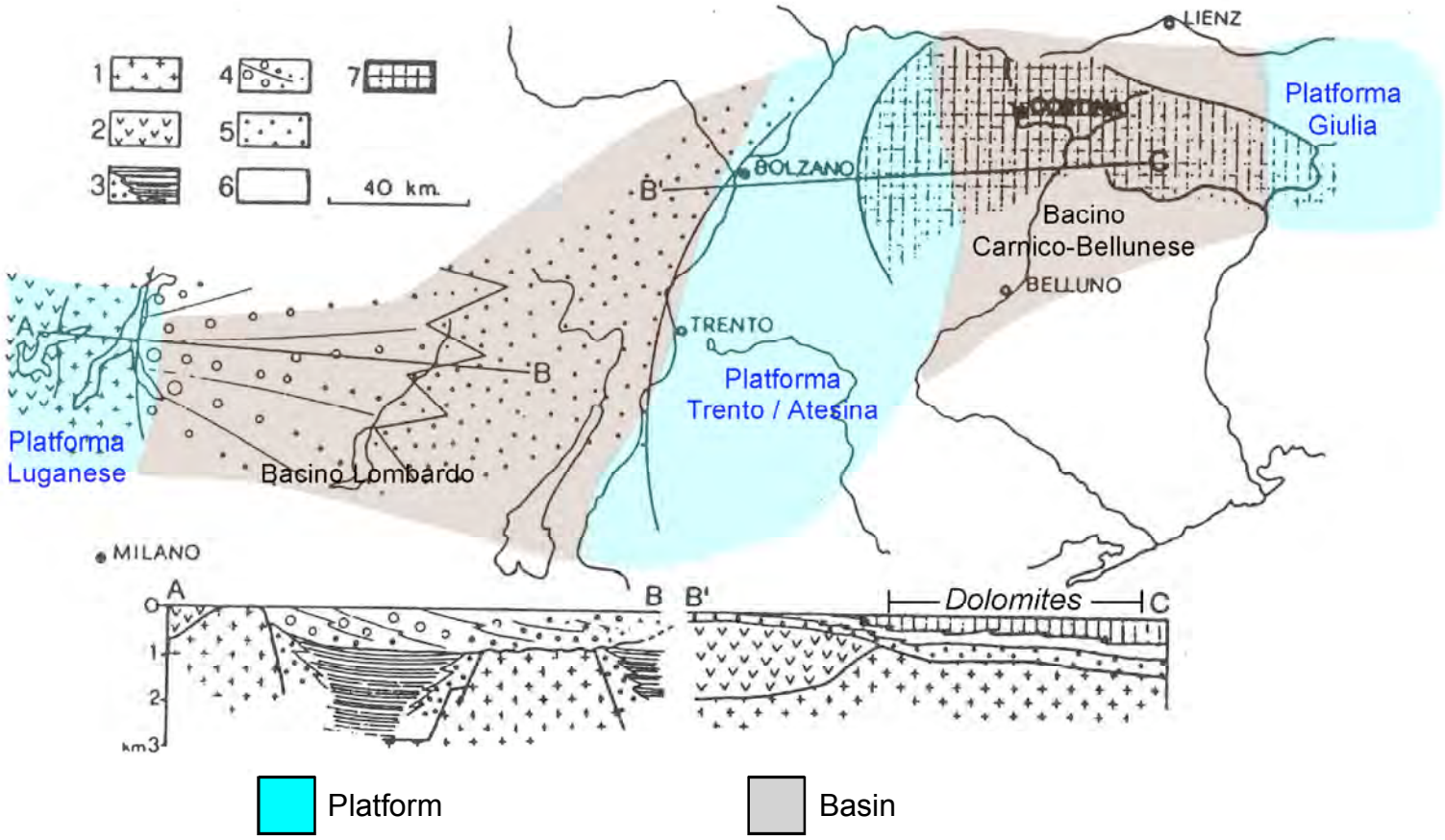

Figure 1.30 Paleogeographic map and cross section of Permo-Triassic deposits in the Southern Alps. 1. Hercynian metamorphics, 2. Permian 'Bozner' volcanics, 3. Lacustrine deposits, 4. Conglomeratic alluvial fans, 5. Fluvial deposits, 6. Shallow marine dolomites and evaporites (tidal flat and sabkha), 7. Shallow marine limestones. Note NS structural grain of platforms and basins, as well as Permian volcanic core of platforms. Figure modified from Winterer and Bosellini (1981) by adding platform and basin labels and colors.

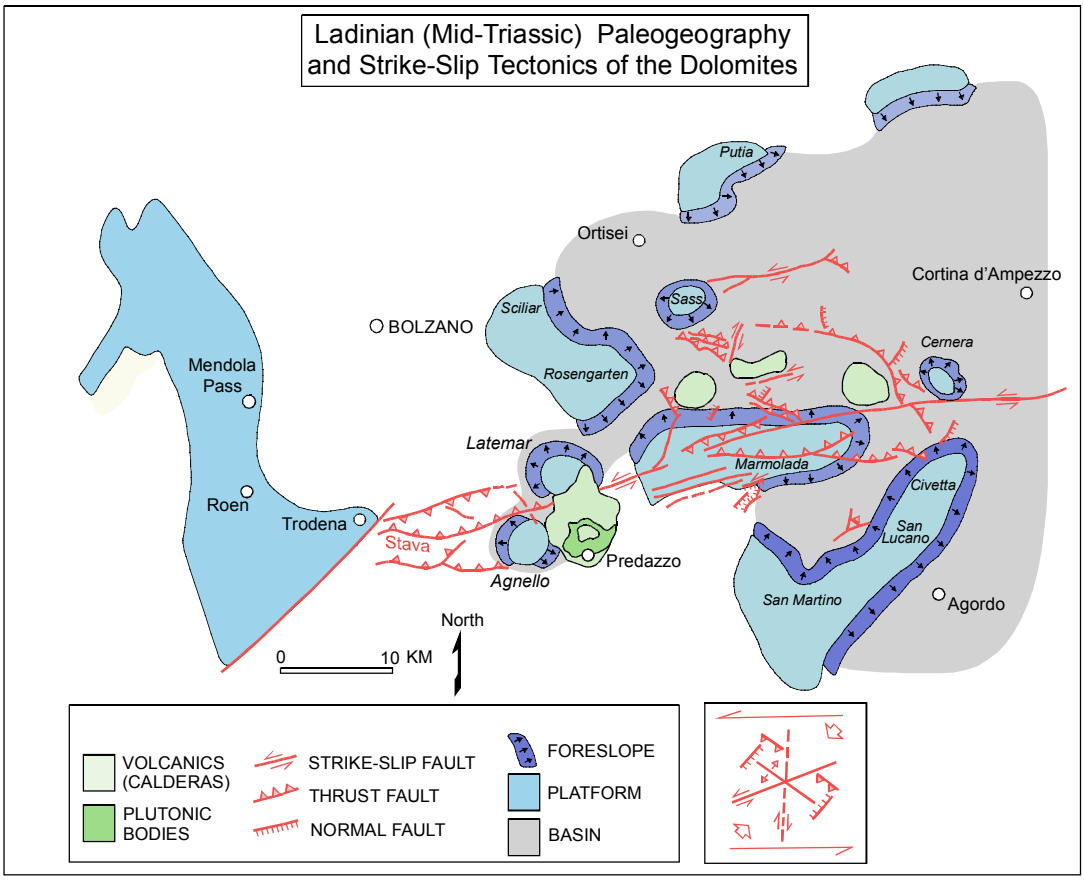

Figure 1.31. Ladinian (Mid-Triassic) paleogeography and tectonics of the Dolomites. During the Mid-Triassic, local mini-basins and antiformal highs form due to sinistral strike slip and block faulting, likely related to regional sinistral transpression related to the rifting of Pangaea (Doglioni, 1984,1985).

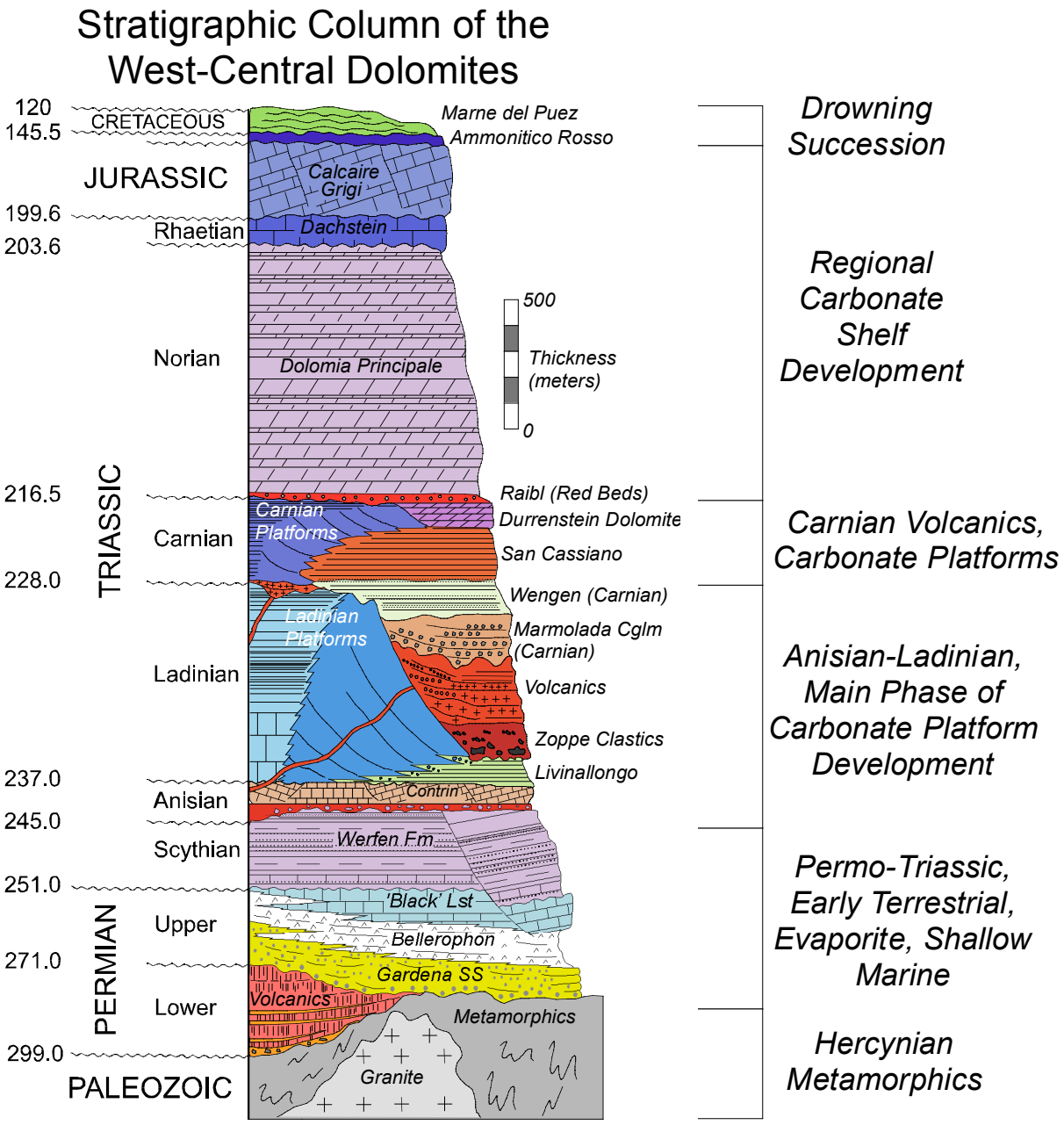

Section modified from Bosellini (1991), dates from Gradstein et al., (2005)

Figure 1.32. Stratigraphic column of the general sedimentary succession preserved in the Dolomite alps of Northern Italy. The Dolomia Principale, a regional carbonate complex of Norian age, is the focus of this study. Dates are stage boundary dates from Gradstein et al (2005) and should be taken as generalized age brackets rather than dates of unconformities.

Figure 1.33. Outcrop photograph of basal “Bozner porphyry”. Photograph taken looking north in the Adige Valley, approximately 10 km north of the city of Bozen (Bolzano).

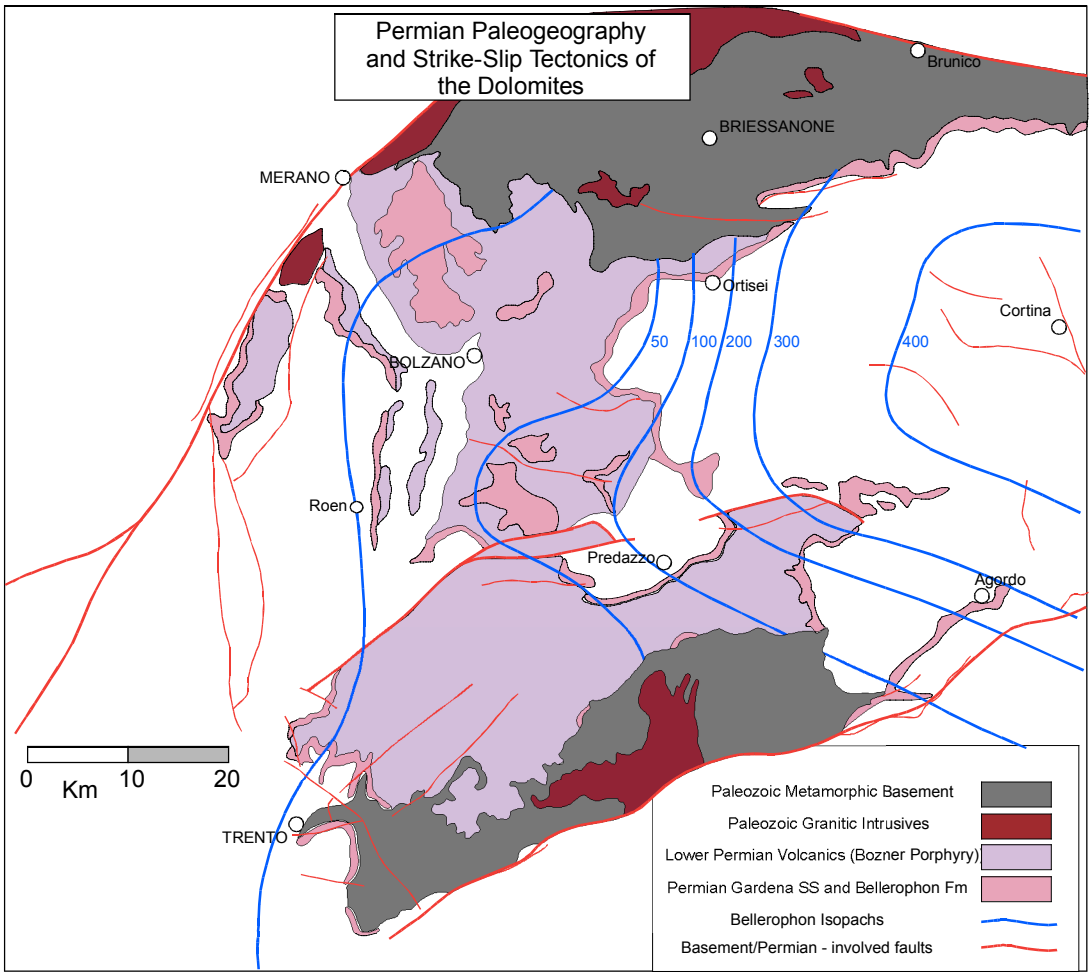

Figure 1.34. Permian deposits in the Dolomites are a record early rifting in the Southern Alps. Rift-related volcanism (Bozner Porphyry) forms a approximately NS striking structural high (Trento/Atesina platform) that is flanked by sedimentary basins to the west (Lombard basin) and east (Carnico-Bellunese basin). Deposition of volcanics is followed by terrestrial fluvial (Gardena SS) and evaporite (Bellerophon) deposits. Fluvial and pedogenically altered beds of the Gardena formation have been interpreted by Massari et al. (1988) as syndepositional early rift fill deposited in a semi-arid setting. The Gardena sandstone thins and fines up, eventually intertonguing with Bellerophon formation encroaching from the Paleotethys to the east (Massari et al., 1988). The Bellerophon formation consists of deposits interpreted as coastal sabkha evaporite grading into shallow shelf carbonate near the top. Note the thickening of the Bellerophon evaporites to the west of the Bozner porphyry, likely the result of Tethyan marine incursion from the east as well as the development of the Carnico-Bellunese basin.The succession is capped by scythian subtidal and supratidal carbonates (Werfen formation) (Channell and Doglioni, 1994). Map after Bosellini (1989).

Figure 1.35. Typical outcrop exposure of the Gardena Formation. In this photograph, paleosols with indurated gypsic and calcic horizons are clearly visible (marked with arrows), suggesting pedogenesis in an arid environment dominated by evaporation. Dr. R.K. Goldhammer for scale.

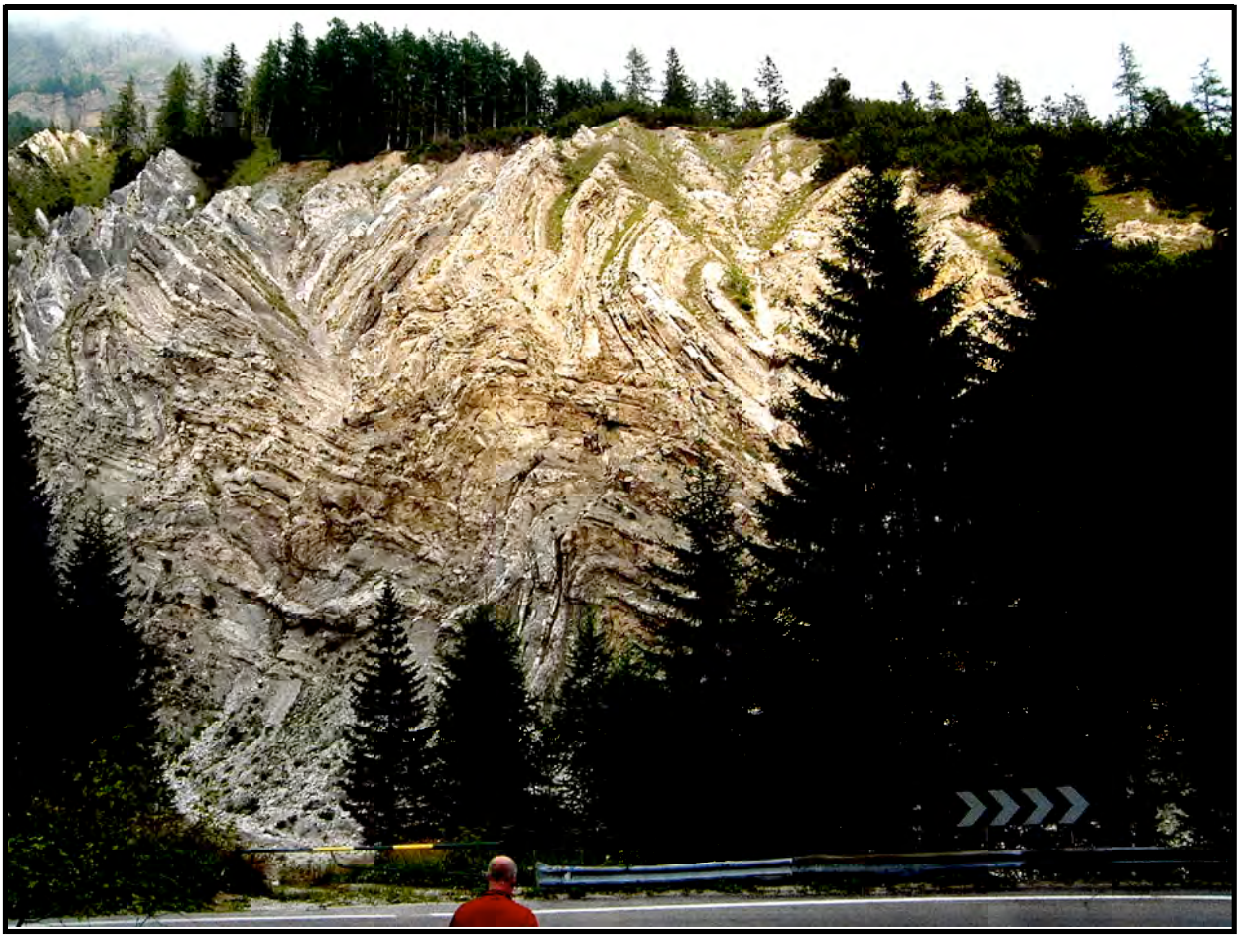

Figure 1.36. Outcrop example of the Bellerophon evaporite package. This deformed example of alternating beds of evaporite and shallow marine dolomites found not far from the Latemar. Dr. R.K. Goldhammer for scale.

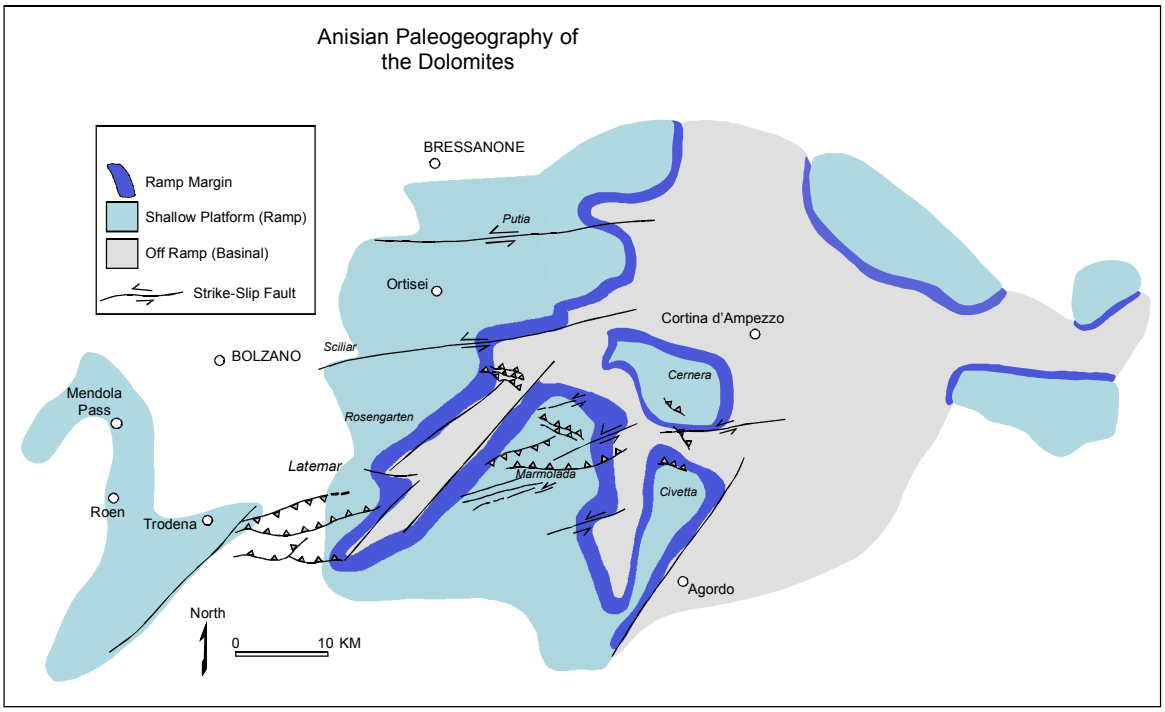

Figure 1.37. Paleogegraphic map of the Dolomites during the Anisian (lower Triassic). Carbonate platforms grew on tectonically controlled bathymetric highs that were likely affected by EW sinistral strike-slip faulting. Map after Bosellini (1989), tectonic interpretation from Doglioni (1985).

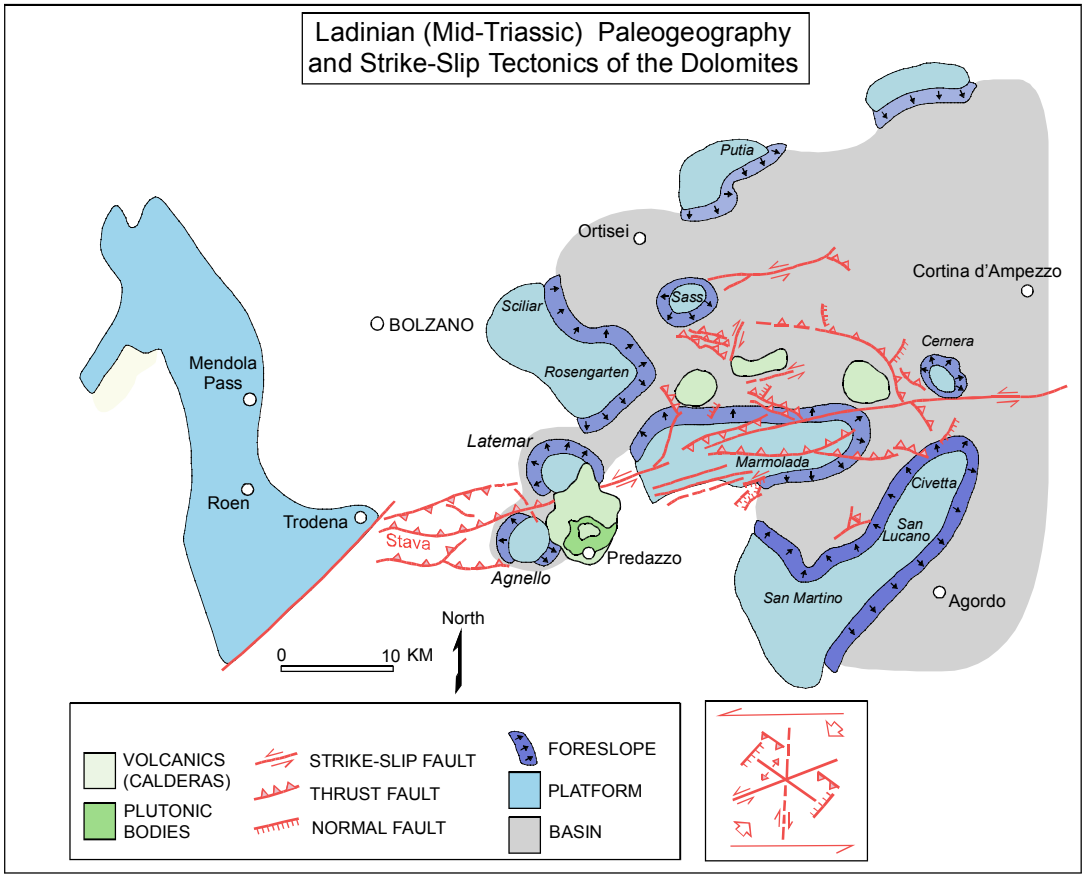

Figure 1.38. Ladinian (Mid-Triassic) paleogeography and tectonics of the Dolomites. During the Mid-Triassic, local mini-basins and antiformal highs form due to sinistral strike slip and block faulting, likely related to regional sinistral transpression related to the rifting of Pangaea (Doglioni, 1984,1985). Bathymetric highs were sites of carbonate platform development (Hsu and Bernoulli, 1978; Hardie et al., 1991). Carbonate platforms in the Dolomites typically have thick, cyclic platform interior nuclei surrounded by narrow margins and steep, radially dipping foreslopes (Bosellini and Stefani, 1991; Hardie et al., 1991). Initial aggradation of platform interiors during early, strong subsidence markedly outpaced time-equivalent basinal sedimentation by approximately 40:1, leading to the formation of steeply-dipping clinoformal breccias upon the onset of progradation (Bosellini, 1991; Bosellini and Stefani, 1991). Volcanics and volcaniclastics buried the entire area in the late Ladinian, which both suffocated and preserved the platforms in their late Ladinian morphology. Map after Bosellini (1989), tectonic interpretation by Doglioni (1985).

Figure 1.39. Platform interior of the Anisian/Ladinian Latemar platform. The high peak in the distance is the Cimon del Latemar. Photograph taken near Rif. Torre de Pisa, looking north, courtesy of Sarah Penniston-Dorland, 2005.

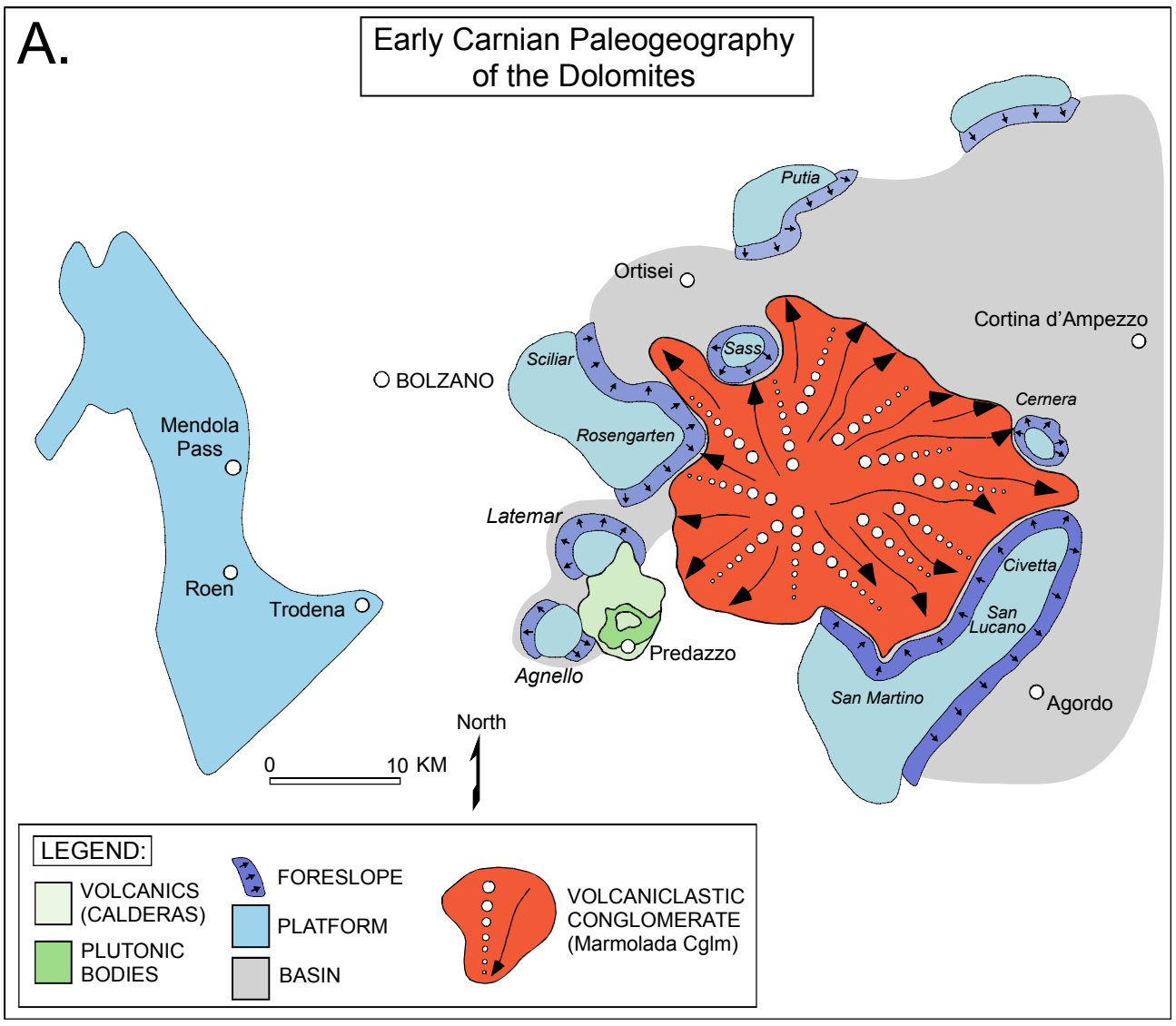

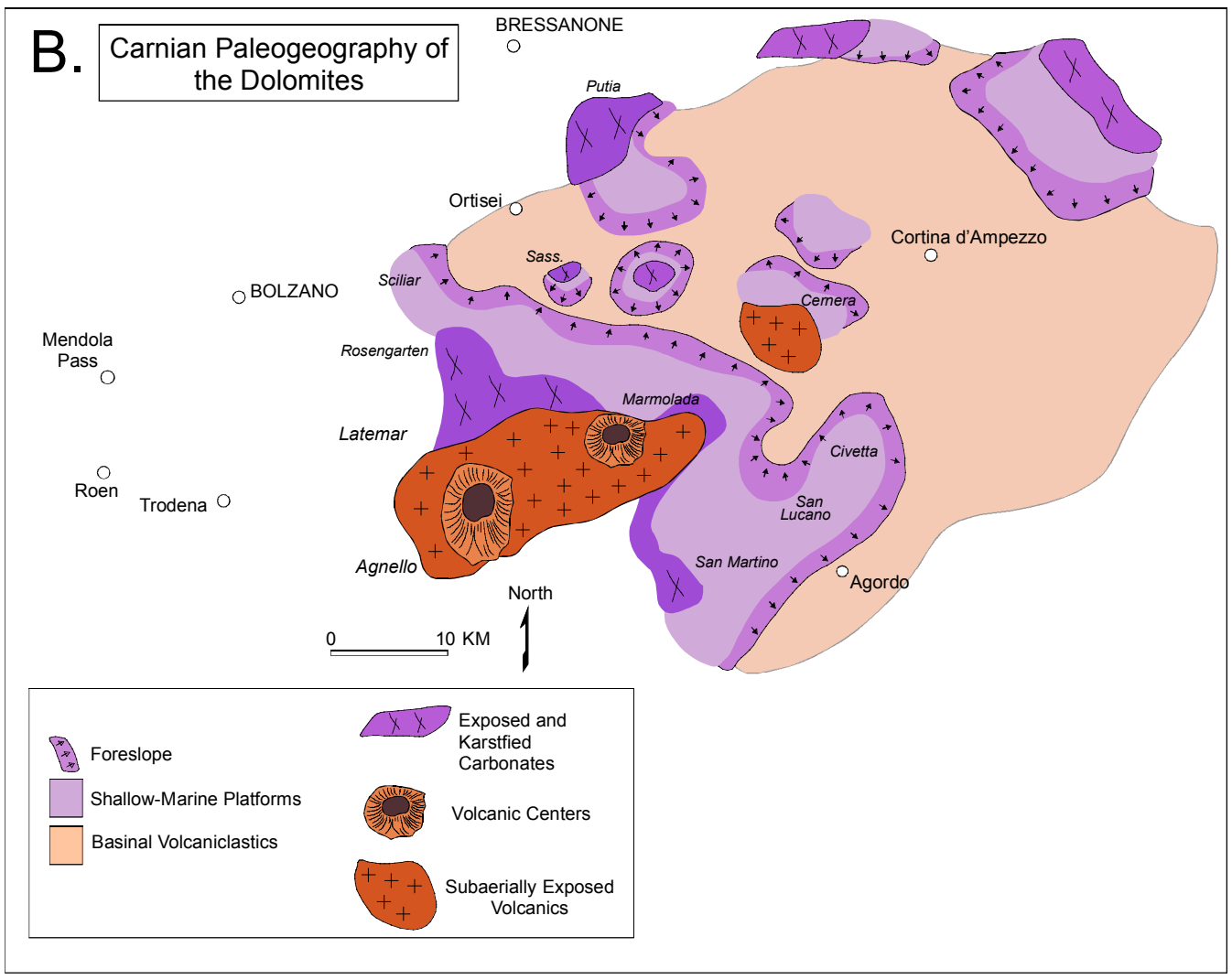

Figure 1.40. A. Early Carnian and B. Late Carnian paleogeography of the Dolomites. Following late Ladinian and early Carnian volcanic infill (Marmolada group), subareal exposure, and erosion, carbonate sedimentation resumed in Carnian time by "grafting and nucleation" on older Ladinian platforms (Bosellini, 1991). Relative stillstand in sea level gave rise to dominantly progradational geometries among later Carnian platforms. Subsequent lowstand in the late Carnian exposed and killed many carbonate platforms, with volcaniclastics and the Durrenstein dolomite filling remaining basinal lows (Bosellini, 1991). Lowstand-to-transgressive siliciclastics and evaporites of the Raibl formation unconformably overlie the Carnian succession. Maps after Bosellini (1991).

Time	Platform	Rate (μm/yr)	Source
Devonian (Givetian/Frasnian)	Canning Basin	30	Playford and Lowrie (1966)
Devonian-Mississippian (Kinderhookian-Meramecian)	Rocky Mountains	50–80	Rose (1976)
Mississippian (Meramecian-Chesterian)	Rocky Mountains	100–150	Rose (1976)
Pennsylvanian Permian	Sverdrup Basin (Nansen Fm.)	30–40	Davies (1977)
Permian (Guadalupian)	Delaware Basin (Capitan Fm.)	75	Harms (1974)
Triassic (Late Anisian–Ladinian)	Northern Limestone Alps	100	Ott (1967)
(Early Carnian)	Dolomites (Picco di Vallandro)	300–500	Schlager and others, unpub. data
Late Jurassic	Southern Alps (Friuli Platform)	30–45	Winterer and Bosellini (1981)
Cretaceous (Late Albian–Cenomanian)	Tampico Embayment	60–90	Enos (1977, p. 279–286)

Note: Calculated from stratigraphic age bracket reported for the formation, applying absolute time spans indicated in the Phanerozoic time scale, 1964; Cohee (1978); accumulation rates are not corrected for compaction.

Figure 1.41. Table 2 from Schlager (1981). Reported accumulation rates are equivalent to mm/kyr. Although the data used to generate this figure has not been published,the Early Carnian of the Dolomites apparently has some of the highest accumulation rates on record for shallow marine carbonate deposits.

Figure 1.42. Carnian toplap relationships preserved above Gardena Pass at the Sella massif. One can clearly see the Carnian platform interior stratigraphy top-lapping over the marginal reef, indicating a stillstand in sea level prior to relative sea level fall.

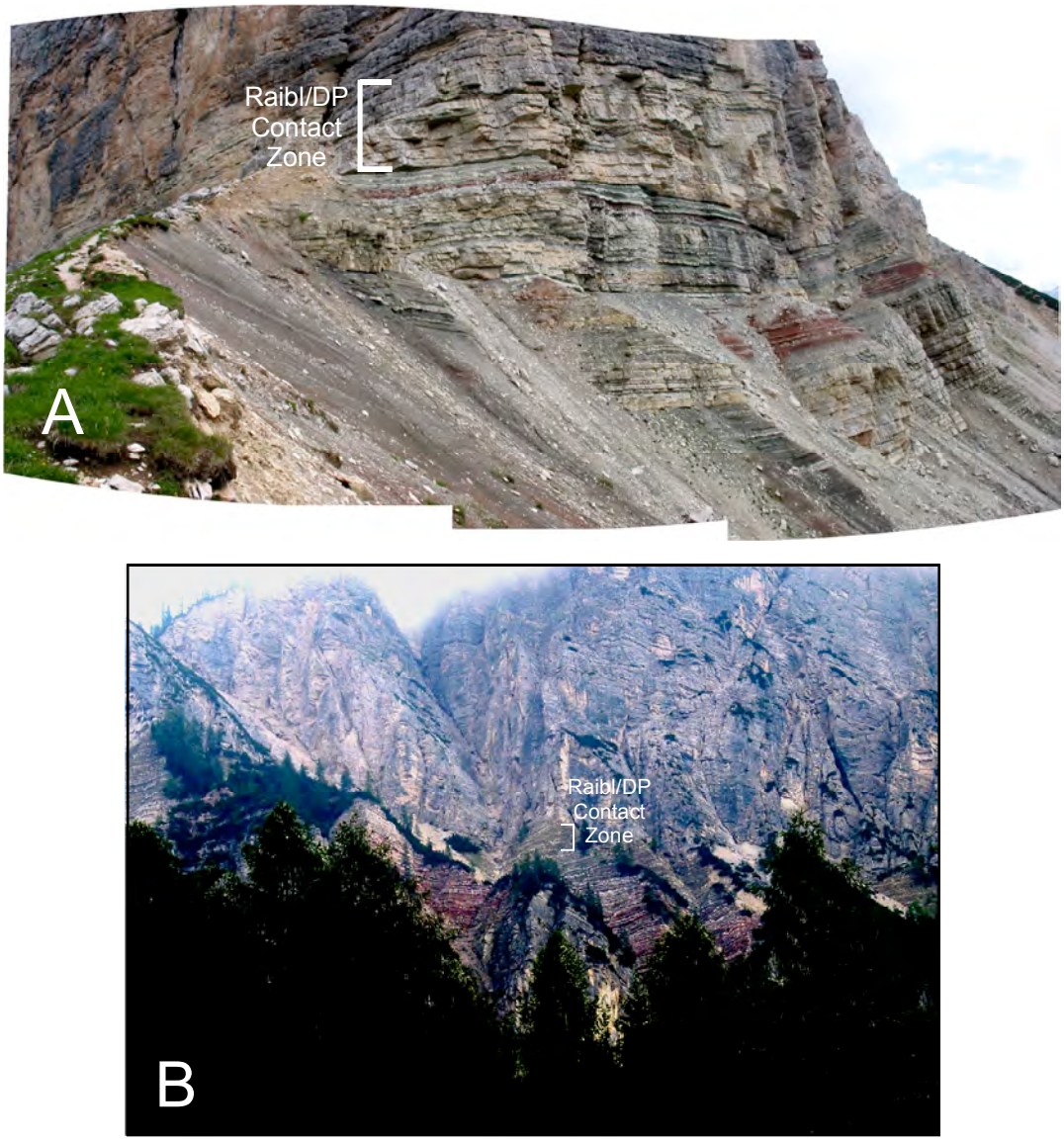

Figure 1.43. Photographs of the Raibl formation at its contact with the Dolomia Principale. A. Raibl-DP contact at the Tofana di Mezzo. Here the Raibl is mixed clastic and marly carbonate and is faulted (see non-correlative strata in Raibl of A).
B. Raibl-DP contact near the base chair lift of the Monte Cristallo ski area (photo B taken ca. 20 km east of photo A). Here the Raibl is far more gypsiferous, possibly reflecting comparably more marine influence in sections to the east.

Figure 1.44. Photograph of the Dolomia Principale outcropping at the Fanes group, with the Raibl outcropping beneath. This photograph is of Tofana di Rozes, the mountain in the center of the photo containing several hundred DP cycles. View from Col dei Bos looking east towards the Fanes group.

Chapter 2: On the Allocyclic Interpretation of the 'Latemar Cycles' (M. Triassic) of the Dolomites, Italy and Implications for High-frequency Cyclostratigraphic Forcing

ABSTRACT

The Middle Triassic Latemar Platform in northern Italy is a ca. 5 km wide, 700 m thick isolated carbonate platform containing a succession of approximately 600 depositional cycles (ca. 1 m avg. thickness), which have been attributed to allocyclic forcing by periodic Milankovitchian and/or sub-Milankovitchian eustasy. These interpretations are based on the facies composition of the cycles: thicker subtidal units overlain abruptly by thinner, cm-scale, subaerial caps- as well as the 5:1 bundling of the 'fundamental' m-scale cycles into lower-frequency 'megacycles'. Spectral analyses of cycle thickness and depth-rank series match calculated Milankovitchian periodicities. The influence of periodic Milankovitchian composite eustasy (whether pure Milankovitch or mixed Milankovitch and sub-Milankovitch) on the development of the Latemar cyclic succession has been questioned based on the dating of ashfall tuffs, paleomagnetic analysis of the platform, and correlation to biostratigraphic markers in nearby basinal deposits. In order to test the interpretation of allocyclic forcing for Latemar cycles, a cyclic succession preserved at Mendola Pass (located 30 km NW from the Latemar) was measured and analyzed. The Mendola cycles (avg. 0.70 m/cycle) are also bundled into upward-thinning

packages with a ca. 5:1 ratio. However, unlike the subtidal deposits immediately overlain by vadose diagenetic caps found at the Latemar, Mendola cycles consist of a mud-rich subtidal unit gradationally overlain by a cryptomicrobial (peritidal) laminite cap. A measured section from Mendola Pass of 36 cycles correlates biostratigraphically and statistically to a unique interval within the Latemar succession. Although laminite-capped cycles may attributed to autocyclicity the similarity of the stacking patterns of the Mendola cycles to those of the Latemar support an allocyclic interpretation. In addition, depositional rates calculated from dated Holocene shallow water carbonate facies equivalent to those at the Latemar and Mendola Pass are shown to be consistent with Milankovitchian or multi-millennial periodicities rather than millennial (ca. 1 kyr) cycle periods. In conclusion, biostratigraphic correlations, in addition to comparative sedimentology, indicate that the Latemar and Mendola cycles were deposited under the control of an allogenic forcing mechanism, and that this mechanism generated depositional cycles with multi-millennial individual periodicities.

AUTHOR'S NOTE

An expanded version of Chapter 2 of this dissertation was accepted for publication as:

Forkner, R.M., Hinnov., L.A., Goldhammer., R.K., and Hardie, L.A., 2006, On the Allocyclic Interpretation of the 'Latemar Cycles' (M. Triassic, The Dolomites, Italy) and Implications for High-frequency Cyclostratigraphic Forcing. SEPM Special Publication in Honor of the Career of R.N. Ginsburg

While this manuscript was drafted in its entirety by the author, the conception of this particular study represents the last body of work leading to a publication by the late Prof. Robert K. Goldhammer in the Dolomite Alps of Northern Italy. Bob had a great love of fieldwork in the Alps due to the excellent preservation of cyclic carbonate stratigraphy at various localities there. Bob also had deep respect for his scientific forebears. Bob would commonly refer to publications and ideas put forth by "the Gins" when teaching to remind students of the many ideas within the scientific community regarding the origin of carbonate rock fabrics and depositional cycles. What we present here is a written attempt to steward his latest ideas to the geologic and broader scientific community.

INTRODUCTION: THE PROBLEM

Investigation of the cyclic succession of platformal carbonate deposits at the Latemar began over 20 years ago and has subsequently stirred a vigorous debate regarding the driving mechanisms and depositional environments required to generate the succession. Goldhammer et al. (1987) proposed that the cyclic succession of approximately 600 depositional cycles (ca. 1 m avg. thickness) at the Latemar platform (the Dolomites, N. Italy) is a sedimentary record of composite glacio-eustasy, driven by Milankovitchian orbital forcing. This interpretation is based on several lines of evidence, including a) the shallowing-upward facies succession within each cycle (thicker subtidal unit overlain abruptly by a thin cm-scale, subaerial cap); b) a prevalent 5:1 bundling of the

'fundamental' m-scale cycles into lower-frequency 'megacycles', and c) time-series analysis of the cyclic succession showing agreement with predicted Triassic astronomical frequencies (Goldhammer et al., 1987, 1990; Goldhammer and Harris, 1989; Hinnov and Goldhammer, 1991; Hinnov et al., 1997; Preto et al., 2001; Preto et al., 2004).

The Goldhammer et al. (1987) interpretation that the high-frequency cyclicity at the Latemar is attributable to Milankovitchian forcing was challenged by the dating of zircons extracted from time-equivalent basinal deposits and ash-fall tuffs preserved in the Latemar platform interior, as well as relative dating provided by biostratigraphy (Brack et al., 1996; Mundil et al., 2003; Zühlke, 2004). These authors conclude that the entire Latemar succession was deposited in ca. 2.2 m.y. (in contrast to the 12 m.y. by the Milankovitchian interpretation), which demands much shorter periodicities for composite cyclic drivers, i.e., the fundamental shallowing-upward cycles are taken out of the Milankovitchian frequency bands (ca. 4.2 kyr/cycle) (Zühlke et al., 2003). As a result, the mechanism for the Latemar cycles was reinterpreted to be a periodic sub-Milankovitchian process and the mechanism for the megacycle bundling as Milankovitchian (Zühlke, 2004).

Most recently, Kent et al. (2004) concluded that most, if not all, of the ca. 700 m thick Latemar cyclic succession is restricted to a single magnetochron and

that the entire succession represents no more than 0.8 myrs, with individual Latemar cycles representing 1.7 kyr cycle durations. Independently, Emmerich et al. (2005) attempted to correlate the U-Pb age dates from tuffs in the basinal Buchenstein beds (by Mundil et al., 1996) to dates in the Latemar platform interior (by Mundil et al., 2003) using the biostratigraphic markers of Brack and Rieber (1993). These results suggest that individual Latemar cycles represent 0.90-1.97 kyr (Emmerich et al., 2005). Both works effectively place both the Latemar cycles and megacycles into the sub-Milankovitch band. In particular, the 'millennial model' of Emmerich et al. (2005) is set apart from the previous models in that no link to Milankovitchian forcing of Latemar cycles or megacycles is implied. Since publication of these works, Hinnov (2006) has questioned the interpretation of the paleomagnetic data in Kent et al. (2004) as a primary magnetic polarity signal, as volcanic dikes that cut the Latemar platform were not analyzed for their magnetic polarity, leaving the question of remagnetization unanswered. Further, the correlation of Emmerich et al. (2005) results in a Latemar chronostratigraphy with two age reversals (see Figure 7b in Emmerich et al., 2005), an increasingly problematic issue that casts serious doubt on the validity of the millennial hypothesis. These questions, and other issues raised by these millennial models, will be explored further below in the *Discussion*.

While arguments surrounding the origin and drivers of cyclic sedimentation at the Latemar continue within the pure Milankovitch, sub-

Milankovitch, and millennial camps, the conclusion that the Latemar cycles are a sedimentological record of an extrabasinal forcing mechanism was never questioned (for a summary of the 3 sets of Latemar cycle period interpretations, see **Figure 2. 1**). Blendinger (2004), however, challenged the validity of recognizing shallowing-upward cycles in the Latemar altogether, proposing that cycle-capping facies (dolomitic caliches, pisoids, tepees, etc.) are the products of post-burial hydrothermal diagenesis rather than the products of early diagenesis in the vadose zone. Blendinger (2004) states (p. 21) that "an alternative interpretation to eustatically controlled cyclicity and repeated subaerial exposure is provided by diagenesis in a hydrothermal field." However, the interpretations of Blendinger (2004) are clearly open for discussion (Preto et al., 2005; Peterhänsel and Egenhoff, 2005; Blendinger, 2005a,b).

If the deposits at the Latemar (as well as other time-equivalent platforms with similar platform-interior facies successions) cannot be confidently determined to be allogenic through sedimentologic and cyclostratigraphic analysis internal to the platform, validation of an allogenic driver may be accomplished through identification of cyclic deposits elsewhere that are temporally and stratigraphically equivalent. In this case, a succession of lower Ladinian cyclic platform interior stratigraphy located approximately 30 km NW of the Latemar at Mendola Pass has been identified, measured, and analyzed for possible periodic signals. Identification of comparable stacking (ca. 5:1 bundling)

and a cross-correlative statistical fit of Latemar and Mendola sections supports the hypothesis for an inter-platformal (hence allocyclic) forcing mechanism.

LOCATION AND GEOLOGIC SETTING

The Latemar platform is a ca. 5 km diameter carbonate platform of Anisian/Ladinian age located in the Dolomites of Northern Italy near the town of Predazzo (**Figure 2. 2**). While the platform is of comparative importance in this study, in order to investigate the possibility of an allocyclic driver for the Latemar cycles we focus our attention on the cyclic succession preserved at Mendola Pass (located 30 km NW from the Latemar near Bolzano), where approximately 500 m of Ladinian-age cyclic platform interior strata of the Dolomia della Val d'Adige Fm. are exposed (Venzo and Fuganti, 1965; Prosser and Selli, 1991). The absolute geometry of the Anisian/Ladinian carbonate buildup at Mendola Pass is not known, but appears to have involved a broad shelf, and allowed for the deposition of low-energy carbonates (e.g. mud-prone lagoons and tidal flats).

Anisian/Ladinian buildups in the Dolomites are common, most of which are limited to isolated buildups 10s of km^2 in area. During the Anisian/Ladinian, active faulting related to incipient rifting of Pangaea was ongoing (Doglioni, 1987, 1988). Most of the Anisian/Ladinian-age structures have been interpreted in relation to a regional N70^{o}E structural grain that includes extensive left-lateral strike slip faulting (e.g. Stava fault) and associated flower structures, many of

which are cut by Late Ladinian volcanic intrusions (Doglioni, 1988). Such an active tectonic regime almost certainly provided unique subsidence histories from locality to locality. Differential subsidence affecting active carbonate platforms in the Alpine Triassic is discussed in a number of studies spanning middle and late Triassic ages, including Bosellini and Hardie, (1985), Doglioni (1987, 1988), Jadoul et al. (1992), Carulli et al. (1998), Brack and Muttoni (2000), and Cozzi (2000).

FACIES AND CYCLES

The platform interior cycles at Mendola Pass and the Latemar share the general trend of having a shallowing-upward facies succession within each cycle. However, the facies internal to the cycles at the two localities are notably different.

Latemar Cycles

At the Latemar, facies within cycles “shallow-upward” from a peloidal wackestone/packstone through an oncolitic, intraclastic grainstone that is capped by a dolomitic caliche crust indicative of subaerial exposure (Goldhammer et al., 1987; Egenhoff et al., 1999; Zühlke et al., 2003; Preto et al., 2001; 2004) (**Figure 2. 3**). This succession was originally interpreted by Goldhammer et al. (1987) as shallowing up from shallow subtidal through subaerial exposure cap, but without a consistent, well-defined intertidal facies. The absence of a clear intertidal

facies was taken as direct evidence of rapid exposure of the platform top to the vadose zone - a "Waltherian skip" in the shallowing-upward facies succession as a direct result of rapid sea level fall (Goldhammer et al., 1987; Goldhammer et al., 1990). Paleobathymetric relations between the platform interior and reef margin facies estimated the reef top to be 2-3 meters deeper than the platform interior (Goldhammer and Harris, 1989). The absence of subaerial exposure diagenesis in the margin therefore constrains the high-frequency sea level amplitudes to ca. 2-3 meters.

This interpretation was modified by Egenhoff et al. (1999) who re-interpreted the oncolitic / bioclastic grainstones beneath exposure caps as intertidal deposits (Figure 2. 3, Microfacies 4), as oncoids have been associated with tidal channels (Demicco and Hardie, 1994). Preto et al. (2004) went on to recognize peloidal pack-to-grainstones with weakly developed fenestral cyanobacterial laminae in several cycles (see Preto et al., 2004, lithofacies 2), interpreting their presence as a record of supratidal conditions.

The recognition of an intertidal/peritidal facies in the Latemar cycles is important because it affects the fundamental conclusion held earlier (e.g. Goldhammer et al., 1987) that the cycles were a record of eustatic oscillations because of the Waltherian skip in facies succession. The interpretation by Egenhoff et al. (1999) for a full shallowing-upward suite of environments allows

for Ginsburgian autocyclicity as a possible driver and does not require eustatic oscillations (Ginsburg, 1971). This makes confirmation of an allocyclic driver for the Latemar all the more pertinent.

Mendola Cycles

A total of 36 complete shallowing-upwards cycles were measured along a road cut section below Mendola Pass (**Illustration 2. 1**). The facies succession internal to the Mendola Pass cycles is fundamentally different than that of the platform interior cycles at the Latemar. Rather being capped by vadose dolomitic caliche fabrics, Mendola Pass cycles are laminite-capped cycles, similar in many ways to the Late Triassic Dolomia Principale and Lofer cycles of the Dachstein Limestone (Fischer, 1964; Bosellini and Hardie, 1985; Goldhammer et al., 1990; Haas, 1994, 2004; Cozzi et al., 2005). The typical Mendola Pass cycle has an erosive base consisting of mm to cm-scale flat laminated intraclasts ripped up from the underlying cycle cap. Erosion of cycle tops is interpreted to be the result of reworking of the substrate during high-energy events prior to the re-initiation of carbonate sedimentation during relative sea level low. Similar base-of-cycle intraclastic breccias can be observed in the laminite-capped cycles of the Dolomia Principale and the Dachstein Limestone, where they are also interpreted as transgressive or storm reworking of the substrate (Fischer, 1964; Bosellini and Hardie, 1985; Cozzi, 2002).

Erosive bases grade upward into a dolomitized peloidal mud-to-wackestone with fine bioclastic debris and intermittent lenses of dasycladacean grainstone (storm beds), interpreted to have been deposited within a shallow (<10 m) restricted lagoon. Work done in the Holocene by Ginsburg et al. (1977) and Shinn (1986) describes offshore sediment in the modern of Andros Island, Bahamas, that closely matches the description of the peloidal wackestones observed in Mendola Pass cycles. Cores taken 4 km offshore from the tidal flats of Andros Island show well-churned, burrowed sediments that notably lack recognizable physical sedimentary structures (Hardie and Ginsburg, 1977). Texturally, these sediments may be described as highly bioturbated, gray pelletal/peloidal mud to wackestones containing benthic forams and skeletal debris (Shinn, 1986). The modern shallowing-upward tidal flat cycle of Enos and Perkins (1979) and Shinn (1986), assigns this subfacies to the subtidal realm, up to ca. 10 meters deep. A similar interpretation applies to the peloidal wackestone facies within the Mendola Pass cycles, with the caveat that a general lack of diversity of faunal remains may be indicative of restriction.

Subtidal wackestone facies within Mendola cycles characteristically coarsen up to a coarse dasycladacean pack-to-grainstone prior to being capped by microbial laminites (**Figure 2. 4**). Dasycladacean grainstones are interpreted as evidence of shallow-water (perhaps intertidal) reworking resulting from sedimentary fill of accommodation space and aggradation into a comparatively

energetic depositional environment. This facies may represent a shallow subtidal depositional setting within the influence of high-energy events (e.g. storms) that reworked algae into partially-articulated bioclasts.

All Mendola Pass cycles are capped by mm-scale, crinkly laminated mud to- wackesone with intercalated discontinuous layers of intraclastic and bioclastic grainstone. Laminae also have rare v-shaped polygonal cracks and horizontal elongate fenestrae. Laminites are interpreted to be evidence of a supratidal flat-type environment similar to the modern tidal flats of Andros Island, Bahamas. Original studies by Black (1933) on Andros Island, Bahamas, identified near shore surface mats of sticky, filamentous blue-green algae that bind and trap sediment washed in from the offshore subtidal carbonate "factory", creating laminated sediments. Later studies by Hardie and Ginsburg (1977) on Andros Island found that thinly-laminated sediments are typically found in low energy, flat, supratidal environments that are exposed subaerially 85% of the time or more. Sediments associated with these mats may contain fenestrae of various subtypes, thin-bedded storm deposits, and well-laminated muddy, organic-rich layers (microbial mat) that alternate with layers of soft peloidal sand (Hardie and Ginsburg, 1977; Demicco and Hardie, 1994). By comparison, it is likely that the laminated subfacies within Mendola pass cycles formed in a supratidal flat-type environment via binding and trapping of transported subtidal sediments onto filamentous microbial mats. Additionally, certain examples (e.g. Mendola Cycle

28 laminites) show evidence of biological origin, including cm-scale stromatolite heads.

Comparison of Latemar vs. Mendola Cycles

The difference in subfacies successions in Mendola and Latemar cycles has several possible explanations. First, it may be that the larger size of the Mendola platform allowed for the development of “protected” tidal-flat environments. Isolation from open marine conditions would have allowed for the accumulation of muddy cycles with flat laminite caps, similar to those observed in the modern tidal flats of Andros Island, Bahamas (Hardie, 1977). This would be in contrast to the Latemar, which appears to have been a smaller isolated platform. By comparison, the interior of the Latemar platform was affected by current and wave energy, winnowing out mud and transporting more sediment off-platform, thereby creating the grainier facies successions preserved there.

It is also possible that differential subsidence affected vertical accommodation space at each location. A slightly lower rate of subsidence at the Latemar during the interval under investigation may have allowed high-frequency sea level oscillations to “touch down” directly onto the subtidal and form diagenetic caps while a slightly faster-subsiding Mendola remained in submerged or in peritidal settings. A slightly faster subsiding Mendola Pass during this interval serves to explain the 0.26 m difference in average cycle

thicknesses between the two localities (average cycle thickness of the Latemar interval = 0.52 m; average cycle thickness of the Mendola interval = 0.73 m). A tectonic arrangement of this type would fit with the sinistral transpressive model of Doglioni (1987, 1988), who recognizes compressive tectonic features of both Anisian and Ladinian age near the Latemar platform, which may have limited subsidence at the Latemar as compared to Mendola (*see* Doglioni, 1988, p. 294, Fig. 1). It should be noted that this phase of compression was both pre- and post-dated by rifting phases that generated differential thickness in sedimentary cover in the Dolomites, resulting in an overall thickening of the Triassic section by at least 3 times from the west near Mendola pass to the east near Tre Cime di Lavaredo (Laubscher and Bernoulli, 1978; Doglioni, 1987, 1988).

While subfacies within Latemar and Mendola cycles are notably different the cycles nonetheless share several common traits. One distinct similarity is that the facies within both successions “shallow-up”, i.e., the cycles at both localities record a progressive filling of accommodation space recorded by vertically shallower facies types within each cycle. Further, the depositional fabrics preserved within the cycles are indicative of deposition within 0-10 m of water depth (Hardie and Ginsburg, 1977; Shinn, 1986). Deposition in the shallow marine realm made these localities sensitive to environmental shifts, most notably sea level oscillations. Finally, the Latemar and Mendola cycles are both of similar vertical scale (ca. 1 meter), and are “bundled” into thinning-upward

packages of predominantly 5 cycles, suggesting that the same process driving the high-frequency stratigraphic development was recorded at both localities (**Figure 2. 5**).

STRATIGRAPHIC CORRELATION OF THE MENDOLA AND LATEMAR SECTIONS

Background

The "Mendel Dolomit" was originally defined lithologically by Richthofen (1874), but since that time little published data has become available with reference to its depositional age. However, a recently published a geologic map includes clues to the age of the Mendola Dolomite (Avanzini, 2002). Notes from the map indicate that the "Mendola Formation" is a platform carbonate body of Late Anisian-Early Ladinian age (Avanzini, 2002). Portions of the map's notes are paraphrased below (translated by N. Preto, personal communication).

Within the Mendel Dolomit, Ogilvie Gordon (1927) recognized a lower member with dasycladacean alga *Diplopora anullatissima* and *Physioporella paucifoliata* corresponding with the Sarl-Dolomit, and an upper member with *Diplopora annulata* corresponding with the Schlern-Dolomit. These conclusions were later corroborated by von Klebelsberg (1935) and Van Hilten (1960). Further stratigraphic studies carried out for the purpose of geological mapping of the area distinguished two informal units within the Mendola Formation. The first is the subtidal member, corresponding to the Upper Serla Dolomite and Contrin Dolomite of the eastern Dolomites. The second is the Peritidal member. The lower boundary of the peritidal member is marked by a paleosol and sometimes associated with tepee horizons. The upper boundary is more variable. At Mendola pass, strongly karstified portions are infilled with andesitic and basaltic volcanics that are laterally equivalent with the basinal Roen Limestones. Additionally, a few ammonoids of the *avisianum* subzone occur at the base of the

peritidal member (Preto, personal communication). The sedimentary environment is that of an aggrading, periodically exposed carbonate platform.

The section measured in this study belongs to the “peritidal member” of the Mendola Fm, which overlaps with Latemar platform interior biostratigraphy (**Figure 2. 6**). The assemblage of dasycladacean algae extracted from the Mendola section includes *Physoporella leptotheca* (Cycle 7), *Diplopora annulata annulata* (Cycles 7, 8, and 20) and *Gyroporella ladinica* (Cycle 20). Dasycladacean algae of the subtidal member of the Mendola formation, including *D. annullatissima* and *P. paucifoliata* were not found within the study interval (N. Preto and O. Piros, personal communication). In terms of correlation to the Latemar, *D. annullatissima* occurs only in the lowermost part of Latemar (Gaetani et al., 1981), and *P. paucifoliata* is even older. However, *D. annulata* was found within the study interval and is consistent with the biostratigraphy of Ogilvie Gordon (1927) for the upper peritidal member of the Mendola formation. The lowermost portion of the peritidal member is reported to contain ammonoids of the *avisianum* subzone indicating late Anisian age, which is consistent with a 175 m thick succession of cycles in the Latemar that includes the upper portion of the Lower Tepee Facies, the entirety of the lower cyclic facies, and the lower half of the Middle Tepee Facies (*see* Manfrin et al., 2005, p. 480, fig. 3). The upper portion of the peritidal member of the Mendola formation may correlate to portions of the Latemar stratigraphy above this interval, including the upper portion of the middle tepee facies and/or the upper cyclic facies. In sum, while biostratigraphy does not tie the Mendola succession to a specific interval within

the Latemar, it does indicate that there is a biostratigraphic overlap of the Mendola and Latemar cyclic successions.

STATISTICAL CORRELATION OF THE MENDOLA AND LATEMAR SECTIONS

Statistical time series analysis of the Latemar and Mendola cycles sheds light on the stratigraphic patterns in the sections and their interrelationships. A more in depth set of statistical analyses, including *running cross-correlation analysis, harmonic analysis, spectral coherency* and *cross-phase analysis* is included in Forkner et al. (2007), but is omitted in this manuscript as the analysis was done by Dr. Linda Hinnov of the Johns Hopkins University. The analyses serve to pinpoint the most likely position of the Mendola section within the Latemar's extended cyclic stratigraphy and to investigate specific cyclic patterns (i.e. bundling frequencies) shared by the two sections.

Running cross-correlation analysis

Forkner et al., (2007) published the results of running cross correlation analysis between Mendola and the Latemar cyclic series measured at Cima Forcellone (**Figure 2. 7**). While the Mendola cyclic series was relatively short (only 36 cycles), an extremely high correlation coefficient value of +0.6, greatly exceeding the 95% confidence limit of 0.375 for 36 degrees of freedom, occurs between the Mendola and the Cima Forcellone series from Cycles 351-386 (*see*

Forkner et al, 2007, fig. 6). This correlation is within the range of correlation provided by Dasycladacean algal biostratigraphy and is the basis for the cyclostratigraphic correlation between the Latemar and Mendola platforms.

Fischer plots

Charts plotting the cumulative deviation from mean cycle thickness (i.e., "Fischer plots", after Fischer, 1964) highlight relative accommodation trends in platform cycle successions. The Fischer plot of the Mendola section (**Figure 2. 8A**) shows clear bundling of cycles into megacycles with an average grouping of 5 depositional cycles into 1 bundle or megacycle (5:1). The Fischer plot of the correlative Latemar section (**Figure 2. 8B**) is remarkably similar, with both bundling and overall stacking trends synchronized with those at Mendola Pass. Both Fischer plots suggest a regressive interval over the first 15 cycles (cycles thinning upward). This trend is particularly pronounced in the Latemar section and is followed by the deposition of a 2.5 meter-thick tepee-capped depositional cycle (a.k.a., Cycle 366, see Goldhammer, 1987) that is the thickest cycle in the study interval. The equivalent cycle at Mendola Pass is also the thickest in the study interval (3.06 meters-thick), but is laminite-capped. The remaining, upper 21 cycles are the most strongly bundled in both sections, and both have a long-term thickening trend suggestive of lower-frequency transgressive to high-stand conditions.

Spectral Analysis

The most advanced statistical methods used for analysis of cycle stacking and bundling trends is spectral analysis of the cyclic successions from the Mendola and Latemar platforms. Essentially, examination of sections as a time series means treating depositional cycles as a representation of cyclic behavior with temporal periodicity, which can be viewed as a combination of waveforms of different frequencies superimposed one on the other. In this case, relative sea level change (whether eustatic or subsidence-driven) are recorded by carbonate rocks as depositional cycles in the rock record. The purpose of the analysis is to identify prominent cyclic frequencies in the data (Bloomfield, 1976). A plot of the spectrum of a cyclic series allows analysis of the cyclic succession in a frequency domain. The spectrum itself is treated as a Fourier transform that re-expresses the depositional cycle thickness series in terms of a sinusoidal function relating thickness to time (Bloomfield, 1976; Jenkins and Watts, 1968). In other words, spectral analysis of a cycle thickness series essentially transforms the series (here represented by the thickness of cycles in meters) into a frequency spectrum based on cyclic sinusoids (in cycles/meter), thereby decomposing the entire time series into individual frequencies (Bloomfield, 1976). The frequencies of the waveforms may represent individual cycles (e.g., a frequency peak of 1 cycle per meter in a series with average cycle thickness of 1 meter), or groups of cycle bundles into a lower-frequency wave (e.g., a frequency peak of 0.2 cycles per meter in a series with average cycle thickness of 1 meter, equaling a 5m

“megacycle”, or bundle of 5 ca. 1 meter cycles). In this case, software packages Analyseries v 1.2 and KaleidaGraph were used in constructing time series plots.

The full suite of statistical bundling patterns in the sections is revealed through time series analysis. In this case, the multitaper method (MTM), which is an exceptional tool for frequency assessment of short, highly noisy time series (Thomson, 1982; Hinnov, 2000; Forkner et al., 2007). A more detailed series of statistical analyses appears in Forkner et al. (2007) while a shortened version appears here. Spectral analysis of the Mendola and Latemar thickness series shows that bundling frequencies similar in the two sections, although their relative amplitudes are different (**Figure 2. 9**). This may be due to low-frequency subsidence-related (tectonic) influences on the development of the Mendola vs. Latemar platforms. The lowest frequency peak (Mendola at 1/18.9 and Latemar at 1/27.0), while measured with a high confidence (F-test) in both sections, is based on only two repetitions in the only 36-cycle long Mendola section, and less than two repetitions in the Latemar section. This means that these peaks cannot be taken represent a sustained bundling at this frequency, but would require additional data from longer measured sections to confirm. The next to lowest peak (Mendola at 1/8.5 and Latemar at 1/9.8) may represent the same process in both sections, as examination of the Fischer plots indicates that one source of this peak in both of the sections appears to involve a single bundle of 8 to 9 cycles (Cycles 7 to 15). The cause of this bundling is not known, but in either

case is present in both sections. Surprisingly, the 5:1 bundling frequency, while prevalent in the Fischer plots, has a very low confidence (ca. 60-75%) in both sections. This suggests that the 5:1 bundling. while quite visible in the Fischer plots of both series, is somewhat variable about 5:1 (e.g., 4:1 and 6:1), resulting lower confidence. Finally, both sections show a bundling at 1/2.4; again, these bundles can be observed in the Fischer plots (e.g., Mendola Cycles 19 to 20, or Latemar Cycles 14 to 15).

DISCUSSION

Shallowing-upward cycles

The Mendola and Latemar cycles are late Anisian / early Ladinian-aged shallowing-upward, meter-scale peritidal platform carbonate cycles that formed as a result of repetitive environmental changes over time. The presence of the shallowing-upward cycles allows for physical measurement and statistical analysis of their stacking trends (i.e., trends in the vertical arrangement of cycle thicknesses). The cyclic successions have stacking patterns that appear similar to the eye (*see* **Figure 2. 8**), but cross-correlate with a correlation coefficient exceeding 95% (*see* **Figure 2. 7**), suggesting a shared external driver. Site-specific controls (e.g., autogenic sedimentary processes, local subsidence) exerted comparably less influence on the development of the cyclic successions, but could explain the differing average cycle thicknesses between the

successions (average cycle thickness of the Latemar interval = 0.52 m; average cycle thickness of the Mendola interval = 0.73 m).

Recording of cyclic processes

Both Mendola and Latemar successions formed in environments conducive to recording rhythmic, cyclic sea level oscillations. The shallow marine realm (<5 m water depth) is almost certainly the depositional environment that these deposits formed in, where repeated flooding and exposure of the sediment-water interface was recorded within each depositional facies succession. This is especially true at Mendola Pass, where facies within shallowing-upward cycles are consistent with those found on modern carbonate tidal flats (e.g., Hardie and Ginsburg, 1977). Strong and consistent sedimentologic evidence for early subaerial exposure of Latemar cycle caps provides evidence for a similar facies/ water depth relationship at the Latemar (e.g., Preto et al., 2004). The significant statistical correlation between the Mendola section and a specific interval at the Latemar indicates that sea level oscillations equally affected both depositional environments. This observation is important, because constantly deep-submerged environments, as favored by Blendinger (2004) for the Latemar cycles, would "miss beats", not have a non-random bundling pattern, and not be readily correlatable to a clearly-peritidal counterpart at Mendola (Preto et al. 2005). The presence of Mendola cycle cap laminites and Latemar cycle cap dolomite crusts indicating subaerial exposure

during sea level fall means that the Latemar was not only able to “keep up” with subsidence, but also undergo extended periods of time with the platform top in peritidal and supratidal conditions, environments not known for rapid accumulation rates (Ginsburg et al., 1977).

The case for allocyclicity

The fact that correlated cycle stacking patterns are recognized at separate locations that are constrained by biostratigraphy is strong evidence for the existence of a common allocyclic mechanism driving the development of both successions. The presence of allocycles at the Latemar and Mendola Pass requires that mechanisms existed during the mid-Triassic that acted to generate both sea level oscillations and resultant carbonate depositional cycles at both localities. In the case of the Latemar controversy, what can be established to a first order is that shallowing-upward depositional cycles have been identified and cross-correlated to Mendola pass, implying that the driving mechanism is at the very least regional (and perhaps global) in its stratigraphic influence.

Comparative Sedimentology

The comparison of Holocene and Pleistocene dated allocycles to ancient depositional cycles is useful for several reasons. First, composite sea level oscillations regarded as drivers for shallow marine carbonate sedimentation in the Holocene and Pleistocene are grouped into 5 ca. 20 kyr oscillations per 100

kyr oscillation (Broecker et al. 1968; Bloom et al. 1974), a pattern that conspicuously matches the vertical stacking at the Latemar and Mendola Pass. The fact that the pattern of sea level oscillations within the Milankovitch band matches the vertical stacking of carbonate depositional cycles demands the consideration of Milankovitchian processes as possible cycle-generating mechanisms. Second, if the composite allocyclic forcing mechanisms that formed depositional cycles in the mid-late Triassic were still active in the Pleistocene and Holocene, then those same mechanisms ought to be recorded as depositional cycles in the Pleistocene and Holocene. Discovery of modern or recent depositional cycles with millennial periodicities and bundling patterns similar to that of the Latemar would better point the cyclostratigraphic community toward identifying the correct forcing mechanism. However, this has yet to occur. Third, shallowing-upward facies successions similar to those at Mendola Pass are found in Florida Bay, the Bahamas, and the Persian Gulf. Comparing the rates at which these deposits form in the modern, is a basis for estimating cycle durations for similar deposits in the geologic past.

Recent publications offer new insights into sea level change during the past 20 kyr. Two compilations are provided here. **Table 2. 1** summarizes Pleistocene and Holocene cyclic climatic processes operating at sub-Milankovitch periodicities. While many types of variations are listed, not every process is tied (observationally or otherwise) to meter-scale sea level change at

these periodicities, and none are tied to the formation of shallowing-upward depositional cycles in modern marine carbonate sedimentary settings. Table 2 compiles literature involving the dating of Pleistocene and Holocene carbonate shallowing-upward successions. This suggests that in most cases, the sediments making up the Holocene carbonate successions- most of which are not yet complete shallowing-upward successions- formed over the past 5-7 kyr as the result of a longer-term sea level rise over the past 10-20 kyr. While a few examples of dated shallowing-upward facies successions from the modern appear to have formed within the last 1,000 years (*see* Strasser and Samankassou, 2003), dating and analyses of Holocene and Pleistocene carbonate successions from around the world has found no example of a correlatable stack of meter-scale shallowing-upward carbonate depositional cycles with millennial (1-2 kyr) periodicity.

Holocene and Pleistocene “icehouse” conditions, so-called due to the presence of major land-locked ice sheets, store and release large amounts of water. This causes high-frequency sea level oscillations with amplitudes of several tens of meters. As an example, dating of coral reef terraces in Barbados by Bloom et al. (1974) suggests that six major sea level oscillations have occurred over the past 130 kyr, with rise/fall amplitudes of 20+/- meters superimposed on the overall 120m rise since the last glacial maximum (Bloom et al. 1974; Chappell and Shackleton, 1986). Shallow marine carbonate cycles

produced by 20+/- meter sea level oscillations are thicker than those found in the Alpine Triassic (e.g., Goldhammer et al., 1990). Pleistocene depositional cycles identified in Florida and the Bahamas are on the order of 5 – 15 meters thick, and consist of subtidal carbonate capped by laterally correlative red soil crusts (Goldhammer and Kaufman, 1995). Both modern carbonate shallowing-upward successions as well as the record of Pleistocene and Holocene sea level oscillations operate at cyclic frequencies that are in tune with known orbital periodicities (**Table 2. 2**; Logan et al., 1969; Bloom et al., 1974; Tudhope, 1989; Parkinson, 1989; Goldhammer and Kaufman, 1995; Strasser and Samankassou, 2003).

The early to mid-Triassic is thought to have occurred during a greenhouse (or possibly transitional icehouse-greenhouse) climatic regime, lacking major continental ice sheets and therefore have lower amplitude (ca. 10 m or less) high-frequency sea level oscillations (Vail et al., 1976; Goldhammer et al. 1990; Wright, 1992; Read, 1995). Consequently, shallowing-upward depositional cycles are relatively thin (1-2 meters), but in many cases still form stacks that reflect orbitally driven eustasy. Many workers have suggested that Triassic depositional cycles formed as the result of Milankovitch-band high-frequency/low-amplitude eustatic oscillations related to rhythmic orbital perturbations that affected the spatial and temporal distribution of solar energy to the Earth's surface (Fischer, 1964; Schwarzacher, 1975; 1993; 2005; Goldhammer et al.

1990; Goldhammer and Kaufman, 1995; Yang and Lehrmann, 2003; Zühlke, 2004; Maurer et al. 2004, Cozzi et al., 2005).

Obviously, the geoclimatic conditions of the Holocene and Pleistocene stand in contrast to those of the early to mid-Triassic. However, observations from modern sediments suggest that cyclic climatic perturbations with millennial periodicities are not being recorded as shallowing-upward carbonate depositional successions, even in areas where carbonate sediments have infilled available accommodation space (e.g. tidal flats of Andros Island). Instead, most shallowing-upward facies successions dated from the Holocene and Pleistocene seem to have formed with periodicities that are commensurate with Milankovitchian and/or other multi-millennial processes. It is possible that the processes driving Triassic depositional cycles were unique to that period of geologic time and that comparison between modern and ancient is not warranted. However, the presence of Triassic allocycles that have an apparent statistical profile that is consistent with Milankovitchian orbital parameters- a link that is temporally justified through comparative rate studies of Holocene facies successions- leaves two main options regarding their origin, discussed as follows:

I. The successions of carbonate depositional cycles at the Latemar and Mendola Pass record periodic, allogenic processes directly linked to Milankovitchian composite eustasy.

The case for Milankovitchinan composite eustasy driving the deposition of either fundamental cycles (e.g., Goldhammeret al., 1987) and/or megacycles (e.g., Zühlke 2004) at the Latemar and Mendola Pass is based on extensive sedimentological and statistical analyses. While the two main models supporting the presence of Milankovitchian composite eustasy involve different time scales (*see* Figure 1), both studies strongly argue for the presence of multi-millennial astroclimatic forcing in the development of carbonate depositional cycles. Here, we recognize that both of these models, Goldhammer et al. (1987) and (Zühlke et al. (2003) argue that the development of Latemar cyclicity is linked to orbital forcing.

From a comparative-sedimentological standpoint, Latemar and Mendola cyclic stratigraphy agrees with known parameters of Milankovitch band sedimentation. Dating of shallowing-upward successions from modern carbonate settings indicates that most have over the past 5-7 kyr in response to Holocene sea level rise (**Table 2. 2**). The fact that many platforms have not yet aggraded to sea level and/or formed exposure caps suggests that the periodicity associated with the cyclic driver is longer than the time in which the depositional

cycle actually sediments. Additionally, sea level inferred from coral reefs and deep-sea sediments confirm that 5 oscillations with amplitudes of 20+/- meters occurred over the past 100 kyr (Broecker et al., 1968; Bloom et al., 1974; Chappell and Shackleton, 1986). The frequencies of these oscillations match those of the precession and eccentricity, and they provide a driver for the bundling of depositional cycles that is fundamentally linked to carbonate sedimentation.

Additional sedimentological evidence for Milankovitch band forcing of depositional cycles relates to the rates at which complete carbonate cycles form, particularly vadose diagenetic facies. While the cycles measured at Mendola Pass do not have diagenetic caps, many of the cycles in the equivalent Latemar succession do have well-developed diagenetic caps. The presence of these diagenetic caps must be accounted for in a temporal sense for the Latemar cycles and in a time-correlative sense for Mendola cycles. The caliche that caps Latemar cycles ranges in thickness from 1-30 cm, averaging 6 cm in thickness (Goldhammer et al. 1987). Radiocarbon-calibrated rates of Holocene caliche formation average 2-4 cm/kyr (James, 1972; Robbin and Stipp, 1974; Handford et al. 1984; Demicco and Hardie, 1994), and several studies suggest even lower rates, at 0.4-1 cm/kyr (Lucia, 1968; Davies, 1970; Evamy, 1973). If Holocene examples are used as a temporal benchmark, rapid, millennial scale sea level oscillations do not provide adequate time for observed vadose diagenetic

features to form. In order for diagenetic caliche caps to form within a millennial cyclic framework (entire cycle in 0.9-1.97 kyr), rates of caliche formation must be much higher than those in the Holocene. Additionally, studies of Holocene tepees at Lake MacLeod, Western Australia by Handford et al. (1984) show that sediment buckles and is tilted into tepee antiforms at an average rate of 4 cm/kyr, and void-filling aragonite cements within tepees grow at extremely slow rates of 0.2-0.4 cm/kyr. Goldhammer et al. (1987) and Hardie et al. (1991) report tepee zones at the Latemar with thicknesses varying from 1 to 13 meters, with individual cement bands up to 20 cm thick. Individual tepee antiforms are typically onlapped by sediments from subsequent cycles, suggesting that tepees were completely formed prior to the deposition of the next cycle(s). If Holocene rates of tepee formation from Lake Macleod are even close approximations of rates of tepee development at the Latemar, the multi-meter tepee structures at the Latemar alone represent several hundreds of kyr of time. In order for these same tepee structures to have formed caps on millennial cycles, both tepee antiforms and cements would have to form at rates that are at least two orders of magnitude faster (40-400 cm/kyr antiform; 20-40 cm/kyr cement) than those documented at Lake MacLeod.

In addition to sedimentologic evidence, spectral analysis of Latemar cycle thickness and rank series indicates a close match between bundling frequencies of Latemar cycles and Milankovitchian orbital cycles. The clarity of the record

and the non-trivial nature of the match is especially apparent in studies using rank series analysis, where plots of depth ranked units appear to have formed in lock-step synchroneity with Milankovitchian insolation (*see* Figure 8 of Preto et al. 2004). However, tuning the Latemar cycles to a sub-Milankovitch component (i.e., 4.2 kyr, Zühlke et al., 2003) also preserves Milankovitchian frequency components, but at a different order (*see* Figures 11 & 12 and Table 2 of Zühlke, 2004), first noted by Schwarzacher, 1998. The difference lies in the assignment of the precession: the pure Milankovitch interpretation suggests that the precession has driven fundamental cycle formation (i.e., 20 kyr Latemar cycles / 100 kyr megacycles), while the mixed Milankovitch/sub-Milankovitch interpretation suggests that precession drove formation of megacycles (i.e., 4 kyr Latemar cycles / 20 kyr megacycles).

In light of this "tuning" equivalence, the mixed Milankovitch/sub-Milankovitch model deserves closer attention. Thus far, no proposed driver of eustatic sea level change is identified to operate at a millennial scale of ca. 4 kyrs. However, we note recent work on Pleistocene eustasy that may lead to the identification of such a driver: Chappell (2002) reports ca. 6 kyr recurrent coral terraces uplifted in the Late Pleistocene of Papua, New Guinea suggestive of sea level oscillations with amplitudes as large as 15 m. Possibly this is the analog to the 4.2 kyr Latemar driver. There is also evidence of similar eustatic behavior in the uplifted Pleistocene coral terraces of Barbados (Thompson and Goldstein,

2005). However, both locations are situated in tectonically active areas, involving rapid uplift of the islands related to the geodynamics of adjacent convergence zones. In particular, the rather large (>10 m) amplitudes that have been suggested for these millennial eustatic changes depend on the accuracy of the uplift rates that have been estimated for these islands. It is also important to note that these measurements were taken from fast-growing corals, not from stacked peritidal depositional cycles.

In either case, (pure Milankovitch or mixed Milankovitch/sub-Milankovitch) both models rely on an astroclimatic forcing mechanism as a cyclic driver for carbonate sedimentation. The hallmark of this forcing is recognized via statistical analysis of Latemar cycles and cross-applied to the Mendola succession. Comparative sedimentology indicates that Holocene carbonate successions formed at rates commensurate with multi-millennial processes, providing further evidence for a link between an allocyclic, Milankovitchian process and the sedimentary record.

II. The successions of carbonate depositional cycles at the Latemar and Mendola Pass record periodic, allogenic processes operating at millennial periodicities.

Emmerich et al. (2005, p. 11) write "radiometric age dating on detrital zircons in air-borne tuff layers intercalated within the cyclic succession of the

Latemar solved the controversy". This statement, however, is by no means an agreed-upon fact. Indeed, their correlation scheme (see Fig. 7b in Emmerich et al., 2005) results in two age-reversals (i.e. older-upward rather than younger-upward) the first occurring from "Tc" (241.2+0.8/-0.6 Ma) to LAT-31 (242.6±0.7 Ma) and the second occurring between the platform-interior ash beds LAT-30 (241.2+0.7/-0.6 Ma) and LAT-32 (241.7+1.5/-0.7 Ma). If these age reversals in zircon crystal ages are accurate, then these ages cannot reflect the age of the sediments they bracket in an absolute sense unless maximum error limits are taken into account.

Emmerich et al. (2005), and independently, Kent et al. (2004), suggest that both cycles and megacycles at the Latemar operate at sub-Milankovitchian frequencies, i.e., ca. 0.9-1.97 kyr/cycle and ca. 3.5-10 kyr/megacycle. As a result, the accumulation of the entire Latemar buildup was calculated to be ca. 1 myr. The prevalent 5:1 megacycle bundling originally identified by Goldhammer et al. (1987) is not recognized by Kent et al. (2004).

Periodic drivers for Triassic millennial shallowing-upward cycles are not identified. No such process operated to generate stacked shallowing-upward cycles in the Holocene or Pleistocene (see previous discussion). Kent et al. (2004) argue for tidal forcing operating at ca. 1.8 kyr, citing a theoretical tide at the periodicity identified by Munk et al. (2002). However, Munk et al. (2002, p.

382) state that “the equivalent tidal amplitude of the millennial term is estimated at 0.04 mm-” which is clearly not enough to generate the meter-scale Latemar cycles. Similarly, there is a disconnect between millennial-period Dansgaard-Oeschger climate cycles and Heinrich-type warming events cited by Emmerich et al. (2005) as possible cycle drivers. No link has yet been established between these cycles and formational periodicities of shallowing-upward carbonate successions of the Holocene and Pleistocene. Recently, Roth and Reijmer (2005) identified oxygen isotope excursions in a 30-m long core from the leeward margin of the Great Bahama Bank that have both centennial and millennial (ca. 1.7 kyr) periodicities. While this discovery establishes a link between centennial and millennial cyclic processes and carbonate sedimentation, the cycles are not linked to the depositional periods of platform-interior shallowing-upward depositional successions. The identification of periodic megacycle drivers within the millennial model is likewise problematic. Studies from the Holocene and Pleistocene have yet to identify a lower-frequency (ca. 5-10 kyr) cyclic process by which millennial tides, Bond cycles, or other climatic processes will produce bundled shallowing-upward carbonate megacycles.

While the rates of eustatic rise and fall required for millennial cyclic carbonate deposition are rapid, rates for subsidence and sediment accumulation required for the development of depositional cycles within this context are likewise very high. The subsidence required to generate 700 m of section in ca.

1 myr is approximately 0.7 m/kyr. As both the Latemar and Mendola sections preserve cyclic successions of similar stacking and bundling trends, subsidence would have operated at near-equal rates at both localities during the study interval in question. In addition, accumulation rates (including time for sedimentation and subaerial exposure) of platform interior and tidal flat sediments would need to be extraordinarily high in the millennial framework – requiring a sustained accumulation rate in excess of 0.7 m/kyr, approaching the growth rates of Holocene corals - to generate both successions (*see* Schlager, 1981 for rates). If one considers low energy carbonate tidal flats as sediment sinks rather than sediment sources (e.g., Ginsburg et al., 1977), source sediments would need to be produced at rates that are yet again even higher than 0.7 m/kyrs in order to generate enough sediment to fill the tidal flat sink.

The paucity of evidence for millennial cyclicity of shallowing-upward carbonate successions in the Holocene and Pleistocene, however, must be tempered with the realization that biotic, climatic, and oceanic conditions have changed throughout geologic time. It is possible that the cyclic drivers in the Triassic were unique to that period and cannot be compared to those operating in the Holocene and Pleistocene. Indeed, it may be that in this case comparative sedimentology has met its limit as a temporal reference, and that its only appropriate use in mid-Triassic carbonates is as a tool for identifying facies and depositional environments.

The conclusion that processes with millennial periodicities formed the depositional cycles at the Latemar is the result of paleomagnetic analysis, the dating of platform interior ash beds, and the correlation of these dates to basinal deposits proximal to the Latemar platform. The decision to rely on these techniques to a greater degree than comparative sedimentology and/or statistical analyses of the cyclic succession is one that must be made in order to accept the millennial model.

CONCLUSIONS

This work has undertaken a new examination of the issue of allocyclicity in the origin of the Latemar platform cycles of the Middle Triassic of the Dolomites, northern Italy. This involved the measurement and analysis of a coeval cyclic platform carbonate formation external to the Latemar locality, 30 km to the northwest at Mendola Pass. The objective was to determine if the Mendola Pass succession contained a stratigraphic record comparable to the one found in the Latemar succession. Both successions have meter-scale cyclic bedding with a shallowing-upward depositional theme, with each cycle exhibiting subtidal (<10 m water depth) to supratidal successions of subfacies. Biostratigraphic ties were established between the two successions; statistical correlation analysis of measured cycle thickness series from the two localities allowed for stratigraphic placement of the shorter Mendola Pass section within the Latemar succession. Harmonic analysis identified the full suite of stacking pattern frequencies in both

sections, and cross-correlation analysis confirmed a significant match between the cyclic signals of both localities.

These results have the following implications for high-frequency cyclostratigraphic forcing of the Latemar platform:

• The current state of knowledge regarding Holocene and Pleistocene composite eustasy, the formation of shallowing-upward cycles, and the rates at which these cycles and their component facies form indicate that carbonate allocycles in the modern form as the result of multi-millennial processes (*see* Table 1, Table 2). If the drivers and depositional rates that have been identified for these cycles can serve as a comparative model, it is then likely that the depositional cycles at Mendola Pass and the Latemar, as well as their conspicuous bundled stacking patterns, formed as the result of composite eustatic forcing.

• Resolving the issue of millennial forcing vs. composite Milankovitch forcing of depositional cycles by comparative sedimentology alone difficult because stacked carbonate allocycles millennial periodicities remain undiscovered in modern carbonate sedimentary settings. In addition, a purely sub-Milankovitchian cyclic driver that would act to form bundled carbonate megacycles remains undiscovered in modern settings.

• At the present time, eustatic oscillations involving Milankovitchian composite eustasy are still the most likely explanation for the record of cyclic stratigraphy observed at Mendola Pass and the Latemar- either in the form of pure Milankovitchian forcing (Goldhammer et al., 1987) or mixed Milankovitch-subMilankovitch forcing (Zühlke et al., 2003).

• If one accepts the conclusion that Latemar and Mendola allocycles and allocycle bundles were formed at millennial periodicities, one must accept one of the following conclusions:

a. That the controls on the sedimentary system, including amplitudes and periodicities of composite eustatic drivers and sustained, very high (0.7 m/kyr+) sedimentation rates in areas of rapid subsidence are unique to mid-Triassic carbonates systems or,
b. That drivers for Triassic cycles also operate in the Holocene and Pleistocene but do not generate carbonate depositional cycles.

ACKNOWLEDGEMENTS

I gratefully acknowledge Nereo Preto and Olga Piros for identification of dasycladacean algae collected from the Mendola cycles, and for sharing important references and ammonite finds relating to the Mendola's stratigraphic framework. R. M. Forkner was supported by The R.K. Goldhammer Mesozoic

Margins Consortium, ConocoPhillips, and The John A. and Katherine G. Jackson School of Geosciences

REFERENCES

Anderson, R.Y. and Kirkland, D.W., 1966, Intrrabasin varve correlation, Geological Society of America Bulletin, Vo. 77, pp. 241-256.

Avanzini, M., 2002. Tavola 26 III - Fondo, Note Illustrative. Provincia Autonoma di Trento, Servizio Geologico, pp., 159, Trento (Italy).

Bendat, J.S. and Piersol, A.G., 1986, Random Data, 2nd Edition, John Wiley and Sons, New York, 566 pp.

Black, M., 1933, The algal sediments of Andros Island, Bahamas, Royal Society of London Philosophical Transactions, series B, v. 122, p. 165-191.

Blendinger, W., 2004, Sea level changes versus hydrothermal diagenesis: Origin of Triassic carbonate platform cycles in the Dolomites, Italy, Sedimentary Geology, v. 169, pp. 21-28.

Blendinger, W., 2005a, Sea level changes versus hydrothermal diagenesis: Origin of Triassic carbonate platform cycles in the Dolomites, Italy: Reply, 178, 141-144.

Blendinger, W., 2005b, Sea level changes versus hydrothermal diagenesis: Origin of Triassic carbonate platform cycles in the Dolomites, Italy: Reply, 178, 151-153.

Bloom, A.L., Broecker, W.S., Chappell, J.M.A., Matthews, R.K., and Mesolella, K.J., 1974, Quaternary sea level fluctuations on a tectonic coast: Quaternary Research, v. 4, p. 185-205.

Bond, G., Kromer, B., Beer, J., Muscheler, R., Evans, M.N., Showers, W., Hoffman, S., Lotti-Bond, R., Hajdas, I., and Bonani, G., 2001, Persistent solar influence on North Atlantic climate during the Holocene: Science, v. 294, p. 2130-2136.

Bond, G., Showers, W., Cheseby, M., Lotti, R., Almasi, P., deMenocal, P., Priore, P., Cullen, H., Hajdas, I., and Bonani, G., 1997, A Pervasive millennial-scale cycle in North Atlantic Holocene and glacial climates: Science, v. 278, p. 1257-1266.

Bosellini, A., and Hardie, L.A., 1985, Facies e cicli della Dolomia Principale delle Alpi Venete. Memorie della Societa Geologica Italiana, Vol. 30, pp. 245-266.

Bosellini, A., 1991, Geology of the Dolomites: An introduction. Dolomieu Conference on carbonate platforms and dolomitization. Ortisei, 43 p.

Brack, P., and Rieber, H., 1993, Towards a better definition of the Anisian/Ladinian boundary: new biostratigraphic data and correlations of boundary sections from the Southern Alps, Eclogae Geologicae Helvetiae, Vol. 86, pp. 415-527.

Brack, P., Mundil, R., Oberli, F., Meier, M., and Reiber, H., 1996, Biostratigraphic and radiometric age data question the Milankovitch characteristics of the Latemar cycles (Southern Alps, Italy), Geology Boulder, v. 24, is. 4, p. 371-375.

Brack, P., and Muttoni, G., 2000, High-resolution magnetostratigraphic and lithostratigraphic correlations in Middle-Triassic pelagic carbonates from the Dolomites (Southern Alps, Italy). Palaeogeography, Paleaoclimatology, and Palaeoceanography, vol. 161, pp. 361-380.

Broecker, W.S., Thurber, D.L., Goddard, J., Ku, T., Matthews, R.K., Mesolella, K.J., 1968, Milankovitch hypothesis supported by precise dating of coral reefs and deep sea sediments: Science, v. 159, no. 3812, p. 297-300.

Carter, G.C., Knapp, C.H., Nuttall, A.H., 1973. Estimation of the magnitude-squared coherence function via overlapped fast Fourier transform processing. IEEE Transactions, Audio and Electroacoustics 21, p. 337-344.

Carulli, G.B.; Cozzi, A.; Salvador, G.L,; Ponton, M.; and Podda, F., 1998, Evidence of synsedimentary tectonic activity during the Norian-Lias (Carnian Prealps, Northern Italy). Memorie della Societa Geologica Italiana, Vol. 53, pp. 403-415.

Chappell, J., 2002, Sea level changes forced ice breakouts in the Last Glacial cycle: New results from coral terraces, Quaternary Science Reviews, Vol. 21, pp. 1229-1240.

Chappell, J. and Shackleton, N.J., 1986, Oxygen isotopes and sea level. Nature, 324, 137-140

Cozzi, A., 2000, Synsedimentary tensional features in the Upper Triassic shallow-water platform carbonates of the Carnian Prealps (northern Italy) and their importance as paleostress indicators. Basin Research, Vol. 12, pp. 133-146.

Cozzi, A., 2002, Facies Patterns of a Tectonically-Controlled Upper Triassic Platform-Slope Carbonate Depositional System (Carnian Prealpls, Northeastern Italy). Facies, Vol. 47, pp. 151-178.

Cozzi, A., Hinnov, L.A., and Hardie, L.A., 2005, Orbitally forced Lofer cycles in the Dachstein Limestone of the Julian Alps (NE Italy), Geology, 33, p. 789-792.

Davies, G.R., 1970, Algal laminated sediments, Gladstone embayment, Shark Bay, Western Australia. American Association of Petroleum Geologists Memoir 13, p. 169-205.

Dean, W.E., and Anderson, R.Y., 1974, Application of some correlation coefficient techniques to time-series analysis, Mathematical Geology, Vol. 6, pp. 59-75.

Demicco R.V., and Hardie, L.A., 1994, Sedimentary structures and early diagenetic features of shallow marine carbonate deposits, SEPM Atlas Series No. 1, 265 p.

Doglioni C., 1988, Examples of strike-slip tectonics on platform-basin margins: Tectonophysics, v. 156, p. 293-302.

Doglioni C., 1987, Tectonics of the Dolomites (Southern Alps, Northern Italy): Journal of Structural Geology, v. 9, no. 2, p.181-193.

Dunn, P.A., 1991, Cyclic stratigraphy and early diagenesis: an example from the Triassic Latemar platform, northern Italy: unpublished Ph.D. dissertation, Johns Hopkins University, Baltimore, Maryland, 836 pp.

Egenhoff, S.O., Peterhänsel, A., Bechstädt, T., Zühlke, R., and Grötsch, J., 1999, Facies architecture of an isolated carbonate platform: tracing the cycles of the Latemar (Middle Triassic, northern Italy), Sedimentology, v. 46, pp. 893-912.

Emmerich, A., Glasmacher, U.A., Bauer, F., Bechstädt, T., and Zühlke, R., 2005, Meso-/Cenozoic basin and carbonate platform development in the SW-Dolomites unraveled by basin modeling and apatite FT analysis: Rosengarten and Latemar (Northern Italy): Sedimentary Geology, v. 175, is. 1-4, p.415-438.

Enos, P., and Perkins, R.D., 1979, Evolution of Florida Bay from island stratigraphy. Geological Society of America Bulletin, Vol. 90, pp. 59-83.

Evamy, B.D., 1973. The precipitation of aragonite and its alteration to calcite on the Trucial Coast of the Persian Gulf *in* Purser, B.M., ed., The Persian Gulf. Berlin, Springer-Verlag, p. 329-342.

Fischer, A.G., 1964, The Lofer Cyclothems of the Alpine Triassic. Kansas Geological Society Bulletin, Vol. 169, pp.107-149.

Forkner, R.M., Hinnov., L.A., Goldhammer., R.K., and Hardie, L.A., 2007 On the allocyclic interpretation of the 'Latemar cycles' (M. Triassic, The Dolomites, Italy) and implications for high-frequency cyclostratigraphic forcing. *Accepted for Publication,* GSA Special Publication in Honor of the Career of R.N. Ginsburg.

Gaetani, M., Fois, E., Jadoul, F. and Nicora, A., 1981, Nature and evolution of Middle Triassic carbonate buildups in the Dolomites (Italy), Vol. 44, p. 25-57.

Ginsburg, R.N., 1971, Landward movement of carbonate mud: new model for regressive cycles in carbonates [abs.], American Association of Petroleum Geologists Bulletin, v. 55, p. 340.

Ginsburg, R.N., Hardie, L.A., Bricker, O.P., Garrett, P., Wanless, H.R., 1977, Exposure Index: A quantitative approach to defining position within the tidal zone. In: Hardie, L.A., ed., Sedimentation on the Modern Carbonate Tidal Flats of Northwest Andros Island, Bahamas. The Johns Hopkins University Studies n Geology, No. 22. pp. 7-11.

Goldhammer, R.K., Dunn, P.A., and Hardie, L.A., 1987, High-frequency glacio-eustatic sea level oscillations with Milankovitch characteristics recorded in Middle Triassic platform carbonates in Northern Italy, American Journal of Science, v. 287, pp. 853-892.

Goldhammer, R.K., Dunn, P.A., and Hardie, L.A., 1990, Depositional cycles, composite sea level changes, cycle stacking patterns, and the hierarchy of stratigraphic forcing: Examples from the Alpine Triassic platform carbonates, Geological Society of America Bulletin, v. 102 pp. 535-562.

Goldhammer, R.K., and Harris, M.T., 1989, Eustatic controls on the stratigraphy and geometry of the Latemar buildup (Middle Triassic), the Dolomites of northern Italy, SEPM Special Publication 44, pp. 232-338.

Goldhammer, R.K., and Kaufman, J., 1995, Astronomical climatic cycles, Pleistocene glacio-eustasy, and the origin of Pleistocene platform cycles in Florida: Exxon Production Research Company Advanced Carbonates Field Report

Haas, J. 1994, Lofer cycles of the Upper Triassic Dachstein platform in the Transdanubian mid-Mountains, Hungary, in De Boer, P.I. and Smith, D.L., eds., Orbital Forcing and Cyclic Sequences, IAS Special Publication 19, p. 303-322.

Haas, J., 2004, Characteristics of peritidal facies and evidences for subaerial exposures in Dachstein-type cyclic platform carbonates in the Transdanubian Range, Hungary, Facies, 50, p. 263-286.

Handford, C.R., Kendall, A.C., Prezbindowski, D.R., Dunham, J.B., and Logan, B.W., 1984, Salina-margin tepees, pisoliths, and aragonite cements, Lake MacLeod, Western Australia; Their significance in interpreting ancient analogs, Geology, v. 12, p. 523-527.

Hardie, L.A., and Ginsburg., R.N., 1977, Layering: The origin and environmental significance of lamination and thin bedding. In Hardie, L.A., ed., Sedimentation on the Modern Carbonate Tidal Flats of Northwest Andros Island, Bahamas. The Johns Hopkins University Studies in Geology, No. 22. pp. 50-123.

Hardie, L.A., Bosellini, A., and Goldhammer, R.K., 1986, Repeated subaerial exposure of subtidal carbonate platforms, Triassic, northern Italy: evidence for high-frequency sea level oscillations on a 10^4 year scale, Paleoceanography, v. 1, p. 447-457.

Harris, M.T., 1996, The carbonate factory of the Middle Triassic buildups in the Dolomites, Italy: A quantitative analysis – Comment, Sedimentology, v. 43, 401-402.

Hinnov, L.A., 2000, New perspectives on orbitally forced stratigraphy. Annual Review of Earth and Planetary Sciences, v. 28, pp. 419-475.

Hinnov, L.A., 2006, Discussion of "Magnetostratigraphic confirmation of a much faster tempo for sea level change for the Middle Triassic Latemar platform carbonates' by D.V. Kent, G. Muttoni, and P. Brack [Earth Planet. Sci. Lett. 228 (2004), 369-377], Earth and Planetary Science Letters, v. 243, p. 841-846.

Hinnov, L.A. and Goldhammer, R.K., 1991, Spectral analysis of the Middle Triassic Latemar Limestone, Journal of Sedimentary Petrology, vol. 61, pp. 1173-1193.

Hinnov, L.A., Cozzi, A., and Bazykin, D.A., 1997, The Milankovitch origin of the Middle Triassic Latemar platform cycles: a review of the sedimentologic criteria and results of a new evolutive spectral analysis of the entire Latemar succession, IAS Regional Meeting Abstracts, Gaia Heidelbergensis, 3, pp. 164-165.

Holland, S.M., Meyer, D.L., and Miller, A.I. (2000), High-resolution correlation in apparently monotonous rocks: Upper Ordovician Kope Formation, Cincinnati Arch, Palaios, Vol. 15, p. 73-80.

Jacobs, D.K., and Sahagian, D.L., 1993, Climate-induced fluctuations in sea level during non-glacial times, Nature, vol. 361, p. 710-712.

Jadoul, F.; Berra, F.; and Frisia, S., 1992, Stratigraphic and paleogeographic evolution of a carbonate platform in an extensional tectonic regime: the example of the Dolomia Principale in Lombardy (Italy). Rivista Italiana Paleontolgia e Stratigrafia, Vol. 98, No.1, pp. 29-44.

James, N.P., 1972, Holocene and Pleistocene calcareous crust (caliche) profiles: criteria for subareal exposure, Journal of Sedimentary Petrology, v. 48. p. 817-836.

Kent, D.V., Muttoni, G., and Brack, P., 2004, Magnetostratigraphic conformation of a much faster tempo for sea level change for the Middle Triassic Latemar platform carbonates, Earth and Planetary Science Letters, 228. p. 369-377.

Klebelsberg R., von., 1935, Geologie von Tirol. Borntraeger, Berlin, 872 pp.

Laubscher, H., and Bernoulli, D., 1978, Mediterranean and Tethys, *in* Nainn, A.E.M., Kanes, W.H., and Stehli, F.G., (eds.), The ocean basins and margins, 4A: New York, Plenum Press, p. 1-28.

Logan, B.W., Read, J.F., and Davies, G.R., 1969, History of carbonate sedimentation, Quaternary epoch, Shark Bay, Western Australia: *in* American Association of Petroleum Geologists – Memoir 13, p. 38-84.

Lucia, F.J., 1968, Recent sediments and diagenesis of Bonaire, Netherlands Antilles. Journal of Geology, v. 78, p. 352-362.

Manfrin S., Mietto P., and Preto N., 2005, Ammonoid biostratigraphy of the Middle Triassic Latemar platform (Dolomites, Italy) and its correlation with Nevada and Canada. Geobios, v. 38, is. 4, p. 477-504.

Maurer, F., Hinnov, L.A., and Schlager, W., 2004, Statistical time-series analysis and sedimentological tuning of bedded rhythms in a Triassic basinal succession (Southern Alps, Italy): SEPM Special Publication no. 81, p. 83-99.

Mundil, R., T., Brack, P., Meier, M., Reiber, H., and Oberli, F., 1996, High resolution U-Pb dating of Middle Triassic volcaniclastics; time-scale calibration and verification of tuning parameters for carbonate Sedimentation, Earth and Planetary Science Letters, v. 141, is. 1-4, p. 137-151.

Mundil, R., Zühlke, R., Bechstadt, T., Brack, P., Egenhoff, S., Meier, M., Oberli, F., Peterhänsel, A., and Rieber, H., 2003, Cyclicities in Triassic Platform Carbonates: synchronizing radio-isotopic and orbital clock: Terra Nova, v. 15/2, p. 81-87.

Munk, W., Dzieciuch, M., and Jayne, S., 2002, Millennial climate variability: Is there a tidal connection? Journal of Climate, v. 15. p.370-385.

Niggemann, S., Mangini, A., Mudelsee, M., Richter, D.K., and Wuth, G., 2003, Sub-Milankovitch climatic cycles in Holocene stalagmites from Sauerland, Germany, Earth and Planetary Science Letters, v. 216, is. 4, p. 539-547.

Ogilvie Gordon, M.M., 1927, Das Groedener- Fassa- und Enneberggebiet in den Suedtiroler Dolomiten. I und II Teil, pp. 376, III Teil, pp. 89, Geol. Bundesanstalt, Wien

Parkinson, R.W., 1989, Decelerating Holocene sea level rise and its influence on southwest Florida coastal evolution: A transgressive/regressive stratigraphy: Journal of Sedimentary Petrology, v. 59, no. 6, p. 960-972.

Peterhänsel, A. and Egenhoff, S.O., 2005, Sea level changes versus hydrothermal diagenesis: Origin of Triassic carbonate platorm cycles in the Dolomites, Italy: Discussion, Sedimentary Geology, 178, p. 145-149.

Piros O., Preto N., 2003, A tentative correlation of dasycladacean biozones with ammonoid standard zones in the Anisian-Ladinian Latemar succession, Italy. Triassic Geochronology and Cyclostratigraphy field symposium, September 11-13, 2003, St. Christina, Italy

Preto, N., Hinnov, L.A., Hardie, L.A., and De Zanche, V., 2001, Middle Triassic orbital signature recorded in the shallow-marine Latemar carbonate buildup (Dolomites, Italy), Geology, v. 29 no. 12, p. 1123-1126.

Preto, N., and Hinnov, L.A., (2003), Unravelling the origin of carbonate platform cyclothems in the Upper Triassic Dürrenstein Fm. (Dolomites, Italy), Journal of Sedimentary Research, 73(5), p. 774-789.

Preto, N., Hinnov, L.A., De Zanche, V., Mietto P., and Hardie, L.A.., 2004, The Milankovitch interpretation of the Latemar platform cycles (Dolomites, Italy): implications for geochronology, biostratigraphy, and middle Triassic carbonate accumulation, SEPM Special Publication No. 81, pp. 167-182.

Preto, N., Hinnov, L.A., Hardie, L.A., and Harris M.T. (2005), Sea level changes versus hydrothermal diagenesis: origin of Triassic carbonate platform cycles in the Dolomites, Italy - Discussion, Sedimentary Geology, 178, p. 135-139.

Prosser, G., and Selli, L., 1991, Thrusts of the Mezzocorona-Mendola Pass area (Southern Alps, Italy): Structural analysis and kinematic reconstruction: Bolletino della Societa Geologica Italiana, v. 110, p. 805-821.

Read, J.F. and Sriram, S., 1990, A computer program for generation of Fischer plots: Compass, 66, 73-78.

Read, J.F.,1995, Overview of carbonate platform sequences, cycle stratigraphy and reservoirs in greenhouse and icehouse worlds: in Read, J.F., Kerans, C., Weber, L.J., Sarg, J.F., and Wright F.W., Milankovitch sea level changes, cycles and reservoirs on carbonate platforms in greenhouse and icehouse worlds, SEPM Short Course Notes No. 35, 1-102.

Richthofen F. vonc., 1874, Ueber Mendola- und Schlern Dolomite. Zeitschr. Deutsch. Geol. Gesell., Berlin, 26, p. 225-256

Robbin, D.M., and J.J. Stipp, J.J., 1974, Depositional rate of laminated soilstone crusts, Florida Keys, Journal of Sedimentary Petrology, v. 49. p. 175-180.

Roth, S., and Reijmer, J.J.G., 2005, Holocene millennial to centennial carbonate cyclicity recorded in slope sediments of the Great Bahama Bank and its climatic implications, Sedimentology, v. 52, is. 1, p. 161-181.

Schlager, W., 1981, The paradox of drowned reefs and carbonate platforms, Geological Society of America Bulletin, vol. 92, p. 197-211.

Schwarzacher, W., 1975, Sedimentation Models and Quantitative Stratigraphy: New York, Elsevier, 382 p.

Schwarzacher, W., 1993, Cyclostratigraphy and the Milankovitch theory, Developments in Sedimentology, v. 52, 225 p.

Schwarzacher, W., 1998, Bed thickness measurements and the cyclostratigraphy of the Latemar Limestone, 15th International Sedimentological Congress of the IAS, 12-17 April, Alicante, Spain, p. 707.

Schwarzacher, W., 2005, The stratification and cyclicity of the Dachstein Limestone in Lofer, Leogang and Steinernes Meer (Northern Calcareous Alps, Austria), Sedimentary Geology, v. 181, is. 1-2, p. 93-106

Shinn, E.A., 1986, Modern carbonate tidal flats: their diagnostic features., in Hardie, L.A., and Shinn, E.A., Carbonate Depositional Environments, Modern and Ancient, Colorado School of Mines Quarterly, Vol. 81, No. 1, pp. 7-33.

Strasser, A., Hillgärtner, H., Hug, W., and Pittet, B., 2000, Third-order depositional sequences reflecting Milankovitch cyclicity. Terra Nova, Vol. 12, p. 303-311.

Strasser, A., and Samankassou, E., 2003, Carbonate sedimentation rates today and in the past: Holocene of Florida Bay, Bahamas, and Bermuda vs. Upper Jurassic and Lower Cretaceous of the Jura Mountains (Switzerland and France): Geologica Croatica, v. 56, no. 1, p. 1-18.

Taft, W.H., 1968, Lithification of modern marine carbonate sediments at Yellow Bank, Bahamas, Bulletin of Marine Science, v. 18, is. 4, p.762-828

Taylor, J.K., 1990, Statistical Techniques for Data Analysis, Lewis Publishers, Inc., Chelsea, Michigan, 200 p.

Thompson, D.J., 1982, Spectrum estimation and harmonic analysis, IEEE Proceedings, v. 70, p. 1055-1096.

Thomson, D.J., and Chave, A.S., 1991, Chapter 2: Jackknifed error estimates for spectra, coherences and transfer function, in, Haykin, S.S., ed., Advances in Spectrum Analysis and Array Processing, Prentice-Hall, New York, p. 58-113.

Thompson, W.G., and Goldstein, S.L., 2005, Open-system coral ages reveal persistent suborbital sea level changes, Science, Vol. 308, pp. 401-404.

Tudhope, A.W., 1989, Shallowing-upwards sedimentation in a coral reef lagoon, Great Barrier Reef of Australia: Journal of Sedimentary Petrology, v. 59, no. 6, p. 1036-1051.

Vail, P.R., Mitchum jr., R.M., Thompson III, S., 1977, Seismic stratigraphy and global changes of sea level, part 4: Global cycles of relative changes of sea level: *in* Payton, C.E., ed., Seismic Stratigraphy – Applications to Hydrocarbon Exploration: American Association of Petroleum Geologists Memoir 36, p.83-97.

Van de Plassche, O., van der Borg, K., and de Jong, A.F.M., 1998, Sea level-climate correlation during the past 1400 yr: Geology, v. 26, no. 4, p. 319-322.

Van Hilten D., 1960, Geology and Permian paleomagnetism of the Val di Non area. Geologica Ultraiectina, 5, p. 1-95, Utrecht

Venzo, G.A., and Fuganti, A., 1965, Il Trias della Mendola (Trentino – Alto Adige): Studi Trentini di Scienze Naturali, Sez. A, Vol. XLII, N. 1, p. 55-86.

Wright, V.P., 1992, Speculations on the controls on cyclic peritidal carbonates: Ice-house versus greenhouse eustatic controls. Sedimentary Geology, v. 76, p. 1-5.

Yang, W., and Lehrmann, D., 2003, Milankovitch climatic signals in Lower Triassic (Olenekian) peritidal carbonate successions, Nanpanjiang Basin, South China, Palaeogeography, Palaeoclimatology, Palaeoecology, v. 201, is. 3-4, p. 283-306.

Zühlke, R., Bechstädt, T., and Mundil, R., 2003, Sub-Milankovitch and Milankovitch forcing on a model Mesozoic carbonate platform – the Latemar (Middle Triassic, Italy), Terra Nova, v. 15, no. 2, 69-80.

Zühlke, R, 2004, Integrated cyclostratigraphy of a model Mesozoic carbonate platform - the Latemar (Middle Triassic, Italy). in D´Argenio, B., Fischer, A., Premoli Silva, I. and Weissert, H., eds., Multidisciplinary Approach to Cyclostratigraphy, Society for Sedimentary Geology, Special Publication, v. 81, p.183-212..

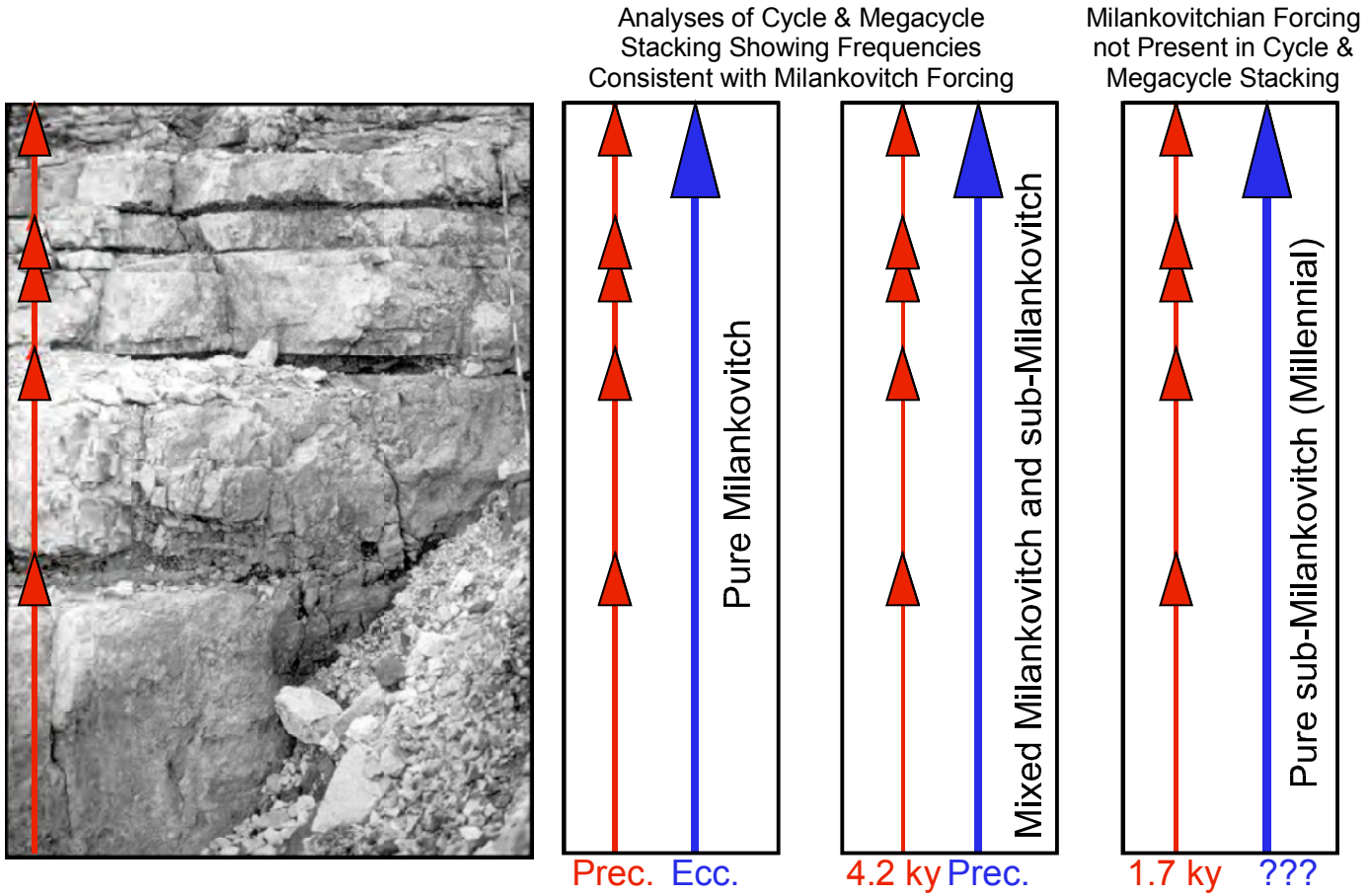

Figure 2.1. Comparison of proposed cyclic driver periodicities for individual cycles and megacycles at the Latemar. Both “Pure Milankovitch” (e.g., Goldhammer et al., 1987; Preto et al., 2004) and “Mixed Milankovitch and sub-Milankovitch” (e.g., Zühlke, 2004) interpret Milankovitchian composite eustasy to have influenced the development of Latemar cycle stacking. The millennial model does not recognize the influence of Milankovitchian forcing on the development of cycles or megacycles at the Latemar. (Note: “Prec” refers to the Precession, and “Ecc.” refers to the Eccentricity.)

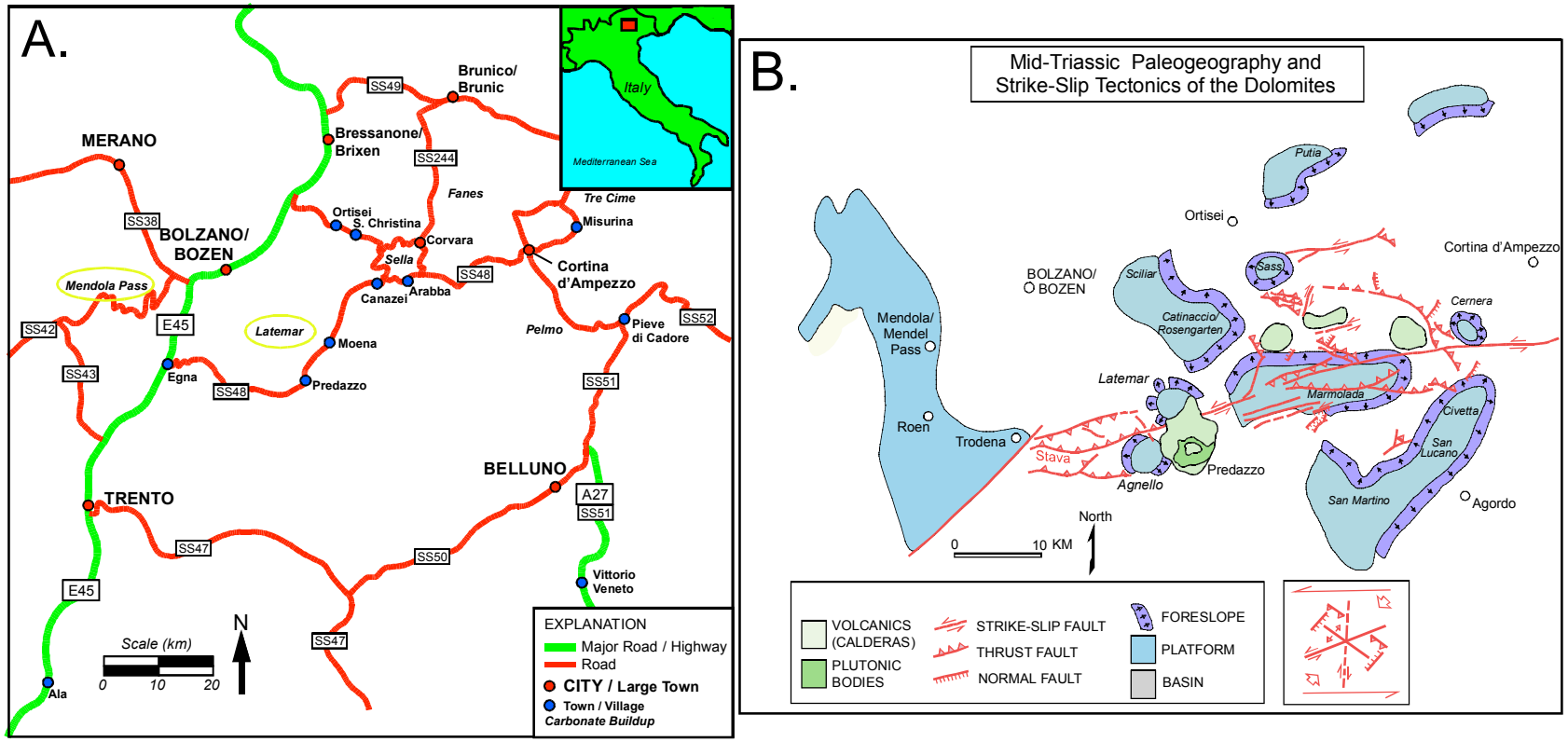

Figure 2.2. A. Location and road map for Dolomites region showing the locations of both the Latemar platform and Mendola Pass. B. Paleogeography of mid-Triassic carbonate platforms in the Dolomites.

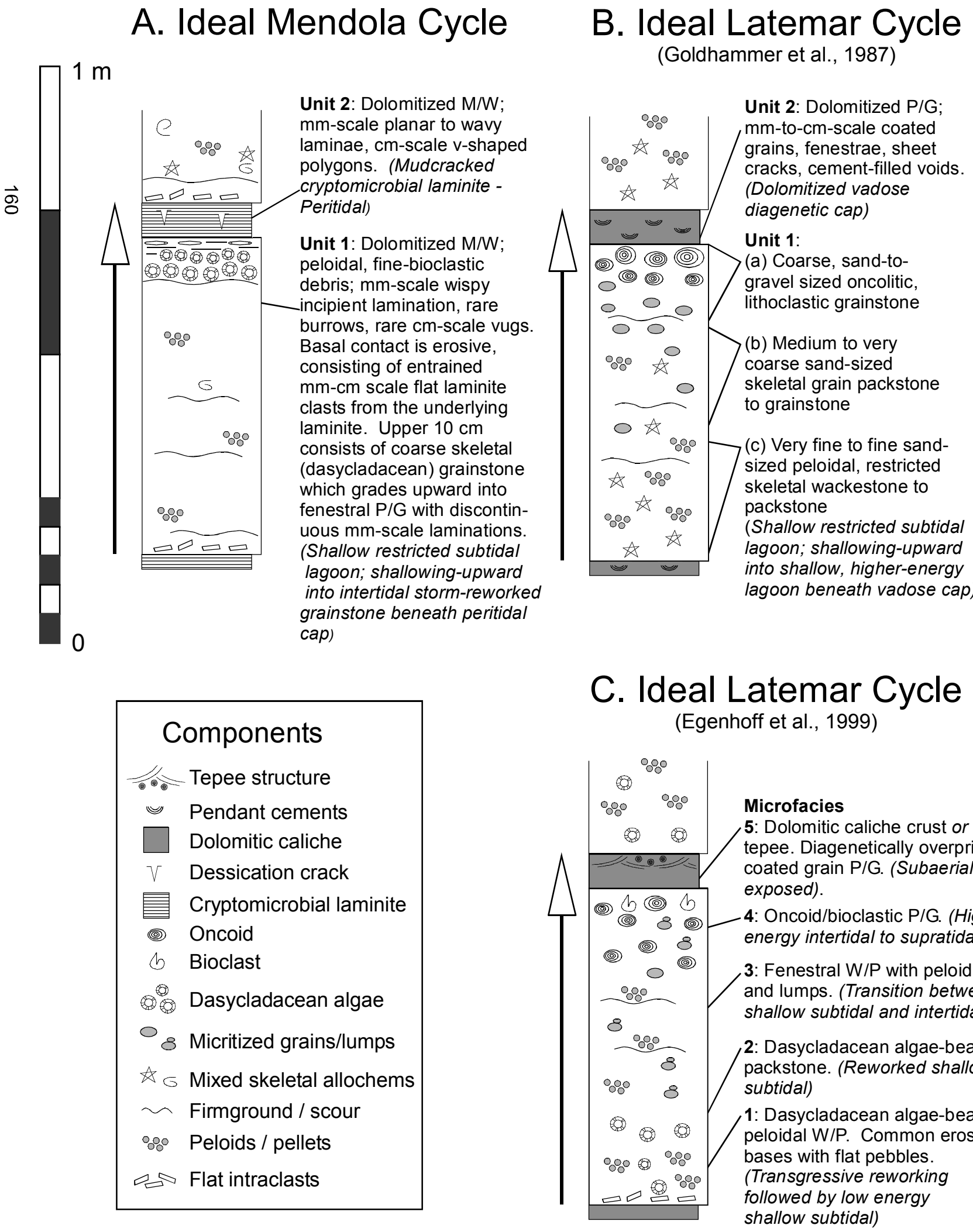

Figure 2.3. Comparison of ideal shallowing-upward cycles as observed at A. Mendola Pass (this study) and at the Latemar buildup by both B. Goldhammer et al. (1987) and C. Egenhoff et al. (1999). Latemar cycles are grain-dominated successions with diagenetic caps while Mendola cycles are muddy with laminite caps.

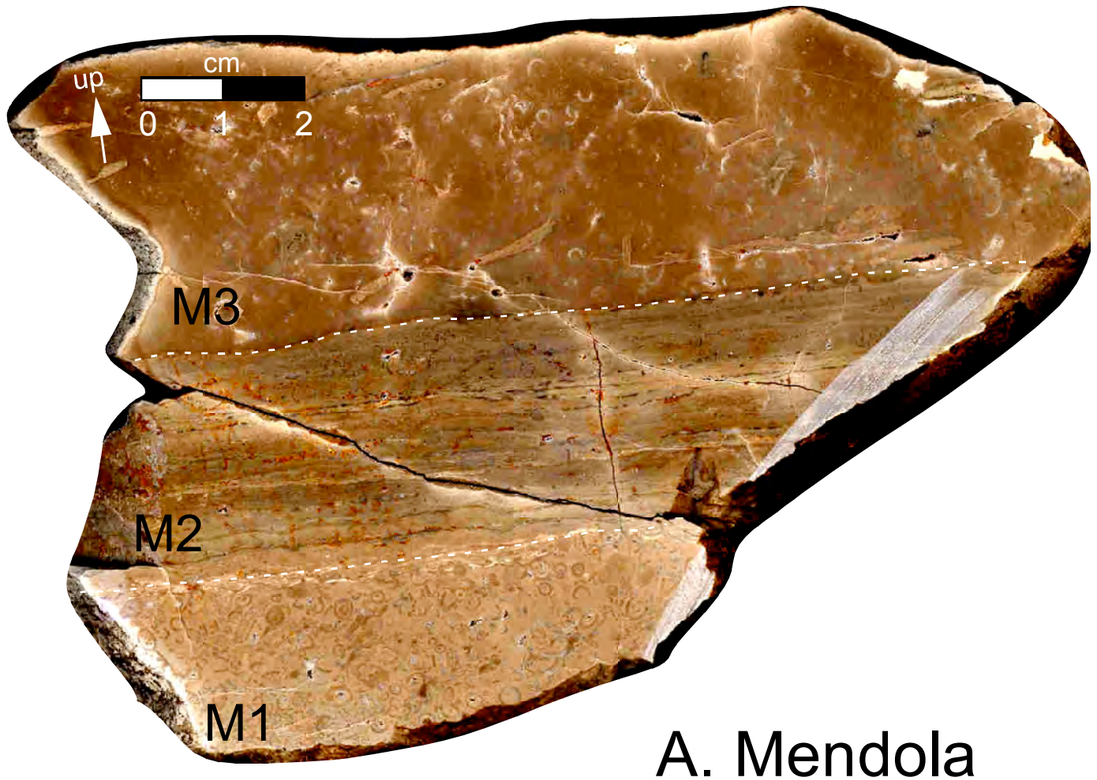

A. Mendola

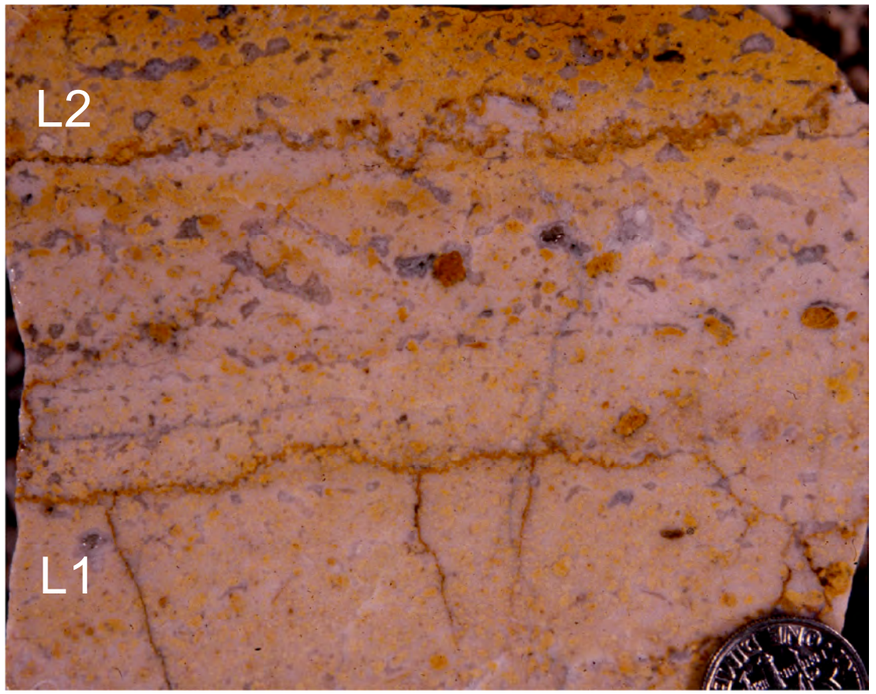

B. Latemar

Figure 2.4. Polished hand specimens of cycle tops from A. Mendola Pass and B. the Latemar. A. Mendola subfacies include: M1, dasycladacean algal packstone; M2, cryptomicrobial laminite cap; and M3, mixed skeletal / intraclastic peloidal wackestone.Note flat clasts ripped up from M2 laminite. B. Latemar subfacies include: L1, fenestral oncolitic / coated grain packstone / grainstone, and L2, dolomitic exposure cap (diagenetically overprinted L1). Direct diagenetic overprinting of L1 subfacies indicates sea level drop, or “Waltherian skip” between regularly submerged facies and subaerial exposure. Mendola facies succession displays a comparably more Waltherian succession from shallow subtidal / intertidal (M1) to intertidal / supratidal facies (M2).

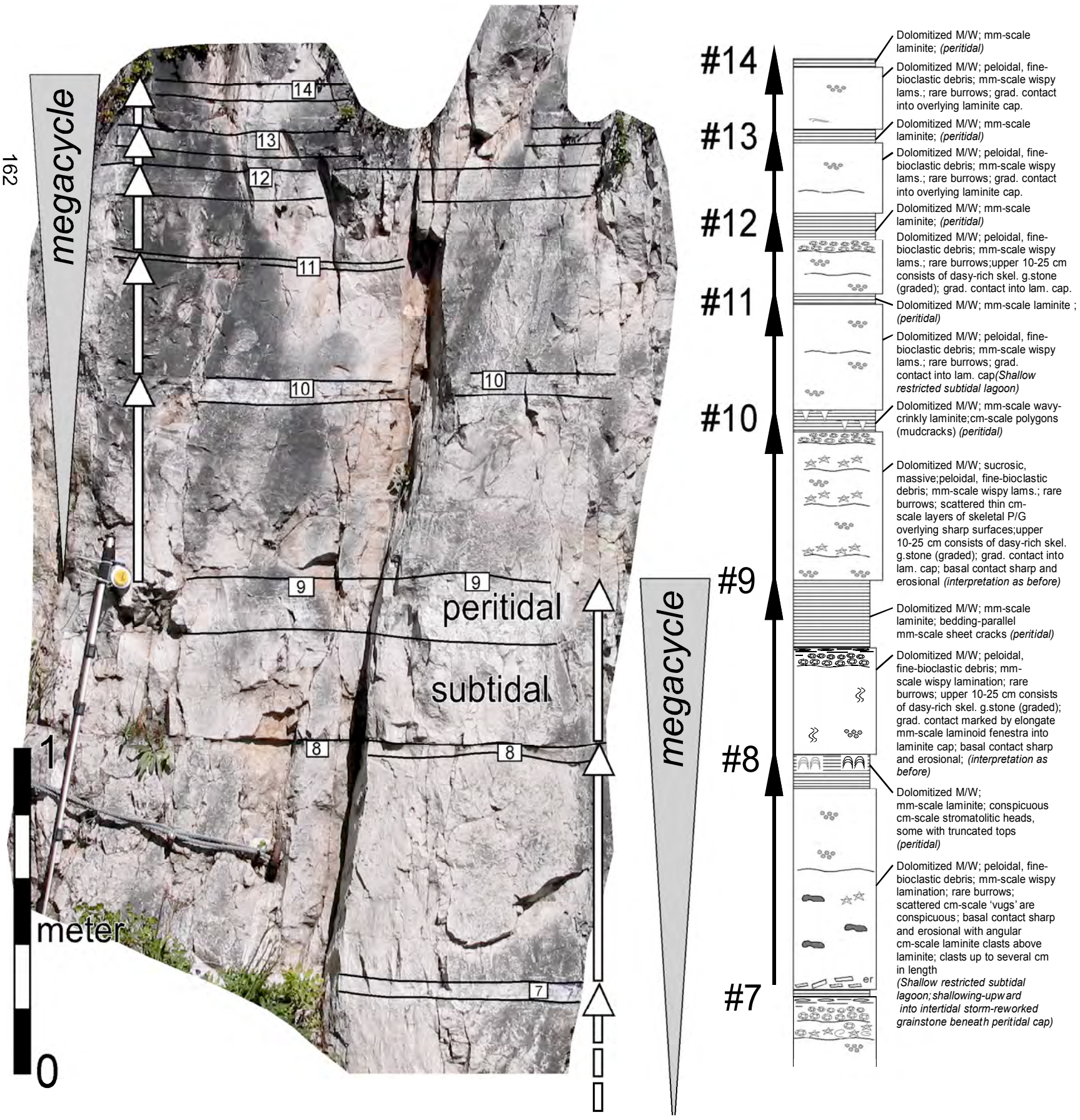

Figure 2.5. Photograph of Mendola road cut section showing cycles 7-14, as well as facies descriptions and megacycle bundling interpretation. Cycles are meter-scale, dolomitized, laminite-capped peritidal deposits likely formed in environments similar to modern carbonate tidal flats. In this example, two megacycles are shown, a 3:1 megacycle (cycles 7-9) and a 5:1 megacycle (cycles 10-14).

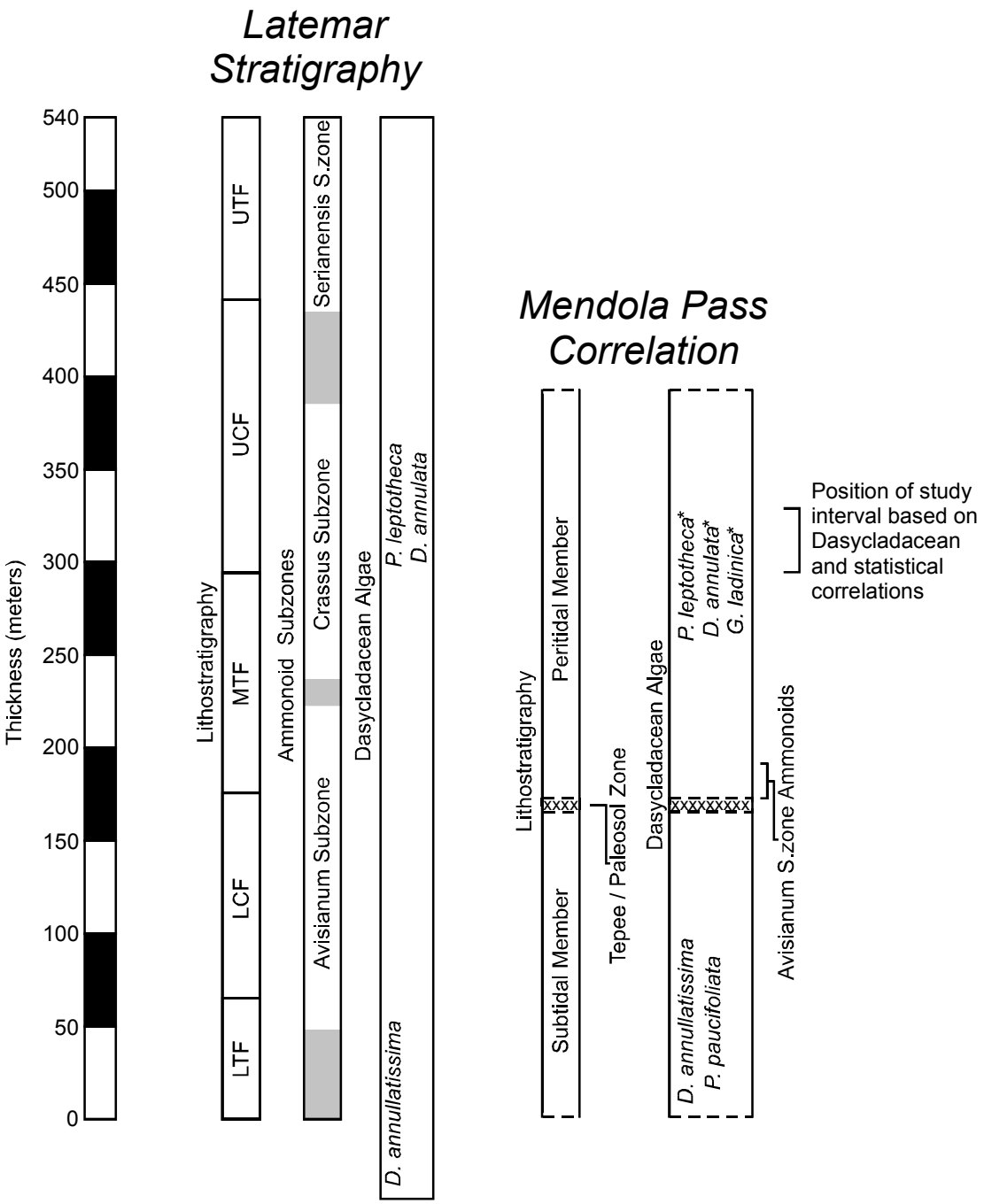

Figure 2.6. Stratigraphic column of the Latemar platform modified from Egenhoff et al. (1999), Preto et al. (2001) and Manfrin et al. (2005) on the left and proposed correlative stratigraphic chart from Mendola pass to the right. Dasycladacean algae from the Latemar are reported in Gaetani et al. (1981). LTF: Lower Tepee Facies; LCF: Lower Cyclic Facies; MTF: Middle Tepee Facies; UCF: Upper Cyclic Facies; UTF: Upper Tepee Facies. Dasycladacean algae and lithostratigraphy from Mendola Pass are reported in Ogilvie Gordon (1927) and Avanzini (2002). Dasycladacean algae marked with an asterisk were identified in this study. Approximate location of study interval based on Dasycladacean biostratigraphy and statistical correlation to the Latemar platform cycles.

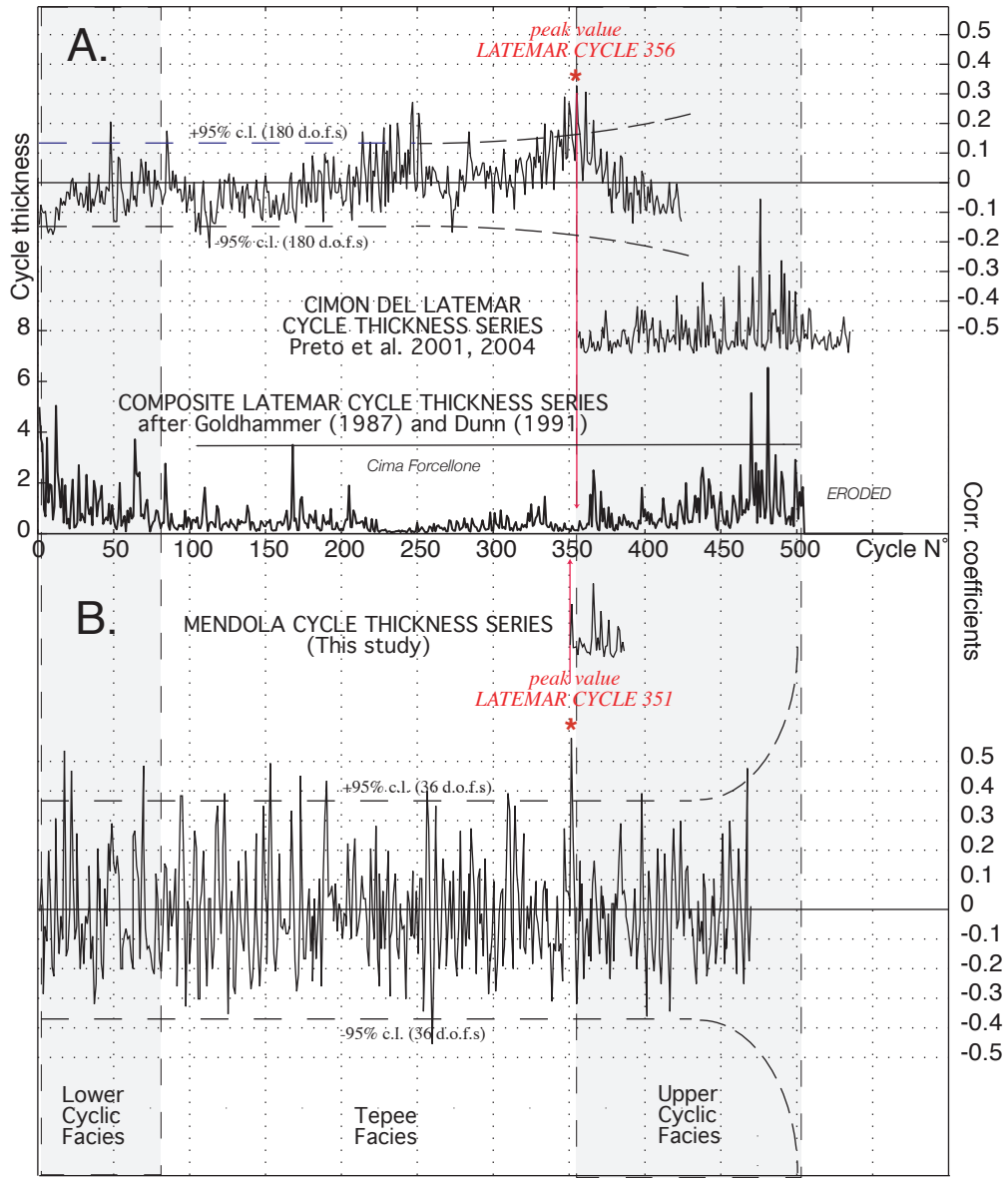

Figure 2.7. Figure from Forkner et al. (2007), constructed by L. Hinnov. Running cross-correlation analysis of cycle thickness series within the Latemar platform (CDL section and Goldhammer/Dunn section), and between Mendola Pass section and the Goldhammer/Dunn Latemar section. The 95% confidence limits were estimated by interpolating the "95% Confidence Belt" of Taylor (1990, p. 139) to sample sizes (i.e. degrees of freedom) of 180 (for CDL/Goldhammer Latemar correlation) and 36 (for Mendola-Latemar correlation). A. Pearson correlation coefficients obtained by progressively shifting the Cimon del Latemar (CDL) cycle thickness series of Preto et al. (2001, 2004) relative to the cycle thickness series at Cima Forcellone of Goldhammer (1987), with 57 additional cycle measurements within the Tepee Facies from Dunn (1991). A singular peak correlation occurs between the CDL series and Cima Forcellone Cycles 356 to 504. B. Correlation coefficients obtained by progressively shifting the Mendola Pass cycle thickness series (this study) against the Cima Forcellone cycle thickness series. Peak correlation occurs at a unique interval of 36 cycles in the Cima Forcellone series, cycles 351 to 386, which corresponds to the lowermost 30 cycles of the CDL series. In both A and B the 95% confidence limits widen at the top of the section as the shifting shorter series (CDL or Mendola) rolls off the upper end of the longer (Cima Forcellone) series, resulting in ever-decreasing degrees of freedom in the calculated coefficients.

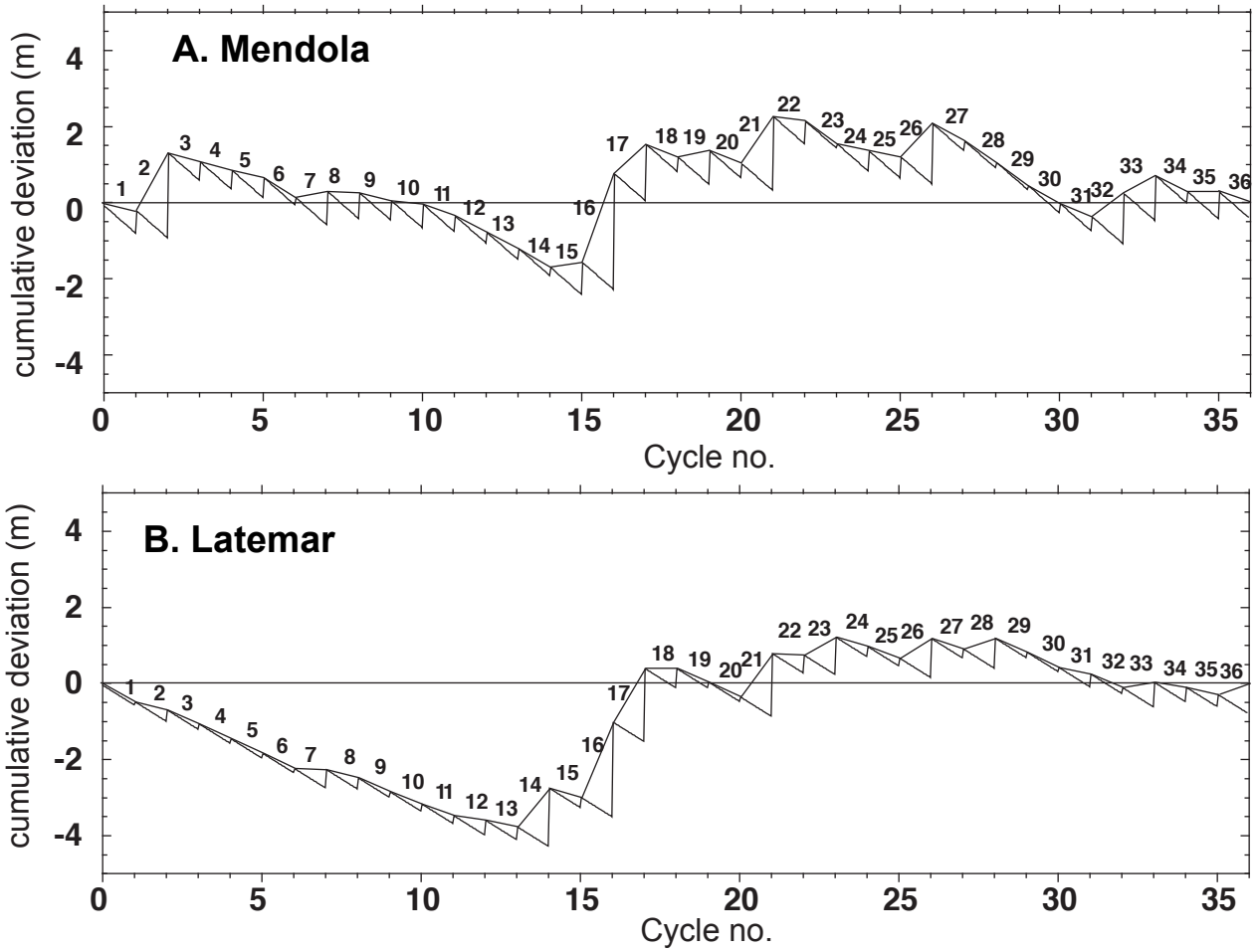

Figure 2.8. Accommodation (Fischer) plots for A. the Mendola Pass cycle thickness series (Cycles 1-36) and B. the correlative Latemar cycle thickness series (Cycles 351-386 from the Cima Forcellone section). Note the striking similarity in accommodation trends over the length of the thickness series.

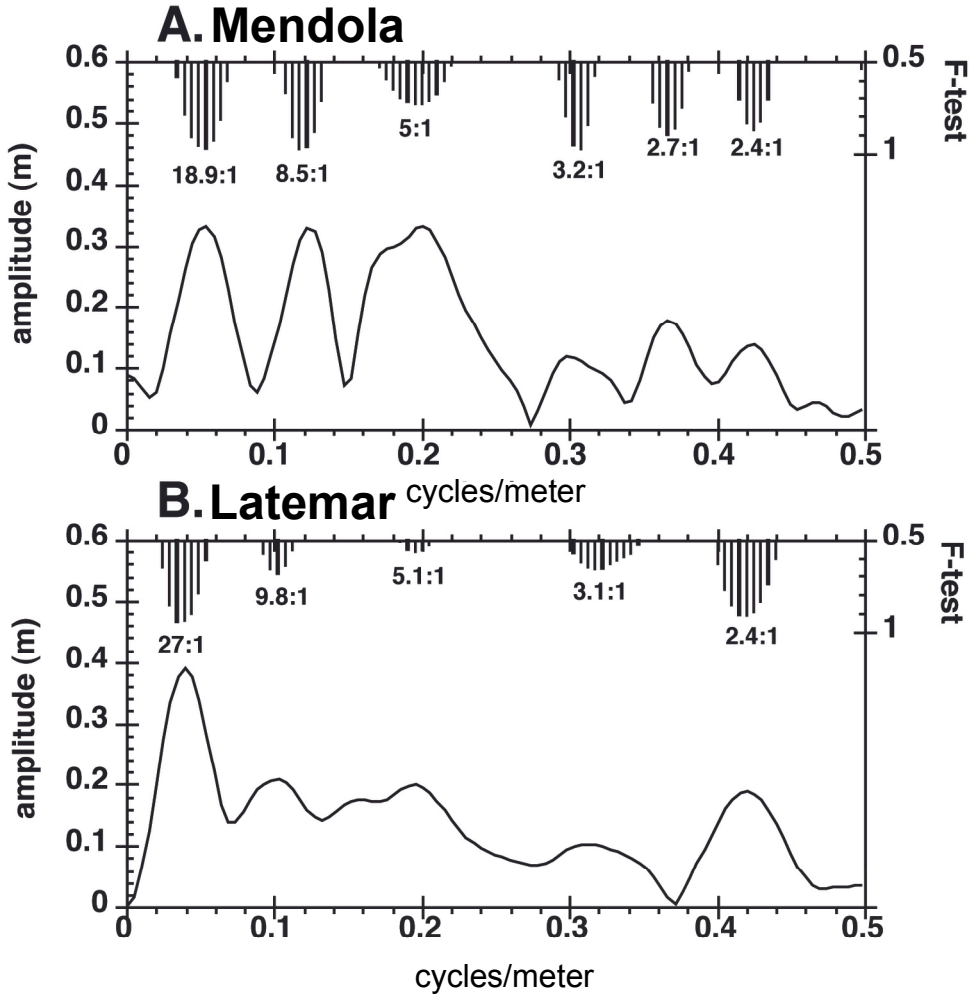

Figure 2.9. MTM spectral analysis of the Mendola and Latemar cycle thickness series (adapted from Forkner et al., 2006, fig. 8, by Hinnov). Plots are of A. the Mendola series and B. Latemar series. For both A and B, the black curves are the amplitude spectra, and refer to the y-axis to the left. The bars descending from the top are F-test (confidence) results for the amplitude spectra, reported as a percentage (50% to 100%), on the y-axis on the top right. Numbers below confidence plots

Study	Cycle Type	Cycle Period
Roth and Reijmer, 2005	Oxygen isotope excursions in a 30 m-long core from the leeward margin of the Great Bahama Bank related to aragonite content	Multi-millennial
		1.725 kyr
		0.54 kyr
Niggemann et al., 2003	Oxygen isotope excursions in 61-cm stalagmite	ca. 1.450 kyr
Bond et al., 1993, 1997, 2001	Oxygen isotope excursions & Ice-rafted sediment cycles	1.5 kyr DO Cycle 5-6 kyr Bond Cycle
Munk et al., 2001	Tidal forcing - Millennial Scale	1.795 kyr
van de Plassche et al., 1998	Mean high water marks from Hammock River marsh, Clinton, Connecticut, USA	Century-scale

Table 2.1. Compilation of dated modern and recent cyclic climatic processes and behaviors with millennial periodicities.

Study	Locality	Depositional Cycle Type	Age of Most Recent S.U. Succession
Strasser and Samankassou, 2003	Florida Bay Bahamas Bermuda	Variable. Shoaling, tidal flat, and subtidal facies successions.	Variable, oldest 5630 bp youngest 680 bp
Gischler, 2003	Belize platforms	Variable. Reefal, shoaling, and subtidal facies successions.	4.5 kyr
Chappell, 2002	Huon Peninsula, Papua New Guinea	Coral Terraces	6-7 kyr
Parkinson 1989	Southwest coast of Florida	T-R cycle, capped by red mangrove peat	ca. 7 kyr
Tudhope 1989	Davies Reef, central Great Barrier Reef complex	Shallowing-up from: gravel lag; bioturbated muddy sand; shoal or exposure cap	Mid-cycle sediments dated at ca. 3 kyr. Actual cycle must be older
Logan et al., 1969	Shark Bay, Western Australia	Shallowing-up from: grainstone; skel. m/w; laminite cap	ca. 5 kyr
Taft et al., 1968	New Providence Platform, Bahamas	Coarsening-up from mud; Skel. P/G; Grapestone GS	6.7 kyr

Table 2.2. Compilation of dates of modern carbonate shallowing-upward facies successions. Most have not yet filled accommodation, and none of these examples exhibit stacking of shallowing-upward facies successions at millennial periodicities.

Chapter 3: Forward modeling of platform-interior carbonate stratigraphy using Milankovitchian solar insolation as a proxy for high-frequency eustasy

ABSTRACT

Eustatic oscillations driven by Milankovitchian astro-climatic forcing have been identified as drivers of sea level change that cause carbonate depositional cyclicity in studies dating from the mid-1960s (e.g., Fischer, 1964). Accurate forward modeling of these processes with respect to their true affects on the development of carbonate depositional cycles and their stacking patterns has only been attempted using generalized inputs for Milankovitchian forcing. The development of increasingly advanced forward modeling software, coupled with the availability of formulas quantifying solar insolation on the earth's surface as a function of orbital cyclicity allows for the ability to test Milankovitchian parameters against rocks interpreted to have formed as the result of Milankovitch forcing. In this case, Milankovitchian solar insolation curves were used as proxy sea level curves in Carb 3d+, a forward modeling program used to create synthetic carbonate platforms based on user inputs. These synthetic platforms were designed as models of the Latemar platform (mid-Triassic, Northern Italy), which is thought by some to contain one of the most complete records of orbitally-forced platform carbonate cyclostratigraphy yet discovered. While identification of the temporal rhythm of cyclic drivers that generated the Latemar stratigraphy is

still a point of vigorous debate among stratigraphers, the use of the Milankovitchian proxy sea level curves in this study was successful in modeling Latemar-like stratigraphy using both pure Milankovitchian and mixed Milankovitchian-to-subMilankovitchian temporal paradigms. Results from this study suggest that use of Milankovitchian solar insolation curves as proxy sea level curves generate synthetic stacks of stratigraphy that closely replicate the stratigraphy observed in outcrop at the mid-Triassic Latemar platform, and may be useful as high-frequency sea level curves for further forward modeling applications.

AUTHOR'S NOTE

Chapter 3 of this dissertation was published in-house by ExxonMobil Upstream Research Company as:

Forkner, R.M., Hinnov. L.A., Smart, P., and Oldham, D., 2006., Forward modeling of high-frequency platform-interior carbonate cyclic stratigraphy using Milankovitchian solar insolation as a proxy for high-frequency composite eustasy. ExxonMobil Upstream Research Company Internal Report.

All of the text and figures were generated by R.M. Forkner. Hinnov, Smart, and Oldham gave technical advice and aided in software programming. The project was devised, implemented, and results written by R.M. Forkner. All of the work (text and figures) that appears here is the original work of R.M. Forkner.

THE ANISIAN-LADINIAN LATEMAR CYCLES

The Latemar Platform (ca. 5 km diameter, 700 m thick) is a relict Middle Triassic carbonate atoll containing well-preserved internal lagoon, reef, and slope facies (**Figure 3. 1**) (Gaetani et al., 1981; Goldhammer et al., 1987; Goldhammer and Harris, 1989; DeZanche et al., 1995; Egenhoff et al., 1999; Preto et al., 2001, 2004; Zühlke, 2004). The platform interior of the Latemar contains a succession of approximately 600 depositional cycles (ca. 1 m avg. thickness), which have been attributed to eustatic sea level change (Goldhammer et al., 1987; Hinnov and Goldhammer, 1991; Preto et al., 2004; Zühlke, 2004; Emmerich et al., 2005). The original time-frequency interpretation for the genetic driver of the cycles was that of Milankovitchian eustasy (Goldhammer et al., 1987; Goldhammer et al., 1990; Hinnov and Goldhammer, 1991). This interpretation is based on the 5:1 bundling of the 'fundamental' m-scale depositional cycles into lower-frequency 'megacycles' as well as extensive spectral analysis confirming a match between Latemar time series and modeled Middle Triassic Milankovitchian orbital parameters (Hinnov and Goldhammer, 1991; Preto et al., 2001; 2004). However, the original allocyclic Milankovitchian interpretation has been questioned as the result of U/Pb series dates from ash-fall zircons extracted from the platform interior, paleomagnetic data, and biostratigraphic correlations to adjacent basinal deposits (Brack et al., 1996; Mundil et al., 2003; Zühlke, 2004; Emmerich et al., 2005). The debate has yet to be resolved, as both hypotheses (pure Milankovitch vs. mixed Milankovitch and

sub-Milankovitch) present strong evidence in defense of their conclusions. The specifics of the debate are detailed below.

The Latemar Problem

Investigation and analysis of the cyclic succession of platform carbonate deposits at the Latemar began over 20 years ago and has subsequently stirred a debate (the "Latemar Controversy") regarding temporal framework behind the driving mechanisms required to generate the cyclic succession (*see* Preto et al., 2004 and Zühlke, 2004 for summaries of both sides of the controversy). Seminal work by Goldhammer et al. (1987) concluded that the cyclic succession of approximately 600 bundled depositional cycles (ca. 1 m avg. thickness) is a sedimentary record of composite Milankovitchian orbital forcing at the 4th-order (ca. 100 kyr) and 5th-order (ca. 20 kyr) time scales. This interpretation is based on several lines of evidence, including a) the shallowing-upward facies succession within each cycle (thicker subtidal unit overlain abruptly by a thin, centimeter-scale, subaerial cap, suggesting deposition was controlled by sea level oscillations); b) the asymmetric ca. 5:1 bundling of the 'fundamental' m-scale cycles into lower-frequency 'megacycles' or 'bundles', c) the discovery of time-equivalent platform-interior carbonates at Mendola Pass (ca. 30 km to the east) bearing a statistically-correlatable stacking pattern and d) time-series analysis of the cyclic succession that is in agreement with Milankovitchian orbital processes (Goldhammer et al., 1987, 1990; Goldhammer and Harris, 1989;

Hinnov and Goldhammer, 1991; Hinnov et al., 1997; Preto et al., 2001; and Preto et al., 2004, fig. 8). Since that time, and possibly as a direct result of this work, many publications have concluded that bundling of platform cycles may record Milankovitchian controls on eustatic cyclicity (e.g., Koerschner and Read, 1989; Hinnov, 2000; Yang and Lehrmann, 2003; Hinnov and Preto, 2003).

The interpretation that the record of cyclicity at the Latemar is dominantly of astronomical forcing was originally challenged via the dating of zircons extracted from adjacent basinal deposits and later from ash-fall tuffs preserved within the Latemar platform interior, as well as relative dating provided by biostratigraphy (Brack et al., 1996; Mundil et al., 2003; Zühlke, 2004). U-Pb dating from ashfall zircons suggests that the entire Latemar succession was deposited in ca. 2.2 m.y. (in contrast to the 10-12 m.y. of Goldhammer et al., 1987 or the 9.14 m.y. of Preto et al., 2004), which demands much shorter periodicities of composite cyclic drivers, such that the driver for fundamental shallowing-upward cycles must operate more rapidly than allowed by Milankovitchian drivers, i.e., the ca. 20 kyr cycle of Goldhammer et al., 1987 instead becomes a ca. 4.2 kyr cycle (Zühlke et al., 2003). This interpretation considers Milankovitchian precession (Zühlke et al., 2003 concludes the megacycles at periodicities of 18-21.5 kyr) as the driver for megacycle bundles. While the sub-Milankovitch driving mechanism for the fundamental Latemar

cycles is defined temporally by Zühlke et al. (2003), it is left unidentified with regards to cause.

More recently, work by Kent et al. (2004) and Emmerich et al. (2005) suggested that individual cycles represent 1.7 kyr or 0.90-1.97 kyr sea level oscillations, respectively, effectively assigning both cycles and bundled megacycles to sub-Milankovitch periodicites. Kent et al. (2004) base their conclusion on paleomagnetic measurements that indicate the ca. 600 m platform interior succession of the Latemar occupies only one magnetic polarity zone (Kent et al., 2004, fig. 2). Emmerich et al. (2005) base their conclusion on an attempt to better correlate platform-interior stratigraphy to adjacent basinal deposits, suggesting that the best correlation occurs if the cyclic stratigraphy of the Latemar were deposited in a total of ca. 1 myr (Emmerich et al., 2005, fig. 4). (**Figure 3. 2**). As a result, both Kent et al. (2004) and Emmerich et al. (2005) suggest that composite sea level drivers operating at millennial (ca. 1-2 kyr) periodicities also formed the fundamental depositional cycles at the Latemar. Proposed drivers include tidal forcing at millennial frequencies (Munk et al., 2001), Bond cycles and/or Dansgaard-Oeschger cycles (Bond et al., 1997; 2001; Chappell, 2002; Lambeck et al., 2002). Schulz and Schäfer-Neth (1997) show an increase in deep-water temperature of approximately 2°C can generate a sea level rise of 1.7 m by thermal expansion via increased formation of warm deep waters in low latitudes (**Table 3. 1**). However, it must be noted that no link

between sea level oscillations with millennial periodicities and the formation of shallowing-upwards carbonate depositional allocycles has yet been established. Most modern carbonate depositional sequences only date from approximately 6 kyr and are one coherent shallowing-upward succession of facies (i.e., un-stacked, or in other words, no stacked periodic millennial scale cycles) many having not yet aggraded to sea level (**Table 3. 2**). While arguments surrounding the origin and drivers of cyclic sedimentation continue within both the pure Milankovitch and sub-Milankovitch camps, neither has refuted the conclusion that the Latemar cycles are an exceptional sedimentological record of an extrabasinal forcing mechanism.

Significance of Stratigraphic Studies at the Latemar: Cyclic Models

The concept of a hierarchy of depositional cyclicity is now well established and is commonly used in both industry and academia (Vail et al., 1987; Haq et. al., 1987). The widely-used (and oft-criticized) Exxon cycle chart originally identified of 3 temporal “orders” of cyclicity: (1) first order cycles with durations of 200-300 m.y.; (2) second order cycles with durations of 10-80 m.y.; and (3) third-order cycles with durations of 1-10 m.y. (Vail et al., 1987; Haq et al., 1987). Miall (1984) expanded this hierarchy in order to connect seismic scale cycles to outcrop-scale “high resolution” cycles, defining fourth-order cycles as those with durations of 0.2 and 0.5 m.y. The hierarchy was expanded via work in high-frequency cyclostratigraphy aided in large part by the work of Goldhammer et al.

(1987, 1990) at the Latemar, where fundamental shallowing-upwards cycles were interpreted to be a record of the ca. 20 kyr precession, and therefore fifth-order cycles (cycles with durations of 0.01-0.1 m.y.). The hierarchical model is still widely used in carbonate stratigraphy, and many stratigraphers use the order hierarchy if the bundling of cycles can be recognized- whether or not absolute age or measure of cycle duration can be determined (Goldhammer, 2003). This is likely a result of the recognition of the "building block" arrangement of cycle stacking that can be observed in outcrop and core from around the world. Thus, the working use of the cyclic hierarchy is many times a relative use and is not accompanied by evidence of temporal periodicity.

Recent work at the Latemar is an excellent example of the results of the problems that can arise with defining temporal periodicity. The 4.2 kyr/cycle model of Zühlke et al. (2003) and the 0.9-1.97 kyr/cycle model of Emmerich et al. (2005) would define a new allocyclic order: 7^{th}-order allocycles (6^{th}-order cycles were defined by Vail et al., 1991 and also by Grammer et al. 1996 as those cycles with durations of 0.01 and 0.03 m.y.) (Goldhammer, 2003). This is important to realize because these same Latemar cycles were identified by Goldhammer et al. (1987, 1990) as 5th-order cycles. The commonplace assignment of "5^{th}-order" temporal periodicity to fundamental high-frequency cycles is reflected in the default settings for sea level drivers in Carb 3d+ (the forward modeling software package used in this study) (**Figure 3. 3**). Clearly,

additional evaluation of the assumptions about high-frequency depositional periodicity are necessary, as are every day assumptions about the temporal nature or forcing mechanisms of high-frequency cycles.

Significance of Modeling Latemar Cyclicity

Initial work on the Latemar by Goldhammer et al. (1987) identified cycles and megacycles interpreted to have formed by global sea level change operating as the result of Milankovitchian astronomical forcing. However, that interpretation was limited to ca. 20 kyr precession as a driver for individual cycles and ca. 100 kyr eccentricity for cycle bundles. More recent depth-rank analysis of a resampled section at the Latemar indicates a full bandwidth of Milankovitch-like frequencies exist in vertical facies stacking (Preto et al., 2004, fig. 8) (**Figure 3. 4**). Unfortunately, quantified amplitudes of sea level oscillations resulting from composite Milankovitch forcing (for each individual orbital process) has not yet been established. However, since a conspicuous frequency match exists between the carbonate depositional record at the Latemar and Milankovitchian orbital cyclicity, it is at least appropriate to test for a linkage between the full bands of astronomical cyclicity (precessions, obliquity and eccentricity), sea level change, and carbonate sedimentation. To test for a link, this study will use a Milankovitchian solar insolation curve generated in the time-series software package AnalySeries 1.2 (Paillard et al., 1996) based on the orbital calculations of Laskar (1990) as a proxy for high-frequency sea level change.

The use of a solar insolation curve as a first-order proxy for high-frequency eustatic oscillations is significant for several reasons. First, it will serve as a cross check for the plausibility of an astro-depositional linkage. This may prove interesting not just for considering solar insolation as a driver for sea level change (astro-climatic forcing), but may also put forth a linkage between solar insolation and carbonate production, particularly in systems dominated by photosynthetic and other light and heat-sensitive carbonate producers. Second, it may provide forward modelers with a more process-based set of sea level curves for assessment of the effects of high-frequency eustasy. This is of inherent importance when constructing a forward model that is designed to be predictive rather than inverse (e.g., generating a sea level curve based on processes affecting sea level rather than using measured rock thickness as a proxy for eustasy).

In addition to being a subject of geological debate, the cyclic stratigraphy of the Latemar provides a real-world locality that serves as a "ground truth" for synthetic output from Carb3d+. This may be achieved through comparison of Carb 3d+ output sections and stacking patterns to those measured, analyzed, and published by other workers (e.g., Preto et al., 2004; Zühlke et al., 2004). The theorized sedimentary input parameters for the Latemar cyclic succession have been defined and tabulated per author (**Table 3. 3**). A simple, one-dimensional set of test models of the Latemar cyclic succession using these input

parameters was also attempted using the program 'Mr. Sediment' (written by Paul Dunn, used in Goldhammer et al., 1990) and is also presented here in a brief format (**Table 3. 4**). Modeling the platform using published rates of eustatic change, sedimentation, and subsidence will serve as a test for these input parameters. Perhaps most importantly, however, the use of an independent, process-based proxy sea level curve (the Milankovitchian solar insolation curve of Lasker, 1990) for high-frequency composite eustasy may generate a more accurate population of facies types and depositional thicknesses within output datasets.

Methods

Generating a Milankovitchian Solar Insolation Curve

In order to generate a proxy sea level curve based on Milankovitchian solar insolation, an insolation curve created. The curve was calculated in the freeware time-series analytical package AnalySeries v.1.2 using the Milankovitchian solar insolation solution of Laskar (1990) (Paillard et al., 1996). Inputs required include orbital model, latitude, and declination from celestial equator (or solar path in the local sky as a function of season) (**Figure 3. 5**). For the purposes of this study, an equatorial latitude was chosen, as well as a seasonal path at the summer solstice. Equatorial latitude was chosen not only because modern carbonates form at near equatorial latitudes (+/- 30 degrees), but also because the position of the Dolomites in the Triassic was near equatorial

(Tucker and Wright, 1990; Scotese, 2003). Output is given in two columns, the first being time step in the series (in years), and the second being insolation (in W/m^2). The data can be copied out of AnalySeries v.1.2 and pasted directly into MS Excel or any other spreadsheet program for further manipulation. A sample plot of output data for 1 million years using a 1 kyr time step at 0 degrees latitude is presented here as (**Chart 3. 1**).

Once the curve is generated, it must be re-calibrated such that the mean (or baseline of the curve) is at zero and the oscillations extend to the eustatic maxima and minima thought to have existed at the time. In the example used here, the mean value for the input insolation curve is 400 W/m^2. To re-center in this example, all of the data points were subtracted by 400 in MS Excel. Next, desired maximum and minimum amplitudes for the curve must be set. The insolation data in this case has maximum and minimum values of +/- 50 W/m^2, and in this case, the desired sea level curve ought to have maximum and minimum oscillations of +/- 5m, which requires division of all data by a factor of 10. The resulting proxy sea level curve is presented here as (**Chart 3. 2**).

Generating additional curves

Using Milankovitchian insolation as a proxy sea level curve generates sea level oscillations at 5^{th}-order periodicities. 4^{th}-order periodicity is inherent to the oscillations in the form of frequency and amplitude modulations. In order to add

higher or lower frequency oscillations to the curve, one must define the curve to be added, and add the two curves together in order to create a composite curve that can be loaded into Carb 3d+. An example is provided below.

In this case, a 3rd-order oscillation will be added to the re-centered proxy curve that is shown in chart 2. The 3rd-order curve will have a period/wavelength of 1 million years, will have an amplitude of +/- 40 meters, and will be represented by a sinusoid. The equation for the sinusoid is:

$$y = A \sin [w(x-a)]+C \text{ , where}$$

A is the amplitude of the resulting curve; w is the angular frequency, given by $w=2\pi/\text{period}$; x is the point along the x-axis the curve is being defined for (in this case equal to the time step values of 0, 1000, 2000, and so on); a is the phase shift; and C is the vertical offset of the baseline from zero. In this case, we do not require a or C for the definition of the curve so those variables can be ignored. Therefore, the equation for this example becomes:

$$y = 40 \sin [(2\pi/1{,}000{,}000)(\text{time step value})]$$

This can be quickly and easily defined in any spreadsheet program using the series of time step values already generated by AnalySeries for the insolation curve (**Figure 3. 6, Chart 3. 3**). Once the values for the second curve have been generated, simply add the two data sets together to generate the composite curve (**Chart 3. 4**).

Loading Sea-level Curve Data into Carb 3d+

Loading sea level curves created using AnalySeries v.1.2 or MS Excel into Carb 3d+ is a straightforward procedure. This can be done by simply cutting and pasting data points into an existing Carb 3d+ .slv file, which can usually be found in any Carb 3d+ project folder. A flow chart detailing the methodology can be see in (**Figure 3. 7**). Before loading the new .slv file into Carb 3d+, be sure that the age at the start and end of the run as well as the calculation increment are set to be equivalent to the data in the .slv file. This can be done in the "Space and Time" window in Carb 3d+ under the "time" tab.

Extracting Cycle Data from Carb 3d+

Extracting cycle/parasequence thickness data from lengthy completed runs of Carb 3d+ has been a difficult process prior to this study. In order to make this process easier for the Carb 3d+ user, Drs. Peter Smart and Dave Oldham (both from the University of Bristol) wrote output code that generates a succession of cycle/parasequence thickness data at any user-defined position on a synthetic platform. The cycle data can be retrieved by using the Carb3d+ display window called "Parasequences". If desired, parasequence data can be exported as an ASCII file for further analysis. Parasequece data is given in 3 columns, the first giving the thickness of the parasequence in meters, the second giving the height of the upper surface of the parasequence relative top of the well

log, and the third whether or not the top of the parasequence underwent subaerial exposure.

Spectral Analysis

Advanced statistical methods used for analysis of cycle stacking and bundling trends involve spectral analysis of the cyclic series generated by Carb 3d+. Examination of sections as a time series means treating depositional cycles as a representation of cyclic behavior with temporal periodicity. The purpose of the analysis is to identify the frequencies of prominent variations in the cycle cycle thickness series (Bloomfield, 1976). In this case, software packages Analyseries v 1.2 and KaleidaGraph were used in constructing time series plots.

Spectral analysis of the thickness series generated by the Carb 3d+ model was performed for comparison to thickness spectra from Latemar sections. The multitaper method of Thompson (1982), available in Analyseries 1.2, was used for the analysis due to its efficacy in detecting bundling in thickness series (*see* Hinnov and Goldhammer, 1991 for detailed explanation and justification).

Model Inputs for Simulations

Each set of model inputs used in Latemar test runs was derived mainly from publications written by authors associated with each depositional paradigm. Input parameters used for each Carb3d+ simulation are presented in (**Appendix**

A). Since the focus of this study was to test for replication of stratigraphic packaging of depositional allocycles, inputs for subaerial diagenesis and erosion were kept at minimal levels as to preserve cycle thickness as generated by eustasy alone.

Milankovitch Model

Data inputs for the Milankovitch model (pure Milankovitch forcing) were assumed from Goldhammer et al. (1987) and are summarized in Appendix A. The Milankovitch Model uses Milankovitchian solar insolation as a proxy high-frequency sea level driver and a +/- 40 m oscillation with a 10 myr periodicity as a 3rd-order driver. Duration and amplitude of the 3rd-order scale oscillation were calculated from accommodation plots (Fischer plots) of the entire Latemar measured section (Harris and Goldhammer, 1989; Goldhammer et al., 1990).

Milankovitch / sub-Milankovitch model

Data inputs for models using the depositional parameters defined by Zühlke (2004) and the carbonate research group from Heidelberg, Germany are tabulated in Appendix A. The Milankovitch / sub-Milankovitch model employs either a +/- 2.5 meter or +/- 5 meter sinusoidal oscillation with 4.2 kyr periodicity atop a Milankovitchian solar insolation curve. Problems generating an accurate model with this forced the inclusion of a 3rd-order scale oscillation that was not

originally defined by Zühlke (2004). This oscillation has an amplitude of +/- 40 m and a period of 2.95 myr.

Millennial Model

Data inputs for the millennial model (Kent et al., 2004; Emmerich et al., 2005) are tabulated in Appendix A. The Millennial model only argues for one sea level driver of 0.9-1.97 kyr in periodicity (Kent suggests 1.7 kyr). Clearly, this driver acting alone will not generate bundling of depositional cyles. In the literature, those arguing for millennial periodicity of cycles suggest that there is a great deal of difficulty and uncertainty in identifying accurate 3rd-order drivers (either periodicity or amplitude) (Emmerich et al., 2005). As a result, Emmerich et al. (2005) argue that differential subsidence may have driven the lower-frequency accommodation. Unfortunately, Carb 3d+ does not allow for input of differential subsidence, and so as a proxy, two lower-order drivers were added to the 1.7 kyr oscillation: a Milankovitchian insolation curve to provide a driver for megacycle bundling, and a lower frequency oscillation with an amplitude of +/- 40 m and a period of 1 my.

Results

Milankovitch Model

Results from the Milankovitch Model run are surprisingly consistent with real-rock measurements of Harris and Goldhammer (1989) and Goldhammer et

al. (1990). As an initial test for consistency, a plot of the cumulative deviation from mean cycle thickness (also known as “Fischer plots” after Fischer, 1964, or “accommodation plots” after Schwarzacher, pers. commun.) of cycles was compared to a plot of the Latemar cycles. Thicknesses of cycles without exposure caps were added to the thickness of subsequent cycles until exposure was attained. Comparison of Fischer plots of both the entire simulation and of shorter windows through the simulation show striking similarities to stacking and accommodation trends present in Latemar measured sections (**Figures 3. 8, 3. 9, and 3. 10**). In the “lower cyclic facies” portion of the accommodation curve (3^{rd}-order rise), a magnified comparison of model data to measured section data from Goldhammer shows notable similarities in stacking, including asymmetric 5:1 bundling of cycles in both the real-rock and modeled sections (the model drivers were symmetric curves), as well as similarities in lower-frequency thickening and thinning trends (Figure 3. 9). The same can be said for cycles in the “middle tepee facies” portion of both accommodation curves (3^{rd}-order fall). At the Latemar, portions of the “middle tepee facies” are disrupted into multi-meter-scale tepee structures that consume multiple thin depositional cycles. While the Carb 3d+ model did not model marine vadose diagenesis and the formation of tepee structures, the portion of the dataset commensurate with the middle tepee facies did include thin, condensed cycles resulting from multiple “missed beats” of sea level rise (Figure 3. 10).

Spectral analysis of thickness series taken from the Carb 3d+ Milankovitch model has power spectral peaks that are consistent (although shifted to lower power) with a spectrum of measured section thickness data obtained by Goldhammer (1987) for the same interval (**Figure 3. 11**). Both sets of data are from the first half of the 3rd-order oscillation, commensurate with the lower cyclic facies and middle tepee facies of Goldhammer et al. (1987). The shift is spectral peaks of the model data relative to the measured section data likely occurred as a result of Carb 3d+ counting every shallowing-upward facies succession produced by a sea level oscillation as a cycle, whether or not sea level fall was large enough in magnitude to expose the platform top and form a diagenetic cap at the top of the cycle. The measured section data, however, defined cycle tops on the basis of the presence of a dolomitized exposure cap (*see* Goldhammer et al., 1987; Preto et al., 2004). As a result, there are more "cycles" delineated in the model data (229) than were counted in the measured section (210). The "extra" cycles also affect the number of cycles counted per megacycle bundle. For example, the measured section spectrum shows dominant "eccentricity" bundling at 5:1 and 6:1, the Carb 3d+ spectrum shows these same bundles with peaks commensurate with 5.6:1 bundles and 7.8:1 bundles because successions without exposure caps were counted as cycles. Overall, however, bundling trends highlighted by spectral analysis appear consistent between both datasets. The similarities in bundling trends taken alongside very similar trends in

accommodation plots suggests that there is a close match between the Milankovitch model cycle stacking to that of the cycle stacking at the Latemar.

Milankovitch / sub-Milankovitch model

Several modeling runs using the parameters defined by Zühlke (2004) were undertaken in order to attain an output dataset that came close to matching the Latemar stratigraphy. Initial runs used only the input parameters found in Zühlke (2004) (Milankovitch forcing along with a 4.20 kyr oscillation at +/- 5m), which was problematic because these parameters include differential subsidence (not possible to model in Carb 3d+), but do not include a 3rd-order scale sea level driver (**Figure 3. 12**). As a result, a 3rd-order driver was added as a variable subsidence proxy in a second modeling run (*see* Appendix A). The addition of this curve improved the number of output cycles generated for what ought to be the first half of the Latemar's history (approximately 200 cycles) as well as the geenral thickening-thinning trend in accommodation (**Figure 3. 13**). Unfortunately, however, accommodation trends still did not match the trends from the measured sections (see Figure 12). Success in generating a close match in accommodation trends came with decreasing the amplitude of high-frequency oscillations from +/- 5 m to +/- 2.5 m and plotting all cycles, whether or not exposure occurred at the caps of the cycles. Comparing these accommodation trends to those from measured section cycle thickness data shows surprising matches in cycle stacking patterns through the succession (**Figure 3. 14**).

However, comparison of cycle frequency spectra from Carb 3d+ Milankovitch / sub-Milankovitch model output data and measured section cycle thickness data from the same stratigraphic interval does not show favorable comparability (**Figure 3. 15**). The Milankovitch / sub-Milankovitch model spectrum differs from the measured section spectrum in several ways. First, the Latemar measured section spectrum has a dominant bundling peak at ca. 30:1, while the Milankovitch / sub-Milankovitch model spectrum has a ca. 30:1 peak, but at much lower power. Second, the megacycle bundes present in the measured section data are focused on 5:1 bundels (dominant) and 6:1 bundles (interpreted as precession 1 and 2). Milankovitch / sub-Milankovitch model megacycle bundles are centered on 7.7:1 bundles (the dominant peak in the spectrum) and 6.6:1 bundles, indicating that there are more cycles per megacycles in the Zühlke model than in the Latemar measured section data. In addition, the Zühlke Carb 3d+ model made far too many depositional cycles (278) over this stratigraphic interval than are allowed by measured section data (210). Again, this is likely because Carb 3d+ counts all successions, whether or not exposure caps formed, as depositional cycles. While overall accommodation trends in Milankovitch / sub-Milankovitch model data and measured section data are comparable, bundling trends between the two datasets do not compare well.

Millennial Model

Parameters for Latemar platform development as defined by Kent et al. (2004) and Emmerich et al. (2005) failed to generate a model platform that is similar to the Latemar. Both studies conclude a millennial-frequency driver with a period of 0.9-1.97 kyr (Kent suggests 1.7 kyr) as the formative driver for fundamental Latemar cyclicity and ignore bundling altogether. In addition, Emmerich et al. (2005) suggest that differential subsidence was the true accommodation driver for the Latemar, and does not assume any lower-frequency sea level drivers were operating. While Carb 3d+ cannot model a differentially subsiding platform, it is already clear from the above description that these drivers will not generate a platform containing equivalent bundling characteristics to those preserved within the Latemar platform, as no driver is included to modulate the high-frequency oscillations into ca. 5:1 bundles. As a result, a 1.7 kyr oscillation was created and added to a Milankovitchian insolation curve as well as a lower-frequency oscillation (**Figure 3. 16**). Unfortunately, these inputs also fail to create an accurate accommodation plot and do not generate an output dataset that has comparable power spectra to Latemar measured section data (**Figure 3. 17**). In addition, most of the cycles generated using the millennial model remain unexposed at their tops. This problem may be addressed by increasing the amplitude of the high-frequency driver. However, sea level oscillations totaling 5 m (+/- 2.5 m) already require the introduction and removal of seawater into the oceans at a volume greater than that of the

Greenland ice sheet – in this case at a periodicity of every 1.7 kyr in near-peak greenhouse conditions (Jacobs and Sahagian, 1993). A process by which the introduction and removal of that quantity of seawater from the oceans at millennial periodicities is not known to science. It is unrealistic to increase the amplitudes of 1.7 kyr oscillations to +/- 5 m (10 m total), even if that would generate stacking more consistent with Latemar stratigraphy. Further work is required to identify the mechanisms behind the proposed millennial-scale drivers in Latemar cyclostratigraphy. At this time, however, they have not been effectively modeled.

Discussion

The interpretations of Milankovitchian forcing of Latemar carbonates, either in the Milankovitchian form of Goldhammer et al. (1987) or the mixed sub-Milankovitch form of Zühlke (2004) relied on analyses of the stacking patterns of depositional cycles at the Latemar to conclude that astronomical forcing played a role in the formation of mid-Triassic platformal carbonates. Preliminary modeling using “Mr. Sediment” by Goldhammer et al. (1987) showed that 5:1 bunding of cycles could be produced using a simplified precessional sea level oscillation with a 20 kyr periodicity superimposed on a eccentricity driver of ca. 100kyr (Goldhammer et al., 1990). However, megacycle stacking at the Latemar is not consistently 5:1, and may be masked altogether in amalgamated tepee belts. The purpose of this study was to take a forward-modeling approach to the

question of Milankovitchian effects on the stratigraphy of the Latemar by using the full suite of Milankovitchian orbital processes (Precessions 1 and 2, Obliquity, and all Eccentricities). These processes were used to construct a proxy sea level curve that was then used in Carb 3d+ in order to grow synthetic carbonate platforms. While previous studies had identified stacking trends consistent with Milankovitch forcing, none had used forcing mechanisms derived from calculated Milankovitchian orbital periodicities to test for a match.

Both the published conclusions of Goldhammer et al. (1987) and Zühlke (2004) produced sedimentation inputs that, when married with the calculations for Milankovitchian orbital processes, produced synthetic stratigraphy that resembled that of the Latemar platform. In particular, the Milankovitch model (i.e., Goldhammer et al., 1987) produced stacking patters consistent with “missed beats” in both LPF and MTF facies, as well as ca. 5:1 bundling that conspicuously matches measured sections in the LCF of the Latemar (see Figures 8, 9, and 10). In addition, spectral analysis of the synthetic thickness series shows similar trends in bundling between both series (see Figure 11). Similarities between Latemar stratigraphy and the Milankovitch / sub-Milankovitch model (i.e., Zühlke, 2004) are also worth attention. Indeed, the visual match in Fischer plots between the synthetic and real stratigraphy (see Figure 14) is striking. However, the match in bundling trends from synthetic stratigraphy to the real stratigraphy is somewhat more problematic.

Conclusions

Several conclusions can be drawn from the use of the Carb 3d+ modeling package to test periodic cycle drivers for the Latemar platform. First, the use of a Milankovitchian insolation curve as a proxy for high-frequency sea level oscillations is a process-based approach to forward modeling of sedimentary systems that is sensitive to high-frequency sea level oscillations of even a few meters in amplitude. Second, the use of a Milankovitchian insolation curve as a proxy for high-frequency sea level oscillations can produce synthetic sedimentary successions with asymmetric stacking, similar bundling frequencies, and similar thicknesses to those observed at the Latemar platform. This is true at both the 4^{th}- and 5th-order scales. Third, the use of a combined sub-Milankovitch-Milankovitchian insolation proxy curve can also produce stacking patterns and accommodation plots that are similar to those of the Latemar platform. Fourth, accurate synthetic stratigraphy generated using millennial-scale drivers has not yet been successfully modeled using Carb3d+. It is possible that the limitations to this paradigm are centered around an incomplete definition of all hypothetical drivers, their frequencies, and causes.

The success of modeling Latemar-like stratigraphy using Milankovitchian insolation curves as proxy sea level drivers provides a base from which to continue this research. Hopefully the methodologies can be refined and cross-applied to other settings and modeling projects to generate more accurate

modeled stratigraphic data. In the future, this may include increasingly accurate prediction of cycle thicknesses, distribution of facies types, and distribution of early diagenetic environments. Carb 3d+ is a powerful modeling tool that stands to become an increasingly reliable asset as refinements and cross checks are made to both sea level curves and timing of sedimentary processes.

References

Alsharhan, A.S., and Kendall, C.G.St.C., 2003, Holocene coastal carbonates and evaporites of the southern Arabian Gulf and their ancient analogues: Earth-Science Reviews, v. 61, p. 191-243.

Black, M., 1933, The algal sediments of Andros Island, Bahamas: Philosophical Transactions of the Royal Society, London, Series B, v. 222, p. 165-192.

Blendinger, W., 2004, Sea level changes versus hydrothermal diagenesis: Origin of Triassic carbonate platform cycles in the Dolomites, Italy: Sedimentary Geology, v. 169, p. 21-28.

Blendinger, W., Brack, P., Norborg, A.K., and Wulff-Pedersen, Erik, 2004 Three-dimensional modeling of an isolated carbonate buildup (Triassic, Dolomites, Italy): Sedimentology, v. 51, p 297-314.

Bloom, A.L., Broecker, W.S., Chappell, J.M.A., Matthews, R.K., and Mesolella, K.J., 1974, Quaternary sea level fluctuations on a tectonic coast: Quaternary Research, v. 4, p. 185-205.

Bloomfield, Peter 1976, *Fourier Analysis of Time Series*, John Wiley and Sons.

Bond, G., Kromer, B., Beer, J., Muscheler, R., Evans, M.N., Showers, W., Hoffman, S., Lotti-Bond, R., Hajdas, I., and Bonani, G., 2001, Persistent solar influence on North Atlantic climate during the Holocene: Science, v. 294, p. 2130-2136.

Bond, G., Showers, W., Cheseby, M., Lotti, R., Almasi, P., deMenocal, P., Priore, P., Cullen, H., Hajdas, I., and Bonani, G., 1997, A Pervasive millennial-scale cycle in North Atlantic Holocene and glacial climates: Science, v. 278, p. 1257-1266.

Bosellini, A., and Hardie, L.A., 1985, Facies e cicli della Dolomia Principale delle Alpi Venete: Memorie della Societa Geologica Italiana, v. 30, p. 245-266.

Brack, P., Mundil, R., Oberli, F., Meier, M., and Rieber, H., 1996, Biostratigraphic and radiometric age data question the Milankovitch characteristics of the Latemar cycles (Southern Alps, Italy): Geology, v. 24, 4, p. 371-375.

Brack, P., and Muttoni, G., 2000, High-resolution magnetostratigraphic and lithostratigraphic correlations in Middle-Triassic pelagic carbonates from the Dolomites (Southern Alps, Italy): Palaeogeography, Paleaoclimatology, and Palaeoceanography, v. 161, p. 361-380.

Broecker, W.S., Thurber, D.L., Goddard, J., Ku, T., Matthews, R.K., Mesolella, K.J., 1968, Milankovitch hypothesis supported by precise dating of coral reefs and deep sea sediments: Science, v. 159, no. 3812, p. 297-300.

Chappell, J., 2002, Sea level changes forced ice breakouts in the last glacial cycle: new results from coral terraces: Quaternary Science Reviews, v. 21, p. 1229-1240.

Cozzi, A., 2002, Facies Patterns of a Tectonically-Controlled Upper Triassic Platform-Slope Carbonate Depositional System (Carnian Prealpls, Northeastern Italy): Facies, v. 47, p. 151-178.

Demicco R.V., and Hardie, L.A., 1994, Sedimentary structures and early diagenetic features of shallow marine carbonate deposits: SEPM Atlas Series No. 1, 265 p.

Doglioni C., 1987, Tectonics of the Dolomites (Southern Alps, Northern Italy): Journal of Structural Geology, v. 9, no. 2, p.181-193.

Doglioni C., 1988, Examples of strike-slip tectonics on platform-basin margins: Tectonophysics, v. 156, p. 293-302.

Egenhoff, S.O., Peterhänsel, A., Bechstädt, T., Zühlke, R., and Grötsch, J., 1999, Facies architecture of an isolated carbonate platform: tracing the cycles of the Latemar (Middle Triassic, northern Italy): Sedimentology, v. 46, p. 893-912.

Emmerich, A., Glasmacher, U.A., Bauer, F., Bechstädt, T., and Zühlke, R., 2005, Meso-/Cenozoic basin and carbonate platform development in the SW-Dolomites unraveled by basin modeling and apatite FT analysis: Rosengarten and Latemar (Northern Italy): Sedimentary Geology, v. 175, is. 1-4, p.415-438.

Enos, P., and Perkins, R.D., 1979, Evolution of Florida Bay from island stratigraphy: Geological Society of America Bulletin, v. 90, p. 59-83.

Fischer, A.G., 1964, The Lofer Cyclothems of the Alpine Triassic: Kansas Geological Society Bulletin, v. 169, p.107-149.

Ginsburg, R.N., 1971, Landward movement of carbonate mud: new model for regressive cycles in carbonates (abs.): American Association of Petroleum Geologists Bulletin, v. 55, p. 340.

Ginsburg, R.N., Hardie, L.A., Bricker, O.P., Garrett, P., Wanless, H.R., 1977, Exposure Index: a quantitative approach to defining position within the tidal zone. *in* Hardie, L.A., *ed*., Sedimentation on the Modern Carbonate Tidal Flats of Northwest Andros Island, Bahamas. The Johns Hopkins University Studies in Geology, no. 22., p. 7-11.

Goldhammer, R.K., Dunn, P.A., and Hardie, L.A., 1987, High-frequency glacio-eustatic sea level oscillations with Milankovitch characteristics recorded in Middle Triassic platform carbonates in Northern Italy: American Journal of Science, v. 287, p. 853-892.

Goldhammer, R.K., Dunn, P.A., and Hardie, L.A., 1990, Depositional cycles, composite sea level changes, cycle stacking patterns, and the hierarchy of stratigraphic forcing: Examples from the Alpine Triassic platform carbonates: Geological Society of America Bulletin, v. 102 p. 535-562.

Goldhammer, R.K., and Harris, M.T., 1989, Eustatic controls on the stratigraphy and geometry of the Latemar buildup (Middle Triassic), the Dolomites of northern Italy: SEPM Special Publication 44, p. 232-338.

Goldhammer, R.K., Hinnov, L.A., and Forkner, R.M., 2003, Resurrection of the allocyclic interpretation of the 'Latemar cycles' (M. Triassic, the Dolomites): view from a coeval platform: American Association of Petroleum Geologists Annual Meeting Abstracts, Salt Lake City, Utah.

Goldhammer, R.K., and Kaufman, J., 1995, Astronomical climatic cycles, Pleistocene glacio-eustasy, and the origin of Pleistocene platform cycles in Florida: Exxon Production Research Company Advanced Carbonates Field Report.

Hardie, L.A., and Ginsburg., R.N., 1977, Layering: The origin and environmental significance of lamination and thin bedding. *In* Hardie, L.A., *ed*., Sedimentation on the Modern Carbonate Tidal Flats of Northwest Andros Island, Bahamas. The Johns Hopkins University Studies in Geology, no. 22. p. 50-123.

Hinnov, L.A., 2000, New perspectives on orbitally forced stratigraphy: Annual Review of Earth and Planetary Sciences, v. 28, p. 419-475.

Hinnov, L.A. and Goldhammer, R.K., 1991, Spectral analysis of the Middle Triassic Latemar Limestone: Journal of Sedimentary Petrology, v. 61, p. 1173-1193.

Hinnov, L.A., Cozzi, A., and Bazykin, D.A., 1997, The Milankovitch origin of the Middle Triassic Latemar platform cycles: a review of the sedimentologic criteria and results of a new evolutive spectral analysis of the entire Latemar succession: IAS Regional Meeting Abstracts, Gaia Heidelbergensis, v. 3, p. 164-165.

Hinnov, L.A. and Preto, N., 2003, Analyzing the depositional signal of the Latemar Limestone (Dolomites, Italy): a multiple working hypothesis approach. in Brack, P., Schlager, W. and Stefani., M., eds., Abstract Volume, Triassic Geochronology and Cyclostratigraphy - a Field Symposium, St.Christina/Italy, September 11-13, p. 10.

Jacobs, D.K., and Sahagian, D.L., 1993, Climate-induced fluctuations in sea level during non-glacial times, Nature, vol. 361. P.710-712.

Jenkins and Watts, (1968), Spectral Analysis and Its Applications, Holden-Day. New York, NY, 288 p.

Kent, D.V., Muttoni, G., and Brack, P., 2004, Magnetostratigraphic confirmation of a much faster tempo for sea level change for the Middle Triassic Latemar platform carbonates: Earth and Planetary Science Letters, v. 228, p. 369-377.

Koerschner III, W.F., and Read, J.F., 1989, Field and modeling studies of Cambrian carbonate cycles, Virginia Appalachians: Journal of Sedimentary Petrology, v. 59, p. 654-687.

Lambeck, K., Yokoyama, Y. & Purcell, T. 2002. Into and out of the Last Glacial Maximum: sea level change during Oxygen Isotope Stages 3 and 2.: Quaternary Science Reviews v. 21, p. 343-360.

Laskar, J., 1990, The chaotic motion of the solar system: A numerical estimate of the chaotic zones: Icarus, v. 88, p. 266-291.

Logan, B.W., Read, J.F., and Davies, G.R., 1969, History of carbonate sedimentation, Quaternary epoch, Shark Bay, Western Australia: *in* American Association of Petroleum Geologists – Memoir 13, p. 38-84.

Maurer, F., Hinnov, L.A., and Schlager, W., 2004, Statistical time-series analysis and sedimentological tuning of bedded rhythms in a Triassic basinal succession (Southern Alps, Italy): SEPM Special Publication no. 81, p. 83-99.

Mundil, R., Zühlke, R., Bechstadt, T., Brack, P., Egenhoff, S., Meier, M., Oberli, F., Peterhänsel, A., and Rieber, H., 2003, Cyclicities in Triassic Platform Carbonates: Synchronizing radio-isotopic and orbital clock: Terra Nova, v. 15/2, p. 81-87.

Niggemann, S., Mangini, A., Mudelsee, M., Richter, D., and Wurth, G., 2003, Sub-Milankovitch climatic cycles in Holocene stalagmites from Sauerland, Germany: Earth and Planetary Science Letters, v. 216, p. 539-547.

Paillard, D., L. Labeyrie and P. Yiou, 1996, Macintosh program performs time-series analysis, Eos Trans. AGU, Vol. 77, p. 379. An electronic supplement of this reference is available at: http://www.agu.org/eos_elec/96097e.html

Parkinson, R.W., 1989, Decelerating Holocene sea level rise and its influence on southwest Florida coastal evolution: A transgressive/regressive stratigraphy: Journal of Sedimentary Petrology, v. 59, no. 6, p. 960-972.

Peltier, W.R., 2001, On eustatic sea level history: Last glacial maximum to Holocene: Quaternary Science Reviews, v. 21, p. 377-396.

Preto, N., Hinnov, L.A., Hardie, L.A., and De Zanche, V., 2001, Middle Triassic orbital signature recorded in the shallow-marine Latemar carbonate buildup (Dolomites, Italy): Geology, v. 29, no. 12, p. 1123-1126.

Preto, N., Hinnov, L A., De Zanche, V., Mietto, P.,, and Hardie, L.A., 2004, The Milankovitch interpretation of the Latemar platform cycles (Dolomites, Italy): implications for geochronology, biostratigraphy, and middle Triassic carbonate accumulation: SEPM Special Publication No. 81, p. 167-182.

Prosser, G., and Selli, L., 1991, Thrusts of the Mezzocorona-Mendola Pass area (Southern Alps, Italy): Structural analysis and kinematic reconstruction: Bolletino della Societa Geologica Italiana, v. 110, p. 805-821.

Rankey, E.C., and Morgan, J., Quantified rates of geomorphic change on a modern carbonate tidal flat, Bahamas: Geology, v. 30, no. 7, p. 583-586.

Read, J.F., and Goldhammer, R.K., 1988, Use of Fischer plots to determine third-order sea level curves in Ordivician peritidal carbonates, Appalachians: Geology (Boulder), v. 16, no. 10, p.895-899.

Roth, S., and Reijmer, J.J.G., 2005, Holocene millennial to centennial carbonate cyclicity recorded in slope sediments of the Great Bahama Bank and its climatic implications: Sedimentology, v. 52, p. 161-181.

Schlager, W., 1999, Scaling of sedimentation rates and drowning of reefs and carbonate platforms: Geology, v. 27, no. 2, p. 183-186.

Schlager, W., 1981, The paradox of drowned reefs and carbonate platforms: Geological Society of America Bulletin, part I, v. 92, p. 197-211.

Schwarzacher, W., 1975, Sedimentation Models and Quantitative Stratigraphy: New York, Elsevier, 382 p.

Shinn, E.A., 1986, Modern Carbonate Tidal Flats: Their Diagnostic Features., in Hardie, L.A., and Shinn, E.A., Carbonate Depositional Environments, Modern and Ancient: Colorado School of Mines Quarterly, v. 81, No. 1, p. 7-33.

Steno, Nichlaus, 1669, De Solido Intra Solidium Naturaliter Contento Dissertationis Prodromus

Strasser, A., and Samankassou, E., 2003, Carbonate sedimentation rates today and in the past: Holocene of Florida Bay, Bahamas, and Bermuda vs. Upper Jurassic and Lower Cretaceous of the Jura Mountains (Switzerland and France): Geologica Croatica, v. 56, no. 1, p. 1-18.

Thompson, D.J., 1982, Spectrum estimation and harmonic analysis: Institute of Electrical and Electronics Engineers, proceedings, v. 10, p. 1055-1096.

Thompson, D.J., 1990, Time series analysis Holocene climate data: Royal Society (London), Philosophical Transactions, v. A 330, p. 601-616.

Tudhope, A.W., 1989, Shallowing-upwards sedimentation in a coral reef lagoon, Great Barrier Reef of Australia: Journal of Sedimentary Petrology, v. 59, no. 6, p. 1036-1051.

Vail, P.R., Mitchum Jr., R.M., Thompson III, S., 1977, Seismic stratigraphy and global changes of sea level, part 4: Global cycles of relative changes of sea level: *in* Payton, C.E., ed., Seismic Stratigraphy – Applications to Hydrocarbon Exploration: American Association of Petroleum Geologists Memoir 36, p.83-97.

Van de Plassche, O., van der Borg, K., and de Jong, A.F.M., 1998, Sea level-climate correlation during the past 1400 yr: Geology, v. 26, no. 4, p. 319-322.

Venzo, G.A., and Fuganti, A., 1965, Il Trias della Mendola (Trentino – Alto Adige): Studi Trentini di Scienze Naturali, Sez. A, Vol. XLII, N. 1, p. 55-86.

Wright, V.P., 1992, Speculations on the controls on cyclic peritidal carbonates: Ice-house versus greenhouse eustatic controls: Sedimentary Geology, v. 76, p. 1-5.

Yang, W., and Lehrmann, D.J., 2003, Milankovitch climatic signals in lower Triassic (Olenekian) peritidal carbonate successions, Nanpanjiang Basin, South China: Paleogeography, Paleoclimatology, Paleoecology, v. 201, p. 283-306.

Zühlke, R., 2004, Integrated cyclostratigraphy of a model Mesozoic carbonate platform - the Latemar (Middle Triassic, Italy). in D´Argenio, B., Fischer, A., Premoli Silva, I. and Weissert, H., eds., Multidisciplinary Approach to Cyclostratigraphy: Society for Sedimentary Geology, Special Publication 44.

Zühlke, R., Bechstädt, T., and Mundil, R., 2003, Sub-Milankovitch and Milankovitch forcing on a model Mesozoic carbonate platform – the Latemar (Middle Triassic, Italy): Terra Nova, v. 15, no. 2, p. 69-80.

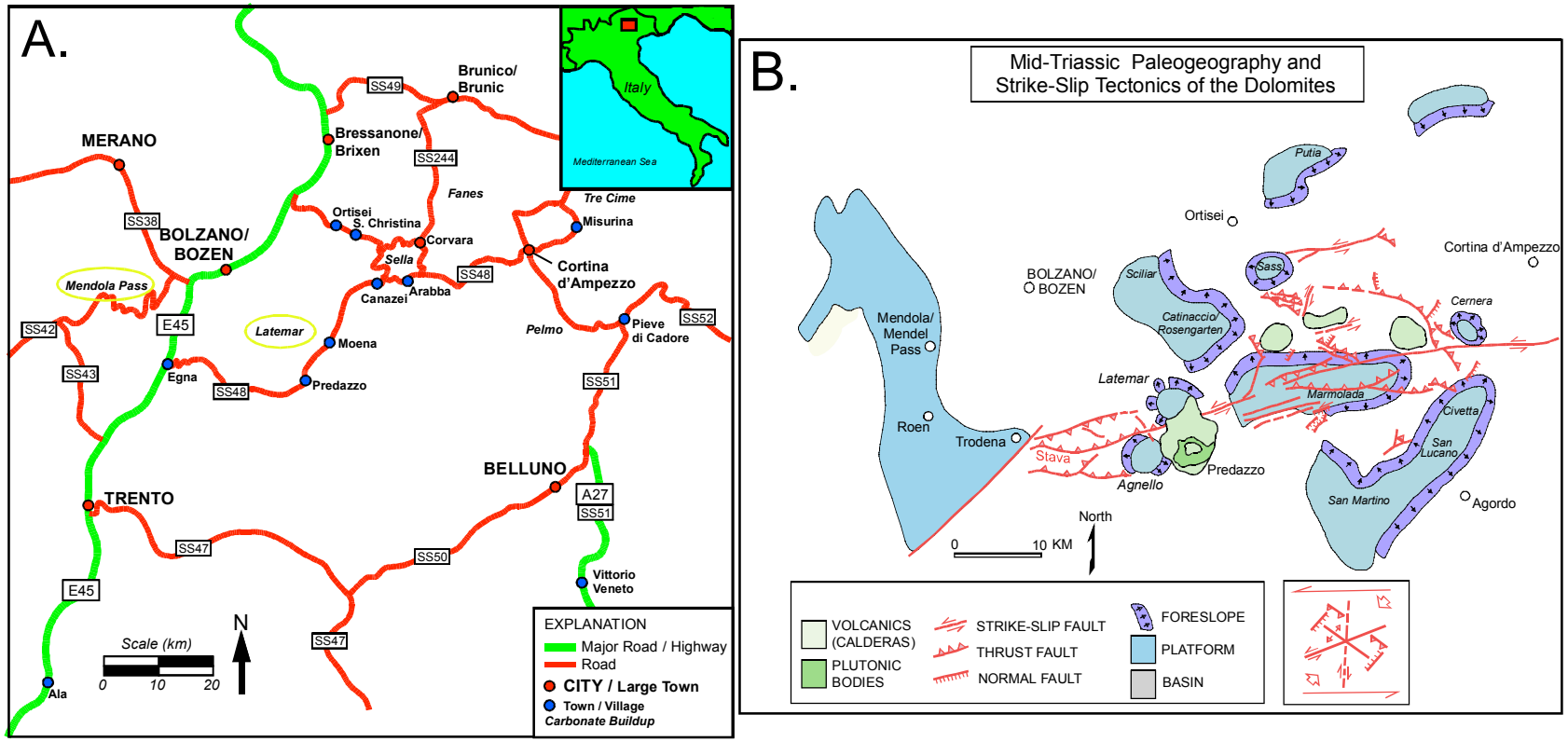

Figure 3.1. A. Location and road map for Dolomites region showing the locations of both the Latemar platform and Mendola Pass. B. Paleogeography of mid-Triassic carbonate platforms in the Dolomites.

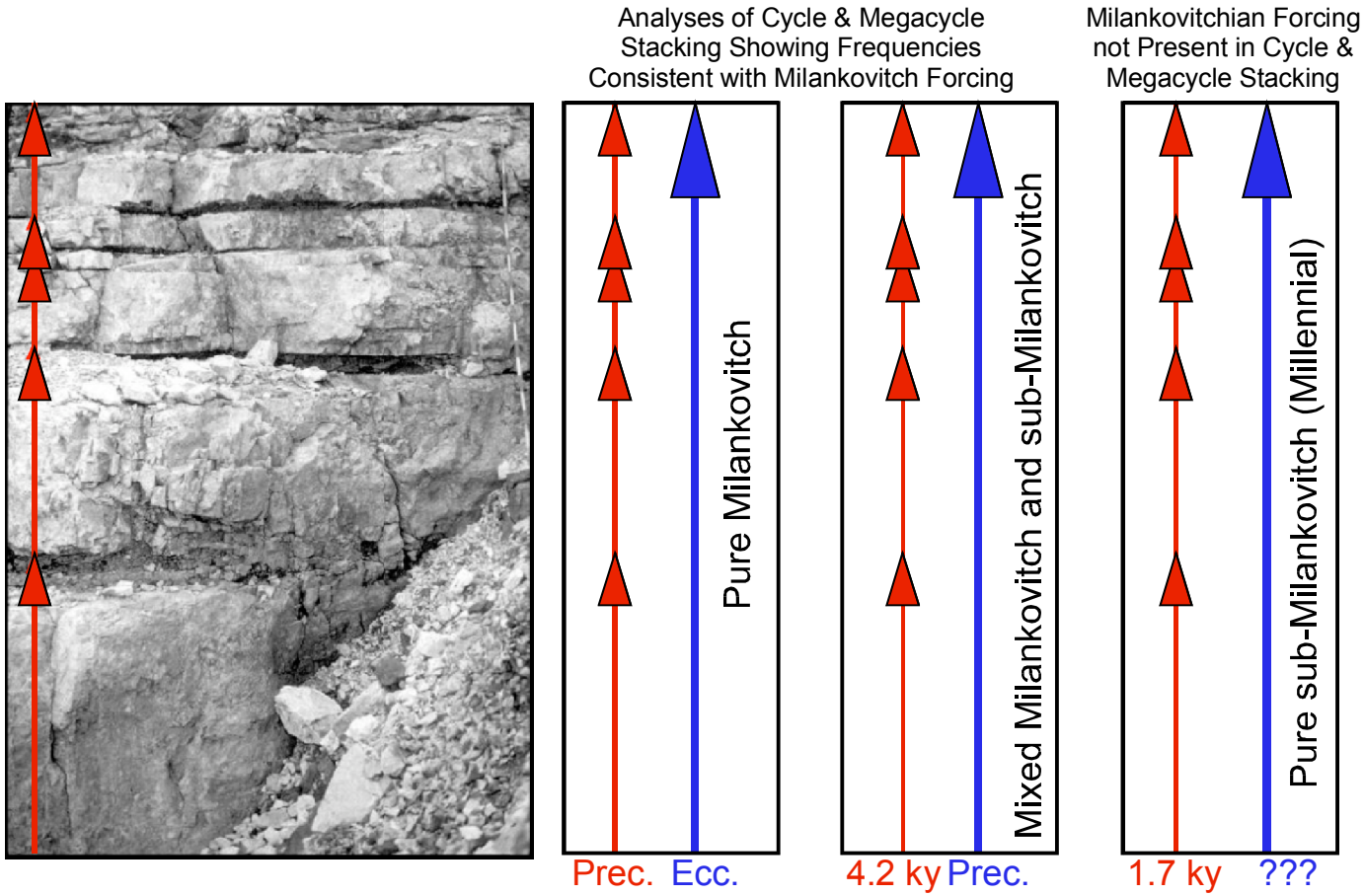

Figure 3.2. Comparison of proposed cyclic driver periodicities for individual cycles and megacycles at the Latemar. Both “Pure Milankovitch” (e.g., Goldhammer et al., 1987; Preto et al., 2004) and “Mixed Milankovitch and sub-Milankovitch” (e.g., Zühlke, 2004) interpret Milankovitchian composite eustasy to have influenced the development of Latemar cycle stacking. The millennial model does not recognize the influence of Milankovitchian forcing on the development of cycles or megacycles at the Latemar. (Note: “Prec” refers to the Precession, and “Ecc.” refers to the Eccentricity.)

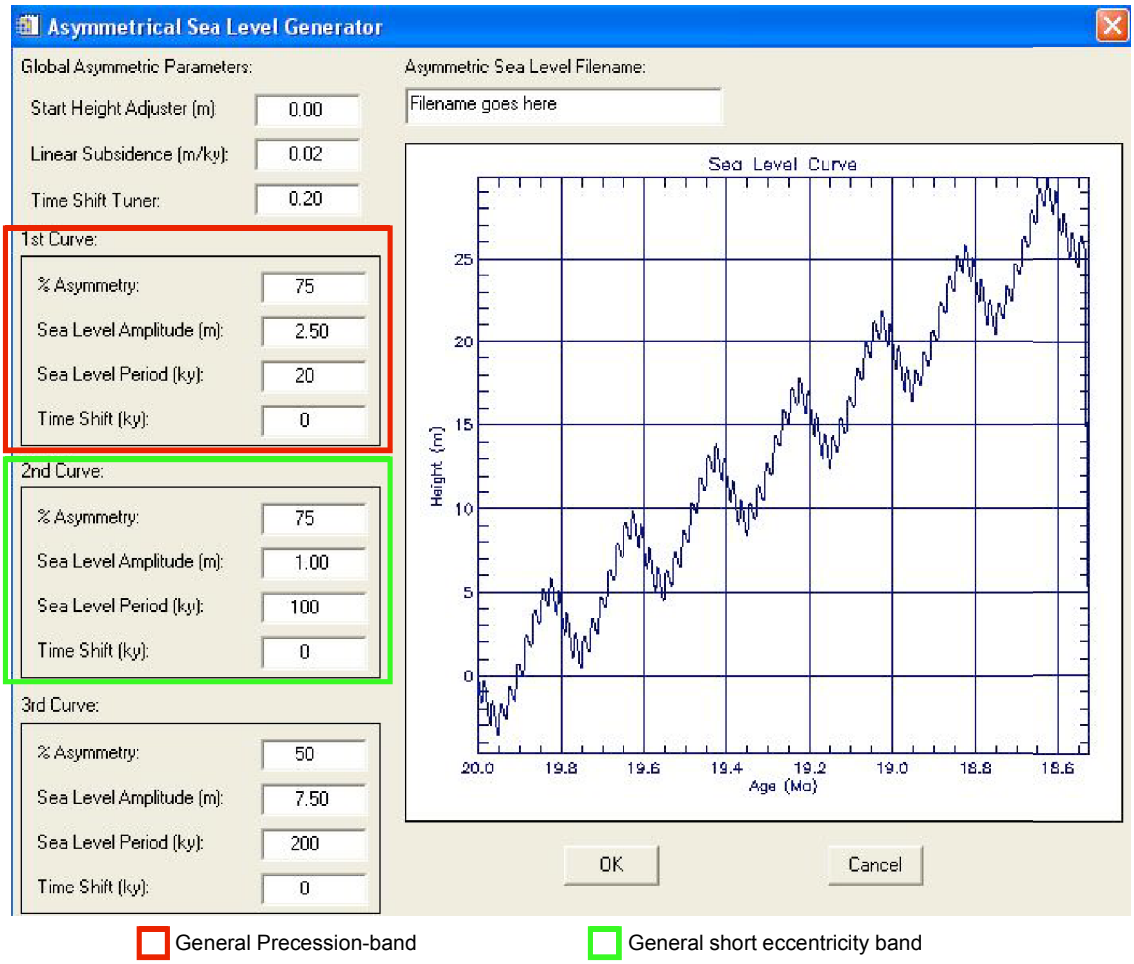

Figure 3.3. Default parameters for sea level oscillations in Carb 3d+ that show reflect the influence of studies suggesting a relationship between sea level change, astro-climatic forcing, and carbonate sedimentation. These input parameters are pre-defined in the program, but can be changed as the user deems necessary. Unfortunately, only three curves can be input in this interface.

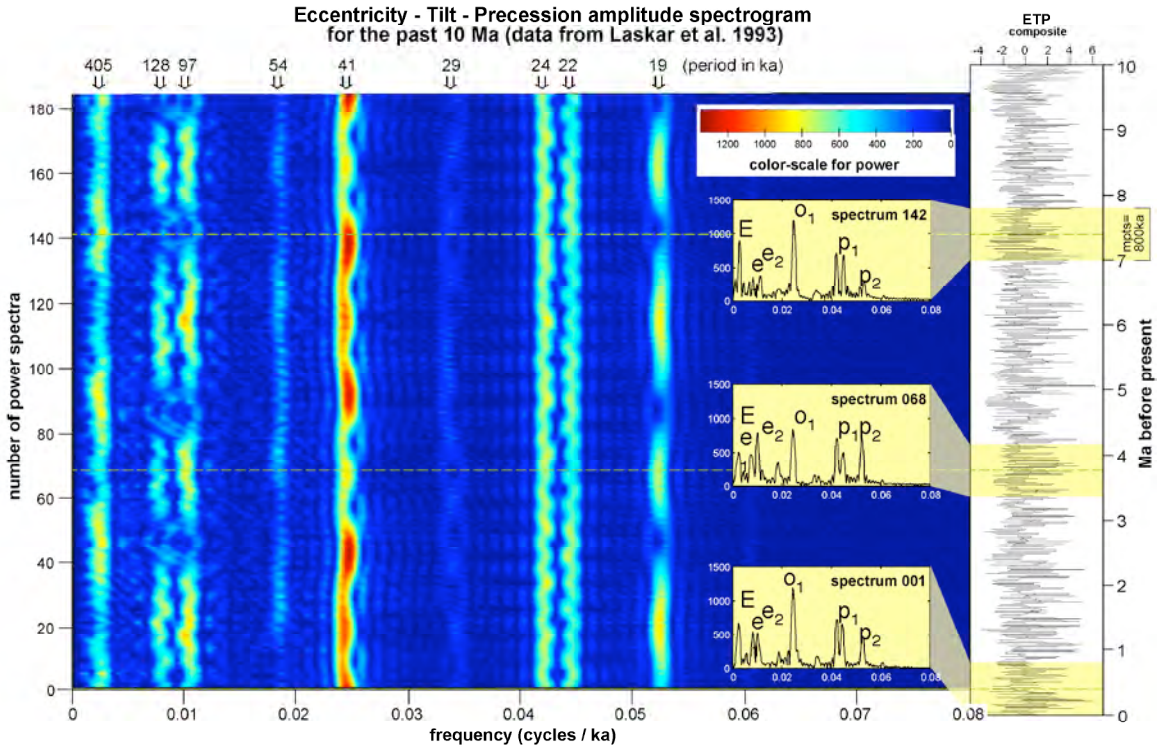

Figure 3.4. Time-frequency landscape (map) view of orbital cycles (eccentricity, obliquity and precession) modeled for the past 10 m.y. courtesy of F. Maurer and L. Hinnov (unpub.). The ETP curve on the right is the sum of standardized eccentricity (E), obliquity (or tilt, T), and precession (P). For the purposes of this study, this diagram serves to illustrate the multiple periodicities and power modulations (density of the spectrum) that the full suite of Milankovitch cycles contains. The frequency content of the cycles are modulated though time, with relative power increasing or decreasing as a function of lower-frequency modulations (see the 3 yellow spectra).

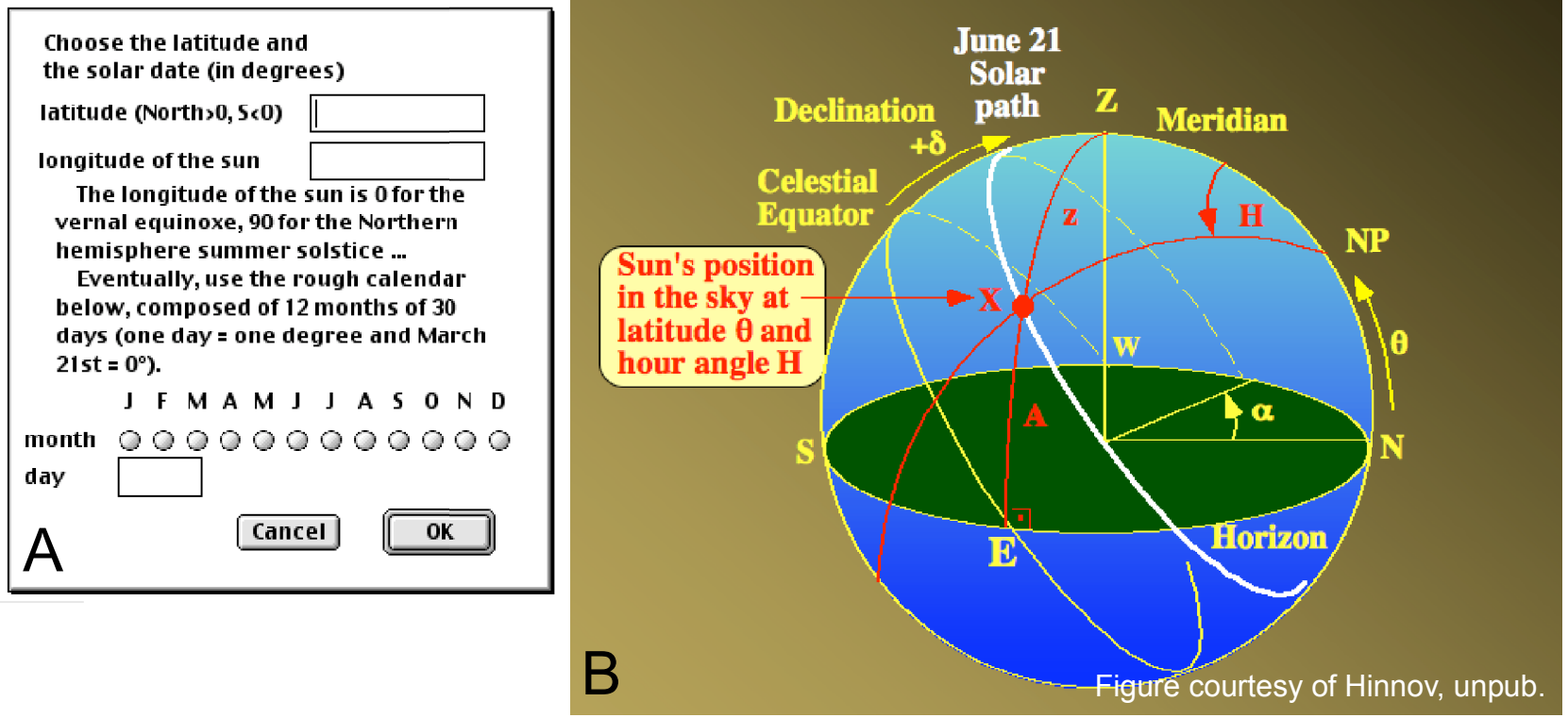

Figure 3.5. Input interface and explanation for generating orbitally forced insolation curves in AnalySeries A. Input window from AnalySeries v 1.2 showing input for latitude and longitude. The longitude entry actually relates to a relative "solar path" in the local sky as a function of season (shown in B), which is at a maximum distance from the celestial equator at solstices (June 21st and December 22nd) and at the celestial equator during the equinoxes (March 21st and September 23rd). Therefore, the date chosen for input in AnalySereies relates to a position on the Earth's surface at which insolation will be calculated.

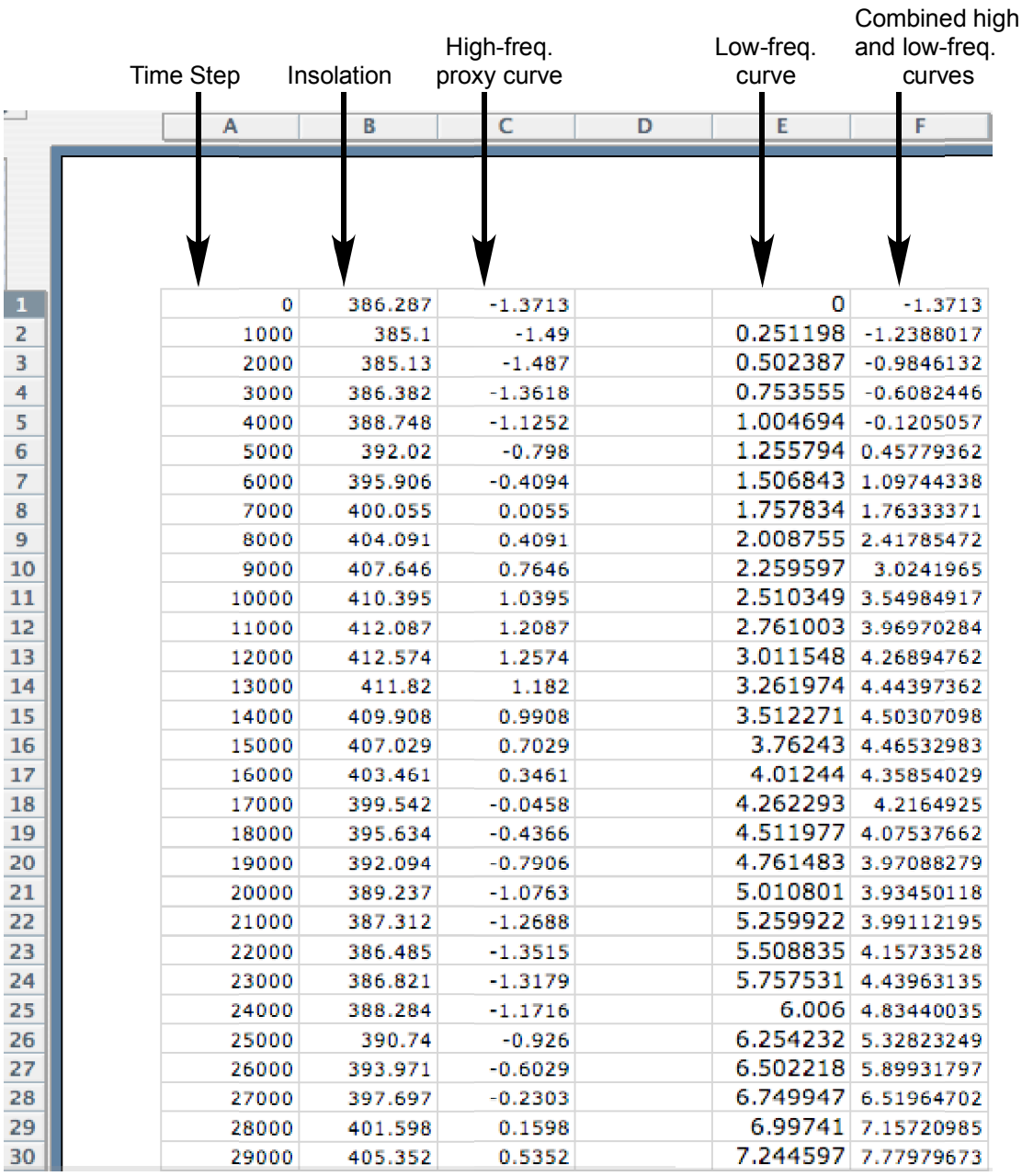

	A	B	C	D	E	F
1	0	386.287	-1.3713		0	-1.3713
2	1000	385.1	-1.49		0.251198	-1.2388017
3	2000	385.13	-1.487		0.502387	-0.9846132
4	3000	386.382	-1.3618		0.753555	-0.6082446
5	4000	388.748	-1.1252		1.004694	-0.1205057
6	5000	392.02	-0.798		1.255794	0.45779362
7	6000	395.906	-0.4094		1.506843	1.09744338
8	7000	400.055	0.0055		1.757834	1.76333371
9	8000	404.091	0.4091		2.008755	2.41785472
10	9000	407.646	0.7646		2.259597	3.0241965
11	10000	410.395	1.0395		2.510349	3.54984917
12	11000	412.087	1.2087		2.761003	3.96970284
13	12000	412.574	1.2574		3.011548	4.26894762
14	13000	411.82	1.182		3.261974	4.44397362
15	14000	409.908	0.9908		3.512271	4.50307098
16	15000	407.029	0.7029		3.76243	4.46532983
17	16000	403.461	0.3461		4.01244	4.35854029
18	17000	399.542	-0.0458		4.262293	4.2164925
19	18000	395.634	-0.4366		4.511977	4.07537662
20	19000	392.094	-0.7906		4.761483	3.97088279
21	20000	389.237	-1.0763		5.010801	3.93450118
22	21000	387.312	-1.2688		5.259922	3.99112195
23	22000	386.485	-1.3515		5.508835	4.15733528
24	23000	386.821	-1.3179		5.757531	4.43963135
25	24000	388.284	-1.1716		6.006	4.83440035
26	25000	390.74	-0.926		6.254232	5.32823249
27	26000	393.971	-0.6029		6.502218	5.89931797
28	27000	397.697	-0.2303		6.749947	6.51964702
29	28000	401.598	0.1598		6.99741	7.15720985
30	29000	405.352	0.5352		7.244597	7.77979673

Figure 3.6. Example dataset used to generate Charts 1-4. Data in columns A & B were pasted directly from AnalySeries v.1.2. Data in column 3 were calculated from the data in column be and werere-centered and given +/- 5m maxima and minima (see text for explanation) using the formula "=((400-B1)/10)" which was then filled down the column. Data in column E are for a low-frequency curve with an amplitude of 40 m and period of 1 my, and was defined using the timesteps in column A. The formula used to generate the data in column E was "=40*(SIN((A1:A1)*0.00000628))" which was then filled down the column. Column F is the data for the combined low and high-frequency curves and is a sum of columns C and E.

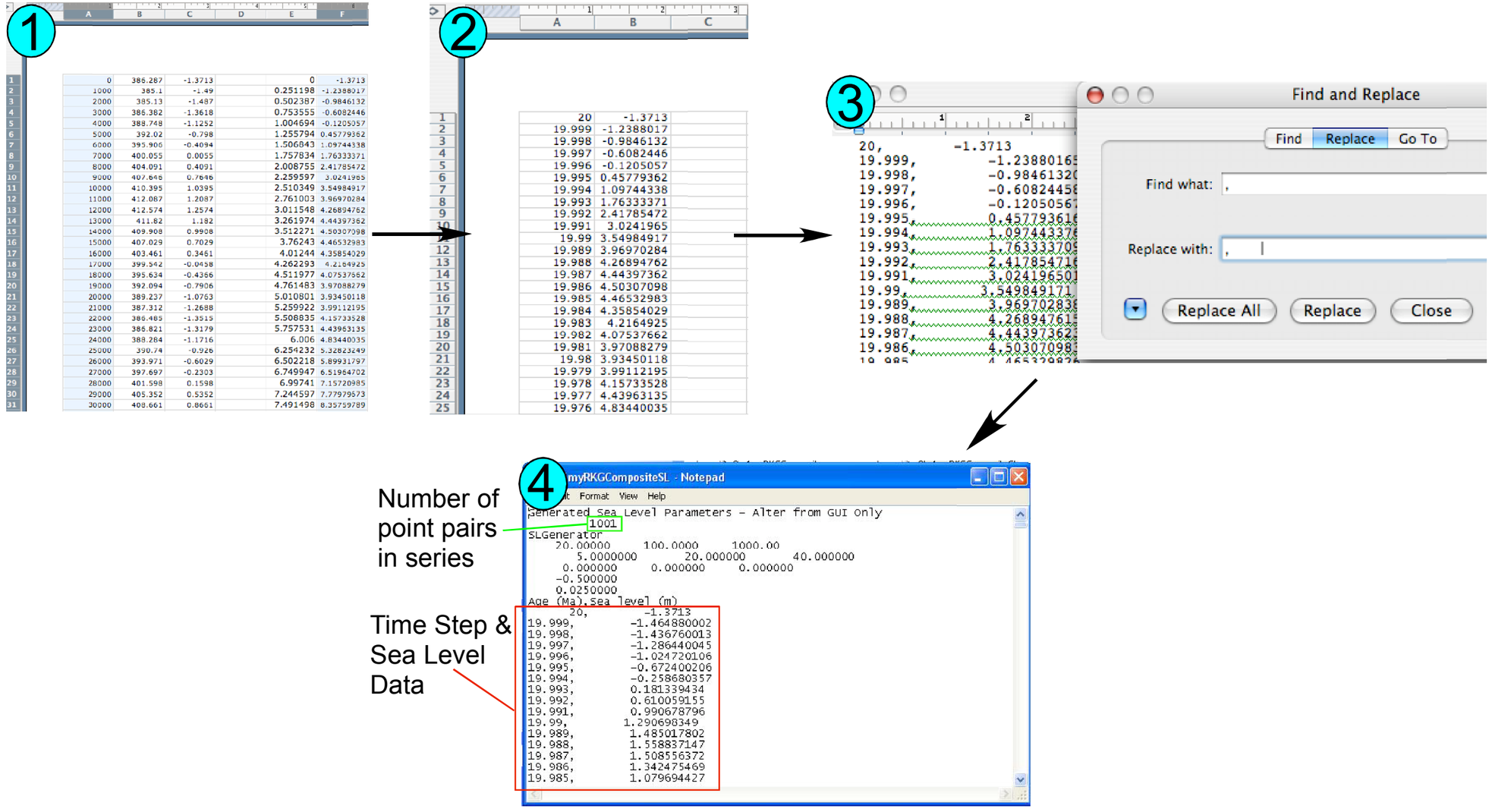

Figure 3.7. Flow chart depicting the method by which one can load externally generated sea level data into Carb 3d+. The method is as follows: 1) Once you have the final composite curve data points generated, copy the series (in the example this would be the data in column F. 2) Open a new Excel worksheet and paste the data in column B. In column A, you must write a new time step series counting down from 20 (x 1 million years) through the data series. The new time steps must be at the same frequency as that used to initially calculate the insolation series. AnalySeries calculates the insolation curve from the present time into the past, and Carb 3d+ will model from the past into the future, so the ordering of the time steps must be reversed as shown in the screen shot 2. 3) Save the data as a comma delimited (.csv) file. Open the .csv file in a text editor. Use the "replace" command to replace all commas with a comma followed by 8 spaces. 4) Open a copy of any sea level file that you choose from any Carb 3d+ project file. Highlight the time step and sea level data in the .slv file and delete it. Then paste in your time step and sea level data in the same location (red box area in screen shot 4). Be sure to also change the number of data point pairs in the series to reflect the number of point pairs in the series you just pasted in (green box area in screen shot 4). All other information in the file can remain the same. Hit the save button, then re-name the file in after saving, making sure it is still a .slv file. The file is now ready to be used by Carb 3d+.

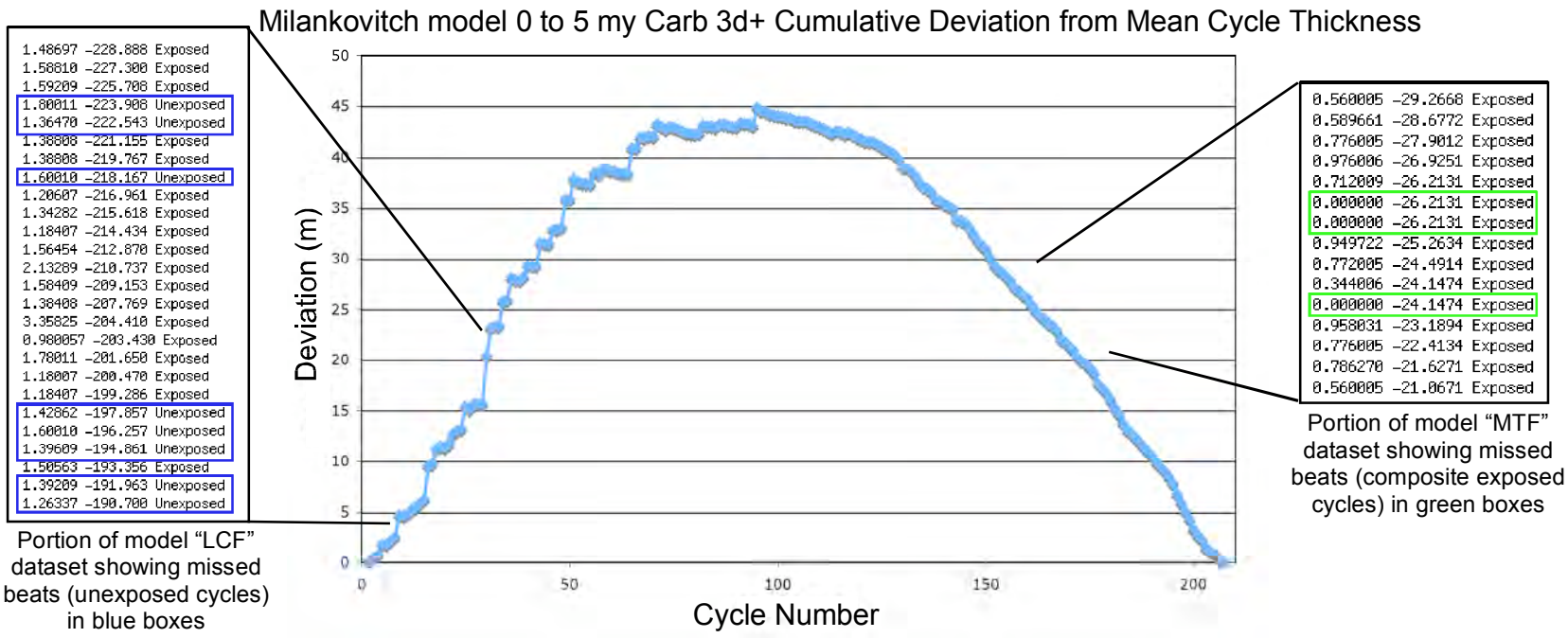

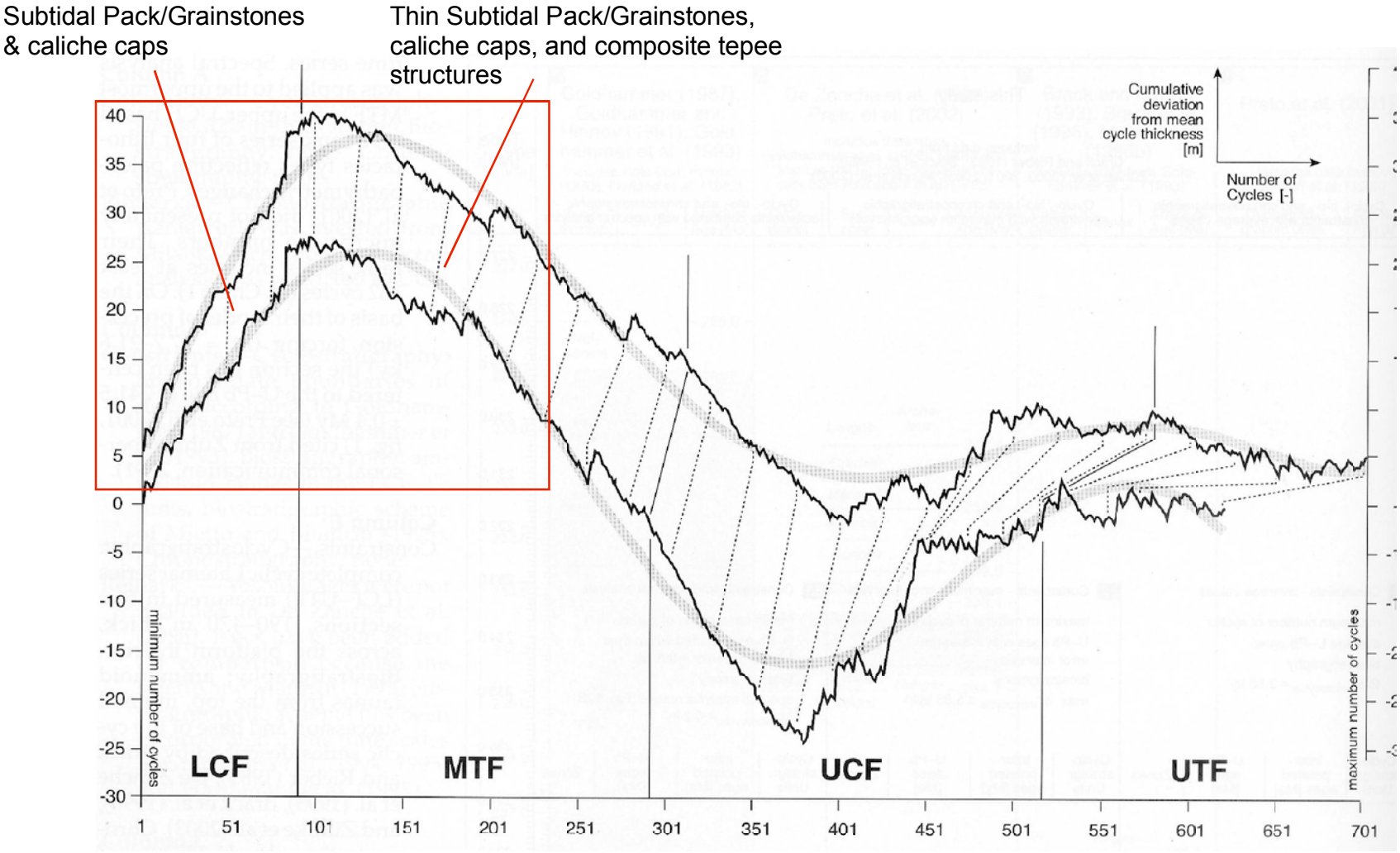

Fischer plot of entire Latemar cyclic series at Cimon del Latemar (North Latemar) from Zuehlke, (2004)

Figure 3.8. Fischer plots of Latemar data. Top) Fischer plot of Milankovitch model exposed cycle data generated in Carb 3d+. Bottom) Measured section data from the entire Latemar cyclic series from Zuehlke (2004). The two curves represent maximum and minimum cycle thickness relative the recognition of true cycle caps. The red box approximates the equivalent series modeled in Carb 3d+. During accommodation gain, thicker bundles result from composite rises in sea level, as do "missed beats" of rhythmic sea level oscillatory touchdown, yielding the slight asymmetry present in both curves (steeper rise than fall) during the LCF (lower cyclic facies). During long term accommodation loss, cycles become thinner and missed beats may also occur due to sealevel high frequency sea level rise amplitudes being overcome by long term fall and being unable to flood the platform.

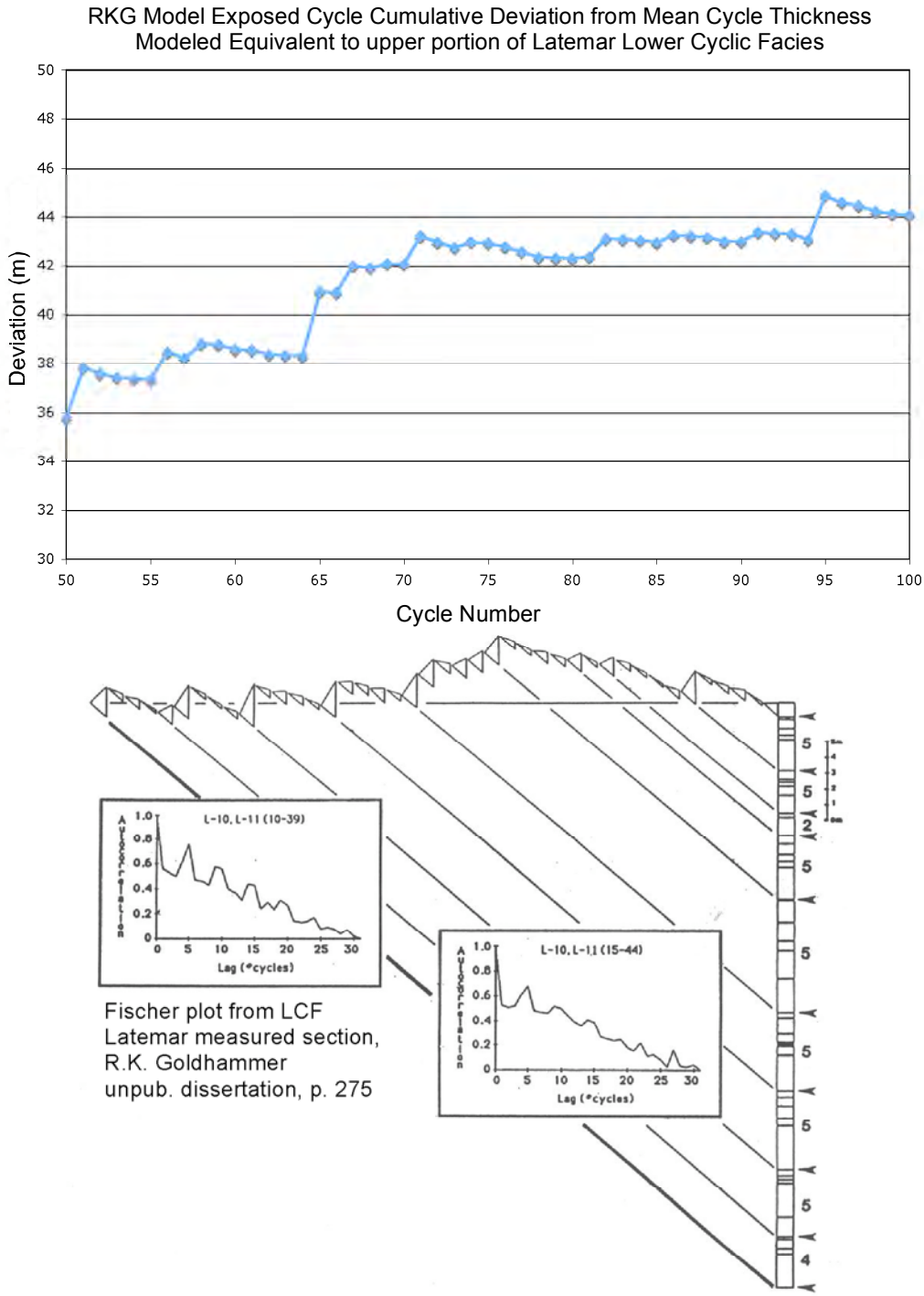

Figure 3.9. Comparison of Fischer plots from "Lower Cyclic Facies" in both Milankovitch modeled output data (top) and Latemar measured section data from Cima Forcellone (West Latemar) (bottom). High-frequency stacking trends show clear similarities in overall stacking trends, including asymmetric bundling of cycles into groups of appx. 5. This is an important point, because while the modeled cycles show an asymmetrical stacking pattern, the sea level driver that formed them was not asymmetric.

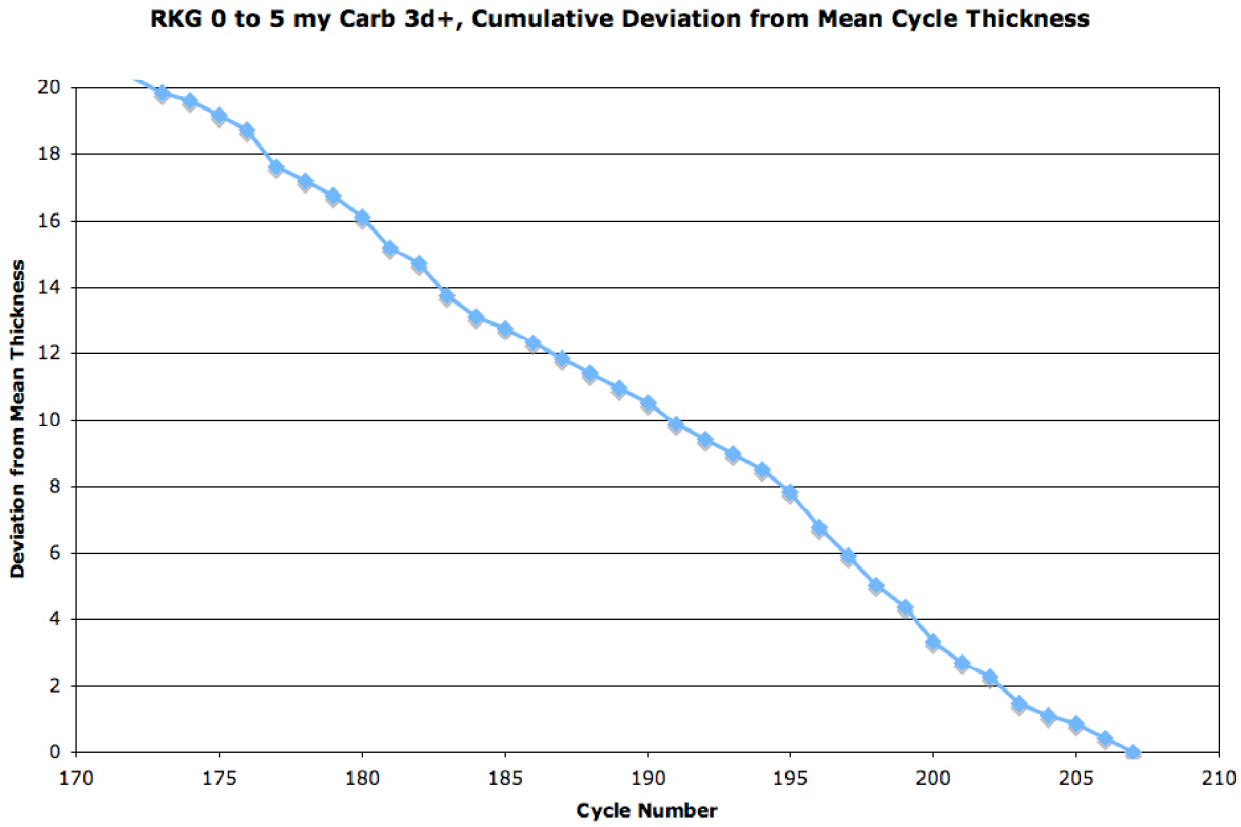

Figure 3.10. Fischer plot from Carb 3d+ run using the Goldhammer model. This portion of the larger scale Fischer plot is commensurate with “Middle Tepee Facies” of Goldhammer et al., (1987) (see Figure 8). Facies within this interval are thin, condensed, accommodation limited cycles with multiple missed beats of rhythmic sea level touchdown resulting from overall low-frequency accommodation loss overpowering the high frequency driver’s ability to make space. At the Latemar, facies in this interval are commonly altered by early marine/vadose diagenesis into composite tepee zones.

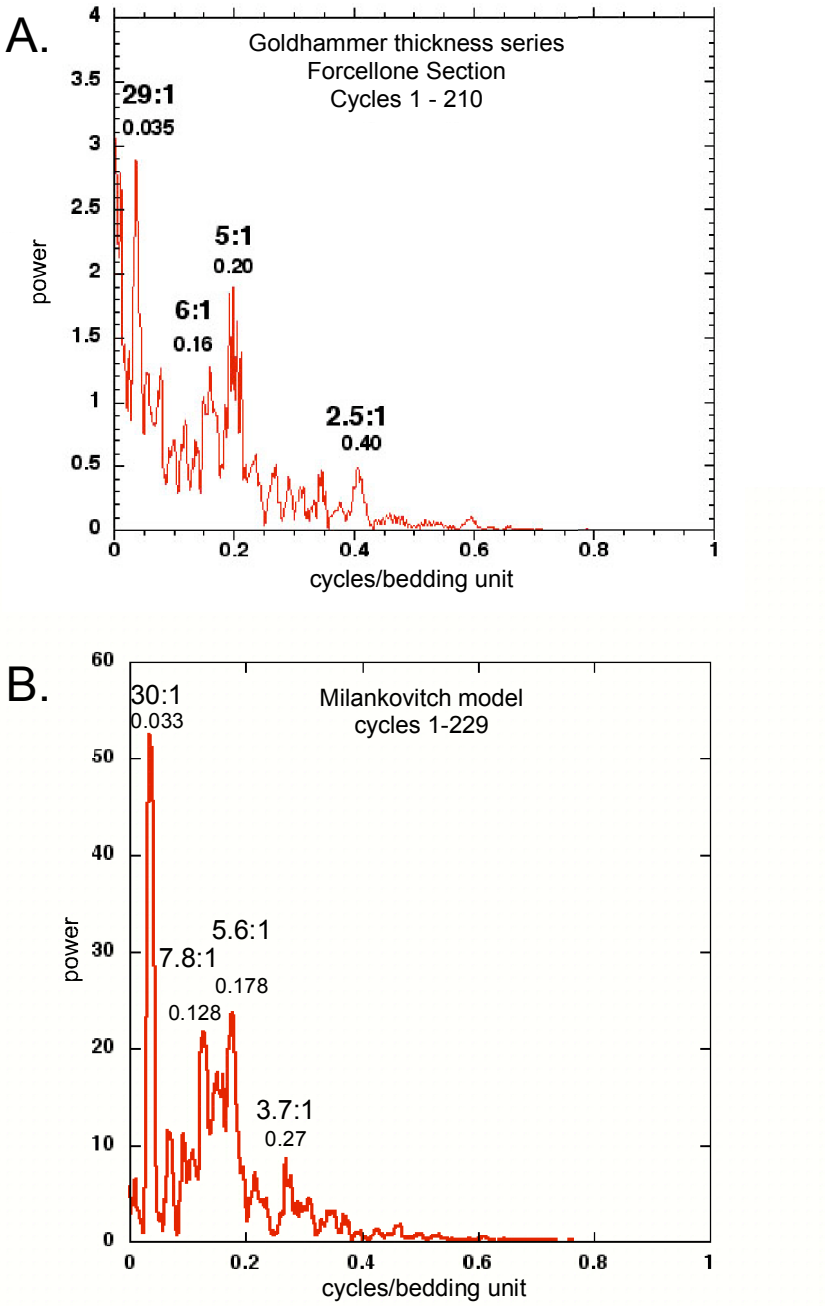

Figure 3.11. Comparative spectra of cycle thickness series measurements from: A. Latemar measured section cycle thickness data for lower cyclic facies and middle tepee facies (210 cycles total). Data from Cima Forcellone section measured by R.K. Goldhammer (1987), and B. Carb 3d+ Milankovitch / sub-Milankovitch model output cycle thickness data for the first half of the third order wave (in this case 229 total cycles occupying the same stratigraphic position as the lower cyclic facies and middle tepee facies of Goldhammer, 1987). Bundling patterns are quite similar in both examples. However, model output data counts all shallowing-upward facies successions as a cycle, even if the cycle lacks a subaerial exposure cap. Goldhammer's (1987) section only counted cycles with exposure caps. As a result, the Milankovitch model spectral power is shifted towards lower frequencies (as compared to the measured section data), as a greater number of cycles are counted per megacycle.

A.

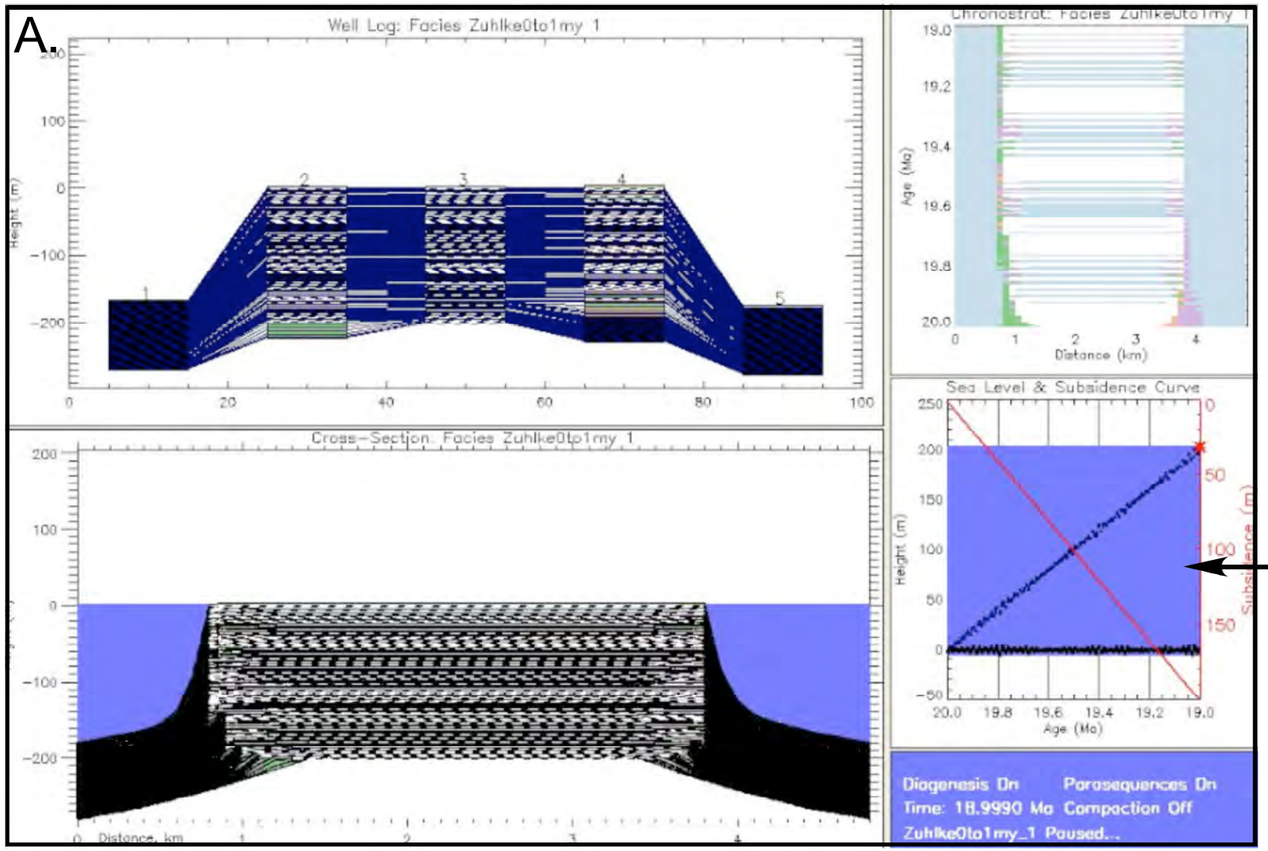

No 3rd-order scale oscillation assumed. Instead, differential subsidence is assumed, but cannot be modeled in Carb 3d+ as of yet.

B.

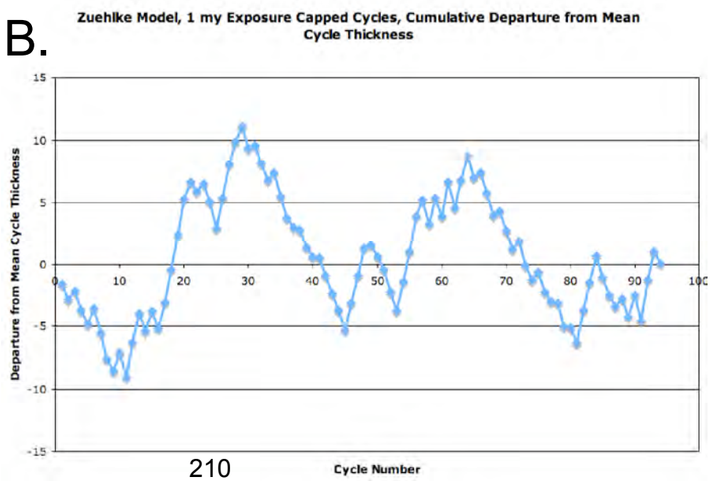

Figure 3.12. A. Carb 3d+ model of the Latemar platform using the input parameters of Zuhlke / Heidelberg group (Milankovitch / sub-Milankovitch model). Several problems exist with this model when comparing the output dataset to real Latemar stratigraphy. Most of these problems stem from the non-inclusion of differential subsidence or a 3rd-order sea level oscillation in the inputs. Problems in output data include too few exposed cycles generated for a time scale that ought to equal half of the history of the platform (see Fischer plot at right- over 200 cycles are expected). B. Fischer plot of cycle data does not produce the slightly asymmetric bell-shaped curve that is expected, but rather appears to reflect modulations in long and short eccentricity drivers. Changing amplitudes of high-frequency sea level oscillations as well as sedimentation rates may improve the output dataset.

A.

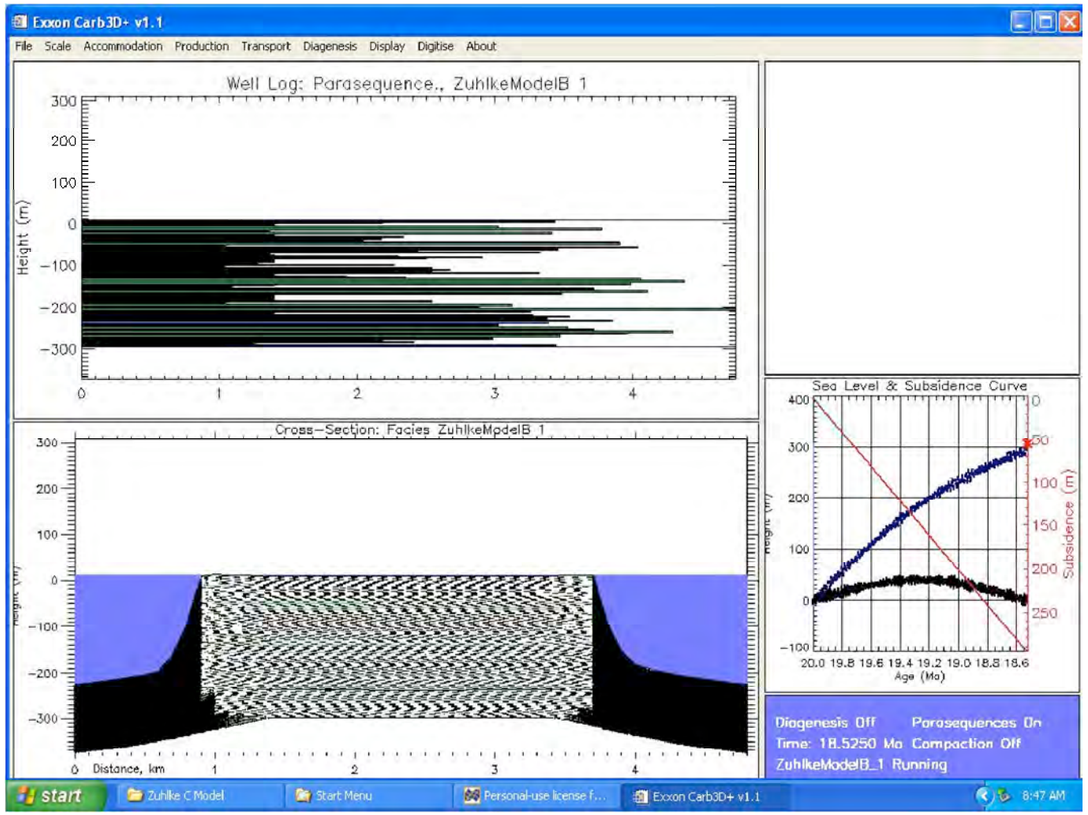

B.

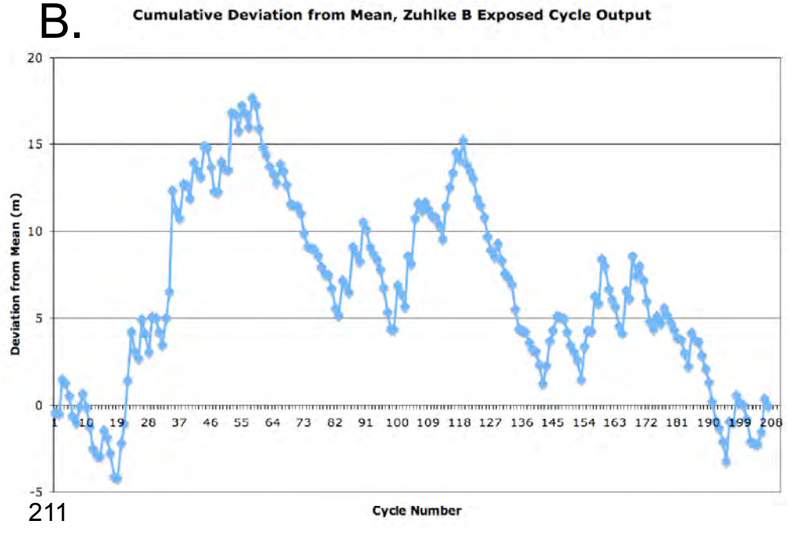

Figure 3.13. A. Screenshot and B. Fischer plot of Milankovitch / sub-Milankovitch model B data. The inclusion of a 3rd-order driver aided generating a more accurate dataset with respect to real-rock stratigraphy. However, a Fischer plot (B) of exposed cycles still lacks a pronounced bell-shaped accommodation trend as shown from real-rock measurements. This may have to do with the relatively large amplitudes of highest-frequency oscillations (+/- 5 m). Further tests were performed with +/- 2.5 m amplitudes.

A.

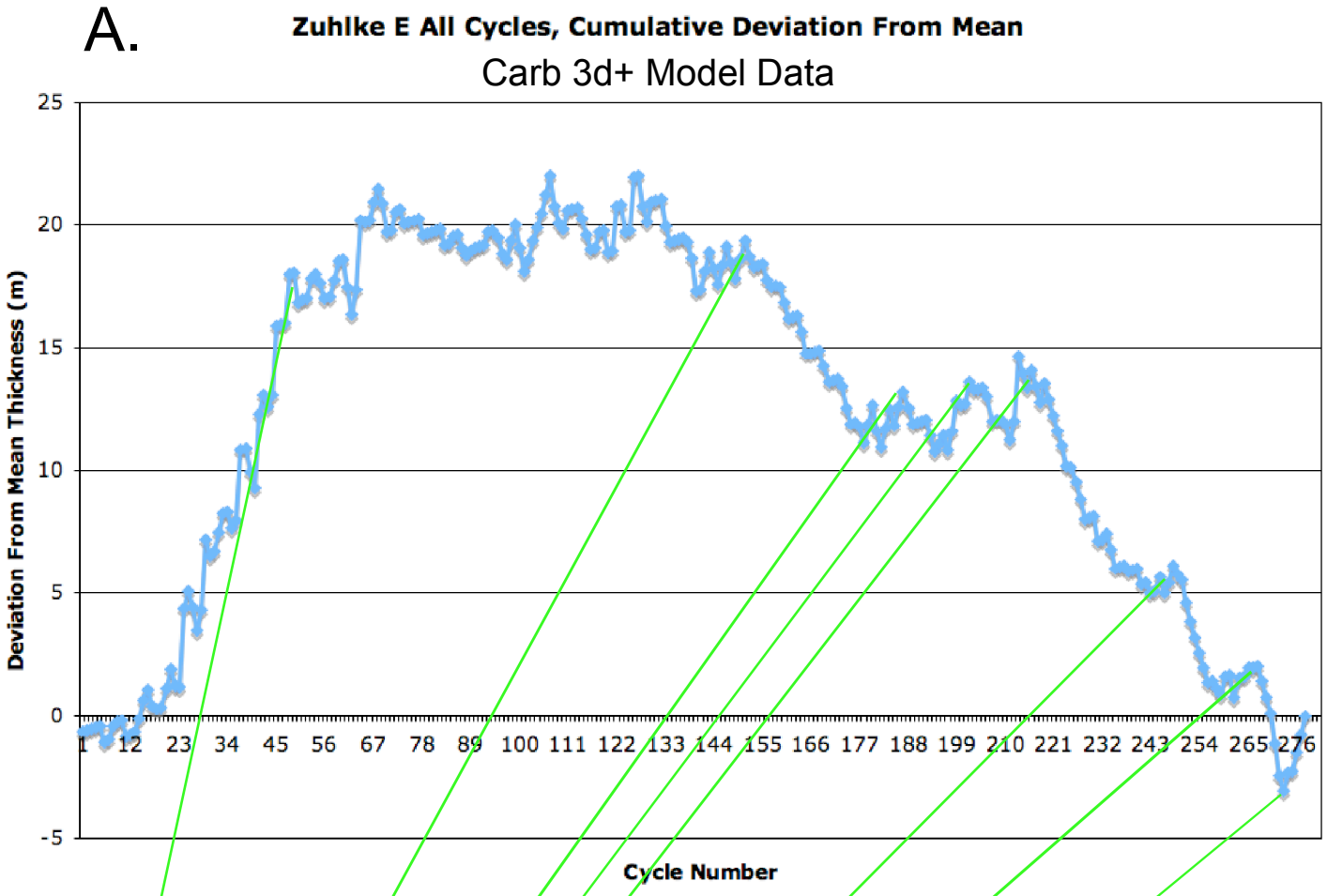

B.

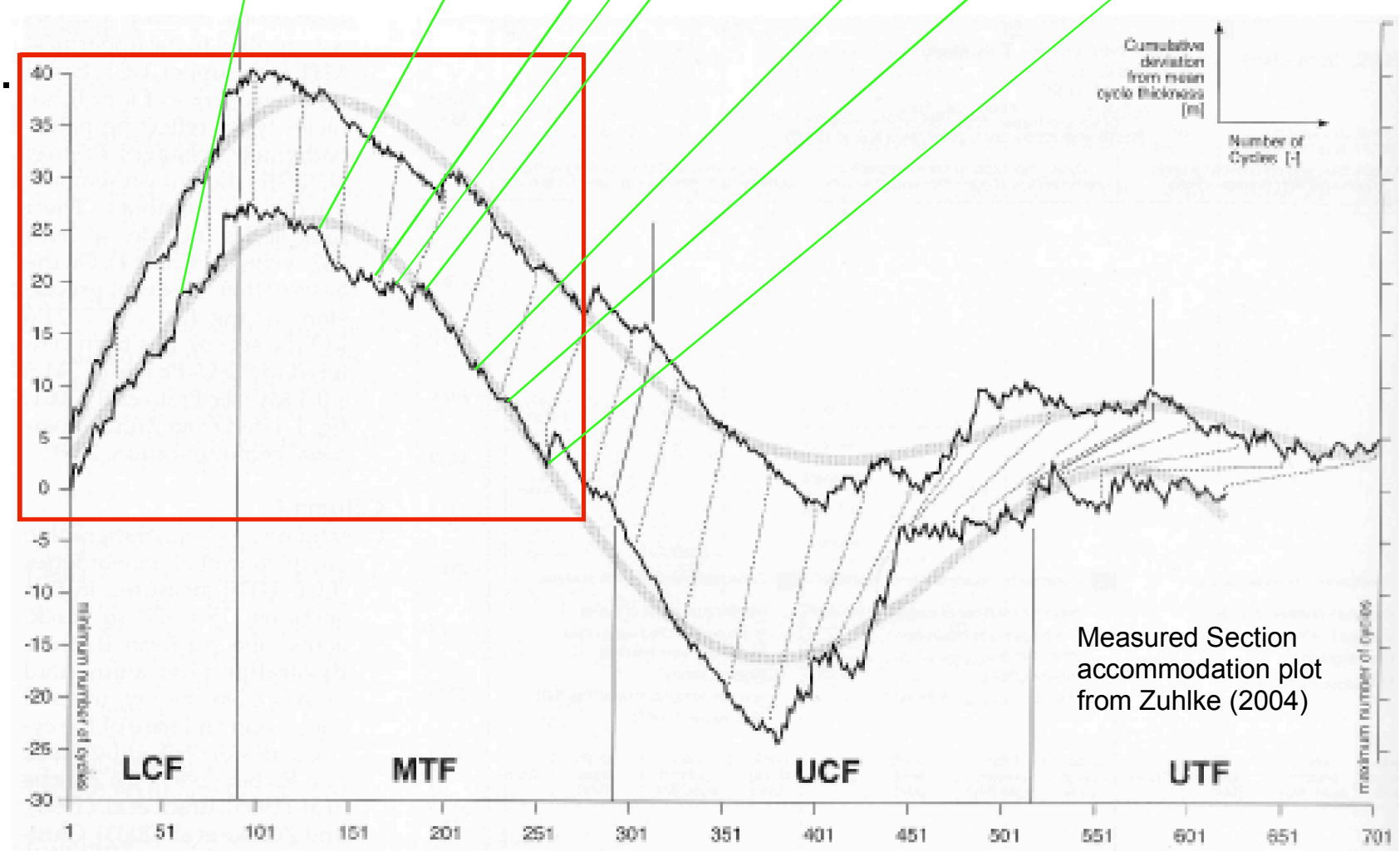

Figure 3.14. A. Accommodation plot from Zuehlke E Model and B. Latemar measured section. Model accommodation plot includes all cycles (parasequences) regardless of having exposed tops. Many similarities exist in accommodation trends between plots (highlighted), which again suggests the possibility of a theoretical match between model drivers in Zuhlke Model E and actual rock.

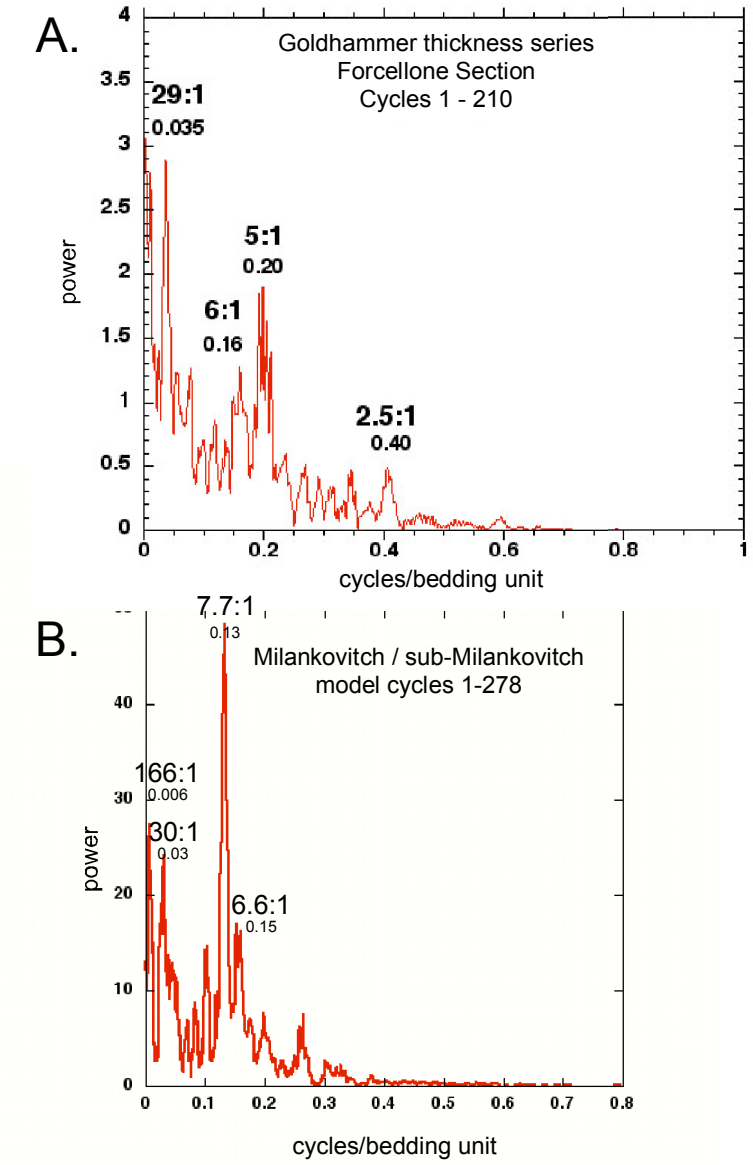

Figure 3.15. Comparative spectra of cycle thickness series measurements from: A. Latemar measured section cycle thickness data for lower cyclic facies and middle tepee facies (210 cycles total). Data from Cima Forcellone section measured by R.K. Goldhammer (1987), and B. Carb 3d+ Milankovitch / sub-Milankovitch model output cycle thickness data for the first half of the third order wave (in this case 278 total cycles occupying the same stratigraphic position as the lower cyclic facies and middle tepee facies of Goldhammer, 1987). The Milankovitch / sub-Milankovitch model spectrum differs from the measured section data in many ways. In the measured section spectrum, the 29:1 peak is dominant, followed by the 5:1 and 6:1 pair. In the model spectrum, the 30:1 peak (likely commensurate with the 29:1 peak) is not as strong, and the 5:1 and 6:1 pair are replaced by a 7.7:1 and 6.6:1 pair with the 7.7:1 peak dominant over the entire series. By comparing the two spectra, it is clear that the bundling present in the model output data is inconsistent with that identified at the Latemar.

A.

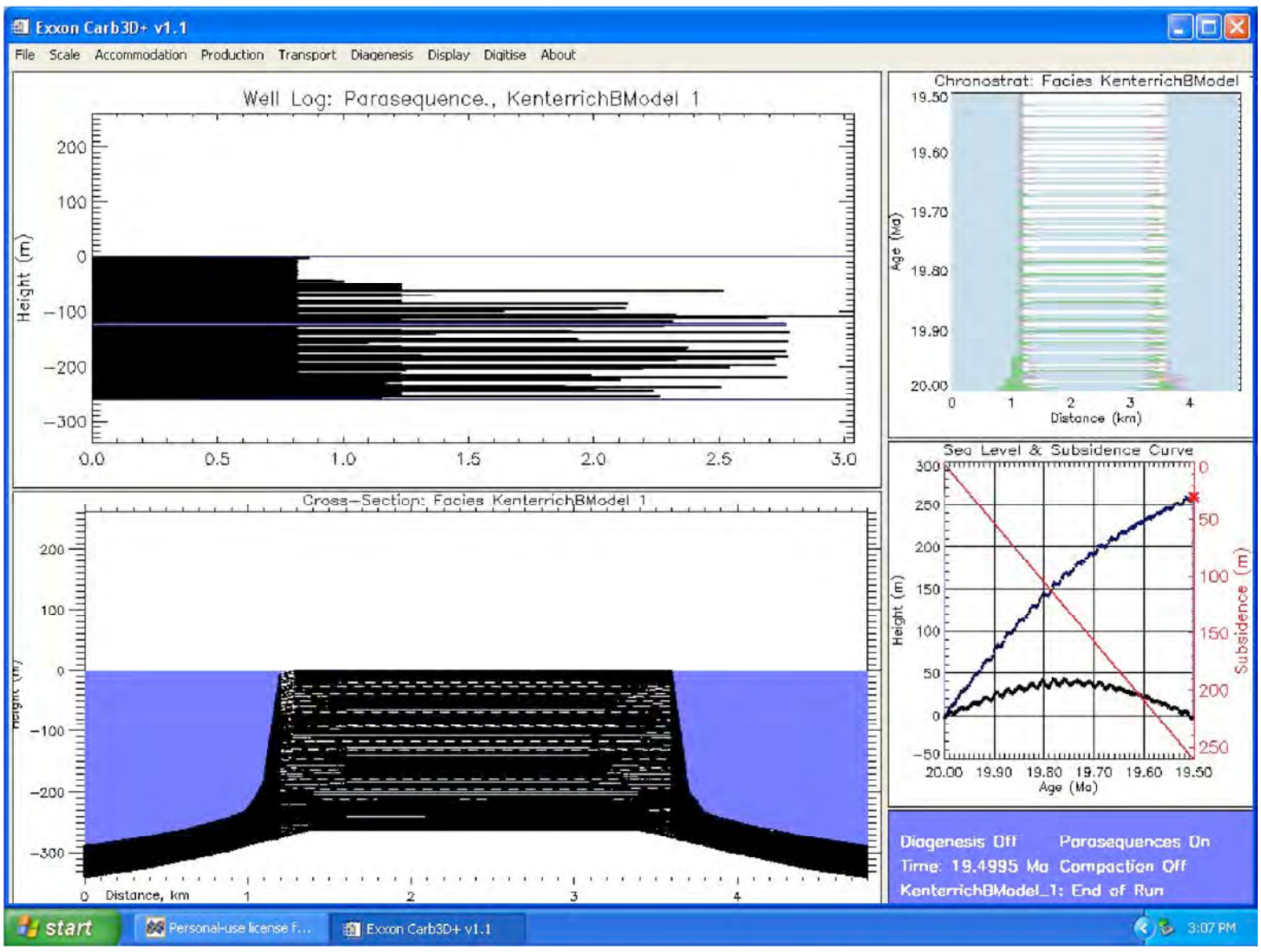

B.

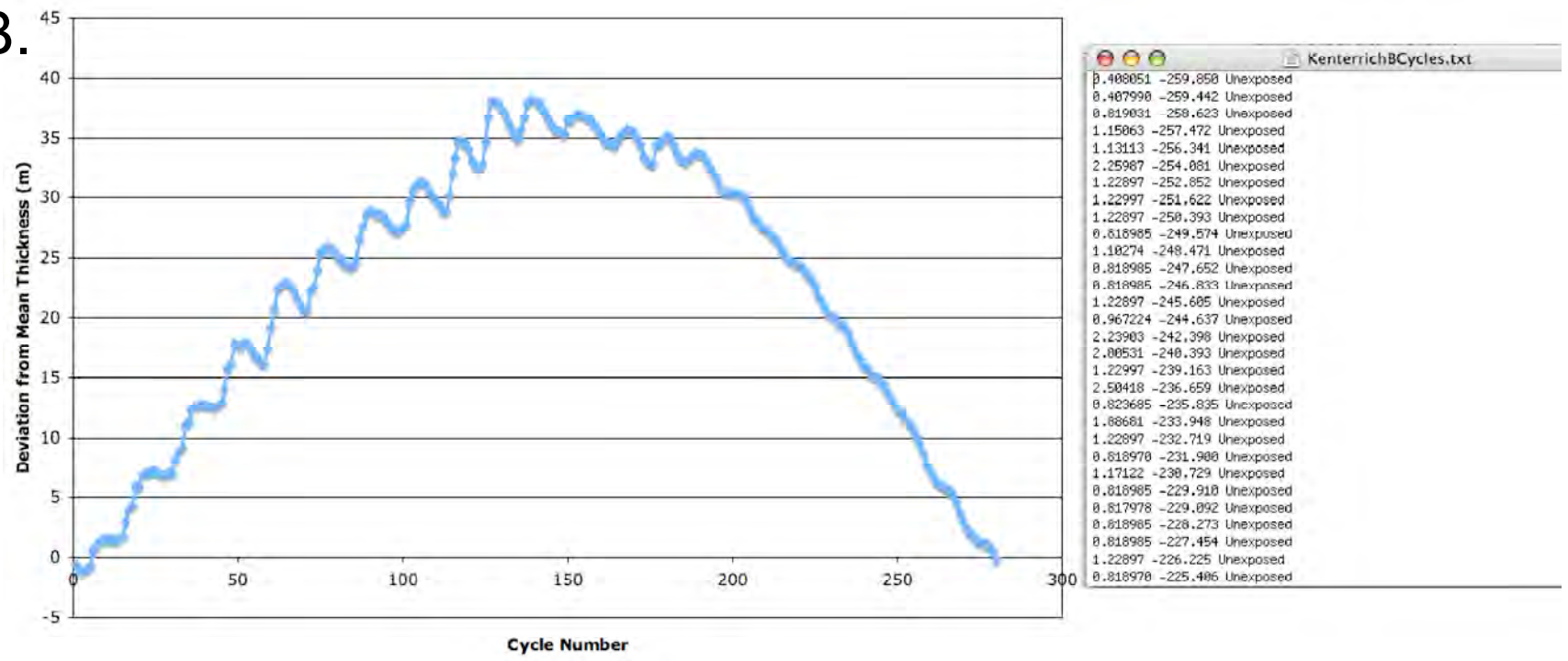

Figure 3.16. A. Screenshot of completed millennial model using modified inputs from Kent et al. (2004) and Emmerich et al. (2005). Modifications include inclusion of a Milankovitchian sea level curve (to generate bundling) and a low frequency oscillation with a total period of 1 myr and amplitude of 40 m. Also shown is B. a Fischer plot of model output data. While the general shape of the plot is consistent with the bell-shape of the true Latemar cumulative deviation from mean cycle thickness through the platform, the sawtooth appearance is not, and is a reflection of the precession modulating the high frequency 1.7 kyr cycles. These fine scale trends are at odds with Fischer plots drawn from true rock data (see Figures 12 & 18 for comparison). In addition, raw data taken from the Carb 3d+ model shows that the great majority of cycles within the millennia model are not exposure cycles. This is also inconsistent with data from measured sections at the Latemar, which suggests most of the cycles in the platform were exposed at their tops.

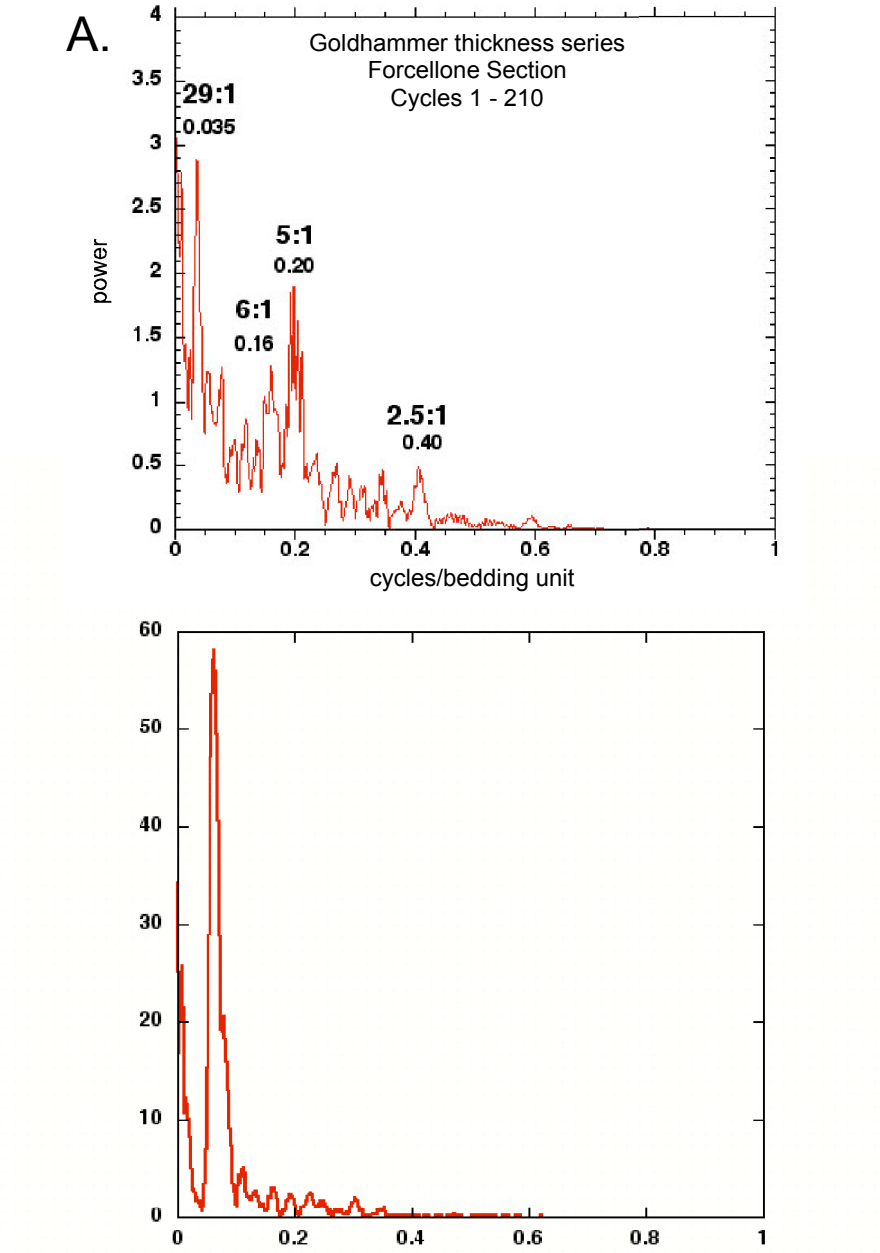

Figure 3.17. Comparative spectra of cycle thickness series measurements from: A. Latemar measured section cycle thickness data for lower cyclic facies and middle tepee facies (210 cycles total). Data from Cima Forcellone section measured by R.K. Goldhammer (1987), and B. Carb 3d+ Millennial model output cycle thickness data for the first half of the third order wave (in this case 281 total cycles occupying the same stratigraphic position as the lower cyclic facies and middle tepee facies of Goldhammer, 1987). Clearly, there is a disparity between the two plots. The model data spectrum shows most of the power concentrated at ca. 16 meters/cycle, which is likely a reflection of the bundling of the 1.7 kyr cycles into the precession, generating cycles of 12-18 cycles per megacycle. This is clearly inconsistent with the measured section spectrum from the Latemar platform.

Study	Cycle Type	Cycle Period
Roth and Reijmer, 2005	Oxygen isotope excursions in a 30 m-long core from the leeward margin of the Great Bahama Bank related to aragonite content	Multi-millennial
		1.725 kyr
		0.54 kyr
Niggemann et al., 2003	Oxygen isotope excursions in 61-cm stalagmite	ca. 1.450 kyr
Bond et al., 1993, 1997, 2001	Oxygen isotope excursions & Ice-rafted sediment cycles	1.5 kyr DO Cycle 5-6 kyr Bond Cycle
Munk et al., 2001	Tidal forcing - Milennial Scale	1.795 kyr
van de Plassche et al., 1998	Mean high water marks from Hammock River marsh, Clinton, Connecticut, USA	Century-scale

Table 3.1. Compilation of dated modern and recent climate-related cyclic processes and behaviors with millennial periodicities.

Study	Locality	Depositional Cycle Type	Age of Most Recent S.U. Succession
Strasser and Samankassou, 2003	Florida Bay Bahamas Bermuda	Variable. Shoaling, tidal flat, and subtidal facies successions.	Variable, oldest 5.63 kyr youngest 0.68 kyr
Gischler, 2003	Belize platforms	Variable. Reefal, shoaling, and subtidal facies successions.	4.5 kyr
Chappell, 2002	Huon Peninsula, Papua New Guinea	Coral Terraces	6-7 kyr
Parkinson 1989	Southwest coast of Florida	T-R cycle, capped by red mangrove peat	ca. 7 kyr
Tudhope 1989	Davies Reef, central Great Barrier Reef complex	Shallowing-up from: gravel lag; bioturbated muddy sand; shoal or exposure cap	Mid-succession sediments dated at ca. 3 kyr. Basal sediment must be older
Logan et al., 1969	Shark Bay, Western Australia	Shallowing-up from: grainstone; skel. m/w; laminite cap	ca. 5 kyr
Taft et al., 1968	New Providence Platform, Bahamas	Coarsening-up from mud; Skel. P/G; Grapestone GS	6.7 kyr

Table 3.2. Compilation of dates of modern carbonate shallowing-upward facies successions. Most have not yet filled accommodation, and none of these examples exhibit stacking of more than one shallowing-upward facies succession.

	Hopkins Group/ Goldhammer et al., (1987)	Heidelberg Group/ Zuhlke et al., (2003)	Kent et al., 2004 Emmerich et al., 2005
Cycle Periodicity	19-23 kyr	4.2 kyr	0.9 - 1.97 kyr
Amplitude	ca. 2 meters	Not defined	Not defined
Megacycle Periodicity	100 kyr	18.1 - 21.5 kyr	Not defined
Amplitude	ca. 1 meter	Not defined	Not defined
3rd Order Periodicity	10 myr	Not defined	Not defined
Amplitude	ca. 60 meters	Not defined	Not defined
Subsidence	passive margin: 0.05 m/kyr	LPF = 0.65 m/kyr	LPF = 0.78 m/kyr
		LCF = 0.27 m/kyr	LCF = 0.62 m/kyr
		MTF = 0.14 m/kyr	MTF = 0.34 m/kyr
		UCF = 0.19 m/kyr	UCF = 0.45 m/kyr
		UTF = 0.185 m/kyr	UTF = 0.43 m/kyr
Sedimentation Rates	0.05 - 0.10 m/kyr	0.65 - 0.70 m/kyr	0.78 - 0.85 m/kyr
Diagenetic Cap/ Caliche Rates	1-2 cm/kyr modern = 2-4 cm/kyr	Not defined	Not defined
Tepee Rates	Not stated, but is consistent with modern rates: Antiform buckling 4 cm/kyr cement fill 0.2-0.4 cm/kyr	Not defined	Not defined

Table 3.3. Rates of sea level oscillation, subsidence, sedimentation, and diagenesis for the Latemar platform interior as defined per research group. Subsidence rates have been calculated per facies group in some instances. LPF = Lower Platform Facies; LCF = Lower Cyclic Facies; MTF = Middle Tepee Facies; UCF = Upper Cyclic Facies; UTF = Upper Tepee Facies. Diagenetic cap / tepee formation rates are not defined by the Heidelberg group or by the Kent / Emmerich studies, but require rates of caliche formation of ca. 25. cm/kyr; rates of antiform bucking of 0.4-4.0 m/kyr and cement fill rates of 0.2-0.4 m/kyr.

RUN		P	Q	R	S	T
Sine wave	period 1000 y	18.4	20	20	18.4	18.4
	amp (m)	2	3	3	2	3
Asymmetric variation	period 1000 y	103	104	104	103	103
	amp (m)	2	3	3	2	3
	sl rise (%)	17	17	33	33	33
sed. rate (m/1000 y)		0.1	0.1	0.1	0.1	0.1
sub. rate (m/1000 y)		0.05	0.05	0.05	0.05	0.05
RESULTS						
5m						
0						
run time (1000 y)		620	620	615	608	608

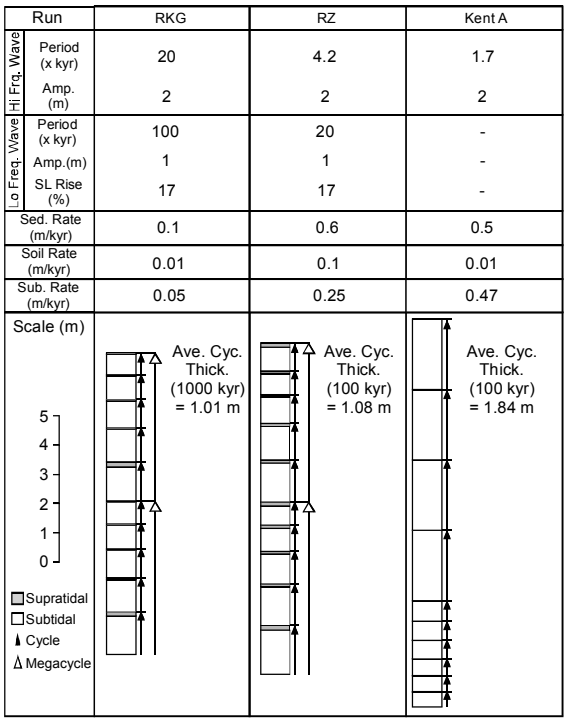

Table 3.4. Modeling of Latemar cycles using " Mr. Sediment" , a 1-D modeling program developed in the late 1980s by Paul Dunn at the Johns Hopkins University. Top: 1D models of Latemar cycle stacks from Goldhammer et al., (1987) generated in " Mr. Sediment. Each run is individually numbered and input variables listed. Bottom: 1D stratigraphic models generated for this study using the published sea level, subsidence, and sediment production inputs of Goldhammer/Hopkins (RKG); Zuhlke/ Heidelberg (RZ); and Kent / Emmerich (Kent A). In this case, only RKG and RZ models generate Latemar-like stacking (e.g. 5:1 bundles).

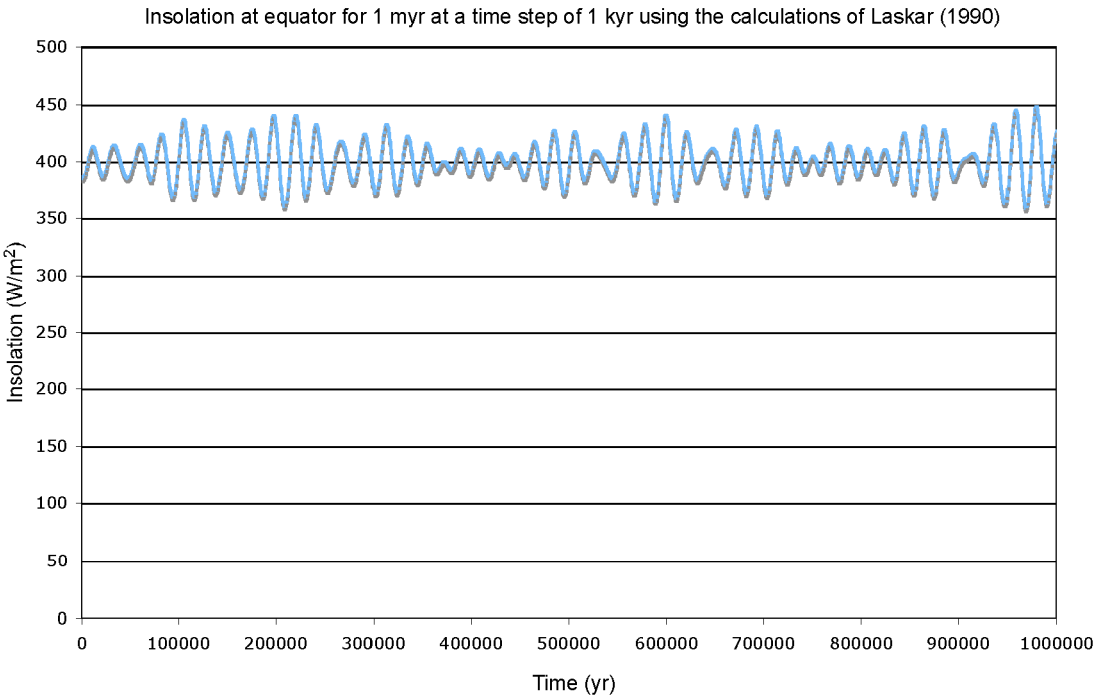

Chart 3.1. Plot of Milankovitchian solar insolation at the equator over a 1 million year period, sampled at 1 kyr, using the calculations of Laskar (1990) and AnalySeries v. 1.2.

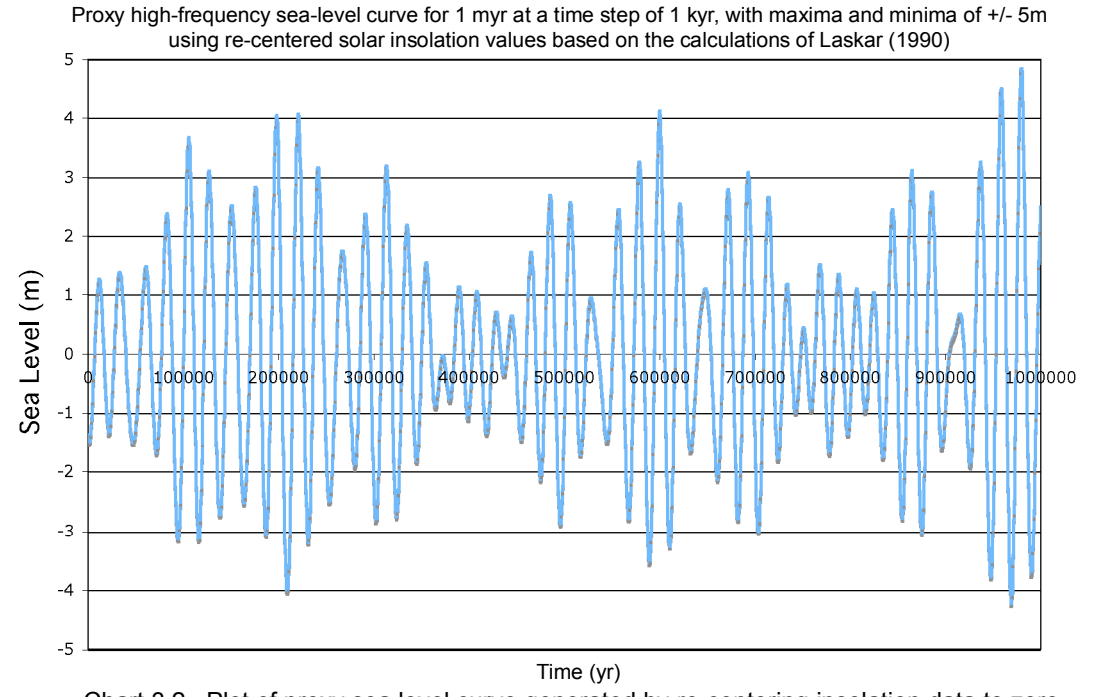

Chart 3.2. Plot of proxy sea level curve generated by re-centering insolation data to zero and making maxima and minima +/- 5 meters.

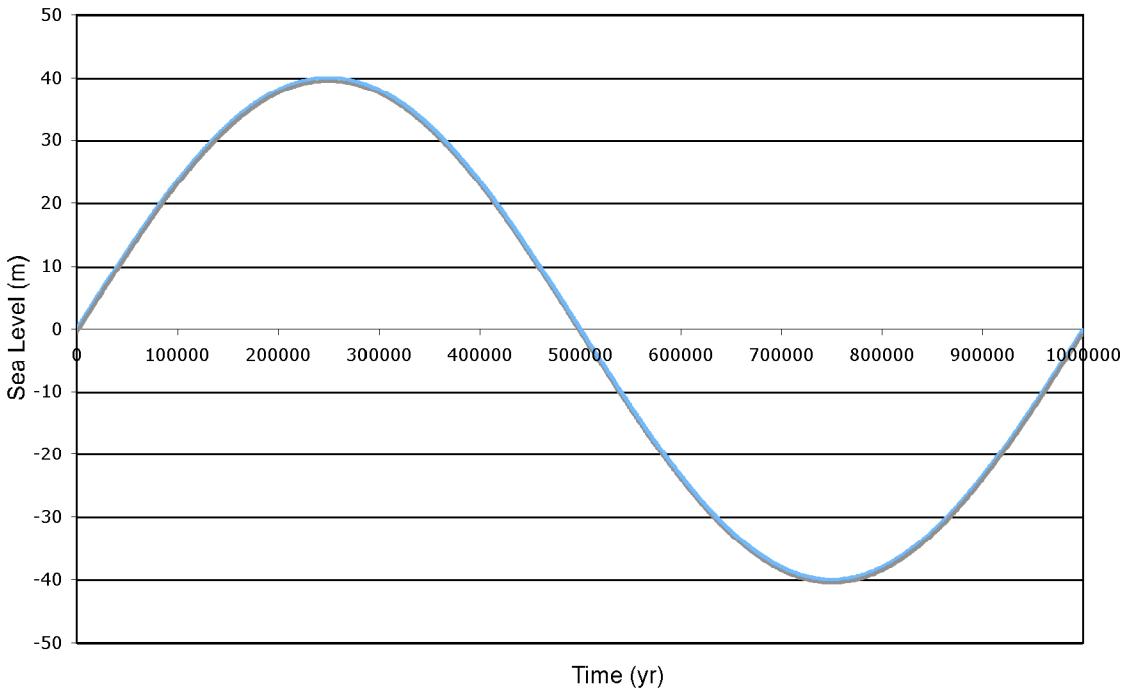

Chart 3.3. Plot of synthetic 3rd-order scale sinusoidal sea level curve

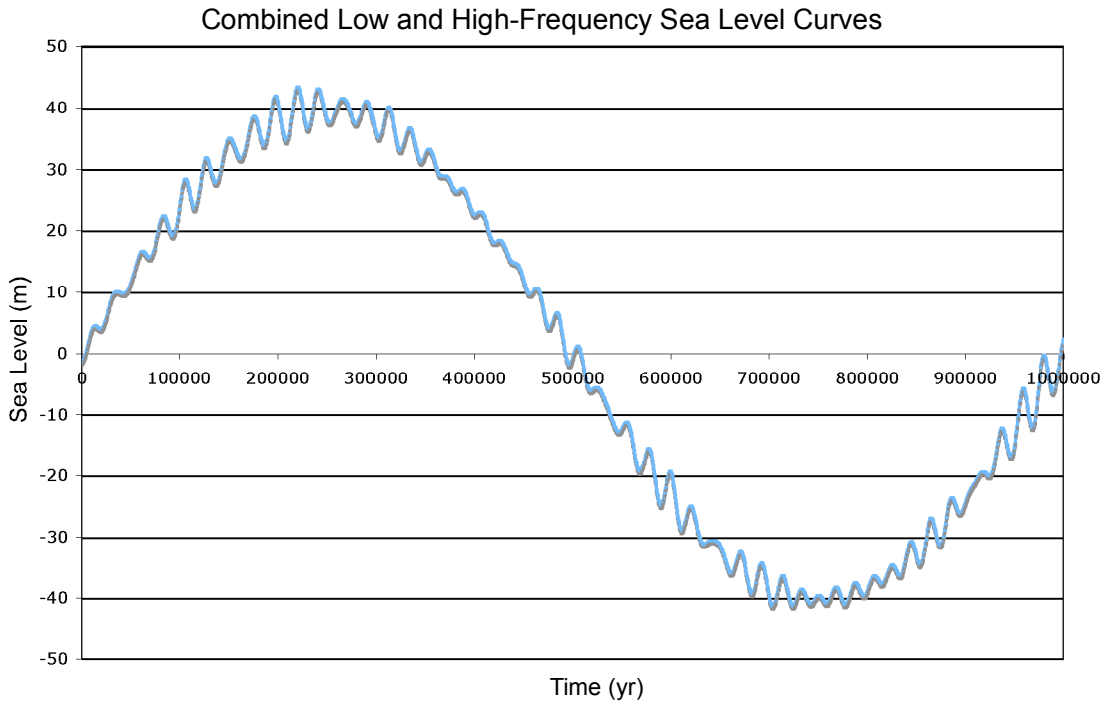

Chart 3.4. Plot of combined high-frequency and low-frequency curves (sum of data in charts 2 and 3)

A.

Sea Level Drivers			
	Highest Frequency	Mid Frequency	Low Frequency
Goldhammer	Milankovitchian Insolation, +/- 5 m	-	10 myr Oscillation at +/- 40 m
Zuhlke Model A	4.2 kyr Oscillation at +/- 5 m	Milankovitchian Insolation, +/- 5 m	-
Zuhlke Model B	4.2 kyr Oscillation at +/- 5 m	Milankovitchian Insolation, +/- 5 m	2.95 myr Oscillation at +/- 40 m
Zuhlke Model C	4.2 kyr Oscillation at +/- 2.5 m	Milankovitchian Insolation, +/- 5 m	2.95 myr Oscillation at +/- 40 m
Zuhlke Model D	4.2 kyr Oscillation at +/- 2.5 m	Milankovitchian Insolation, +/- 5 m	2.95 myr Oscillation at +/- 40 m
Zuhlke Model E	4.2 kyr Oscillation at +/- 2.5 m	Milankovitchian Insolation, +/- 5 m	2.95 myr Oscillation at +/- 40 m
Millennial Model A	1.7 kyr Oscillation at +/- 2.5 m	Milankovitchian Insolation, +/- 5 m	-
Millennial Model B	1.7 kyr Oscillation at +/- 2.5 m	Milankovitchian Insolation, +/- 5 m	

B.

Input Parameters for Carb 3d+ Runs									
Menu Parameter	Subset	Goldhammer Model	Zuhlke Model A	Zuhlke Model B	Zuhlke Model C	Zuhlke Model D	Zuhlke Model E	Millennial Model A	Millennial Model B
Space and Time	Length X	5 km	5 km	5 km	5 km	5 km	5 km	5 km	5 km
	Langth Y	5 km	5 km	5 km	5 km	5 km	5 km	5 km	5 km
	Cell resolution	100 m	100 m	100 m	100 m	100 m	100 m	100 m	100 m
	Model X Margin	0m	0m	0m	0m	0m	0m	0m	0m
	Model Y Margin	0m	0m	0m	0m	0m	0m	0m	0m
	Age at Start	20 Ma	20 Ma	20 Ma	20 Ma	20 Ma	20 Ma	20 Ma	20 Ma
	Age at End	15 Ma	19 Ma	18.525 Ma	18.525 Ma	18.525 Ma	18.525 Ma	19 Ma	19.5 Ma
	Calculation Increment	2 kyr	1 kyr	0.5 kyr	0.5 kyr	0.5 kyr	1 kyr	0.5 kyr	0.5 kyr
Accommodation	Sea Level File	Loaded	Loaded	Loaded	Loaded	Loaded	Loaded	Loaded	Loaded
	Load Subsidence	0.05 m/kyr	0.2 m/kyr	0.2 m/kyr	0.2 m/kyr	0.2 m/kyr	0.25 m/kyr	0.52 m/kyr	0.52 m/kyr
Production	Reef Max Rate	0.7 m/kyr	3.0 m/kyr	3.0 m/kyr	3.0 m/kyr	3.0 m/kyr	3.0 m/kyr	3.0 m/kyr	3.0 m/kyr
	Depth of Max Production	3 m	3 m	3 m	3 m	3 m	3 m	3 m	3 m
	Fall off depth	10 m	10 m	10 m	10 m	10 m	10 m	10 m	10 m
	Initial Porosity	40 (default)	40 (default)	40 (default)	40 (default)	40 (default)	40 (default)	40 (default)	40 (default)
	Bioerosion % coarse	20%	20%	20%	20%	20%	20%	20%	20%
	Margin Max Rate	1.0 m/kyr	1.0 m/kyr	1.0 m/kyr	1.0 m/kyr	1.0 m/kyr	1.0 m/kyr	1.0 m/kyr	1.0 m/kyr
	Depth of Max Production	3 m	3 m	3 m	3 m	3 m	3 m	3 m	3 m
	Fall off depth	10 m	10 m	10 m	10 m	10 m	10 m	10 m	10 m
	Interior Max Rate	0.1 m/kyr	0.7 m/kyr	0.7 m/kyr	1 m/kyr	.35 m/kyr	.7 m/kyr	0.82 m/kyr	0.82 m/kyr
	Restriction Distance	0.5 km	0.5 km	0.5 km	0.5 km	0.5 km	0.5 km	0.5 km	0.5 km
	Restriction Depth	5 m	5 m	5 m	5 m	5 m	5 m	5 m	5 m
	Pelagic Max Rate	0.01 m/kyr	0.1 m/kyr	0.1 m/kyr	0.1 m/kyr	0.1 m/kyr	0.1 m/kyr	0.1 m/kyr	0.1 m/kyr
Transport	Roughness Scale	default	default	default	default	default	default	default	default
	Boundary Current Speed	default	default	default	default	default	default	default	default
	Current Direction	default	default	default	default	default	default	default	default
Diagenesis	Hydrology	all default	all default	all default	all default	all default	all default	all default	all default
	Depositional Mineralogy	Default 70/30 Arag/Calc	Default 70/30 Arag/Calc	Default 70/30 Arag/Calc	Default 70/30 Arag/Calc	Default 70/30 Arag/Calc	Default 70/30 Arag/Calc	Default 70/30 Arag/Calc	Default 70/30 Arag/Calc
	Diagenesis Rates	Arag to Dolo in vadose 5%/kyr	Arag to Dolo in vadose 5%/kyr	Arag to Dolo in vadose 5%/kyr	Arag to Dolo in vadose 5%/kyr	Arag to Dolo in vadose 5%/kyr	Arag to Dolo in vadose 5%/kyr	Arag to Dolo in vadose 5%/kyr	Arag to Dolo in vadose 5%/kyr
	Surface Dissolution Rate	2mm/kyr	2mm/kyr	2mm/kyr	2mm/kyr	2mm/kyr	2mm/kyr	2mm/kyr	2mm/kyr

Appendix A. A. Eustatic drivers for Carb 3d+ Runs and B. Input values for Carb 3d+ runs

Chapter 4: Structural Analysis of Dolomia Principale fault zones near Passo Falzarego, the Dolomites, N. Italy

ABSTRACT

Previous workers have identified and interpreted the effects of synsedimentary extension on the development of the Norian Dolomia Principale (DP) a in the Dolomite Alps, Lombard Alps, and Carnian PreAlps of Northern Italy (Doglioni, 1986, 1992; Bosellini and Hardie, 1985; Jadoul et al., 1992; Carulli et al., 1998; Cozzi and Podda, 1998; and Cozzi, 2000). These interpretations conclude that the Dolomia Principale underwent EW-directed extension as a result of Late Triassic rifting related to the breakup of Pangaea and the opening of the Tethyan/Ligurian ocean system. The effects of synsedimentary extension were interpreted to have affected the stratigraphic development of the DP by Bosellini and Hardie (1985) concluding that the DP was locally block-faulted, with each block having differing subsidence histories such that the cyclic stratigraphy from one locality to the next is both uncorrelatable as a thickness series and deviates from expected facies trends at the third-order scale. However, quantified evidence of deformation (measurement of fault orientations, kinematic indicators, or amount of fault offset) was not presented in the publications listed above, and quantification of the amount of synsedimentary extension has not been published. While the topic of this dissertation is far more stratigraphically oriented, the possibility that synsedimentary faulting affected the DP demands justification by observational evidence rather than interpretation from a distance.

This manuscript presents the first measured evidence for structural synsedimentary extension and deformation of the Dolomia Principale in the Passo Falzarego region of the Dolomite Alps, as well as reactivation of these faults by orogenic processes later in their history.

BACKGROUND

Location

While exposures of the Dolomia Principale can be found throughout the Southern Alps (Lombardian Alps, Dolomite Alps, Carnian PreAlps, etc.), the locality of this study is the Dolomite Alps. The Dolomites are a mountain chain located in the north of Italy and are bordered by the Adige valley to their west, to the north by the Insubric lineament, and to the south by the south-vergent Valsugana overthrust (Doglioni, 1986; Bosellini, 1991) (**Figure 4. 1**). While the Dolomia Principale is exposed throughout a large area of the Dolomites, the bulk of the quantitative structural analyses in this study focuses on outcrops near Passo Falzarego, including a ca. 25 km^2 area between Passo Falzarego and Tofana di Mezzo to the east (**Figure 4. 2**). General observations relating to formational thickness and scaling of structural features were made on a wider scale, from the Sella massif in the west through to Tre Cime di Lavaredo approximately 50 km to the east.

Geologic Setting

The sedimentary history of the Dolomites begins in the Late Permian and continues through the Early Cretaceous, although the most volumetrically significant portion of sedimentary geology spans Triassic time, when two phases of rifting related to the breakup of Pangaea and development of the Tethyan ocean system occurred (Bernoulli and Lemoine, 1980; Doglioni, 1986; Bosellini, 1991). The stratigraphy of the Dolomites preserves a classic “rift-drift” succession of volcanics, redbeds, evaporites, marine carbonates and clastics and a final drowning succession through the development of the Tethyan passive margin (**Figure 4. 3**). The depositional record of the Dolomites begins in the Permian, when early rifting associated with the breakup of Pangaea and opening of the Tethys resulted in the emplacement of a volcanic complex with porphyritic ignimbrites locally exceeding 2000 meters in thickness (Bosellini, 1991). Rift-related sinistral transtension was active throughout the Southern Alps from the late Permian through the early to mid-Triassic (Doglioni, 1986). Block faulting associated with strike-slip movement led to the development of N-S trending highs (e.g., the Trento/Atesina Platform of the western Dolomites), and sedimentary basins (e.g., the Ligurian and Belluno basins) (Bernoulli and Lemoine, 1980; Doglioni, 1986; Bosellini, 1991) (**Figure 4. 4**). Nucleation and growth of Anisian and Ladinian carbonate platforms within the Belluno basin is thought to have been the result of continued strike-slip block faulting and emplacement of magma (sourcing later Ladinian volcanics), creating localized

bathymetric relief necessary for carbonate development (Winterer and Bosellini, 1981; Doglioni, 1986; Boselini, 1991). Subsequent sea-level drop and volcanic activity in the late Carnian led to an influx of siliciclastic and volcaniclastic sediments, which buried the Anisian-Ladinian platform-and-basin system and flattened depositional bathymetry (Bosellini, 1991; Bertotti et al., 1993). Upon sea-level rise, subsequent successions of carbonates were regional in extent (hundreds of km^2), nucleating on relatively flat, land-attached topography, as evidenced by the presence of dinosaur trackways in Norian carbonate tidal flat successions throughout the Dolomites. The Norian Dolomia Principale (DP) is the first of these regional peritidal carbonate packages, and reaches local thickness in excess of 1 kilometer in the Dolomites and upwards of 2.5 kilometers in the Carnian Prealps (Bosellini, 1967; Winterer and Bosellini, 1981; Boselini, 1991, Bertotti et al., 1993; Cozzi, 2000). The DP is overlain by equally broad subtidal carbonate packages, the Calcari Grigi and Dachstein, which are in turn overlain by a drowning succession of deep-water carbonates (Jurassic Ammonitico Rosso and Cretaceous Puez marl) and pelagic shales (Bosellini, 1991). The Dolomites are currently part of a large pop-up synclinorium of Neogene age constituting a relatively coherent slab of crust carried south 8-10 km during Alpine orogenesis (Doglioni, 1986, 1991; Bosellini, 1991). Neogene deformation created the present elevation of the Dolomites, causing 3-5 km of uplift via the formation of a 60 km-wide south-vergent “pop-up” synclinorium (Doglioni, 1987; 1992). Neogene deformation did not significantly shorten the

sedimentary cover in the synclinorium, with areal balances by Doglioni (1987) of folds and faults in both basement and sedimentary cover totaling no more than 10% (ca 5 km) shortening from north to south. The uplift of the synclinorium that includes the Dolomite Alps left the sedimentary units minimally deformed with previous deformations intact, preserving a record of magmatic, tectonic, and sedimentary events from post-Hercynian rifting through Alpine collision (Bosellini, 1991). In the Passo Falzarego area, however, the dip of formerly flat-lying tidal flat beds is approximately 25 degrees to the north.

Previous Work

While a detailed structural analysis of the DP has never been published, it is of utility to briefly describe what has been published so that the reader has a frame of reference both to approach the subject and the new data presented in this study. Five publications are briefly discussed below.

Bosellini and Hardie (1985)

In a study of the Norian Dolomia Principale (DP), Bosellini and Hardie (1985) concluded that shallowing-upward depositional cycles developed independent of each other (from locality to locality) as a result of being on separate fault blocks with individual, unique subsidence histories. The input of localized subsidence on depositional accommodation space led to the development of depositional successions that differ so greatly from locality to

locality (1-10 km apart) that they cannot be correlated using stacking pattern analysis. The difficulty in correlating the vertical thickness series of cycles within the DP suggests that even if a eustatic driver had been acting, irregular subsidence was far stronger a driver for the development of sedimentary successions in a vertical sense, likely resulting in differential thickness of individual sedimentary successions and/or different numbers of shallowing-upward successions from locality to locality. As a result, individual fault blocks likely record a unique mixture of tectonic autocycles and eustatic allocycles, making correlation by comparative cycle stacking impossible. Bosellini and Hardie (1985) is regarded in the carbonate stratigraphic community as one of the seminal publications in the concept of depositional “tectonic” cylicity. However, the evidence for tectonic activity posited in this publication comes directly from the assumption that sections within the DP would have formed correlatable sequences of carbonate depositional cycles were it not for differential subsidence. Therefore, no structural analysis of the study areas is presented.

Doglioni (1992)

Prof. Dr. Carlo Doglioni published a field trip guidebook for AGIP petroleum company in 1992. The volume is written entirely in Italian and is comprised primarily of field photographs and interpretive drawings, along with excerpts of publications. Several of the faults that cut the DP in both the Sella and Passo Falzarego areas are photographed in this volume. However, no

kinematic data are presented, such that the interpretive drawings are inferred from the structural geometry seen at a distance.

Jadoul et al. (1992)

Stratigraphic and sedimentologic studies of the Dolomia Principale of the Lombard basin (directly west of the Dolomites, see Figure 4) indicate that the area was offset by six synsedimentary faults with over 100 meters of throw during Norian time. Specifically, Jadoul et al. describe 5 phases of tectono-stratigraphic development in the DP of the Lombard basin. These phases include: 1) Restricted lagoon and tidal flat development at the Carnian/Norian boundary. 2) A thick (up to 700 m) succession of platform interior tidal flat cycles. This succession is cut by a NNE/SSW-striking normal fault near Idro Lake, in the eastern Lombard basin (nearest to the Dolomites) generating an intraplatform basin 100-200 m in bathymetric relief during the early Norian. Tensional features, such as Neptunian dykes, are reported in the upper portions of this succession, although kinematic data are not presented. 3) The middle and upper DP is dissected by six mapped NNE/SSW-striking normal faults with 200-1000 m of displacement. Intraplatform basin, margin, and slope facies are associated with each of these faults (**Figure 4. 5**). 4) In the uppermost Dolomia Principale, the surviving inner platform facies begin to prograde over the intraplatform basins. 5) Carbonate production ceases and sedimentation is dominated by terrigenous material. It is hypothesized that both clay pollution and

high subsidence rates led to the destruction of the DP carbonate factory in the Lombard basin. This model for the development of the DP in the Lombard basin invokes strong tectonic control on sedimentation (**Figure 4. 6**). However, no high-resolution (meter or sub-meter-scale) measured sections are presented, nor are any numerical data on faults or associated slickensides. Instead, field relationships and identification of facies trends on the 10-100 meter scale were used to infer the tectono-stratigraphic process.

Cozzi and Hardie (2003)

In a study of the Dolomia Principale of the Carnian Prealps (directly adjacent and to the east of the Dolomites) Cozzi and Hardie (2003) conclude that the formation-scale stratigraphic development of the Dolomia Principale was driven by accommodation space provided by tectonic subsidence rather than eustasy. Rather than recording two successive sea level lowstands in the Norian and Rhaetian (as predicted by the Haq curve) the DP of the Carnian Prealps records only long-term sea level rise through the formation. Cozzi and Hardie interpret this discrepancy as a result of plate-scale rifting in the NW Tethys preceding oceanic spreading later in the Jurassic. Additional evidence for tectonic influence includes sediment and cement-filled fractures, numerous normal faults (no number given) with 0.30-0.50 meter displacements, meter-scale breccia-filled fractures, and Neptunian dykes. Cozzi (2000) also reports these findings, as well as identification of normal faults and Neptunian dykes, all of

which strike NNE/SSW. However, kinematic indicators are not reported, nor are sections measured at the meter-scale. Cozzi and Hardie (2003) close by concluding that extensional tectonics can produce, via pulses of normal faulting, transgressive-regressive sequences that develop on a timescale similar to that predicted for third-order sequences (1-10 million years).

Fantoni and Scotti (2003)

Fantoni and Scotti (2003) analyzed organic matter maturity of rock samples to calculate the peak temperatures of sedimentary basins in the Southern Alps during Mesozoic extensional phases. Data from 41 representative samples are reported. Maturity was determined through vitrinite reflectance and records heating events (60-200^{o}C) experienced by the samples after burial. Fantoni and Scotti refer to the same tectonic model for the development of Mesozoic Alpine extension as Bertotti et al. (1993), specifically that the area was broken into NS-striking grabens and EW dipping normal faults. Through analysis of samples, Fantoni and Scotti conclude that the distribution of organic material maturity is controlled by burial during the Norian-Liassic extensional phase (**Figure 4. 7**).

Sum of Published Data on DP Structure

Very little data has been published on the kinematics of extensional structures in the Dolomia Principale. Stratigraphic data (Bosellini and Hardie,

1985; Jadoul et al., 1992; Cozzi and Hardie, 2003), thermochronology data (Fantoni and Scotti, 2003) and interpreted photographs (Doglioni, 1992) are presented as evidence that the Dolomia Principale underwent synsedimentary extension in the Norian. While this dissertation is not a comprehensive structural analysis of the Dolomia Principale, any claim of structural deformation ought to be based on observable data preserved in the rock. The Dolomia Principale has experienced at least two major tectonic events (the development of the Tethyan passive margin via rifting and the development of the Alps via destruction of the Tethys and collision of Africa and Europe) that left a structural record of deformation in the rock. If faults are synsedimentary and related to extension, they ought to show normal motion, have similar strikes, and be depositionally overlapped assuming overlying stratigraphy is preserved. Structures formed during Alpine orogenesis would more likely show NS displacement, and may include thrust faults and synsedimentary normal faults reactivated with strike-slip overprint. The purpose of this study is to document the nature of structural features in Dolomia Principale of the Dolomites near Passo Falzarego, where spectacular exposures of hundreds of meters of late Triassic platform carbonate cycles are exposed (*see* Figure 2). The major questions of concern are whether measurements of structures in the area are indicative of synsedimentary extension, and if so, how synsedimentary extension affected the stratigraphic development of late Triassic carbonates deposited there.

Methods

Faults were identified in the field during reconnaissance and when measuring sections for stratigraphic analysis. Fault patterns and thickness trends were identified along a west-to-east transect, which the basinward direction of thickening of the DP (Doglioni, 1991; Cozzi, 2000). Faults were photographed and locations mapped. Data collected include faults and slickenside orientations and strike and dip of nearby bedding. Orientation data were collected using a Brunton compass. Fault data were tabulated and plotted on stereonets using the Stereonet 6.3.2 software package by Allmendinger, (2002).

EXTENSIONAL FEATURES

Differential thickness of the DP in the Dolomites

In the Dolomites, the Dolomia Principale thickens from ca. 250 m on the Sella Massif to over 700 m at Tre Cime di Lavaredo over a ca. 40 km west-to-east transect (**Figure 4. 8**). The stratigraphic thickness appears to abruptly change across valleys approximately 10 km wide. As a result, valleys are inferred to be locations of major fault zones, as the faults responsible for the 100s of meters of offset are not exposed in outcrop. For example, the thickness of the Dolomia Principale roughly doubles from the Sella group to the Fanes group across Val Badia. Normal faults dipping into Val Badia can be observed in the Puez group above Corvara. The offset on these exposed faults is small (1-10

meters) and cannot account for the change in stratigraphic thickness across the valley (**Figure 4. 9**). The Dolomia Principale also thickens from ca. 600 m at the Fanes group to at least 700 m (section incomplete) at Tre Cime di Lavaredo 20 km to the east. Major faults responsible for this offset are not exposed.

The thickening of the DP from west to east was the result of differential subsidence that generated additional accommodation space for carbonate sediment to fill eastward. If major faults (e.g., faults with 100 meters + offset) were the loci for the differential thickness of the DP, those faults are not exposed and their existence must be inferred. However, if differential subsidence from west to east generated the majority of differential stratigraphic thickness in the DP major faults would not be required. Instead, differential subsidence, whether driven tectonically or through gravitation, could have generated differential thickness in the DP from 250 m at the Sella to approximately 700 m at Tre Cime. However, Cozzi and Hardie (2003) report that the Dolomia Principale is 2 km in thickness in the Carnian Prealps, directly east and adjacent to the Dolomites, indicating a regional trend of increasing subsidence eastward over ca. 100 km (*see* Figure 4. 7). These observations are consistent with regional studies that include reconstructed cross sections of the Mesozoic Tethyan margin, including those published by Laubscher and Bernoulli (1978) (*see* Chapter 1, Figure 21) and Fantoni and Scotti (2003) (*see* Figure 7 this chapter).

Scaling of Extensional Features

In addition to stratigraphic thickness changes of the Dolomia Principale in the Dolomites, extensional features can be observed at numerous scales (mm, cm, m, dm) in outcrop (**Figure 4. 10**). At the millimeter scale, clasts incorporated into breccias can be observed to have open-mode fractures that stop at the boundary of the clast and do not extend into the breccia matrix. Depositionally-overlapped normal faults at the cm and m-scales with EW displacement have also been observed in the Passo Falzarego area (*see* Figure 2). Meter-scale faults with depositional overlap are also identified as well as more obvious displacements at the dm-scale. In addition, faults with radial "fanning" of strata thickening into the hanging wall were observed at Forcella Averau (Carnian San Cassian Fm.) and at Tofana di Mezzo above Rifugio DiBona (late Carnian Dürrenstein Fm.). Photographs, measurements, and locations of structures identified in the Passo Falzarego area are shown in Figures 4. 11 - 4. 18. All of the features indicate that synsedimentary extension was active both immediately prior to and during the deposition of the Dolomia Principale.

Orientations of Faults and Sense of Slip

123 fault orientation measurements were taken in the Passo Falzarego area (5-10 measurements per fault) and provide quantification of fault orientation and displacement associated with their formation. Over 90% of the measured faults strike within 30 degrees west of north (**Figure 4. 11**). Fault dips vary from

50 degrees to near vertical, with the majority of faults dipping between 60 and 80 degrees. The average fault orientation calculated from all measurements is N5W, 70W, although faults were measured at opposite sides of graben structures and dip both east and west. A map view of many of the faults on the south side of the valley between the Fanes Group and Cinque Torri can be seen from the top of the cablecar lift at Cima Lagazuoi. Measurements of these faults indicate strikes within 30 degrees of NS, with slickensides on faults indicating both normal and strike-slip motion (**Figures 4. 12 & 4. 13**).

A normal fault across the valley from the Fanes Group can be seen at Forcella Averau exposed over a vertical distance of approximately 50 meters (**Figure 4. 14**). In this case, the fault cuts late Carnian stratigraphy that in turn dips and thickens into the hanging wall of the fault in a fanning geometry, indicating that the fault was active concurrent with sedimentation. Slickensides were observed and measured at the base of the exposure and are oriented horizontally, indicative of strike-slip movement. Slickensides measured near the top of the fault exposure, however, are near-vertical in orientation and are indicative of normal motion.

A fault with almost identical geometry and slip indicators can be seen cutting the Dürrenstein and Raibl formations at the base of Tofana di Mezzo above Rifugio di Bona (**Figure 4. 15**). Nereo Preto (unpublished dissertation,

2001) interpreted the fanning geometry of the beds to be sedimentary structures associated with the migration of a submarine dune. However, the abrupt termination of beds against a listric fault marked by vertical slickensides indicates that the fanning geometry in the Dürrenstein is more likely the result of growth faulting.

Additional faults with slickensides were identified in the Dürrenstein and Raibl formations near Cima Lagazuoi and Col dei Bos. These fault scarps are 3-5 meters in height and extend across the exposure (**Figures 4. 16 and 4. 17**). Both of these faults have slickensides oriented subvertically indicative of normal motion.

A composite stereonet of all fault and slickenside data indicates that faults strike within 35-40 degrees of NS (most striking roughly NNW) with two main sets of slickensides: one set (and accompanying antithetics) oriented subvertically and indicative of normal motion and the second set oriented subhorizontally and indicative of strike-slip motion on the fault plane (**Figure 4. 18**).

DISCUSSION

Analysis of structural data collected in the late Carnian and early Norian stratigraphy of the Dolomites indicates that the Dolomia Principale underwent a period of normal faulting and a period of strike-slip faulting. However, the

amount of extension near Passo Falzarego is small (meter-scale fault offsets) when compared to studies of the DP elsewhere (e.g., Lombard basin) where structures record hundreds of meters of offset (Jadoul et al., 1992). Understanding the relationship of different faults to each other is best done through understanding their orientations and timing. Over 90% of the measured faults strike within 30 degrees of north, due to undulating graben scarps identified in the valley opposite the Fanes group from Cima Lagazuoi (*see* Figures 4. 12 and 4. 13). Twelve of the seventeen faults have slickensides that indicate normal motion. Eight of the seventeen faults measured also have slickensides that indicate strike-slip motion.

Determining the timing of the fault movements is accomplished in light of tectono-stratigraphic architecture of the localities themselves and of the region as a whole. The NS-striking EW dipping faults measured in the Passo Falzarego area with both normal and strike slip slickensides are either depositionally overlapped on the down-dropped side (flat-lying stratigraphy draping the fault) or radially-filled with either late Carnian or early Norian sediments (e.g., Forcella Averau, Tofana di Mezzo, Tofana di Rozes, *see* Figures 4. 14 and 4. 15). These geometries prove that in the Passo Falzarego area, faults of equivalent geometries with indicators of normal motion formed contemporaneous to carbonate sedimentation. On the larger scale, the Dolomia Principale thickens over short intervals from west to east (*see* Figure 4. 8) indicating that subsidence

increased in magnitude from west to the east in the Dolomites. Relationships in fault geometry, timing of faulting via sedimentary overlap, and increase in thickness of the DP from west to east are support the conclusion the DP underwent synsedimentary extension. However, data from this study alone does not prove whether or not all of these features are tectonic (i.e., rooted in the basement) or are all limited to sedimentary cover (e.g., compaction or gravitationally-driven).

The timing of strike-slip motion on DP faults is not constrained, although two distinct possibilities exist. The southern Alps, and in particular the Dolomites, underwent two periods of inversion due to plate convergence (Doglioni, 1986). Both episodes are related to changing directions of relative motion between Africa and Eurasia. The first period of convergence, Paleogene in age, is related to the formation of the Dinaric foreland and generated N-S and NNW-SSE trending thrusts and fold axes and W and WSW striations on fault surfaces (*see* Figure 4 from Doglioni, 1992 & Figure 6 from Doglioni, 1986). The second period of convergence (Neogene) is thought to have been more significant, and formed the majority of the present elevation of the Dolomites (Doglioni, 1986). NS-directed shortening related to the northward migration of Africa is thought to have generated 3-5 km of uplift via the formation of a 60 km-wide south-vergent "pop-up" synclinorium that currently comprises the Dolomite Alps (*see* Figure 8 of Doglioni, 1986) (Doglioni, 1986, 1992). Either of these periods of convergence

may have reactivated NS striking normal faults, superimposing strike-slip kinematic indicators on indicators of normal motion.

CONCLUSIONS

Analysis of structural data collected in Carnian and Norian deposits of the Dolomites supports the hypothesis that the Dolomia Principale was affected by synsedimentary extension. Evidence for synsedimentary extension identified in this study includes the formation of fractures and faults at various scales (*see* Figure 4. 10) that strike 30^{o} West of North, have a dip of >45^{o}, and have normal displacements to the east and west (*see* Figure 4. 18). These similarities in fault geometry are indicative of a genetic relationship. It was also observed that the formational thickness of the DP in the Dolomites thickens systematically from west to east from approximately 250 m thick a the Sella Massif to over 700 m thick at Tre Cime di Lavaredo, which is located 40 km to the east (*see* Figure 4. 8). These observations do not detract from the hypothesis that systematic thickening of the DP from west to east in the Dolomites relates to the rifting of Pangaea and development of the Tethys-Ligurian ocean system in the Late Triassic through Jurassic. However, the observations made in this study also do not directly confirm the hypotheses that extensional features observed in the DP are tectonic, as they could have also formed due to deformation of sedimentary cover via gravitational sliding. Normal faults identified and measured in this study are, however, oriented with NS strike and EW displacement, which is in

agreement with the orientation of regional extensional structures. The effect of these faults on the development of the DP is still debatable however, as none of the faults identified totaled more than 10's of meters of offset. Instead, normal faults are likely a manifestation of a regional trend of differential subsidence increasing from west to east (**Figure 4. 19**). A regional structural analysis of the Triassic of the Dolomites, including recording of kinematic data and analysis of thermal history is needed to make this determination. In either case, examples of fanning geometries in faults and depositional overlap do indicate that the structures observed in the Passo Falzarego area are synsedimentary extensional features. This is the first time that quantitative structural data supporting the hypothesis that the DP of the Dolomites underwent synsedimentary extension has been published.

While the presence of synsedimentary extensional features in the DP has been posited in the literature, the presence of strike-slip faults in the DP has not been reported by other workers. Based on the tectonic history of the area (i.e., extension followed by two phases of orogenesis) as well as the geometry of most faults being consistent with synsedimentary normal motion, the strike slip features observed on the faults in the Passo Falzarego area are interpreted as the effects of reactivation of normal faults during Alpine orogenesis. NS- directed shortening related to the northward migration of Africa is properly oriented to reactivate NS-striking normal faults via strike slip. Doglioni (1987) calculates the

total shortening of the Dolomites region via orogenesis to be no more than 10% (5 km total shortening), of which these strike slip faults are a portion. Strike-slip features identified in the DP of the Passo Falzarego area of the Dolomites are interpreted as post-depositional reactivation features associated with Alpine orogenesis.

A complete structural analysis of the Dolomia Principale in the Dolomites and elsewhere is required in order to determine the regional heterogeneity in syndepositional structural styles preserved in late Triassic outcrops across the Southern Alps. In addition, dating of late Triassic carbonates would aid in determination of subsidence and accumulation rates through time. A better understanding of the structural development of carbonate shelves in passive margin settings is key to understanding similar Mesozoic deposits formed around the world during the rifting of Pangaea.

REFERENCES

Allmendinger, R.W., 2002, Stereonet v. 6.3.3 for Mac OS X

Bernoulli, D., and Lemoine, M., 1980, Birth and early evolution of the Tethys: the overall situation: Memorie della BRGM, no. 115, p. 168-179.

Bertotti, G., Picotti, V., Bernoulli, D., and Castellarin, A., 1993, From rifting to drifting: tectonic evolution of the South-Alpine upper crust from the Triassic to the Early Cretaceous: Sedimentary Geology, v. 86, p. 53-76.

Bertotti, G., Seward, D., Wijbrans, J., ter Voorde, M., and Hurford, A.J., 1999, Crustal therman regime prior to, during, and after rifting: A geochronological and modeling study of the Mesozoic South Alpine rifted margin: Tectonics, v. 18, no. 2, p. 185-200.

Bosellini, A., 1991, Geology of the Dolomites: An introduction: Dolomieu Conference on carbonate platforms and dolomitization. Ortisei, 43 p.

Bosellini, A., 1967, La tematica deposizionale della Dolomia Principale (Dolomiti e Prealpi Venete: Bolletino della Societa geologica Italiana, v. 86, is. 2, p. 133-169

Bosellini, A., and Hsu, K.J., 1973, Mediterranean plate tectonics and Triassic paleogeography: Nature, v. 244, p. 144-146.

Bosellini, A., and Hardie, L.A., 1985, Facies e cicli della Dolomia Principale delle Alpi Venete: Memorie della Societa Geologica Italiana, v. 30, p. 245-266.

Carulli, G.B., Cozzi, A., Longo Salvador, G., Ponton, M., and Podda, F., Evidence of synsedimentary tectonic activity during the Norian-Lias (Carnian PreAlps, northern Italy): Memorie della Societa Geologica Italiana v. 53, p. 403-415.

Cozzi, A., 2000, Synsedimentary tensional features in Upper Triassic shallow-water platform carbonates of the Carnian PreAlps (northern Italy) and their importance as paleostress indicators: Basin Research, v. 12, p. 133-146.

Cozzi, A., 2002, Facies Patterns of a Tectonically-Controlled Upper Triassic Platform-Slope Carbonate Depositional System (Carnian Prealpls, Northeastern Italy): Facies, v. 47, p. 151-178.

Cozzi, A., and Hardie, L.A., 2003, Third-order depositional sequences controlled by synsedimentary extensional tectonics: evidence from Upper Triassic carbonates of the Carnian PreAlps (NE Italy): Terra Nova, v. 15, p. 40-45.

Cozzi, A., and Podda, F., 1998, A platform to basin transition in the Dolomia Principale of the M. Pramaggiore area, Carnian PreAlps, northern Italy: Memorie della Societa Geologica Italiana, v. 53, p.387-402.

Doglioni, C., 1992, Relationships between Mesozoic extensional tectonics, stratigraphy, and Alpine inversion in the Southern Alps: Eclogae geol. Helv., v. 85, no. 1, p. 105-126.

Doglioni C., 1988, Examples of strike-slip tectonics on platform-basin margins: Tectonophysics, v. 156, p. 293-302.

Doglioni C., 1987, Tectonics of the Dolomites (Southern Alps, Northern Italy): Journal of Structural Geology, v. 9, no. 2, p.181-193.

Emmerich, A., Glasmacher, U.A., Bauer, F., Bechstädt, T., and Zühlke, R., 2005, Meso-/Cenozoic basin and carbonate platform development in the SW Dolomites unraveled by basin modeling and apatite FT analysis: Rosengarten and Latemar (Northern Italy): Sedimentary Geology v. 175, is. 1-4, p.415-438

Fantoni, R., and Scotti, P., 2003, Thermal record of the Mesozoic extensional tectonics in the Southern Alps: Atti Ticinensi di Scienze della Terra, no. 9, p. 96-101.

Favre, P., and Stampfli, G.M., 1992, From rifting to passive margin: The examples of the Red Sea, Central Atlantic, and Alpine Tethys: Tectonophysics, v. 215, p. 69-97.

Hsu, K.J., and Bernoulli, D., 1978, Genesis of the Tethys and the Mediterranean: DSDP, v. 42, p. 943-949.

Jadoul, F.; Berra, F.; and Frisia, S., 1992, Stratigraphic and paleogeographic evolution of a carbonate platform in an extensional tectonic regime: the example of the Dolomia Principale in Lombardy (Italy): Ri. It. Paleont. Strat., v. 98, no.1, p. 29-44.

Laubscher, H., and Bernoulli, D., 1978, Mediterranean and Tethys, *in* Nainn, A.E.M., Kanes, W.H., and Stehli, F.G., (eds.), The ocean basins and margins, 4A: New York, Plenum Press, p. 1-28.

Lemoine, M., and Trumpy, R., 1987, Pre-oceanic rifting in the Alps: Tectonophysics, v. 133, p. 305-320.

Winterer, E.L., and Bosellini, 1981, Subsidence and sedimentation on Jurassic passive continental margin, Southern Alps, Italy: AAPG Bulletin, v. 65, is. 3, p. 394-421

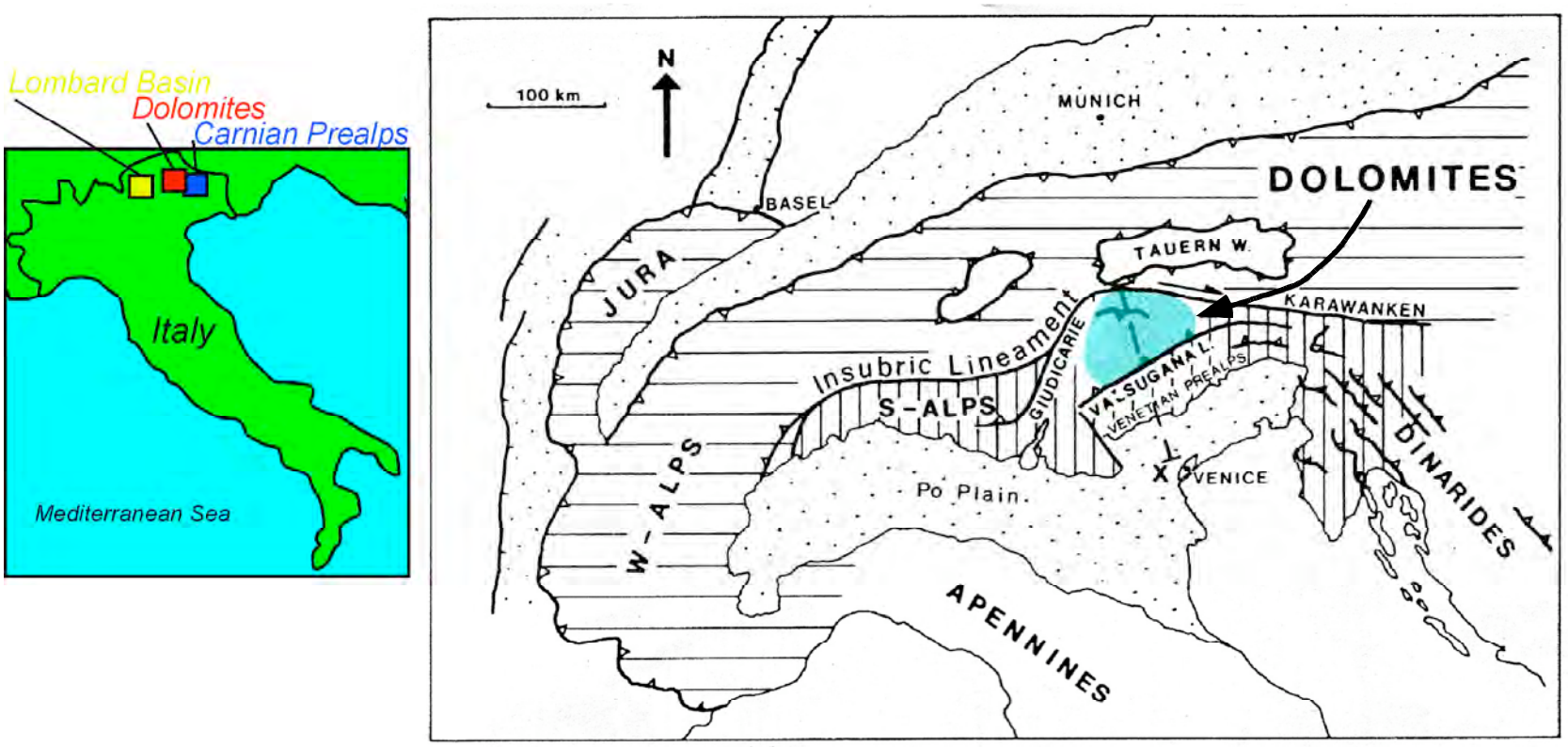

From Doglioni, (1986)

Figure 4.1. Location of the Dolomite Alps. The Dolomites are located in the eastern portion of northern Italy in the 'Southern Alps', which are bordered to the north by the Insubric lineament (dextral). The Dolomites proper are also bordered by the Valsugana overthrust to the south and by the Adige valley to the west.

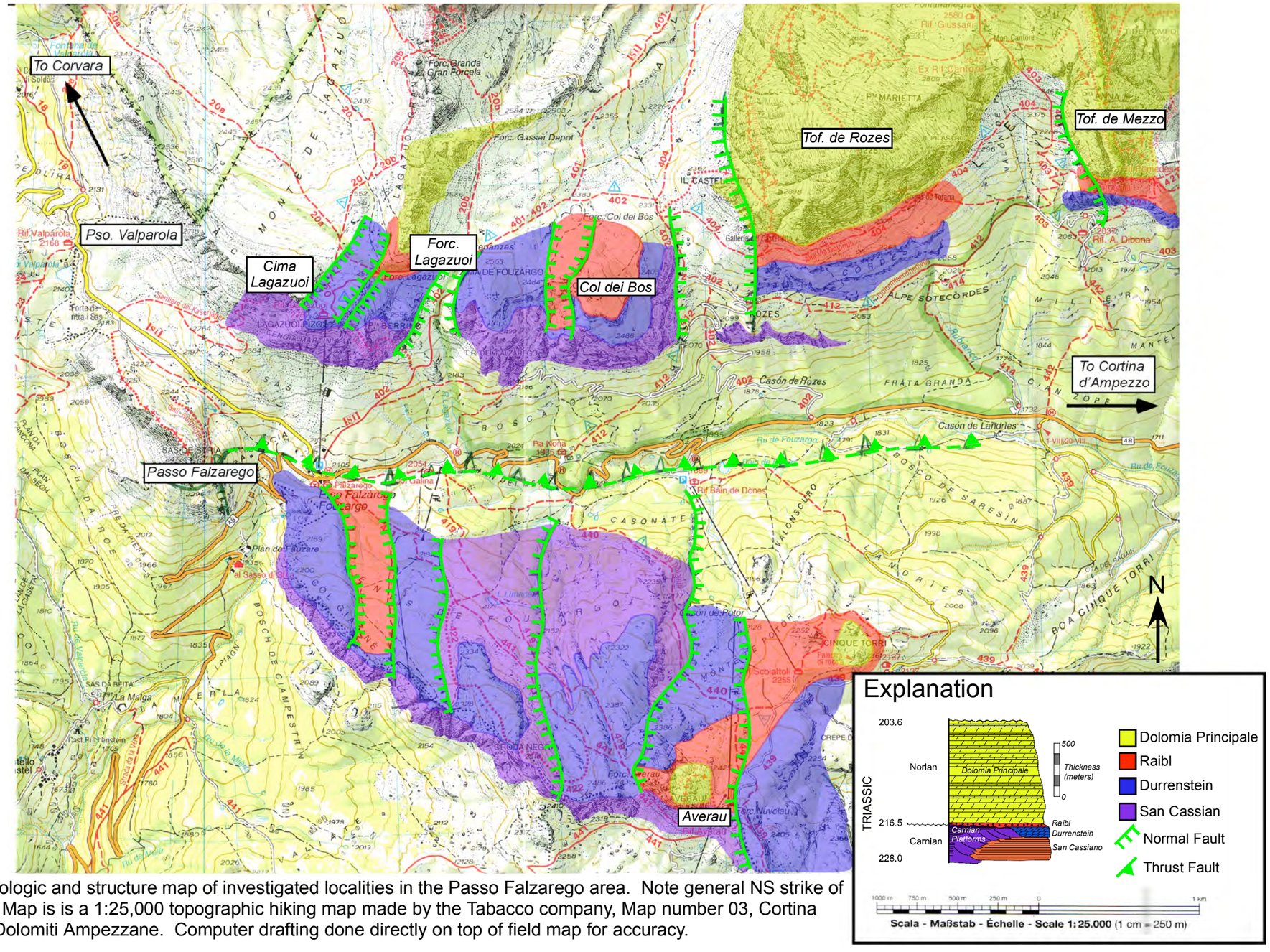

Figure 4.2. Geologic and structure map of investigated localities in the Passo Falzarego area. Note general NS strike of normal faults. Map is is a 1:25,000 topographic hiking map made by the Tabacco company, Map number 03, Cortina d'Ampezzo e Dolomiti Ampezzane. Computer drafting done directly on top of field map for accuracy.

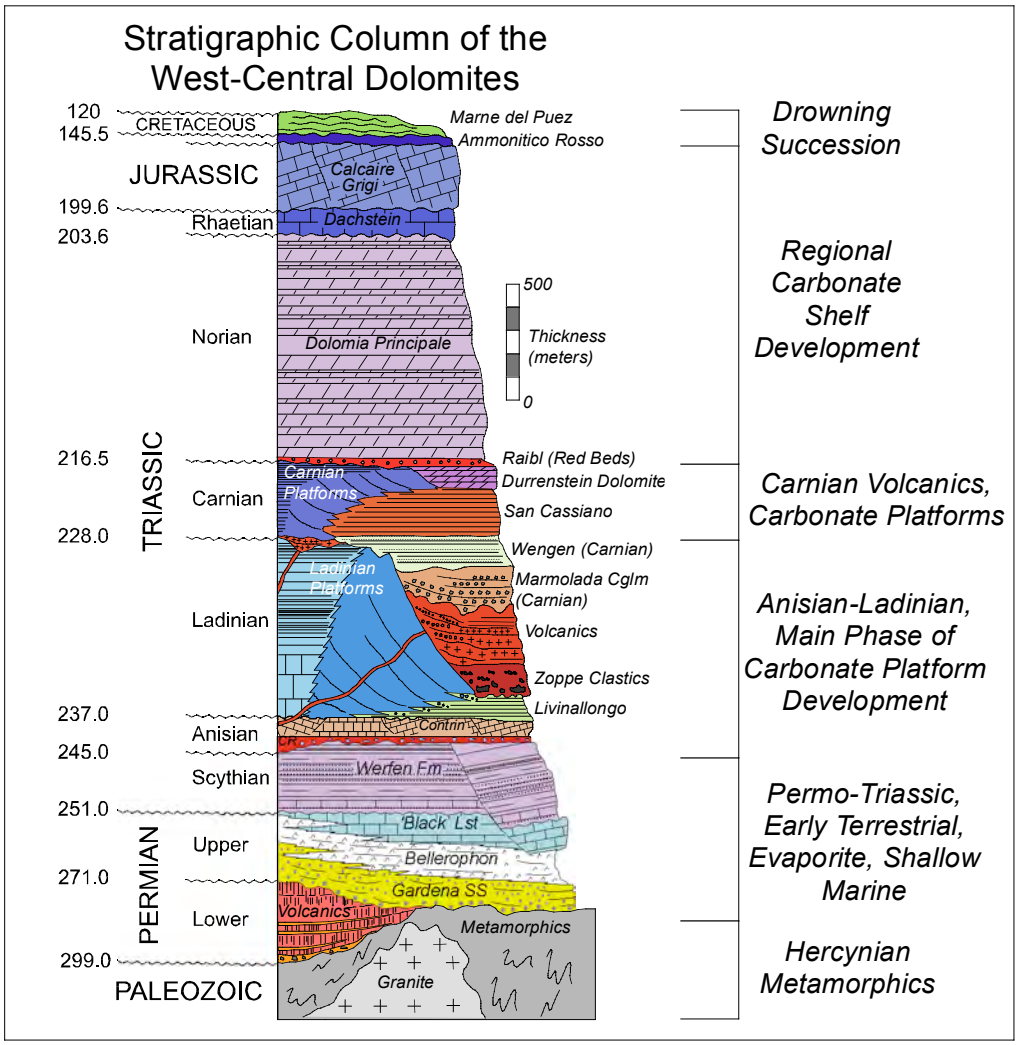

Section modified from Bosellini (1991), dates from Gradstein et al., (2004)

Figure 4.3. Stratigraphic column of the general sedimentary succession preserved in the Dolomite alps of Northern Italy. The Dolomia Principale, a regional carbonate complex of Norian age, is the focus of this study.

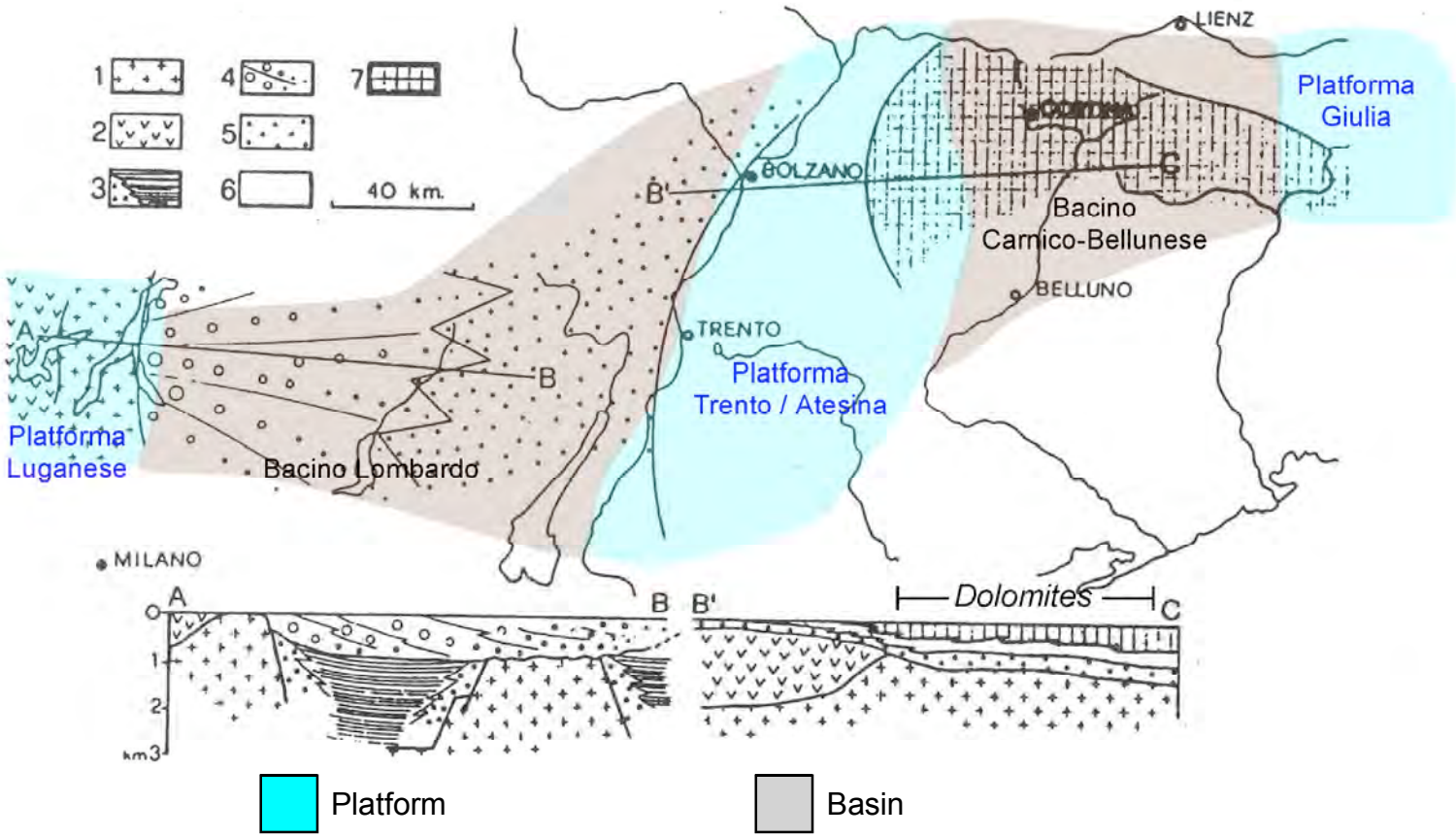

Figure 4.4 Paleogeographic map and cross section of Permo-Triassic deposits in the Southern Alps. 1. Hercynian metamorphics, 2. Permian 'Bozner' volcanics, 3. Lacustrine deposits, 4. Conglomeratic alluvial fans, 5. Fluvial deposits, 6. Shallow marine dolomites and evaporites (tidal flat and sabkha), 7. Shallow marine limestones. Note NS structural grain of platforms and basins, as well as Permian volcanic core of platforms. Figure modified from Winterer and Bosellini (1981) by adding platform and basin labels and colors.

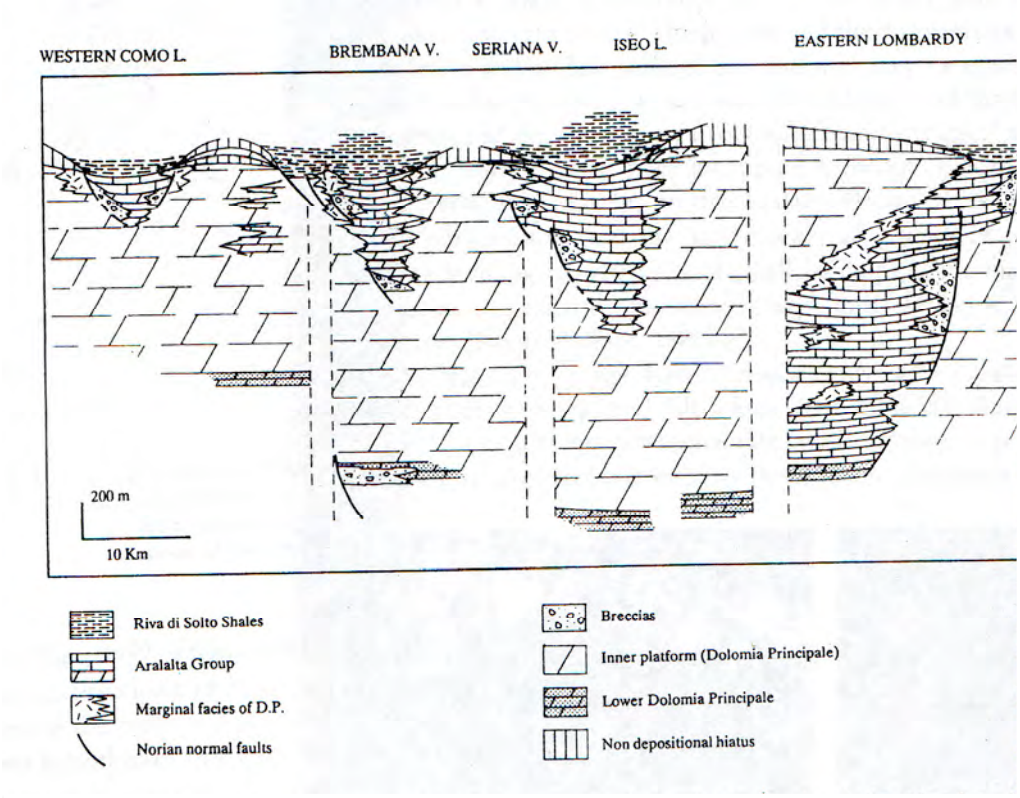

Figure 4.5. Schematic cross-section across the Norian Dolomia Principale of the Lombard basin, directly adjacent (west) of the Dolomites from Jadoul et al. (1992). Fault scarps developed intraplatform breccia zones while marginal facies developed on the opposite side of intraplatform basins.

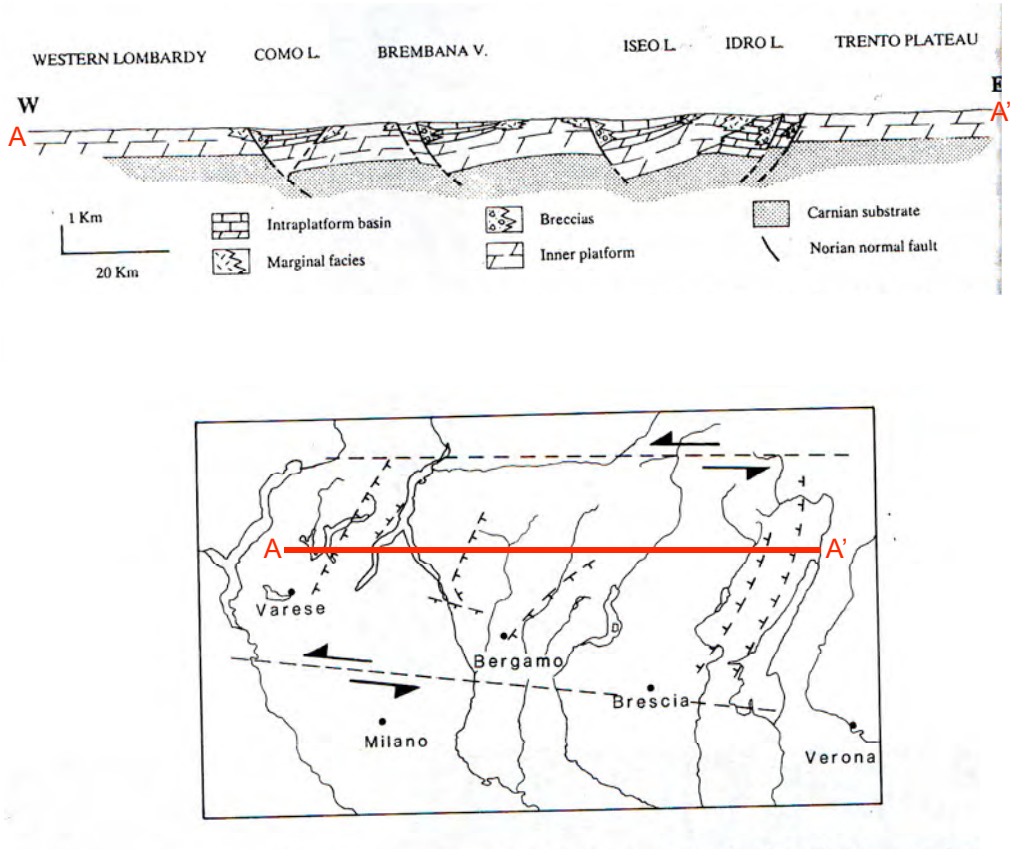

Figure 4.6. Rifting model proposed by Jadoul et al. (1992) for the Dolomia Principale of the Lombard Basin, directly adjacent (west) to the Dolomites. The synsedimentary normal faults are thought to have been generated via the development of a sinistral strike-slip pull apart basin, based on the studies of Doglioni (1987).

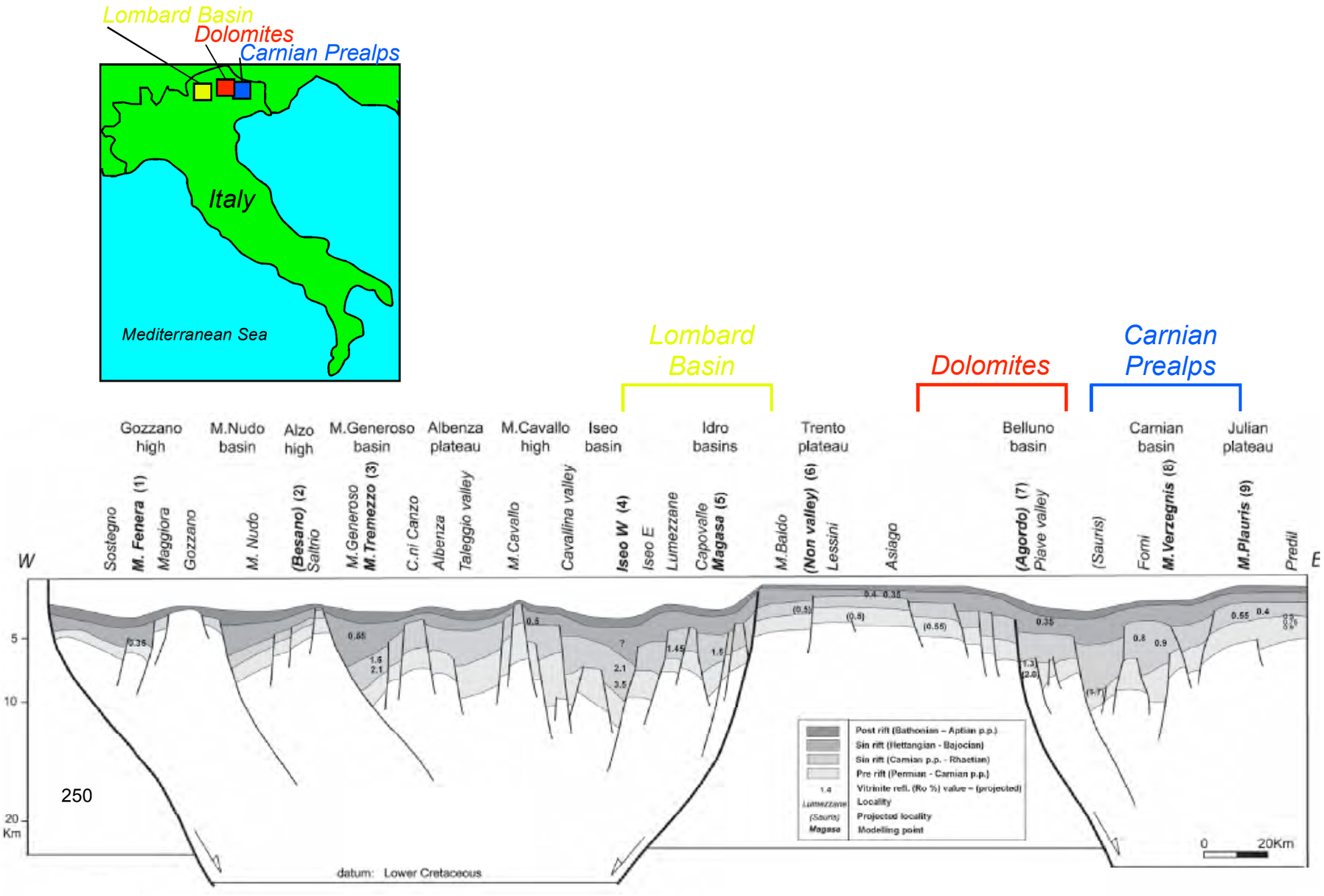

Figure 4.7. Sketch by Fantoni and Scotti (2003) of the extensional Mesozoic architecture of the Southern Alps. Vitronite reflectance analysis indicates that organic material was heated to its highest temperatures during the Norian-Liassic, thought to be a period of active rifting. No structural data was presented. Formation thickness data were measured in the field.

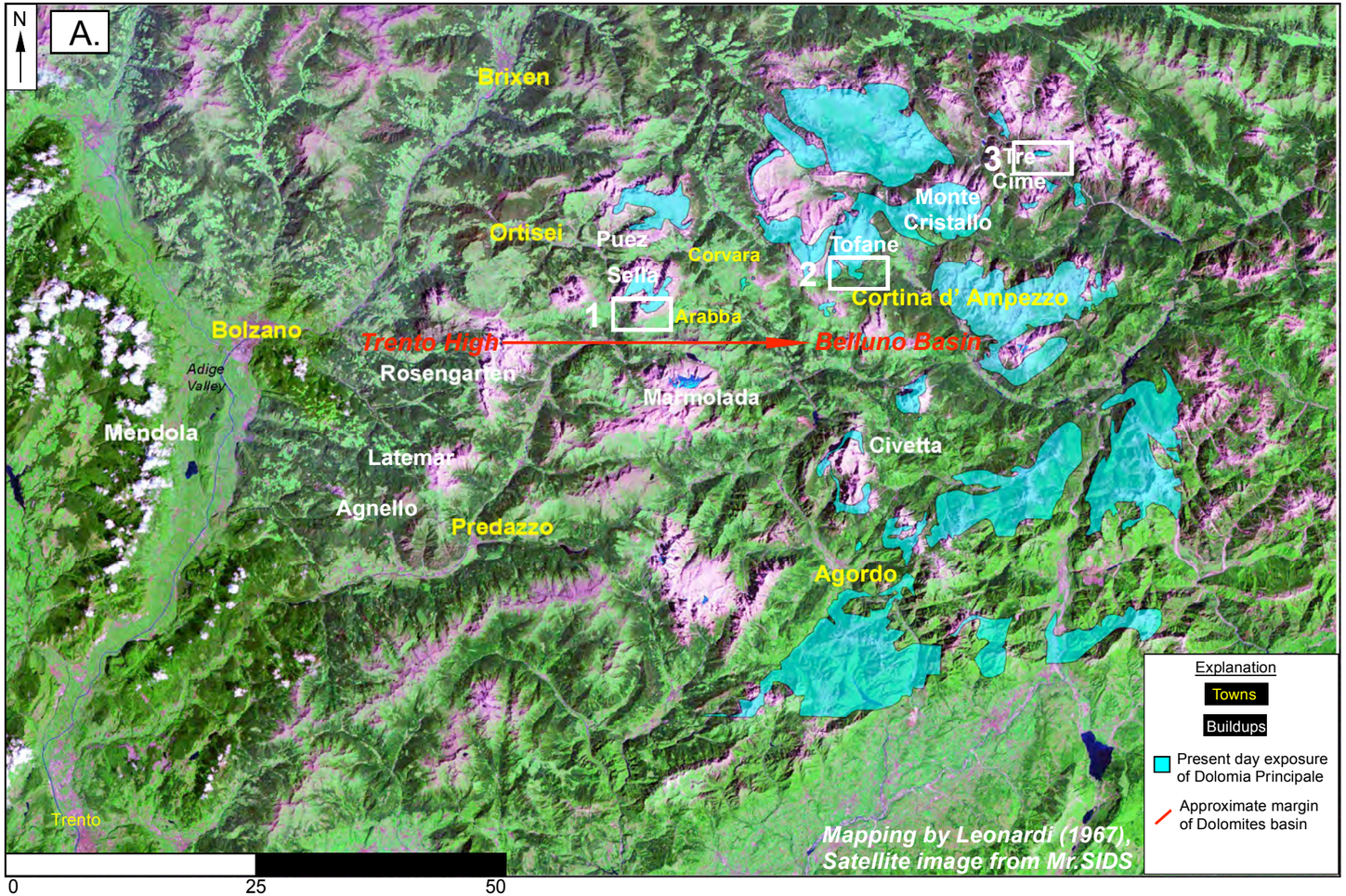

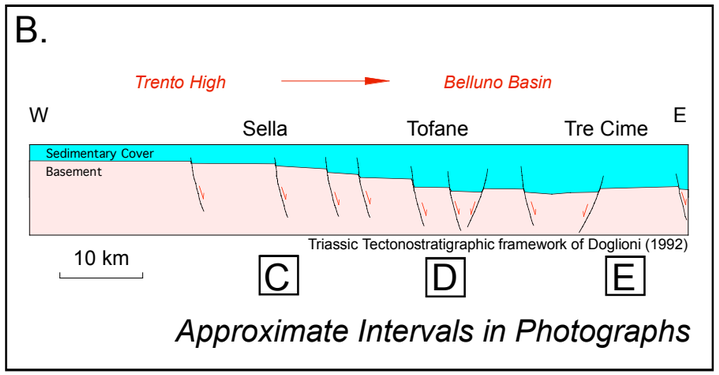

Figure 4.8. A. Geologic map, and B. thickness variability between outcrops of the Dolomia Principale. Doglioni, (1992) concluded that late Triassic and early Jurassic sediments of the Dolomites underwent synsedimentary extension. Apart from normal faults identified in outcrop, the Norian Dolomia Principale can be observed to thicken from west to east in the Dolomites from C. the Sella, to D. the Fanes group, to E. Tre Cime di Lavaredo (other authors report thickening of the DP from east to west in the Lombard basin, adjacent to and directly west of the Dolomites). In the examples presented here, the DP nearly triples in thickness (250 m to 700 m) from west to east over ca. 40 km. Photographs of representative outcrops are presented at the bottom of the figure and keyed to B. an interpretive cross-section.

W — 20 km — 20 km — E

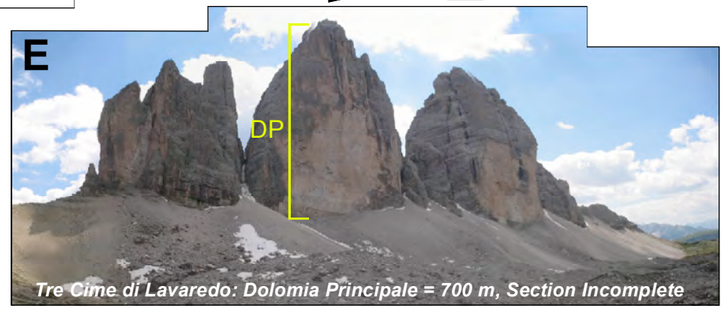

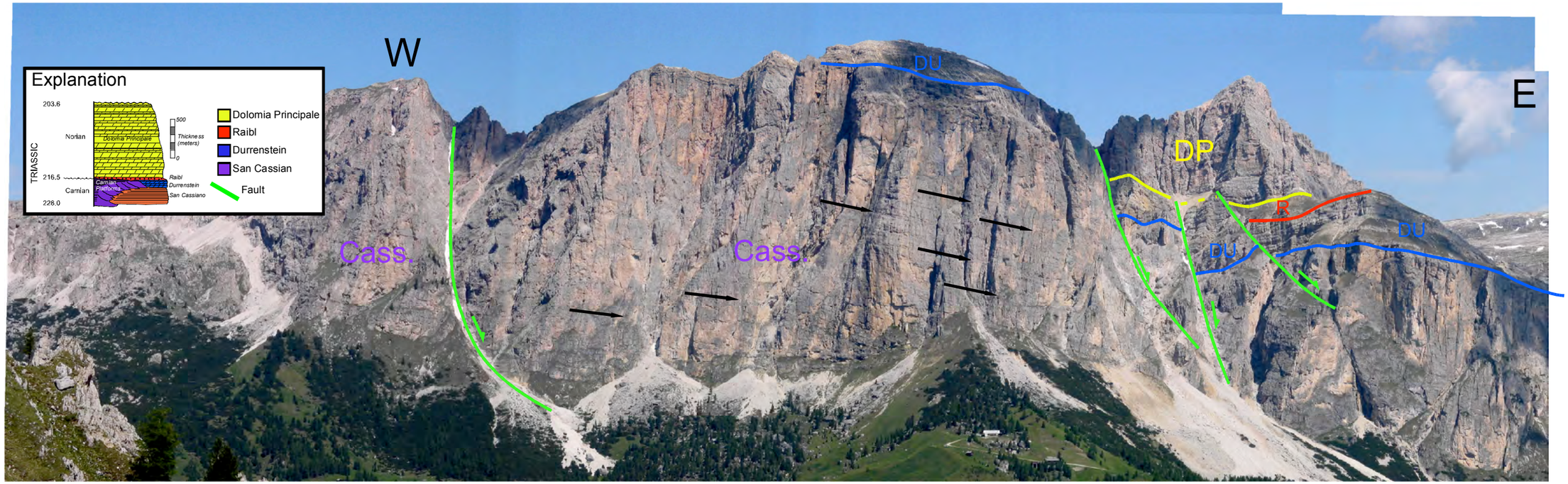

Figure 4.9. NS-striking normal faults in the Puez Group outcropping above the town of Corvara. Faults have apparent offset of approximately 10 meters. Photo taken from the Sella Massif, looking north towards the Puez group. Arrows indicate direction of Cassian slope progradation. Cass = Carnian San Cassian carbonate slope deposits; R = upper Carnian Raibl formation; DP = Norian Dolomia Principale

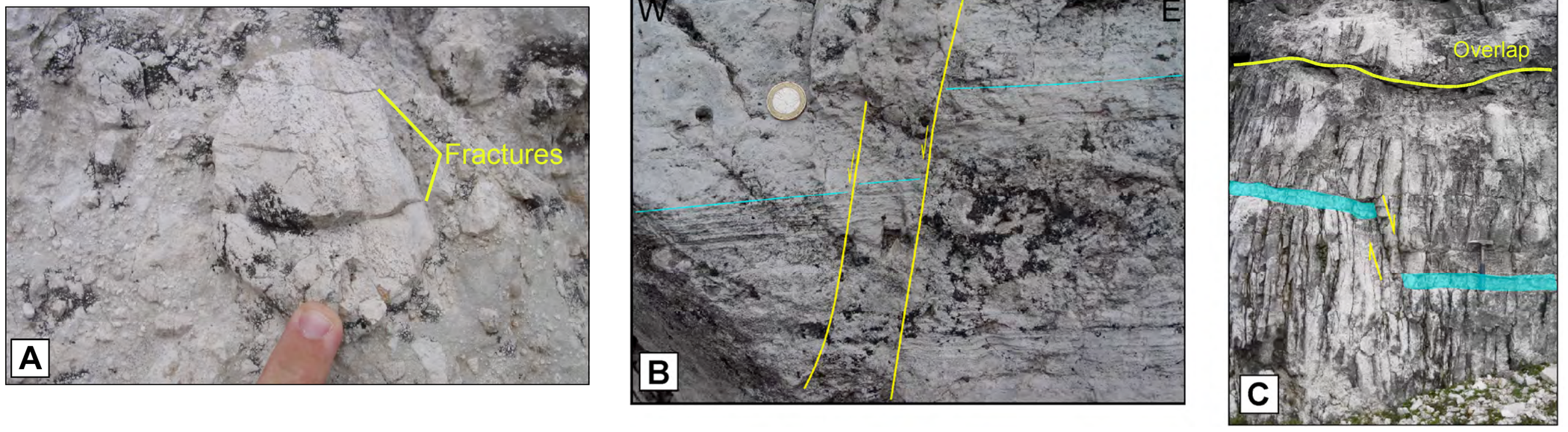

Figure 4.10. Scaling of extensional features in the Dolomia Principale. A. Breccia with fractured clasts. Note fractures in the clasts are of similar orientation (roughly perpendicular to fenestral lamination) and do not extend past the edge of the clast, indicating that the fractures predate the breccia and may have been present in the clast before re-sedimentation. B. Centimeter-scale offset in a cryptomicrobial laminite at Forcella Averau. C. Normal fault with ca. 40 cm of offset at the base of Tofana di Rozes, adjacent to Grotta di Tofana. Note that the fault is depositionally overlapped. D. Multi-meter scale offset in the DP preserved at the Sella group. Original interpretation of D by Doglioni, (1992).

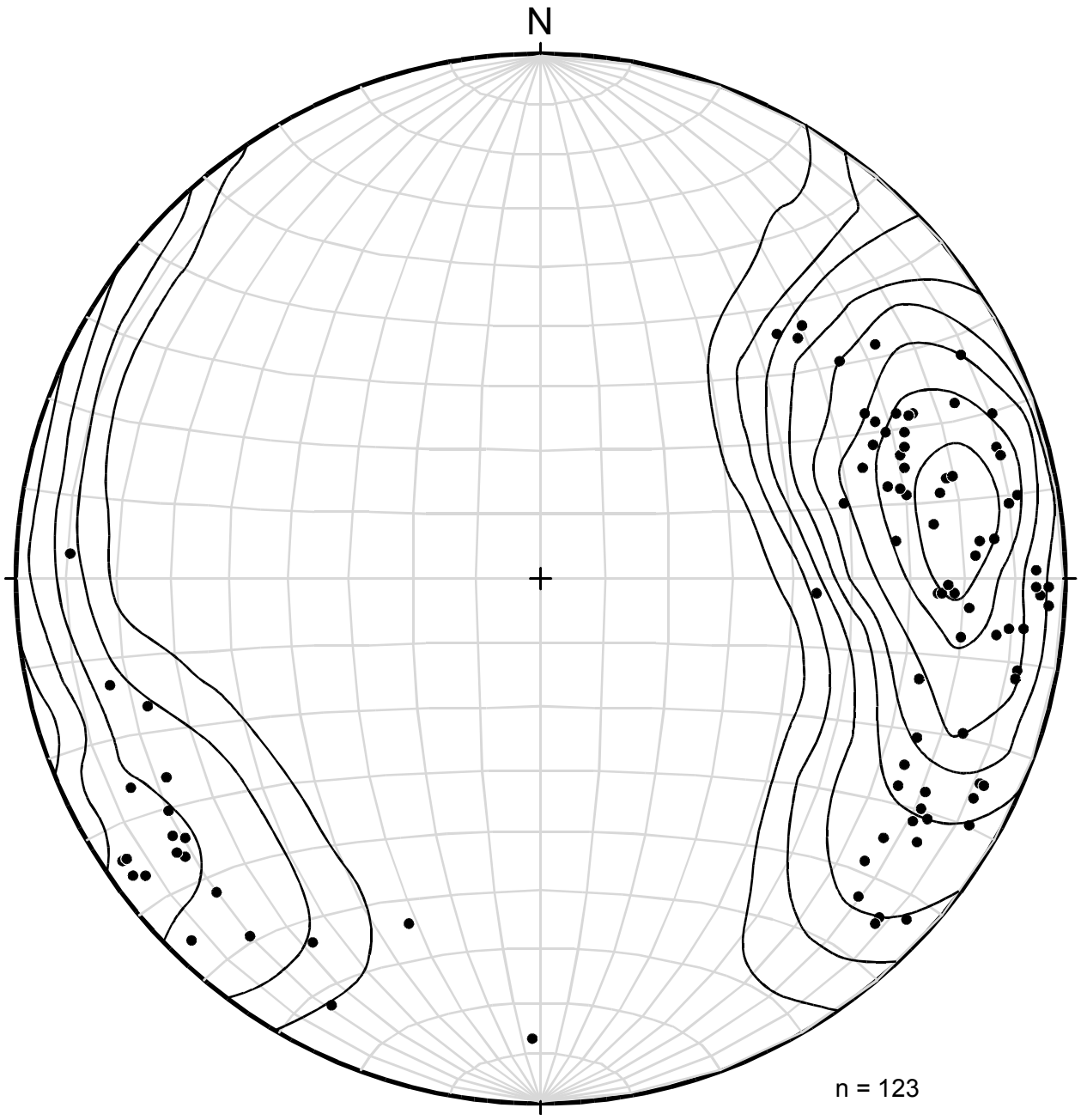

Figure 4.11. Plot of 123 poles to fault planes measured in the Passo Falzarego area. Faults strike within 30 degrees west of north. The “bulls eye” orientation of all poles is approximately N85E, 20E, indicating a mean fault trend oriented N5W, 70W. Data were contoured using Richard Allmendinger’s StereoNet software package.

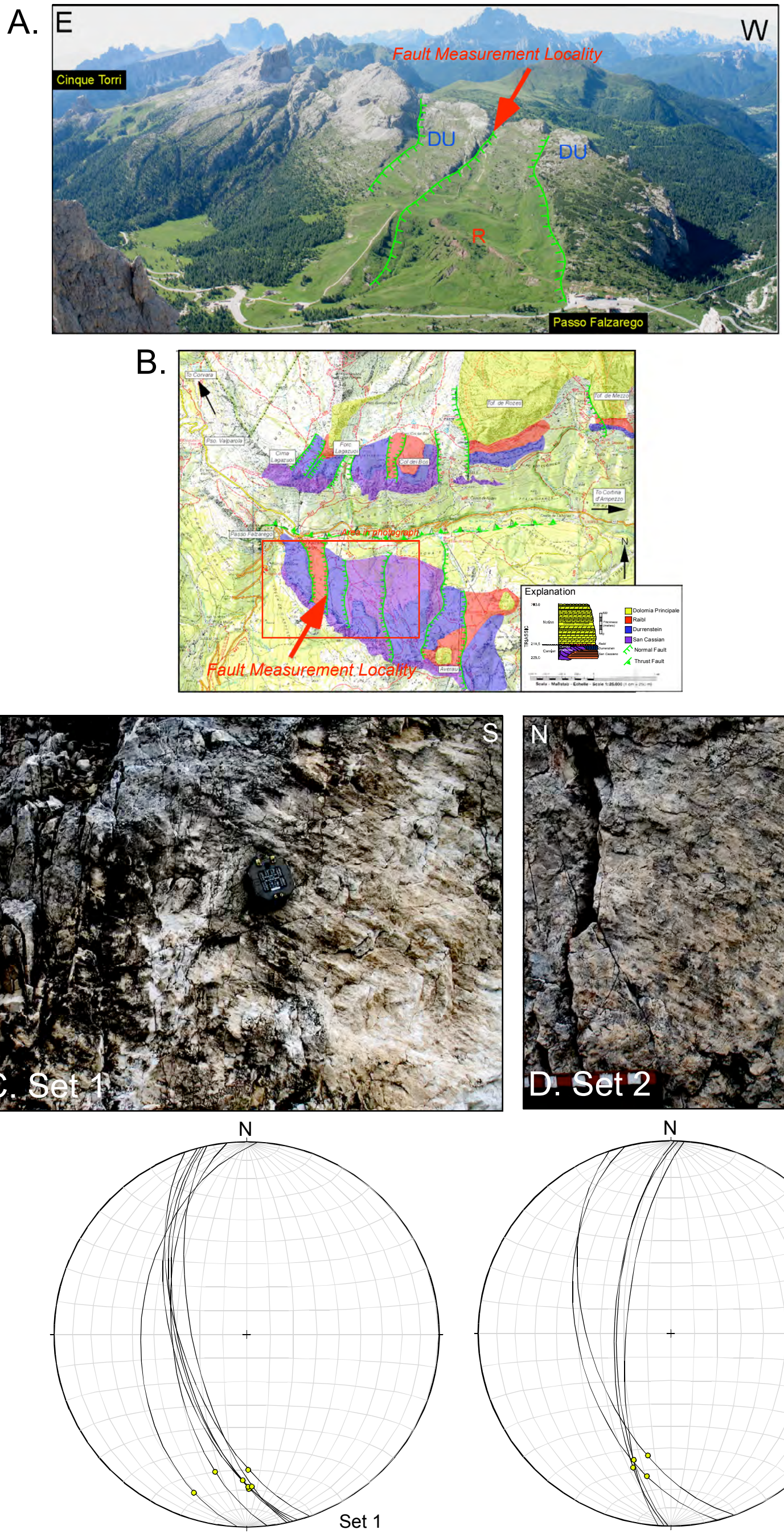

Figure 4.12. Kinematic data from Falzarego graben fault 1. A. Photograph of location of fault measurement taken from Cima Lagazuoi looking south. B. Location of location of fault measurement on wanderkarte. C&D. Photographs and stereonets of fault planes and slickensides collected 3 meters apart at the location shown in A&B. Data are presented as measured and are un-rotated. Slickensides indicate strike-slip motion to the NNW.

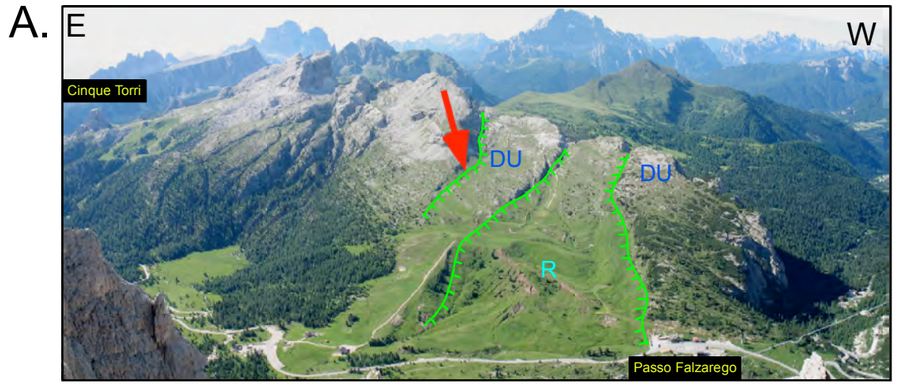

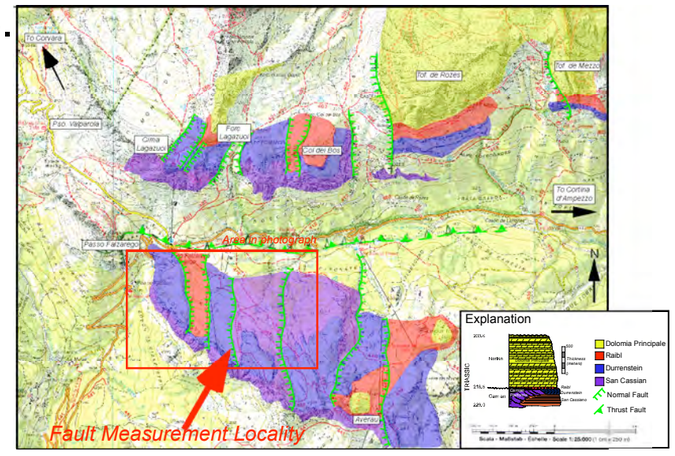

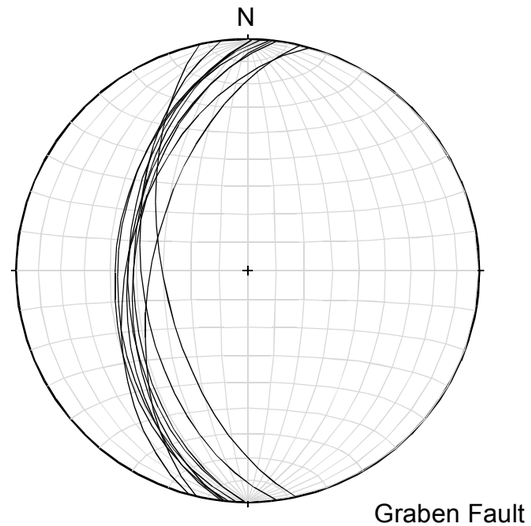

Graben Fault

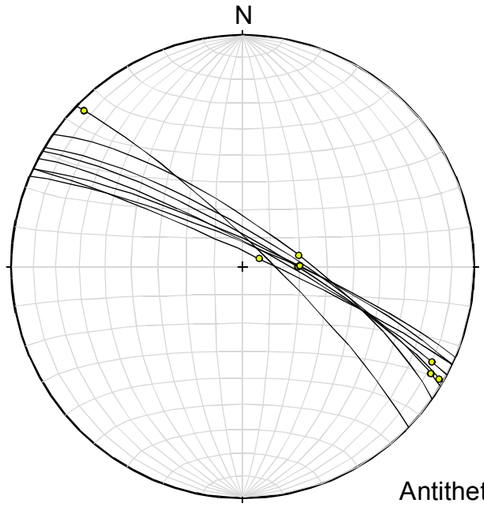

Antithetic Fault

Figure 4.13. Kinematic data from Falzarego graben fault 2. A. Photograph of location of fault measurement taken from Cima Lagazuoi looking south. B. Location of fault measurement on wanderkarte. C&D. Photographs and stereonets of fault planes and slickensides collected at the location shown in A&B. Data are presented as measured and are un-rotated. No slickensides were identified from the face identified as a fault. Indeed, the lack of motion indicators may indicate that the face is representative of an eroded open-mode joint rather than a normal fault. However, two sets of slickensides were measured along what would be an antithetic fault identified along in the graben wall. Slickensides record two distinct directions of motion- normal and left-lateral strike-slip.

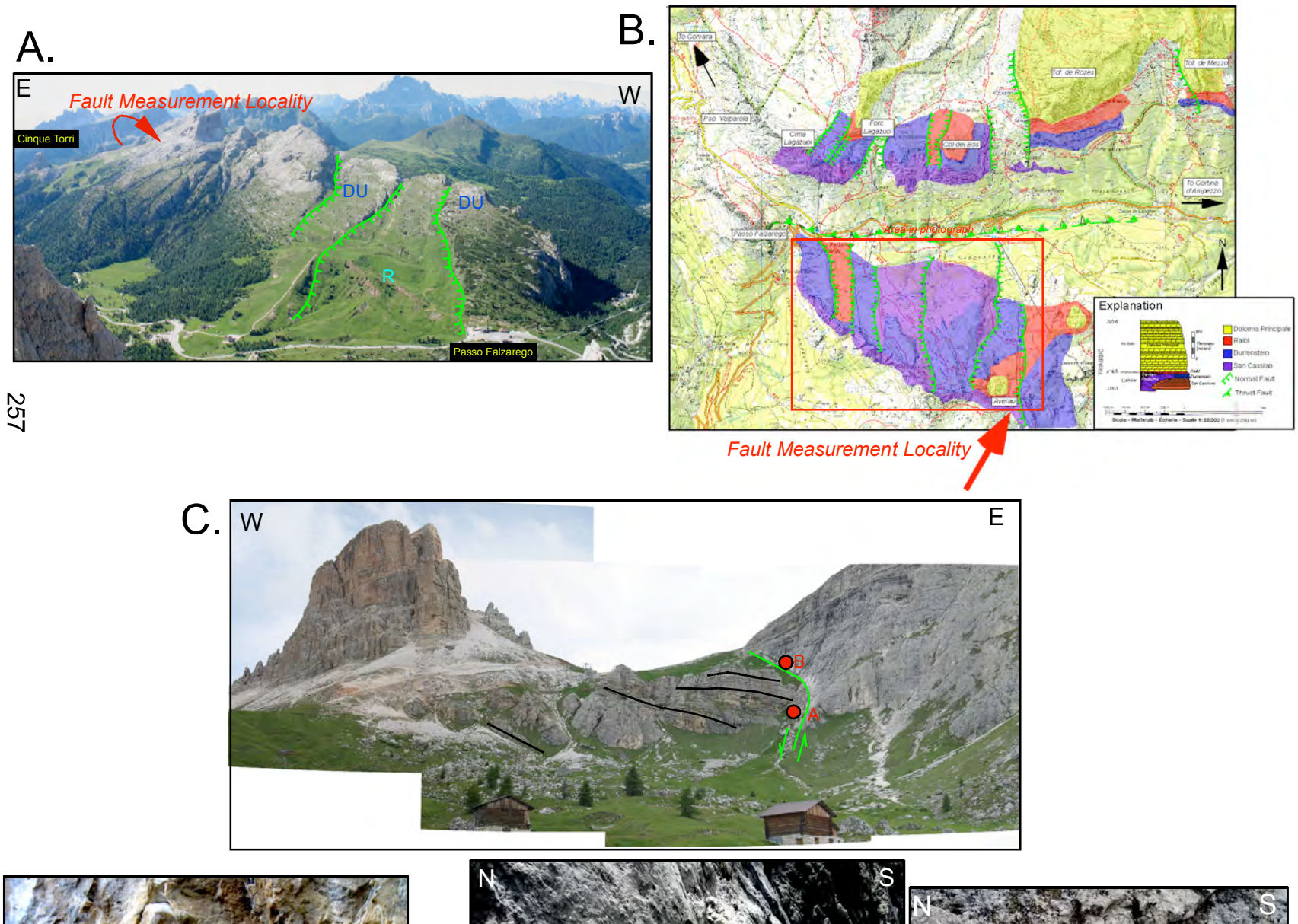

Figure 4.14. Kinematic data from Forcella Averau. A. Photograph of location of fault measurement taken near Passo Giau looking north. B. Location of fault measurement on wanderkarte. C. The fault is located directly under Forcella Averau, with the footwall forming a cliff on the eastern side of the ski piste. The stratigraphy cut by the fault radially "fans" and thickens into the hanging wall. This indicates that the fault was active during sedimentation. Photographs and stereonets of fault planes and slickensides collected at the location shown in A&B. Data are presented as measured and are un-rotated. Photographs and stereonets of fault and slickenside orientation data from locations A&B on Photograph C are presented at the base of the figure. Measurements of fault orientation show general NS strike, with slickensides recording both normal and strike slip motion. Note set 3 is data from a fault antithetic to the main fault.

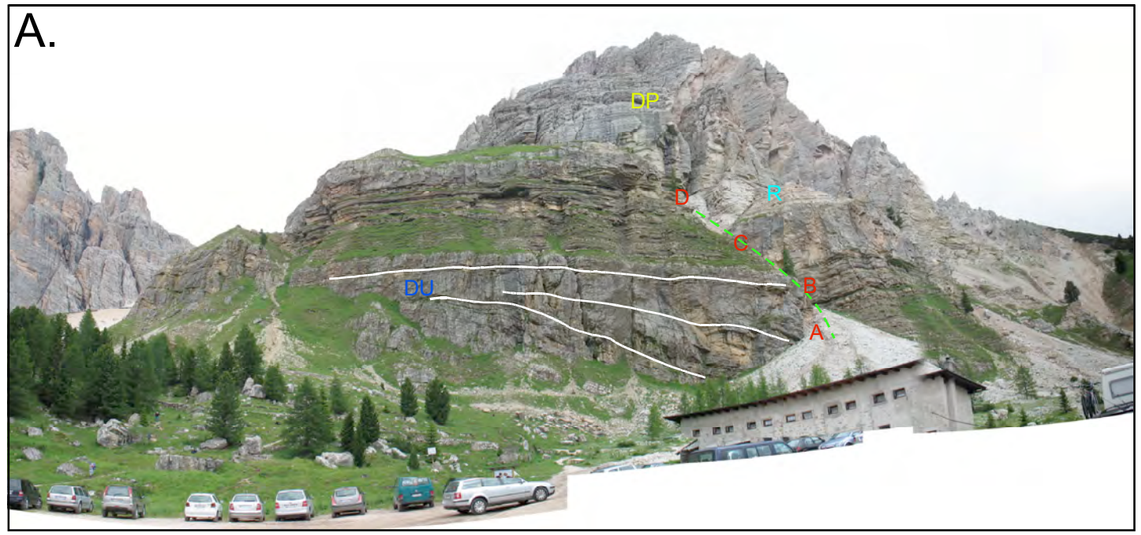


Sub-horizontal slickensides at locality A

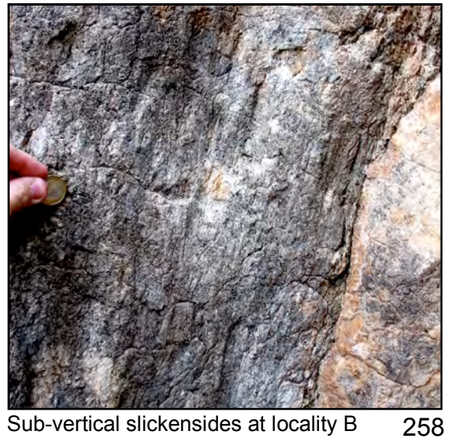
Sub-vertical slickensides at locality B

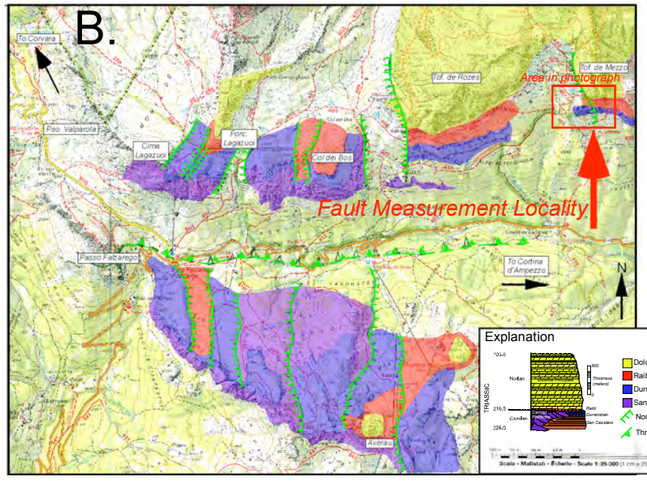


Sub-vertical slickensides at locality C

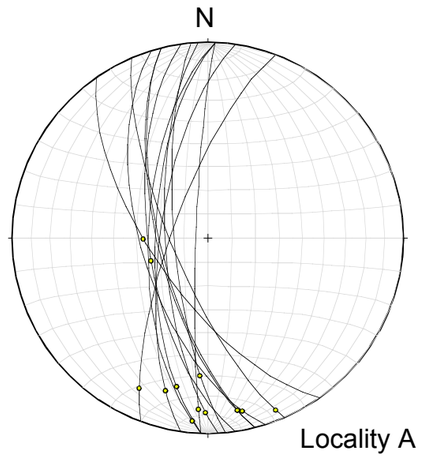

Locality A

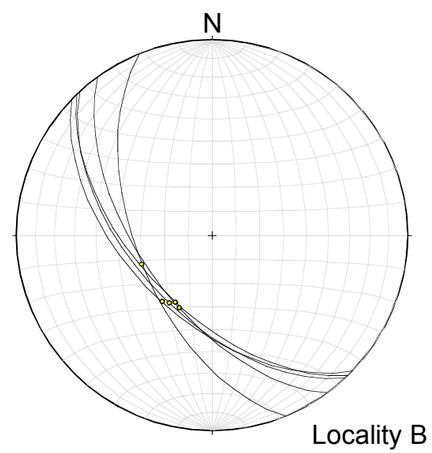

Locality B

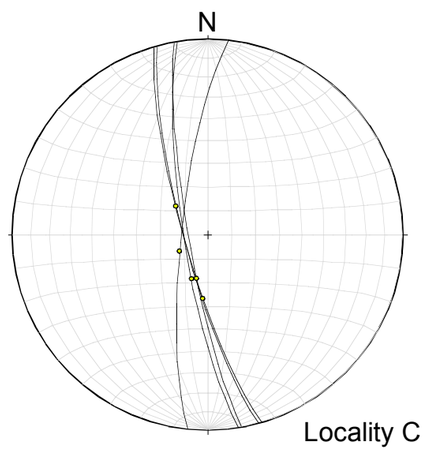

Locality C

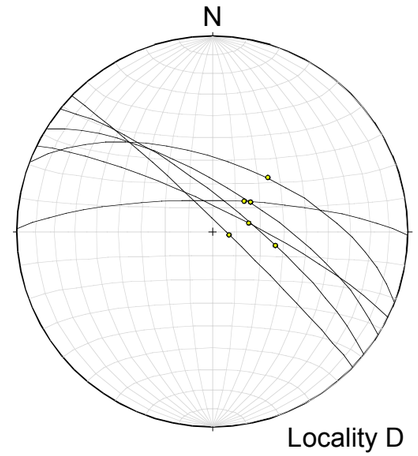

Locality D

Figure 4.15. Kinematic data from Tofana di Mezzo. A. Photograph of location of fault measurement taken from Rifugio Dibona looking north. B. Location of fault measurement on wanderkarte. The fault is located at the base of Tofana di Mezzo above Rifugio Dibona. Fault has a “fan” or radial geometry of beds thickening into the hanging wall, indicative of syn-sedimentary deformation. Photographs and strereonets of slickensides keyed to photograph A. Slickensides record two general movements- both normal and strike-slip. Slickensides measured at the base of the exposure are sub-horizontal, and indicate strike-slip motion, while slickensides measured at the top of the exposure are sub-vertical and indicate with normal motion.

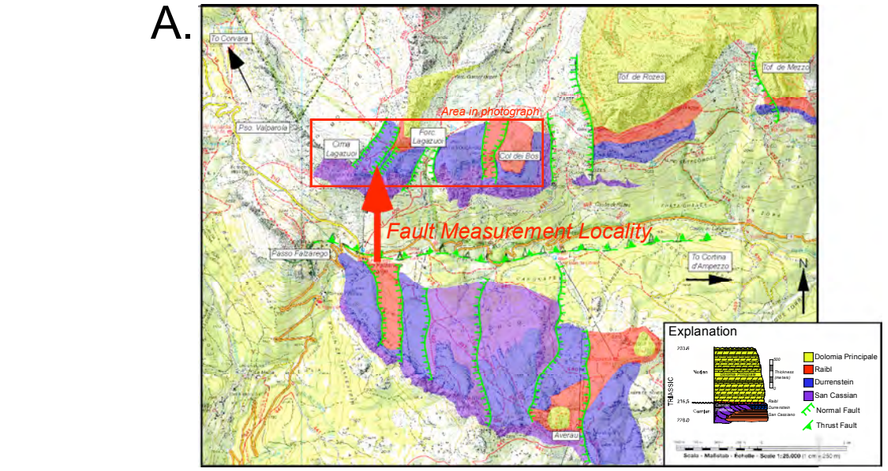

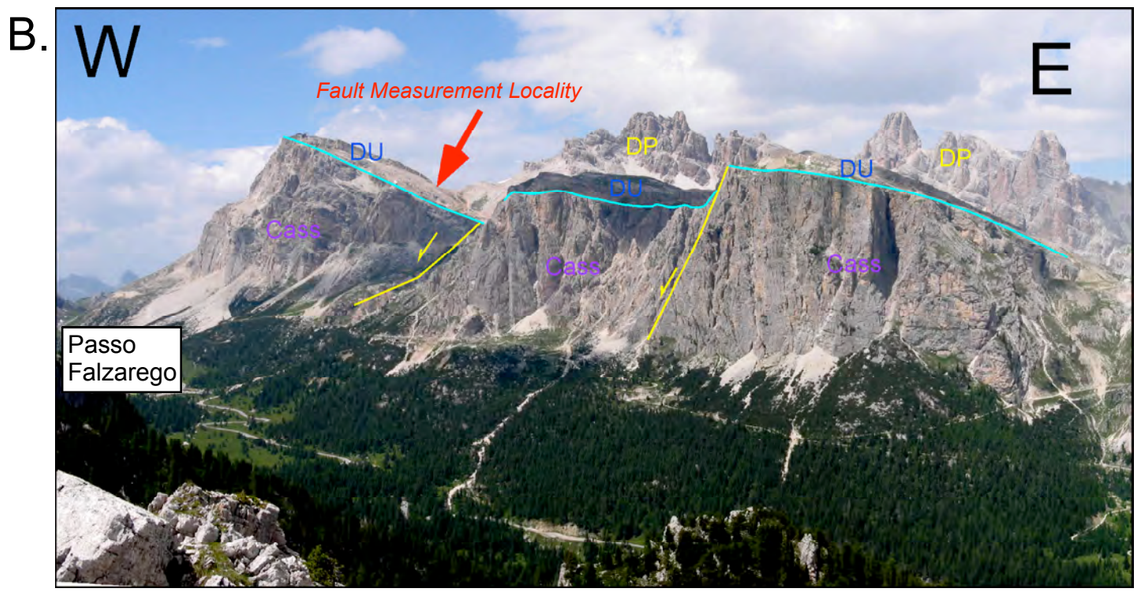

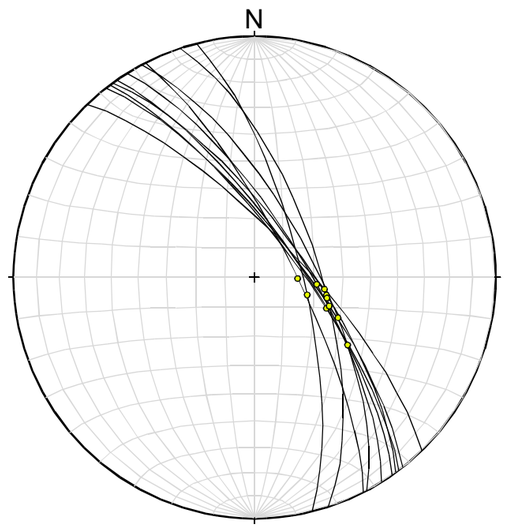

Figure 4.16. Kinematic data from Cima Lagazuoi. A. Location of fault measurement on wanderkarte. B. Photograph of location of fault measurement taken from Cinque Torri looking north. C. Photograph, fault orientation and slickenside data for the normal fault located near Cima Lagazuoi, at a former WW1 Austro-Hungarian entrenchment known as “the rocky wall”. The eastern face of the rocky wall is a fault scarp where slickensides could be measured. Slickensides are subvertical and indicative of normal motion.

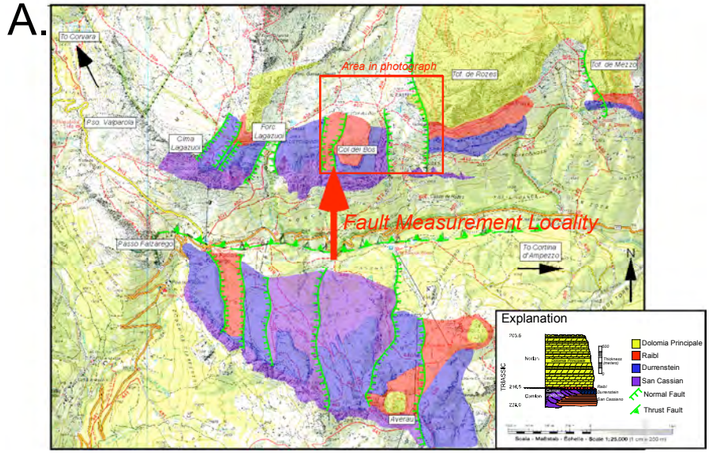

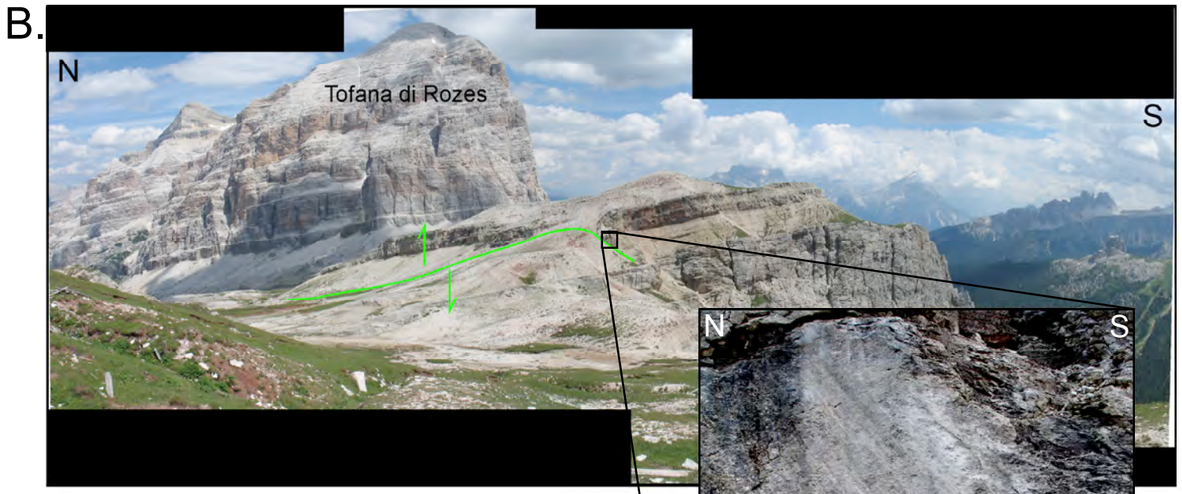

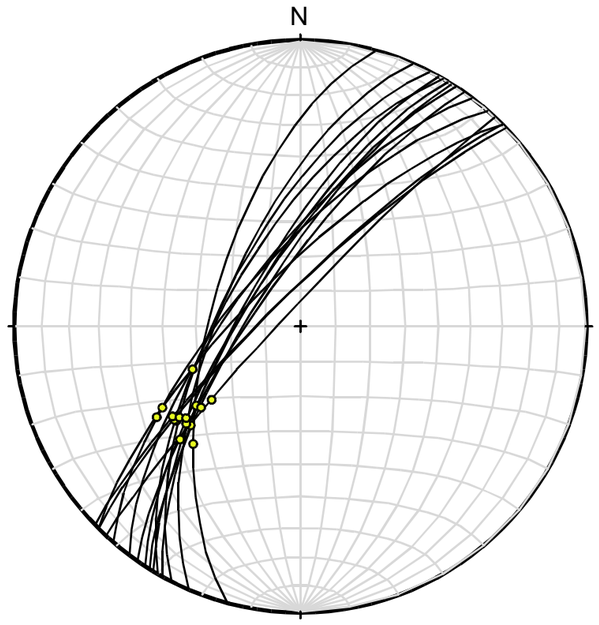

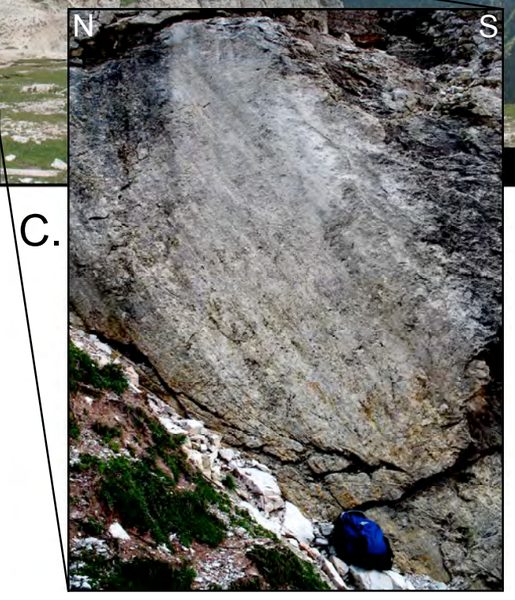

Figure 4.17. Kinematic data from Col dei Bos A. Location of fault measurement on wanderkarte. B. Photograph of location of fault measurement taken from Cima Lagazuoi looking east. C. Photograph, fault orientation and slickenside data for the normal fault located at Col dei Bos. Slickensides are oriented subvertically (note the regional dip of approximately 20 degrees to the north) and are indicative of normal motion.

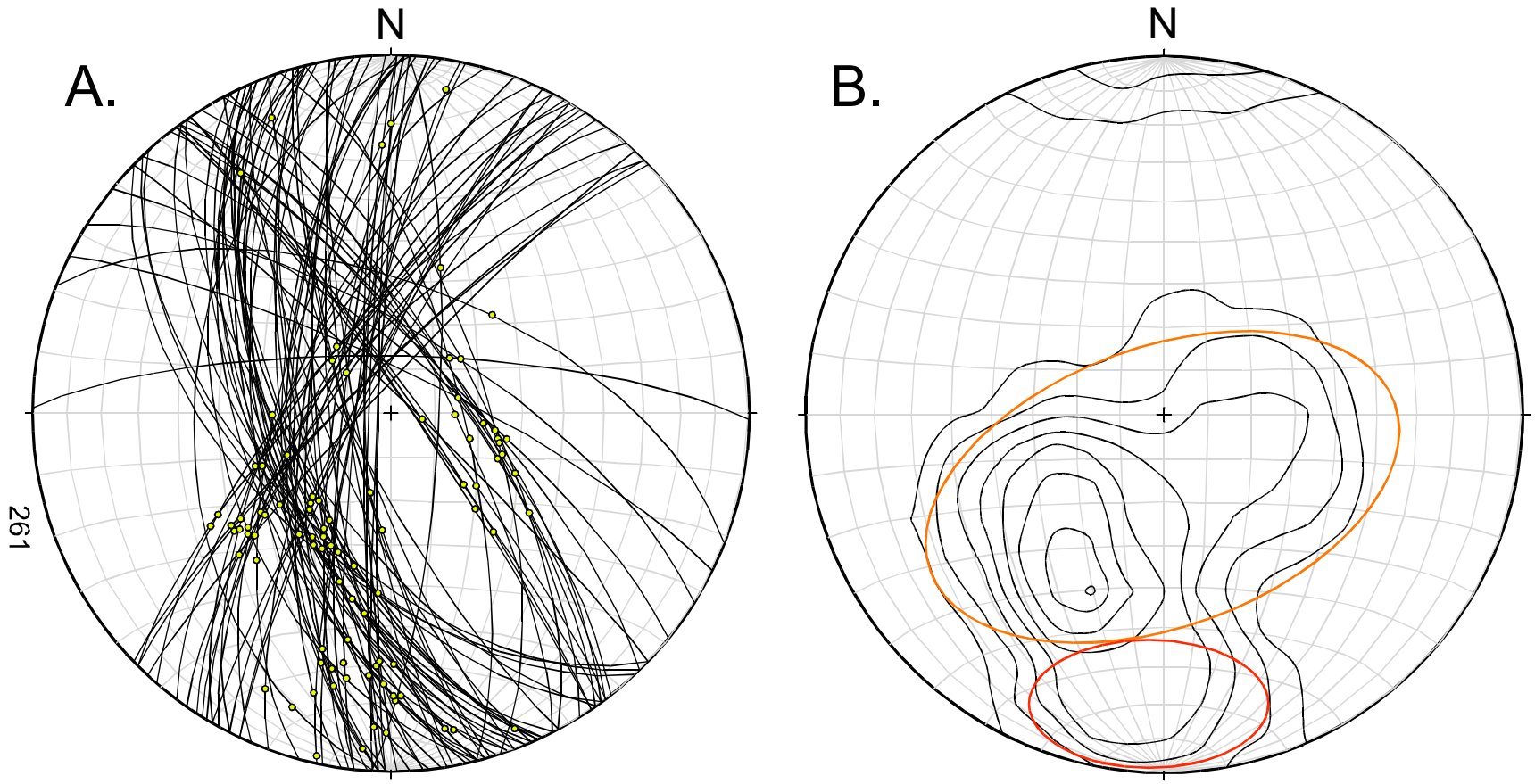

Figure 4.18. A. Sum of all measured fault data from Falzarego area and B. Kamb contour of the trend and plunge of slickenside rakes. Patterns in the data are interpreted as follows- two sets of motion are recorded on the faults displayed here- normal motion and strike slip motion. Normal motion is can be seen on faults dipping either east or west and striking approximately 30 degrees from north (this "double" set of normal indicators reflect the faults and their antithetics, highlighted with the orange circle on the contoured stereonet). A second set of indicators are those recording strike-slip motion, highlighted with the red circle.

A

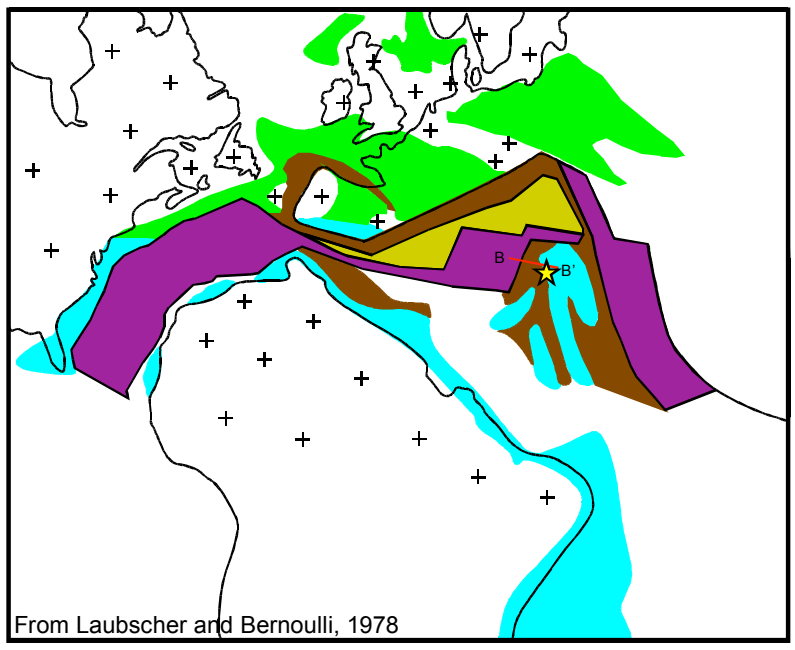

Continental basement with associated terrestrial clastics
Thin, shallow marine marls, sandstones, and limestones
Thick (> 1km) carbonate deposits
Block-faulted areas with thin pelagics or locally restricted limestones
Basinal clastics
Tethyal oceanic crust
Location of Dolomites

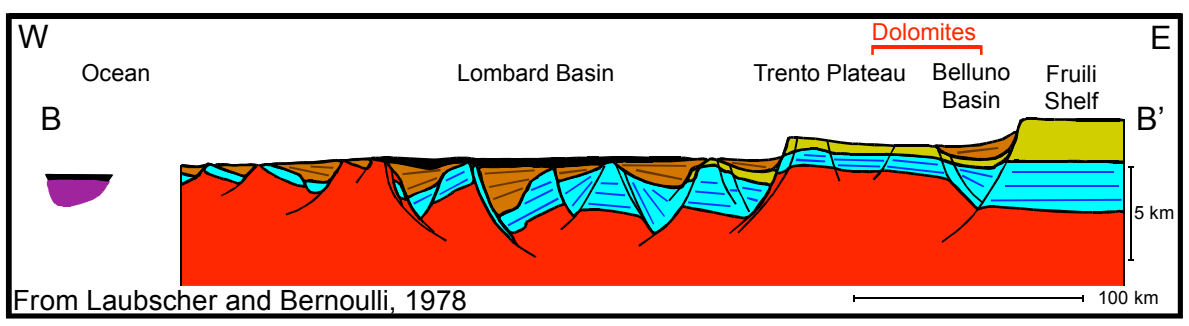

Late Jurassic Pelagics
Oceanic Crust
Early / Mid Jur. Pelagics and Turbidites
Early Jurassic Shallow Water Carbonates
Triassic Carbonates
Paleozoic Continental Basement

B

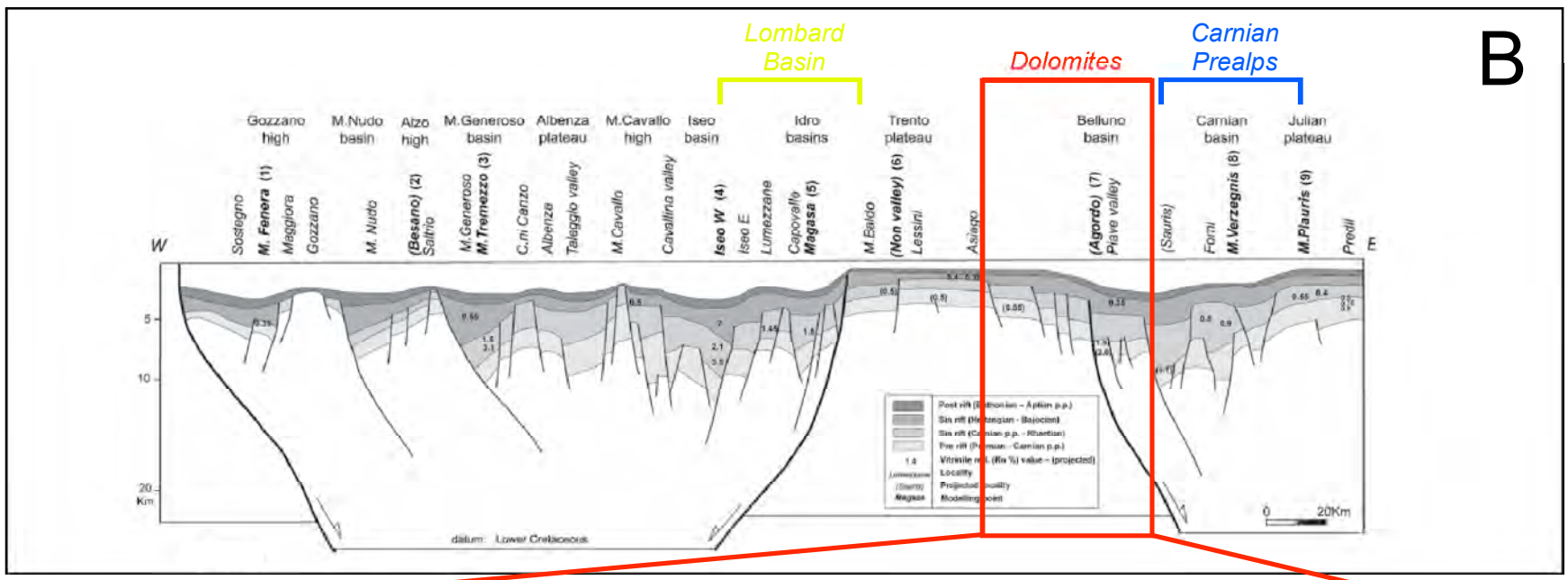

C

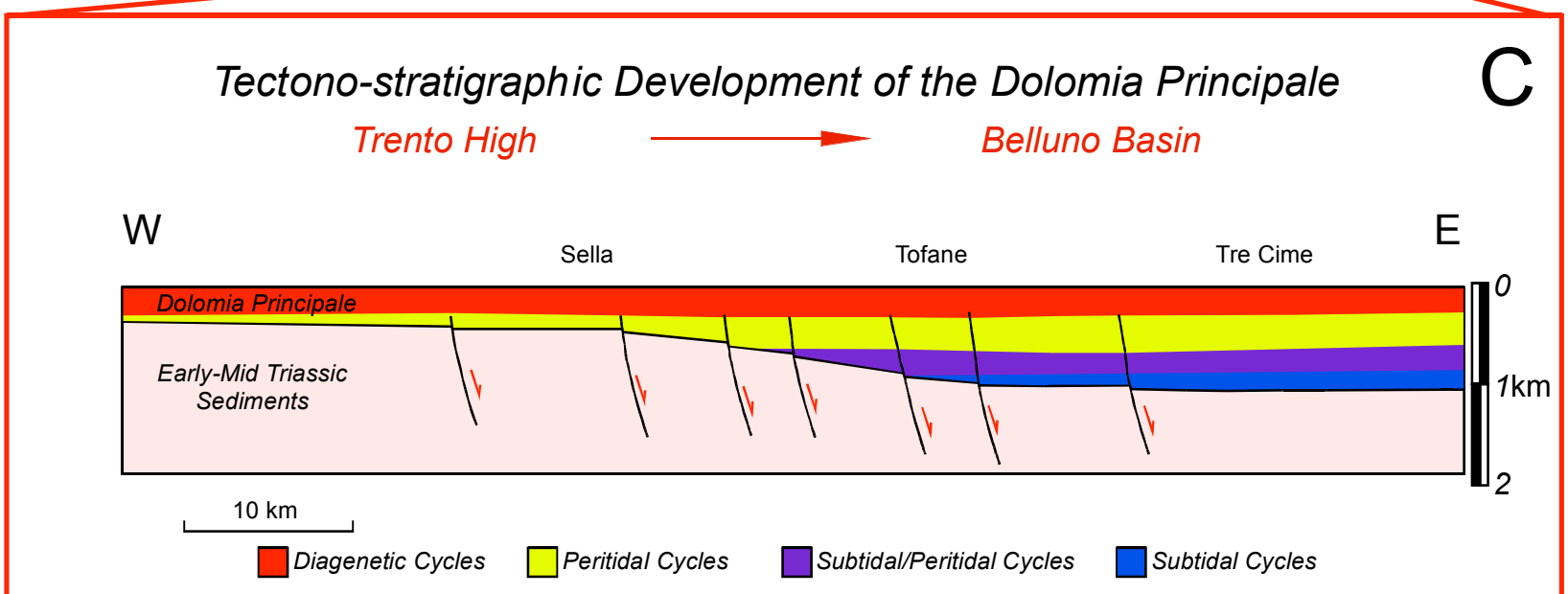

Figure 4.19. Tectonostratigraphic reconstructions of the Southern Alps Early Jurassic paleogeography of the southern Alps (A & B) and of the Dolomia Principale of the Dolomites (C). A. Tectonostratigraphic reconstruction of the Southern Alps by Laubscher and Bernoulli, 1978. Early Jurassic paleogeography of the southern Alps and cross section based on field mapping and formation thicknesses. B. Sketch by Fantoni and Scotti (2003) of the extensional Mesozoic architecture of the Southern Alps included as Figure 7 in this chapter and shown again here for comparison. Cross section was reconstructed using formational thicknesses and vitronite reflectance analysis indicates that organic material was heated to its highest temperatures during the Norian-Liassic rifting. C. Cross section showing tectono-stratigraphic development of the Dolomia Principale in the Dolomites. While synsedimentary faults can be observed in outcrop (see Figures 12-18) offset on observed faults is not more than a few tens of meters. Additional work is required to determine whether or not the faults were tectonic in origin. Differential subsidence controlled the stratigraphic development of the DP in a regional sense (east-west thickness and facies trends).

Chapter 5: Stratigraphic Analysis of the Lower Dolomia Principale, the Dolomites, N. Italy

ABSTRACT

The Norian (Late Triassic, 216.5 Ma-203.6 Ma) Dolomia Principale (DP) is a broad carbonate shelf preserved across much of the Southern Alps, with particularly good exposures outcropping in the Dolomites of N. Italy. The purpose of this study is to analyze the cyclic stratigraphy of the Dolomia Principale of the Dolomites of N. Italy in order to identify any trends in vertical thickness series that may aid in identification of a formative mechanism. The study area is comprised of a transect across the Dolomites from west to east, totaling approximately 100 km. Results of the study indicate several trends from west to east in the Dolomite Principale of the Dolomites, including: an increase in the thickness of the DP from 250 m to over 700 m, and increase in the number of cycles per megacycle from 3:1 to 5-6:1, and a progressively "Milankovitchian" character to cycle stacking frequencies. These trends are interpreted to be the result of regional-scale differential subsidence that may be related to rifting and the development of the Tethyan ocean system. Differential subsidence of the DP in the Dolomites acted to drive carbonate production from mainly supratidal environments in the west to increasingly subtidal environments in the east, rather than acting to drown carbonates altogether as can be observed in the Lombard basin directly to the west of the Dolomites. As a result, sections through the DP

in the eastern Dolomites preserve a cyclic record that is consistent with Milankovitch forcing while sections in the west are condensed due to prolonged subaerial exposure.

INTRODUCTION

The Norian (Late Triassic, 216.5 Ma-203.6 Ma) Dolomia Principale (DP, also known as the 'Hauptdolomit') was a broad peritidal carbonate shelf deposited on a regional scale (several hundreds of km^2), and is preserved atop several mid-Triassic carbonate platforms in the Southern Alps (Gradstein et al., 2005) (**Figure 5. 1**). Early studies by Bosellini and Hardie (1985) recognized vertically repetitious of shallowing-upward facies successions throughout the DP. Laminate-capped peritidal facies successions composing the basal two-thirds of the total thickness, and massive subtidal dolostones with diagenetic exposure caps dominating the top one-third. These cyclic successions were interpreted by Bosellini and Hardie (1985) to have formed as the result of Milankovich-driven glacio-eustasy, requiring repetitive meter-scale sea level oscillations with frequencies of 10^3-10^5 years. However, Bosellini (1967) and Bosellini and Hardie (1985) also recognized that correlation of cycle thickness series from one locality to another (km-scale) was difficult to achieve and suggested that spasmodic subsidence on individual structural blocks may have affected the stratigraphic development of the DP. Jadoul et al. (1992) and Cozzi (2000) recognized depositionally overlapping faults at the cm and multi-meter scales, thickness

variability in the DP, and intrashelf mini-basins within the DP complex in the Lombard basin (adjacent to and directly west of the Dolomites) and the Carnian Prealps (adjacent to and directly east of the Dolomites) as the result of syndepositional extension associated with the opening of the Tethys. Chapter 4 of this dissertation details similar features identified in the Dolomites, specifically near Passo Falzarego. No published study of DP cyclicity in the Dolomites, includes multiple sections measured at the meter-scale. This study is an investigation to document the cyclic stratigraphy of the DP in the Dolomites in order to identify what mechanisms acted on the development of late Triassic platform interior carbonate strata.

PURPOSE AND SIGNIFICANCE

The purpose of this study is twofold: (1) document the regional cyclostratigraphy of the Dolomia Principale and (2) to quantify the stratigraphic response of the Dolomia Principale to synsedimentary extension. There are two significant reasons why a stratigraphic study of the DP is important. First, the study of the DP stratigraphy provides the opportunity to examine the stratigraphic response of platform carbonates to differential subsidence at a high (meter-scale) resolution. Examination of cyclic successions across fault zones can reveal whether accommodation created by differential subsidence affected the number of depositional cycles generated at each locality, whether the cycle thickness differs from locality to locality, or both. Quantifying stratigraphic response to

synsedimentary extension is based on 6 measured sections (approximately 700 meters total, measured at the cm-scale) along a 100 km east-west transect. Faults separate all of the sections measured.

The second reason why a study of the DP is important relates to the timing of periodic depositional cyclicity from the middle through the late Triassic. The “Latemar controversy” (discussed in Chapters 2 and 3) centers around three competing hypotheses relating to the timing of depositional periodicity in the middle Triassic, with depositional cycles forming in response to either Milankovitchian eustasy, mixed Milankovitchian and sub-Milankovitchian eustasy, or purely sub-Milankovitchian eustasy (Goldhammer et al., 1987; Zühlke, 2004; Kent et al., 2004; Emmerich et al., 2005). Current empirical datasets from dated zircons support the hypothesis that the Latemar platform cycles formed at rapid, millennial-scale periodicities. In addition to the hypothesis that mid-Triassic platform carbonate cycles formed at millennial periodicities Muttoni et al. (2005) has proposed new dates of 227.5 Ma to 208 Ma for the Norian stage (the Norian is currently dated from 216.5 Ma to 203.6 Ma, according to the International Commission on Stratigraphy 2004), thereby adding 7 million years to the Norian. This “long Norian” hypothesis, along publications dealing with depositional cyclicity in the late Triassic, argue strongly for Milankovitch periodicity of depositional cycles in Norian time (Fischer, 1964; Bosellini and Hardie, 1985; Goldhammer et al., 1990; Olsen and Kent, 1999; Muttoni et al., 2004;

Schwarzacher, 2005). Taken together, millennial-scale periodicitiy of mid-Triassic depositional cycles and Milankovitch control of late Triassic depositional cycles requires a shift in cyclic depositional periodicity from the mid Triassic (1-2 kyr/depositional cycle) to late Triassic (20 kyr/cycle). Therefore, stratigraphic analysis of multiple DP sections is important in order to decipher whether or not Milankovitch forcing affected the deposition of the DP in the Dolomites.

LOCATION AND GEOLOGIC SETTING

Exposures of the Dolomia Principale can be found throughout the Southern Alps (e.g. Lombardian Alps, Dolomite Alps, Carnian Prealps). The locality of this study is the Dolomite Alps. The Dolomites are a mountain chain located in the North of Italy and are bordered by the Adige valley to their west, to the north by the Insubric lineament, and to the south by the south-vergent Valsugana overthrust (Doglioni, 1986; Bosellini, 1991) (**Figure 5. 2**).

The sedimentary history of the exposures in the Dolomites begins in the upper Permian and continues through the lower Cretaceous. The most volumetrically significant portion of sedimentary geology spans Triassic time, when two phases of rifting related to the breakup of Pangaea and development of the Tethyan ocean system are thought to have occurred (Bernoulli and Lemoine, 1977; Doglioni, 1986; Bosellini, 1991). The stratigraphy of the Dolomites preserves a classic “rift-drift” succession of volcanics, redbeds, evaporites, marine carbonates and clastics and a final basinal drowning

succession. Rifting associated with the breakup of Pangaea and opening of the Tethys resulted in the emplacement of a volcanic complex with porphyritic ignimbrites locally exceeding 2000 meters in thickness (Bosellini, 1991). Rift-related sinistral transtension was active throughout the region from the late Permian through the early to mid-Triassic (Doglioni, 1986). Block faulting associated with strike-slip movement led to the development of N-S trending highs (e.g. the Trento/Atesina Platform), and sedimentary basins (e.g. the Ligurian and Belluno basins) (Bernoulli and Lemoine, 1980; Doglioni, 1986; Bosellini, 1991) (**Figure 5. 3**). Nucleation and growth of Anisian and Ladinian carbonate platforms within the Belluno basin is thought to have been the result of strike-slip block faulting and emplacement of magma (sourcing later Ladinian volcanics), creating the bathymetric highs on which carbonate strata accumulated (Winterer and Bosellini, 1981; Doglioni, 1986; Bosellini, 1991). Sea level drop and volcanic activity in the late Carnian led to an influx of siliciclastic (Raibl Fm.) and volcaniclastic sediments, which buried the Anisian-Ladinian platform-and-basin system and leveled depositional bathymetry (Bosellini, 1991; Bertotti et al., 1993). Upon sea level rise, carbonates nucleated on the near-level surface and developed into regional-scale carbonate shelves (hundreds of km^2). The Norian Dolomia Principale (DP) is the first of these regional peritidal carbonate packages, and reaches thickness in excess of 1 kilometer in the Dolomites and upwards of 2.5 kilometers in the Carnian Prealps directly adjacent to and east of the Dolomites (Bosellini, 1965, 1967; Winterer and Bosellini, 1981;

Bosellini, 1991, Bertotti et al., 1993; Cozzi, 2000). The DP is overlain by broad subtidal carbonate units, the Dachstein limestone and Calcari Grigi formations, which are in turn overlain by a succession of deep-water carbonates (Jurassic Ammonitico Rosso and Cretaceous Puez marl) and pelagic shales (Bosellini, 1991). The Dolomites are currently part of a large pop-up synclinorium of Neogene age constituting a relatively coherent slab of crust carried south 8-10 km during Alpine orogenesis (Doglioni, 1986, 1992; Bosellini, 1991). As a result, the Dolomites are relatively undeformed, preserving a record of magmatic, tectonic, and sedimentary events from post-Hercynian rifting through Alpine collision (Bosellini, 1991).

METHODS

The data generated in this study were collected in the form of 6 sections totaling over 700 vertical meters measured at the centimeter-scale. The sections were collected along an east-west transect across the Dolomites, beginning near the town of Ala and ending at Tre Cime di Lavaredo, roughly 100 km to the east/northeast (*see* Figure 5. 1). The transect was devised in relation to previously mapped Triassic-age faults, which strike roughly North-South and with displacements downdropped to the east (Doglioni, 1992). Five of the six sections were measured from the Raibl-DP lithostratigraphic contact. It is recognized that this may be a diachronous contact between localities, it is at least a recognizable demarcation of lithologic change, and easily identified from a distance.

Section Identification and Measurement

Most exposures of the DP in the Dolomites are in the form of vertical cliffs several hundred meters in height. In order to measure sections through the DP, localities had to be identified where either roadcuts or talus slopes flank the exposures such that an ascent through the section was negotiable. Sections from the Raibl-DP contact were measured upwards to the furthest accessible height. In discussions with Dr. Carlo Doglioni (U. Roma) as well as Dr. Andrea Cozzi (ETH Zurich), the common definition of the base of the DP formation over the Raibl is at the first occurrence of a “loferite”, or laminite capped shallowing-upward carbonate cycle (*see* Fischer, 1964). However, the Raibl is not lithologically homogeneous from locality to locality, and in some locations it was difficult to determine where the Raibl formation ends and where the DP begins (**Figure 5. 4).** The Raibl becomes both thicker and increasingly dominated by marine sediments from west to east in the Dolomites. For example, at the Sella massif the Raibl is quite thin (a few meters thick to absent), and actually is missing from the section entirely near the center of the buildup. Further east at the Fanes group, the Raibl is silty sandstone at the base, alternating with skeletal/megalodont wackestones upwards, before grading into partially brecciated carbonate tidal flat beds in the DP. Still further east at Monte Cristallo near Cortina d'Ampezzo, the Raibl is dominated by clastics at the base and evaporites near the top. Finally, at Monte Pelmo and Tre Cime di Lavaredo, the

Raibl transitions from clastics into a 20-30 m thick succession of subtidal carbonate cycles (possibly an equivalent to the Monticello formation of Cozzi and Hardie, 2003). The transition from thin/absent clastic-prone Raibl at the Sella to carbonate dominated Raibl at Tre Cime occurs over an east-west transect of approximately 50 km. This presented a fundamental problem relating to where measured sections ought to begin, as the Raibl-DP contact is not lithostratigraphically consistent from locality to locality. To resolve the problem, sections were started at least 10 meters below the occurrence of the first shallowing-upward carbonate tidal flat cycles (also known as Lofer cycles).

Section measurement included describing lithology, texture (Dunham, 1962), presence or absence of fossils, and vertical thickness of individual facies at the centimeter-scale. The thinnest beds measured were approximately 3.0 mm shale partings between peloidal wackestones at Tre Cime di Lavaredo. Cycle boundary interpretations were made after each bed/facies was individually measured and described. Photographs keyed to measured sections were taken, and 150 representative samples were taken at regular intervals (nearly 1200 pounds total) for hand sample and thin-section analysis. Forty samples were sawn and polished as both hand specimens and thin section blanks for facies identification.

Structural Methods

The general structural framework of the area under investigation was determined via literature search, with introductory field excursions provided by Dr. Carlo Doglioni from the University of Rome. The greatest concentration of faults thought to be synsedimentary (Carnian-Norian) were found in Val Falzarego, where numerous N-S trending grabens were identified. Structural analysis of the area is detailed in Chapter 4.

SEDIMENTOLOGY

Introduction

Correct interpretation of facies and depositional environment is key to understanding Waltherian relationships in facies distribution in a landward-to-basinward sense (Middleton, 1973). Analysis and interpretation of facies is crucial to deciphering evolution of depositional environments and facies belts through time. In this case, analysis and interpretation of facies within the DP of the Dolomites indicates that the repetitious shallowing upward successions are carbonate deposits formed in shallow water (10 m) to exposed (tidal flat) settings. This interpretation is based on careful identification of facies in both hand sample and thin section based on comparative sedimentology. In fact, facies descriptions of DP facies are similar to the Holocene shallowing-upward tidal flat succession described by Hardie (1977) (**Figure 5. 5**).

The depositional cycles of the Dolomia Principale are organized vertically into repetitive shallowing-upward facies successions. Complete cycle thicknesses vary per locality from 0.8 m to 1.4 m. From base to top, the subfacies are: 1) intraclastic breccia with common clasts eroded from the underlying bed; 2) peloidal mud-to-wackestone with worm burrows and common oxide framboids; 3) mixed-skeletal bioturbated megalodont wacke-to-packstone with mollusks, gastropods, echinoderms and dasycladales, becoming fauna-poor and incipiently laminated towards the top; 4) crinkly fenestral laminites with both tubular and elongate fenestrae and laminated tufts; laminae become thinner and smoother upwards, with cm-scale mudstone interbeds observed, and; 5) disrupted zone with buckled and antiformally-displaced mother rock with void space filled by fibrous carbonate cement and red silt; 6) yellow and red “karst breccia” with dissolution tubes. This facies has a chaotic, brecciated fabric (larger blocks of cm to 10s of cm scale in silty dolomicritic matrix), which is also generally cut into by overlying intraclastic breccias (**Figure 5. 6, fold-out**). While the above outlines all facies that may occur in a DP depositional cycle, most do not contain every facies. For example, successions deposited in deeper water settings will contain 3 or 4 subfacies from the deeper water environments, while successions deposited in shallower environments tend to be dominated by repetitive successions of 3 or 4 shallower-water facies.

The vertical succession of facies within each depositional cycle in the DP are strikingly similar to those identified by Fischer (1964) as a "Lofer cycle" (laminite capped carbonate cycle), as well as the classic shallowing-upwards tidal flat succession known from studies of modern tidal flats from Andros Island, Bahamas (Fischer, 1964; Bosellini and Hardie, 1985; Hardie and Shinn, 1986; Goldhammer et al., 1990; Demicco and Hardie, 1994) (**Figure 5. 7**). In particular, the facies-to-facies similarity between shallowing-upwards successions in the DP and those from the Holocene of Andros Island serve as indicators of depositional environment for each facies. Facies 1-6 identified through hand sample, thin section, and comparative sedimentologic analysis are examined individually and in greater detail below.

Facies I. Intraclastic Breccia

Observations

Base-of-cycle breccias are common within the DP, occurring in approximately 50% of the shallowing-upward cycles measured. In general, breccias are composed of cm-scale clasts suspended in micritic matrix (**Figure 5. 8**). Clasts within intraclastic breccias show some degree of rounding, likely a result of edges having been nicked off during transport. Clasts are predominantly composed of microbial laminite facies, but clasts from other facies types have been identified. Most clasts appear to have been ripped from underlying beds and are between 2 cm and 5 cm long, with long-direction parallel to internal

lamination of the clast. In rare cases, clasts over 30 cm in length can be observed. Breccias may fine up into blue-green massive mudstone or pelleted wackestone that are littered with oxide framboids.

In thin-section, intraclastic breccias typically show a dual composition of rounded clasts and micritic matrix (**Figure 5. 9**). The majority of the clasts within brecciated facies are consistent with facies described as cryptomicrobial laminites (described in detail in Facies 4 section). However, other types of intraclasts can be found, and include skeletal, pelleted wacke-to-packstones, and clasts of lithified intraclastic breccia. The presence of clasts of multiple facies types indicates that the breccia-generating event was either a) deeply erosive, or b) areally extensive enough to have incorporated and transported portions of the contemporaneous subtidal substrate (**Figure 5. 10**).

Interpretation

Depositional environments associated with each facies are well documented in the literature. Early studies of carbonate intraclastic breccia and flat-pebble conglomerate deposits cited storms (tempestites) as the usual cause of both erosion of the substrate and the deposition of breccia facies (Aigner 1982, Einsele and Seilacher 1982, Sepkoski 1982, and Wanless at al., 1988). Tempestite stratification, as defined by Aigner (1982), is the result of a high-energy event, probably most commonly a storm, that initially is erosive and

becomes depositional as energy wanes. Aigner (1982) recognized that storm scour may erode down to a previous coarse cemented layer (removing all other material) whose presence may inhibit further scour (**Figure 5. 11**). Bedded breccia deposits of this type may have multi-event geneses.

In studies of modern shallow water carbonate and tidal flat environments in the Bahamas (e.g., Hardie 1977; Hardie and Shinn, 1986; and Demicco and Hardie, 1994) suggest three main generative mechanisms for intraclastic breccias: 1) lateral accretion lags from migration of tidal channels; 2) storm lags; and 3) transgressive lag (**Figure 5. 12**). Where breccias are stratiform and/or non-channelized, the latter two mechanisms are favored. Subtidal intraclastic conglomerates – both carbonate and siliciclastic – are commonly interpreted to be storm or swell lags deposited in shoreface-type environments. These may form the base of hummocky cross-stratified, planar-stratified, graded beds that fine upward into wave rippled and bioturbated sands. Transgressive lags however, may be brecciated at the bases and have subsequent physical sedimentary structures masked by bioturbation as a result of the environment shifting to deeper water.

According to Demicco and Hardie (1994), intraclastic breccias and conglomerates are a ubiquitous component of modern and ancient shallow marine carbonate deposits, with many appearing to be generated during storm

events (**Figure 5. 13**). High current energy may also form intraclastic breccias, and many examples can be found flooring intertidal channels. Early descriptions of the facies and cycles in the DP also included descriptions of intraclastic breccias at the bases of cycles. Bosellini and Hardie (1985) observed that upper and lower boundaries of cycles are typically sharp, while transitions within inter-cycle subfacies are comparatively gradational. Bottoms of cycles are typically erosive, with reworking of the upper part of the underlying cycle suggested by the presence of mud chips and flat laminate pebbles. This is followed upwards by bioturbated mud-to-wackestone, recording subtidal environmental conditions.

In all likelihood, the breccias observed in the bases of cycles within the DP of the study area were generated by high-energy events that eroded and re-deposited lithified and partially-lithified clasts of intrabasinal material. It is difficult to determine whether these breccias always represent a eustatic "transgressive lag" as might be expected from shoreface ravinement, storm-type events that were erosive, or some combination of both. If intraclastic breccias represent transgressive lags, then either a) the flooding event leading to the generation of the next cycle must have been a high-energy event, or b) the lag time between flooding of the platform and re-initialization of carbonate sedimentation allowed for reworking of the substrate during storm events. Alternatively, intraclastic breccias may represent storm re-working of the substrate that may not be related to eustatic rise. This conclusion seems equally plausible, because a) breccias

within the DP are not absolutely exclusive to cycle bases, and b) not every cycle boundary is marked by an intraclastic breccia, which might be expected if intraclastic breccias were to only reflect eustatic rise in sea level. In addition, circum-granular cracks around caliche clasts indicate that some degree of desiccation took place after deposition, suggesting that whatever event formed the breccias was not necessarily related to long term flooding of the environment (see Figures 5. 9 & 5. 10). In three cases, channelized breccia deposits are identified as the remnants of tidal channels within the DP tidal flat complex (**Figure 5. 14**).

Facies 2. Massive Peloidal Mud-to-Wackestone

Observations

Carbonate mudstones in the DP typically weather as recessive intervals that are observable from a distance (**Figure 5. 15**). These intervals are sometimes referred to as "shales" by local people, due to the fact that the rock may be dark colored and is easily broken apart into porcelain-like shards. Massive mudstones are typically green to dark gray, generally lack recognizable fossil forms, are commonly found above intraclastic breccias, and underlie mixed skeletal wackestone (**Figure 5. 16**). Small (< 1 cm), sub-spherical oxide balls or framboids are common along horizons within mudstone beds.

Most mudstones are dominated by a dolomicrite matrix with intraclastic grains (**Figure 5. 17**). Thin (mm-scale) sub-vertical “worm” tubes are also common in the mudstone facies. In thin section, the tubes are found to be backfilled with geopetal sediment, suggesting that the sediment was cohesive when the tubes formed. It is not known what fauna formed the burrows, but they are reminiscent of *skolithos*-type feeding traces or, more likely, tubes of precipitated calcium carbonate constructed by worms inhabiting the substrate (Frey and Seilacher, 1980). There is a paucity of other allochems or bioturbation within the mudstone facies.

Oxide balls or framboids are common in outcrop and can be observed along horizons in mudstones as small (mm-scale) balls of rust-colored material. In microscopic view, oxides appear are opaque round balls or raspberry-shaped clumps of small cubes (**Figure 5. 18**). In reflected light, oxides are rust-colored, as they are in hand-sample. In either case, both of these forms would be consistent with either pyrite or sphaerosiderite as the formative, pre-oxidized phase.

Interpretation

Massive mudstone beds are usually found above intraclastic breccias and underlie mixed skeletal wackestones. This may imply that the mudstones are suspension sedimentation after a breccia-producing energetic event. However,

physical sedimentary structures have not been identified within massive mudstone facies, nor have any textural trends within the facies, either of which would be expected in suspension sedimentation. It is more likely that the mudstones represent a low energy depositional environment with conditions not amenable to diversity of faunal forms.

The scarcity of fossil remains, moderate bioturbation, lack of physical sedimentary structures, and the presence of oxide blebs are not features of any other facies within the Dolomia Principale. The lack of these features made determination of depositional environment problematic. In a study of Holocene tidal flat environments, Shinn (1986) observed that while subtidal environments vary greatly, the common features of subtidal sediments in anoxic settings are dark, grayish color, a lack of sedimentary structures, and a characteristic rotten egg smell due to the presence of sulfate-reducing bacteria. These environments are typical for low-energy restricted settings, either in ponds or in shallow subtidal environments where sediments are rarely exposed to air (Shinn, 1986). Faunal forms within the system are limited to gastropods and benthic forams that can tolerate low oxygen levels and are attached to organic litter on the substrate (Shinn, 1986). The description of sediments from Holocene anoxic subtidal settings is very similar to the massive mudstone facies of the Dolomia Principale.

In addition to DP massive mudstones being similar in appearance and texture to sediment formed in shallow anoxic environments in the Holocene, the presence of oxide balls (likely former framboidal pyrite) also testifies to the presence of reducing conditions at the time of deposition. Work by Wilken and Barnes (1996), Wilken at al. (1997) and Bellanca et al. (1999) in both modern and ancient settings identify framboidal pyrite forming in anoxic marine sediment, with iron and sulfur sourced from seawater. In addition, studies by R.L. Folk describe petrified nannobacterial cells forming the framework of framboidal pyrite masses, suggesting an organic origin for pyrite framboids in reducing marine conditions (Folk, 2005).

Facies 3. Mixed Skeletal Wacke-to-Packstone

Observations

Massive, bioturbated mixed skeletal wackestone-to packstone (or biomicrite) facies make up the thickest individual subfacies within shallowing upward depositional cycles in the Dolomia Principale (**Figure 5. 19**). Skeletal wacke-to-packstones typically overlie intraclastic breccias and grade upwards into microbial laminites. This facies is characterized by massive, fossil-rich beds, typically without physical sedimentary structures. Evidence of bioturbation may be in the form of a nodular fabric or open tubular fenestrae. Fossils within this facies are numerous, and include megalodont pelecypods ranging in size from 5 cm to 30 cm long, gastropods, dasycladacean algae, benthic forams, oncoids and echinoderm debris. Megalodont pelecypods increase in size eastwards,

reaching their largest size (40 cm) at Cima Ovest. Increasing size of pelecypods to the east may reflect deeper subtidal conditions from west to east. This facies typically becomes faunally restricted upwards, becoming limited to gastropods and dasycladacean algae near the top of the bed. Incipient microbial lamination is also common where this facies is grades upward into laminite facies.

Numerous and varied allochems are identified petrographically in the mixed skeletal facies (**Figure 5. 20**). Texturally, samples vary between wackestone and grainstone. Most samples are dolomitized, with relict textures somewhat difficult to determine where replacement by dolomite was fabric-destructive such that allochem ghosts are the only clue to depositional texture (**Figure 5. 21**). Skeletal grains and associated allochems identified in thin section include Norian Dasycladale *Gyroporella vesiculifera* (**Figure 5. 22**), oncoids (**Figure 5. 23**), megalodont bivalves (**Figure 5. 24**), forams (**Figure 5. 25**), and peloids (**Figure 5. 26**). Other skeletal fragments were also likely present although fabric destructive dolomitization makes accurate identification nearly impossible (**Figure 5. 27**).

Interpretation

The mixed skeletal wacke-to-packstone facies in the DP was generated in a shallow (10 m or less) low-energy subtidal depositional environment with abundant density and diversity of carbonate producing flora and fauna. This

facies is very similar in description to the “Megalodont Limestone” of Fischer (1964) in the Rhaetian Dachstein Formation. Fischer (1964) reported textures ranging from well-winnowed grainstones to massive carbonate mud. Fossil biota within the megalodont limestone is varied, and includes oncoids, red algae, green algae (both codiacean and dasycladacean), sponges, corals, bryozoans, brachiopods, gastropods, pelecypods (rare) ammonites, ostracodes, and echinoderms (Fischer, 1964). Fischer describes the depositional environment that produced the megalodont limestone as a shallow, neritic realm, with diversified biota living near, but decreasing landward of, the reef margin, as a direct response to deviation from normal marine salinities. Goldhammer et al. (1990) interpreted the megalodont limestone as the subtidal member of each shallowing-upward cycle in the Dachstein Formation.

As with each of the previous facies, identification of depositional environment with the mixed skeletal wacke-to-packstone was done through literature comparison. Other workers studying the Dolomia Principale also interpret the mixed-skeletal wacke-packstones as deposited in a low-energy subtidal depositional environment. Early studies by Bosellini (1967) described a subtidal unit within each depositional cycle, identified as a massive crystalline dolomite with megalodonts and gastropods. Bosellini and Hardie (1985) compare their sections to the modern shallowing-upward tidal flat cycle of Enos and Perkins (1979), where mixed skeletal wackestones and packstones formed

in the subtidal realm and microbial laminites occur in the supratidal. Cozzi (2002) observes similar features in the DP of the Carnian Prealps, noting that this subfacies in typically intensely bioturbated and is heavily pelleted/peloidal with sparse intraclasts and common Megalodonts, benthic forams, crinoids, gastropods, and mixed pelecypods. Again, Cozzi (2002) interprets the facies as the subtidal member of a shallowing upward cycle.

The most prominent fossil of this subfacies is the megalodont pelecypod, a pachydont clam, and thought to be an ancestor of the rudistids (Zapfe, 1957) (**Figure 5. 28**). Megalodont molds are the most recognizable fossil form within the subtidal member, and were found in nearly every bed of mixed-skeletal wackestone measured. Shell sizes in the long direction vary from 10 cm to 40 cm. Previous work by Zapfe (1957) suggests that megalodonts lived partially-buried in the substrate, with "beaks down and hinge essentially vertical". Most megalodonts found within the Dolomia Principale were found with the hinge line vertically or sub-vertically oriented, suggesting that this was the living position for the animal. No actual megalodont shells were shells were found, suggesting that the shells may have been constructed primarily of aragonite.

Facies 4. Cryptomicrobial Laminites

Observations

Beds of thinly-laminated carbonate sediment are a common, reoccurring facies within the inner platform of the Dolomia Principale, occurring on approximately 75% of all cycles. These "laminites" are usually carbonate mud-to-wackestone with mm-scale, horizontal, crinkly laminations (**Figure 5. 29**). Laminite facies may have open and/or spar-filled fenestrae throughout. Typically, this facies is weakly laminated (mm to cm between individual laminae) at the base of a bed and more tightly laminated near the top of the bed (mm-scale, straight and undisrupted). "V" shaped infilled cracks may be found in laminites, and intercalated thin mudstone / wackestone beds are common and represent transport and re-deposition of sediment during storms. In rare instances (only one instance observed, although two others are reported on tourist hiking maps), trackways from terrestrial vertebrates can be viewed along bedding-plane exposed blocks of laminate, indicating deposition in very shallow or supratidal settings (**Figure 5. 30**). In other instances when bedding-plane views of laminate facies are exposed, the similarities between modern microbial tufts such as *Scytonema* are striking, and suggests a similar origin in a supratidal setting (**Figure 5. 31**). Laminite facies typically form gradationally atop either mixed skeletal wackestones and packstones or fenestral wackestones to packstones. Laminate facies can be overlain by cement-indurated and/or disrupted tepee zones in upper portions of sections where diagenetic cycle caps

are common. Otherwise laminites show evidence of erosive downcutting and reworking prior to deposition of deeper-water facies.

Petrographic analysis of this facies reveals mm-scale laminations of dolomitized mud that appear to have been colonized by black, subvertical microbial filaments (**Figure 5. 32**). Microbial filaments tend to extend upward from the base of micritic laminae, suggesting that they grew upwards through successive sedimentary laminations, progressively binding and trapping sediment. Microscopic rock fabric of this type was termed "palisade structure" by Hardie and Ginsburg (1977) and can be observed in Holocene freshwater tidal marshes at Andros Island, Bahamas (Cozzi, 2002). Laminae may also display a clotted texture with fenestrae and alternating geopetal and cement fill (**Figure 5. 33**). This clotted texture is a common feature of tufted laminites, in which microbial growth may disrupt or agglutinate sediment into amorphous clots (Demicco and Hardie, 1994). In most instances, laminae alternate between dark micrite, possibly ingrown by black tufted filaments, and clotted, black, organic-rich laminae (**Figure 5. 34**).

Fenestrae are also common in thin section and typically display a succession of fill. Fenestrae are nearly always subparallel to laminations, and are floored by geopetal micrite followed by void-filling cement (**Figure 5. 35**). Fenestrae were an early feature that formed as a result of biogenic gasses from

microbial mat decomposition, shrinkage of the mat during dessication, or in some cases, the propagation of expansive cement through cracks (Demicco and Hardie, 1994). The presence of preserved fenestral fabric is additional evidence for deposition in a supratidal setting.

Microscopic-scale fracturing was also observed in thin sections taken from laminite facies (**Figure 5. 36**). Fractures are typically filled with micrite and cement. Fractures could have multiple causes, including dessication and erosion.

Interpretation

Laminite facies within the Dolomia Principale are interpreted as algal or microbial in origin and to have formed in the supratidal zone. This interpretation is based on comparison of hand sample and thin section observations with those of other workers who have identified like facies both in the modern and in the DP. Bosellini (1967) included a description of a "lower intertidal unit consisting of biogenic dolomite with stromatolites, associated with various structures of subaerial dessication". This description identifies and gives a genetic context to those beds in the Dolomia Principale that are interpreted as microbial in origin. Bosellini and Hardie (1985) described the laminite facies as “supratidal laminites of probable algal origin". Hardie and Shinn (1986) found similar blue-green algal laminae in the supratidal zone of the Holocene tidal flats of Andros Island,

Bahmas. Cozzi (2002) also observes a unique microscopic 'palisade' growth form in some laminate facies of the DP, consisting of vertically-branching filamentous algal tube molds. In every case, laminites have been interpreted as algal or microbial in origin and to have formed in the supratidal zone, which is consistent with observations from the modern.

In the tidal flats of Andros Island, Bahamas Hardie and Ginsburg (1977) generated a dataset detailing layering and lamination type which they related to exposure index and depositional subenvironment within the tidal flat (**Figure 5. 37**). thinly-laminated sediments are found in modern tidal flat subenvironments that are exposed subaerially (or to freshwater) over 85% of the time. Two kinds of mats predominate- "smooth" and "crinkly" immotile fleshy mats composed of various combinations of filamentous forms of blue-green algae (Demicco and Hardie, 1994). Sediments associated with these mats contain fenestral laminae, thin-bedded (mm to cm-scale) storm deposits, and well-laminated muddy, organic-rich layers (microbial mat) that alternate with layers of soft peloidal sand (Hardie, 1977; Demicco and Hardie, 1994). The descriptions of these tidal flat deposits match the descriptions of laminite facies within the DP, and are interpreted as equivalent depositional settings.

Facies 5. Tepee Zones and Cement Disruption

Field Observations

Antiformal, silty, brittley deformed, cement-filled beds within the Dolomia Principale are common in upper portions of sections that are dominated by supratidal facies. In outcrop, these beds are characterized by large (decimeter-scale) flat, broken and up-arched blocks with intervening void space filled by fibrous cement and red silt (**Figures 5. 38 and 5. 39**). Up-arched blocks typically meet as opposing "limbs", and then flatten within a meter or two of the central axis. Spacings between broken, uparched blocks are typically two to four meters. The antiformal geometry of these structures has led to their being called "tepee structures" (Demicco and Hardie, 1994). Incipient mm-scale cement bands occur parallel to depositional/microbial laminations (sheet cracks). Individual tepee zones are stratiform, with undeformed beds at base and top

Petrographic Observations

Hand samples of tepee zone sediments display a spectacular array of features associated with marine/vadose diagenesis, including cement-lined sheet cracks, voids filled with several generations of cement and red internal sediment, and a high percentage (in some cases over 50%) cement and internal sediment phases to host rock (**Figure 5. 40**). Host rock facies are either cryptomicrobial laminite or fenestral wacke-to-packstone that has been broken into flat clasts.

Clasts of host rock are usually displaced via expansive-cement fill of fractures in the rock.

Petrographic analysis of tepee sediments revealed several features related to the formation of the facies via the precipitation of two forms of carbonate cements (**Figure 5. 41**). The first is an isopachous cement with conspicuously square crystal terminations (orthorhombic system) interpreted to have formerly been aragonite. Rinds of these cements are stacked at ≈1 mm thicknesses within sheet cracks. These cements also have conspicuous micritic laminae at crystal terminations or at zoned intervals within the crystals. Micritic laminae are evidence for biogenic activity either aiding in aragonite precipitation, or halting it through colonization and boring of crystal terminae during hiatus in precipitation (Demicco and Hardie, 1994). The other type of cement common to the tepee facies occurs as bands of radially-oriented calcite crystals (the length-slow “coconut meat” calcite of Assereto and Folk, 1980). This type of cement is thought to have been precipitated in either the vadose of phreatic zone, and represents alternating influence of marine and non-marine conditions on the precipitation of tepee cements (Demicco and Hardie, 1994). Thin sections of host rock in tepee zones show fenestrae in tilted blocks filled with tilted geopetal sediment and cement (**Figure 5. 42**). Tilted geopetals indicate that stabilization of geopetal sediment by cement infill occurred before the block was tilted.

Curiously, no pisoids were identified in any tepees in the lower DP. This is in contrast to numerous tepees in the underlying Dürrenstein formation (as well as other middle-Triassic deposits in the Dolomites) that are full of pisoids. The reason for the absence of pisoids in DP tepee structures is unknown.

Interpretation

Facies associations in modern and ancient examples indicate that most displasive, marine vadose diagenesis takes place in the vadose zone in areas subject to infrequent wetting and subsequent evaporation of seawater. Disruptive fabrics are found within the Dolomia Principale are found in association with other facies interpreted as intertidal or supratidal, including fenestral wackestones and cryptomicrobial laminites. The interpretation of depositional environment for cement-disrupted facies within the Dolomia Principale is within the supratidal zone, in areas infrequently flooded by marine waters and therefore affected by both early marine and vadose diagenetic processes.

Early marine-vadose diagenetic features have long been recognized in the Dolomia Principale. The tepee structures identified in this study of the DP are also interpreted as early marine-vadose diagenetic features that formed in a supratidal setting. Bosellini (1967) describes beds with early cement fracture fill, pisoids, and intercalated silt, which he interprets to be related to early subaerial

diagenesis. Bosellini and Hardie (1985) note that the upper Dolomia Principale consists of massive beds of subtidal dolostones with diagenetic caps of pisolitic breccia and tepee structures. According to Bosellini and Hardie (1985), the diagenetic caps of the upper Dolomia Principale record repeated subaerial exposure of subtidal sediments, which can only be through a drop in relative sea level. Cozzi and Podda (1998) also recognize early marine/vadose diagenetic features within the interior platform of the Dolomia Principale. These include mudcracks, and cm-scale antiformal micro-tepee structures formed by expansive cement growth within fenestral pores. Cozzi and Podda (1998) also identified sheet cracks filled with multiple generations of cement fill, the first being of early vadose character (meniscus and pendant fabrics) and the latter being sparry calcite that likely formed later, possibly replacing former aragonite or high-Mg calcite cements.

Observable products of early diagenesis of carbonate rocks in the Holocene environments are the basis for interpreting similar features in the ancient. Most tidal flats in the modern are subject to diagenesis in the "marine vadose" realm (i.e., exposed to vadose conditions 85% of the time, and to marine conditions 15% of the time, though this varies from place to place), where evaporating seawater leads to the superconcentration of $CaCO_3$ and subsequent precipitation of carbonate cements in void space (Tucker and Wright, 1990). Incipient cementation of surface mats is a common feature of the supratidal zone

of the tidal flats in the Bahamas (Demicco and Hardie, 1994). Crusts consist of aragonite, high-Mg calcite and non-stoichiometric proto-dolomite that form rock-hard pavements out of former peloidal muds in areas above mean high tide (exposed over 85% of the time) (Demicco and Hardie, 1994). Crusts typically preserve original depositional fabric, but may be broken apart during energetic events or bioturbation (e.g., storms, root penetration), thus serving as a source for intraclasts (Demicco and Hardie, 1994). Cement fabrics within crusts may be light colored acicular aragonite banding around vug margins, as well as meniscus and pendant cements along peloid margins. Additional early post-depositional diagenetic processes in the marine vadose zone that are known to modify tidal flat sediments are micritization of grains by boring endolithic algae, dissolution, and dolomitization (Tucker and Wright, 1990).

As void-filling cementation progresses in the supratidal environment, sediments buckle and crack due to cement-growth pressures, creating up-tilted blocks and additional void space for cement nucleation. Initial cracks commonly form along subhorizontal zones that contain fenestrae. Fenestral voids serve as an open nucleation site for carbonate cement growth, which can lead to the rupture of the rock along fenestral void spaces as cementation progresses. These subhorizontal cement-filled voids are then termed "sheet cracks" (Assereto and Kendall, 1977; Demicco and Hardie, 1994). Progressive, superimposed phases of cementation and sheet crack formation eventually lift

and deform the host rock into rigid, uparched polygons (Assereto and Kendall, 1977) (**Figure 5. 43**). Zones of displasive cementation of this type were termed "tepee structures" by Adams and Frenzel (1950) to describe the angular, antiformal geometries internal to these types of rocks (Adams and Frenzel, 1950; Demicco and Hardie, 1994). Holocene tepee structures are nearly identical to those in the Dolomia Principale and are the basis for interpreting the depositional environment of the facies.

Facies 6: Karst Breccia

Observations

Breccias are common cycle-bounding sediments within the Dolomia Principale (**Figure 5. 44**). Breccias consist of a matrix of either bright yellow silty dolomicrite or green silty mud (**Figure 5. 45**). The matrix typically supports clasts from mm-scale through 10s of cm-scale, most of which are microbial laminite or a similar peritidal facies. Clasts are typically angular and commonly displaced a few cm from the underlying bed. The bases of breccia beds are usually highly irregular, with dissolution “pipes” of sediment sometimes extending several 10s of cm into the underlying beds (**Figure 5. 46**). Sedimentary structures associated with scour and fill are notably absent, and clasts do not exhibit imbrication, grading, or any other evidence of transport by water. Beds of breccia vary in thickness along strike at the 10s of cm-scale, and may be truncated and incorporated into overlying breccia deposits.

Environmentally-specific petrographic characteristics of this facies are limited. Thin sections reveal fine silt and mud-size dolomite interspersed with variably-sized angular clasts of peritidal sediments (**Figure 5. 47**). In thin section, yellow sediment matrix is identified as silt to mud-sized carbonate sediment void of any other descriptive features. Photomicrographs from samples of fractured clasts with yellow sediment fill do not show dissolution rids or redox halos as expected in pedogenically-altered rock (**Figure 5. 48**). No root traces or bioturbation was identified in this facies, nor other pedogenic features, marine or vadose cements, or fossils. Rather than true paleosols the breccias have the characteristics of physical alteration (e.g., exposure and erosion by dissolution) rather than pedogenic processes which would have altered the sediment both chemically and biologically.

Interpretation

In attempting to decipher the depositional and diagenetic history of the facies, it became clear that there is no unified agreement as to exactly what depositional process generated the facies (e.g. pedogenesis, vs. karst). The original field interpretation of the cycle-capping dolomitic breccia facies was a carbonate paleosol. However after petrographic analysis of seven thin sections and ten hand samples, not a single pedogenic feature was identified, including sepic fabrics, root traces, plant remains, pedogenic carbonate nodules, laminated caliche, or other indicators. However, the presence of dissolution pipes and

bright yellow color (iron oxides) indicates that the facies formed during subaerial diagenesis, and may instead represent windblown infill of subaerial dissolution cavities. The vast size of the DP shelf (100s of km^2) was large enough to have served as a both a sediment source and sink for windblown carbonate sediments during periods of subaerial exposure. Additional interpretation by both Folk and Kerans (pers. commun after examining photographs, hand samples, and thin sections) is in agreement with the conclusion that the bright yellow, and green sediments are likely eolian derived sediment filling 25-50 cm deep karst profiles, although the possibility of a pedogenic link is not wholly discounted.

Goldhammer et al. (1990) includes a description of cycles from the upper Dolomia Principale identifying depositional cycles capped by red, massive, soil-like breccias that, other than the color, are of very similar description to the yellow breccias found capping cycles in the lower DP. These red breccias incorporate centimeter-scale clasts derived from the underlying subtidal unit into red silty dolomicritic sediment. Lower boundaries of the breccias are highly irregular, with matrix-filled dissolution pipes extending nearly 0.5 m into the underlying subtidal units. Goldhammer et al. (1990) noted that red soil-like breccias occur directly atop thick subtidal beds, leading the authors to posit that the red breccias are “paleosols” and represent substantial (1-10kyr) periods of subaerial exposure.

Studies in the cyclic successions of the Dachstein limestone of the Julian Alps by Cozzi et al. (2005) also revealed a suite of facies similar to those found in the DP of the Dolomites, including a succession-capping breccia interpreted to be karstic and/or pedogenic. Cozzi et al. (2005) identify this facies as a "red-green marl" that abruptly overlies microbial laminites with a very irregular dissolution surface that penetrates as far as 2 meters into the underlying deposit. Centimeter-sized fragments of laminite are common within the marls. Cozzi interprets this facies as a paleosol (although curiously, pedogenic features are absent), and attributes the red, green or yellow color of the sediment to oxidation of wind blown dust that collected in karstic dissolution cavities on cycle tops (Cozzi, *pers. commun*.). Cozzi et al. (2005) also interpret cycles as the result of precessional forcing, with the paleosol representing a lengthy hiatus in deposition between sea level oscillations .

It is most likely that the bright yellow cycle-capping breccia facies in the DP represents a karstic dissolution/fill facies. No evidence for pedogenic processes was found in any instance either in the field or during examination of hand specimens or thin sections.

MEASURED SECTIONS

In order to analyze and/or identify a cyclostratigraphic framework for the Dolomia Principale, measured sections through the stratigraphy of the DP are

needed. Six measured sections (approximately 700 meters total, measured at the cm-scale) were measured along an EW- transect in through the Dolomites, with five of the six sections starting at the Raibl/DP lithostratigraphic contact. The section furthest west is located near the town of Ala, on the Trento/Atesina high, and is near where Goldhammer et al. (1990) described facies of the upper Dolomia Principale. This section is an outlier rather than a part of the tighter-spaced transect, as it is ca. 60 kilometers from the next section at Passo Valparola and does not begin at the Raibl/DP lithostratigraphic contact. Nevertheless, access to sections and direction to workable localities is limited and all accessible sections were included. The tightest grouping of sections is in the valley between Passo Falzarego and Cortina d'Ampezzo, where four measured sections are located with EW spacing of less than 10 kilometers total (**Figure 5. 49**). The sections furthest to the east are those at Tre Cime di Lavaredo, located nearly 100 kilometers east of Ala.

Detailed descriptions of each measured section, including mapped location, photograph of ascent route and drafted section can be found in the Appendix of this chapter. A fold-out illustration of all measured sections is included in the back pocket of this volume (**Illustration 5. 1**).

CYCLOSTRATIGRAPHY

Depositional Cycle Definition

The recognition of lithofacies in the DP that correspond to known depositional environments from the Holocene is the basis for interpreting a stratigraphic framework for the DP. Of particular interest to this study are vertical

the arrangement of facies into repetitive shallowing-upward facies successions, also known as ‘depositional cycles’. A "cycle" is a series of connected events that proceed forward, and eventually return to a starting point before repeating (Goldhammer, 2003). In the case of ‘depositional cycles’, the most objective, all-inclusive definition of a depositional cycle within the shallow marine carbonate realm comes from Goldhammer et al. 1991 (*in* Franseen et al., 1991), which is based on Wilson (1975), James (1984), and Hardie and Shinn (1986):

> "A relatively conformable succession of genetically related subtidal subfacies bounded by peritidal subfacies, subaerial exposure surfaces, and/or marine flooding surfaces (very thin intervals characterized by slow rates of deposition). Cycles are the thinnest recognizable allocyclic or autocyclic depositional unit and they may be progradational and/or aggradational and thus subfacies within cycles [shallow] upwards. Individual cycles typically contain both a "transgressive" and a "regressive" component, and the relative proportion of these components within any given cycle is a function of the cycle's position in a lower frequency cycle or sequence."

Of note in this definition is that depositional cycles always shallow-upwards, and that the repetitive vertical organization of facies is not necessarily tied to a temporal periodicity.

Origin of the DP cycles

While no publication exists that includes measured sections and cyclostratigraphic analysis of DP depositional cycles, several authors have recognized that the DP is made up of repetitively stacked shallowing-upward facies successions and have hypothesized about how the DP cycles were

generated. Specifically, the origin of the DP cycles is debated because workers have concluded that the stratigraphic architecture of the DP formed as the result of both eustatic and local tectonic processes. Summaries of three publications are discussed briefly here.

Bosellini and Hardie (1985)

The first attempt to identify a cyclic driver in the DP was by Bosellini and Hardie (1985) who identified two members in the DP, a lower succession, 500-600 m thick, represented by meter-scale cyclic peritidal carbonates (DP Peritidale), and an upper succession, 200-300 m thick, consisting of mainly massive, vuggy dolostone beds with diagenetic caps bearing pisolites and tepee structures (DP Subtidale). Cyclicity within the upper and lower members of the DP is explained in two different ways. Within the DP Peritidale, Bosellini and Hardie (1985) suggest that depositional cycles may have formed either through eustatic oscillations, or may be subsidence-driven autocycles of the type described by Ginsburg (1975). This is primarily because DP Peritidale successions have shallowing-upward facies indicative of a complete suite of environments from the subtidal to supratidal without facies “skipping” (e.g., from subtidal directly to supratidal without intertidal deposits, which imply sea level drop. Bosellini and Hardie (1985) do not identify which mechanism formed the DP Peritidale cycles, however. In the case of the DP Subtidale, however, the presence of diagenetic caps directly atop subtidal deposits indicates repeated

subaerial exposure of subtidal sediments, which would have to be driven by drops in relative sea level. While the authors do not provide any empirical evidence they do invoke Milankovitch glacio-eustasy (10^3-10^5 year frequency) as the cause of sea level oscillations that formed the shallowing-upward successions of the DP Subtidale. In addition to identifying two distinct successions within the DP, Bosselini and Hardie (1985) assert that the DP is uncorrelatable between localities (although neither localities or measured sections are presented). Bosellini and Hardie explain difficulties in correlation as the result of differential subsidence during deposition leading to differential sediment thickness between localities. Differential thickness of shallowing upward successions, they argue, makes correlation of vertical thickness series in the DP very difficult.

Goldhammer et al. (1990)

In a treatise on the hierarchy of stratigraphic forcing in the Alpine Triassic, Goldhammer et al. (1990) hypothesize that differential subsidence likely had an important influence on cyclic sedimentation in the DP. While the majority of the publication is dedicated to the stratigraphic development of the mid-Triassic of the Dolomites, Goldhammer et al. (1990), include one measured section through the upper DP, where they recognize paleosol-capped “condensed megacycles”. Goldhammer et al. (1990) hypothesize that the paleosol-capped cycles measured near Ala formed as the result of Milankovitchian composite eustasy,

with the cycle caps due to prolonged subaerial exposure on the Trento/Atesina topographic high during deposition. As evidence for this, Goldhammer et al. (1990) also note that the thickness of the entire DP section near Ala is 250 m, while DP as the formation reaches an estimated 1.5 km thick in the Belluno basin to the east (Dolomites) and to the west in the Lombard Basin. Goldhammer et al. (1990) hypothesize that DP cycles in the Belluno and Lombard basins have a more complete suite of shallowing upward facies and may be arranged vertically in response to astro-climatic forcing, although no additional sections are described.

Cozzi and Hardie (2003)

In a study of the effects of synsedimentary extension on the record of relative sea level change in the Carnian Prealps, Cozzi and Hardie (2003) show that the depositional record of the DP does not correlate with the Haq sea level curve, and hypothesize that the deviation from the Haq curve was driven purely by subsidence. Specifically, the platform margin succesion of the DP in the Carnian Prealps fails to show a stratigraphic succession consistent with two global sea level drops (ca. 50 meters) that are predicted by the Haq curve for the Norian and Rhaetian. Instead, the platform margin evolves from progradational to aggradational, signaling ever-deepening conditions through the history of the formation. The discrepancy in facies successions in the DP from what is predicted by the Haq curve, as well as the presence of numerous structures

consistent with synsedimentary extension including open mode fractures, shatter breccias, and depositionally-overlapped normal faults (*see* summary in Chapter 4) lead Cozzi and Hardie (2003) to conclude that subsidence was the dominant control on the development of the Dolomia Principale in the Carnian Preapls at the 3rd-order scale. However, Cozzi and Hardie (2003) do not include description or cyclostratigraphic analysis of measured sections in their publication, and no explanation for the timing and/or origin of high-frequency cycles (e.g., 4th and 5th-order) is given.

The need for additional work

While previous studies have provided hypothetical tectonostratigraphic frameworks for the deposition of the Dolomia Principale in the Dolomites, none have presented a dataset including detailed facies descriptions, high-resolution measured sections taken from multiple localities, and identification and measurement of structures consistent with synsedimentary extension. This study includes all of the above (structural data are in Chapter 4). All data are original and as measured in the field and laboratory by the author.

Depositional Cycle Identification in the Dolomia Principale

The definition of a depositional cycle provided by Goldhammer (2003) allows for the demarcation of cycles from measured sections through the DP. Cycles were picked by identifying shallowing-upwards facies successions in

measured sections and noting the thickness of each. Cycles were identified for the purpose of analyzing patterns in vertical thickness trends as well as to aid in correlation between sections.

While the idea of identifying pertitidal and/or supratidal "bounding facies" is conceptually simple, the ability to pick the "shallowest" facies from a succession of peritidal facies is not always straightforward. This issue was recognized by Hardie (1977), who documented overlapping "exposure indices" (percent of total time a facies was exposed subaerially) in tidal flat facies on Andros Island, Bahamas (**Figure 5. 50**). In other words, deciding which facies actually represent the shallowest depositional environment is not straightforward, as multiple facies types might form in environments of nearly equivalent exposure time. Facies described from measured sections in the Dolomia Principale were assigned exposure indices that reflect the mean value of indices shown in Figure 50. This particular technique has not been used before in stratigraphic analysis. Once this procedure was completed, depositional cycles could be picked based on exposure index. For this study, the method of picking cycles based on exposure index was done as follows: Cycle tops were chosen at the facies of highest exposure index in a shallowing upward succession. The definition of the cycle top also required a shift in exposure index of at least 10% from cycle top to subsequent cycle base (e.g., a cycle top would be defined at a bed with a 95% exposure index followed by a bed with 35% exposure index). Defining cycle

series using this method generated two separate datasets- a cycle thickness series (cycles defined by the thickness of the shallowing-upward facies succession) and exposure index rank series (each bed assigned an exposure index, a number that is a quantifiable "rank" of exposure). Both of these series can be analyzed in hopes of recognizing vertical stacking trends that may aid in both correlation of sections and determination of a cyclic driver.

Thickness Series

Cycle thickness series were obtained after cycles were defined through exposure ranking (see above). Thickness series and plots of cumulative deviation from mean cycle thickness (Fischer plots) for all sections measured from the Raibl-DP lithostratigraphic contact were plotted and compared (**Figure 5. 51**). Comparison of these plots does not yield readily identifiable, correlatable trends between the sections. This indicates that the vertical cycle thickness series of each measured section is unique and does not approximate or match the thickness series of nearby sections to the east or west (sections in Passo Falzarego are only a few km apart).

While plots of thickness series do not offer clear, matching trends between sections from east to west, some sections are similar to others when compared individually, particularly in they are spaced closely in an east-west aspect (e.g., Tofana di Rozes and Forcella Averau) (**Figure 5. 52**). Similarities include

position of thick cycles within the thickness series as well as similar general cycle thinning/thickening trends in Fischer plots. While these series do not indicate cycle-for cycle correlation through the entire section, they do provide evidence that subsidence and sedimentation histories between two localities were similar. The plots of thickness trends from sections measured at Tofana di Rozes and Forcella Averau are the most similar. These two sections are spaced ca. 1 km apart in EW distance (ca. 5 km apart in NS distance), with no large (multi-meter) normal fault observed cross-cutting the DP in between. This suggests that these two sections were on one tectonic block (elongate in the NS-directions, as seen in Chapter 4, Figure 4. 2) recording the same subsidence history. The similarity in vertical thickness trends between these two sections lends credence to the idea of using thickness series as a correlative tool. However, sections located apart from each other in east-west directions or separated by recognizable faults do not have thickness series that match. This is worth note particularly in the sections measured at Tofana di Rozes and Tofana di Mezzo, separated from each other by only a few hundred meters of distance from west to east, but with a normal fault present in between (*see* Chapter 4 Figure 4. 15). These sections are spaced the closest together of all sections measured, but do not share recognizably similar vertical stacking trends. This may be the result of differential subsidence along fault blocks that were elongate in the north-south direction, with displacement to the east and the west (*see* Chapter 4). It may also be the result of general deepening of the DP depositional profile from west to east

(changing subenvironments) as compared to similar depositional position from north to south, as the faults identified in outcrop did not have offset of more than a few meters (*see* Chapter 4, Figure 4. 19). However, it is worth noting the cycle-for cycle correlations were possible in between Anisian-Ladinian Mendola Pass and Latemar sections that are 40 km apart with no identified faults in between (*see* Chapter 2). If Middle Triassic depositional cycles can be correlated over 40 km distances, but Norian cycles cannot be correlated over several hundred meters across a fault zone, it stands to reason that synsedimentary faulting and differential subsidence must have modified the cycle thickness series of the Dolomia Principale in the Dolomites.

Exposure Rank Series

Assignment of exposure rank per facies generated a dataset of vertical exposure rank data per bed. This dataset is composed of exposure index data only and does not contain bed thickness data, and is hence called a rank series rather than a thickness series. This was done in the event that differential subsidence generated random differential cycle thickness per locality. Since the rank series does not contain any thickness information, stacking patterns of rank series will only reflect vertical trends in exposure of facies, perhaps preserving correlatable patterns between sections otherwise clouded by differential thickness. Plots were generated for all sections measured from the Raibl-DP contact (**Figure 5. 53**). A moving average was also applied to the plots of raw data, as true exposure ranks are not unique values, but rather ranges and

therefore cannot truly be represented by points (*see* Figure 5. 50). The moving average is used to smooth out short term fluctuations in order to highlight longer term trends or cycles in order to better approximate a trend through a range of values. The moving average is an unweighted mean of the previous *n* data points. In the case of the analyses here, a 10 point moving average was used to define the trendline through the rank series.

There is a common theme to most of the exposure index plots presented in Figure 5. 53. While all sections began within 10 meters of the Raibl-DP lithostratigraphic contact, this contact is not lithologically consistent from locality to locality such that the likelihood of beginning each section at exactly the same bed is improbable, although all sections start either well before the Raibl DP boundary, or are less than ten meters past it. Nevertheless, similar trends in exposure index can be observed between sections. Sections measured near Passo Falzarego (Averau, Tofana di Rozes, and Tofana di Mezzo) begin with either the exposure index at approximately 50% followed by a rapid rise and fall of exposure index (Averau and Tofana di Mezzo) or simply a rapid fall in exposure index (Tofana di Rozes). This reflects late stage near-shore environments (upper Raibl, high exposure index) followed by flooding and establishment of the carbonate factory over the Raibl (marine transgression, falling exposure index). After this stage, beds in all sections quickly become marine dominated, demarcated in each section by an exposure minimum

(maximum flood zone). Subsequent deposits in all sections become increasingly dominated by ever-greater periods of exposure upwards, reflecting progressive infill of accommodation (interpreted as a highstand systems tract). All sections eventually become exposure dominated at their tops, which is indicative of sequence boundary (SB) at the top of each section.

In addition to exposure rank trends reflecting a relative sea level oscillation (flooding through exposure), sections measured in the Passo Falzarego area appear to have similar trends in exposure rank internal to their respective sections (**Figure 5. 54**). Peaks and dips in similar position indicate contemporaneous response to environmental change (water depth/environment relative to sea level and subsidence) irrespective of actual cycle thickness. Trends in exposure rank series in passo Falzarego link the sections, with an overall shallowing-upward trend through each section being obvious. Higher frequency oscillations in exposure index also appear to be generally in-phase between sections, and are the records of high-frequency oscillations in relative sea level

Observable Bundling Trends

Assuming multiple cyclic mechanisms acted to produce sea level oscillations, it is no surprise that depositional cycles formed in response to eustasy are stacked vertically in patterns that reflect the interplay and

modulations of cycle drivers (*see* Chapter 3 for a discussion on Milankovitch forcing). Platform carbonate deposits from the Dolomites are well known for the obvious asymmetric 5:1 bundling present in mid-Triassic platform carbonate deposits (e.g., the Latemar platform and Mendola Pass). However, bundling patterns in the Dolomia Principale are more varied. Three types of cycle bundling trends can be visually observed in the sections measured in the DP of the Dolomites: 3:1 bundling in a section of the upper Dolomia Principale measured in the western Dolomites near Ala; 20:1 bundling present in sections measured near Passo Falzarego, and composite bundling consistent with Milankovitch forcing seen in sections in the eastern Dolomites (Pelmo, Tre Cime di Lavaredo) (*see* measured sections in fold-out pocket).

As with any cyclostratigraphic study, confirmation of the interpretation of cyclic periodicity can only be done with dating. This study contains no dating of cyclic deposits in the DP (although ash beds were searched for) and relies solely on recognition of stacking trends and comparison of these trends to known spectra of cyclic drivers for identification of stratigraphic forcing mechanisms. Interpretation of stacking trends can be found below.

Time Series Analysis

Statistical methods used for analysis of cycle stacking and bundling trends involve spectral analysis of the cyclic series successions in each measured

section. Examination of sections as a time series means treating each shallowing-upward facies succession as a representation of cyclic behavior with temporal periodicity. In order to identify the repetitive frequency of occurrence of each cycle, spectral analysis is used to view the cyclic series in frequency space (in this case cycles/unit).

In this study, the goal is to identify any periodic drivers that may have been recorded in the rock record of the DP cycles. Because dates within the DP are lacking, identification of spectral peaks consistent with Milankovitchian mechanisms is used to identify the signal. For example, if one assumes each depositional cycle is the result of precessional (approximately 20 kyr) forcing, then these cycles also ought to be grouped into "bundles" reflecting the influence of other Milankovitchian components, including the short (approximately 100 kyr cycle, bundle of 5 cycle/unit) and long (approximately 400 kyr cycle, bundle of 20 cycles/unit) eccentricity. If it is assumed that these signals are periodic signals attributable to Milankovitch forcing, then other peaks will represent the sum effects of aperiodic phenomena on the cycle series (e.g., erosion, autocyclicity, etc.).

Classical harmonic analysis decomposes a time series (in this case a stratigraphic section assumed to be formed by periodic forcing) of length N and sampling rate Δt into sine and cosine terms (i.e., a discrete Fourier series) at

discrete frequencies $f_n=n\Delta f$, n=0,…, N/2-1 where $\Delta f=1/(N\Delta t)$, which is the sampling frequency (Hinnov and Goldhammer, 1991). Multitaper spectral analysis was developed by Thompson (1982) specifically for cases where the series is short or the range of the resultant spectrum of frequencies is large. It has been used heavily in scientific field such as paleoclimate analysis and cyclostratigraphy due to the ability to use the F-test to analyze the variance of the spectrum to confidently identify significant spectral lines in a series. In analyzing the DP cyclic series, the software packages Analyseries v 1.2 and KaleidaGraph were used in constructing time series plots of sections. Data were entered into the software package as vertical cycle thickness series. This is the same methodology used in chapters 2 and 3 to identify prominent cycle frequencies in mid-Triassic sections.

Statistical identification of bundling within DP sections was determined through identification of significant (>90% confidence through F-test) frequencies in cycle thickness series (**Figure 5. 55**). Because spectral analysis converts a cyclic series to frequency space, the inverse of significant frequency peaks is multiplied by the mean cycle thickness in order to give an estimate if the number of cycles present per peak, be they individual shallowing upwards successions or bundled shallowing-upward successions. Significant bundling trends in each section were identified as follows: Ala: Avg. Cycle Thickness = 1.43m, cycle bundles of 3-4 cycles per megacycle; Forcella Averau: Avg. Cycle Thickness =

1.0m, cycle bundles of 3-4 and 7 cycles per megacycle; Tofana di Rozes: Avg. Cycle Thickness = 0.94m, cycle bundles of 3-5 cycles per megacycle; Tofana di Mezzo: Avg. Cycle Thickness = 0.84m, cycle bundles of 3-6 cycles per megacycle; Pelmo: Avg. Cycle Thickness = 0.84m, bundles of 3-6 cycles per megacycle; Cima Ovest: Avg. Cycle Thickness = 1.4m, bundles of 5 cycles per megacycle (*see* Figure 55). These trends indicate that in general, there are a greater number of cycles per megacycle in successively eastward DP sections. This discovery is consistent with the tectono-stratigraphic framework of the DP that has been previously discussed- that the DP thickens from west to east as a result of increased accommodation eastward related to differential subsidence.

DISCUSSION

Analysis of data

Tectonics

Normal faults present in the DP are indicative of syndepositional extension (*see* Chapter 4). These structures have a range of size distributions that includes in sub-mm scale open mode fractures in breccia clasts, and depositionally overlapped faults at cm, 10s of cm, meter and 10s of m scale (*see* Chapter 4, Figure 4. 10). In addition, measurement of the orientation of these fault indicates that most strike within 30 degrees west of north and have kinematic indicators (slickensides) that indicate both normal and strike-slip motion. Normal indicators are consistent with structures identified as forming as

the result of synsedimentary extension (EW directed extension commensurate with the opening of the Tethyan system), while strike slip indicators are consistent with Alpine orogenesis, when NS-striking normal faults may have been reactivated (*see* Chapter 4). Two of these faults, near Forcella Averau and above Rifugio DiBona exhibit a radial fanning of the sediment into the hanging wall of faults, indicative of sedimentation during extension (*see* Chapter 4, Figures 4. 14 and 4. 15). In addition, the DP thickens considerably from 250 m thick in the western Dolomites (Trento-Atesina platform) to over 700 meters at Tre Cime di Lavaredo in the eastern Dolomites (Belluno Basin).

In sum, structures observed within the DP of the Dolomites are consistent with those one would expect to find in a body of sedimentary rock being deposited while undergoing differential subsidence, with localities to the east subsiding faster than those in the west. It is likely that faulting and differential subsidence influenced the stratigraphic development of the DP platform with regard to number and/or thickness of depositional cycles from locality to locality.

Stratigraphy

Stratigraphic data were collected from measured sections across an east-west transect through the Dolomites to obtain data on cyclic deposits within platform interior deposits of the DP. Vertical trends in cycle thickness series from various sections are inconsistent from locality to locality, particularly those

separated from each other in east-west directions or with mapped normal faults in between (*see* Figure 5. 51). With the exception of sections measured at Forcella Averau and Tofana di Rozes, cycle thickness series do not correlate well, either by plots of the thickness series or Fischer plots due to increasing rates of subsidence from west to east. Better correlation between sections (particularly in gross overall trends) was achieved using plots of bed number vs. exposure rank per bed and ignoring thickness. This method was used in hopes of avoiding correlation problems that may be related to disparities in accommodation across the platform created by differential subsidence. Sections with the most similar exposure rank series are closely-spaced sections in the Falzarego area (Averau and Fanes sections). Recognition of both gross overall shallowing-upward trends in sections is accompanied by matches in higher frequency oscillations in exposure indices (*see* Figures 5. 53 and 5. 54). However, it must be pointed out that these trends are gross trends and do not match cycle per cycle.

While using exposure rank series for correlation does identify similar facies trends per section in the DP, these methods do not identify any cycle stacking trends within sections. As stated in Chapter 1, multiple processes operating at multiple timescales are known to generate repetitive strata in the rock record, which led to the concept of the "orders of cyclicity" in sedimentology (*see* Chapter 1, Table 1. 1). Time series analysis of sections was completed in

order to identify dominant cyclic frequencies occurring in each thickness series. Analysis of the frequencies at which cyclic events (in this case represented by shallowing-upward facies successions) occur indicates that the DP of the western Dolomites is dominated by cycle bundles of 2-4 cycles per megacycle, while cycle bundles in the central Dolomites are dominated by bundles of 3-5 cycles per megacycle, and cycle bundles in the eastern Dolomites are dominated by bundles of 4-6 cycles per megacycle (*see* Figure 5. 55). The increase in the number of depositional cycles per cycle bundle from west to east may be reflective of increasing accommodation from west to east as related to differential subsidence.

Interpretation of Results

Stacking patterns in DP stratigraphy

The fact that depositional cyclicity within the Dolomia Principale varies in each of the sections measured does not identify a cause for discrepancies in cyclic series. Discrepancies in cycle thickness series may be caused by a number of factors, including missed oscillations in sea level due to position on platform (e.g., environment too deep for sea surface touchdown or too topographically high to be flooded by each oscillation), on-platform diachroneity of sedimentation (e.g., sedimentation beginning in a seaward position and migrating landward through time), variations in carbonate production potential related to health of the biotic system, Ginsburgian autocyclicity and related lateral

sediment transport, and domination of the record by relative sea level changes driven by inherently chaotic processes (e.g., differential subsidence). Any of these processes individually or in combination may have acted to create the depositional record of the Dolomia Principale. However, while each section preserves a unique cyclic record, it is incorrect to conclude that there is no systematic organization of depositional cycles within the Dolomia Principale. Rather, DP cycles are condensed in the western Dolomites due to prolonged exposure, and become increasingly Milankovitchian in their stacking to the east.

The DP platform during the time of deposition was a broad shelf, at least 100 km wide (from shore to margin). The size of the platform may have dictated the irregular stratigraphy from locale to locale. Assuming a near flat-topped platform, with a basinward slope of only 0.01^{o} over ca. 100 km, there would be 17.5 meters of depositional bathymetry across the platform, which is certainly enough to form multiple depositional environments (**Figure 5. 56**). Assuming precession frequency sea level oscillations were on the order of 5-6 m, as they are thought to have been in the Anisian-Ladinian (see Goldhammer et al., 1987, 1990) only higher amplitude oscillations (e.g., eccentricity) would be able to reach far enough across the platform to generate depositional cycles updip. This would leave the platform with a more complete cyclic record marginward and an overly exposed/condensed record landward, can explain why there are fewer cycles per megacycle in the western Dolomites (e.g., Ala) as compared with

localities investigated in the east (e.g., Pelmo). If differential subsidence were able to generate only one degree of slope from Ala to Tre Cime di Lavaredo, ca. 1750 m of accommodation space is created from west to east over a 100 km transect. Differential subsidence would have operated slowly and contemporaneous to deposition, however, such that the platform top appeared relatively flat (only a few meters of relief) at any point during deposition. By the end of the deposition of the DP, differential subsidence would have generated at least 500 additional meters of filled accommodation space in the eastern Dolomites near Tre Cime, as compared to localities on the Trento high (e.g., Ala, Sella). It is likely that differential subsidence increased to the east in the Carnian Prealps (directly east and adjacent to the Dolomites) where the DP is 2.5 kilometers thick (Cozzi and Hardie, 2003).

Bundling in all sections is interpreted to be a record of Milankovitch forcing affecting different portions of the DP shelf, based both on bundling trends observed in sections and statistical analysis of cycle thickness series. Observationally, the easternmost portions of the platform (Pelmo and Tre Cime) cycles are bundled into thinning-upward bundles of 5 that are also grouped into lower frequency bundles of 20 (*see* measured sections). This is interpreted to be a record of Milankovitch forcing- 20 kyr precession forming the fundamental cycles, 100 kyr eccentricity modulating the 20 kyr precession and forming the ca. 5:1 bundles, and the 400 kyr eccentricity forming the 20:1 bundles. In the central

Dolomites, the signal is somewhat suppressed, with clear observational bundling being limited to 20:1 bundling. In western portions of the DP shelf (e.g., Ala), the cyclic record is dominated by cycles grouped into successions of 3 cycles per megacycle with diagenetic exposure caps on the top of each cycle.

Statistical analysis identifies of every resolvable bundling frequency, which is more discriminating than bundling trends identified by eye alone. Statistically, differential west-to-east stacking trends are confirmed, with western sections preserving condensed cyclic records and sections towards the east becoming increasingly Milankovitchian in their stacking (**Figure 5. 57**). This is interpreted to be the result of western sections (e.g., Ala, Fanes group) being at a topographically higher position (the so-called Trento/Atesina high) than sections to the east (Belluno Basin), such that there were missed beats of high-frequency, low amplitude sea level change resulting in an incomplete or condensed cyclic record. In the cyclic succession preserved at Ala, cycles have well-developed diagenetic exposure caps and bundled into megacycles of 3 cycles/megacycle or less, rather than the 5 cycles/megacycle expected to Milankovitch-forced cycle bundling. Eastern sections (Pelmo, Tre Cime) were not located on the same topographic high as the section at Ala, and preserve a comparably “clean” record of periodic sea level oscillations. Spectral analysis of both Pelmo and Tre Cime sections contain bundling peaks consistent with the eccentricity (ca. 5:1 bundling) and long eccentricity (ca. 20:1 bundling). Whether these frequency peaks

actually reflect Milankovtichian forcing on the cyclic succession cannot be confirmed without accurate dating. The similarity in frequency spectra between eastern DP sections and Milankovitchian orbital processes is indicative of a link between cyclic process and the depositional cycles of the eastern DP. In this case, the combination of structural and stratigraphic evidence, taken in the context of differential subsidence leads to the interpretation that DP cycles reflect the combined influence of tectonic and astro-climatic forcing mechanisms (**Figure 5. 58**).

The different cyclic records per locality are interpreted to be a function of position on the DP shelf and the result of differential subsidence per locality affecting the ability of the carbonate factory to record every meter-scale oscillation in sea level. In other words, while interpreting depositional cycles as the results of periodic forcing means that each depositional cycle is and equally spaced time-event, these cycles may not be preserved equally spaced lithologic events due to multiple factors including bathymetric position and depositional environment, amplitude of sea level oscillations, etc. (Schwarzacher, 1975). Individual precessional oscillations in Triassic sea level were interpreted by Goldhammer et al. (1987, 1990) to be +/- 5-6 meters and may not have affected every portion of the platform, depending on depositional slope of the shelf (*see* Figure 5. 56).

The effects of differential subsidence on regional DP stratigraphy

While both the faulty recording of cyclic behavior related to local bathymetry the time-transgressive nature of DP deposits may have worked to different degrees to affect the regional correlatability of DP platform deposits, structural evidence also exists for differential subsidence along an E-W transect through the DP of the Dolomites and the southern alps. Data supporting the conclusion that the DP of the Dolomites underwent synsedimentary extension can be found in Chapter 4 of this dissertation, while data supporting the hypothesis that late Triassic sediments of the entire Southern Alpine region were deformed by synsedimentary extension can be found in Laubscher and Bernoulli 1978; Doglioni 1986, 1992; Bosellini and Hardie 1985; Jadoul et al. 1992; Carulli et al. 1998; Cozzi, 2000; Cozzi and Hardie 2003; and Fantoni and Scotti 2003.

It is difficult to discount the likelihood that differential subsidence related to synsedimentary extension influenced the stratigraphic development of the Dolomia Principale. Agreements in both sedimentary and structural trends are numerous. Thickness changes occur across valleys with identifiable normal faults nearby (*see* Chapter 4, Figure 8), and NS-striking normal faults with EW displacements can be identified at several locations along the DP transect. In addition, formational thickness increases from ca. 250 m on the Trento-Atesina high (Ala) to at least 750 m at Tre Cime di Lavaredo. This trend in gross formation-scale accommodation is matched at the high-resolution cycle scale,

with “condensed” megacycles (2-3 cycles/megacycle with well-developed diagenetic exposure caps) being far more common in updip positions, and “Milankovitch-like” 5:1 bundling of laminite-capped cycles being more common to the east.

CONCLUSIONS

The conclusion that differential subsidence influenced the stratigraphic development of the DP in the Dolomites is novel in terms of the multiple lines of evidence presented. As stated in chapter 4, the structures consistent with synsedimentary extension are identifiable and measurable in Dolomia Principale near Passo Falzarego. Differential subsidence increased the thickness of the Dolomia Principale in the Dolomites from 250 m at the Sella to over 700 m at Tre Cime di Lavaredo. Correlating sections based on thickness series of cyclic deposits is difficult, a fact that may relate to the deposition of the DP on differentially subsiding blocks. Improved correlation may be attempted using exposure rank series, but even this depends on proximity of sections and consistent depositional inputs between locations. Correlation of sections in the DP based on likeness of thickness and rank series is difficult to achieve, with similar trends only being identified between proximal sections. It is most likely that the difficulty in correlating cyclic series is the result of different depositional paleoenvironments between localities driven by both at least 500 meters of differential subsidence, autocyclicity, and eustasy.

While correlation between measured sections based on thickness and rank series is problematic, stacking patterns within the DP differ systematically from locality to locality. Observational differences in stacking patterns include 3:1 bundling of cycles with diagenetic exposure caps in the upper DP of the western Dolomites near Ala, 20:1 bundling of cycles in the Passo Falzarego area, and both 5:1 and 20:1 bundling of cycles in the eastern Dolomites. Spectral analysis of sections indicates that cycles within the DP are bundled into megacycles with increasing numbers of cycles per megacycle occurring from west to east in the Dolomites, as well as an increasingly Milankovitch-like spectrum of cyclic frequencies recorded in sections from west to east. Specifically, megacycles from sections in the west and central portions of the study area (e.g. Ala) are composed of "condensed" megacycles of 3-4 cycles/megacycle. By contrast, sections further to the east (e.g. Pelmo, Cima Ovest) are "Milankovitch-like" in bundling, containing megacycles of 5-6 cycles/megacycle (reflecting eccentricity-modulation of the precessional index). Differential cycle bundling trends observed in measured sections and identified by statistical analyses are consistent with structural observations concluding that the DP underwent west-east directed extension with greater accommodation (reflected by overall formational thickness) to the east.

Without accurate dates, we cannot confirm cycle drivers within the DP were driven by periodic processes. However, frequency analysis of sections in the

eastern Dolomites indicates cycle bundling frequencies consistent with Milankovitch forcing. Bundling of cycles in the west is comparably condensed, while evidence from the Carnian Prealps to the east suggests that subsidence dominated the stratigraphic record there. However, the similarity in bundling trends between measured sections in the DP of the eastern Dolomites and Milankovitchian cyclic processes is compelling.

This study is able to quantifiably show an increase in the thickness of the DP from west to east, a rough correlatability in DP sections based on exposure ranking of facies through measured sections in the Passo Falzarego area, an increase in number of depositional cycles per megacycle from east to west in the DP over a lateral transect of 100 km, and evidence for increasingly Milankovitch-like stacking of DP cycles from west to east in the Dolomites. The combination of these findings, along with structural evidence, supports the long held belief that the Dolomia Principale of the Dolomites was deposited on a broad shelf (hundreds of km^2) that underwent differential subsidence. The cyclic stratigraphy of the DP records both autocyclic and allocyclic processes. Autocyclic processes are related to erosion, sediment transport and Gisnburgian autocyclicity and contribute to the difficulty in correlating DP from different localities in the Dolomites. However, an allocyclic signal consistent with Milankovitchian frequencies has also been identified in the DP of the Dolomites. This signal is modified from eastern portions of the DP shelf where the signal is relatively clean

to western portions of the shelf where is progressively condensed. The Dolomia Principale of the Dolomites records periodic, astroclimatic forcing of shallowing upward facies successions modified by differential subsidence.

REFERENCES

Adams, J.E., and Frenzel, H.N., 1950, Capitan barrier reef, Texas and New Mexico: Journal of Geology, v. 58, is. 4, p. 289-312.

Aigner, T., 1982, Event-stratification in nummulite accumulations and in shell beds from the Eocene of Egypt, *in* Cyclic and event stratification; symposium. Einsele, G., ed., Tuebingen, Federal Republic of Germany, April 25-27, 1980. p. 248-262.

Assereto, R., and Folk, R.L., 1976, Brick-like texture and radial rays in Triassic pisolites of Lombardy, Italy: a clue to distinguish ancient aragonitic pisolites: Sedimentary Geology, v. 16, p. 205-222.

Assereto, R., and Folk, R.L., 1980, Diagenetic fabrics of aragonite, calcite, and dolomite in an ancient peritidal-spelian environment: Triassic Calcare Rosso, Lombardia, Italy: Journal of Sedimentary Petroology, v. 50, no. 2, p. 371-394.

Assereto, R., and Kendall, C.G. St.G., 1971, Megapolygons in Ladinian limestones of Triassic of Southern Alps: evidence of deformation by penecontemporaneous desiccation and cementation: Journal of Sedimentary Petrology, v. 4, no. 3 p. 715-723.

Assereto, R., and Kendall, C.G. St.G., 1977, Nature, origin and classification of peritidal tepee structures and related breccias: Sedimentology, v. 24, p. 153-210.

Bellanca, A., Masetti, D., Neri, R., and Venezia, F., 1999, Geochemical and sedimentological evidence of productivity cycles recorded in Toarcian black shales from the Belluno Basin, Southern Alps, northern Italy: Journal of Sedimentary Research, v. 69, is. 2, p. 466-476.

Bernoulli, D., and Lemoine, M., 1980, Birth and early evolution of the Tethys: The overall situation: Memorie Della Bureau de Recherches Géologiques et Minières, no. 115, p. 168-179.

Bertotti, G., Picotti, V., Bernoulli, D., and Castellarin, A., 1993, From rifting to drifting: Tectonic evolution of the South-Alpine upper crust from the Triassic to the Early Cretaceous: Sedimentary Geology, v. 86, pp. 53-76.

Bloomfield, Peter (1976), *Fourier Analysis of Time Series*, John Wiley and Sons

Bosellini, A., 1967, La tematica deposizionale della Dolomia Principale (Dolomiti e Prealpi Venete: Bolletino della Societa Geologica Italiana, v. 86, is. 2, p. 133-169

Bosellini, A., 1991, Geology of the Dolomites: An introduction: Dolomieu Conference on carbonate platforms and dolomitization. Ortisei, 43 p.

Bosellini, A., and Hardie, L.A., 1985, Facies e cicli della Dolomia Principale delle Alpi Venete: Memorie della Societa Geologica Italiana, v. 30, p. 245-266.

Carulli, G.B., Cozzi, A., Longo Salvador, G., Ponton, M., and Podda, F., Evidence of synsedimentary tectonic activity during the Norian-Lias (Carnian Prealps, northern Italy): Memorie della Societa Geologica Italiana v. 53, p. 403-415.

Cozzi, A., 2000, Synsedimentary tensional features in Upper Triassic shallow-water platform carbonates of the Carnian Prealps (northern Italy) and their importance as paleostress indicators: Basin Research, v. 12, p. 133-146.

Cozzi, A., 2002, Facies patterns of a tectonically-controlled upper Triassic platform-slope carbonate depositional system (Carnian Prealpls, Northeastern Italy): Facies, v. 47, p. 151-178.

Cozzi, A., Hinnov, L.A., and Hardie, L.A., 2005, Orbitally forced Lofer cycles in the Dachstein Limestone of the Julian Alps (northeastern Italy): Geology, v. 33, is. 10, p. 789-792.

Cozzi, A., and Podda, F., 1998, A platform to basin transition in the Dolomia Principale of the M. Pramaggiore area, Carnian Prealps, northern Italy: Memorie della Societa Geologica Italiana, v. 53, p. 387-402.

Demicco R.V., and Hardie, L.A., 1994, Sedimentary structures and early diagenetic features of shallow marine carbonate deposits: SEPM Atlas Series No. 1, 265 p.

Doglioni C., 1987, Tectonics of the Dolomites (Southern Alps, Northern Italy): Journal of Structural Geology, v. 9, no. 2, p. 181-193.

Doglioni, C., 1992, Relationships between Mesozoic extensional tectonics, stratigraphy, and Alpine inversion in the Southern Alps: Eclogae Geologica Helvetica, v. 85, no. 1, p. 105-126.

Dunham., R.J., 1969, Vadose pisolite in the Capitan reef (Permian), New Mexico and Texas: Special Publication – Society of Economic Petrologists and Minerologists, v. 14, p. 182-191.

Einsele, G., Ricken, W., and Seilacher, A. (eds.), 1991, Cycle and Events in Stratigraphy. New York: Springer-Verlag.

Emmerich, A., Glasmacher, U.A., Bauer, F., Bechstädt, T., and Zühlke, R., 2005, Meso-/Cenozoic basin and carbonate platform development in the SW Dolomites unraveled by basin modeling and apatite FT analysis: Rosengarten and Latemar (Northern Italy): Sedimentary Geology v. 175, is. 1-4, p.415-438

Enos, P., and Perkins, R.D., 1979, Evolution of Florida Bay from island stratigraphy: Geological Society of America Bulletin, v. 90, is. 1, p. 59-83.

Fischer, A.G., 1964, The Lofer Cyclothems of the Alpine Triassic: Kansas Geological Society Bulletin, v. 169, p.107-149.

Folk, R.L., 2005, Nannobacteria and the formation of framboidal pyrite: Textural evidence: Journal of Earth System Science, v. 114, no. 3, p. 369-374.

Ginsburg, R.N., 1971, Landward movement of carbonate mud: new model for regressive cycles in carbonates (abs.): American Association of Petroleum Geologists Bulletin, v. 55, p. 340.

Ginsburg, R.N., Hardie, L.A., Bricker, O.P., Garrett, P., Wanless, H.R., 1977, Exposure Index: a quantitative approach to defining position within the tidal zone. *in* Hardie, L.A., *ed*., Sedimentation on the Modern Carbonate Tidal Flats of Northwest Andros Island, Bahamas. The Johns Hopkins University Studies in Geology, no. 22., p. 7-11.

Gischler, E., 2003, Holocene lagoonal development in the isolated carbonate platforms off Belize: Sedimentary Geology, v. 159, p. 113-132.

Goldhammer, R.K., 2003, Cyclic Sedimentation, *in* Middleton, G.V., ed., Encyclopedia of Sediments and Sedimentary Rocks, Springer-Verlag, Netherlands p. 173-185.

Goldhammer, R.K., Dunn, P.A., and Hardie, L.A., 1990, Depositional cycles, composite sea level changes, cycle stacking patterns, and the hierarchy of stratigraphic forcing: Examples from the Alpine Triassic platform carbonates: Geological Society of America Bulletin, v. 102 p. 535-562.

Goldhammer, R.K., Dunn, P.A., and Hardie, L.A., 1987, High-frequency glacio-eustatic sea level oscillations with Milankovitch characteristics recorded in Middle Triassic platform carbonates in Northern Italy: American Journal of Science, v. 287, p. 853-892.

Goldhammer, R.K., and Harris, M.T., 1989, Eustatic controls on the stratigraphy and geometry of the Latemar buildup (Middle Triassic), the Dolomites of northern Italy: SEPM Special Publication 44, p. 232-338.

Gradstein, F.M., Ogg, J.G., and Smith, A.G., Agterberg, F.P., Bleeker, W., Cooper, R.A., Davydov, V., Gibbard, P., Hinnov, L.A., House, M.R., Lourens, L., Luterbacher, H.P., McArthur, J., Melchin, M.J., Robb, L.J., Shergold, J., Villeneuve, M., Wardlaw, B.R., Ali, J., Brinkhuis, H., Hilgen, F.J., Hooker, J., Howarth, R.J., Knoll, A.H., Laskar, J., Monechi, S., Plumb, K.A., Powell, J., Raffi, I., Röhl, U., Sadler, P., Sanfilippo, A., Schmitz, B., Shackleton, N.J., Shields, G.A., Strauss, H., Van Dam, J., van Kolfschoten, T., Veizer, J., and Wilson, D., 2004. A Geologic Time Scale 2004. Cambridge University Press, 589 p.

Hardie, L.A., 1977, Sedimentation on the modern carbonate tidal flats of Northwest Andros Island, Bahamas. Johns Hopkins University Studies in Geology, is. 22, 202p.

Hardie, L.A., and Ginsburg., R.N., 1977, Layering: The origin and environmental significance of lamination and thin bedding. *In* Hardie, L.A., *ed*., Sedimentation on the Modern Carbonate Tidal Flats of Northwest Andros Island, Bahamas: The Johns Hopkins University Studies in Geology, no. 22. p. 50-123.

Hardie, L.A., and Shinn, E.A., 1986, Carbonate depositional environments, modern and ancient, 3, Tidal Flats: Colorado School of Mines Quarterly, v. 81, p. 1-74.

Hinnov, L.A., 2000, New perspectives on orbitally forced stratigraphy: Annual Review of Earth and Planetary Sciences, v. 28, p. 419-475.

Hinnov, L.A. and Goldhammer, R.K., 1991, Spectral analysis of the Middle Triassic Latemar Limestone: Journal of Sedimentary Petrology, v. 61, p. 1173-1193.

Jadoul, F.; Berra, F.; and Frisia, S., 1992, Stratigraphic and paleogeographic evolution of a carbonate platform in an extensional tectonic regime: the example of the Dolomia Principale in Lombardy (Italy): Ri. It. Paleont. Strat., v. 98, no.1, p. 29-44.

James, N.P., 1984, Shallowing-upward sequences in Carbonates: in Walker, R.G., (ed.), Facies Models. Geoscience Canada reprint series 1, p. 213-228.

Jenkins and Watts, (1968), Spectral Analysis and Its Applications, Holden-Day.

Kendall, G.St.C. and Schlager, W.,1981, Carbonates and relative changes in sea level: Marine Geology, v. 44, p 181-212.

Kent, D.V., Muttoni, G., and Brack, P., 2004, Magnetostratigraphic conformation of a much faster tempo for sea level change for the Middle Triassic Latemar platform carbonates: Earth and Planetary Science Letters, v. 228, p. 369-377.

Middleton, G.V., 1973, Johannes Walther's Law of the Correlation of Facies: Geological Society of America Bulletin, 1973, v. 84, is. 3, p.. 979-987.

Muttoni, G., Meco, S., and Gaetani, M., 2005, Magnetostratigraphy and biostratigraphy of the Late Triassic Guri Zi section, Albania; constraint on the age of the Carnian-Norian boundary: Rivista Italiana di Paleontologia e Stratigrafia, v. 111, is. 2, p.233-245.

Paillard, D., L. Labeyrie and P. Yiou, 1996, Macintosh program performs time-series analysis: Eos Trans. AGU, v. 77: p. 379.

Preto, N., Hinnov, L.A., Hardie, L.A., and De Zanche, V., 2001, Middle Triassic orbital signature recorded in the shallow-marine Latemar carbonate buildup (Dolomites, Italy): Geology, v. 29, no. 12, p. 1123-1126.

Preto, N., Hinnov, L A., De Zanche, V., Mietto, P.,, and Hardie, L.A., 2004, The Milankovitch interpretation of the Latemar platform cycles (Dolomites, Italy): implications for geochronology, biostratigraphy, and middle Triassic carbonate accumulation: SEPM Special Publication no. 81, p. 167-182.

Read, J.F., and Goldhammer, R.K., 1988, Use of Fischer plots to determine third-order sea level curves in Ordivician peritidal carbonates, Appalachians: Geology, v. 16, no. 10, p. 895-899.

Sander, B., 1951, Contributions to the study of depositional fabrics; rhythmically deposited Triassic limestones and dolomites. English translation by Eleanora Bliss Knopf, 160 p.

Schulz, M., and Schaefer-Neth, C., 1997, Translating Milankovitch climate forcing into eustatic fluctuations via thermal deep water expansion: a conceptual link: Terra Nova, v. 9, no. 5, p. 228-232.

Schwarzacher, W., 1975, Sedimentation Models and Quantitative Stratigraphy: New York, Elsevier, 382 p.

Sepkoski, J.J., 1982, Flat-pebble conglomerates, storm deposits, and the Cambrian bottom fauna, *in* Einsele, G., ed., Cyclic and event stratification; symposium, Tuebingen, Federal Republic of Germany, April 25-27, 1980, p. 371-385.

Shinn, E.A., 1986, Modern carbonate tidal flats: Their diagnostic features., in Hardie, L.A., and Shinn, E.A., Carbonate Depositional Environments, Modern and Ancient: Colorado School of Mines Quarterly, v. 81, No. 1, p. 7-33.

Suess, E., 1888 Das Anilitz der Erder, Volume 2 (English translation by Sollas, 1906). Oxford: Clarendon Press, p. 1-254.

Tucker, M.E., and Wright, P.V., 1991, Carbonate Sedimentology, Blackwell Sci. Pub., Oxford, United Kingdom, 482 p.

Walker, R.G., and James, N.P., (eds.), 1990, Facies Models: Response to sea level change: Geological Association of Canada.

Wanless, H.R., Tyrrell, K.M., Tedesco, L.P., and Dravis, J.J., 1988, Tidal-flat sedimentation from hurricane Kate, Caicos Platform, British West Indies: Journal of Sedimentary Petrology, v. 58, no. 4, p. 724-738.

Wilkin, R.T., and Barnes, H.L., 1997, Formation processes of framboidal pyrite: Geochimica et Cosmochimica Acta, v. 61, is. 2, p. 323-339.

Wilkin, R.T., and Barnes, H.L., 1997, Pyrite formation in an anoxic estuarine basin: American Journal of Science, v. 297, is. 6, p. 620-650.

Wilson, J.L., 1975, Carbonate facies in geologic history, New York: Springer-Verlag.

Winterer, E.L., and Bosellini, 1981, Subsidence and sedimentation on Jurassic passive continental margin, Southern Alps, Italy: AAPG Bulletin, v. 65, is. 3, p. 394-421

Zapfe, H., 1957, Das Meer der alpinen Trias; seine Organismenwelt und seine Ablagerungen, Universum Horn Österreich, v. 7, p. 193-201.

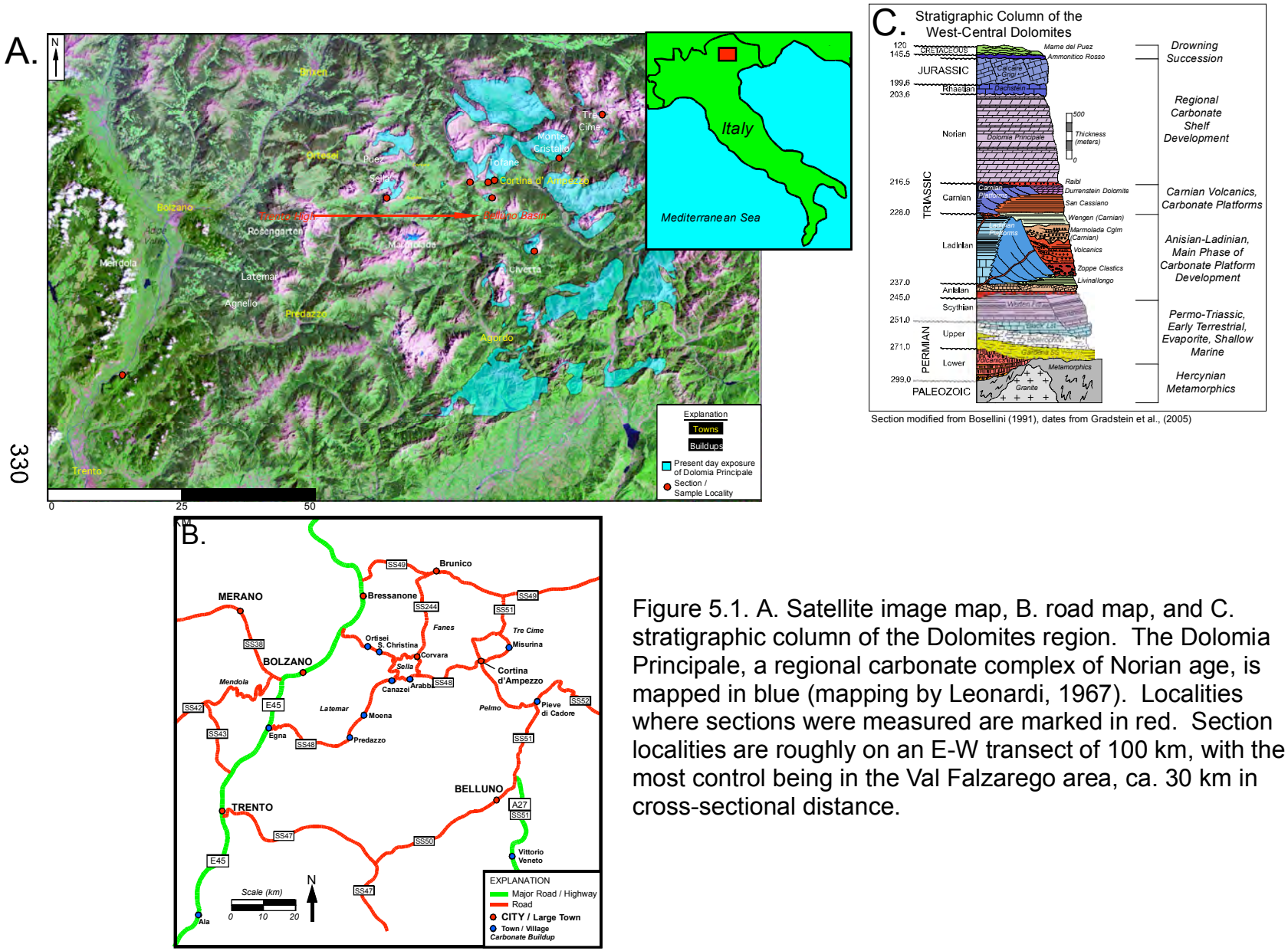

Section modified from Bosellini (1991), dates from Gradstein et al., (2005)

Figure 5.1. A. Satellite image map, B. road map, and C. stratigraphic column of the Dolomites region. The Dolomia Principale, a regional carbonate complex of Norian age, is mapped in blue (mapping by Leonardi, 1967). Localities where sections were measured are marked in red. Section localities are roughly on an E-W transect of 100 km, with the most control being in the Val Falzarego area, ca. 30 km in cross-sectional distance.

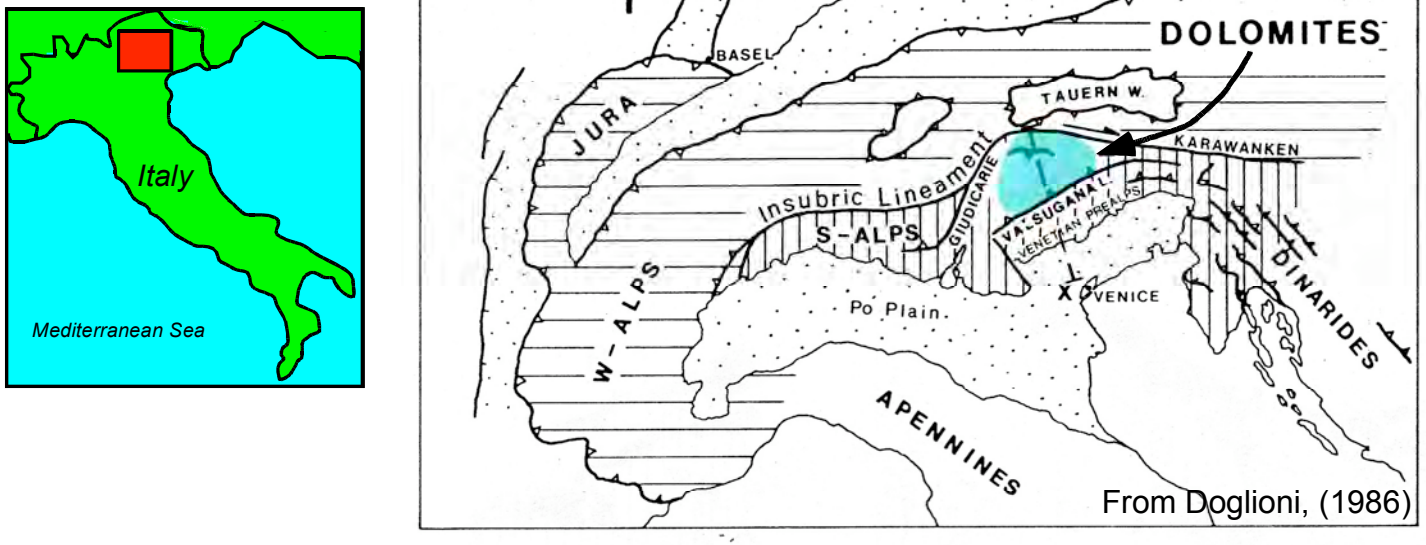

Figure 5.2. Location of the Dolomite Alps. The Dolomites are located in the eastern portion of northern Italy in the 'Southern Alps', which are bordered to the north by the dextral Insubric Lineament. The Dolomites proper are also bordered by the Valsugana overthrust to the south and by the Adige valley to the west.

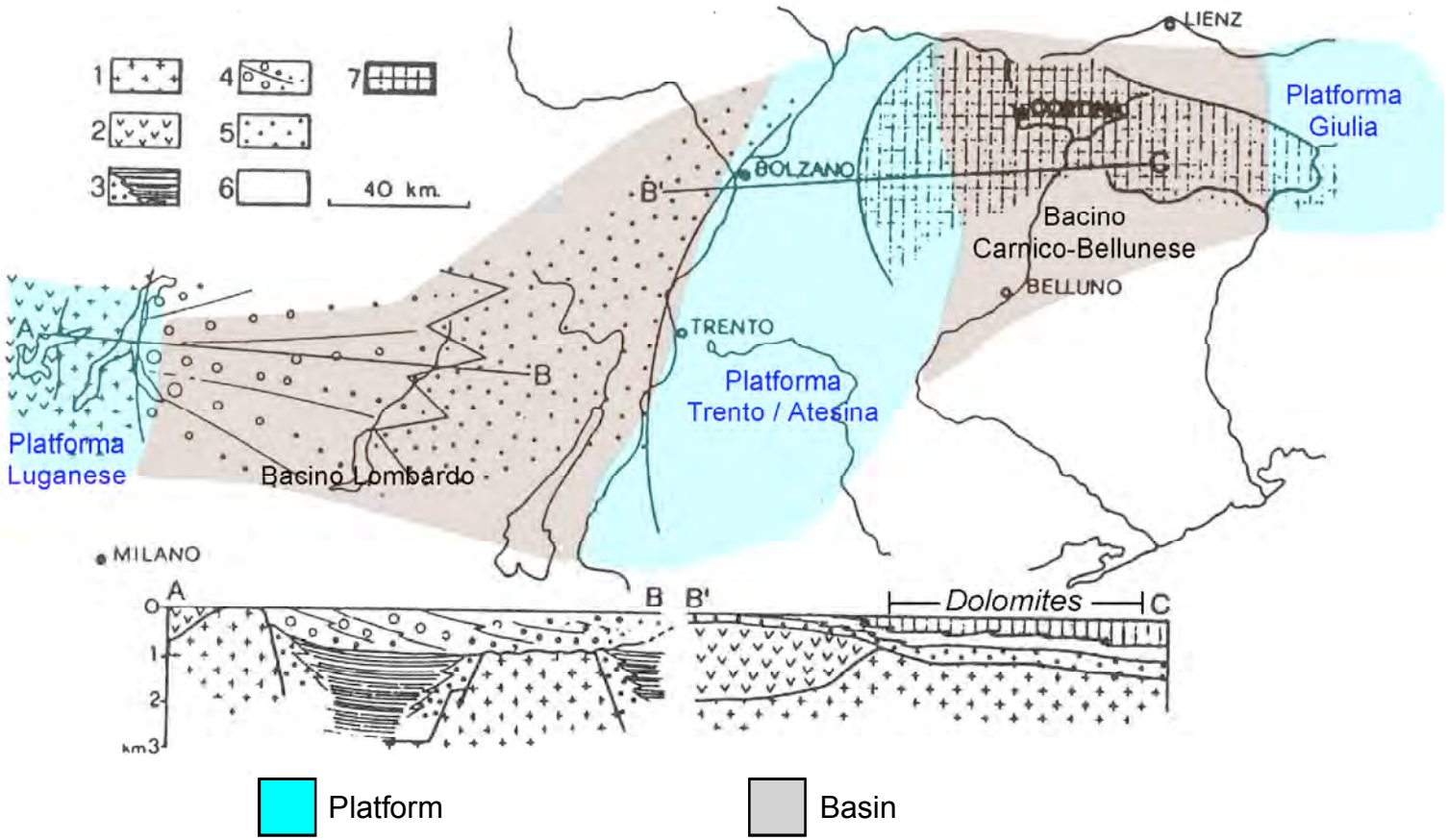

Figure 5.3. Paleogeographic map and cross sections of Permo-Triassic deposits in the Southern Alps. 1. Hercynian metamorphics, 2. Permian 'Bozner' volcanics, 3. Lacustrine deposits, 4. Conglomeratic alluvial fans, 5. Fluvial deposits, 6. Shallow marine dolomites and evaporites (tidal flat and sabkha), 7. Shallow marine limestones. Note NS structural grain of platforms and basins, as well as Permian volcanic core of platforms. Figure modified from Winterer and Bosellini (1981) by adding platform and basin labels and colors.

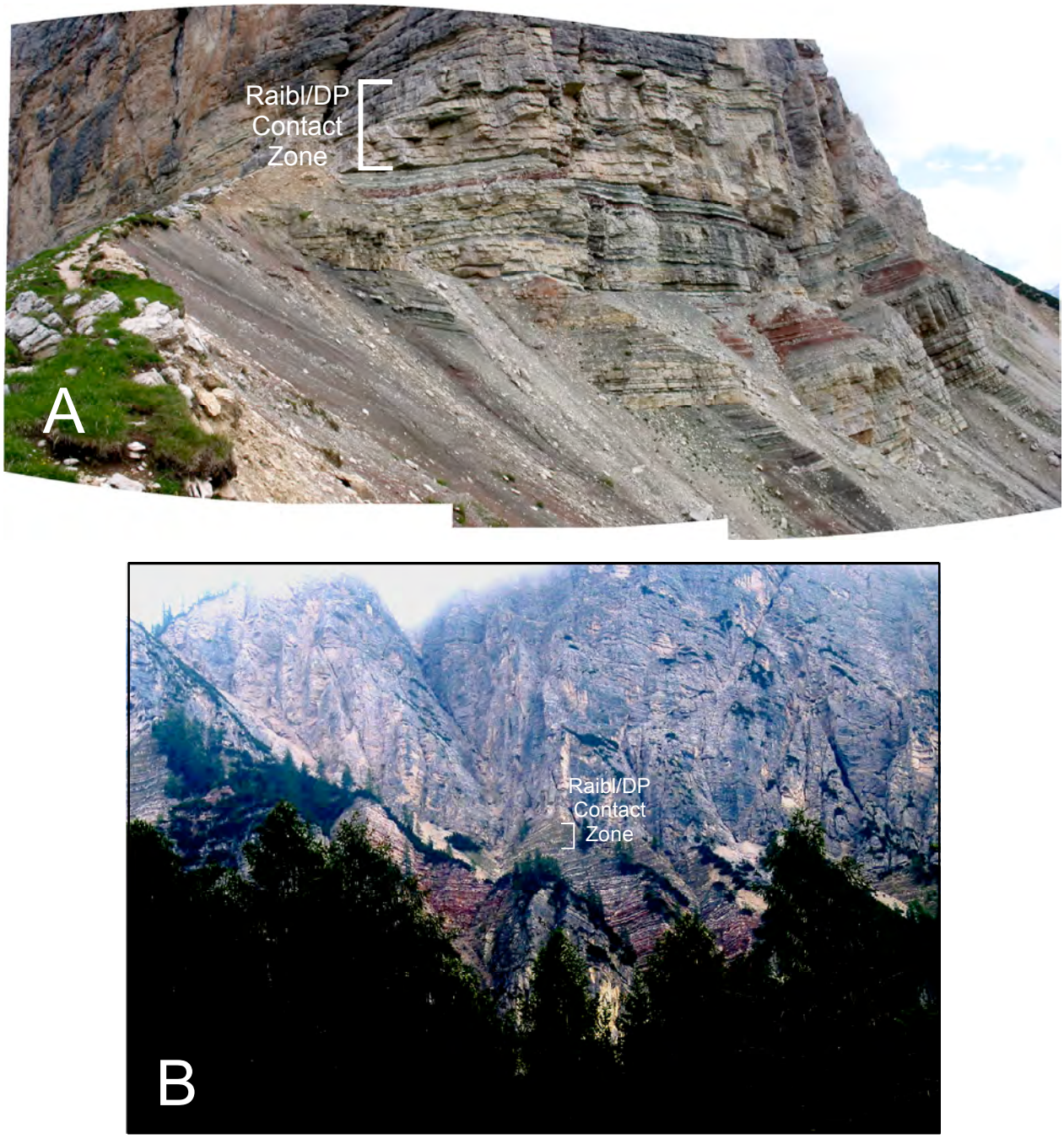

Figure 5.4. Photographs of the Raibl formation at its contact with the Dolomia Principale. A. Raibl-DP contact at the Tofana di Mezzo. Here the Raibl is mixed clastic and marly carbonate and is faulted (see non-correlative strata in Raibl of A).
B. Raibl-DP contact near the base chair lift of the Monte Cristallo ski area (photo B taken ca. 20 km east of photo A). Here the Raibl is far more gypsiferous, possibly reflecting comparably more marine influence in sections to the east.

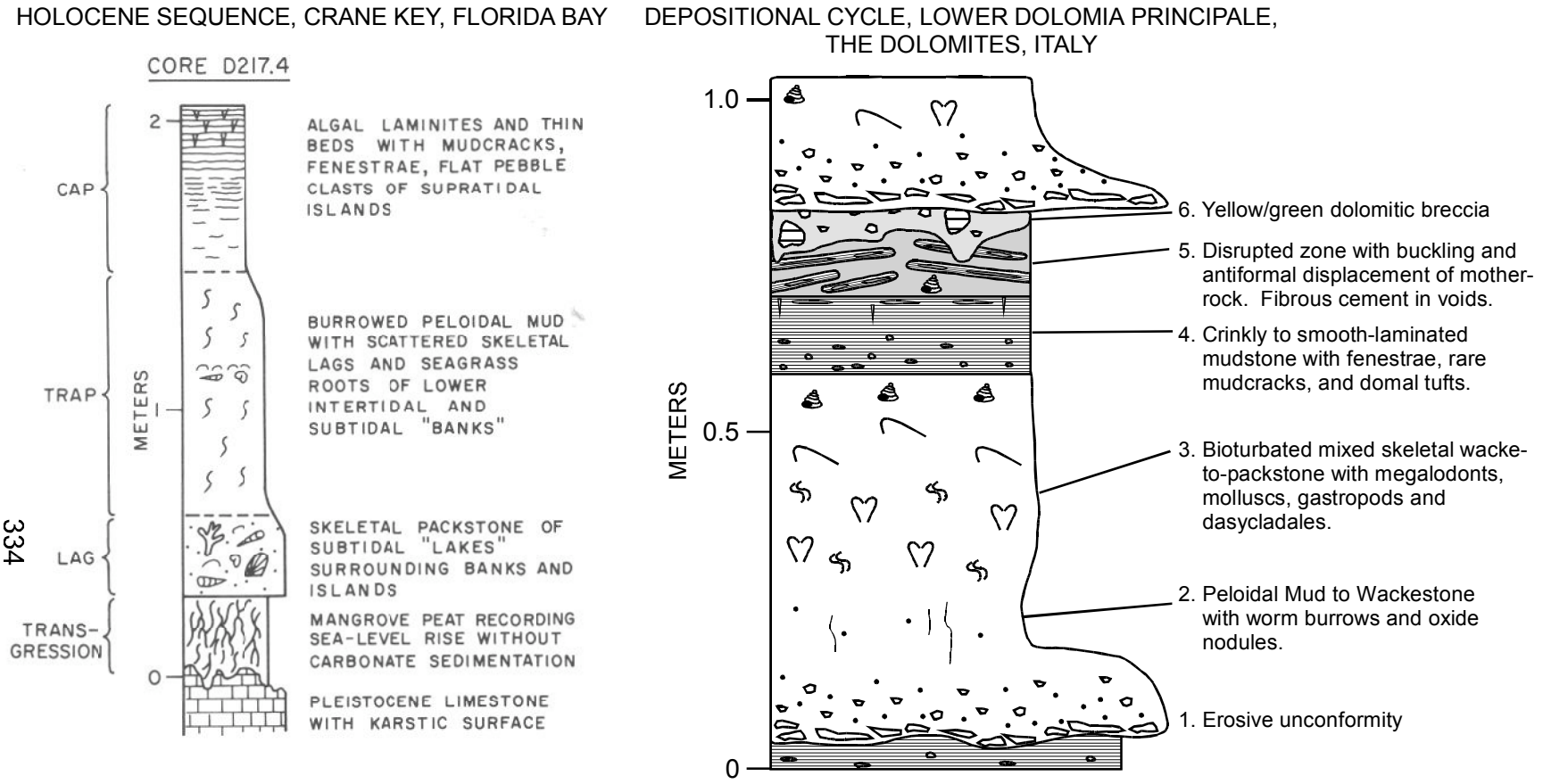

Figure 5.5. Comparison between Holocene shallowing-upward succession in Florida Bay (left, from Hardie, 1977) and an ideal cycle from the Norian Dolomia Principale. Subfacies within Dolomia Principale successionsare stacked into “shallowing-upward” depositional cycles. From base to top, the subfacies are: 1. erosive, intraclastic breccia; 2. peloidal mud-to-wackestone with burrows and oxide framboids; 3. mixed-skeletal megalodont wacke-to-packstone; 4. crinkly fenestral laminite with both tubular and elongate fenestrae; 5. cement-indurated, antiformally-disrupted bed of peritidal and supratidal mother rock; 6. dolomitic “karst breccia”. The succession of facies is indicative of rapid sea level rise and ever-shallower sub-environments upward.

Figure 5.6. Ideal Depositional Cycle, Lower Dolomia Principale, The Dolomites, N. Italy

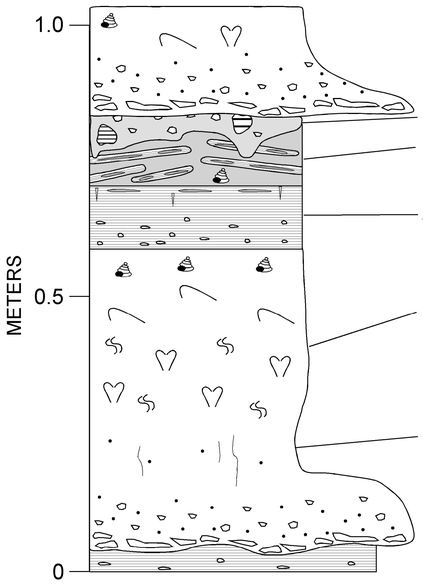

6. Yellow/green dolomitic breccia
5. Disrupted zone with buckling and antiformal displacement of mother-rock. Fibrous cement in voids.
4. Crinkly to smooth-laminated mudstone with fenestrae, rare mudcracks, and domal tufts.
3. Bioturbated mixed skeletal wacke-to-packstone with megalodonts, molluscs, gastropods and dasycladales.
2. Peloidal Mud to Wackestone with worm burrows and oxide nodules.
1. Erosive unconformity

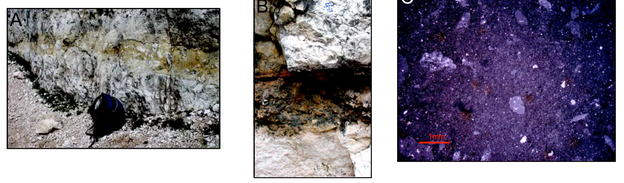

A & B. Diagenetic karst breccia cap consisting of laminite clasts suspended in a dolomicritic matrix. Example A from Forc. Averau, example B from Ala roadcut section.
C. Photomicrograph of anglular breccia clasts in dolomicritic matrix. Note lack of pedogenic features- absence of root and/or animal traces, lack of sepic fabric, and lack of caliche fabrics.

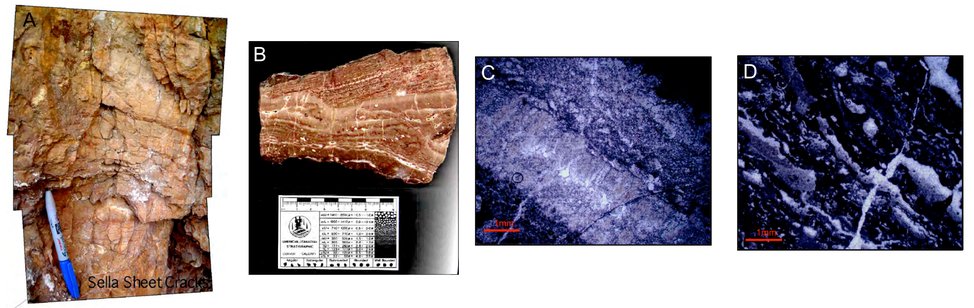

A & B. Diagenetic cap consisting of tepeeized microbial laminite. Precipitation of early expansive marine cements within fenestrae leads to the development of sheet cracks and eventually to antiformal tepee structures and exposure breccias (Demicco and Hardie, 1994). Certain examples may consist of over fifty percent early cement phases relative to displaced mother rock. Facies typically show red terra rossa staining typical of subareal exposure. Pisoids are not abundant in DP exposure caps.
C. Former aragonite botryoids replaced by dolomitie. Note ghosts of square tipped orthorhombic aragonite accentuated by a possible microbial colonization surface (Folk, 1974; personal communication).
D. Tilted cryptomicrobial laminite with geopetals. Tilting of geopetals suggests tepeeization post-geopetal fill and cementation of sediment.

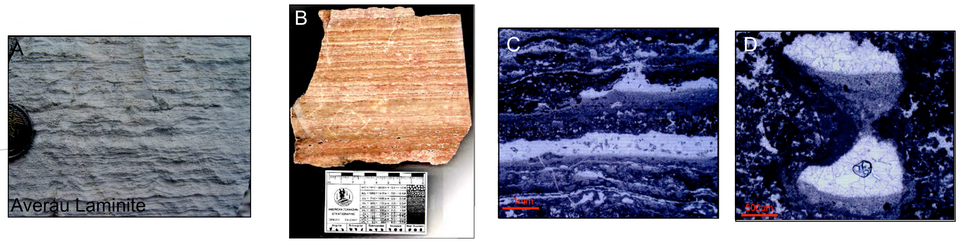

A & B. Cryptomicrobial laminated bindstone. Laminites in the Dolomia Principale typically have abundant fenestrae at the base and become tighter towards the tops. Intercalated thin mudstone/wackestone beds within laminites may represent storm events when lagoonal sediments were transported landward. This facies typically has a gradational base and top.
C. Microscopic view of laminae. Laminae consist of intercalated mud, rip-up clasts and petrified microbial mat. Note geopetal fill in elongate fenestrae.
D. Hourglass fenestrae with geopetal fill.

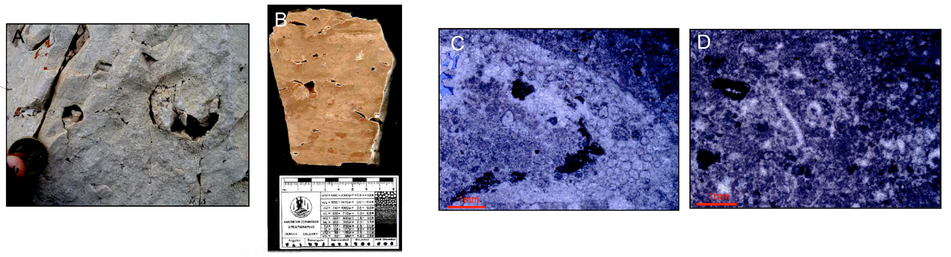

A & B. Mixed skeletal wackestone-packstone. Skeletal debris and fossils are common, including bivalves, gastropods, dasycladacean algae, and megalodont molds. Faunal diversity typically decreases up, being limited to gastropods near the top. Sedimentary structures are typically masked by bioturbation. Whispy microbial lamination can also be observed and increases in abundance upward.
C. Oblique-vertical cross section through a daslcladale. Note the vesiculiferous regions, common to examples of the Norian dasycladale *gyroporella vesiculifera* (Pugliese, 1996).
D. Matrix of dolomitized wack-packstone. Ghosts of peloids and bivalve fragments can be seen through the diagenetic fabric.

A & B Massive mudstone. Carbonate mudstone is common in the DP and typically weathers as a recessive interval. Mudstones are typically green to gray, may have (A) few sub-mm diameter vertical burrows (serpulid worms) and typically have oxide masses weathering out of the profile. B. Oxide framboids may form along horizons and can be upwards of 1 cm in diameter. Oxide masses may be after framboidal pyrite or siderite and may be indicators of restriction / reducing environment.

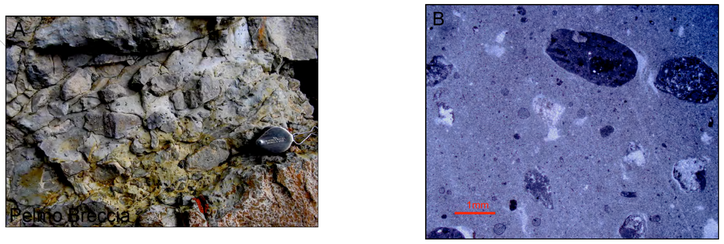

A. Intraclastic breccia. Breccias are common within the DP and may form the base of shallowing-upward cycles. Clasts within breccias are typically lifted from the underlying bed and may be rounded.
B. Microscopic view of an intraclastic breccia with dolomicrite matrix and intraclasts of varying types including cryptomicrobial bindstone, breccia, and clasts replaced by coarse crystalline dolomite. Most of the clasts are rounded, suggesting a moderate amount of transport and reworking.

1

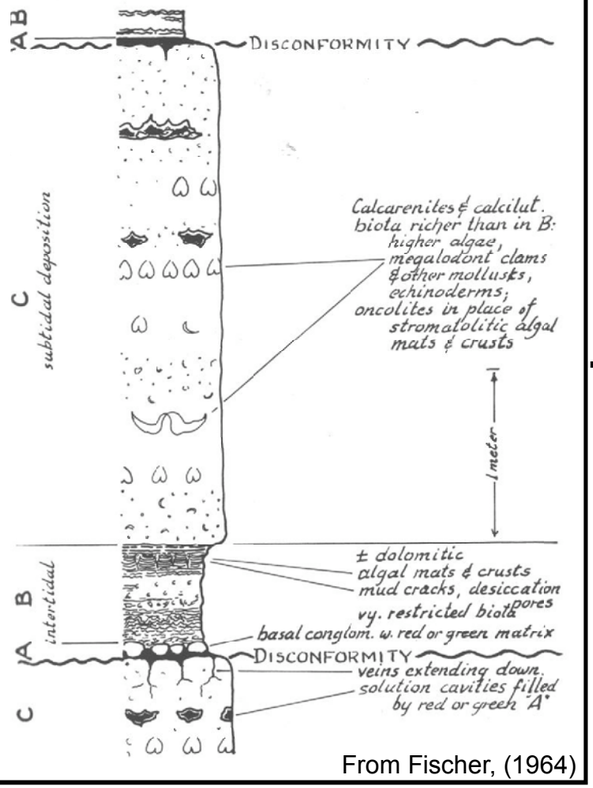

From Fischer, (1964)

2

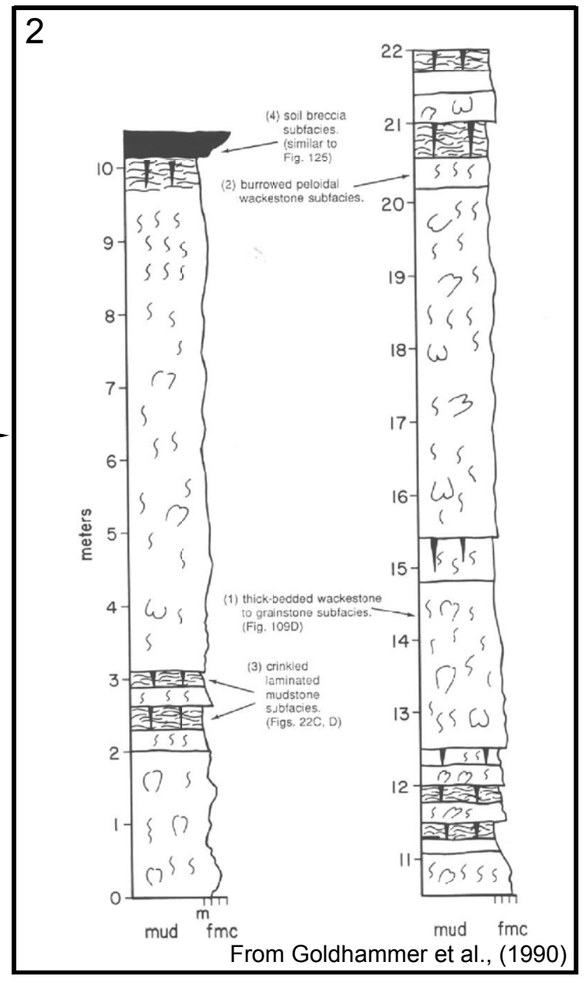

From Goldhammer et al., (1990)

3

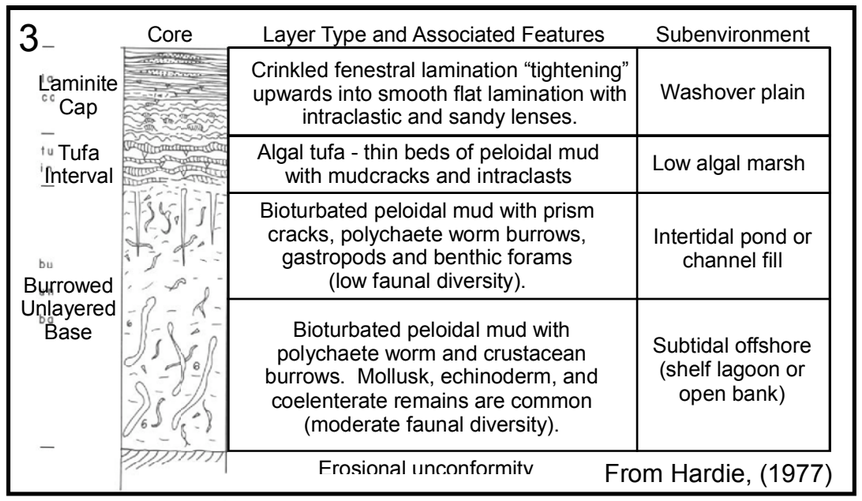

Layer Type and Associated Features	Subenvironment
Crinkled fenestral lamination "tightening" upwards into smooth flat lamination with intraclastic and sandy lenses.	Washover plain
Algal tufa - thin beds of peloidal mud with mudcracks and intraclasts	Low algal marsh
Bioturbated peloidal mud with prism cracks, polychaete worm burrows, gastropods and benthic forams (low faunal diversity).	Intertidal pond or channel fill
Bioturbated peloidal mud with polychaete worm and crustacean burrows. Mollusk, echinoderm, and coelenterate remains are common (moderate faunal diversity).	Subtidal offshore (shelf lagoon or open bank)

From Hardie, (1977)

Figure 5.7. Evolution of the interpretation of cycles in the Alpine Triassic. 1) Diagrammatic representation of Lofer cycle from Fischer, (1964). Fischer recognizes 3 main subfacies: A) a basal unconformity usually capped by a basal red or green argillaceous member, interpreted as a soil; B) an "intertidal" member containing algal mats and dessication features; and C) a massive subtidal member with varied biota. Cycles are bound at base and top by disconformities. 2) Re-interpretation of Lofer cycles by Goldhammer et al., (1990), the main difference between Fischer (1964) and Goldhammer et al., (1990) being that Goldhammer interprets the cycles as capped by the shallowest water facies. Goldhammer recognizes 4 subfacies: a) Thick (up to 20 m) beds of wacke-to-grainstones with hardgrounds and a diverse assemblage of fossils including megalodonts, sponges, corals, and gastropods (Fischer's "C" member); b) Dolomitic, burrowed peloidsl wackestones with restricted fauna of gastropods and ostracods (subfacies of Fischer's "B" member); c) Dolomitic, crinkly-laminated mudstone with common prism cracks, sheet cracks, and fenestrae (subfacies of Fischer's "B" member); and d) An intraformational breccia with green, brown, or red matrix (Demicco and Hardie, 1994). Goldhammer et al., (1990) also state that the breccias, which may be of pedogenic origin, systematically overlie laminites rather than form beneath them, as reported by Fischer (1964). This further suggests that the Lofer cycles are shallowing-upward rather than transgressive. Finally, 3) A schematic drawing through the modern tidal flats of Andros Island Bahamas by Hardie (1977). This diagram bases the subenvironments within the cycle to those observed in the modern. The similarity of facies within both modern and ancient succession is striking (Hardie, 1977).

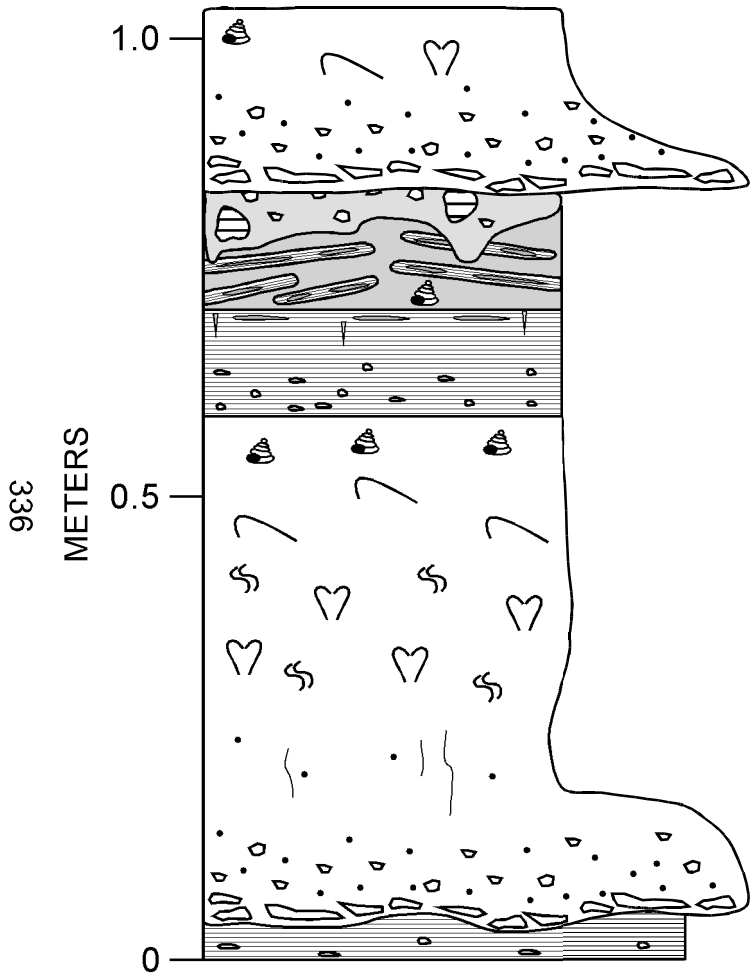

Figure 5.8. Facies 1, Intraclastic breccia from the Pelmo. Note rounding of clasts and comparably fine-grained matrix. In this example, most of the clasts are from a bed of skeletal wackestone, indicating downward erosion of the storm event into an underlying bed or transport and redeposition of partially-lithified clasts from the subtidal.

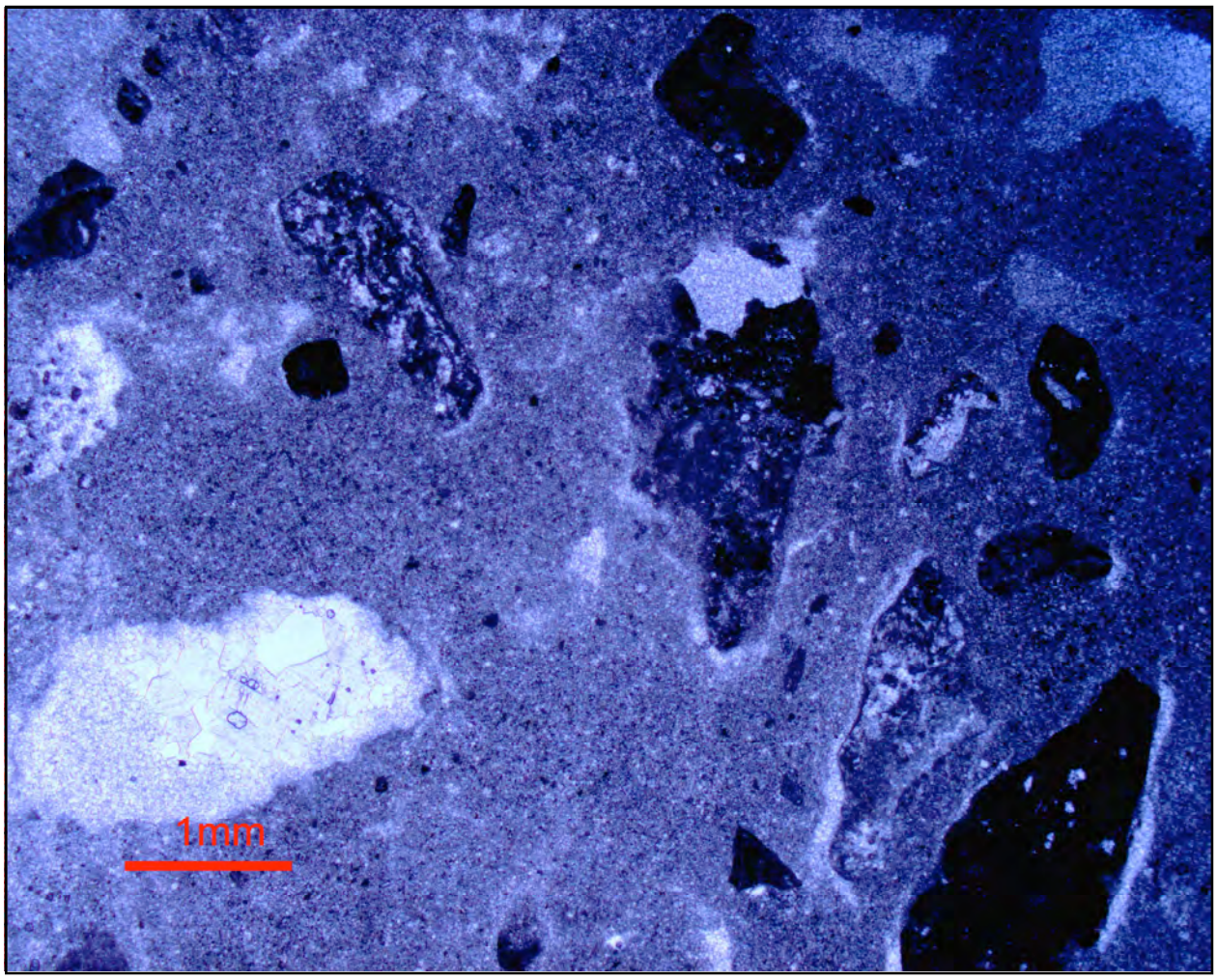

Figure 5.9. Photomicrograph of breccia sample from Tofana di Rozes (Fan 25A). Dolo-micritic matrix supports intraclasts of varying types, including clasts of microbial laminite, peloidal packstone, and cement. Note slight rounding of clasts (transport), possible burrow mottling (colonization), and cracks around clasts (shrinkage due to dessication).

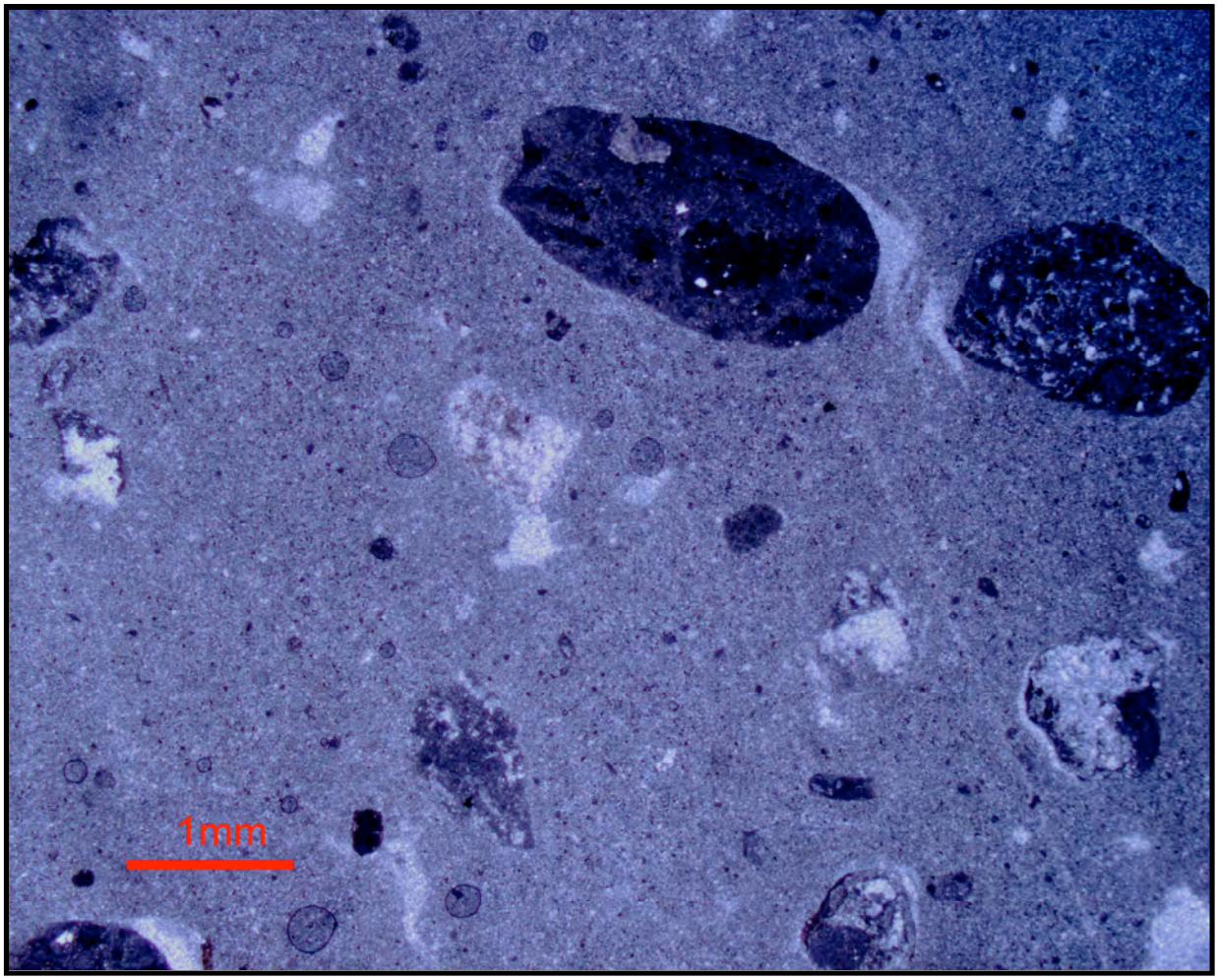

Figure 5.10. Rounded breccia intraclasts from Tofana di Rozes, Sample 25A. In this case, rounded clasts are made of formerly lithified breccia, suggesting that the breccia is multi-generational. Additionally, it is possible that the presence of breccia intraclasts signals subtraction and incorporation of the former substrate (Itself a shallowing-upward cycle). Also note that the breccia clasts are better rounded than the other clasts, which may further testify to the multi-generational interpretation of the intraclasts.

IDEAL TEMPESTITE SEQUENCE
+ HYDRODYNAMIC INTERPRETATION

BEDFORMS	FLOW REGIME	SEDIMENT. RATE
pelitic division	LAMINAR FLOW	very low
wave ripples	LOWER REGIME	moderate - low
plane lamination	UPPER REGIME	high
graded bedding	redeposition of suspended detritus	very high
erosional contact	storm erosion	
pelitic background	sedimentation	very low

Figure 5.11. An idealized tempestite sequence with physical sedimentary structures preserved, after Aigner, (1982). The sequence corresponds closely to the Bouma sequence, suggesting initial erosion during a high energy event, and subsequent deposition as a result of waning energy. In this case, is erosive and depositional event is interpreted to be a storm or hurricane-type event.

Figure 5.12. Core of modern tidal flat sediments from the Caicos tidal flats, Bahamas. At the base, the core shows ripped-up flat laminated intraclasts (red arrows) from an intertidal channel levee bound into a microbial mat. Overlying sediment is mixed skeletal / mangrove peloidal wackestone.

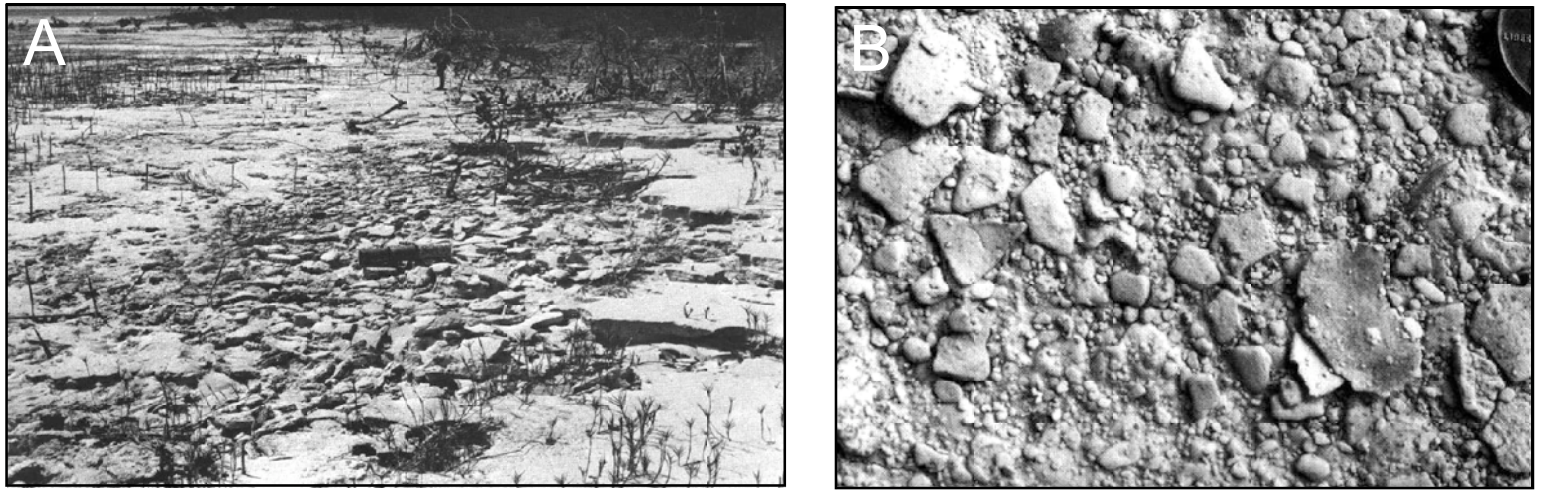

Figure 5.13. Intraclastic conglomerates. A. Algal-bound laminated flat pebbles at the base of a small erosion ledge on a beach terrace. These pebbes were derived in-place from undercutting of the ledge during a severe onshore storm. Scale bar is 30 cm. Figure and description from Hardie, (1977). B. Modern Bahamian mudchip gravel. The mudchips, although rounded by erosion are not cemented and can be ductily deformed when wet. Penny for scale in upper right corner. Photograph and description from Demicco and Hardie (1994).

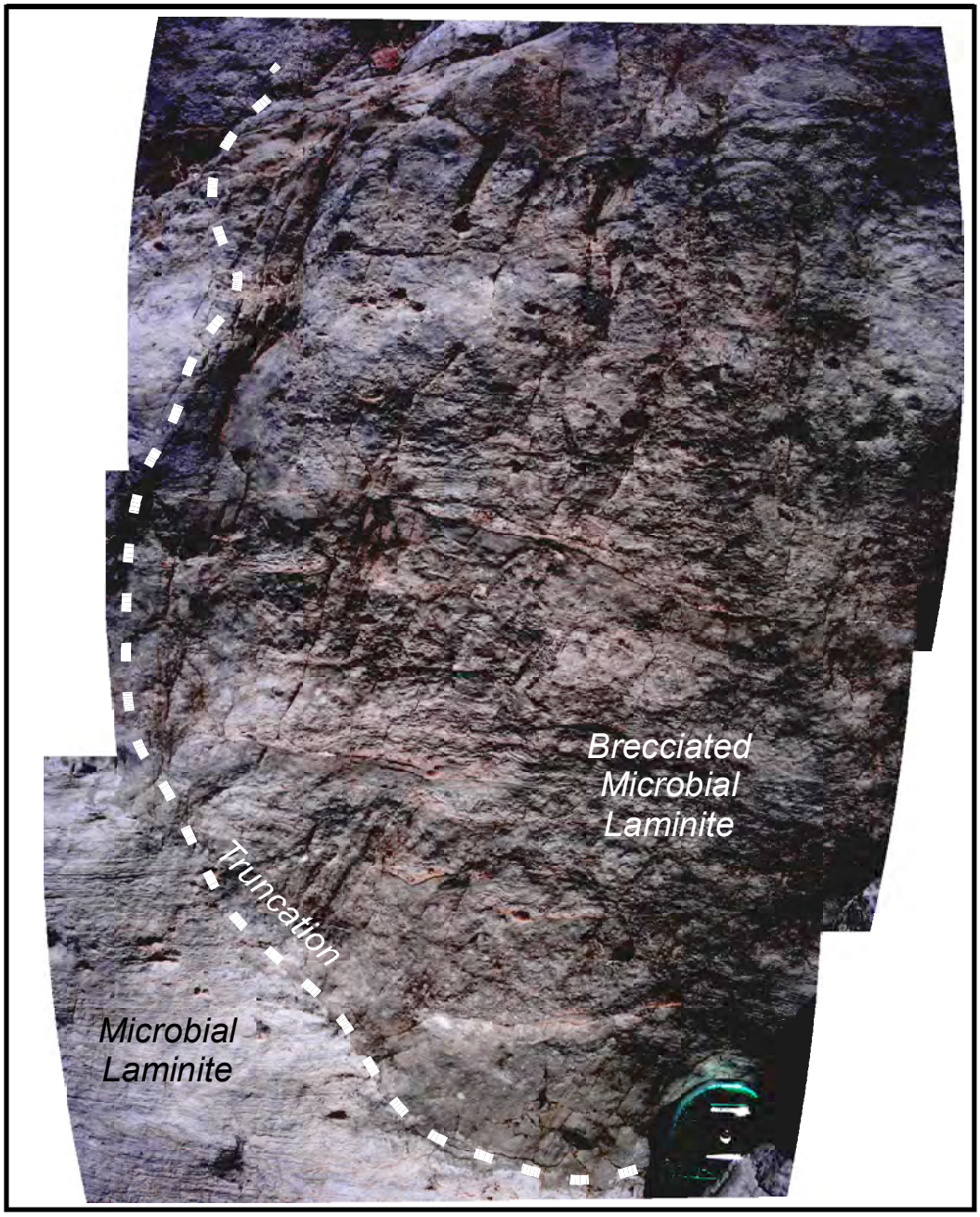

Figure 5.14. Erosive or channelized intraclastic breccia, tape measure for scale. This example from the Pelmo illustrates the down-cutting or erosive nature of some of the breccias within the DP complex. In this case, the depositional event first carved out a channel within a cryptomicrobial laminite in which the breccia clasts and matrix were deposited. Larger breccia clasts in this examples are nearly 30 cm in the long direction.

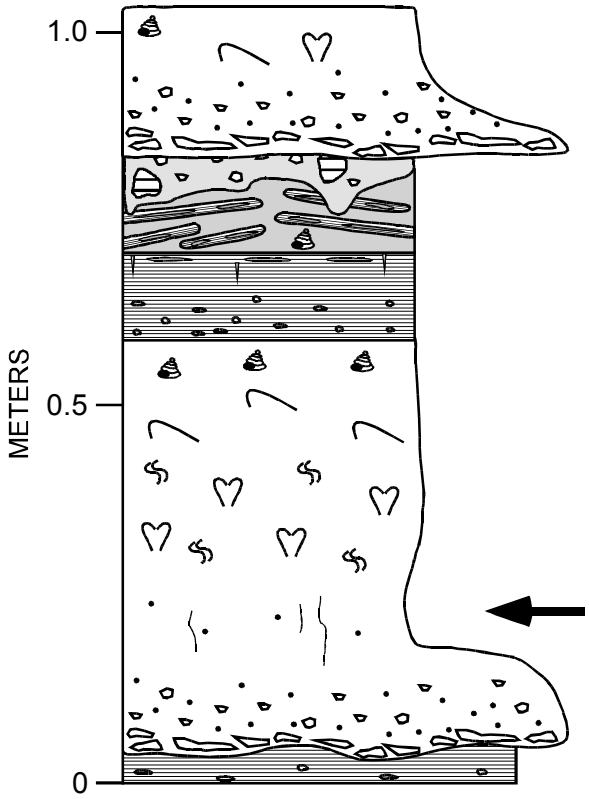

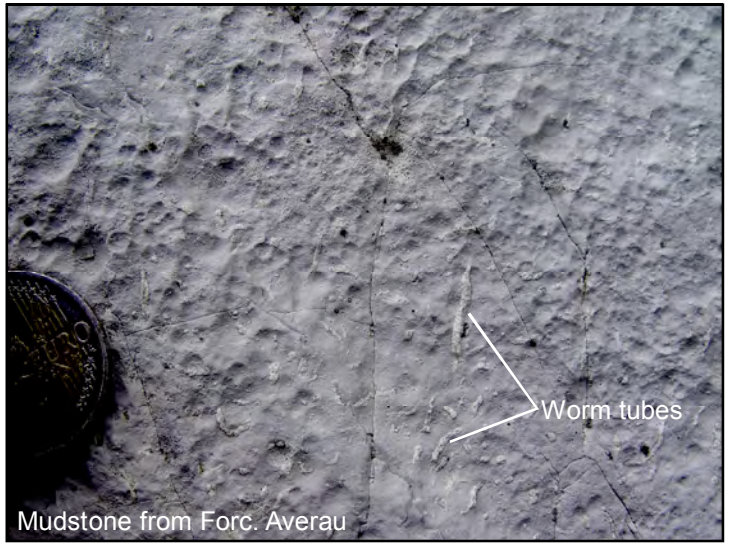

Figure 5.15. Facies 2, Massive mudstone. Carbonate mudstone is common in the DP and typically weathers as a recessive interval. Mudstones are typically green to gray, may have few sub-mm diameter vertical burrows (serpulid worms) and typically have oxide blebs. Oxide blebs may form along horizons and can be upwards of 1 cm in diameter. Oxide blebs may be after framboidal pyrite or siderite and may be indicators of restriction / reducing environment (Folk, personal communication).

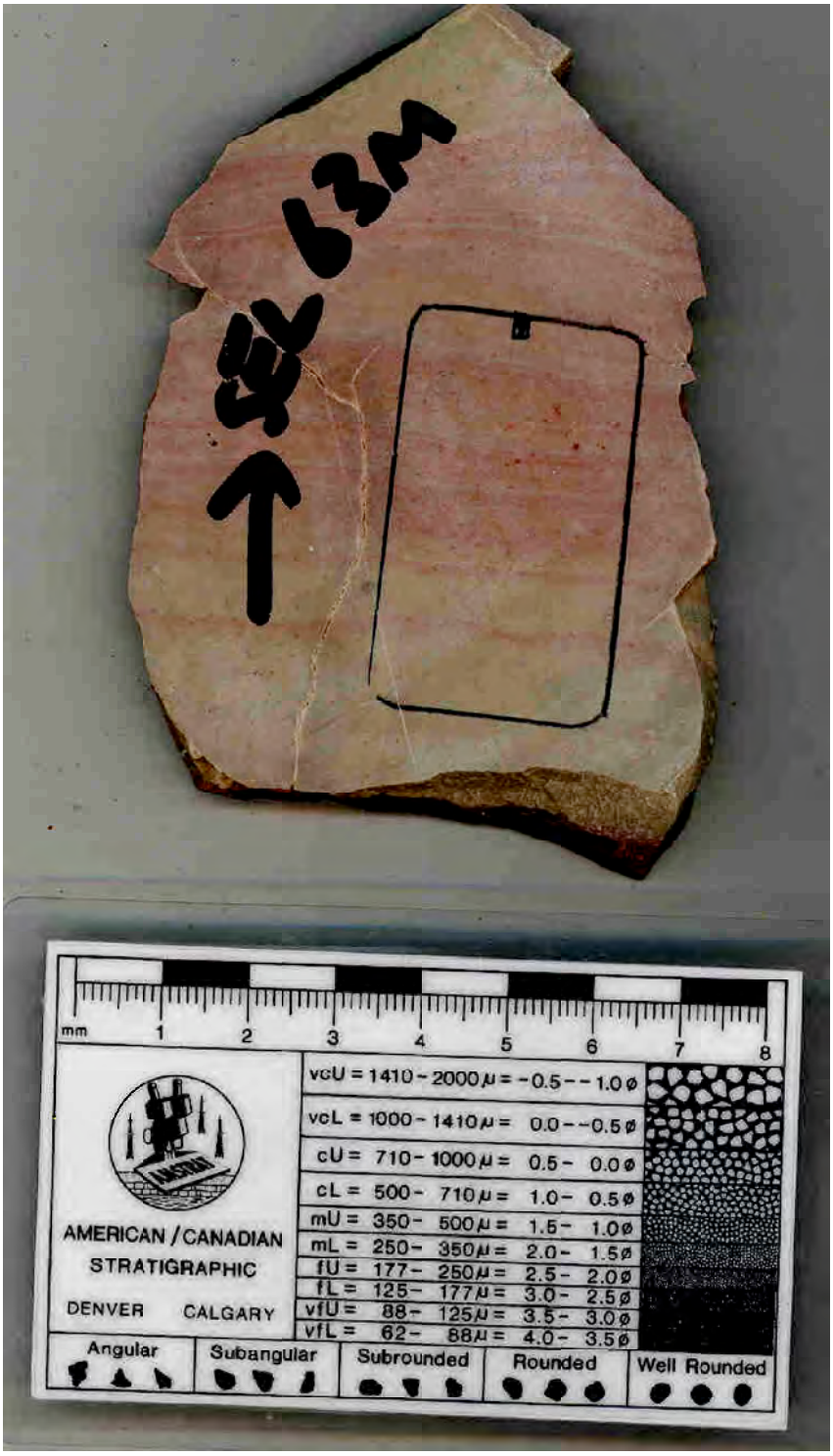

Figure 5.16. Hand specimen of mudstone from the DP of the Sella (Sample 63m). Sample lacks recognizable allochems and has a distinctive red/green color, possibly related to oxidizing/reducing conditions during or shortly after deposition.

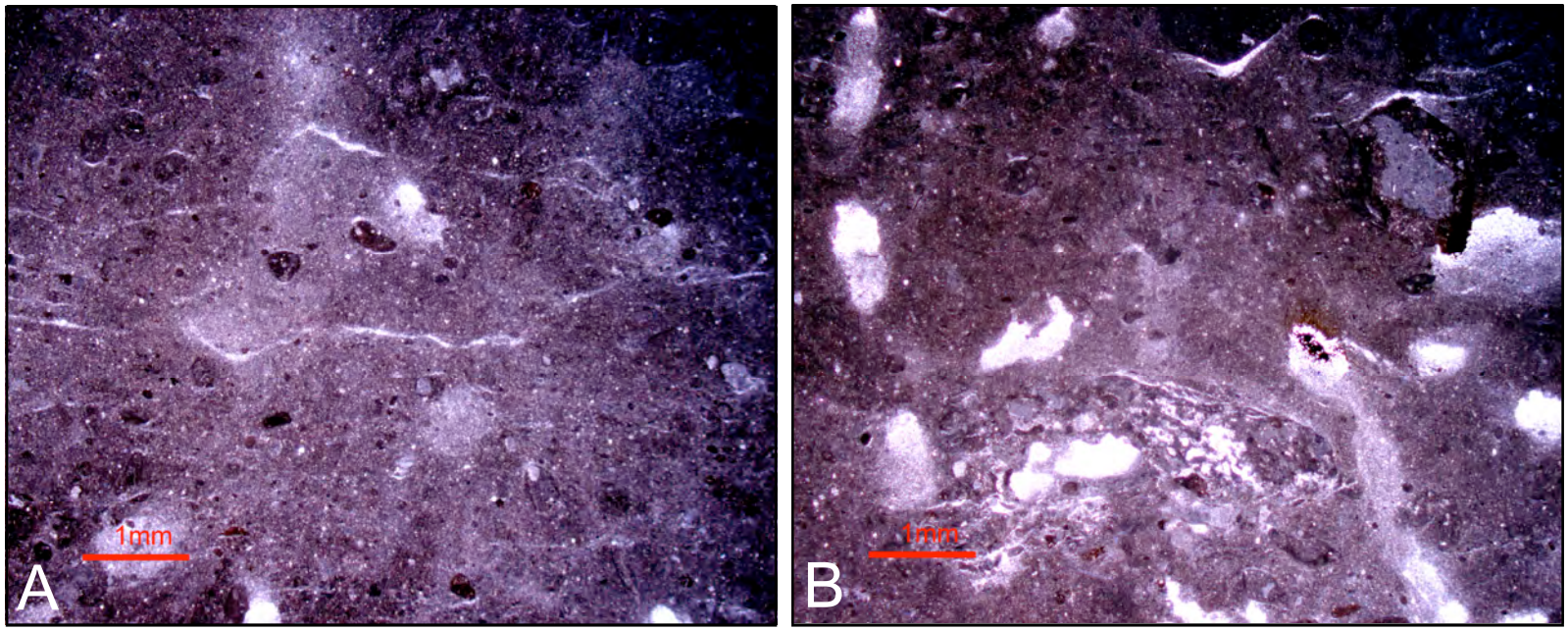

Figure 5.17. Mudstone/Wackestone photomicrographs from the Tofana di Rozes (Sample 31d). Hand sample is mud-dominated with sub-mm clasts entrained in bright yellow dolomicritic matrix that is bioturbated by mm-wide (worm?) burrows. A. Photomicrograph showing fabric of rock. The sample is a mud dominated wackestone with sub-mm-scale clasts. B. Photomicrograph of mm-scale back-filled burrows near the top of the sample.

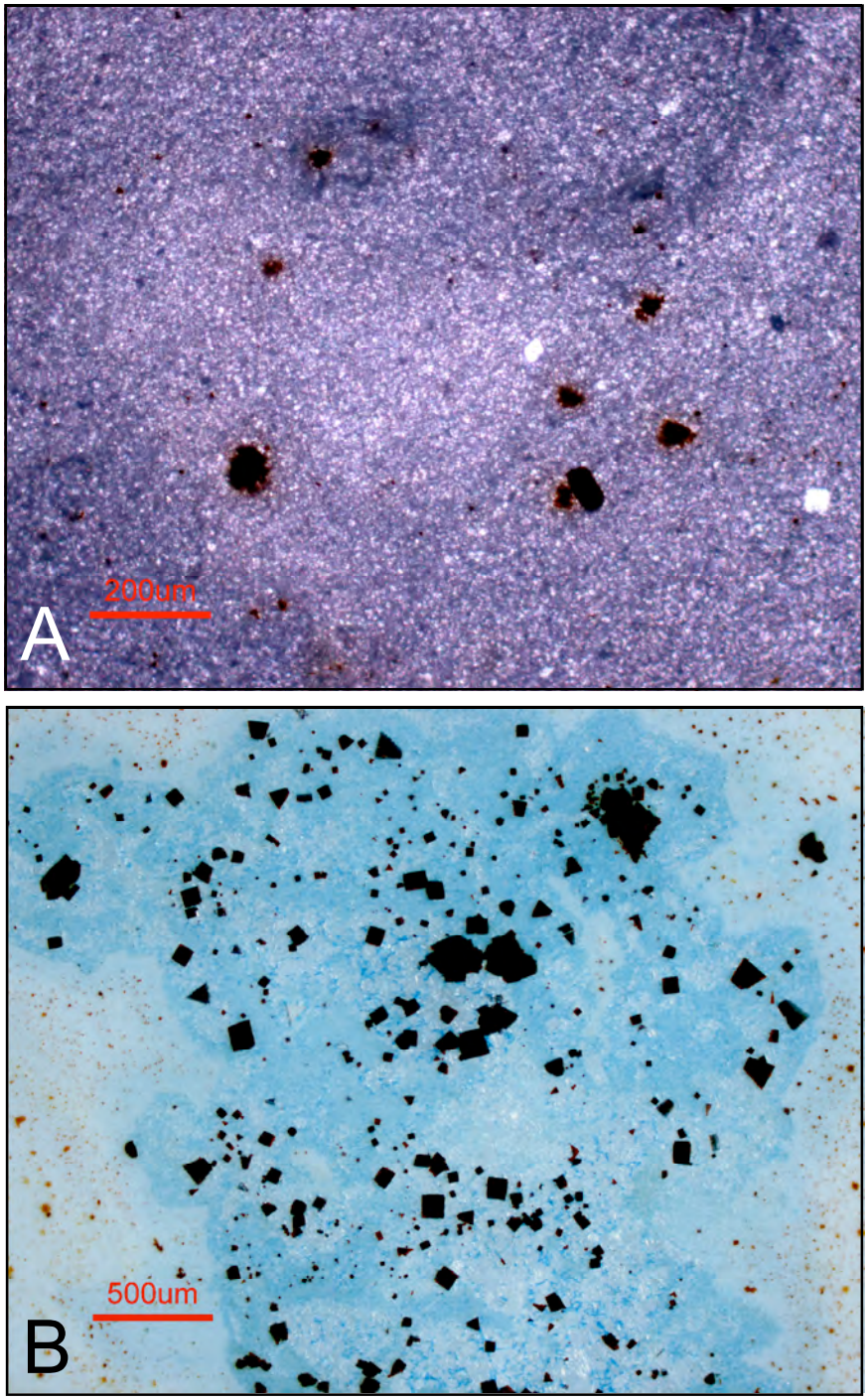

Figure 5.18. Photomicrographs of mudstone samples from Passo Valparola (Sample 1 B). A. Field of view showing dolomicrite and oxides, likely former pyrite. B. Photomicrograph of oxides (thin section backed by a white card and under reflected light), likely former pyrite due to the cubic crystal shapes. Pyrite likely formed during or soon after deposition in reducing conditions (further evidenced by lack of skeletal allochems or trace fossils), and was later oxidized.

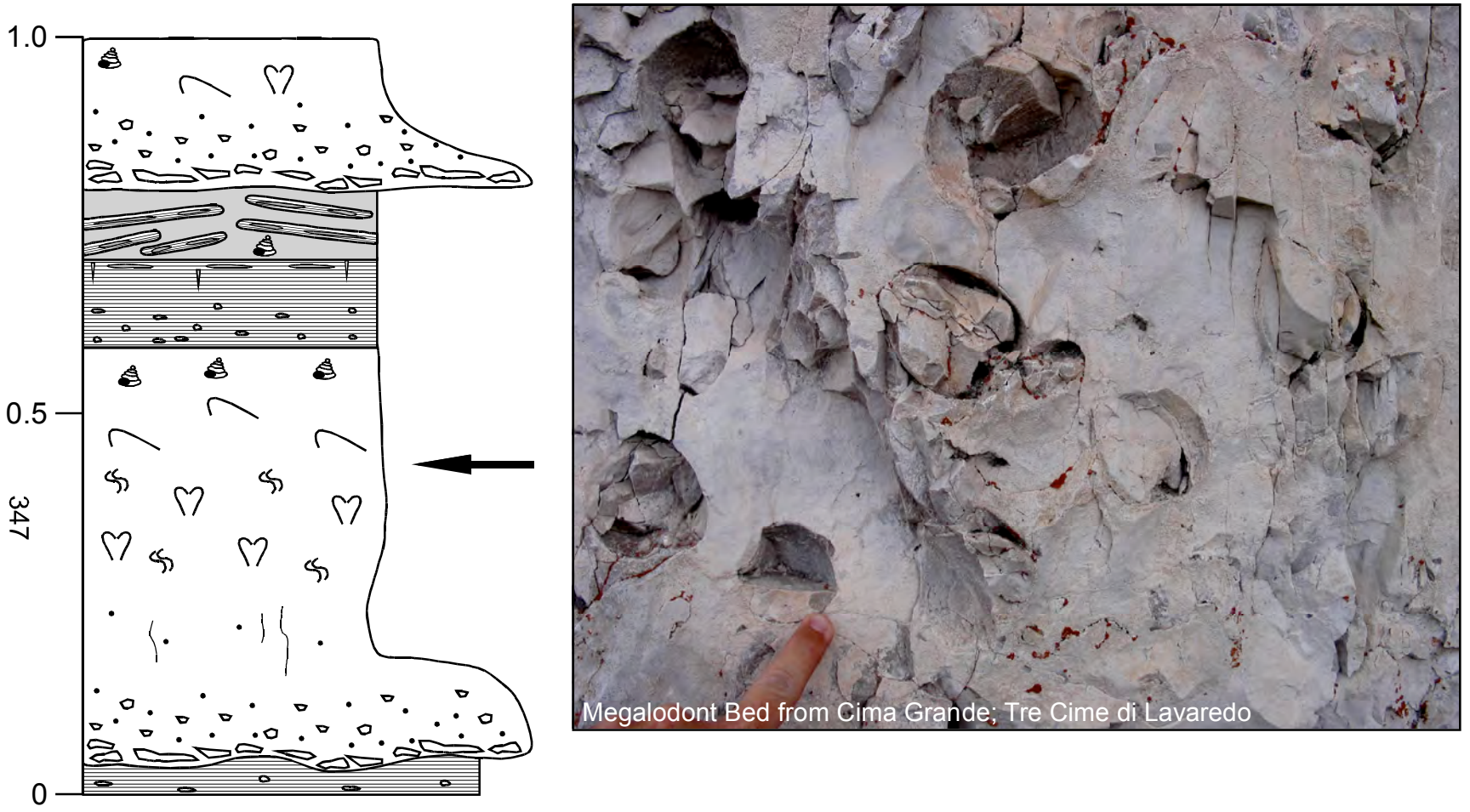

Figure 5.19. Facies 3, mixed skeletal wackestone. Skeletal debris and fossils are common, including bivalves, gastropods and megalodont molds. Faunal diversity typically decreases up the bed, being limited to mainly gastropods near the top. Sedimentary structures are typically masked by bioturbation. Wispy microbial lamination increases in abundance upward, and many times grades into a cryptomicrobial laminite.

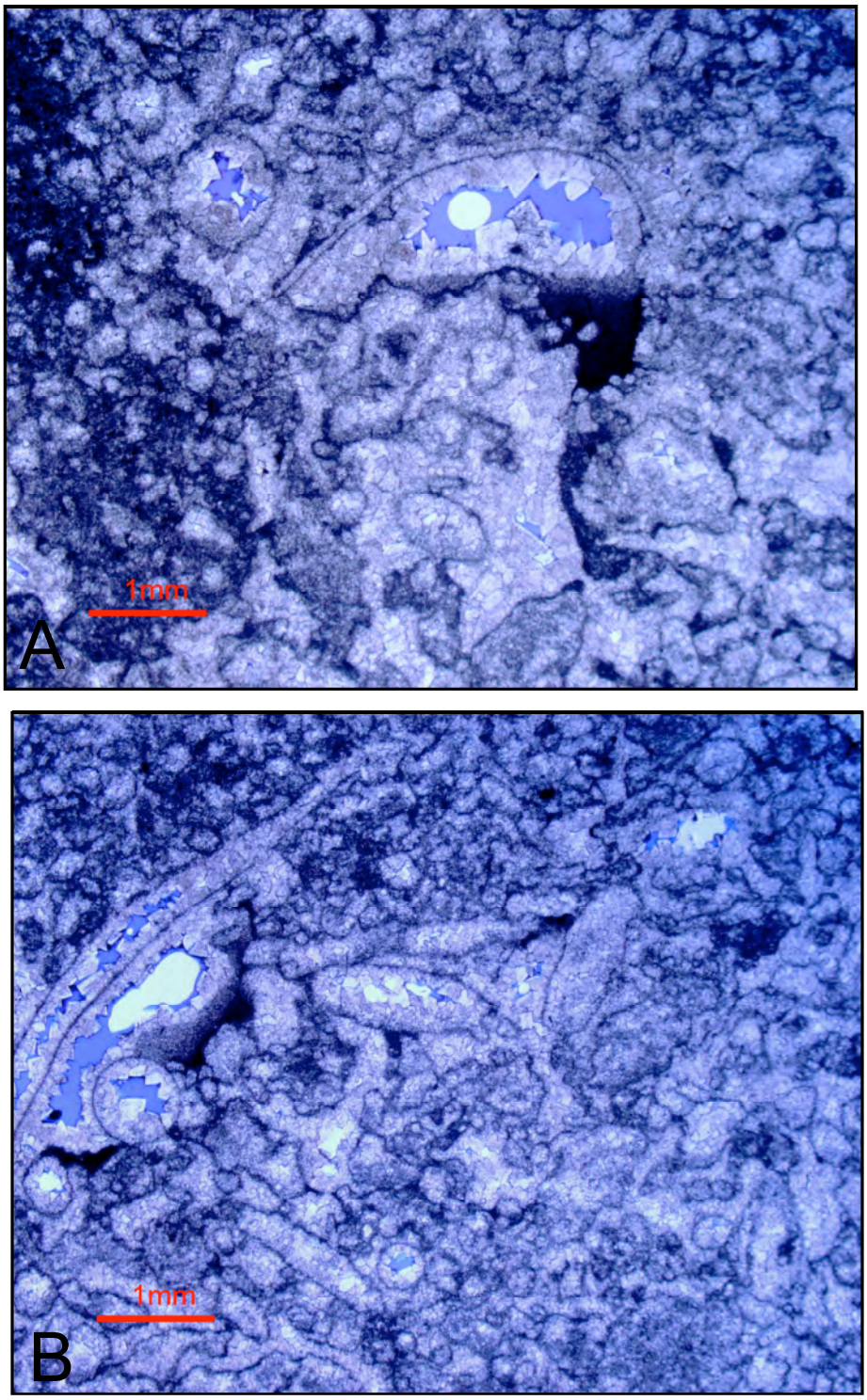

Figure 5.20. Photomicrographs of mixed skeletal packstone from the DP of the Sella Massif (Sel 26A). A. Shelter pore and geopetal fill beneath a former megalodont shell. Note extensive dolomitization of the sample and lack of preserved internal structures of ghost grains. B. Photomicrograph showing variability in allochem size and shape. While most allochems have undergone fabric-replacing dolomitization, the grain ghosts suggest that the parent allochems may have been bivalves, green algae, peloids, composite grains. Other grain types are difficult to confidently identify do to lack of preservation.

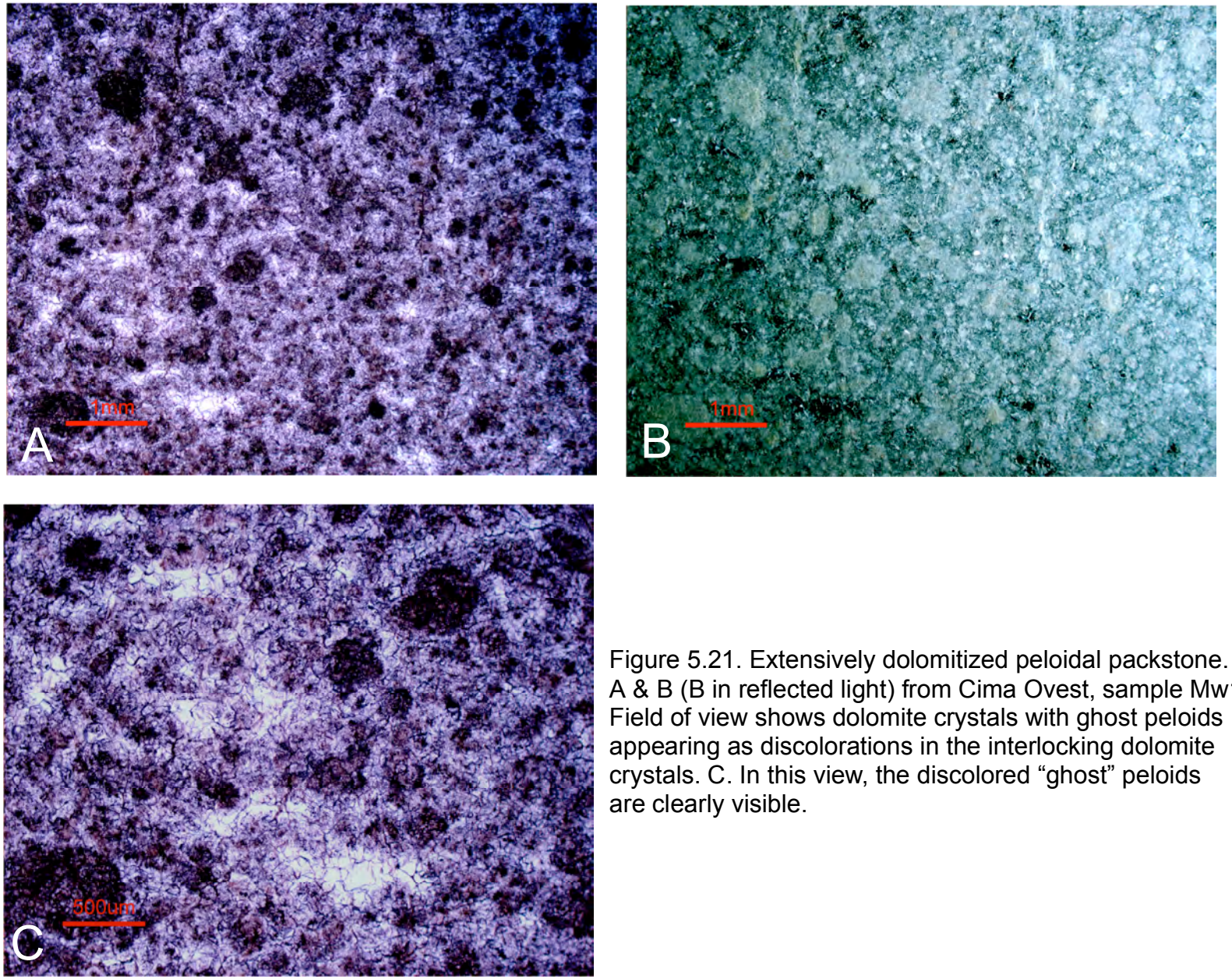

Figure 5.21. Extensively dolomitized peloidal packstone. A & B (B in reflected light) from Cima Ovest, sample Mw1. Field of view shows dolomite crystals with ghost peloids appearing as discolorations in the interlocking dolomite crystals. C. In this view, the discolored “ghost” peloids are clearly visible.

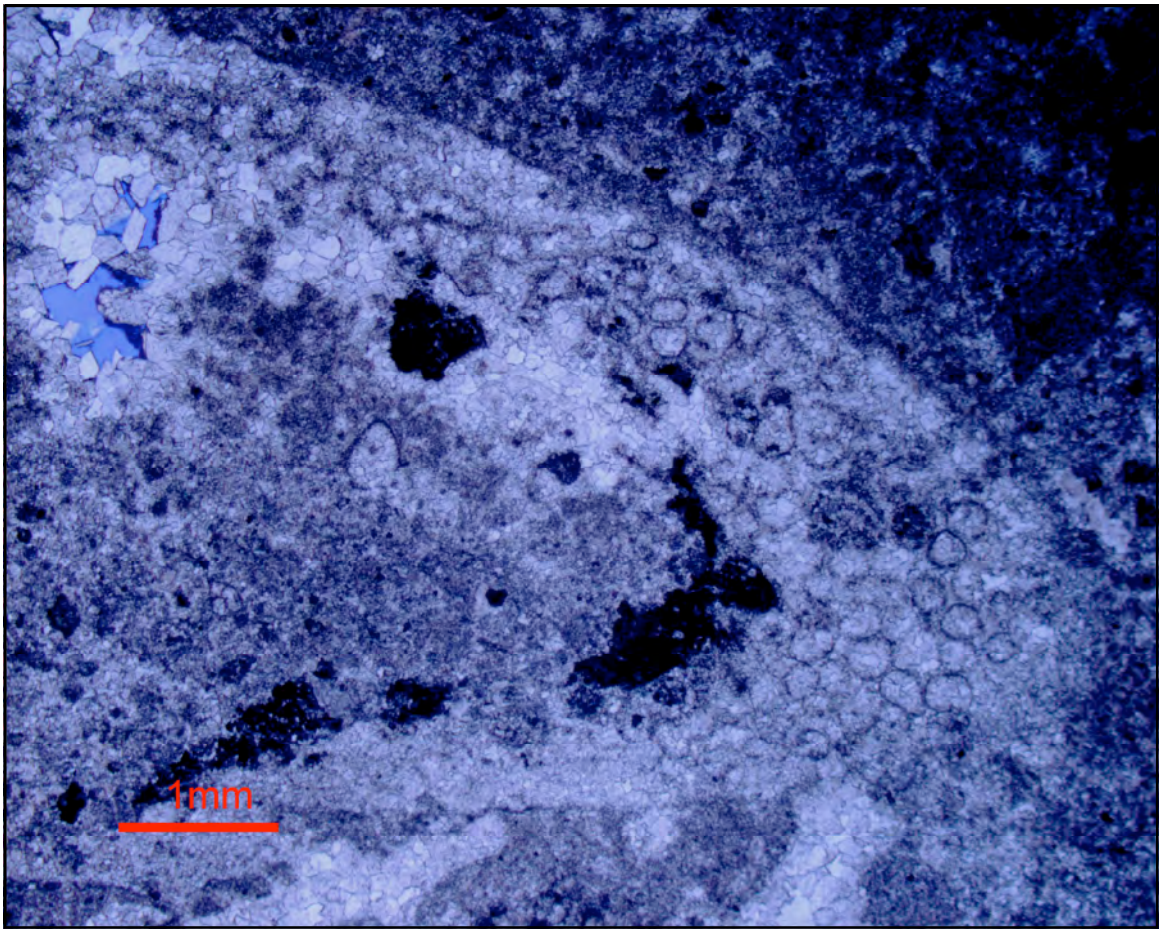

Figure 5.22. Mixed skeletal wacke-to-packstone from Monte Cristallo (Crs 17 Aii). Sample is completely dolomitized. This photomicrograph shows a cross-section through a dasycladacean alga fragment. Note the vesiculiferous regions, common to examples of the Norian dasyclad Gyroporella vesiculifera (Pugliese, 1996)

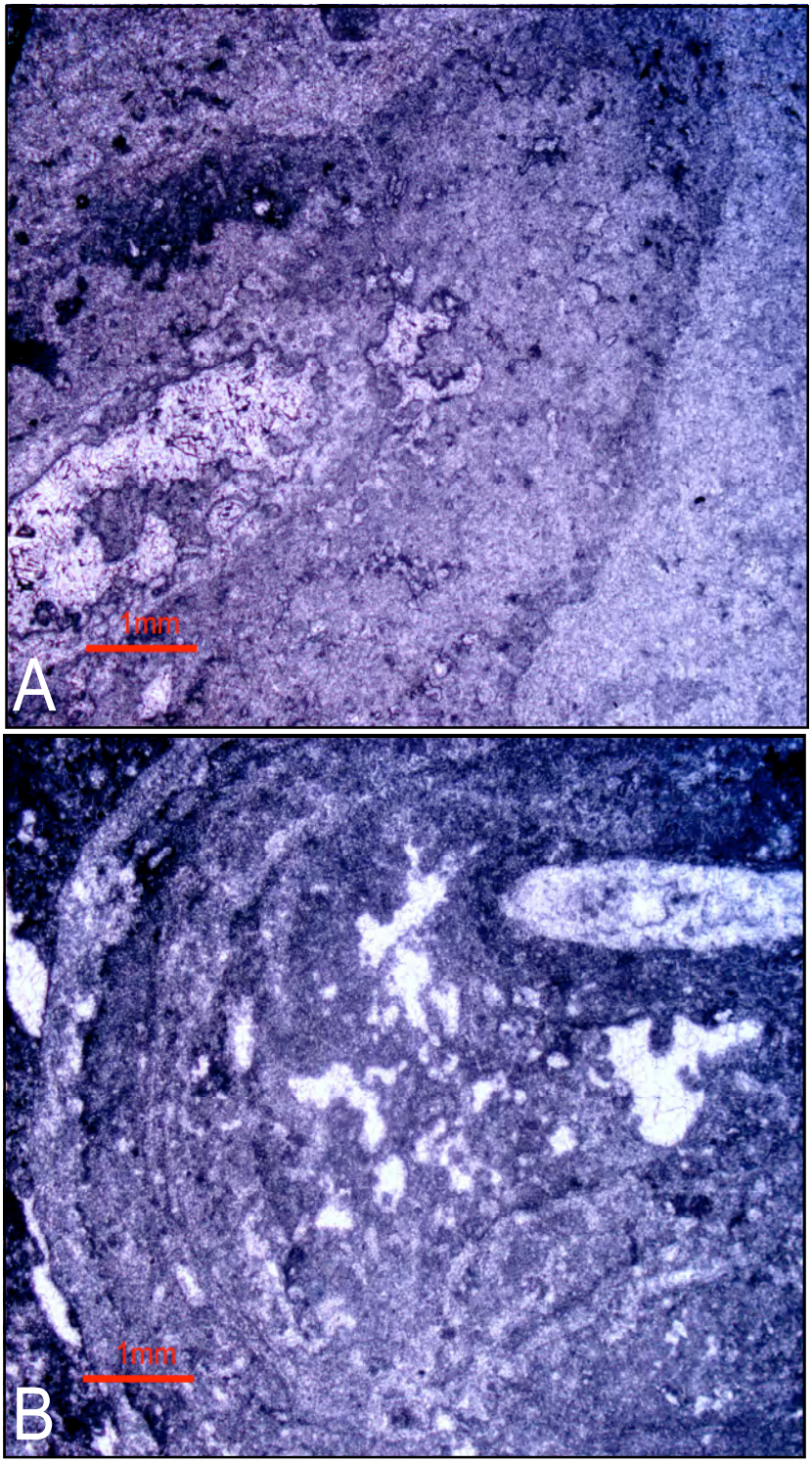

Figure 5.23. Oncoids preserved in (former) mixed skeletal/peloidal wacke-to-packstone from Forcella Lavaredo, sample FC21. A. Note tuft-like micritic laminae around core of dasycladacean alga grain. This structure is more akin to microbial binding and trapping of sediment than chemical precipitation of carbonate that would be expected in a pisolite. B. Oncoid nucleating on an aggragate of skeletal grains, including bivalve fragments and dasycladale fragments.

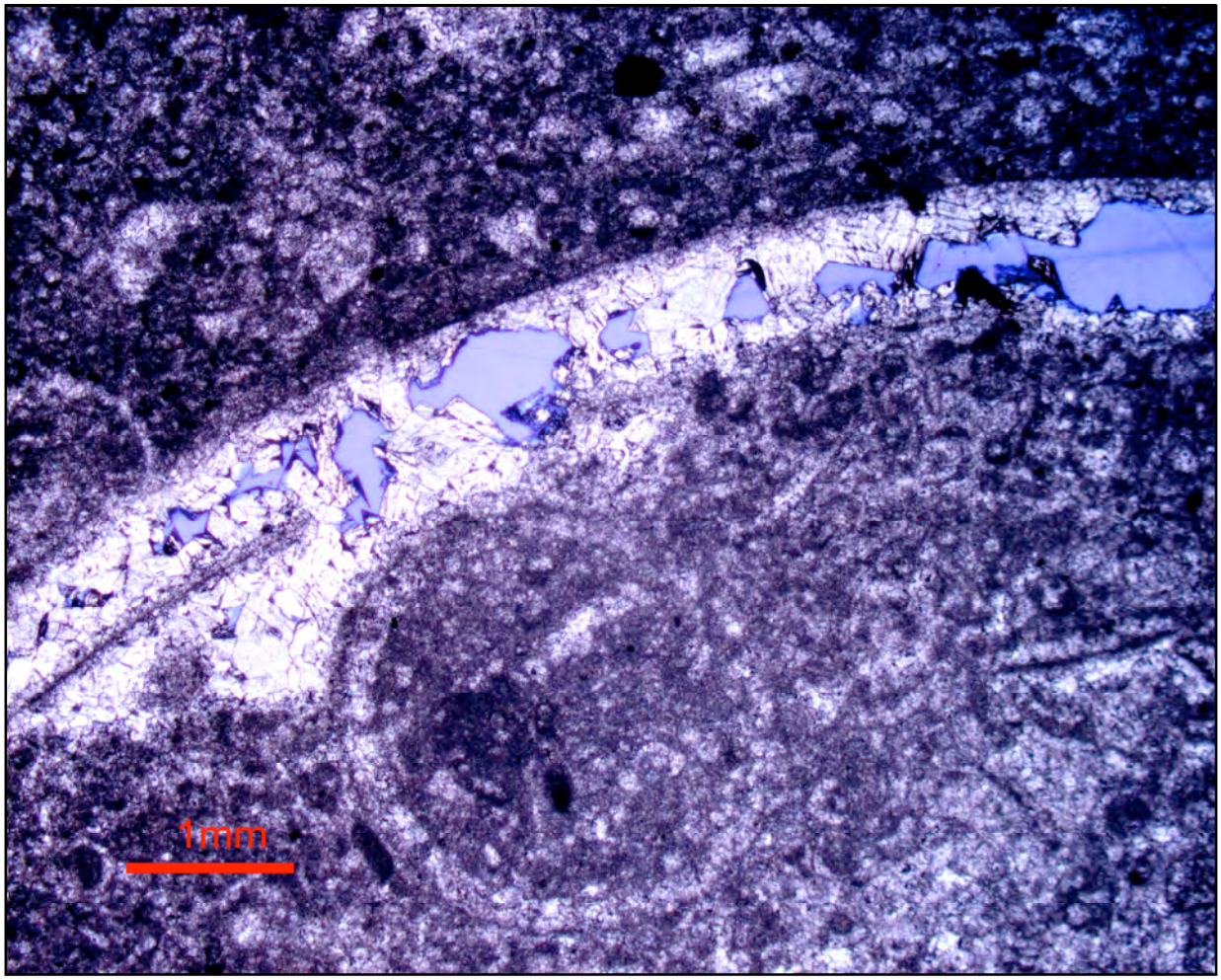

Figure 5.24. Former mixed skeletal pack-to-grainstone from the Pelmo, sample PS1B. Sample was completely dolomitized, leaving only ghosts of original allochems and the remnants of a megalodont bivalve and dasycladacean algae.

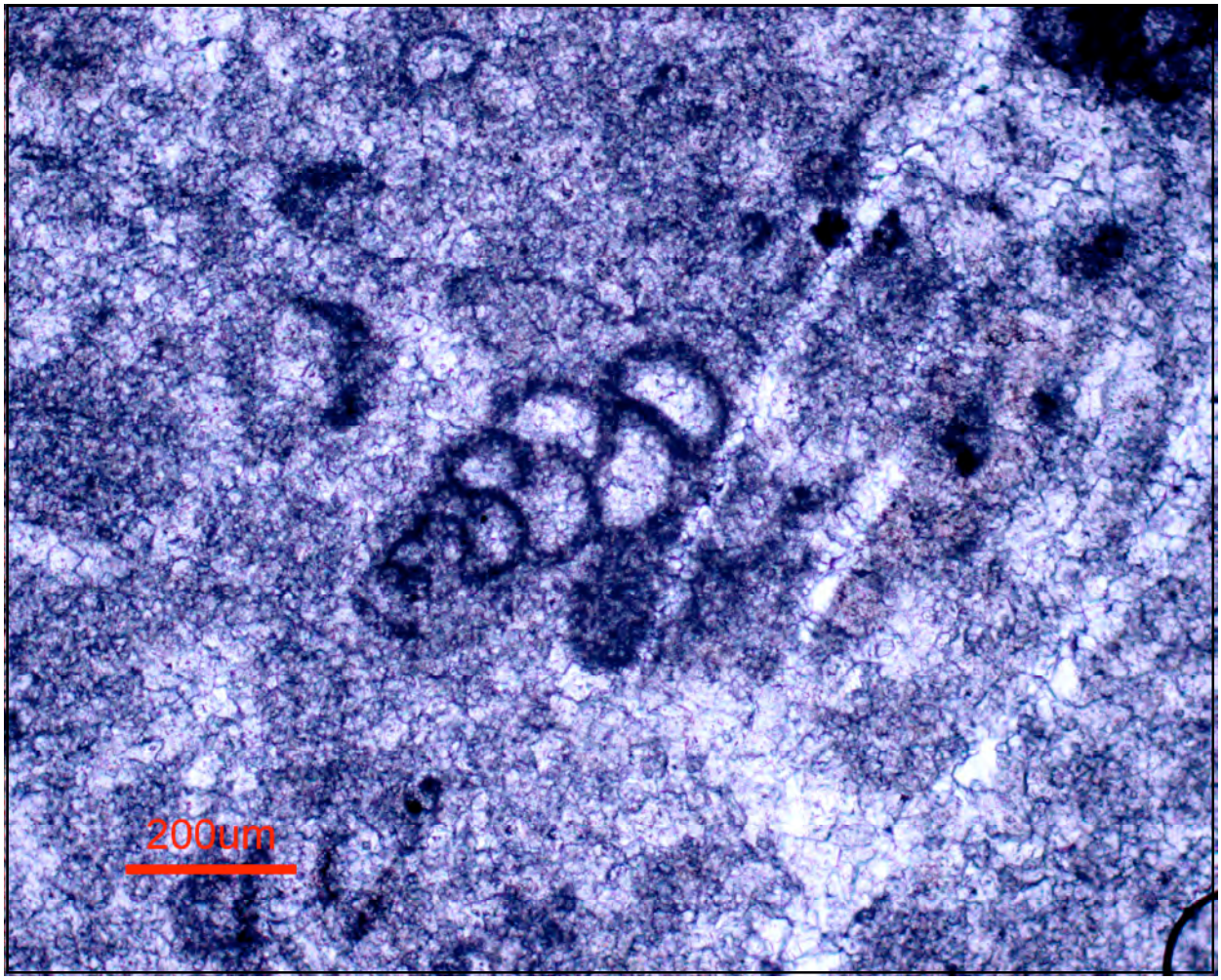

Figure 5.25. Sample of mixed skeletal wacke-to-packstone from Monte Cristallo (Crs 17A). This photomicrograph shows an open-water biserial foram preserved in the sediment. Note that the entirety of the host rock has been replaced and is now crystalline dolomite with only grain/allochem ghosts.

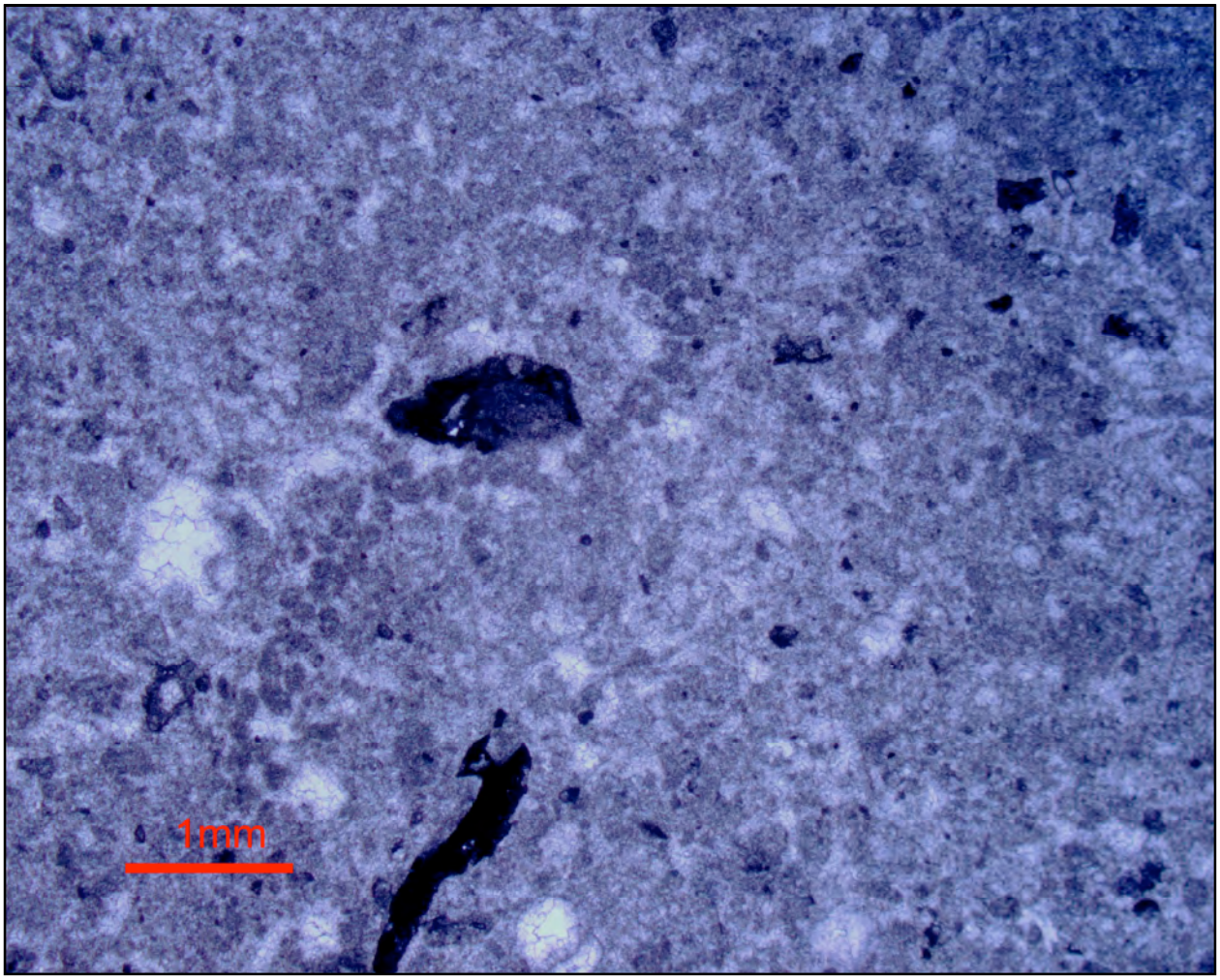

Figure 5.26. Sample of mixed skeletal packstone from Monte Cristallo (Crs 17Aii). This sample appears to have been a peloidal packstone at the time of deposition. Peloid/pellet ghosts are recognizable, but the entire rock has been recrystalized into chiefly dolomite.

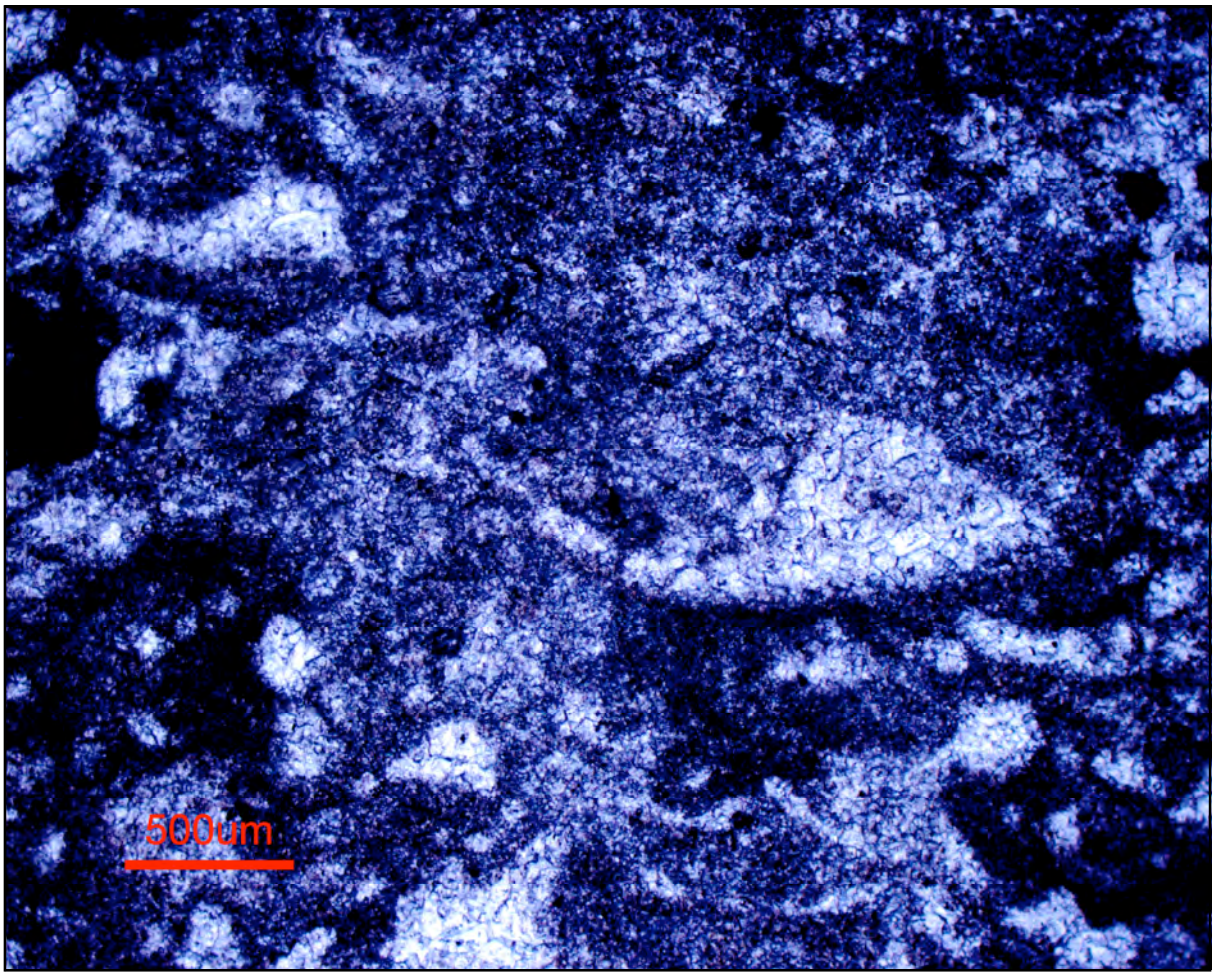

Figure 5.27. Sample from Tofana di Rozes (Fan 57A) showing ghost skeletal allochems in what may have been a mixed skeletal wackestone. The entire rock has been replaced by fine crystalline dolomite, leaving only “ghosts” of original grains.

Figure 5.28. Photographs of megalodonts from Cima Ovest, Tre Cime di Lavaredo. A. Megalodont bed. Megalodonts are found embedded in massive wackestone. Most examples have valves oriented vertically or subvertically, probably in former living position, as indicated by geopetal fill B. Close-up of megalodont fossil with geopetal fill (dashed line).

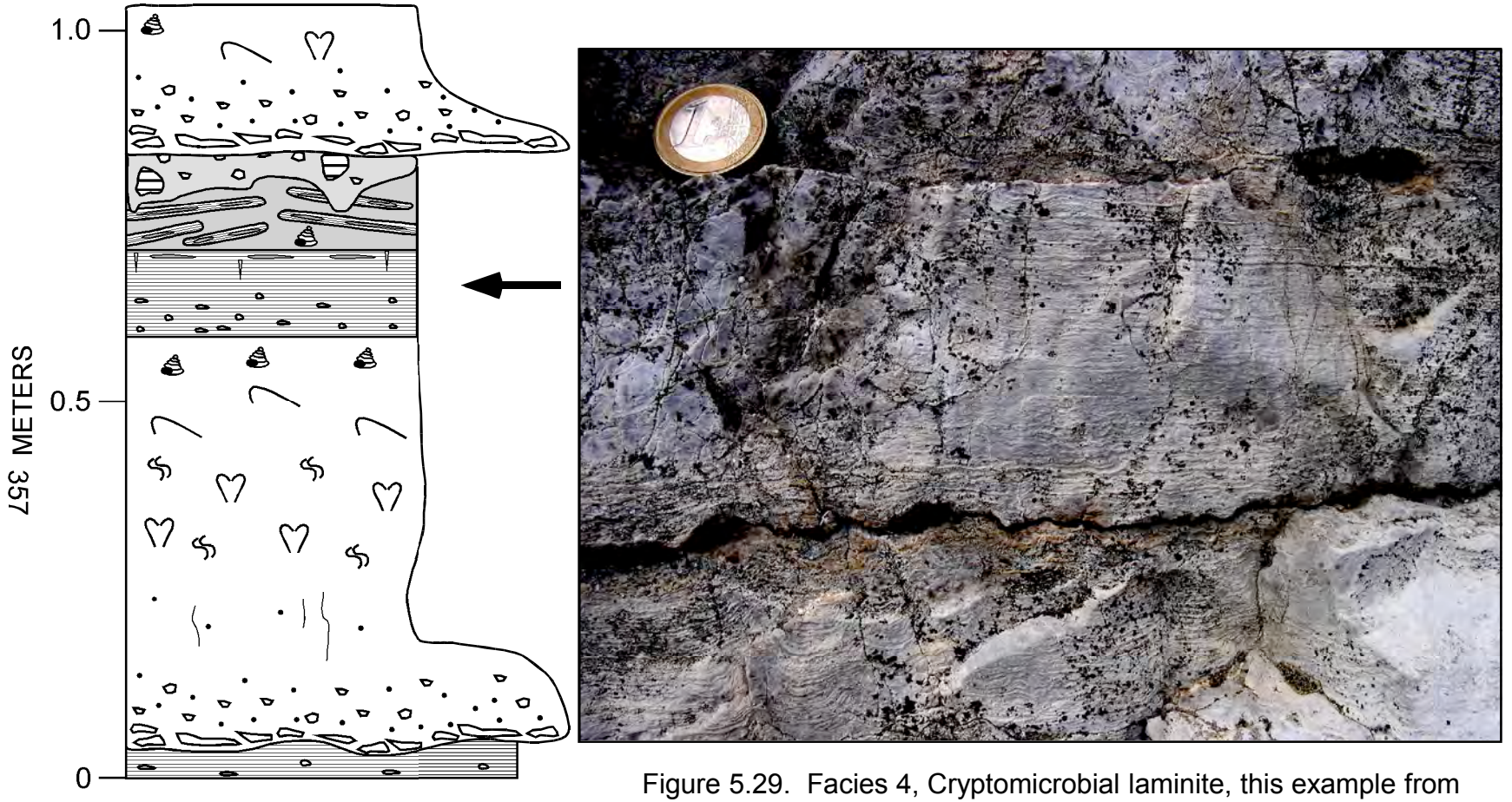

Figure 5.29. Facies 4, Cryptomicrobial laminite, this example from Forcella Averau. 1 Euro coin for scale.

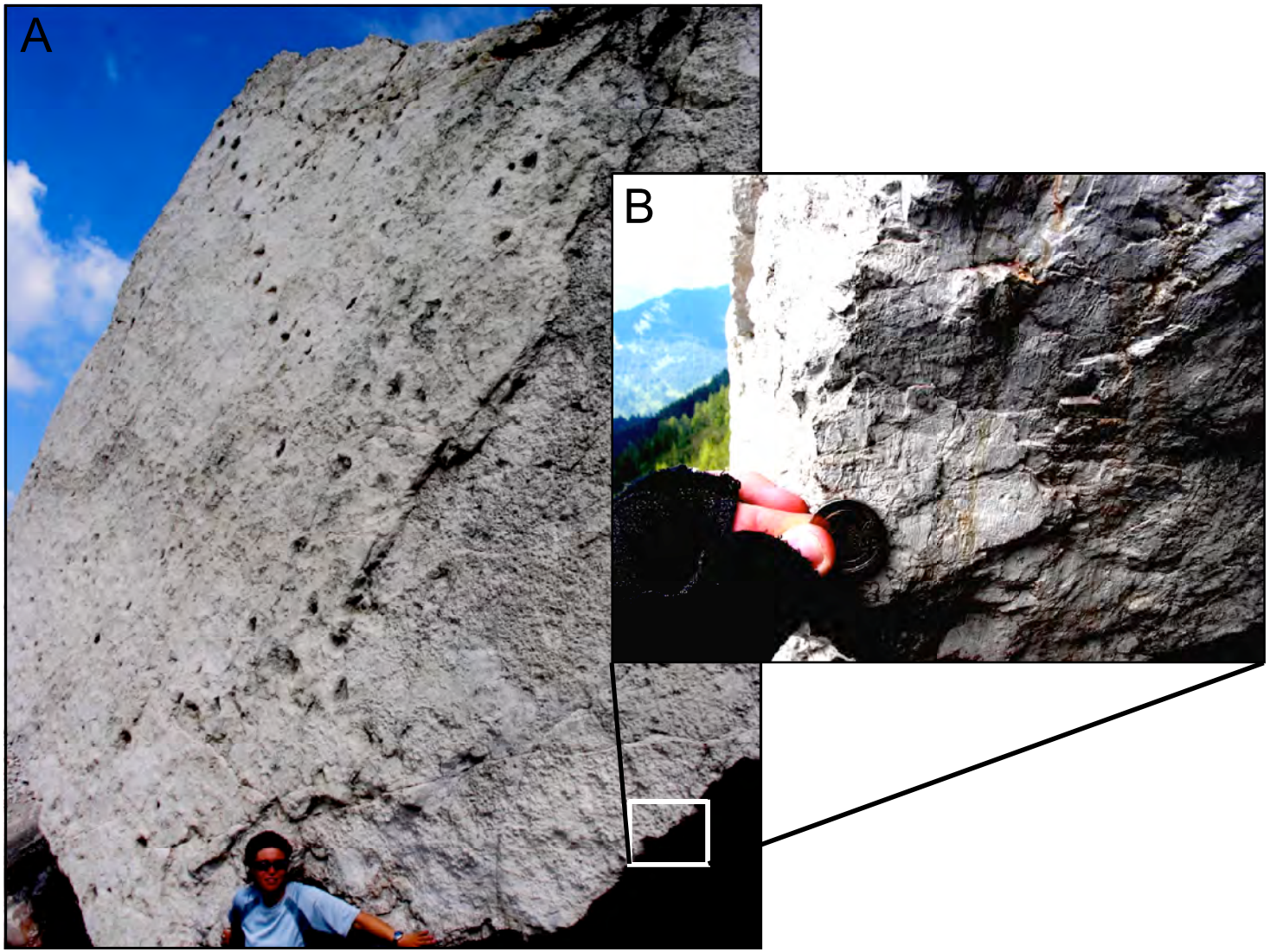

Figure 5.30. Terrestrial trace fossils (dinosaur tracks) preserved in a block of cryptomicrobial laminite at the Pelmo. Dinosaur tacks can be seen in photograph A, above the head of Ms. Stefanie Heins. In cross section (photograph B) crinkly microbial laminae are easily visible.

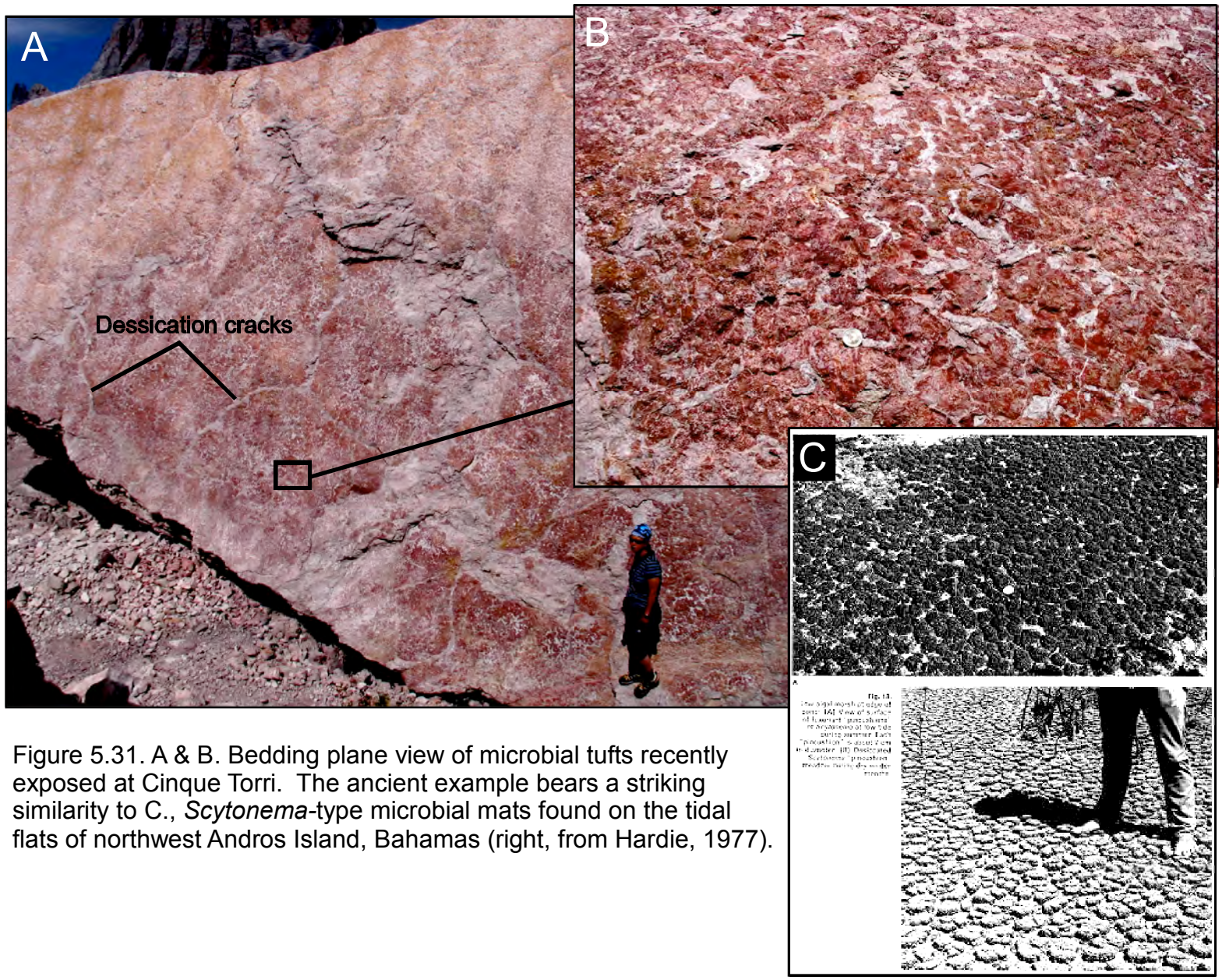

Figure 5.31. A & B. Bedding plane view of microbial tufts recently exposed at Cinque Torri. The ancient example bears a striking similarity to C., *Scytonema*-type microbial mats found on the tidal flats of northwest Andros Island, Bahamas (right, from Hardie, 1977).

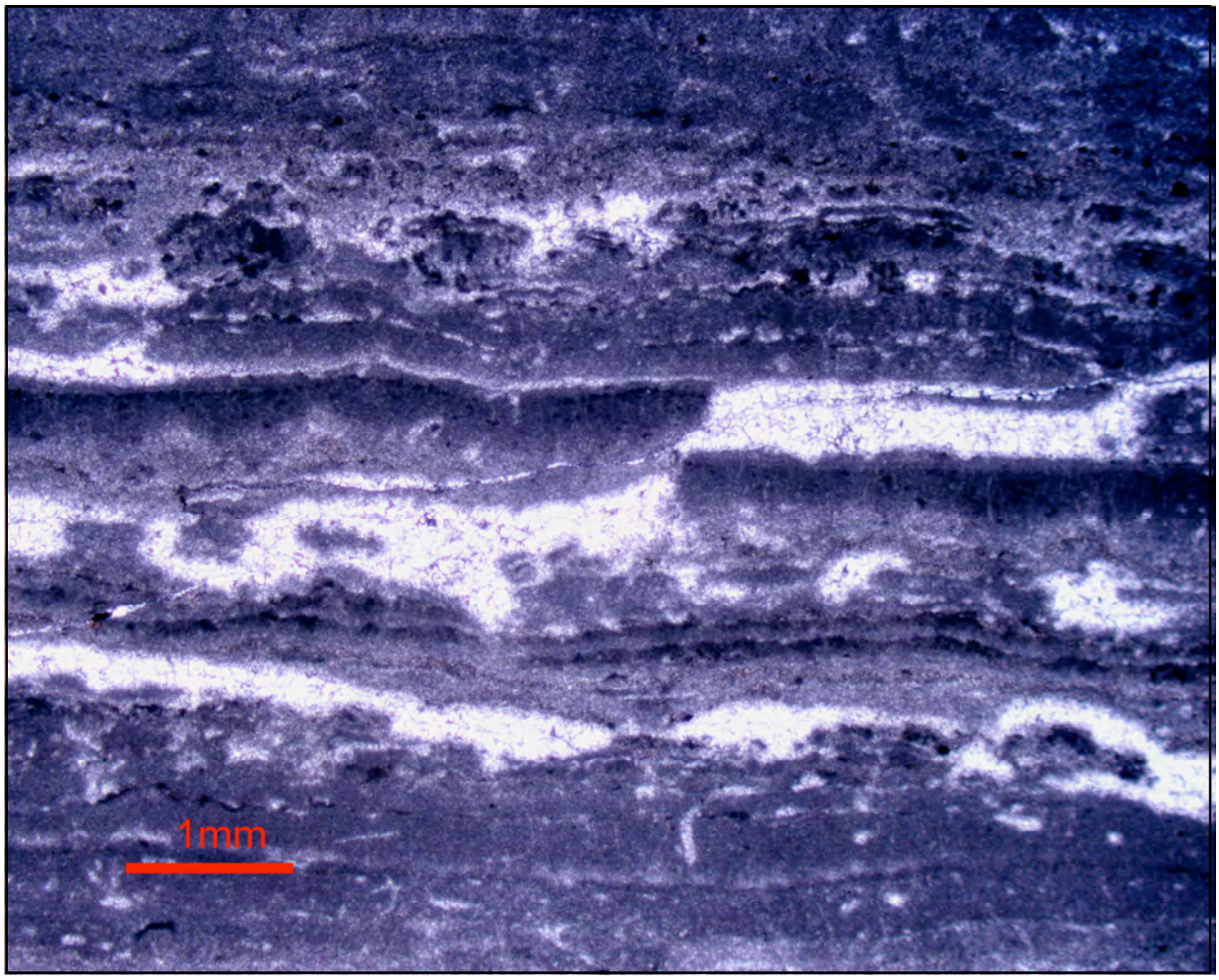

Figure 5.32. Laminite from Forcella Averau (sample V32). Laminae consist of mud with subvertical white, cement/spar filled filaments within horizontal laminae. Laminae also contain dark, micritic, patches and crusts; possibly peloids or columnar microproblematica. Geopetal micrite and cement fill within fenestrae is common, and is possible evidence for early dissolution and/or fill by expansive cement (sheet cracks) that has since been replaced by dolomite.

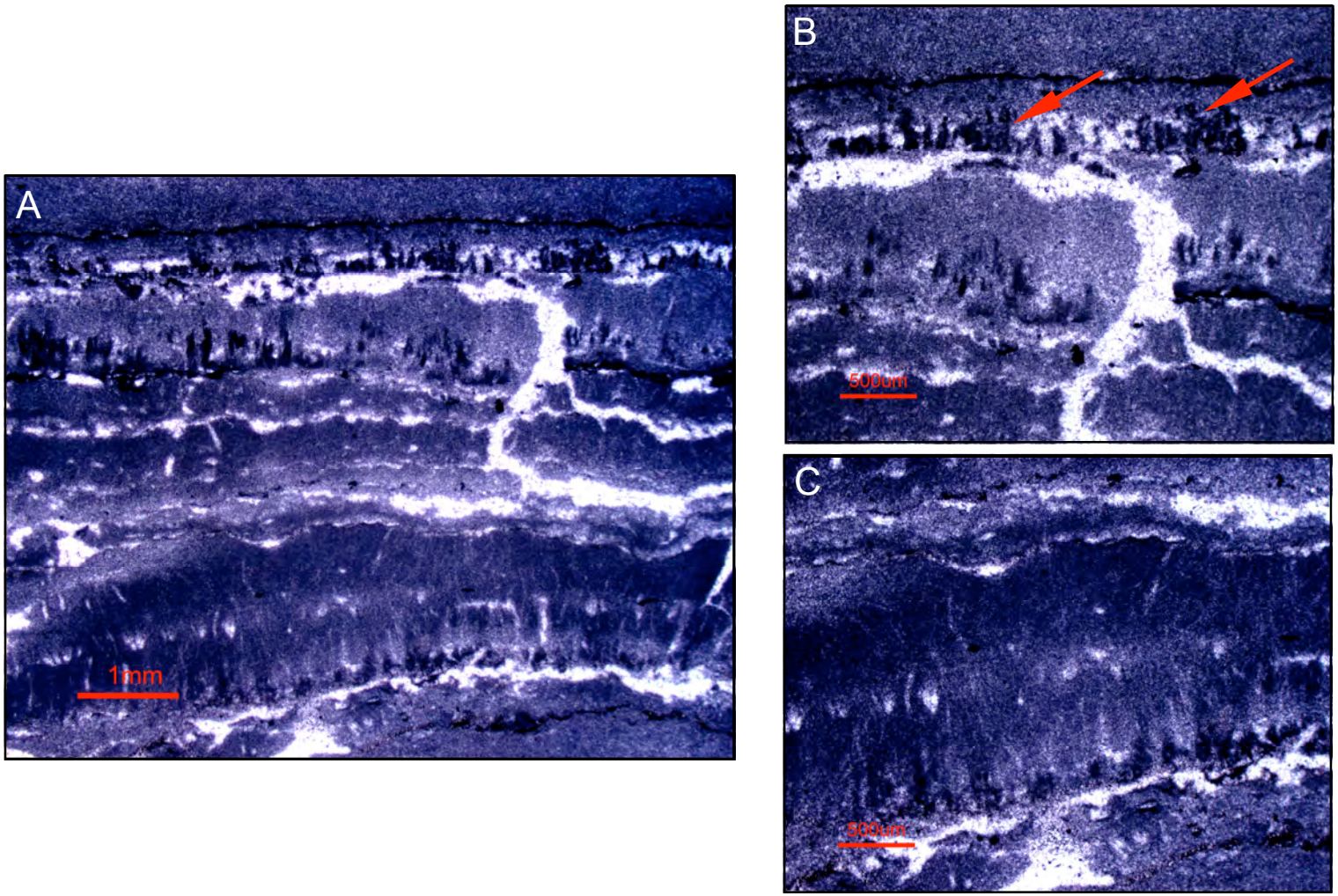

Figure 5.33. Photomicrographs of a microbial laminite from Forcella Averau. A. Field of view showing multiple micritic laminae with cement-filled micro sheet cracks as well as subvertical filaments within laminae. B. Close-up view of dark, stubby columnar tubes, likely *Microtubus communis* (Flugel, 1981; Cozzi, 2002). Note that filaments extend upwards from the base of micritic lamina, suggesting that they are not mud crack infill. Filaments may be the result of the upward growth of microbial mat that have acted as sediment baffles or binding agents. C. Close-up view of thin, whispy, cement/spar-replaced subvertical filaments within micritic lamina. Subvertical "palisade" fabric of microbial filaments is common in tidal flats with low sedimentation rates, where microbes have time to grow upwards through sedimentary laminae subsequent to deposition of sediment (Hardie, 1977).

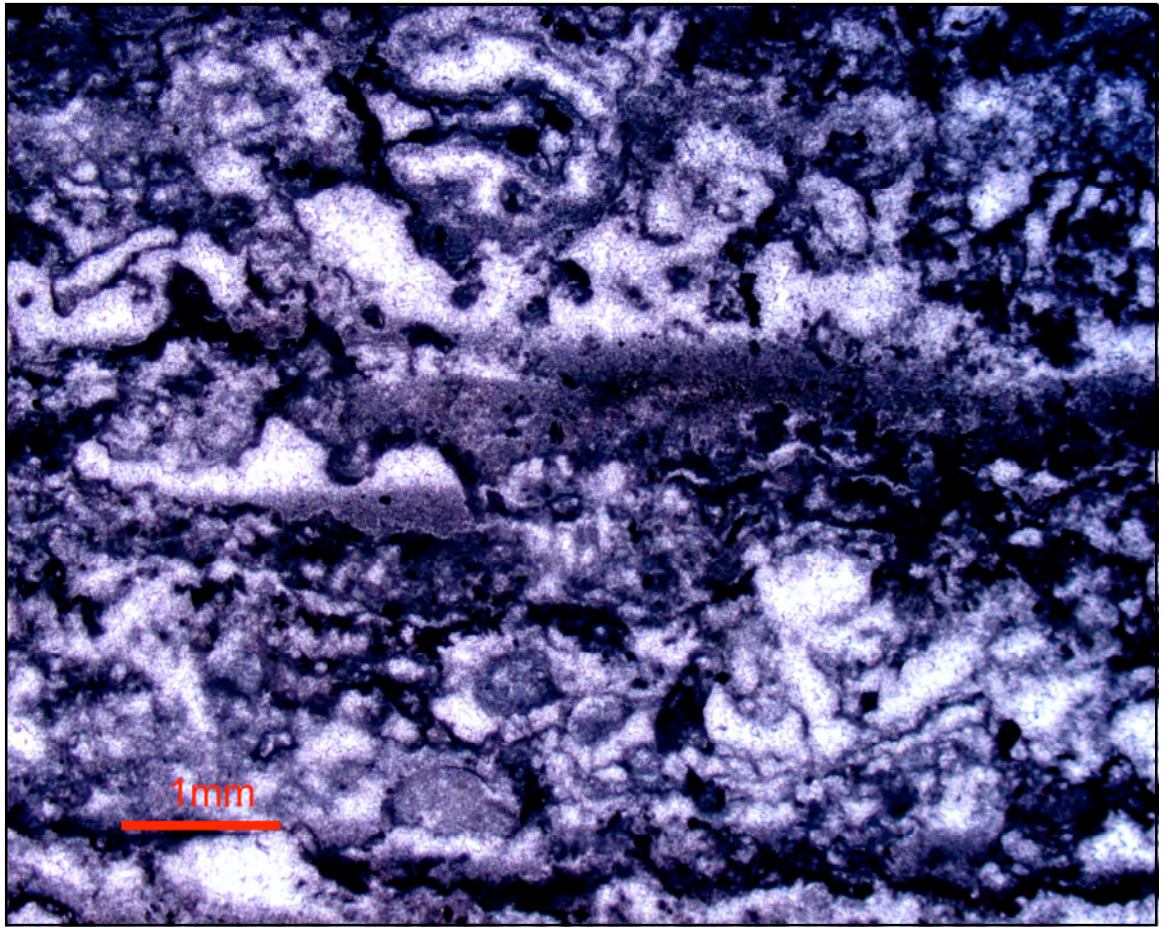

Figure 5.34. Photomicrograph of a laminite from the Pelmo. By comparison, this laminite is far more clotted in appearance than the palisaide-type laminites (e.g. example from Forc. Averau). This may reflect a faster rate of deposition, whereby microbial filaments did not have time to grow upwards through sedimentary laminae before the next deposit occurred. Also note fenestral spaces, now filled with geopetal micrite and secondary cement. The presence of geopetal micrite suggests that the fenestrae were open during micrite deposition, which is possible evidence for early dissolution during exposure in the vadose zone. Fenestrae were subsequently cement-filled such that they were not eliminated by compaction.

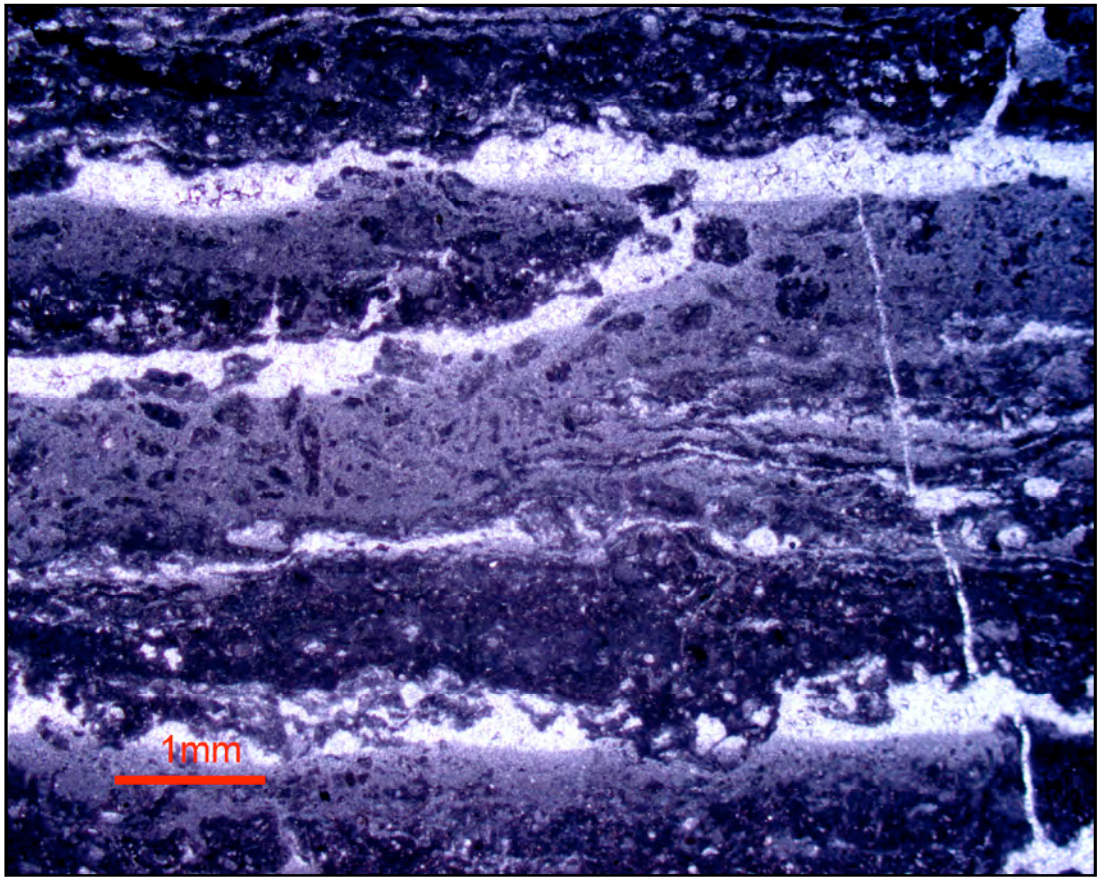

Figure 5.35. Photomicrograph of laminite from Tofana di Rozes. Note brecciated appearance to this laminite suggesting vadose microerosion/solution and refill as a source for geopetal fill. Also note whispy subhorizontal clots of dark micrite within laminae, possibly a former microbial sheet or crust. Sheet cracks are also present, but may represent secondary cement fill of fenestrae already partially filled by geopetal sediment, as geopetals many times form bases of sheet cracks.

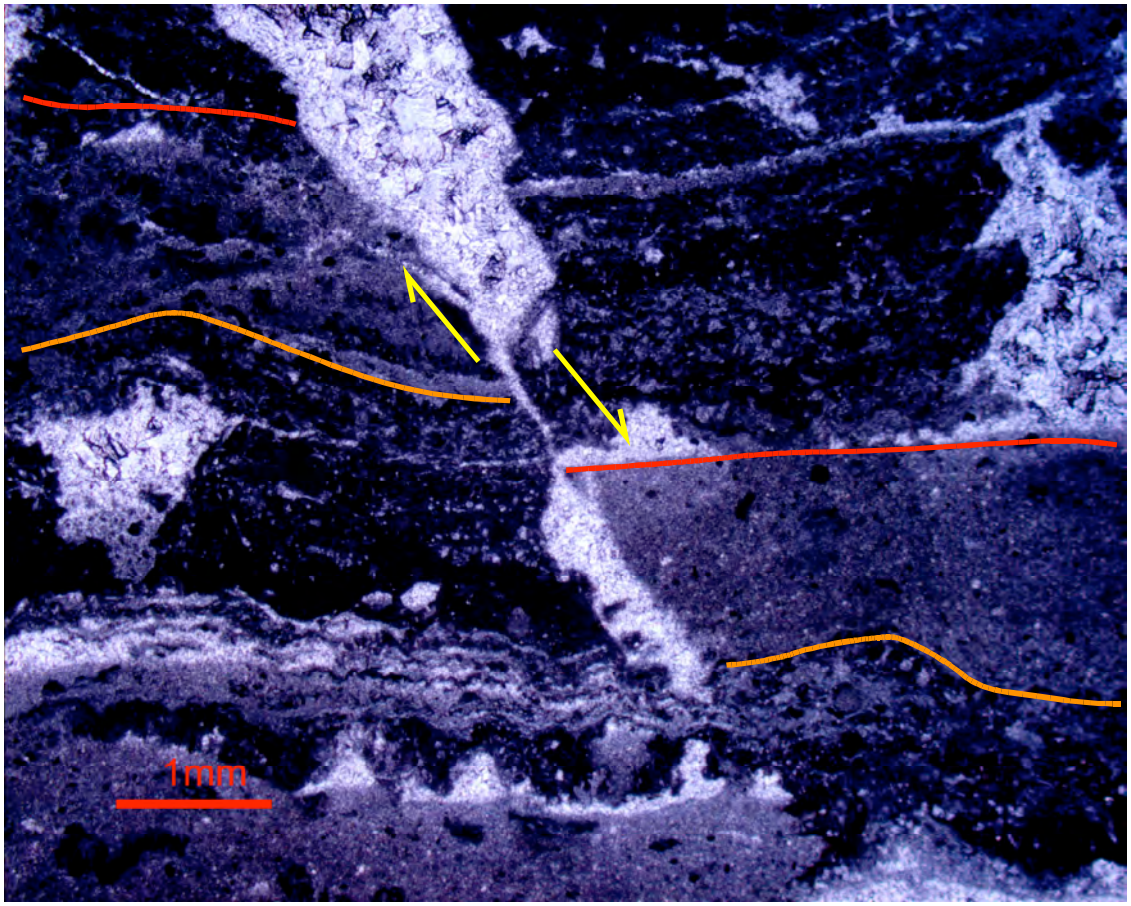

Figure 5.36. Photomicrograph of a fractured laminite from Tofana di Roces (Sample Fan 28iii). Note both micritic (sedimentary) and clotted (organo-sedimentary) laminae, as well as geopetal fill of fenestral pores and subsequent fill by later cement. Note that laminae are cross-cut by a fracture that displaces laminae 3-5 mm to the lower right. Possible micro-scale indicator of early extension.

Layer type	Subenvironment (s)	Exposure Index
I. **Thin lamination**		
A. smooth domal lamination	channel bank	40–90%
B. smooth flat lamination	levee crest, beach terrace, beach ridge washover crest, intertidal channel bar crest	98–99.7%
C. disrupted flat lamination	levee backslope, beach ridge washover backslope	91–98%
D. crinkled fenestral lamination	high algal marsh, inland algal marsh	80–91% (up to 99 in inland marsh)
E. wavy fenestral lamination	high algal marsh-levee backslope boundary, beach terrace	85–95%
F. lamination with "palisade" structure	high algal marsh-levee backslope boundary, inland algal marsh	85–95% (up to 99 in inland marsh)
II. **Thin bedding and thick lamination**		
A. algal tufa-peloidal mud interbeds	inland algal marsh	approx. 70–99%
B. disrupted fenestral bedding	low algal marsh	60–80%
C. flat-pebble gravel	beach ridge washover crest, low algal marsh, inland algal marsh, channel floor, beach	approx. 70–99% (0–5% in channels)
D. round-pebble gravel	beach, channel floor	0–approx. 45%
III. **Thin to thick cross-bedding**		
A. rippled skeletal sands	channel floor	0–5%
B. festooned skeletal sands	beach ridge hummocks	98–99.9%
IV. **Thick to very thick bedding**		
A. bioturbated peloidal mud	pond, subtidal channel bars, beach, offshore	0–60%

From Hardie, 1977

Figure 5.37. Types of layering in the Three Creeks tidal flat sediments

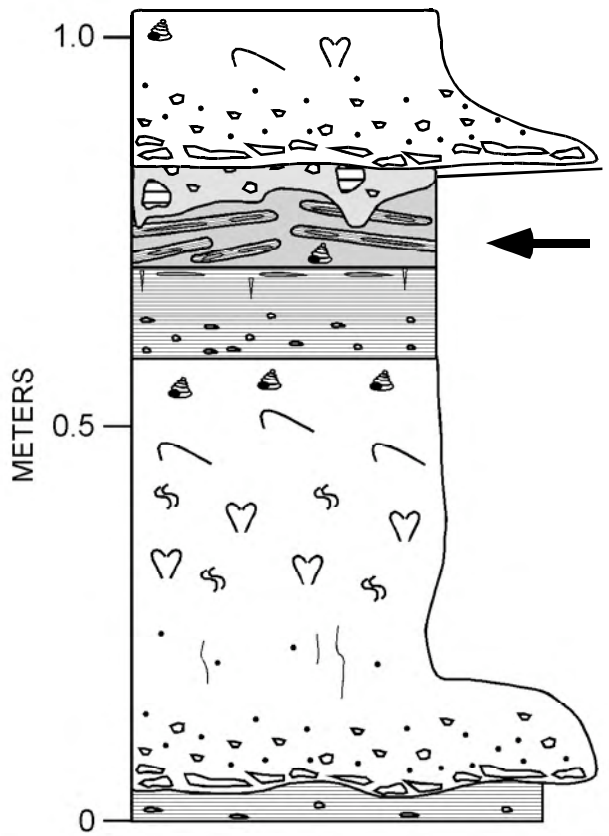

Figure 5.38. Facies 5, diagenetic cap consisting of sheet cracked and/or tepee-ized laminite. Precipitation of aragonite and/or high-Mg calcite cements within voids leads to the development of sheet cracks and eventually to antiformal tepee structures and exposure breccias. Some examples consist of over fifty percent early cement phases relative to displaced mother rock. Facies may show red 'terra rossa' staining typical of Fe oxidation during subareal exposure. Red silt, possibly aolian, is also common. Pisoids were not found in DP exposure caps.

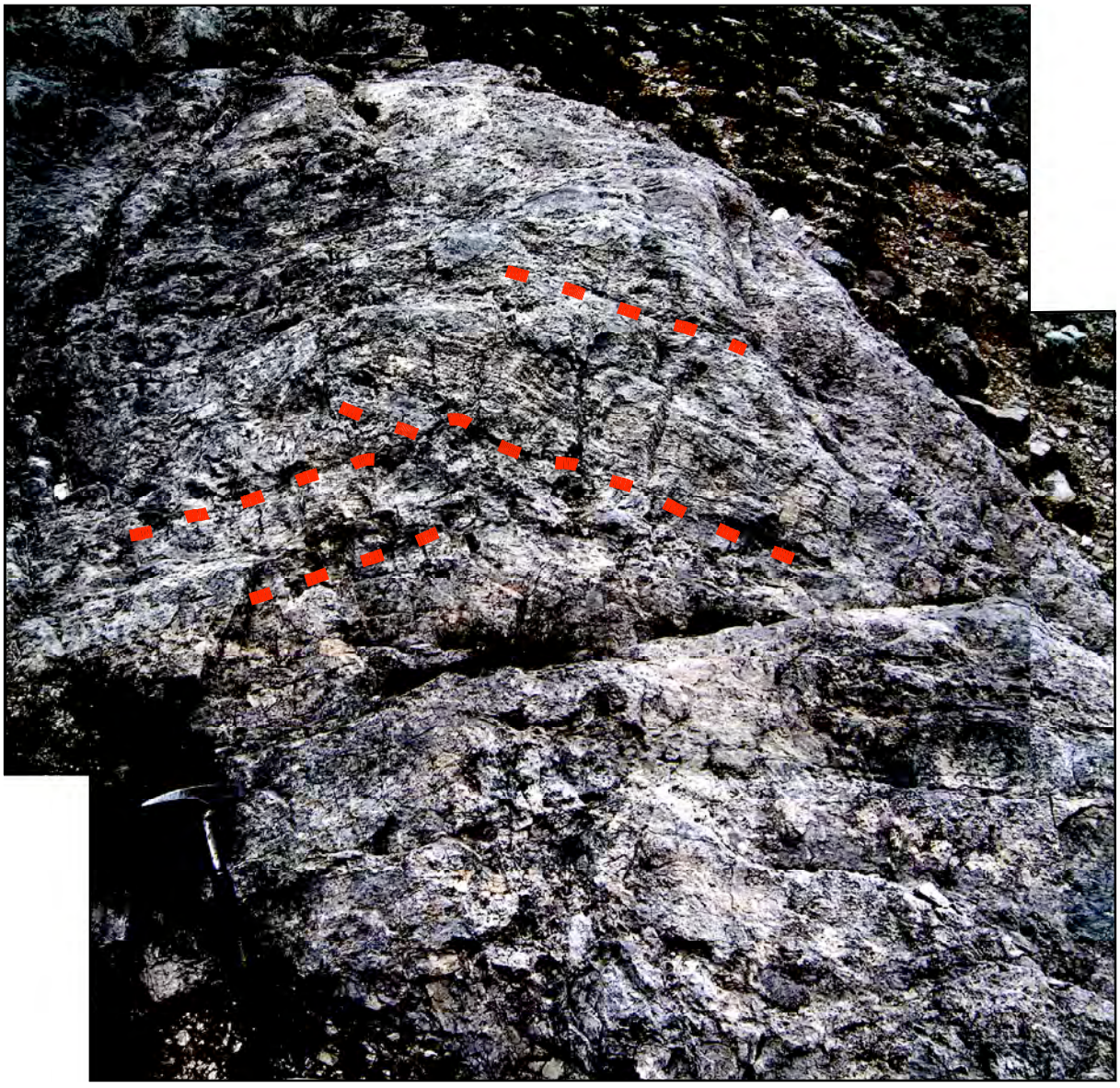

Figure 5.39. Photograph of broken, upturned laminite blocks within a tepee zone. Much of the now-filled void space is oriented parallel to lamination, suggesting origin as inter-lamellar sheet cracks. This example from Monte Cristallo.

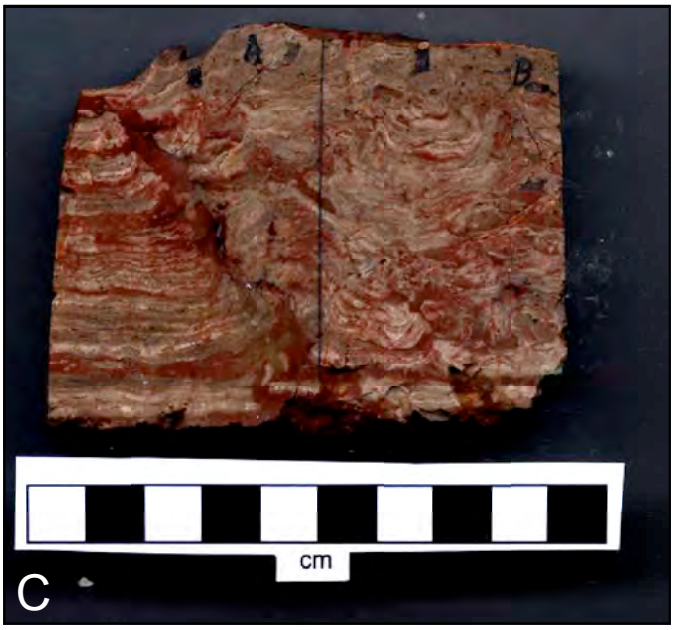

Figure 5.40. Hand specimens of DP tepee facies from: A Monte Cristallo (Crs 23B); B. Tofana di Rozes (Fan 32C); and C. Forcella Averau (AvCS 1A). All specimens show disruption of formerly flat cryptomicrobial laminae via fracture and infill of cement and red “terra rosa” sediments. While other features, such as pisoids, were not found in DP tepees, fracturing and infill by expansive aragonite cements, and the presence of red oxidized sediments over supratidal laminites indicate that these are features consistent with early marine/vadose diagenesis.

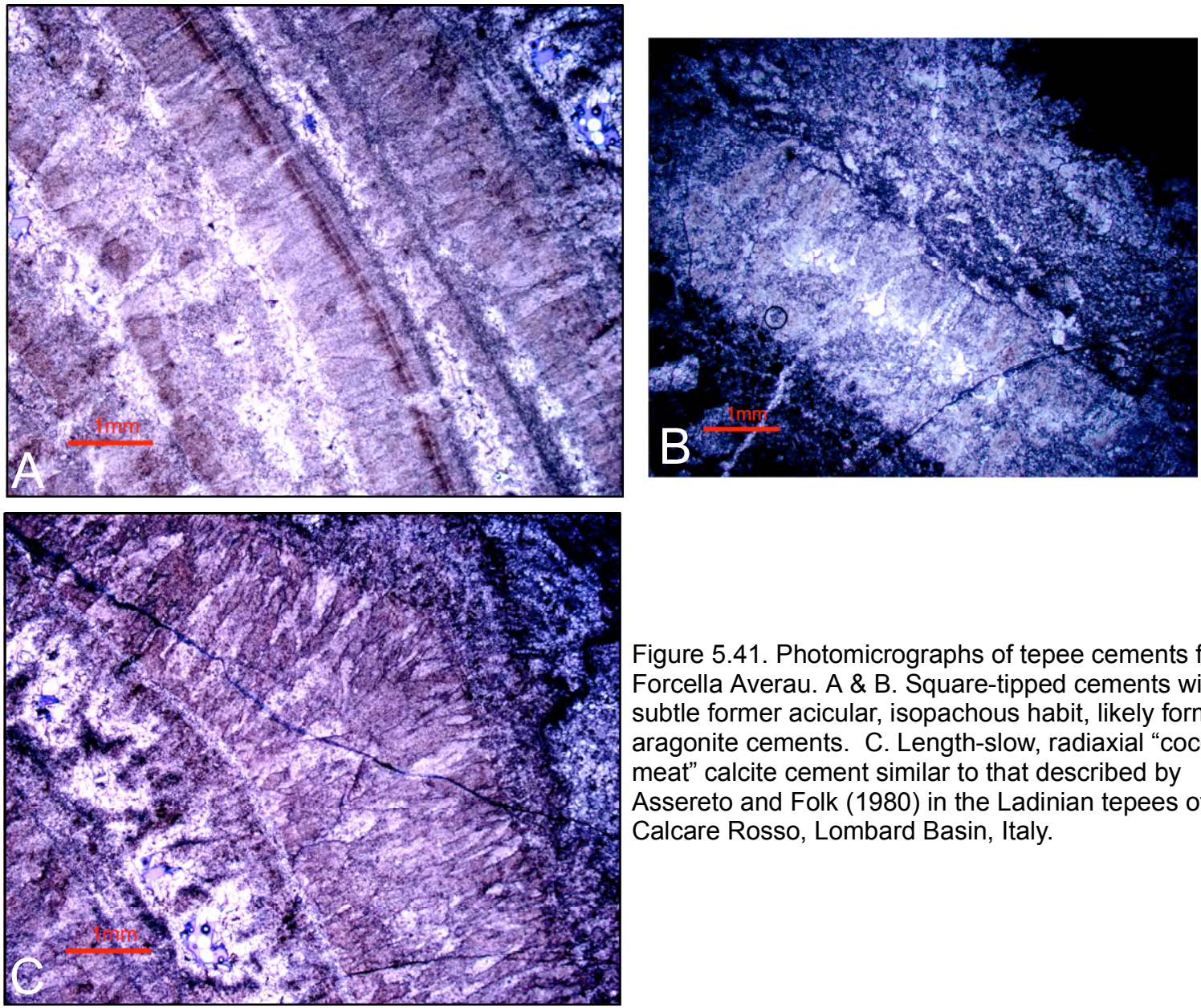

Figure 5.41. Photomicrographs of tepee cements from Forcella Averau. A & B. Square-tipped cements with subtle former acicular, isopachous habit, likely former aragonite cements. C. Length-slow, radiaxial "coconut meat" calcite cement similar to that described by Assereto and Folk (1980) in the Ladinian tepees of the Calcare Rosso, Lombard Basin, Italy.

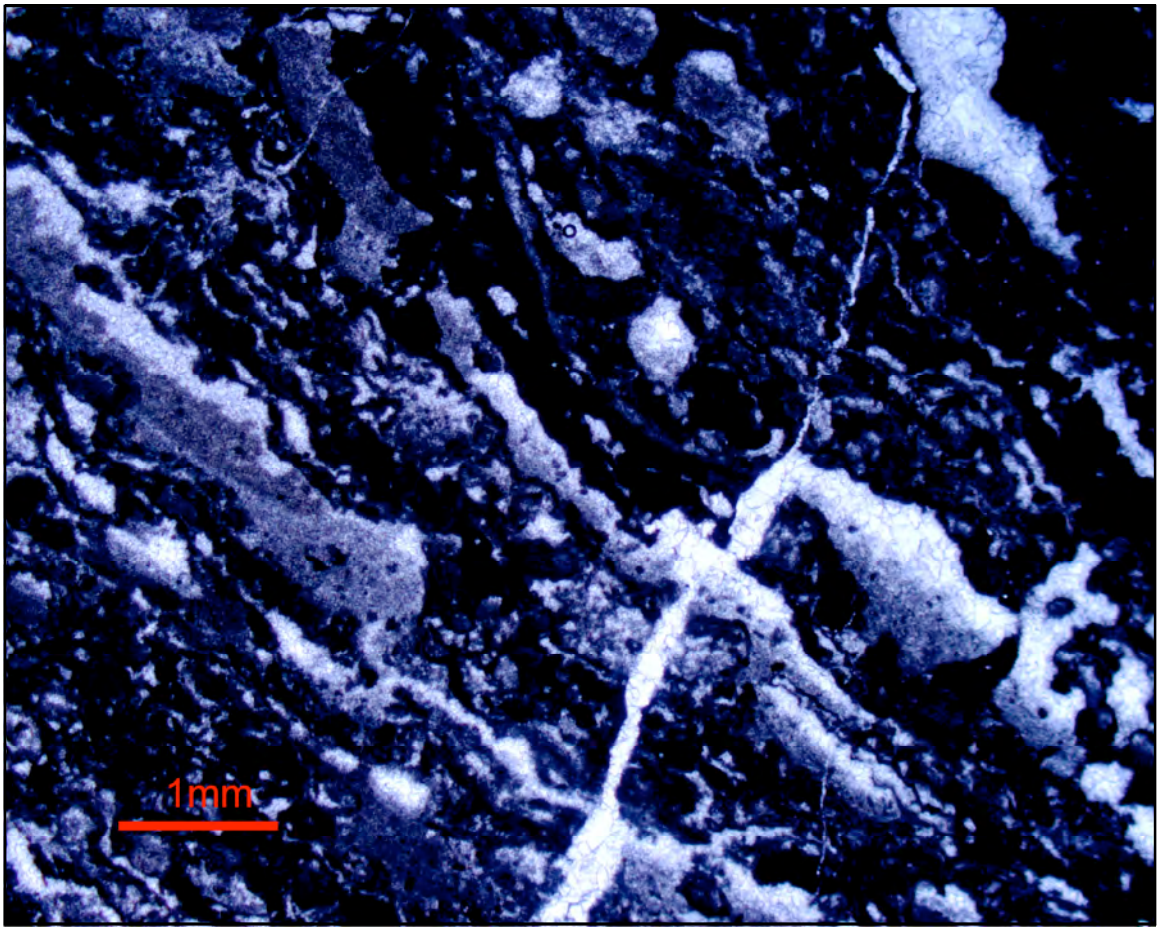

Figure 5.42. Photomicrograph of cycle-capping tepee structure from Monte Cristallo (Crs 23B). In this sample, up is stratigraphic up. Tilting of laminar fabric is the result of expansive cementation. Note tilted geopetals, suggesting a history of 1. fenestrae formation related to decomposition of microbial material; 2. Partial infill of fenestrae by micrite; 3. Cement fill of fenestrae; 4. Expansive cementation, bucking and tilting of tepee.

Figure 5.43. “Juvenile” tepees near Deep lake, South Australia. Tepees define the edges of large polygons several meters in diameter. Photograph courtesy of Dr. Chris Kendall, The University of South Carolina.

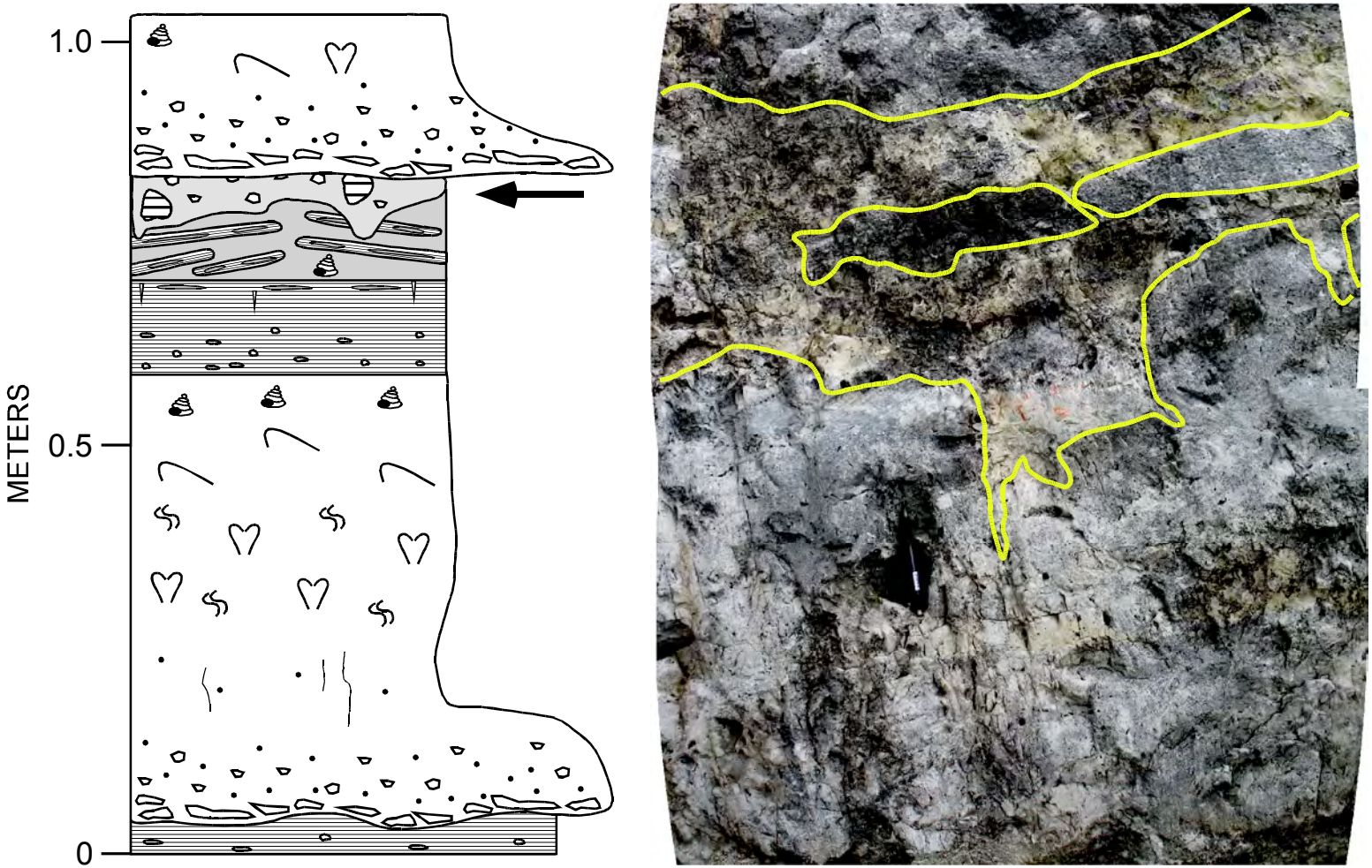

Figure 5.44. Facies 6, karstic breccia/paleosol in depositional context as a cycle cap. The term "karstic" is interpretive, but reflects the likely exposure-related formation of the facies without implying true pedogenesis. Boundaries of breccia beds are nearly always irregular, with silty dolomitic sediment penetrating several 10s of centimeters into underlying beds. The breccia itself typically consists of bright yellow dolomitic silt and blocks of microbial laminite from the underlying bed.

Figure 5.45. An excellent example of a yellow dolomitic “karst breccia” capping a depositional cycle at Forcella Averau. Note the irregularity of the basal and upper contacts of the bed. Basal irregularity likely the result of dissolution and fill of dissolved spaces by breccia and silty sediments. Upper contact irregularity likely caused by truncation of bed during transgression.

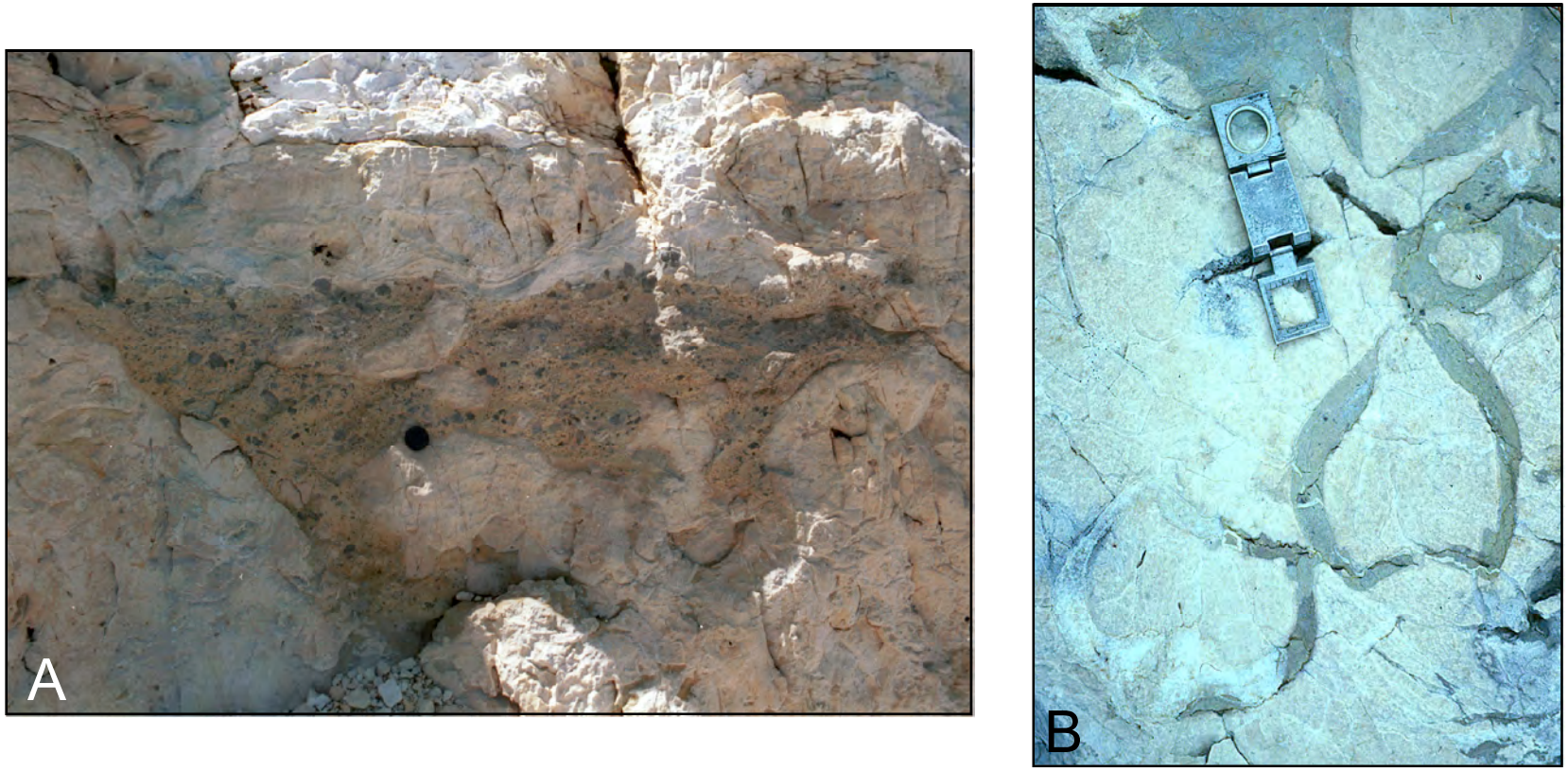

Figure 5.46. “Karst” breccia commonly occurs as a fill sediment in dissolution voids. A. Yellowish-green marly sediment differentially filling a dissolution void in a microbial laminite. B. Green marly sediment and cements filling dissolved megalodont molds. Both photographs courtesy of Andrea Cozzi, ETH Zurich.

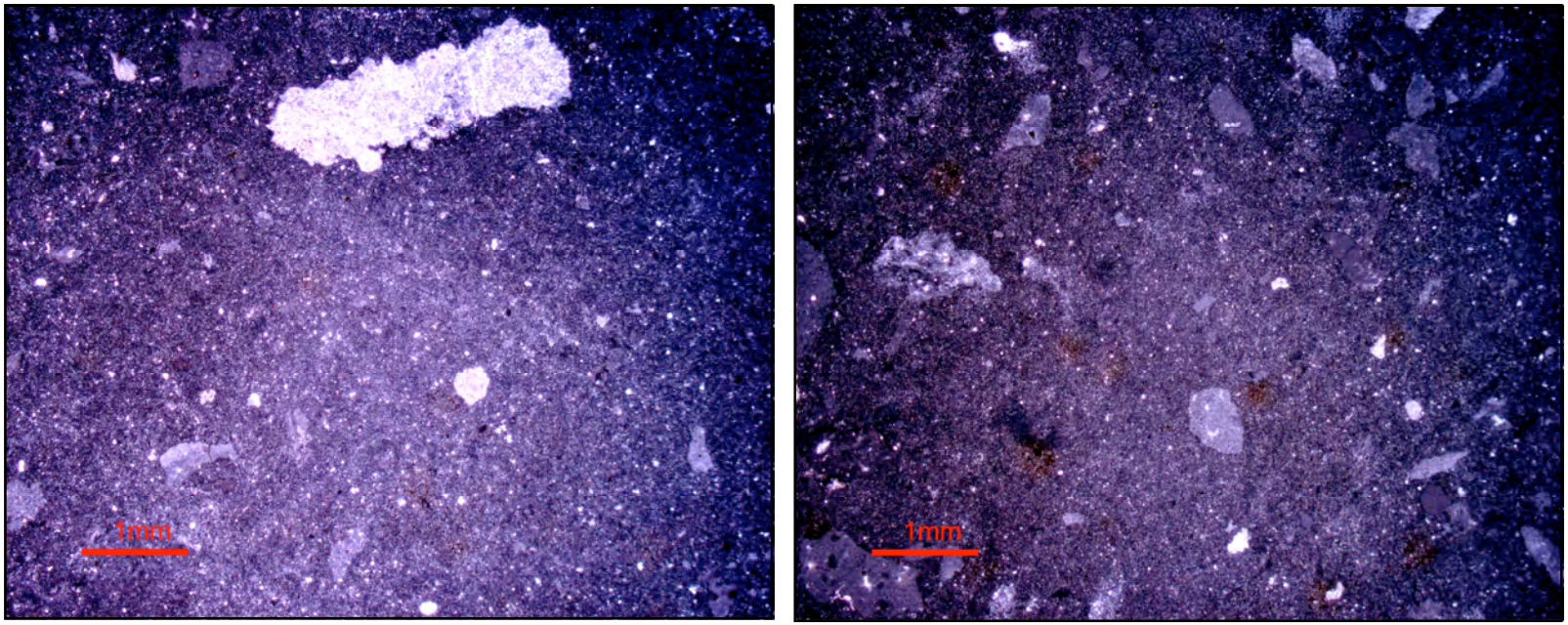

Figure 5.47. Photomicrographs of bright yellow dolomitic “soil” from the Sella (Sel19B). This sample forms a bright yellow layer atop a microbial laminite in outcrop, and has void-filling “solution pipes” extending into the underlying succession ca. 20 cm. In thin section, the sample is recognized as a dolomicritic micro-breccia or a mud-dominated dolo-wackestone. No true sepic fabric can be identified, nor plant root traces or any other evidence that the material formed as the result of pedogenic processes. The sediment is either the product of dissolution and re-sedimentation or soil-forming processes.

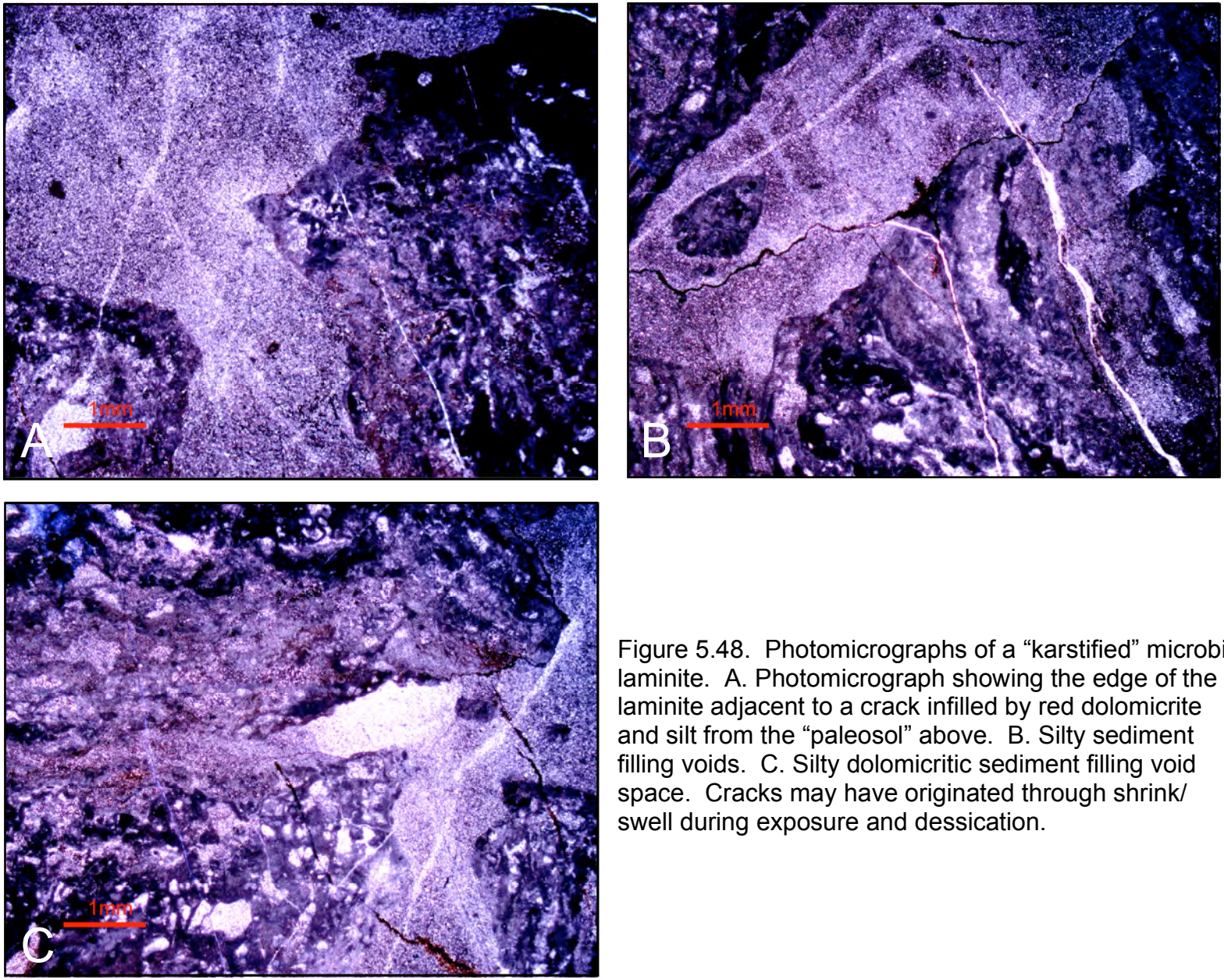

Figure 5.48. Photomicrographs of a “karstified” microbial laminite. A. Photomicrograph showing the edge of the laminite adjacent to a crack infilled by red dolomicrite and silt from the “paleosol” above. B. Silty sediment filling voids. C. Silty dolomicritic sediment filling void space. Cracks may have originated through shrink/ swell during exposure and dessication.

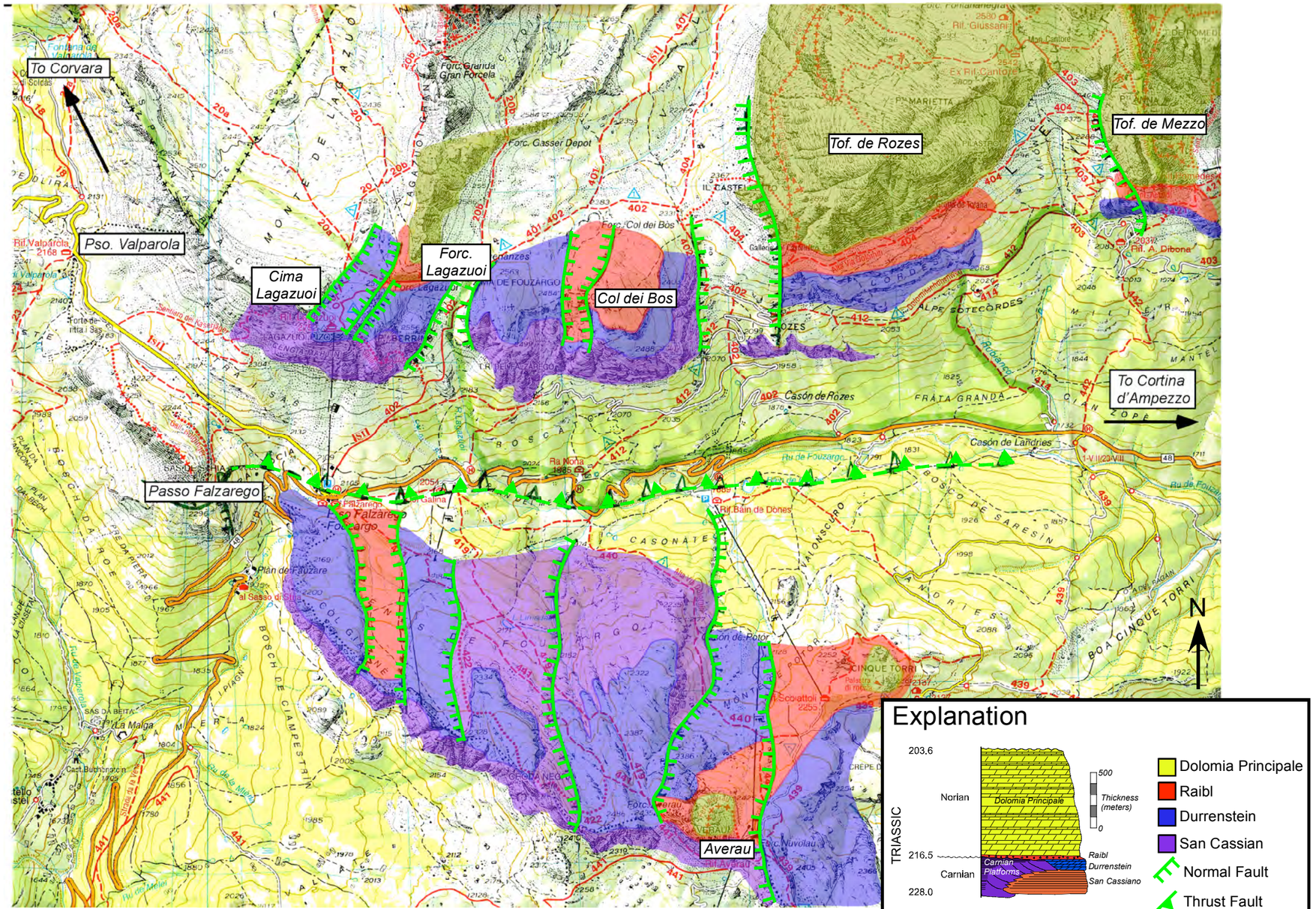

Figure 5.49. Geologic and structure map of investigated localities in the Passo Falzarego area. Note general NS strike of normal faults. Map is is a 1:25,000 topographic hiking map made by the Tabacco company, Map number 03, Cortina d'Ampezzo e Dolomiti Ampezzane. Computer drafting done directly on top of field map for accuracy.

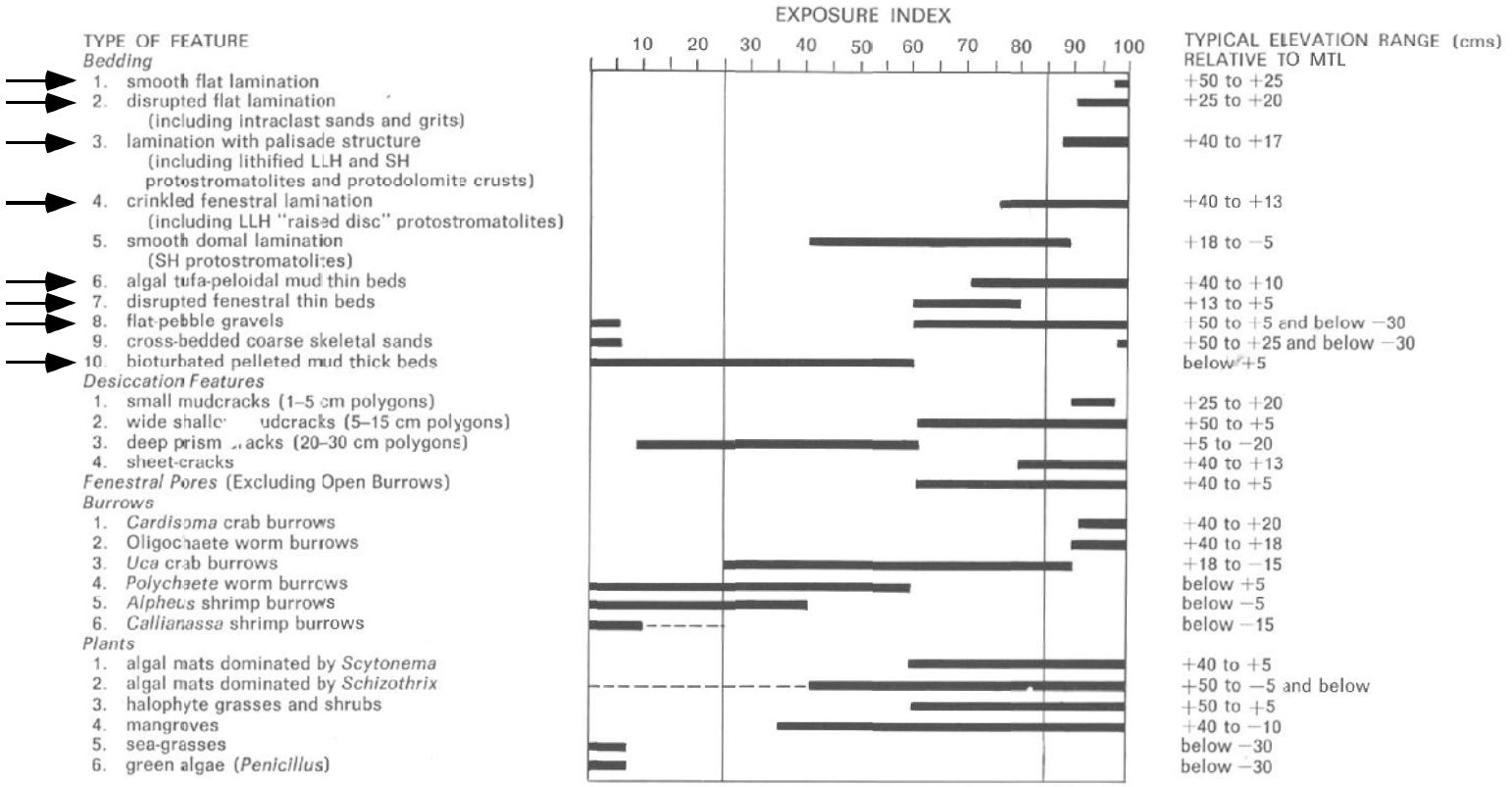

Figure 5.50. Exposure index (% of time exposed subaerially) for Holocene carbonate tidal flat deposits at the Three Creeks area, Andros Island, Bahamas relative to mean tide level (MTL). While facies in the DP can be generally arranged into shallowing-upwards successions, there is a measurable degree of overlap in exposure index between facies (see arrows pointing to like-facies in the DP cycles), which is important when attempting to establish Waltherian relationships between depositional facies. From Hardie (1977).

Locality	Thickness Series	Fischer Plot
Forc. Averau	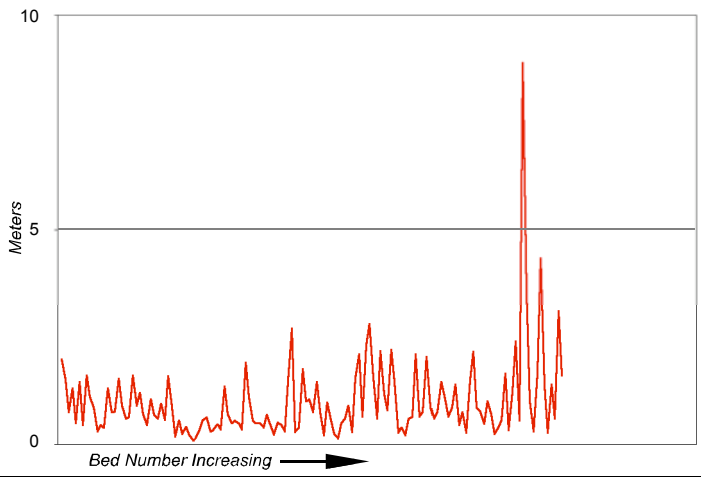	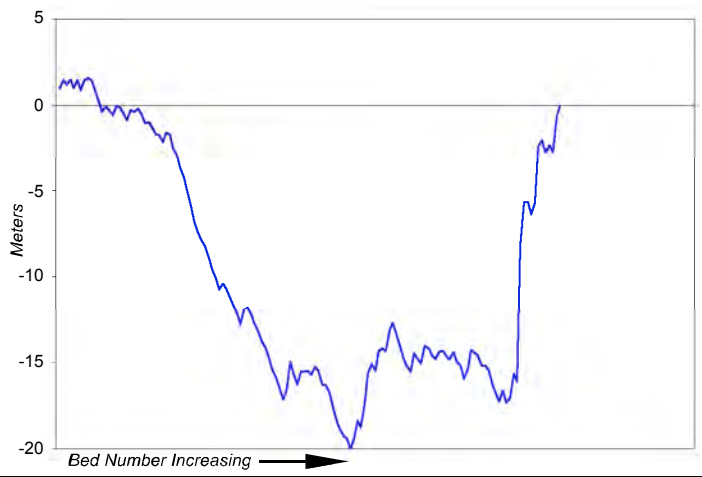
Tofana di Rozes	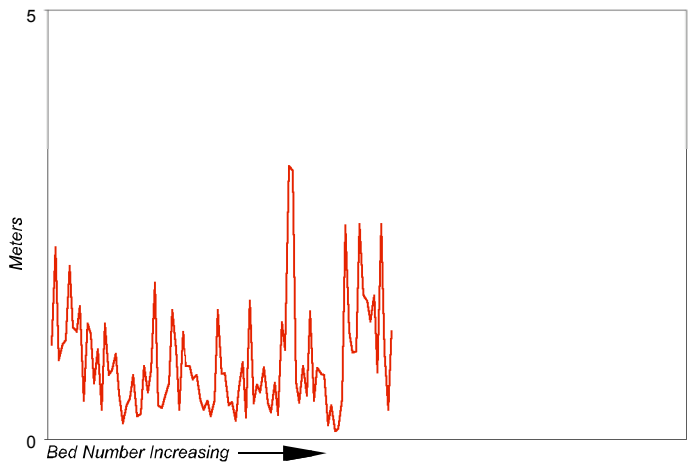	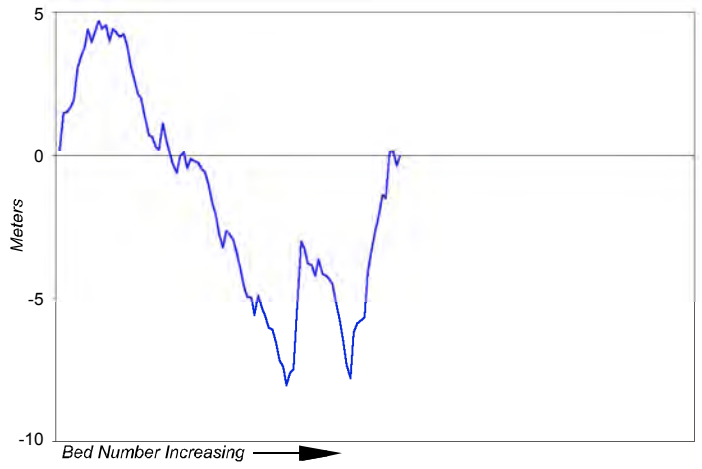
Tofana di Mezzo	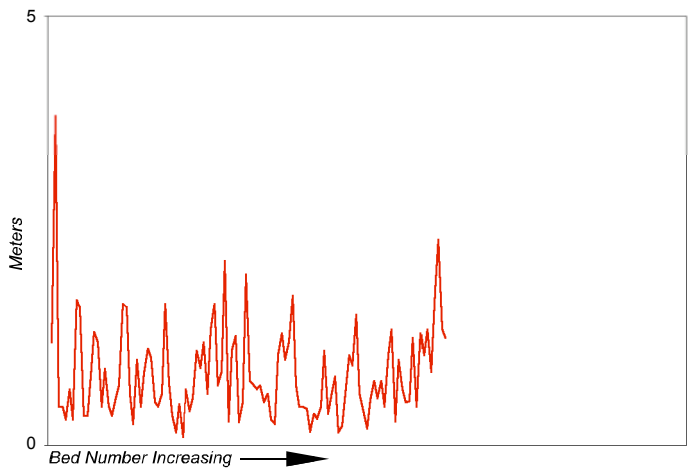	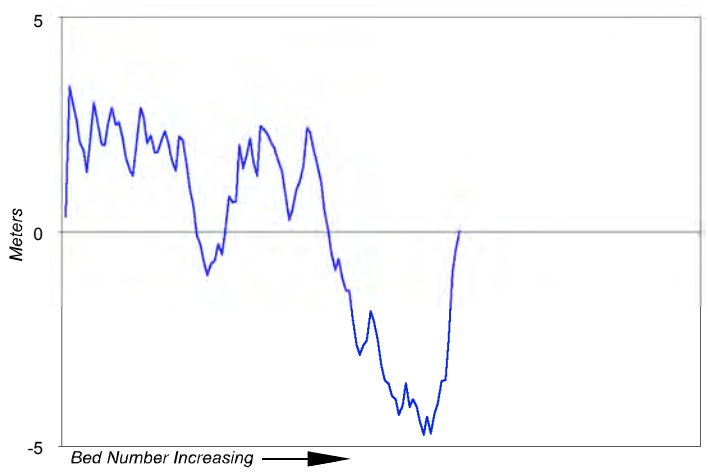
Pelmo	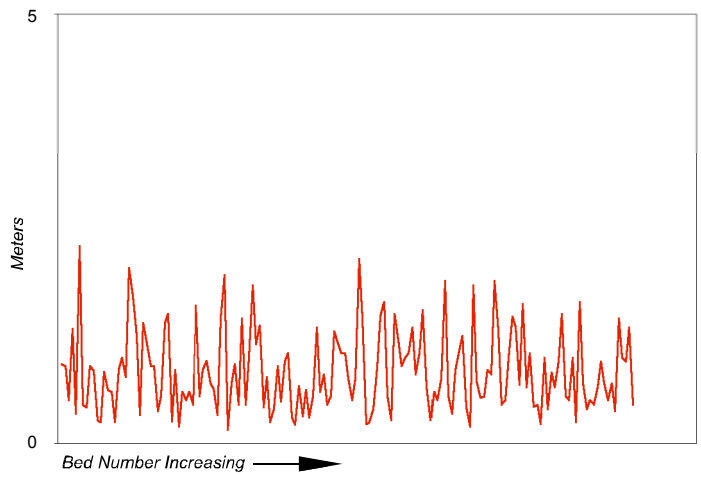	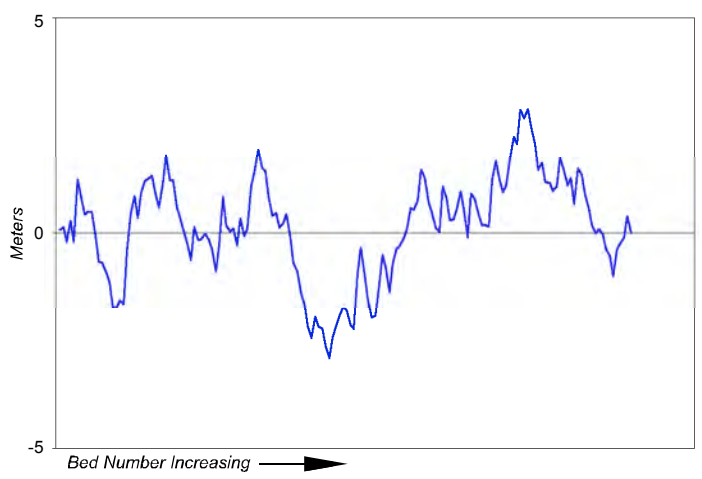
Cima Ovest	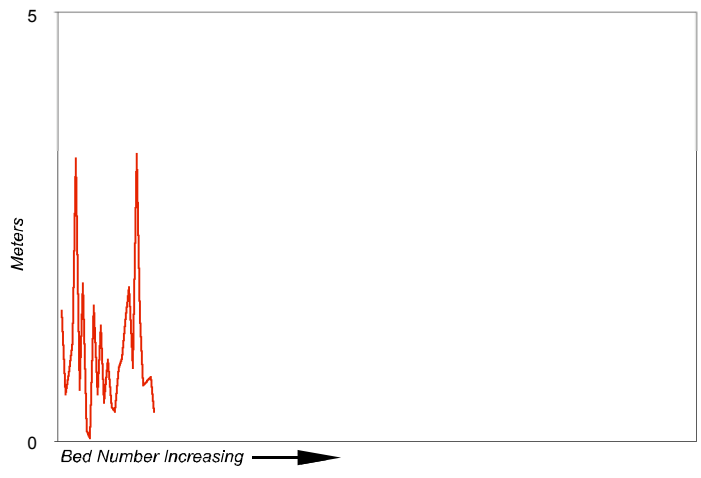	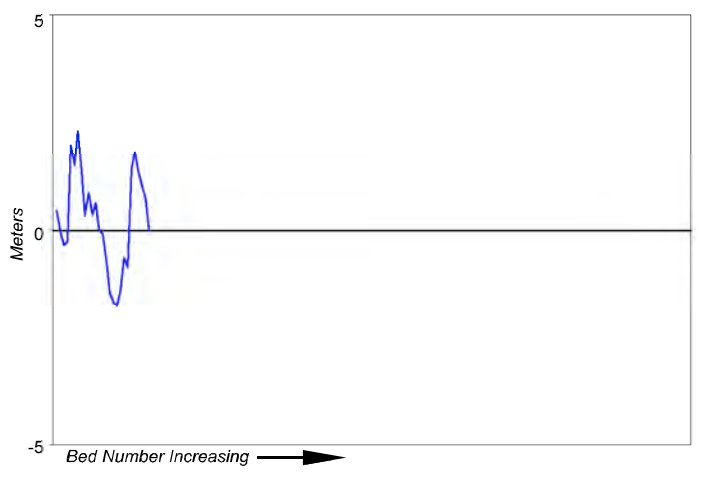

Figure 5.51. Thickness series plots for DP sections measured from the Raibl/DP lithostratigraphic contact. Trends in the thickness series are not consistent from locality to locality. Fischer plots serve to further illustrate these inconsistencies in cycle thickness trends from locality to locality.

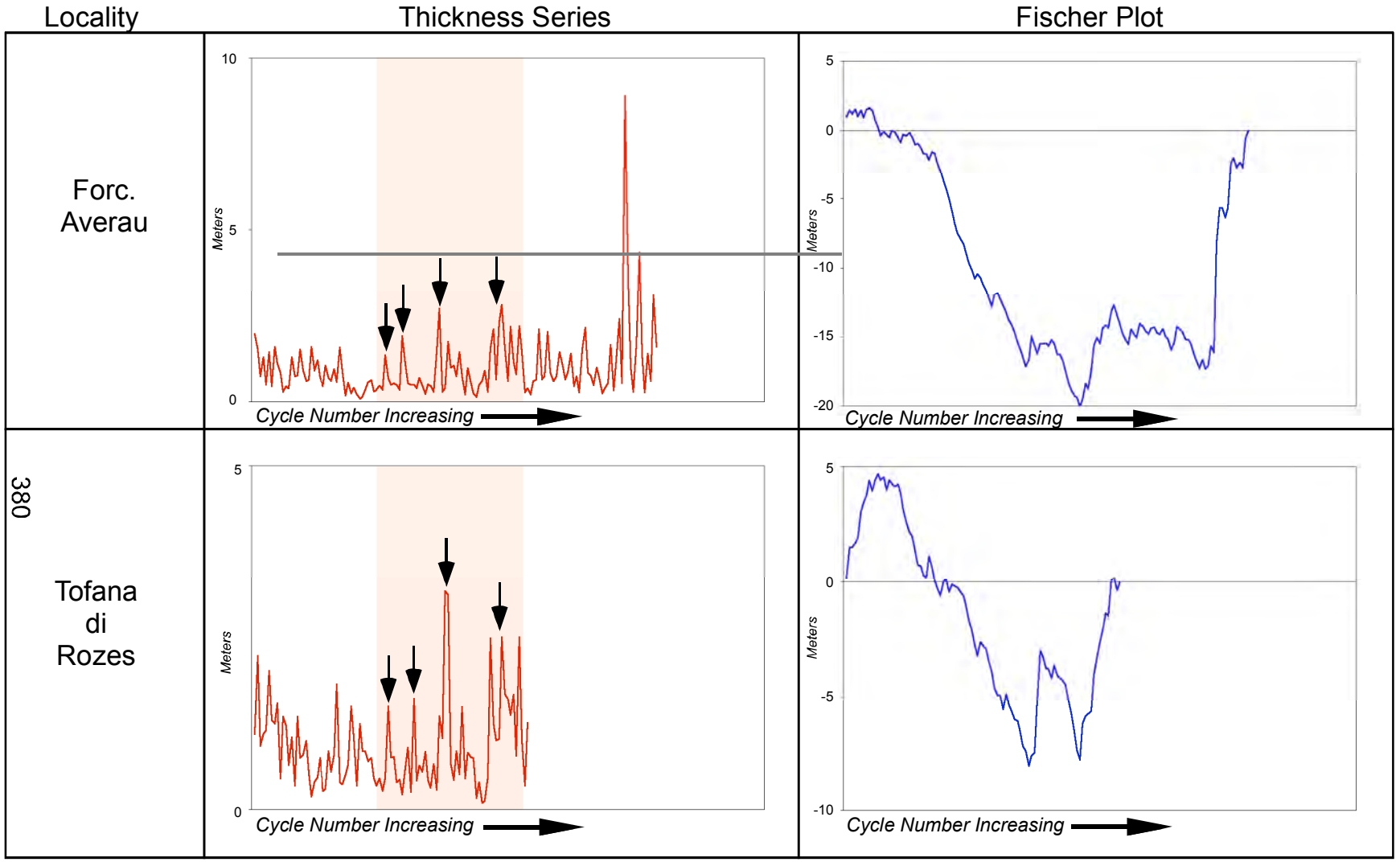

Figure 5.52. Similarities in the thickness series of sections at Forcella Averau and Tofana di Rozes. Similarities in the thickness series are highlighted by arrows. General cycle thinning-thickening similarities can also be noted in Fischer plots. It is possible that these sections underwent similar subsidence histories and may have been grounded on the same NS-striking block.

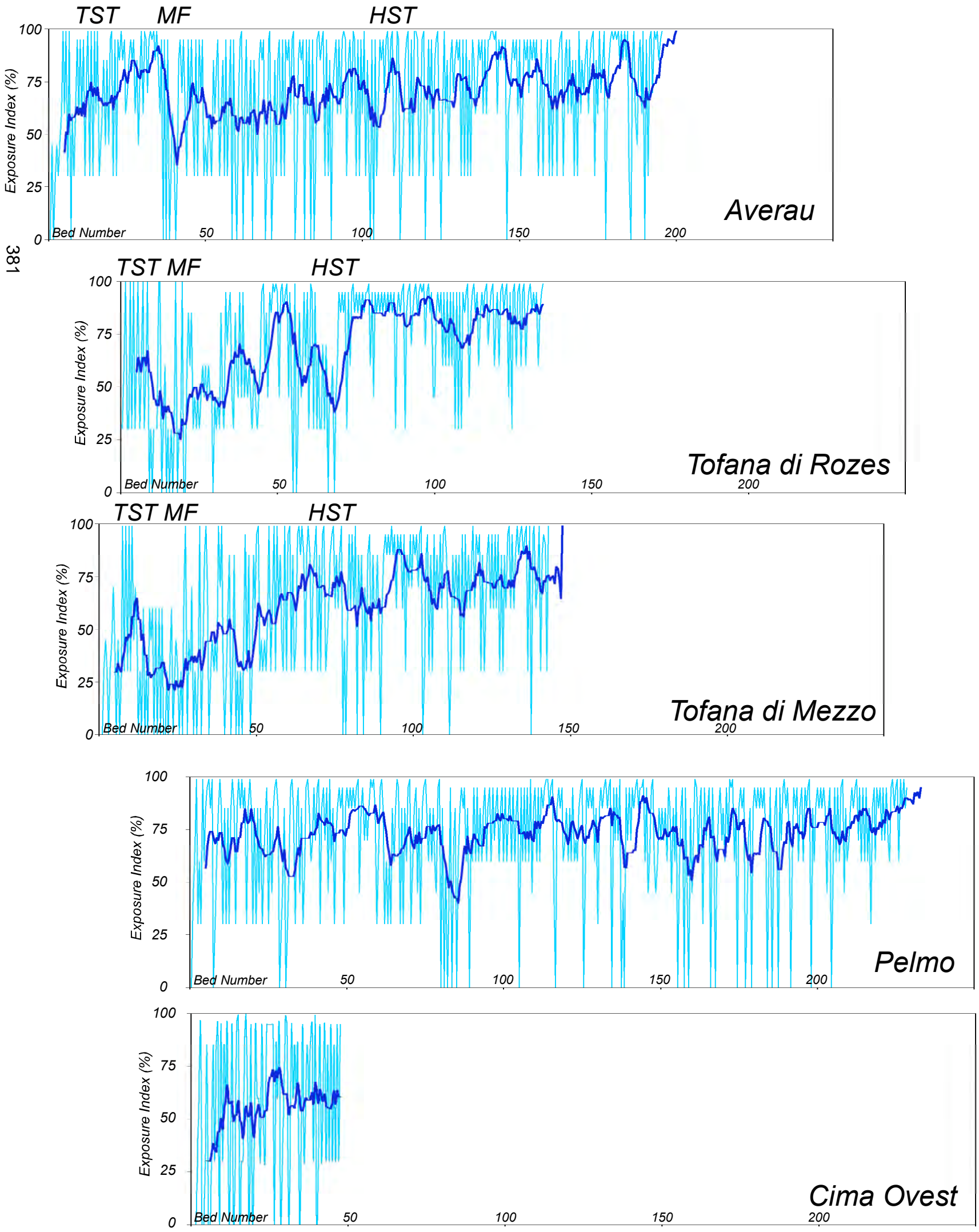

Figure 5.53. Exposure indices plotted for each section measured from the Raibl-DP contact. Plots are of exposure index vs. bed number. Thickness of beds is not included in these plots. Plots are shifted to apparent matches in peak values. Upper 3 plots contain interpretations relative to sequence stratigraphic framework. Lower beds in Falzarego sections are typically karst-brecciated above the Raibl-contact (TST) before becoming marine-dominated (MF) and subsequently becoming dominated by diagenetically-capped cycles (HST to SB). Sections further eastward (Pelmo and Cima Ovest) do not contain these same types of successions in their basal DP cycles, as the transition from marginal marine Raibl to open shallow marine DP carbonate may have been less gradational in a downdip location. Plots are a 10 point moving average of exposure index, reflecting the fact that exposure indices are ranges, not exact percentages. The moving averages serves to smooth short term (i.e., facies to facies) fluctuations and highlight longer term trends or cycles.

Dolomia Principale Exposure Index Plots

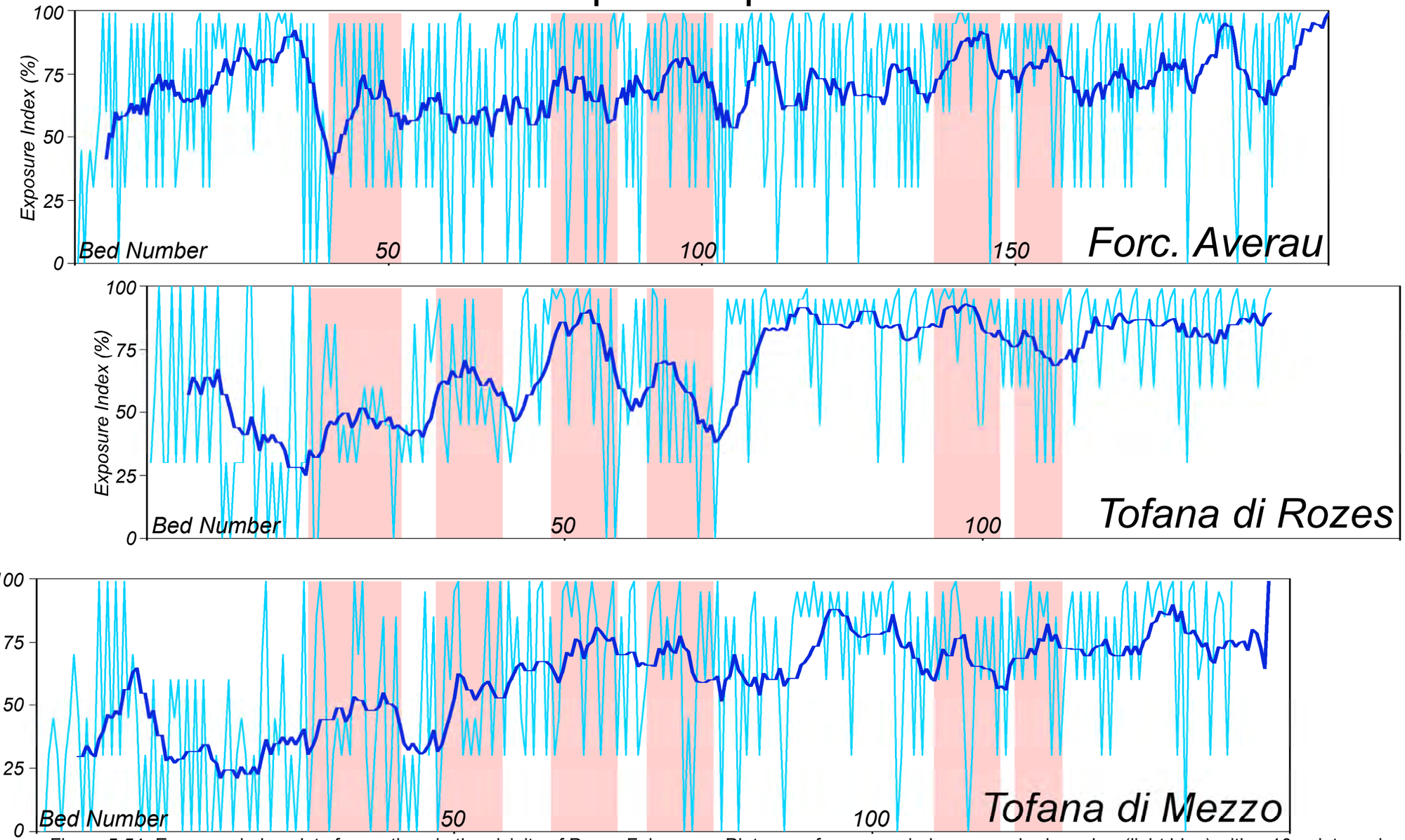

Figure 5.54. Exposure index plots for sections in the vicinity of Passo Falzarego. Plots are of exposure index versus bed number (light blue) with a 10 point moving average applied (dark blue) as exposure indices are actually ranges rather than actual values, with a average of the curves being a more accurate representation of the true evolution of indices than points. Similar trends in exposure indices between sections are highlighted.

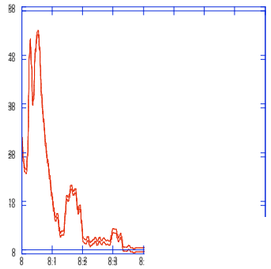

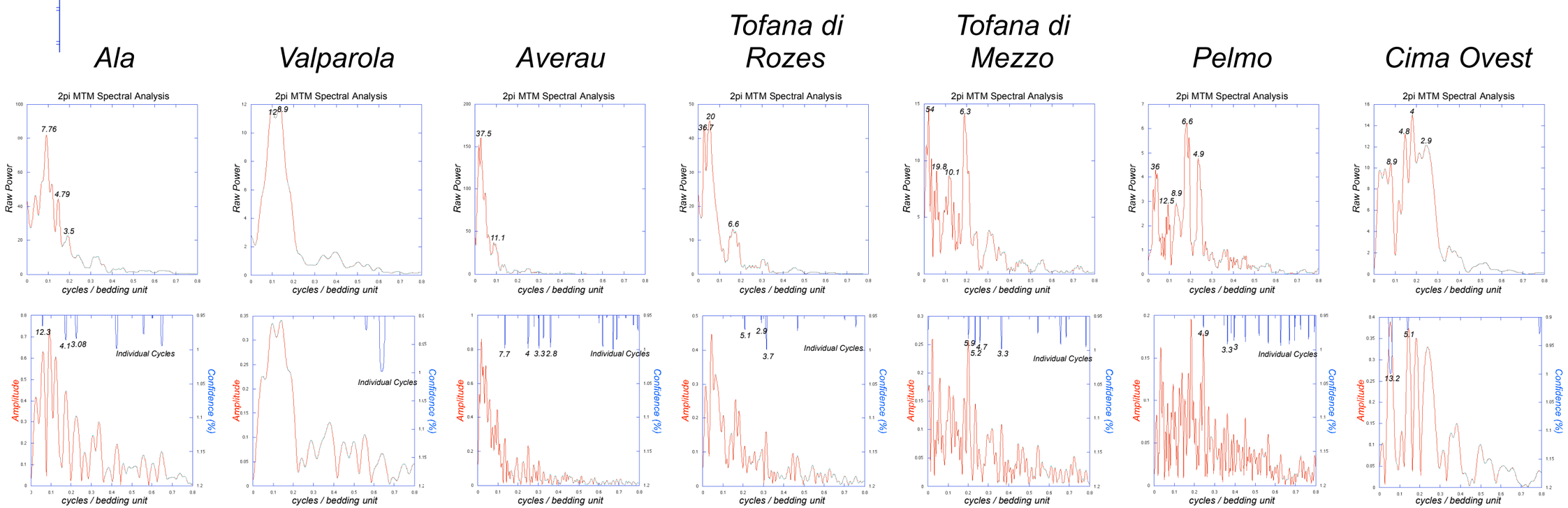

Figure 5.55. Resulting spectra from frequency analysis of Dolomia Principale measured section thickness series. Upper plots is raw power versus frequency, lower plots are amplitude versus frequency, with confidence (F-test) graphed on a secondary y-axis. The upper row of plots record the variance (power) over a preset band of frequencies at every resolvable frequency. The lower row of plots record the mean fitted sinusoid amplitude of every resolvable frequency. AnalySeries v. 1.2 and KaleidaGraph software packages were used in construction of plots.

Of note in the plots is the increasing number of cycles within megacycle bundles from east to west. In this study, cycles are bundled as follows:

Ala: Avg. Cycle Thickness = 1.43 m; cycle bundles of 3-4 cycles per megacycle in TP zones

Forcella Averau: Avg. Cycle Thickness = 1.0 m; cycle bundles of 3-4 and 7 cycles per megacycle

Tofana di Rozes: Avg. Cycle Thickness = 0.94 m; cycle bundles of 3-5 cycles per megacycle

Tofana di Mezzo: Avg. Cycle Thickness = 0.84 m; cycle bundles of 3-6 cycles per megacycle

Pelmo: Avg. Cycle Thickness = 0.84 m; bundles of 3-6 cycles per megacycle

Cima Ovest: Avg. Cycle Thickness = 1.4 m; bundles of 5 cycles per megacycle

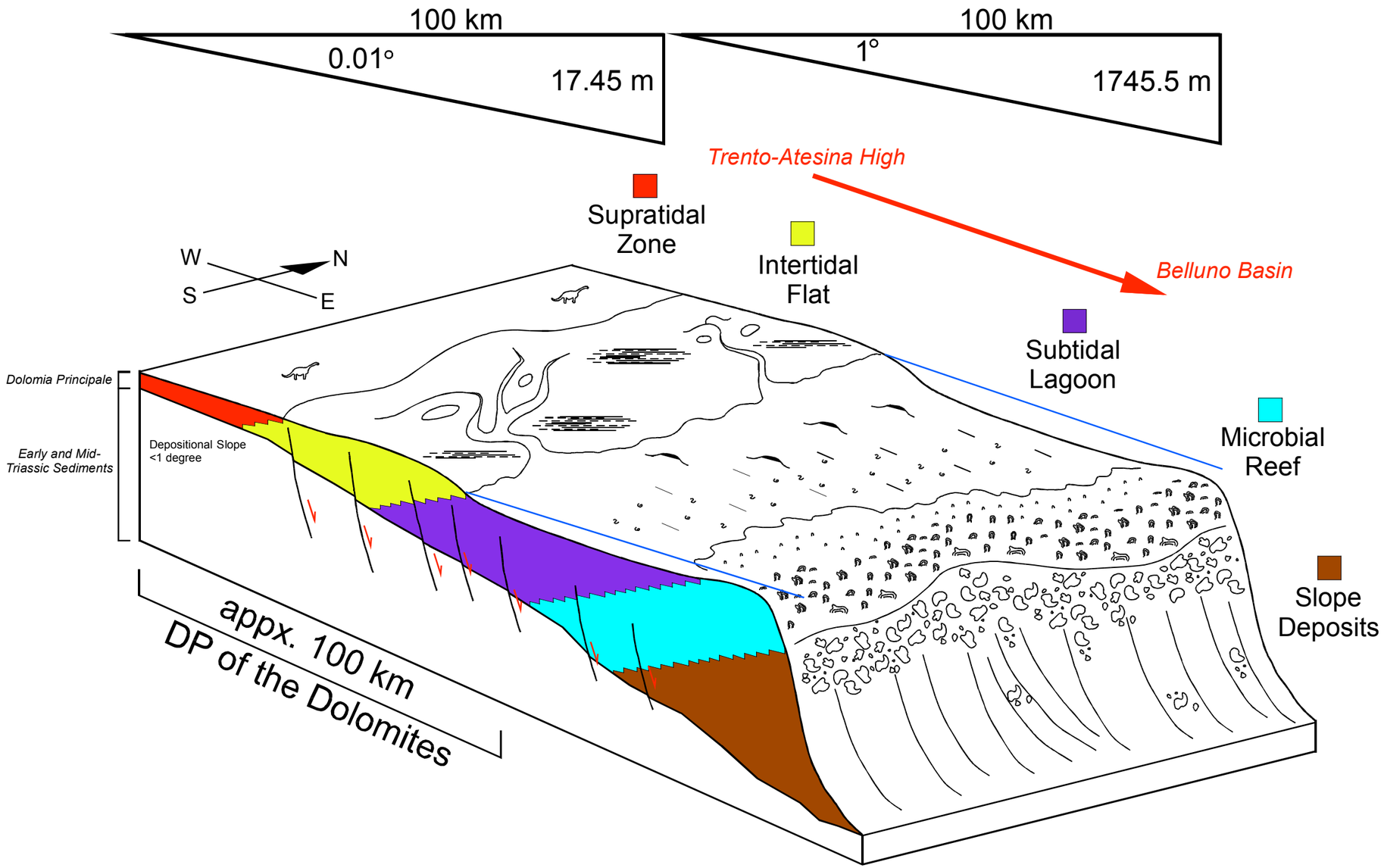

Figure 5.56. Diagram depicting development of the Dolomia Principale as a regional carbonate shelf. The DP of the Dolomites thickens from west to east in the Dolomites and is cut but normal faults with throw at the meter and 10's of meter scales. It is not known whether tectonic extension or gravitational extension and compaction resulted in these trends. However, if a regional dip of only 0.01 degree existed during deposition, 17.6 m of relief would exist over 100 km, easily enough to generate different depositional environments basinward. If a regional dip of 1 degree existed during deposition, 1746 meters of differential relief over 100 km is generated, accounting for the differential thickness of the DP through the Dolomites and into the Carnian prealps. Individual sea level oscillations generated by precessional forcing have been interpreted to have had a range of +/- 5-6 meters, meaning that it is unlikely that every precessional oscillation would have been recorded across the entire platform. DP facies encountered in the Dolomites do not extend to the margin, but are limited to supratidal, tidal flat, and subtidal lagoon facies belts.

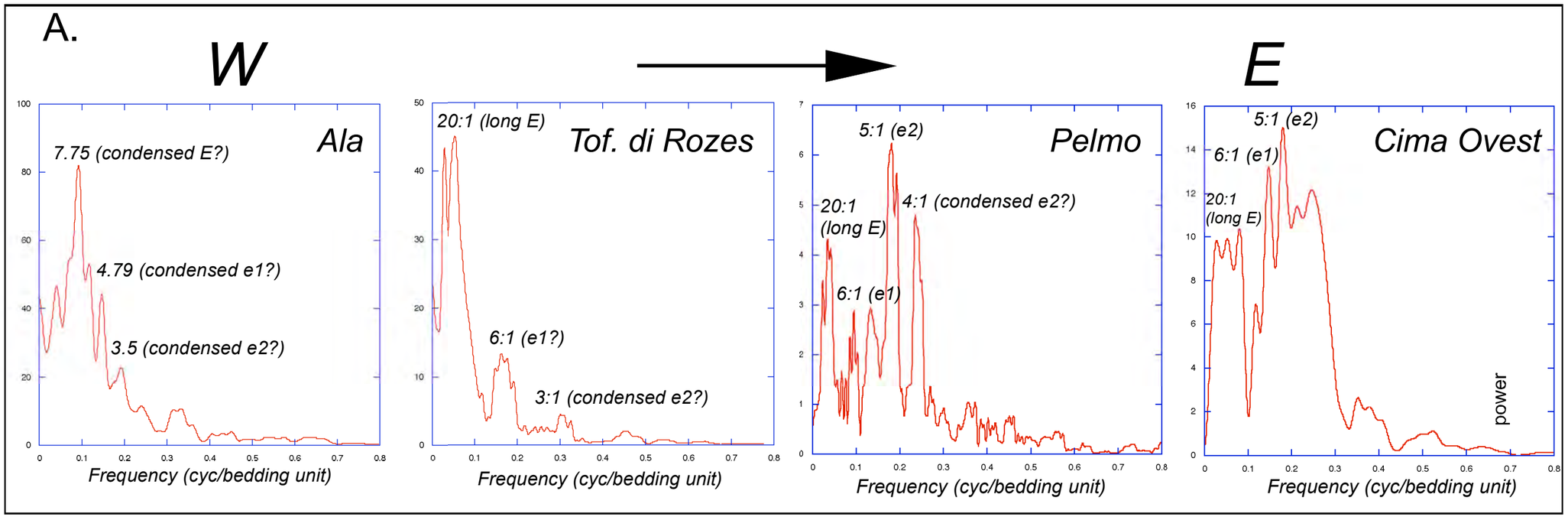

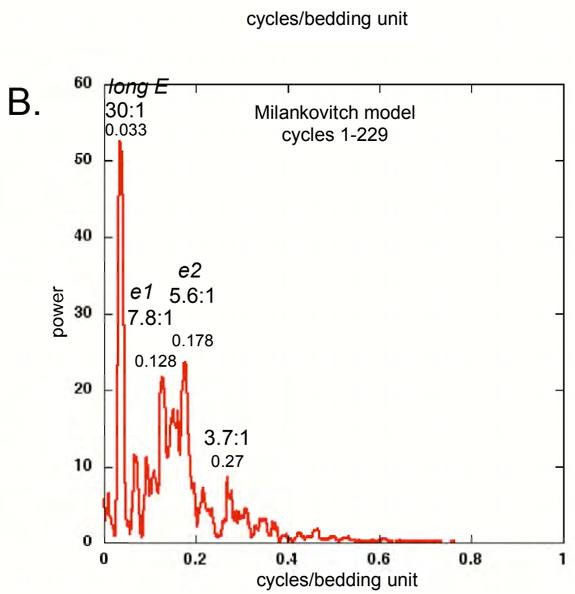

Figure 5.57. A. Comparison of spectra from measured sections of the DP in the Dolomites (west-east transect) showing the development of increasingly Milankovitch-like frequencies to the east. B. A spectrum of synthetic depositional cycles formed using Milankovitchian solar insolation as a proxy for eustasy is included for comparative purposes.

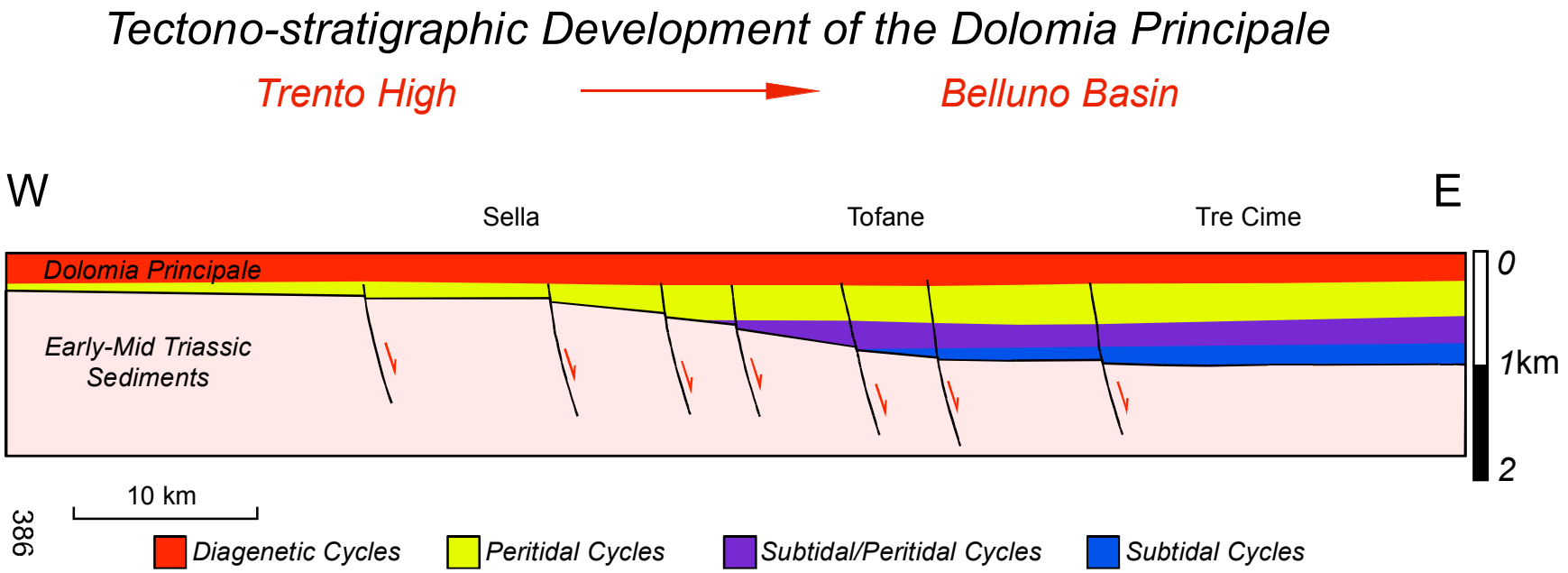

Figure 5.58. The tectono-stratigraphic development of the Dolomia Principale was largely driven by EW-directed regional extension associated with the opening of the Tethyan ocean system (Bosellini, 1984; Doglioni, 1987). Extension led to block faulting and differential subsidence within the DP shelf complex, producing a general thickening of the DP from west to east. Cross- platform subsidence accommodation is reflected in the bundling of depositional cycles, which contain more individual cycles per megacycle from west to east. Carbonate sedimentation was able to keep up with differential subsidence, producing successions dominated by shallow water and peritidal carbonates even in easternmost localities.

APPENDIX B. DP MEASURED SECTIONS

Introduction

In order to analyze and/or identify a cyclostratigraphic framework for the Dolomia Principale, measured sections through the stratigraphy of the DP had to be completed. As stated previously, many workers have identified EW directed extension in the DP (Doglioni, 1987, 1992; Bosellini, 1991; Cozzi, 2000). In order to address this issue sections were measured along an EW- transect in through the Dolomites, with each section starting at the base of the DP (**Figure 5. B1**). The section furthest west is located near the town of Ala, on the Trento/Atesina high. This section was more of an outlier than a part of the tighter-spaced transect, as it is ca. 60 kilometers from the next section on the transect at Passo Valparola. Nevertheless, access to sections and directions to workable localities being limited at best, all possible sections were included. The tightest grouping of sections is in the valley in between Passo Falzarego and Cortina d'Ampezzo, where 4 measured sections are located with EW spacing of under 10 kilometers total. The sections furthest to the east are those at Tre Cime di Lavaredo, located nearly 100 kilometers east of Ala.

All sections were measured beginning at the Raibl/DP lithostratigraphic contact. While it is recognized that this boundary might be time-transgressive from locality to locality, the lack of any other specific marker led to its being used as a control point. Sections were measured from the DP basal contact upwards until measurement could not continue due to extreme relief. Descriptions were made at the highest possible resolution, with any recognizable change in facies

being noted in the log book. Indeed, Italian hikers often looked on in wonder as we measured a mountain with a centimeter-stick.

Below, each section is described in terms of its location on a map and on a panoramic photograph, along with general geologic findings from base to top of the section with trends and irregularities noted. Drafted sections taken from field measurements are also included

Section 1: Roadcut above the town of Ala near Passo Fizzanze.

Location

This approximate section measured and described by Goldhammer et al. (1990) in their foundational paper on the hierarchy of stratigraphic forcing in the Alpine Triassic. Its location on the Trento/Atesina platform (a paleohigh in the Triassic) made it a prime locality for the study of cycles that recorded "missed beats" in sea level to the comparatively high topographic position in the basin. In this case, cycles are interpreted to have missed beats and undergone extended periods of subaerial exposure and tepee/paleosol development (*see* Chapter 5). The Ala section is located on the eastern side of the Adige Valley, and can be easily seen as a roadcut ascending from the valley floor just past the town of Ala while driving southbound on A22 (**Figure 5. B2 and 5. B3**). It is the only such roadcut that was observable anywhere near the area and is visible from the highway.

Section Description

The section through the DP preserved in a roadcut section near Ala is a 55 meter-thick representative section through the upper Dolomia Principale, or "Dolomia Principale Subtidale" according to the scheme of Bosellini and Hardie (1985) and therefore does not correlate time-stratigraphically to the other sections that are part of the study (lower Dolomia Principale, or "Dolomia Principale Peritidale"). The section consists of cycles 0.15 to 5.0 meter thick (avg. 1.5 meters/cycle), each composed of a thick package of subtidal carbonate topped by a comparatively thinner diagenetic cap of either a tepee zone or a red, brecciated "paleosol" (*see* Goldhammer et al., 1990, for their description of similar facies). Subtidal portions of cycles are very thick and have been altered by groundwater diagenesis such that depositional fabrics are very difficult to discern in the field. Subtidal units to consist of massive, vuggy dolomite composed primarily of peloid and composite-grain wacke-to-packstones with burrows and molds of large megalodont bivalves. Subtidal units are capped by either tepee structures (0.25-2.0 m thick) or red brecciated soil-like deposits (0.2 – 1.0 m thick) (**Figure 5. B4**). Tepee-capped cycles tend to be concentrated at the base of the section, whereas paleosol-capped cycles are more common in the upper portion of the upper portion of the section. This distribution of cycle cap-types might be related to long term, low frequency sea level fall occurring as cycles were deposited, leading to increasingly more cycle condensation and "missed beats" up section, resulting in a switch from tepee (marine/vadose) diagenetic caps to soil (purely vadose) diagenetic caps.

Sections: Val Falzarego area - Passo Valparola, Forcella Averau, Tofana di Rozes and Tofana di Mezzo

Location

A series of 4 sections were identified in the Passo Falzarego area, from Passo Valparola in the west to Tofana di Mezzo 7 kilometers away to the east (**Figure 5. B5**). These sections were chosen for measurement based on their relative ease of access and close lateral proximity to each other (from a few hundred meters to a few kilometers spacing). All of the sections measured in the Passo Falzarego area are based at the Raibl/DP lithostratigraphic contact and can be accessed via talus piles that extend through the height of the exposure.

The first (furthest west) of these four sections is located at Passo Valparola, near Passo Falzarego and the well-known Austro-Hungarian WWI fort Tre Sassi. A small outcrop (only a few 10s of meters in height) of Dolomia Principale was identified ca. 200m west of Rifugio Valparola and was measured (**Figure 5. B6**). While the section was not very thick, it did begin at the Raibl-DP contact, made for a quick measure, and serves as a good point of facies comparison to other sections based at the same lithostratigraphic marker.

The second section measured in the Falzarego area can be found at Forcella Averau, directly adjacent from Rifugio Averau and above the Cinque Torri outdoor WWI museum. The section was measured from the base of Forcella Averau and upwards along a talus slope (**Figure 5. B7**).

The two sections measured at the Fanes group were measured at opposite sides of the Valon de Tofana, along the sides of the talus slope extending upwards through the outcrop of DP exposed there (**Figure 5. B8**). The western side of Valon de Tofana extends up the eastern side of Tofana di Rozes, while the eastern side of the valley extends up the western side of Tofana di Mezzo. Both sections were approached from by hiking upwards from Rifugio DiBona, located at the base of the Fanes group

Section Description – Falzarego section group

Nearly all of the DP sections anchored on the Raibl-DP lithostratigraphic contact are highly brecciated at their bases. Indeed, all of the sections in the Passo Falzarego area (Valparola, Averau and Tofana sections) have heavily brecciated bases with both karst breccias and transgressive-lag breccias occurring, many times the differentiation between them being quite difficult to determine. This is not an unexpected occurrence as marine transgression over the Raibl involves flooding of marginal marine and/or fluvial/paleosol successions such that initial high-frequency, low-amplitude sea level oscillations would lead to subaerial exposure and karsting of marginal marine carbonates deposited during transgression.

Continuing upwards, sections become increasingly dominated by subtidal deposits, including mixed skeletal and megalodont pack and grainstones and massive mudstones. These deposits record the stabilization of carbonate production and establishment of a subtidal “carbonate factory” after initial transgression at the Raibl-DP boundary. These deposits are either capped by

microbial laminites, fenestral wackesone with incipient microbial lamination, or intraformational breccias. Further upsection, facies dominance shifts from subtidal to supratidal deposits, with thick (1-2 m) beds of microbial laminites and associated exposure surfaces dominating the cycle thickness series. These laminites eventually give way to tepees and heavily indurated and vertically disrupted tepee zones. Tepee zones themselves cannot be separated into individual cycles, although it is noted that rock in tepee zones belongs to multiple depositonal facies and likely records the deposition of multiple cycles.

In general, facies successions within DP sections in the Falzarego area reflect a “nested”, hierarchical arrangement of shallowing-upward successions, similar to what might be predicted in the “order” model of depositional cyclicity (described by Goldahmmer, 2003). Each individual cycle is made up of facies that vary in thickness according to the cycle’s postion within the lower-order cycle. For example, cycles located within the middle portion of sections have a dominance of subtidal facies as conditions “deepen upwards” overall after transgression and the initiation of marine carbonate sedimentation. In a similar way, cycles located in the upper “supratidal” portion of the section are dominated by supratidal facies. In each instance, sections measured in the Falzarego area record one “third order scale” depositional sequence, deepening upward through basal transgression and maximum flooding zone, followed by a shallowing upward succession of cycles capped by supratidal laminites and finally by marine/vadose diagenetic zones indicative of subaerial exposure.

Section 6: Pelmo

Location

The 3168 meter-high Pelmo (and adjacent 2990 meter peak, the Pelmetto) is a spectacular mountain peak made up, for the most part of Dolomia Principale. Access to sections is variable around the mountains, although a section above a popular hiking stop “impronti dinosauri” (dinosaur footprints) (**Figure 5. B9**). The stop is located above trail 472, at the base of Monte Pelmo. The trail to the section can be accessed directly from Rifugio Staulanza, along road 251, approximatey 5 kilometers southeast of the town of Pescul (**Figure 5. B10**).

Section Description

The Pelmetto section is somewhat problematic at its base due to the somewhat unique transition from “Raibl-like” facies through to the shallowing-upward marine carbonate cycles of the DP. While some contend that the true formational contact occurs at the point where typical Lofer-type cycles can first be recognized, the irregularity of the lithological succession that is the Raibl-DP contact from locality to locality suggests that the depositional environments per locality at the time of the transition were different, and/or that the boundary is time-transgressive from locality to locality. Due to this, the entire Raibl-DP contact was measured and included here for the sake of consistency from locality to locality, in hopes that if Raibl-DP contacts vary in time from locality to locality, that at least the cyclic successions may be recorded regardless of facies type deposited at any given locality.

The section begins in what is likely the Raibl, dominated by clastic mudstones and fissile shales before becoming dominated by marly carbonate about 10 meters up from the base. The section then reverts back to peloidal wackstone/shale couplets, becoming dominated by Lofer-type carbonate cycles about 45 meters from the base of the section. This 45-meter basal section was included because a Raibl-DP transition zone of this type does not occur at any of the other localities, and therefore needed to be recorded to investigate possible cyclic/temporal links to other sections.

Carbonate cycles in the Pelmo section are dominated by subtidal deposits toward the base of the section. Cycles at the base of the carbonate section are composed primarily of mixed skeletal packstones with thin laminite and/or breccia caps. Upward through the section, the facies become more dominated my supratidal deposits, including laminites with karstic breccia caps. Microbial laminites dominate the top of the measured section, some examples being over 2 meters thick. Well developed tepee zones were not observed at the Pelmetto section, but may occur higher on the mountain, which was inaccessible due to our lack of free-climbing skill. However, the general shallowing-upward trend in the Pelmo section is consistent with the other sections analyzed, the lower transition zone between the Raibl and DP being the main difference.

Section 7: Tre Cime di Lavaredo Forcella Lavaredo and Cima Ovest

Location

Sections were measured, where possible and safely accessable, at Tre Cime di Lavaredo, the locality furthest to the east in the study. Tre Cime di

Lavaredo is located ca. 15 km east of Cortina d'Ampezzo off of local road no. 48. The three towering, spire-like peaks are easy to spot from the road, or from Rifugio Auronzo near the base of the three mountains. Two sections were measured at Tre Cime- the first approaching from the eastern side of the three mountains up from Forcella Lavaredo through the base of the first Dolomite cliffs, and the second up ca. 65 meters from the base of the north side of Cima Ovest (**Figure 5. B11**). The section was stopped at 65 meters due to the exteme hazard of falling rocks from above (loosened unintentionally by climbers). Ideally, a section from base to top of Cima Ovest could be measured with enough time and climbing equipment, as the wall face of the mountain is very clean.

Section Description

Two sections were measured at Tre Cime di Lavaredo. The first, at Forcella Lavaredo, records the Raibl-DP transition and the second, at the base of Cima Ovest, records the base of the DP cyclic series preserved there. The Raibl-DP transition was measured at Forcella Lavaredo for the same reason as the transition was measured at the Pelmo- the transition is lithologically unique among other sections measured. The base of the "Raibl" (so-called here due to its clastic-rich, erosive profile and stratigraphic position above the underlying peritidal deposits of the Dürrenstein) at Tre Cime is rich in carbonate deposits, particularly thick (1-2 meter) beds of megalodont wacke-to packstone. The section becomes increasingly carbonate-dominated upwards, with oncoids becoming plentiful near the lithologic transition into Lofer-type DP cycles. However, the deposits remain largely subtidal and lack the heavily brecciated

fabric of transitional breccias found in Falzarego sections. The depositional environment as subtidal marine, which is in marked contrast to gypsum-rich Raibl facies near Monte Cristallo and paleosol-rich facies found near the Fanes group. Again, it is not known whether the difference in Raibl facies reflects different depositional environments within the same temporal framework, or if the entire transition between Raibl and DP is time and environmentally transgressive. Therefore, transition sections were measured in hopes of recording any cyclic behavior that may have a "shallow" equivalent updip.

The section measured from the base of Cima Ovest does not include Raibl-DP transitional facies, although the section likely starts within 10 meters of the lithologic transition. Basal DP cycles at Cima Ovest are conspicuously non-brecciated, and do not exhibit the thick, well-developed karsted caps that basal cycles in the Falzarego area (eg Forcella Averau) display. Rather cycles are composed largely of megalodont pack-to-grainstones with exceedingly large (over 30 cm on the long-axis) megalodont bivalves and have microbially laminated cycle caps. Cycles become increasingly partitioned into microbial laminite facies upwards (at an interval between 40 and 50 meters from the base of the section) before again being dominated by thick (2m +) mixed skeletal megalodont packstones. It is possible that the basal shallowing upward trend at Cima Ovest is equivalent to the basal karsted breccia cycles identified in the Falzarego area. The section then becomes dominated by subtidal facies and has the thickest single beds of subtidal megalodont beds of all sections measured. The section could not be carried higher into the next peritidal zone due to danger of being killed by falling rocks.

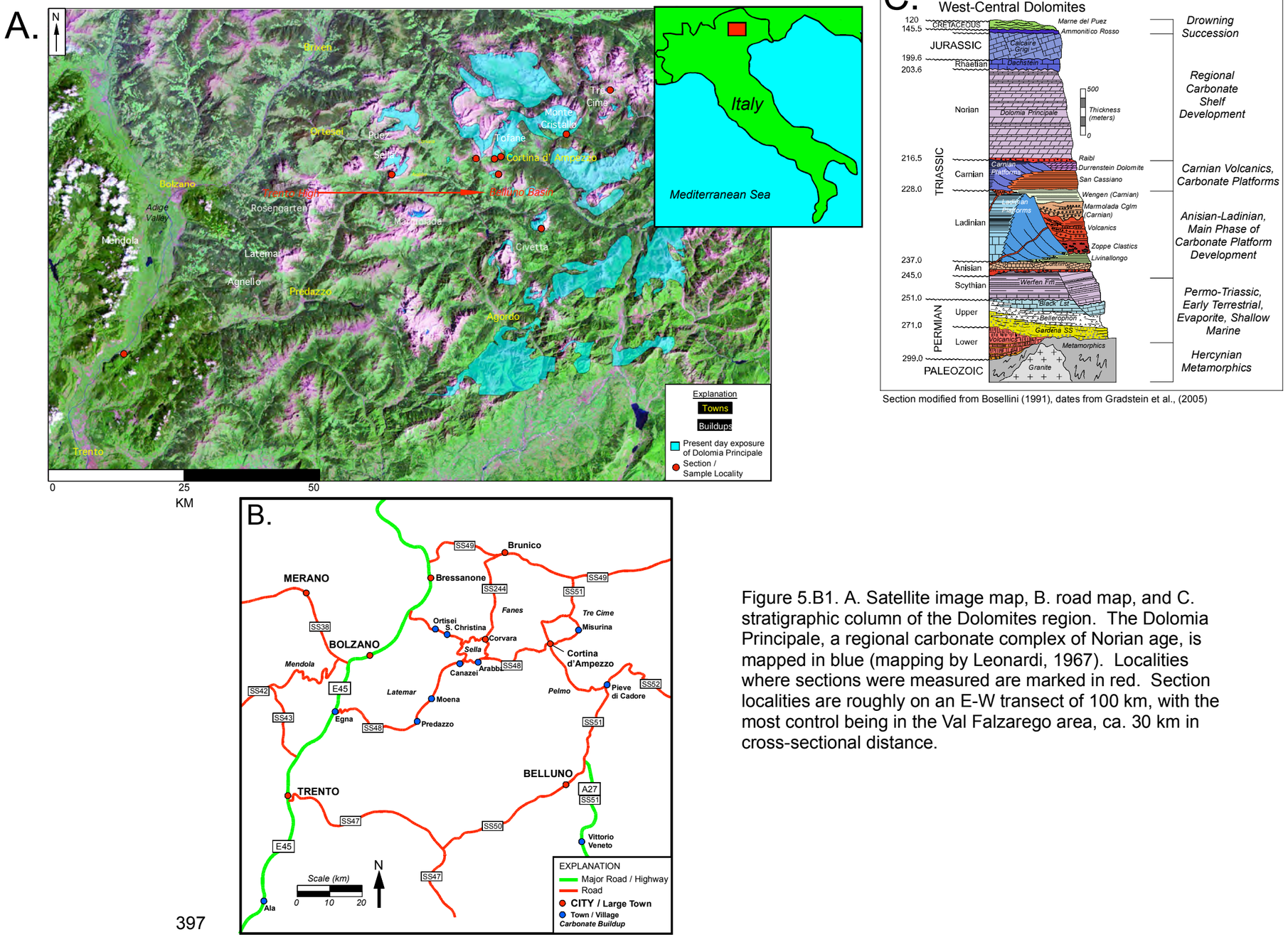

Section modified from Bosellini (1991), dates from Gradstein et al., (2005)

Figure 5.B1. A. Satellite image map, B. road map, and C. stratigraphic column of the Dolomites region. The Dolomia Principale, a regional carbonate complex of Norian age, is mapped in blue (mapping by Leonardi, 1967). Localities where sections were measured are marked in red. Section localities are roughly on an E-W transect of 100 km, with the most control being in the Val Falzarego area, ca. 30 km in cross-sectional distance.

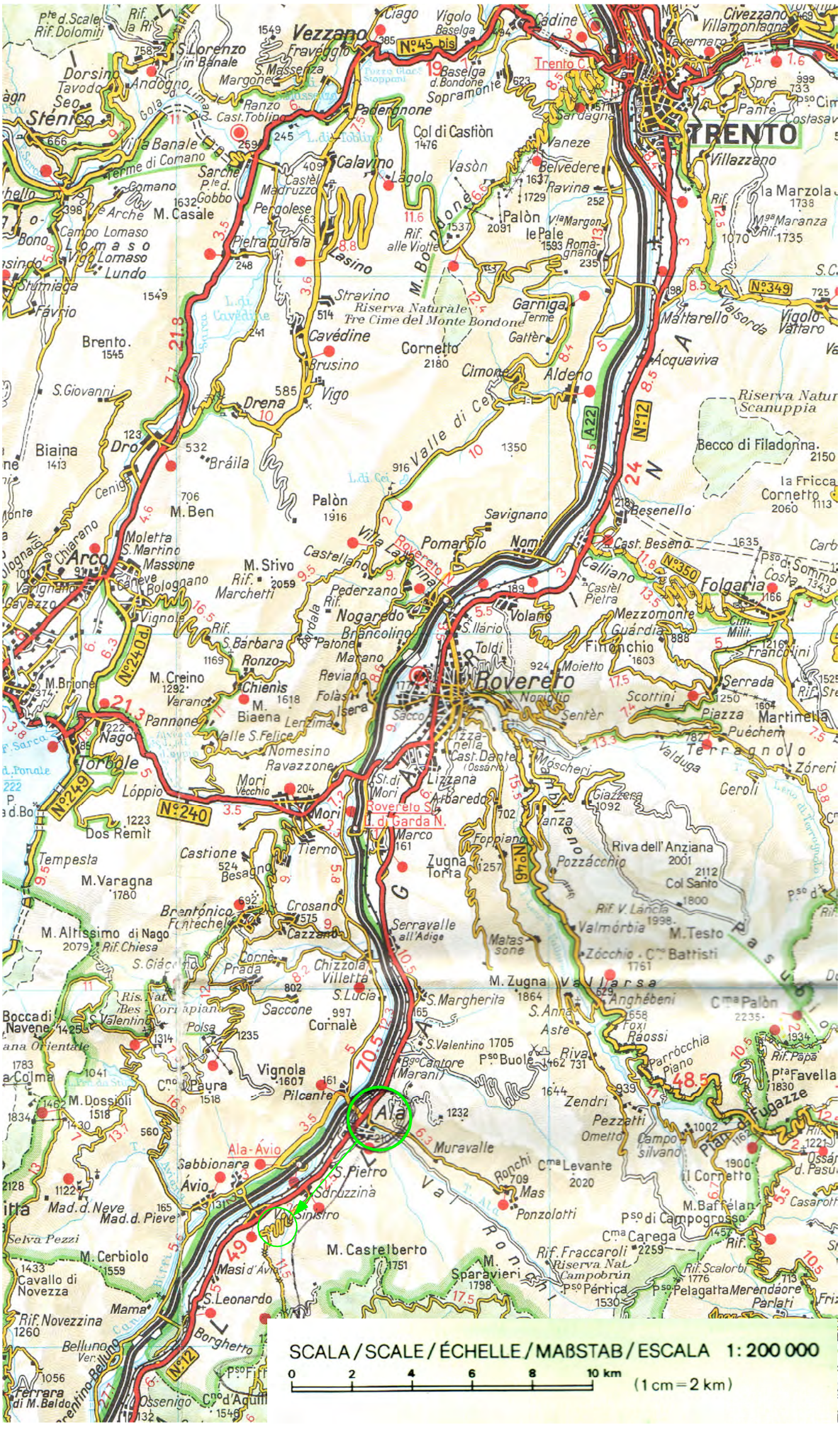
TRENTO
Vezzano
Sténico
Dorsino
Tavodo
Andogno
S.Lorenzo in Banale
Villa Banale
Terme di Comano
Comano
Sarche
Calavino
Lágolo
Vasòn
Belvedere
Ravina
Cadine
Trento C.
Sopramonte
Baselga d.Bondone
Vigolo Baselga
Ciago
Fravéggio
S.Massenza
Margone
Ranzo
Cast.Toblino
Padergnone
Col di Castìon
Vaneze
Villazzano
Sardagna
Spré
Pantè
Civezzano
Villamontagna
la Marzola
M.Casale
Pergolese
Castèl Madruzzo
Pietramurata
Lasino
Campo Lomaso
Lomaso
Lundo
Stumiaga
Favrio
Brento.
S.Giovanni
Drena
Cavédine
Brusino
Vigo
Stravino
Riserva Naturale Tre Cime del Monte Bondone
Cornetto
Cimone
Aldeno
Garniga Terme
Gattèr
Ácquaviva
Maltarello
Valsorda
Vigolo Vattaro
Riserva Natur Scanuppia
Becco di Filadonna.
la Fricca
Cornetto
Besenello
Cast. Beseno
Calliano
Castèl Pietra
Folgaria
Costa
Biaina
Dro
Bráila
Palòn
M.Ben
Arco
Moletta S.Martino
Massone
Bolognano
Vignole
M.Stivo
Marchetti
Rif.
Pomarolo
Savignano
Nomi
Castellano
Pederzano
Nogaredo
Brancolino
Marano
Reviano
Folàs
Isera
Lenzima
Valle S.Felice
Nomesino
Ravazzone
Mori
Vecchio
Mori
Rovereto
Rovereto N.
Rovereto S.
L. di Garda N.
Lizzanella
Cast.Dante
Lizzana
Arboredo
Marco
Zugna Torta
Foppiano
Riva dell' Anziana
Pozzácchio
Col Santo
Rif. V. Lancia
Valmórbia
M.Testo
Zócchio - C.no Battisti
M. Zugna
Val Larsa
Anghébeni
Cima Palòn
Rif. Papa
Fittanze
Ala
Ala-Ávio
Sabbionara
Ávio
S.Pietro
Sdruzzinà
Muravalle
Ponzolotti
Ronchi
Cima Levante
Mas
Il Cornetto
M.Baffelan
Cima Carega
Rif. Fraccaroli
Riserva Nat. Campobrún
M. Sparavieri
M. Castelberto
Passo Pértica
Passo Pelagatta
Merendaore
Parlati
Tugazze
Rif. Scalorbi
Rif. Pian delle Fugazze
Terragnolo
Geroli
Zóreri
Valduga
Serrada
Martinella
Piazza
Puechem
Finonchio
Mezzomonte
Guárdia
Volano
Toldi
Moietto
Scottini
Sentèr
Noriglio
Lizzanella
Cast.Dante
Mascheri
Giazzera
Vanza
Besenello
Calliano
Folgaria
Costa
Nogaredo
Pedersano
Castellano
Villa Lagarina
Rovereto N.
Rovereto S.
Lizzana
Riva
Torbole
Nago
Loppio
Dos Remit
Tempesta
M.Varagna
M.Altissimo di Nago
Rif. Chiesa
Brentonico
Crosano
Cazzano
Serravalle all'Adige
Matassone
Castione
Besagno
Tierno

Figure 5. B3. Photograph of the Ala/Fittanze roadcut easily seen on the eastern side of the Adige valley, traveling southbound on highway A22 near the town of Ala. It is the only ascending road with a visible roadcut ascending from the valley floor anywhere near Ala, and is not difficult to find. This is the location of the DP section measured by Goldhammer and Dunn and published in Goldhammer et al., (1990) and is the western-most section measured in this study.

Figure 5. B4. Typical roadcut outcrop exposure along the road to Passo Fittanze above the town of Ala.

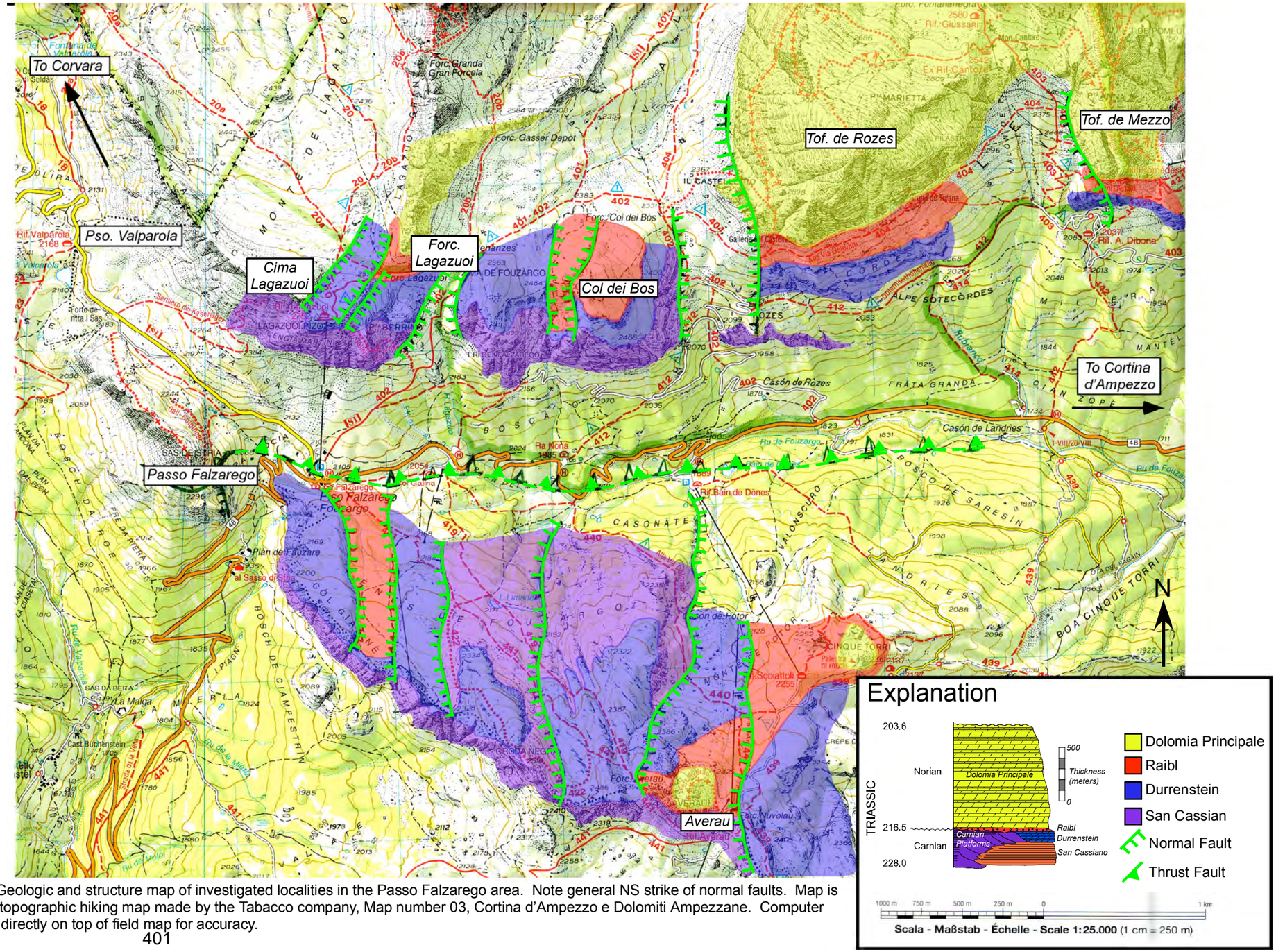

Figure 5.B5. Geologic and structure map of investigated localities in the Passo Falzarego area. Note general NS strike of normal faults. Map is is a 1:25,000 topographic hiking map made by the Tabacco company, Map number 03, Cortina d'Ampezzo e Dolomiti Ampezzane. Computer drafting done directly on top of field map for accuracy.

Figure 5. B6. Dolomia Principale section location at Passo Valparola. Section route in green.

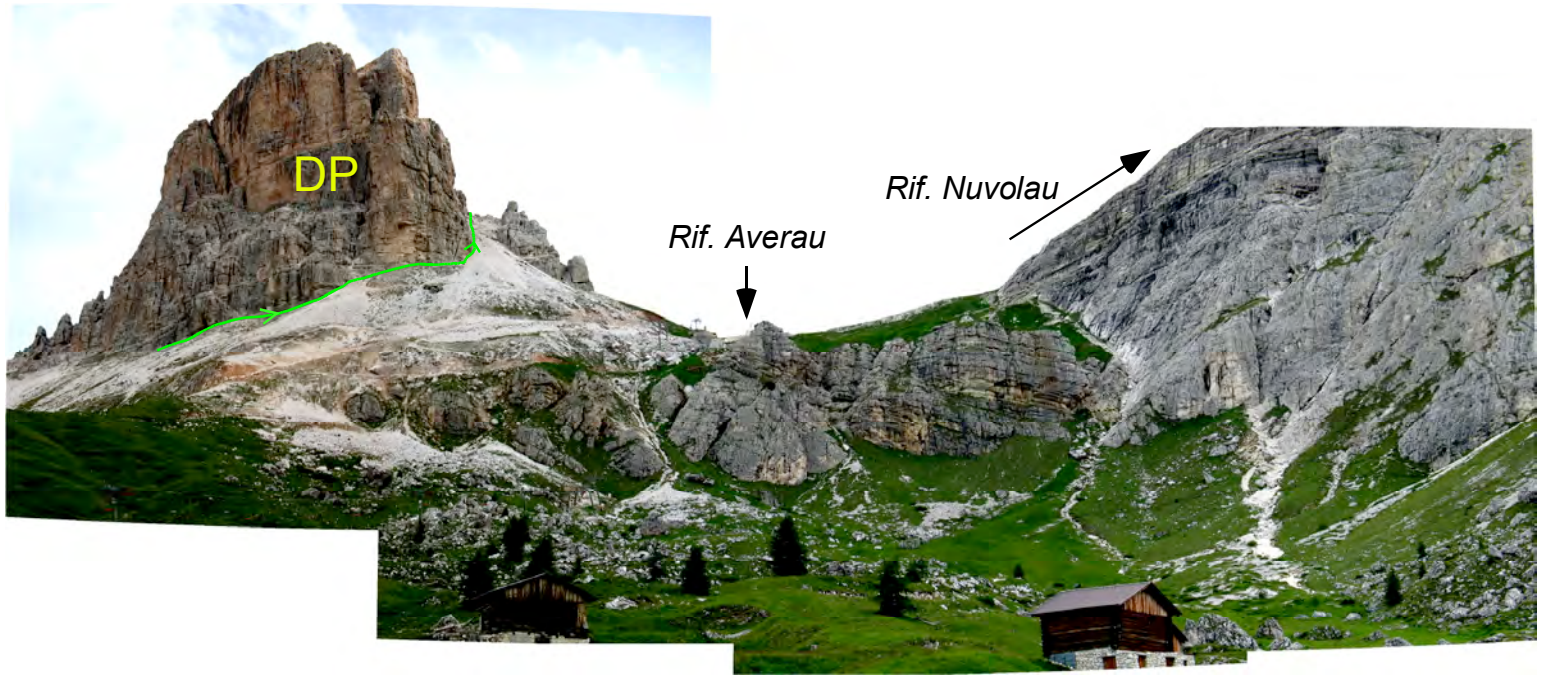

Figure 5. B7. Photograph of location of measured section at Forcella Averau. Section begins at the base of the south side of the block of Dolomia Principale ca. 100 meters east from Rifugio Averau and continues up the talus slope as indicated. Green line denotes path of measured section.

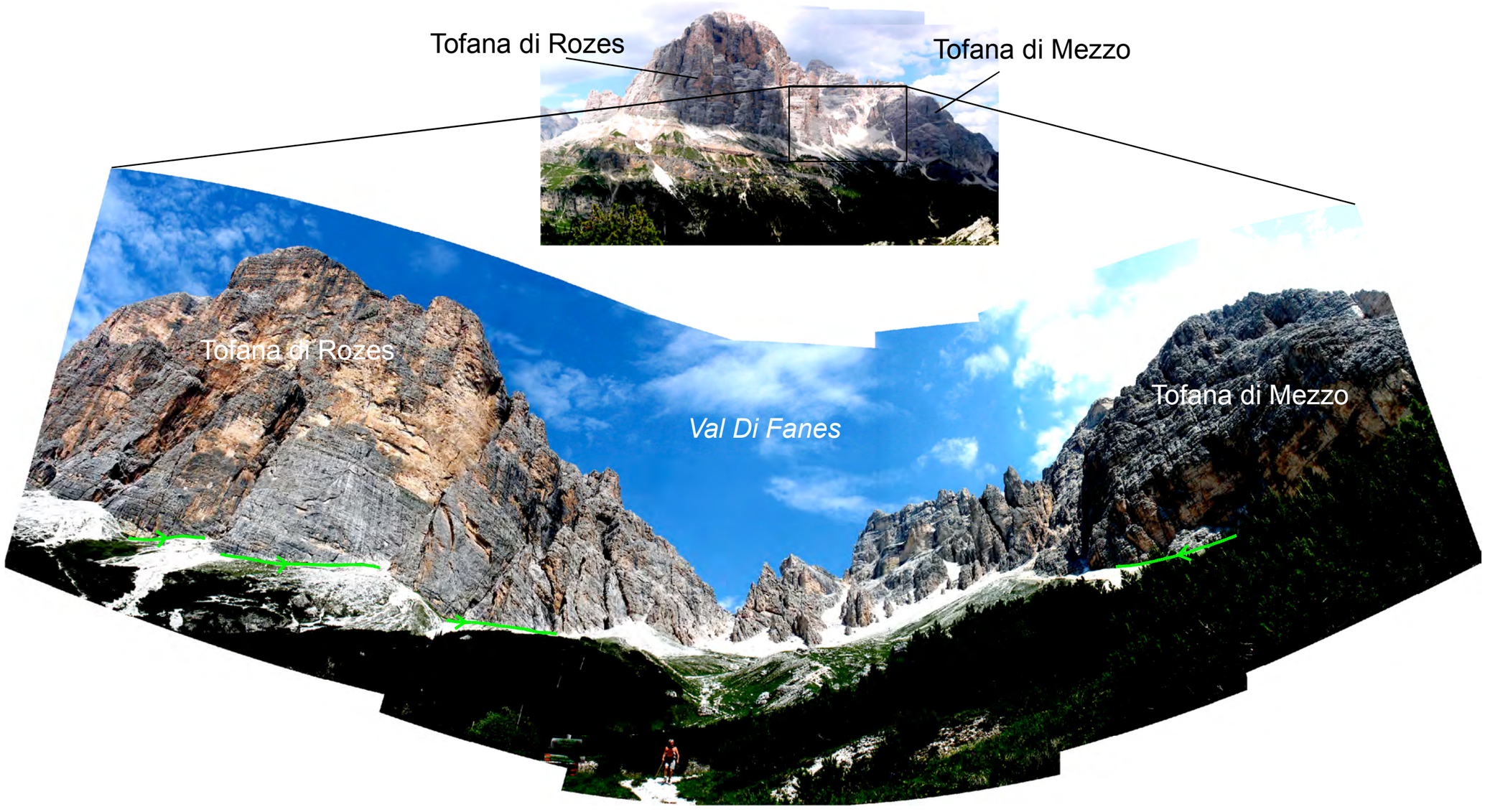

Figure 5. B8. Section locations at the Fanes group. Sections were based at the Raibl/Duerrenstein-DP lithostratigraphic contact on both sides of the Val di Fanes (suspected to be a large normal fault). The section up Tofana di Rozes is sometimes referred to as Tofane (West) and the section up Tofana di Mezzo is sometimes referred to as Tofane (East).

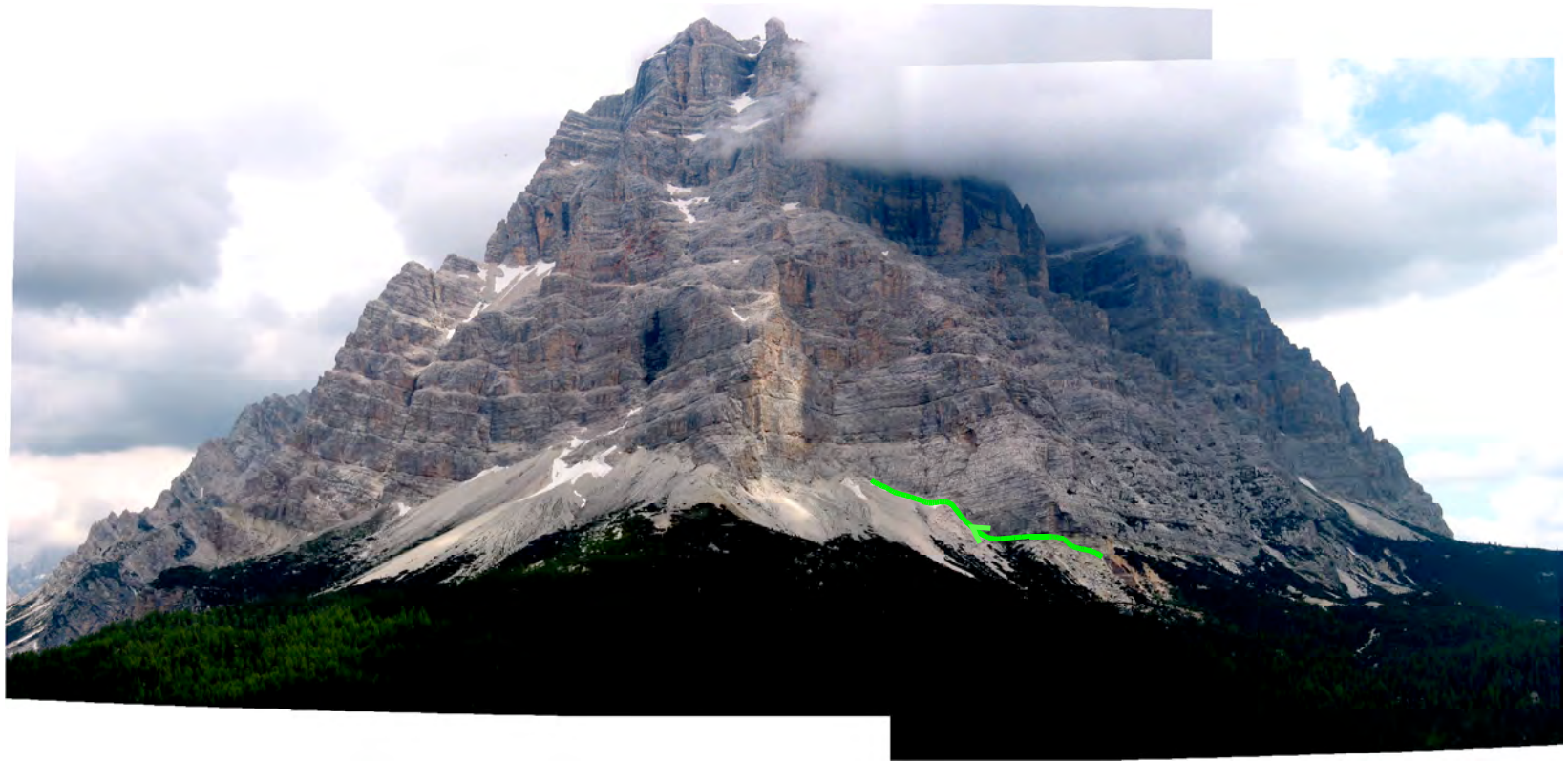

Figure 5. B9. The Pelmo. Section measurement followed the green line, and started at the Raibl-DP contact near the famous block of DP containing the dinosaur footprints.

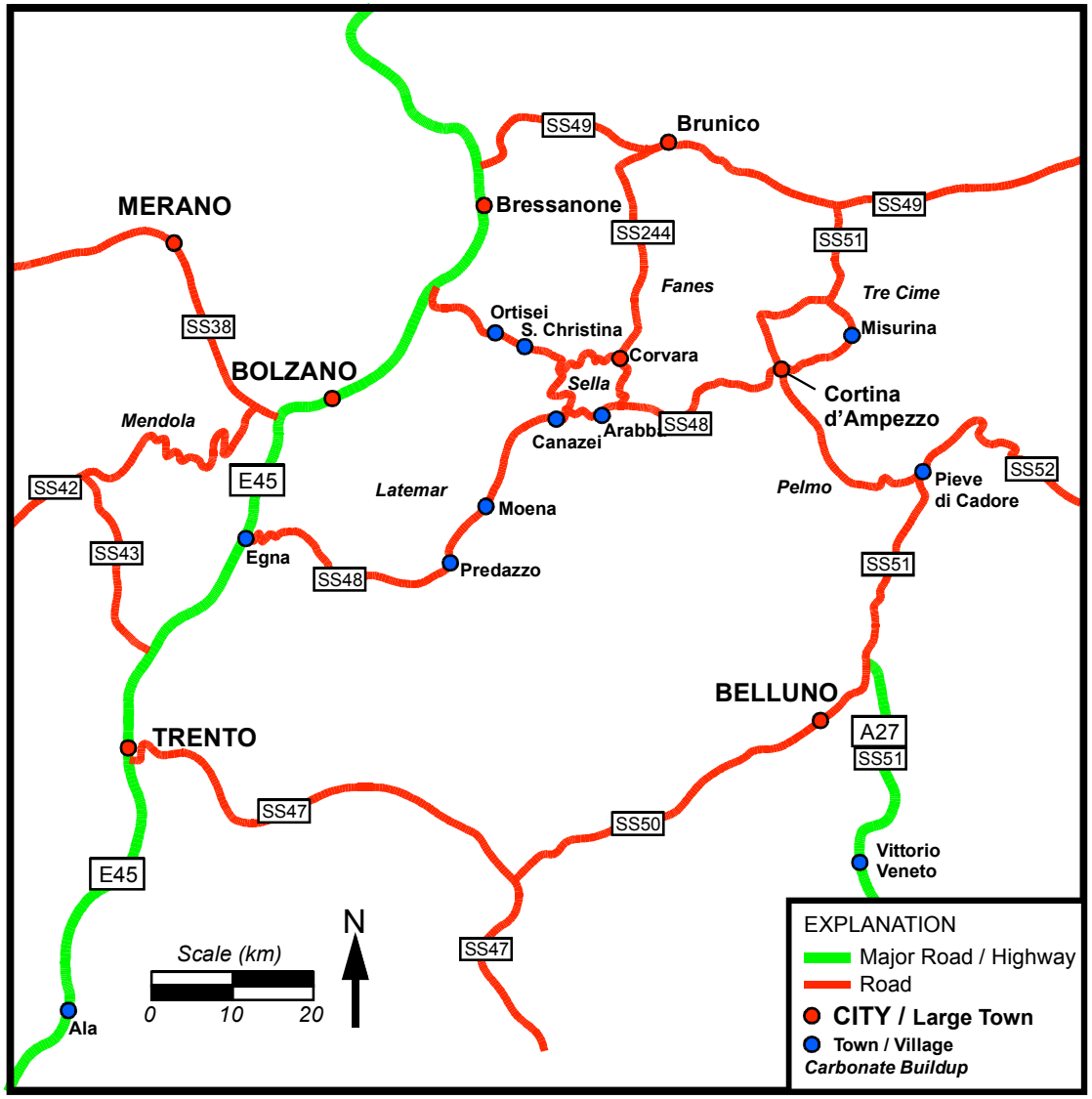

Figure 5. B10. Road and location map for cities, towns, and major carbonate buildups in the Dolomites.

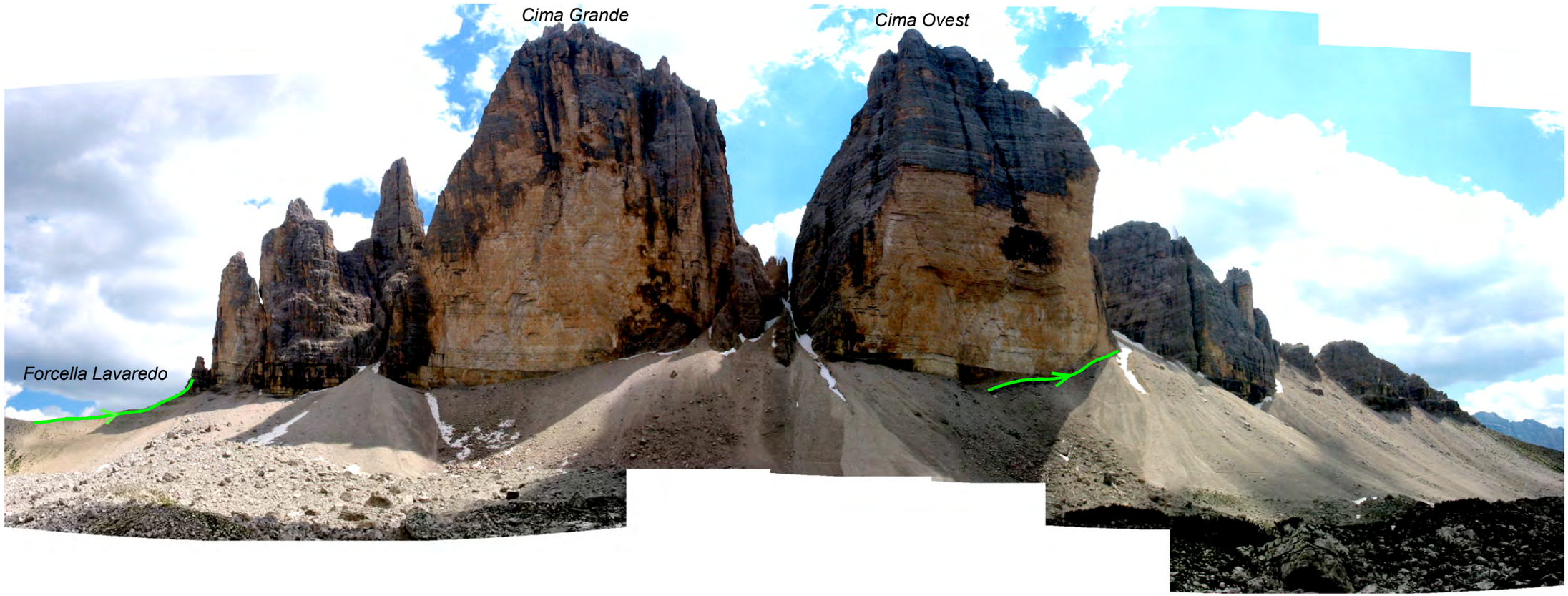

Figure 5. B11. Classic panoramic view of the north faces of Tre Cime di Lavaredo, some of the best-known mountains in the Dolomites. Measured sections follow green lines.

Chapter 6: The Current State of the Hierarchy of Stratigraphic Forcing in the Alpine Triassic

ABSTRACT

In their seminal publication documenting composite cycle stacking patterns in the Triassic carbonate platforms of the Southern Alps, Goldhammer et al. (1990) conclude that a 'hierarchy of stratigraphic forcing' acted to form the depositional cycles present in the many exposures. This hierarchy was driven by eustasy (sea level changes) via astroclimatic forcing related to Milankovitchian orbital processes. As a result, successions with stacking patters consistent with Milankovitchian forcing were interpreted to have been deposited with like periodicities in the absence of constraining dates. Successions with stacking patterns outside of this hierarchy are interpreted to be the result of the "faulty recording mechanism" inherent in the rock record. That is, that equally spaced time events are not necessarily recorded as equally spaced lithologic events because of autocyclicity or erosion.

Currently, there is a debate over the timescale of carbonate depositional cyclicity that fundamentally affects the interpretation of Goldhammer et al. (1990). That is that cyclic carbonate deposits in the mid-Triassic were deposited at millennial periodicities rather than at 20 kyr periodicities. However, deposits in the late Triassic of identical facies composition are interpreted to have Milankovitchian periodicities (*see* previous chapter). If these hypotheses are true, then there must have been a depositional "slowdown" through Triassic time as recorded in the depositional successions of carbonate platforms in the

Southern Alps. A review of the literature provides clues, indicating a long term uptake of CO_2 into the atmosphere, decreasing temperature though the Triassic (dropping 4^{o}C) and a progressive die-off of carbonate producing organisms through the Triassic prior to the end-Triassic extinction. While by no means proven, the combination of the stratigraphic research provided in this volume, as well as a literature review at the very least points towards plausibility for a Triassic depositional slowdown.

INTRODUCTION

Background

In their discussion of the nature of depositional cyclicity in the Triassic of the Southern Alps, Goldhammer et al. (1990) identified 'hierarchy of stratigraphic forcing' in the depositional record of platform carbonates. This stratigraphic hierarchy was interpreted to be the sedimentary response of platform carbonate systems to sea level oscillations operating at multiple periodicities. Goldhammer et al. (1990) analyzed patterns in vertical stacking of thickness series in individual shallowing-upward cycles (thought to represent 0.01-0.1 my cycle periods, so-called '5th-order' cycles), bundles of shallowing-upward cycles (0.1-1.0 my periodicities, or '5th-order' cycles), and lower frequency groupings (1.0-10 my periodicities, or '5th-order' cycles). Goldhammer et al. (1990) identified these cycles on the basis of comparative sedimentology and frequency matching in the absence of high-resolution age dating. For example, cycles bundled into thinning-upwards packages of approximately 5 cycles per bundle were thought to reflect Milankovitchian eustatic oscillations related to the precessional cycle (ca. 20 kyr) and modulated by the eccentricity cycle (ca. 100 kyr). Statistical analyses

of measured sections appears to confirm this supposition, with stacking patterns of both thickness and rank series being comparable to the precessional index (*see* Chapter 2, and Preto et al., 2001, 2004).

Two Triassic carbonate successions thought to record Milankovitchian eustatic oscillations have been examined in this dissertation and include the Anisian/Ladinian Latemar platform and the Norian Dolomia Principale. Central to the interpretation of a record of periodic cyclic drivers within these deposits are the results of statistical time series analysis, confirming bundling trends within successions that are strikingly similar to mathematical solutions for Milankovitchian orbital cycles (*see* Chapter 5, Figure 5. 59) and synthetic stratigraphy created by computer models with sea level drivers operating under composite Milankovitchian forcing (*see* Chapter 2). Both of these carbonate successions have been interpreted to have formed in response to Milankovitch forcing.

Goldhammer et al. (1990) also presents two examples of carbonate successions that do not have 5:1 stacking trends as expected from Milankovitchian cyclicity (Norian Lofer cycles and the Pleistocene of S. Florida). In the case of the Lofer cycles, local tectonics and differential subsidence are thought to have changed relative sea level during the deposition of the Dachstein, causing the depositional record to lack an identifiable Milankovitch signal. In the Pleistocene example, high-amplitude (120 meters rather than 2-5 meters) sea level oscillations in modern “icehouse” times have generated a depositional record of “missed beats” of higher-frequency (ca. 5th-order) sea

level oscillations due to the inability of single oscillations to completely expose submerged platform tops. In either instance, however, the main thrust of Goldhammer et al. (1990) is to assert that a hierarchy of periodic, predictable stratigraphic forcing mechanisms act on carbonate platforms and generate predictable stacking patterns through successions. Goldhammer et al. (1990) quote Sander (1951) and Schwarzacher (1975), who conclude that the presence of a cyclic record in stratigraphy requires a cyclic driver. The absence of a cyclic record does not necessarily discount the presence of a cyclic driver, but that its signature might not be recorded due to any number of processes, including erosion, lateral sediment transport, intrabasinal autocyclicity, etc.

Evidence for Rhythmic Sedimentation

The absence of high-resolution dates for stratigraphic successions studied by Goldhammer et al. (1990) is a fundamental problem when making the argument for a record of temporally periodic cycle drivers within the Alpine Triassic. However, evidence for a eustatic driver in both the Anisian/Ladinian Latemar platform and the Norian DP appears to limit the possibility for dominance of autogenetic forcing within either succession. Interpretation for eustatic forcing stems from a non-Waltherian facies succession within cycles of both Latemar and upper DP deposits, consisting of subtidal deposits as cycle bases that are immediately capped by supratidal deposits (caliches, tepee structures, etc.) without intervening intertidal deposits. This type of succession requires sea level fall in order to place a supratidal environment directly on an exposed subtidal environment, and is indicative of formation via eustatic oscillation. In addition, five-part thinning upward cycle bundles are interpreted by

Goldhammer et al. (1990) as a stacking signature of Milankovitchian composite eustasy, with the ca. 20 kyr precession being modulated by an asymmetric, ca. 100 kyr eccentricity cycle. This was evident through field observations and confirmed through frequency analysis (Preto et al., 2004).

Comparative sedimentology also supports the conclusion that platform interior carbonate depositional cycles form at timescales consistent with Milankovitch forcing. Goldhammer's use of Pleistocene sea level curves from Hays et al. (1976) and Imbrie et al. (1984), sedimentation rates of like-facies from the Pleistocene and Holocene, and the absence of any other known mechanisms that will produce consistent, thinning-upwards 5:1 bundling trends led Goldhammer et al. (1990) to conclude that the nested cycles observed in the Alpine Triassic formed as the result of periodic eustatic oscillations caused by Milankovitchian orbital forcing.

TESTING TEMPORAL PERIODICITY

Early and Mid-Triassic

Since the original work on the Latemar by Goldhammer et al. (1987; 1990), additional studies have been undertaken in order to better understand the nature of depositional cylicity in the Alpine Triassic. A study of the Latemar-equivalent Mendola Pass area was completed in 2005 (Chapter 2 of this dissertation) and documents cycle-for-cycle similarities in thickness trends between Latemar cycles and depositionally-coeval Mendola pass cycles (*see* Forkner et al., *in press*). This study bolstered the conclusion that Latemar cycles were the product of an allocyclic forcing mechanism, as the platforms were

separated by a distance of over 30 km yet retained nearly identical cycle thickness series. While this study delivers additional evidence of allocyclicity in the Alpine Triassic, it does not confirm the temporal periodicity of the cycles.

Identification and dating of zircons extracted from ash beds within the Latemar cyclic succession have provided the first empirical data that directly challenges the conclusion that Latemar cycles have Milankovitchian periodicities (Mundil et al., 1996; Zühlke et al., 2003). Bases on dated zircons extracted from 3 “ash” horizons in the Latemar, Mundil et al. (1996) conclude that the entire Latemar succession was deposited in ca. 2.2 m.y. (in contrast to the 12 m.y. by the Milankovitchian interpretation), which demands much shorter periodicities for composite cyclic drivers, i.e., the fundamental shallowing-upward cycles are ca. 4.2 kyr/cycle rather than the ca. 20 kyr of Milankovitchian precession (Zühlke et al., 2003). As a result, the driving mechanism for the fundamental Latemar depositional cycles was reinterpreted to be a periodic sub-Milankovitchian process with the driver for the megacycle bundling being the precession (Zühlke, 2004).

Most recently, Kent et al. (2004) have argued that most, if not all, of the 540 m thick Latemar cyclic succession is restricted to a single magnetochron, limiting the entire succession to ca. 0.8 myr of time and individual Latemar cycles to 1.7 kyr durations. Independently, Emmerich et al. (2005) attempted to correlate the U-Pb series dates from tuffs in the basinal Buchenstein beds (by Mundil et al.,

1996) to dates in the Latemar platform interior (by Mundil et al., 2003) using the biostratigraphic markers of Brack and Rieber (1993). These results suggest that individual Latemar cycles represent 0.9-1.97 kyr (Emmerich et al., 2005). Both works effectively place both the Latemar cycles and megacycles into the sub-Milankovitch band. In short, while first order frequency analysis suggests that Latemar cycles formed via cyclic drivers operating at frequencies consistent with Milankovitch forcing, dating of the succession has led to two interpretations of cycle periodicity at the Latemar, that cycles formed by a mixture of 20 kyr Milankovitchian and sub-Milankovitchian periodicities (Zühlke, 2004) or that cycles formed at purely sub-Milankovitchian periodicities (Emmerich et al., 2005) (**Figure 6. 1**).

Whether mixed Milankovitch/sub-Milankovitch or pure sub-Milankovitch cycle periodicities are argued for, rates of deposition, subsidence and sea level change must be increased from the Milankovitchain hypothesis in order to fit the Latemar cycles to more rapid periodicities (**Table 6. 1**). The essence of the argument between Milankovitch and sub-Milankovitchian camps comes down to which dataset workers choose to put more weight on. Zircon dates and biostratigraphy are interpreted by Kent et al. (2004) and Emmerich et al. (2005) to indicate purely sub-Milankovitchian cycle periodicities while spectral analysis and comparative sedimentology argue for Milankovitchian (Goldhammer et al., 1987; Hinnov and Goldhammer, 1990) and/or mixed Milankovitchian/sub-Milankovitchian (Zühlke, 2004) periodicities. The possibility that the Latemar cycles are not of

Milankovitchian periodicity calls into question the periodicities, drivers, and sedimentary potential of carbonate platforms that led to the development of the shallowing-upward depositional cycles on the platform.

Sedimentary forward modeling was attempted in order to determine whether or not use of Milankovitch astronomical forcing was able to generate a vertical cyclic platform succession with resemblance to the Latemar successions of the mid-Triassic (*see* Chapter 3). Models were constructed using Milankovitchian solar insolation as a proxy for sea level oscillations. While depositional cycle bundling generated by pure Milankovitichian forcing is more consistent with measurements taken from Latemar sections, mixed Milankovitch/sub-Milankovitch forcing also produced synthetic stratigraphy with close matches to measured stratigraphy from the Latemar. In this case, modeling was not conclusive in either direction, with neither forcing mechanism could be adequately proven or disproven using this modeling technique. However, purely sub-Milankovitchian forcing, which is as of yet poorly defined, was unable to generate stratigraphy with similar stacking or bundling trends to those at the Latemar.

The conclusion that sediment accumulation rates in the mid-to-late Triassic of the Southern Alps are exceptional not entirely new. In a publication concerning the “paradox” of drowned carbonate platforms, Schlager (1981) reports accumulation rates for several carbonate platforms across geologic time. The most rapid accumulation rates for all platforms examined are from the Carnian of the Dolomites, with sustained accumulation rates of 0.3-0.5m/kyr (**Figures 6. 2 &**

6. 3). The dates associated with these calculations have never been published. These findings are, however, corroborated by Keim and Schlager (2001) in a study of the Ladinian and Carnian carbonates of the Sella massif, reporting vertical sedimentation rates in late Ladinian/early Carnian strata as high as 0.6 m/kyr with lateral progradation rates as high as 1.6 m/kyr. While Keim and Schlager do not present the data that led to the calculation of these rates, they do corroborate the Anisian/Ladinian dates of Zühlke (2004) for rapid platform growth at the Latemar.

If the zircon dates mentioned above do reflect and bracket the depositional ages of the carbonates they are found within, it is seemingly possible that while vertically-organized stratigraphy exists in the early to mid Triassic, appearing Milankovitchian in vertical stacking trends, that formative periodicities were much more rapid than concluded by Goldhammer et al. (1987). This hypothesis does not alter the fundamental observation that carbonate cycles are stacked into packages, but it does call into question the reality of timing periodicity of depositional cycles in the Dolomites.

Late Triassic

While evidence of sub-Milankovitch periodicity exists in early and mid-Triassic deposits, Norian deposits from around the world appear to driven either by autocyclic processes or by Milankovitchian eustasy (Olsen and Kent, 1999; Muttoni et al., 2004; Furin et al., 2006). The late Triassic and early Jurassic time scale calibrated to Milankovitchian periodicities was constrained by Olsen and Kent (1999) in their studies of the Newark rift basin, New Jersey. The Newark rift

basin is filled by ca. 15 km of dominantly lacustrine deposits that are profoundly cyclic. Time series analysis using sediment color and depth rank tuned to the 404 kyr eccentricity both indicate frequencies within the series that are equivalent to those expected from Milankovitchian astronomical forcing. Work from the Dolomites corroborates this conclusion. Both Bosellini and Hardie (1985) and Goldhammer et al. (1990) argue for Milankovitchian control over diagenetically-capped megacycles in the upper portion of the Dolomia Principale and Dachstein Limestone. Central to this interpretation (similar in many ways to the Latemar) was the observation that subaerial exposure caps directly overlie subtidal facies in the upper DP, implying a eustatic driver. Indeed, the previous chapter of this volume details the systematic change in bundling trends from landward 3:1 bundles to seaward 5-6:1 “Milankovitch-like” bundles within the DP of the Dolomites.

Radiometric dating within the Dolomia Principale in the Dolomites has never been done. Biostratigraphic correlations based on ammonoids and dasycladales place the DP in the Norian, but empirical data relating to periodicities of depositional cycles remains unobtained. However, new dating of Norian ash deposits in Southern Italy combined with biostratigraphy, magnetostratigraphy and stable isotope stratigraphy has led several workers to conclude that the Carnian-Norian boundary ought to be moved from the current ICS date of 216.5 Ma to 227.5 Ma, thereby shortening the middle Triassic and lengthening the Norian (**Figure 6. 4**) (Muttoni et al., 2004; Furin et al., 2006). In addition, both Muttoni et al. (2004) and Furin et al. (2006) conclude that magnetostratigraphy and biostratigraphy link the late Triassic limestone

successions of both Southern Italy and Sicily with the Milankovitch-tuned Newark series of Olsen and Kent (1999). This “long Norian” time scale certainly allows for (if not fully supports) Milankovitchian forcing through the DP of the Dolomites. Cycle stacking data from this dissertation (*see* Chapter 4) indicates that the DP depositional cycles were generated by a mixture of Milankovitchian orbital forcing and differential subsidence. This presents a conundrum in that early and mid-Triassic deposits appear to have been deposited at sub-Milankovitch periodicities (*see* Mundil et al., 1996, Zühlke, 2004, Kent et al., 2004, and Emmerich et al., 2005) while late Triassic carbonates appear to have been deposited at Milankovitchian periodicities without any change in facies type or stacking patterns. A “short” lower and middle Triassic coupled with a “long” late Triassic has profound implications for the identification of the developmental processes related to the carbonate cycles of the Alpine Triassic.

CHANGING CONDITIONS THROUGH THE TRIASSIC

If the “short” lower/mid Triassic / “long” upper Triassic interpretation is correct, a slowdown in carbonate production must have occurred between the mid Triassic (in this case likely late Carnian) and the late Triassic (likely base Norian) (**Table 6. 2**). This is because age constraints on cyclic successions of Anisian and Ladinian platforms dictate a cyclic driver of sub-Milankovitchian periodicity (ca. 1-4 kyr per cycle), while cyclic successions of Norian and later ages can be shown to have formed at timescales consistent with Milankovitchian periodicities (ca. 20 kyr per cycle). Yet, shallowing-upwards facies successions within many mid-Triassic and late Triassic carbonate platforms are nearly identical (e.g. ,Mendola vs. DP). It is difficult to imagine how nearly identical facies

successions are produced by cyclic drivers with nearly an order of magnitude difference in temporal rhythm. However, a literature search has revealed several trends through Triassic time that may lend credence to the idea of a sedimentary slowdown from middle Triassic to late Triassic time, although additional work will be needed to prove this idea empirically.

In the Dolomites, an obvious difference between carbonate rocks of mid Triassic age and late Triassic age is the platform size upon which carbonates grew. Platforms in the early through mid Triassic of the Dolomites are small, many encompassing no more than a few 10s of km^2 surface area (e.g., Latemar and Cernera platforms) (Bosellini, 1991). By contrast, platforms of late Triassic age were deposited on regional-scales of many 100s to 1000s of km^2 in area. This has been attributed to the infilling of depositional bathymetry by fluvial and marginal marine clastics (Dürrenstein and Raibl formations) prior to the deposition of the Dolomia Principale carbonate shelf (Bosellini, 1991). The flattening of bathymetry eliminated outstanding antecedent topography, leading to the development of a broad carbonate shelf over a relatively flat area. While the area of carbonate production changed from Carnian to Norian, it is unknown how this would have affected the rates of carbonate production. Theoretically, it would be possible, given longer residence times of waters on the shelf, comparably higher rates of evaporation and/or stagnation over a larger area, that the health of the carbonate factory might not have been as robust on a larger shelf.

Demicco and Hardie (2002) suggest that residence time and depth of waters on platform are a major control on rates of $CaCO_3$ deposition on "larger" platforms such as the Great Bahama Bank. They developed a numerical model was created to calculate $CaCO_3$ production using residence time and water as variables with equilibrium thermodynamics used to calculate $CaCO_3$ loss from seawater over the model Bank. Modeling indicates that sediment production is most rapid on platform margins and rapidly falls off into the platform, approaching zero in the shallowest, innermost portions of the platform. In addition, they suggest that in the cases of larger platforms (e.g., the size of the Great Bahama Bank and larger), shallow, peritidal areas may become areas of sediment trapping rather than sediment production due to both shallow conditions and extended residence times of waters in interior areas of the platform. In the case of the Triassic of the Dolomites, smaller early and mid-Triassic platforms may have had the sedimentary "advantage' of being smaller, allowing for shorter residence times and better on-platform circulation. In contrast, late Triassic shelves such as the DP would have had both longer residence times for on-platform waters and a larger overall area in peritidal and supratidal conditions at any given time. These distinct differences in platform size alone may set up a contrast in carbonate sedimentary potential through the Alpine Triassic.

Other environmental changes across Triassic time require isotopic analyses to determine. Estimation of ancient atmospheric carbon dioxide levels has been determined using a carbon isotope record in pedogenic carbonate, and indicates a general trend of rising pCO_2 from early through late Triassic time (**Figure 6. 5**) (Ekart et al., 1999). Atmospheric carbon dioxide levels were determined using a

formula relating the $\delta^{13}C$ of pedogenic carbonate and the $\delta^{13}C$ and pCO_2 of the atmosphere (Ekart et al., 1999). Ekart et al. (1999) report an increase from ca. 1000 ppmV to ca. 2000 ppmV from the early Triassic to the late Triassic. Modern levels of pCO_2 stand at ca. 380 ppmV. Increase in pCO_2 is important, as it relates directly to the precipitation of inorganic carbonate in the marine realm. The dissolution and precipitation of carbonate is controlled by pH, which is directly affected by the amount of CO_2 dissolved in water (Tucker and Wright, 1992). When CO_2 is dissolved in water, pH increases via the following series of reactions:

$$H_2O + CO_2 \longleftrightarrow H_2CO_3 \text{ (carbonic acid)}$$

$$H_2CO_3 \longleftrightarrow H^+ + HCO_3^- \text{ (bicarbonate ion)}$$

$$HCO_3^- \longleftrightarrow H^+ + CO_3^{2-} \text{ (carbonate ion)}$$

This series of reactions causes carbonate to remain in solution rather than precipitate (Tucker and Wright, 1992). If $CaCO_3$ reacts with H_2O and CO_2, the following reaction occurs:

$$H_2O + CO_2 + CaCO_3 \longleftrightarrow Ca^{2+} + 2HCO_3^-$$

If CO_2 is removed, the reaction remains to the left, and $CaCO_3$ precipitates. If excess CO_2 is present in water, the reaction goes to the right and $CaCO_3$ remains in solution. Increased atmospheric pCO_2 drives more CO_2 into seawater while also preventing degassing of water-borne CO_2 into the atmosphere, thus making inorganic precipitation of $CaCO_3$ increasingly difficult (Tucker and Wright, 1992). Increasing atmospheric pCO_2 through the Triassic may have played a role in limiting the sedimentary potential of the carbonate factories of the Dolomites over time. In the same way, the relatively low pCO_2 in the early Triassic may have

aided carbonate production such that high accumulation rates were possible and cycles were able to record sea level oscillations at millennial periodicities.

Along with a general rise in pCO_2 through the Triassic, estimates of mean paleotemperature of ocean water suggest the paleotemperature fell ca. 4°C from the beginning to the end of the Triassic (Veizer et al., 2000, fig. 3) (**Figure 6. 6**). Paleotemperature anomalies were derived from $\delta^{18}O$ values of unaltered marine bivalve shells taken from low-latitude, shallow water, carbonate-producing environments. As with pCO_2, temperature directly affects the ability of waters to precipitate inorganic carbonate. The relationship between dissolved gasses and their concentration in waters is given by Henry's Law, which states that the concentration of gas in a liquid is directly proportional to the partial pressure of the gas above the solution (Atkins and de Paulo, 2002). However, the solubility of gases is temperature-dependent, as the solubility of gases generally decreases with increasing temperature (Atkins and de Paula, 2002). Therefore, the cooling of seawater and increase in pCO_2 means that both more CO_2 is available to go into solution in seawater, and the solubility of that CO_2 will generally increase through the Triassic as temperature drops. Both of these parameters may have limited the ability of carbonate systems to precipitate inorganic carbonate in the late Triassic.

Along with trends in pCO_2 and paleotemperature, trends in the speciation of marine organisms appear to indicate a gradual decline in diversity of flora and

fauna through the Triassic, from the post P-T extinction recovery through to the end-Triassic mass extinction. Three separate groups were examined- Dasycladacean algae, ammonoids, and foraminifera. Dasycladacean algae are a form of green algae common in carbonate producing environments, and may be a major producer of micrite and allochem debris within sheltered lagoonal environments (Tucker and Wright, 1992). Remains of Dasycladacean algae are common in platform-interior cyclic successions of the Dolomites and can be easily identified in both the Latemar and DP successions. With few exceptions, the biodiversity of dasycladacean algae fluctuates in-phase with paleotemperature (Aguirre and Riding, 2005) (**Figure 6. 7**). In this case, biodiversity of Dasycladacean forms decreases through the Triassic with paleotemperature, eventually reaching an all time low (other than during the PT extinction) in the mid-Jurassic (Aguirre and Riding, 2005). It is unknown how species diversity relates to algal density in this case, or if Codiacean algal forms fluctuated in diversity at like phase and amplitude to Dasycladacean forms. What can be said, however, is that the diversity of a commonly found carbonate sediment-producing organism decreases through the Triassic. If the density of the algal community decreased in a likewise fashion, it would undoubtedly affect a carbonate system's ability to sediment at high rates. A study of ammonoid taxonomic and morphologic patterns by McGowan (2004) identified decreases in both number of genera and morphological variance of ammonoid taxa through the Triassic (**Figure 6. 8**). Similar trends of declining rates of speciation and

increasing in rates of extinction in Triassic foraminifera are documented by Marquez (2005) (**Figure 6. 9**).

The culmination of the declines in speciation was the end-Triassic extinction, one of the five largest known extinctions in earth history, in which ca. 80% of all species went extinct (Sepkoski, 1996; Huynh and Poulsen, 2005). In the marine realm, Benton (1995) estimated familial extinction rates at 12.7-16.9 %. Hallam and Goodfellow (1990) suggest that nearly all reef building organisms went extinct, along with significant extinctions in cephalopods, bivalves, gastropods and brachiopods (Hallam and Wignall, 1997; Huynh and Poulsen, 2005). Microorganisms in the marine realm fared little better, with mass extinctions affecting ostracodes, forams, coccoliths, radiolarians, and dinoflagellates (Bown and Lord, 1990; Huynh and Poulsen, 2005). The cause for the end-Triassic extinction is still hotly debated, with several theories proposed, including volcanism, bolide impact, sea level changes, anoxia, and rising pCO_2 (Huynh and Poulsen, 2005). In terms of impact on the marine realm, however, it seems likely that whatever the cause of the extinction, the shallow marine carbonate community may have shown signs of a depositional slowdown in the late Triassic, which may have been an ecological red flag indicating the approach of dire ecological conditions. This idea makes sense in the context of Alpine carbonate deposition, with most of the southern Alpine carbonate system having

been “drowned” or otherwise “foundered” by middle Jurassic time (Bosellini, 1991).

Of additional importance is the biotic composition of mid and late Triassic platforms. In a quantitative compositional analysis of the Carnian portions of the Sella Massif in the Dolomites, Keim and Schlager (2001) identify *automicrite* (in-situ-formed autocthonous micrite appearing as laminoid-peloidal, thrombolitic-peloidal and/or crustal masses of clotted micrite, possibly formed by blue-green algae or in association with sponges), along with associated microorganisms such as *Tubiphytes* and marine cements were shown to have formed the bulk of the sediment from the platform top to toe of slope depth so up to 200 m. Specifically, platform top sediments were shown to contain 41% automicrite and 35% marine cements, margin-upper slope sediments contain 29% automicrite and 48% marine cements, and lower slope sediments contain 28% automicrite and 27% early marine cements. In total, the amount of skeletal grains on the platform is <10%. This is in direct contrast to deposits of the latest Carnian Cassian and Dürrenstein dolomite, which have a much larger composition of skeletal grains (ca. 30%) including branching corals, dasycladacean algae, and various bivalves. Automicrite is thought to have been deposited as a result of organic processes, mainly due to its close depositional relation to various microproblematica including tubiphytes, as well as higher percentages of organic carbon than surrounding deposits. High proportions of automicrite,

microproblematica, and marine cements in all depositional realms of the Sella, from shallow marine platform top to aphotic toe-of-slope environments suggest that the deposition of a majority of Sella carbonates may have been driven by microbial carbonate production that was likely at its highest production peak in the late Ladinian and early Carnian. Unpublished dates from Keim and Schlager (2001) indicate that during this time, the Sella was able to produce sediment at the rate of 0.6 m/kyr in the vertical direction, while slopes prograded at 1.6m/kyr at the same time. These rates are consistent with both modeled and published rates of deposition suggested for the Anisian/Ladinian Latemar platform given the sub-Milankovitchian depositional paradigm of either Zühlke et al. (2003) or Emmerich et al. (2005). The volumetric increase in skeletal allochems in the latest Carnian deposits of the Sella may signal an environmental shift that limited the biotic output of carbonate sediment from automicrite-producing organisms. It is unknown if the increase in proportion of skeletal allochems to microproblematica and automicrite is related to other declines in speciation known to have occurred during the late Triassic.

IMPLICATIONS

If empirical data relating to the timing of mid and late Triassic depositional sequences (e.g., long Norian vs. ICS Norian) and changing environmental conditions across the middle and late-Triassic is correct, a depositional "slowdown" must have occurred from middle Triassic to late Triassic time in the

carbonate factories of the Dolomite Alps. If this is the case, this slowdown has been identified primarily though dating of three ashfall tuffs intercalated within the cyclic carbonates of the Latemar platform and comparing the resultant cycle periodicities to those of the late Triassic. Biostratigraphic and magnetostratigraphic correlations aid in transferring information from one locality to another, which is the case in the circumstance of the "long Norian" as applied to the Dolomites. The "long Norian", boundary ages were determined using biostratigraphy, magnetostratigraphy, and U-Pb series dating of only eight zircon grains from one ash bed in a pelagic carbonate succession in southern Italy (Muttoni et al., 2004; Furin et al., 2006). The accuracy of these ages is critically important to the argument. Bolstering the argument for the long Norian are the dates of Mundil et al. (2003) for the Latemar limestone that indicate that the entire cyclic succession may have been deposited in ca. 2.2 million years. This has led proponents of the long Norian to agree that the Norian can be lengthened at the expense of the Anisian/Ladinian (Muttoni et al, 2004, Figure 10, p. 1055). However, the validity of the Anisian/Ladinian dates and their implications for mid-Triassic cyclostratigraphy are still somewhat controversial. For instance, while Mundil et al. (2003) argue that empirical data indicate the Latemar sedimented with cyclic periodicities of sub-Milankovitch rhythm, Mundil et al. (2001) warns:

"even large suites of very high-quality, single-zircon U–Pb analyses for these tuffs cannot, in most cases, yield objective, reliable, and robust dates with accuracies at the sub-myr level – though the temptation to perform arbitrary selection of subsets of the analyses for that purpose is almost irresistible." (p.131-132)

While this warning sounds reasonable, Mundil et al. (2003) do date beds to sub-million year accuracies, determining the duration of sedimentation in the Latemar platform despite having an age reversal within the series of three dates (Mundil et al., 2003, fig. 2, p. 84). Instead of discounting the reversal, Mundil et al. (2003) perform a linear regression through the data (including error bars) allowing the conclusion to be made that the platform accumulated in ca. 2.2 million (in contrast to the 10-12 m.y. of Goldhammer et al., 1987 or refined 9.14 m.y. timescale of Preto et al., 2004).

The implications of the shortened mid-Triassic on cyclostratigraphy are numerous. Of primary concern is identification of a composite allocyclic driver that can force multi-frequency depositional cyclicity at sub-Milankovitch periodicities. Proposed drivers include tidal forcing at millennial frequencies (Munk et al., 2001, who conclude that while this does occur, the amplitude is mm-scale), Bond cycles and/or Heinrich events (cycles in ice-rafted debris) (Bond et al., 1997; 2001; Chappell, 2002; Lambeck et al., 2002), and thermal expansion of the water column (Schulz and Schäfer-Neth, 1997 indicate that an increase in deep-water temperature of approximately 2°C can generate a sea level rise of 1.7 m by thermal expansion via increased formation of warm deep waters in low latitudes) (**Table 6. 3**).

However, it must be noted that no link between sea level oscillations with millennial periodicities and the formation of shallowing-upwards carbonate depositional cycles has yet been established in any Holocene and Pleistocene setting. Modern carbonate depositional cycles date from approximately 6 kyr, and are one shallowing-upward succession of facies (i.e., un-stacked, or in other words, no stacked periodic millennial frequency depositional cycles are found) many having not yet aggraded to sea level (see Table 3). While arguments surrounding the origin and drivers of cyclic sedimentation continue within both the pure Milankovitch and sub-Milankovitch camps, neither has expressly negated the conclusion that the Latemar cycles are a sedimentological record of an extrabasinal forcing mechanism. Therefore a primary implication of accepting the short mid-Triassic/long Norian ages are that depositional cycles within the early and mid-Triassic record some of the most rapid accumulation rates of platform carbonates in geologic history, followed immediately by a drop-off in accumulation rates in the late Triassic. If this is the case, the accumulation rates of carbonate cycles hinges on the ability of the carbonate-producing community to make sediment and fill accommodation at a rate consistent with a given cyclic driver.

Accepting a sub-Milankovitch driver for early and mid-Triassic cycles and a Milankovitchian driver for both late Triassic and Pleistocene/Holocene cycles also calls the very use of time series analysis in carbonate sedimentology into question. While there seems to be little doubt that many mid-Triassic carbonate

deposits (e.g., Latemar and Mendola successions) formed as the result of a series of eustatic drivers, use of time series analysis originally led to the conclusion that the Latemar cycles formed as a result of Milankovitchain composite eustasy (*see* Hinnov and Goldhammer, 1991; Preto et al., 2004). In this study, it is the use of both published dates for the Norian along with time series analysis on the DP cyclic succession of the Dolomites that has led to the hypothesis that the DP formed as a result of Milankovitch forcing with the rhythmic signal somewhat muted by differential subsidence. However, spectral analysis of the Latemar cyclic series generates frequency plots that are Milankovitchian in their character, as are those of the DP in the eastern Dolomites. What must be established then, is whether frequency matching of depositional successions to Milankovitchian eustatic cycles is evidence enough to suggest a link between depositional cycle and astroclimatic forcing.

There is yet to be resolution to the debate on whether Latemar cycles formed at Milankovitchian periodicities or not. There does, however, seem to be broad (although not proven) consensus that late Triassic platform carbonates did form at periodicities consistent with Milankovitch forcing, which is in apparent agreement with stratigraphic analysis of DP sections presented in this manuscript. The implications of the “short” mid Triassic / “long” late Triassic challenges fundamental concepts related to Alpine cycle periodicity outlined in such publications as Fischer (1964); Bosellini and Hardie (1985) and Goldhammer et al. (1990). Namely, if the “short” mid Triassic / “long” late Triassic date are correct, they imply that a depositional “slowdown” took place in

platform carbonate settings from the mid Triassic through the late Triassic. Interestingly, this “slowdown” appears to have coincided with several environmental shifts that directly affect marine carbonate production, including and increase in atmospheric pCO_2 of ca. 1000 ppmV from mid to late Triassic, a drop in mean shallow water ocean temperature of 4^{o}C through the Triassic, and a drawdown in marine speciation throughout the Triassic that culminated in one of the 5 largest extinctions in earth history. Clearly, additional dates in Triassic platform carbonates successions are necessary before this hypothesis can be confirmed or disproven.

DISCUSSION AND CONCLUSIONS

In order to draw any conclusions about the hierarchy of stratigraphic forcing in the Alpine Traissic based on current data, one must be willing to accept that carbonate sedimentation and the recording of sea level oscillations changed by order of magnitude from the early/mid Triassic to the late Triassic. If carbonate accumulation rate slowdown from mid to late Triassic was indeed caused by multiple environmental issues, then the cyclic mechanisms recorded by shallowing-upward depositional cycles must be of different periodicities – an effect of carbonate’s ability to sediment at rates consistent with relative sea level oscillations. If current dates reported by Mundil et al. (1996), Zühlke (2004), Kent et al. (2004) and Muttoni et al. (2004) are accepted, then early and mid-Triassic carbonate depositional cycles record sea level oscillations with periodicities of ca. 1-4 kyr., while depositional cycles of both the Dolomia Principale and Pleistocene/Holocene formed at periodicities consistent with Milankovitch forcing. This is an important realization for numerous reasons. First, facies successions

of some mid Triassic cycles are nearly identical to those of late Triassic and Pleistocene/Holocene cycles, including mud rich subtidal facies with laminite caps (compare Mendola cycles to DP, Dachstein, or Bahamian tidal flat cycles). In theory, this means that in a comparative sense, depositional facies successions and thicknesses cannot be used for approximation of temporal periodicity with any degree of certainty, even if facies successions are *identical*. This is an important realization because it also suggests that early and mid-Triassic tidal flat deposits had *accumulation rates* approaching the *sedimentation rates* of many modern shoal and reef systems (*see* Schlager, 1981, fig.5). However, if tidal flats function as sedimentary sinks, then these high accumulation rates would actually reflect lagoonal sedimentation rates and onshore transport of sediment rather than actual in-situ growth of supratidal deposits. As a result, high sedimentation rates in early and mid Triassic platformal carbonates would translate into high sedimentation rates of contemporaneous tidal flat deposits, while similar deposits in the late Triassic and Holocene have comparably slower rates of formation.

Whether or not frequency analysis can serve as primary evidence for Milankovitch forcing, the existence of apparent composite, sub-Milankovitchian cyclic successions that have cycle frequencies that appear Milankovitchian requires the existence of eustatic driving mechanisms that are yet unidentified in any Holocene setting. Such sub-Milankovitch eustatic drivers must only be active during certain periods of geologic time (e.g., early and mid Triassic) *or* are only recorded as depositional cycles during times when both the subsidence and sedimentation rates of platform carbonates are particularly high and able to

record them. In either case, no such drivers have yet been discovered in the Holocene record of carbonate depositional cycles. It may be, then, that the early and mid Triassic were particularly unique periods of carbonate sedimentation, perhaps recording some of the most rapid accumulation rates of platform carbonates in geologic history, followed immediately by a drop-off in accumulation rates. The only way to finally solve this problem is to generate datasets from multiple locations that include both dates and measured sections through mid and late Traissic sediments that show like trends in the timing of depositional cycles.

The plausibility of the existence of depositional cycles with sub-Milankovitch periodicities does not necessarily change the fundamental observation that carbonate depositional cycles are nested into cycles of ever-lower frequency. It does, however highlight the importance of obtaining high-resolution age dates before assuming cycles were formed by periodic drivers. In addition, it highlights the complexity of nature and our ability (or inability) to read and understand the history of the geologic record. It is easy to simply conclude that the geologic record is a great “misthaufen” (dung-heap) of badly-recorded cyclic processes of various periodicities (Schwarzacher, *pers. commun*.). However, it is more optimistic to conclude that we are yet to fully understand the true nature of cyclic forcing through time, such that we may not recognize the degree to which the stratigraphic record is a reflection of deterministic forcing versus muddled stochastic processes.

REFERENCES

Aguirre, J., and Riding, R., 2005, Dasycladacean algal biodiversity compared with global variations in temperature and sea level over the past 350 myr: PALAIOS, vol. 20, p. 581-588.

Atkins, P., and de Paula, J., 2002, Physical Chemistry: W.H. Freeman and Co, New York, NY, 1140 p.

Benton, M.J., 1995, Diversification and extinction in the history of life: Science, vol. 268, p. 52-58.

Bond, G., Showers, W., Cheseby, M., Lotti, R., Almasi, P., deMenocal, P., Priore, P., Cullen, H., Hajdas, I., and Bonani, G., 1997, A Pervasive millennial-scale cycle in North Atlantic Holocene and glacial climates: Science, v. 278, p. 1257-1266.

Bond, G., Kromer, B., Beer, J., Muscheler, R., Evans, M.N., Showers, W., Hoffman, S., Lotti-Bond, R., Hajdas, I., and Bonani, G., 2001, Persistent solar influence on North Atlantic climate during the Holocene: Science, v. 294, p. 2130-2136.

Bosellini, A., 1991, Geology of the Dolomites: An introduction: Dolomieu Conference on carbonate platforms and dolomitization. Ortisei, 43 p.

Bosellini, A., and Hardie, L.A., 1985, Facies e cicli della Dolomia Principale delle Alpi Venete: Memorie della Societa Geologica Italiana, v. 30, p. 245-266.

Bown, P.R., and Lord, A.R., 1990, The occurrence of calcareous nannofossils in the Triassic-Jurassic boundary interval: Cahiers de l'Universite de Lyon, Serie Scientifique, v. 3, p. 127-136.

Chappell, J., 2002, Sea level changes forced ice breakouts in the last glacial cycle: new results from coral terraces: Quaternary Science Reviews, v. 21, p. 1229-1240.

Cozzi, A., and Hardie, L.A., 2003, Third-order depositional sequences controlled by synsedimentary extensional tectonics: evidence from Upper Triassic carbonates of the Carnian Prealps (NE Italy): Terra Nova, v. 15, p. 40-45.

Demicco R.V., and Hardie, L.A., 2002, The 'carbonate factory' revisited; a reexamination of sediment production functions used to model deposition on carbonate platforms,: Journal of Sedimentary Research, v. 72, is. 6, p. 849-857.

Ekart, D.D., Cerling, T.E., Montanez, I.P., and Tabor, N.J., 1999, A 400 million year carbon isotope record of pedogenic carbonate: implications for paleoatmospheric carbon dioxide: American Journal of Science, v. 299, p. 805-827.

Emmerich, A., Glasmacher, U.A., Bauer, F., Bechstädt, T., and Zühlke, R., 2005, Meso-/Cenozoic basin and carbonate platform development in the SW-Dolomites unraveled by basin modeling and apatite FT analysis: Rosengarten and Latemar (Northern Italy): Sedimentary Geology, v. 175, is. 1-4, p.415-438.

Fischer, A.G., 1964, The Lofer Cyclothems of the Alpine Triassic: Kansas Geological Society Bulletin, v. 169, p.107-149.

Forkner, R.M., Hinnov., L.A., Goldhammer., R.K., and Hardie, L.A., 2006, On the Allocyclic Interpretation of the 'Latemar Cycles' (M. Triassic, The Dolomites, Italy) and Implications for High-frequency Cyclostratigraphic Forcing. SEPM Special Publication in Honor of the Career of R.N. Ginsburg, *In Review*

Furin, S., Preto, N., Crowley, J.L., Bowring, S.A., Rigo, M., Roghi, G., and Gianolla, P., 2006, A new U-Pb age constraint on the Upper Triassic duration from southern Italy: Geophysical Research Abstracts, v. 8, p. 3610.

Goldhammer, R.K., 2003, Cyclic Sedimentation, *in* Middleton, G.V., ed., Encyclopedia of Sediments and Sedimentary Rocks, Springer-Verlag, Netherlands p. 173-185.

Goldhammer, R.K., Dunn, P.A., and Hardie, L.A., 1990, Depositional cycles, composite sea level changes, cycle stacking patterns, and the hierarchy of stratigraphic forcing: Examples from the Alpine Triassic platform carbonates: Geological Society of America Bulletin, v. 102 p. 535-562.

Goldhammer, R.K., Dunn, P.A., and Hardie, L.A., 1987, High-frequency glacio-eustatic sea level oscillations with Milankovitch characteristics recorded in Middle Triassic platform carbonates in Northern Italy: American Journal of Science, v. 287, p. 853-892.

Gradstein, F.M., Ogg, J.G., and Smith, A.G., Agterberg, F.P., Bleeker, W., Cooper, R.A., Davydov, V., Gibbard, P., Hinnov, L.A., House, M.R., Lourens, L., Luterbacher, H.P., McArthur, J., Melchin, M.J., Robb, L.J., Shergold, J., Villeneuve, M., Wardlaw, B.R., Ali, J., Brinkhuis, H., Hilgen, F.J., Hooker, J., Howarth, R.J., Knoll, A.H., Laskar, J., Monechi, S., Plumb, K.A., Powell, J., Raffi, I., Röhl, U., Sadler, P., Sanfilippo, A., Schmitz, B., Shackleton, N.J., Shields, G.A., Strauss, H., Van Dam, J., van Kolfschoten, T., Veizer, J., and Wilson, D., 2004. A Geologic Time Scale 2004. Cambridge University Press, 589 p.

Hallam, A., and Goodfellow, W.D., 1990, Facies and geochemical evidence bearing on the end-Triassic disappearance of the Alpine reef ecosystem: Historical Biology, v. 4, 131-138.

Hallam, A., and Wignall, P.B., 1997, Mass extinctions and their aftermath: Oxford University Press, Oxford, UK, 320 p.

Hays, J.D., Imbrie, J., and Shackelton, N.J., 1976, Variations in the Earth's orbit: Pacemaker of the ice ages: Science, v. 194, p. 1121-1132.

Hinnov, L.A. and Goldhammer, R.K., 1991, Spectral analysis of the Middle Triassic Latemar Limestone: Journal of Sedimentary Petrology, v. 61, p. 1173-1193.

Huynh, T.T., and Poulsen, C.J., 2005, Rising atmospheric CO_2 as a possible trigger for the end-Triassic mass extinction: Palaeogeography, Palaeoclimatology, Palaeoecology, v. 217, p. 223-242.

Imbrie, J., Hays, J.D., Martinson, D.G., McIntyre, A., Mix, A.C., Morley, J.J., Pisias, N.G., Prell, W.L., and Shackelton, N.J., 1984, The orbital theory of Pleistocene climate: support from a revised chronology of the marine $\delta^{18}O$ record, *in* Berger, A., Imbrie, J., Hays, J., and Kukla, G., and Saltzman, B., eds., Milankovitch and climate. Boston, Massachusetts, Reidel, p. 269-306.

Keim, L., and Schlager, W., Quantitative compositional analysis of a Triassic carbonate platform (Southern Alps, Italy): Sedimentary Geology, v. 139, p. 261-283.

Kent, D.V., Muttoni, G., and Brack, P., 2004, Magnetostratigraphic conformation of a much faster tempo for sea level change for the Middle Triassic Latemar platform carbonates: Earth and Planetary Science Letters, v. 228, p. 369-377.

Lambeck, K., Esat, T.M., and Potter, E.K., 2002, Links between climate and sea levels for the past three million years: Nature London, v. 419, is. 6903, p.199-206.

McGowan, A.J., 2004, Ammonoid taxonomic and morphologic recovery patterns after the Permian-Triassic: Geology, v. 32, no. 8, p. 665-668.

Mundil, R., Brack, P., Meier, M., Rieber, H., and Oberli, F., 1996, High resolution U-Pb dating of Middle Triassic volcaniclastics; time-scale calibration and verification of tuning parameters for carbonate sedimentation: Earth and Planetary Science Letters, v. 141, is. 1-4, p. 137-151.

Mundil, R., Metcalfe, I., Ludwig, K.R., Renne, P.R., Oberli, F., and Nicoll, R.S., 2001, Timing of the Permian-Triassic biotic crisis; implications from new zircon U/Pb age data (and their limitations): Earth and Planetary Science Letters, v. 187, is.1-2, p. 131-145.

Mundil, R., Zühlke, R., Bechstadt, T., Brack, P., Egenhoff, S., Meier, M., Oberli, F., Peterhänsel, A., and Rieber, H., 2003, Cyclicities in Triassic Platform Carbonates: synchronizing radio-isotopic and orbital clock: Terra Nova, v. 15/2, p. 81-87.

Munk, W., Dzieciuch, M., and Jayne, S., 2002, Millennial climate variability: Is there a tidal connection?: Journal of Climate, v. 15. p.370-385.

Muttoni, G., Kent, D.V., Olsen, P.E., Di Stefano, P., Lowrie, W., Bernasconi, S.M., and Hernandez, F.M., 2004, Tethyan magnetostratigraphy from Pizzo Mondello (Sicily) and correlation to the Late Triassic Newark astrochronological polarity time scale: Geological Society of America Bulletin, v. 116, no. 9/10, p. 1043-1058.

Olsen, P.E., and Kent, D.V., 1999, Long-period Milankovitch cycles from the late Triassic and early Jurassic of eastern North America and their implications for the calibration of the early Mesozoic time-scale and the long-term behaviour of the planets: Philosophical Transactions: Mathematical, Physical, and Engineering Sciences, v. 357, no. 1757, p. 1761-1786.

Preto, N., Hinnov, L A., De Zanche, V., Mietto, P.,, and Hardie, L.A., 2004, The Milankovitch interpretation of the Latemar platform cycles (Dolomites, Italy): implications for geochronology, biostratigraphy, and middle Triassic carbonate accumulation: SEPM Special Publication no. 81, p. 167-182.

Sander, B., 1951, Contributions to the study of depositional fabrics; rhythmically deposited Triassic limestones and dolomites. English translation by Eleanora Bliss Knopf, 160 p.

Schlager, W., 1981, The paradox of drowned reefs and carbonate platforms: Geological Society of America Bulletin, v. 92, p. 197-211.

Schlager, W., 1999, Scaling of sedimentation rates and drowning of reefs and carbonate platforms: Geology, v. 27, no. 2, p. 183-186.

Schulz, M., and Schaefer-Neth, C., 1997, Translating Milankovitch climate forcing into eustatic fluctuations via thermal deep water expansion: a conceptual link:. Terra Nova, v. 9, no. 5, p. 228-232.

Schwarzacher, W., 1975, Sedimentation Models and Quantitative Stratigraphy: New York, Elsevier, 382 p.

Sepkoski, J.J., 1996, Patterns of Phanerozoic extinction: a perspective from global databases. *In* Walliser, O.H., ed., Global Events and Event Stratigraphy, Springer-Verlag, New York, p. 35-51.

Tucker, M.E., and Wright, V.P., 1990, Carbonate Sedimentology: Blackwell Science, Oxford, UK, 482 p.

Veizer, J., Godderis, Y., and Francois, L.M., 2000, Evidence for decoupling of atmospheric CO_2 and global climate during the Phanerozoic eon: Nature London, v. 408, is. 6813, p. 698-701.

Zühlke, R., Bechstädt, T., and Mundil, R., 2003, Sub-Milankovitch and Milankovitch forcing on a model Mesozoic carbonate platform – the Latemar (Middle Triassic, Italy): Terra Nova, v. 15, no. 2, p. 69-80.

Zühlke, R., 2004, Integrated cyclostratigraphy of a model Mesozoic carbonate platform - the Latemar (Middle Triassic, Italy). in D´Argenio, B., Fischer, A., Premoli Silva, I. and Weissert, H., eds., Multidisciplinary Approach to Cyclostratigraphy,: Society for Sedimentary Geology, Special Publication No. 44.

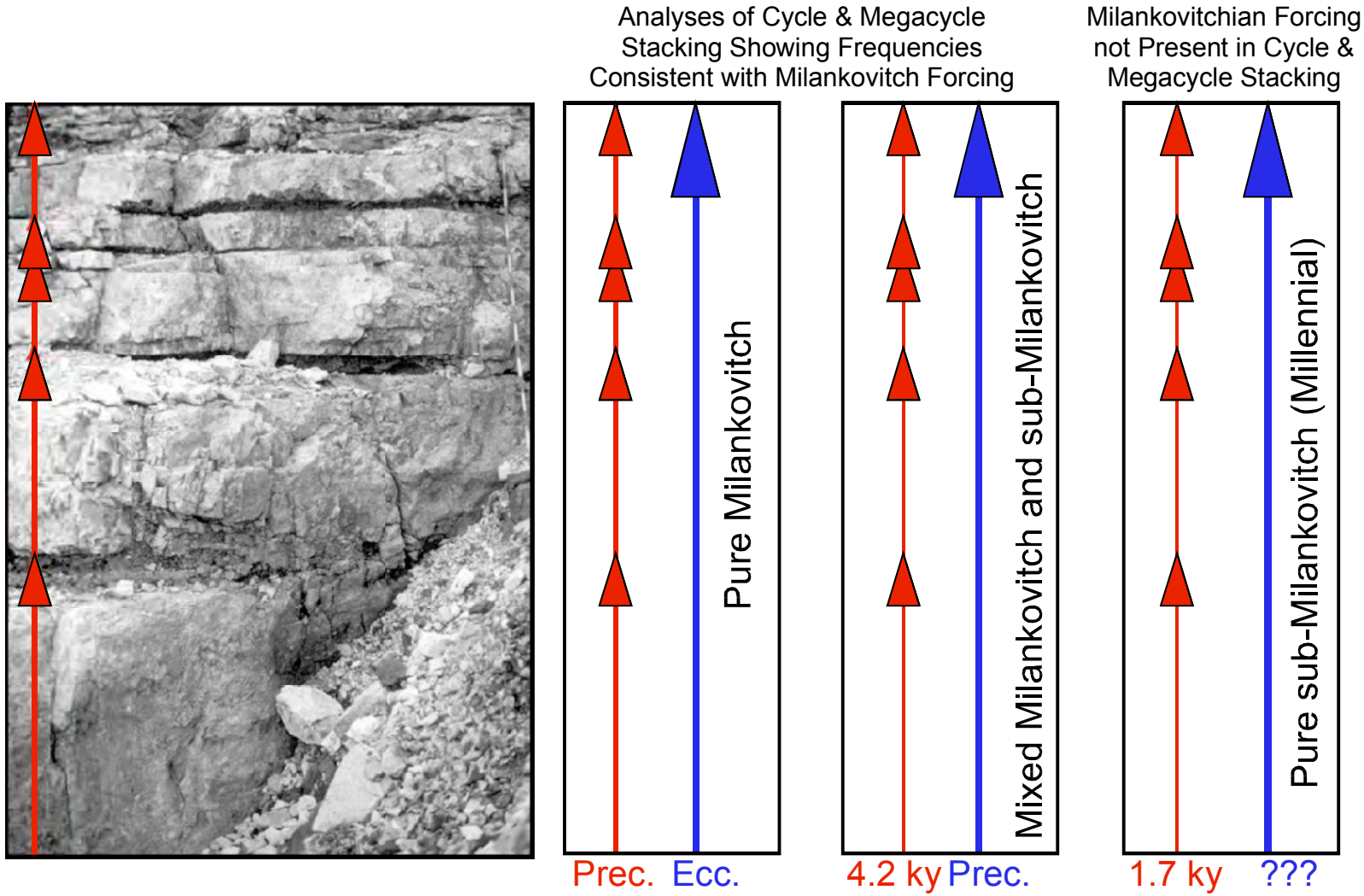

Figure 6.1. Comparison of proposed cyclic driver periodicities for individual cycles and megacycles at the Latemar. Both "Pure Milankovitch" (e.g., Goldhammer et al., 1987; Preto et al., 2004) and "Mixed Milankovitch and sub-Milankovitch" (e.g., Zühlke, 2004) interpret Milankovitchian composite eustasy to have influenced the development of Latemar cycle stacking. The millennial model does not recognize the influence of Milankovitchian forcing on the development of cycles or megacycles at the Latemar. (Note: "Prec" refers to the Precession, and "Ecc." refers to the Eccentricity.)

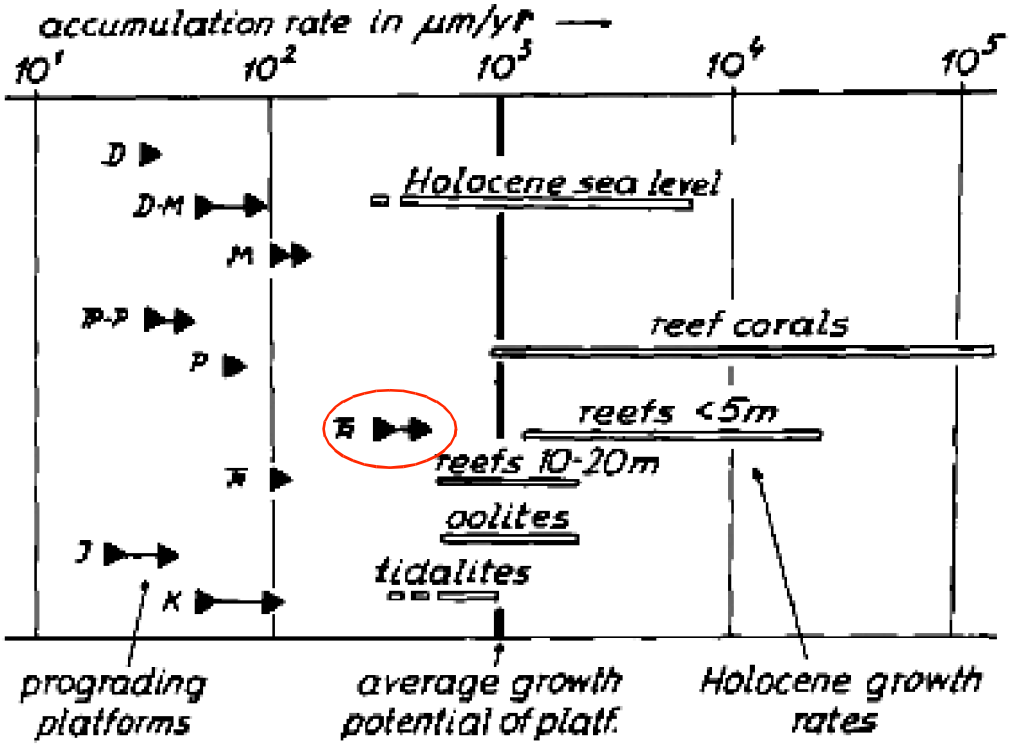

Figure 6. 2. Accumulation rates of carbonate platforms through geologic time plotted against growth rates of Holocene facies groups (recall total accumulation rate and growth rate are not equivalent). The circled data point represents the Carnian of the Dolomites, with the highest reported accumulation rates. Chart from Schlager (1981).

Time	Platform	Rate (μm/yr)	Source
Devonian (Givetian/Frasnian)	Canning Basin	30	Playford and Lowrie (1966)
Devonian-Mississippian (Kinderhookian-Meramecian)	Rocky Mountains	50–80	Rose (1976)
Mississippian (Meramecian-Chesterian)	Rocky Mountains	100–150	Rose (1976)
Pennsylvanian Permian	Sverdrup Basin (Nansen Fm.)	30–40	Davies (1977)
Permian (Guadalupian)	Delaware Basin (Capitan Fm.)	75	Harms (1974)
Triassic (Late Anisian–Ladinian)	Northern Limestone Alps	100	Ott (1967)
(Early Carnian)	Dolomites (Picco di Vallandro)	300–500	Schlager and others, unpub. data
Late Jurassic	Southern Alps (Friuli Platform)	30–45	Winterer and Bosellini (1981)
Cretaceous (Late Albian–Cenomanian)	Tampico Embayment	60–90	Enos (1977, p. 279–286)

Note: Calculated from stratigraphic age bracket reported for the formation, applying absolute time spans indicated in the Phanerozoic time scale, 1964; Cohee (1978); accumulation rates are not corrected for compaction.

Figure 6.3. Rates of accumulation of carbonate platforms through geologic time, from Schlager, (1981). Note that the highest reported accumulation rates presented are from the mid-Triassic of the Dolomites, although the data upon which the rates are based is not included.

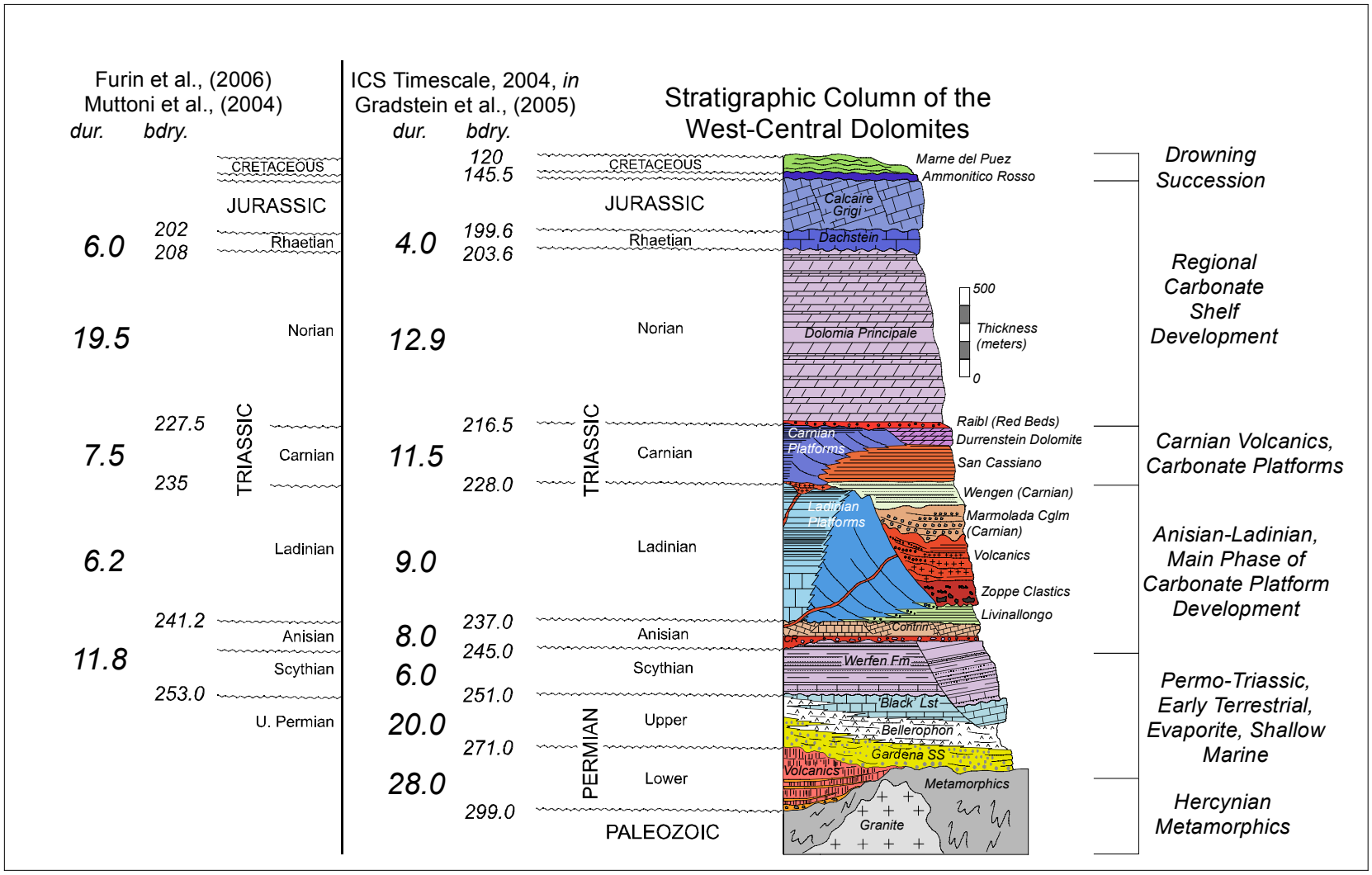

Section modified from Bosellini (1991)

Figure 6.4. Triassic stage dates tabulated per author.

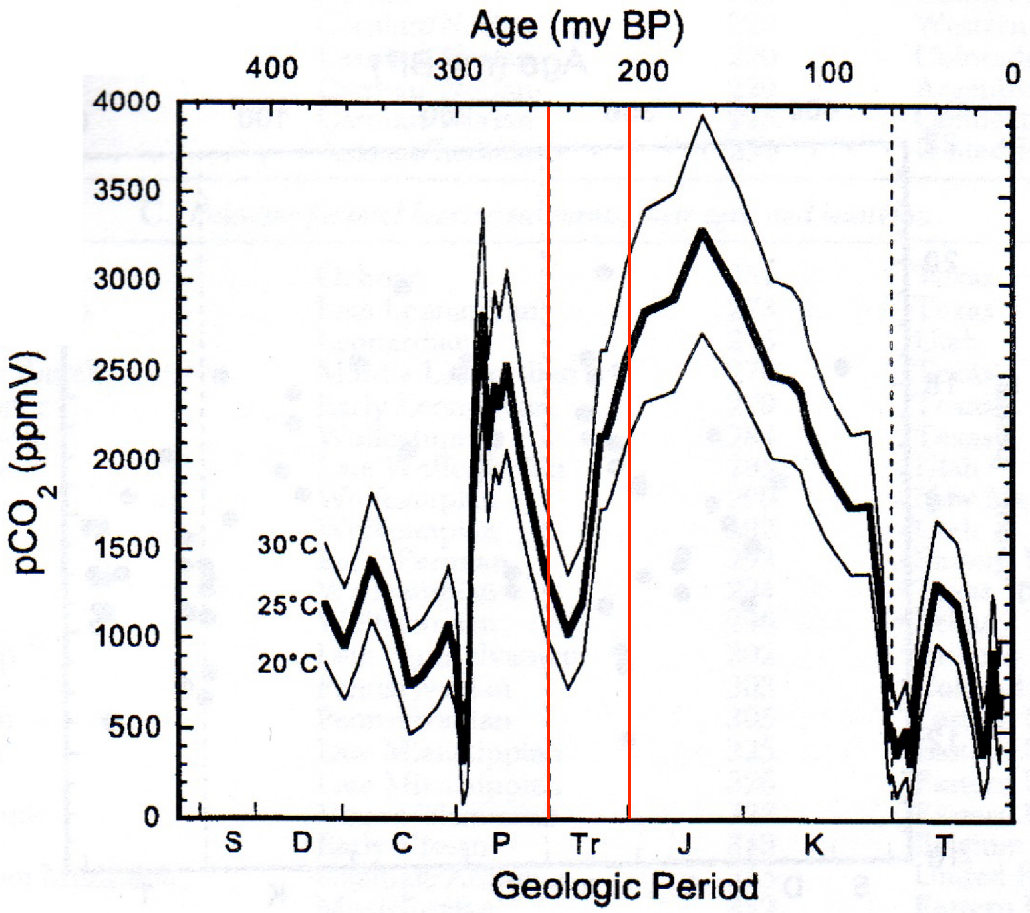

Figure 6. 5. Atmospheric pCO2 calculated from paleosol carbonate nodules, given estimated temperatures of formation of 20, 25, and 30 degrees celsius. While pCO2 levels fall in through the early Triassic, the majority of the Triassic is characterized by increasing pCO2. Increasing pCO2 may limit the precipitation of inorganic carbonate from seawater. From Ekart et al. (1999).

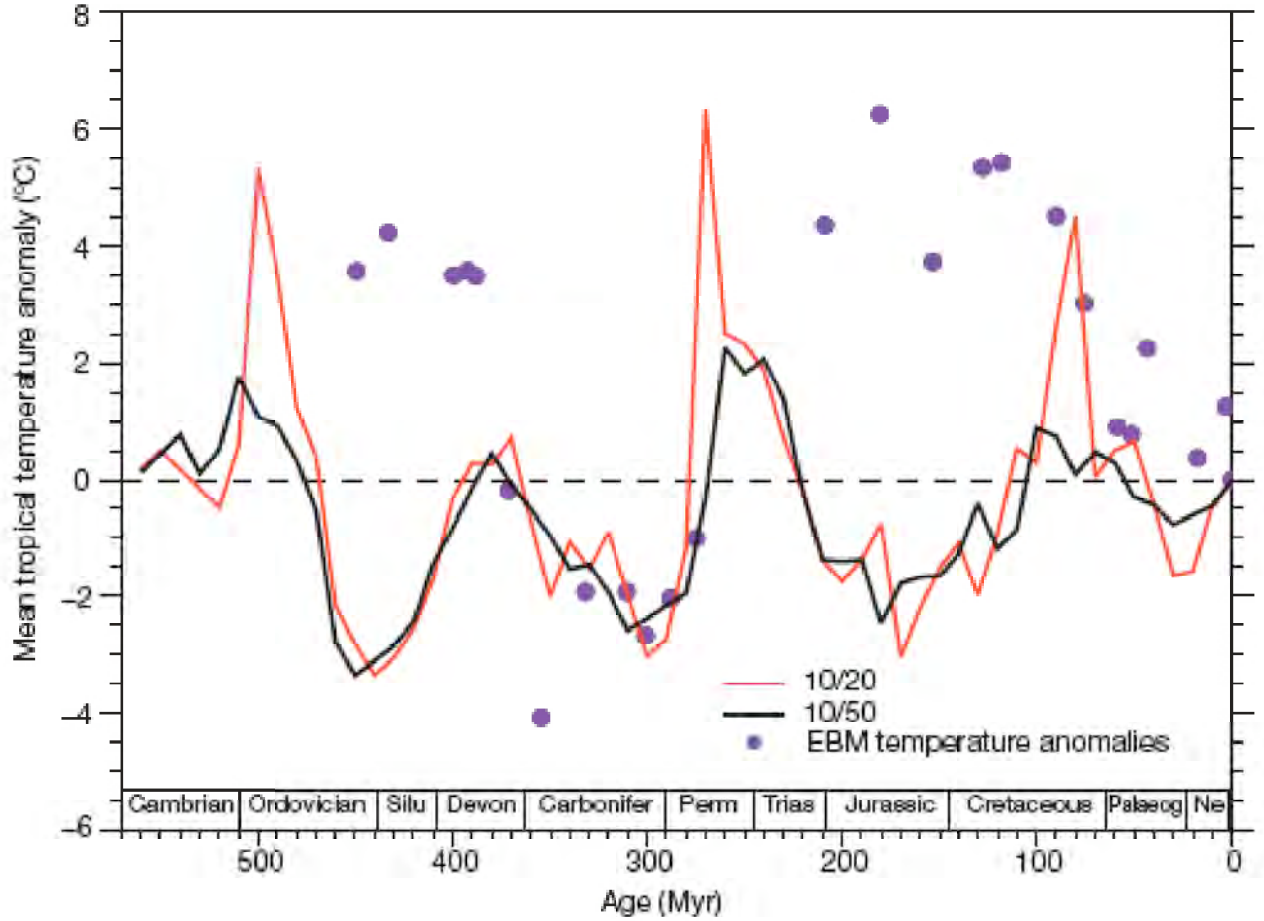

Figure 6. 6. Tropical sea surface paleotemperatures from Veizer et al., (2000). Plot shows temperature data calculated from delta 18O measurements taken from unaltered marine bivalve shells. Red line is a plot of the running mean of the data spread, using a 10 myr step and a 20 myr window. The black line uses a 10 myr step and a 50 myr window. Purple points represent temperature anomalies. Note ca. 4 degree temperature drop through the Triassic.

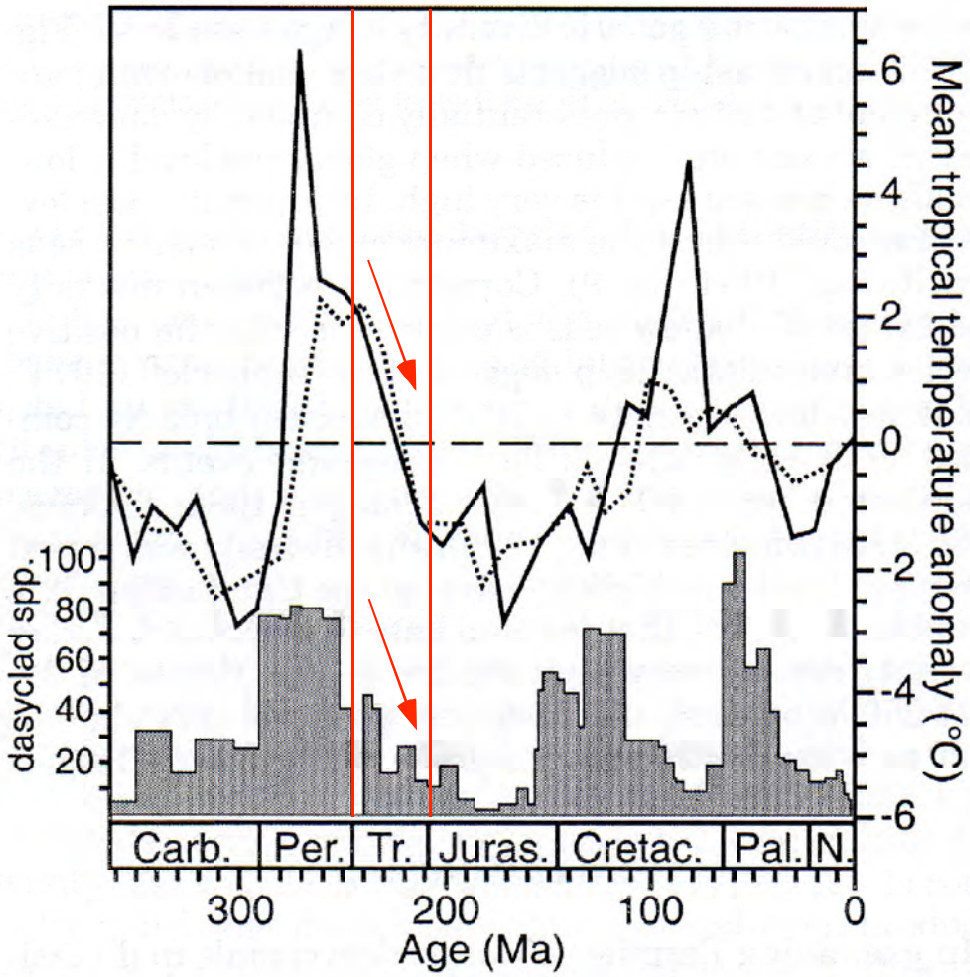

Figure 6. 7. Composite plot of species number data of Dasycladacean algae and ocean paleotemperature data. Triassic time bracketed by red bars. During Triassic paleotemperature dropped by ca. 4 degrees C while the number of species of Dasycladacean alga drops by over 50% (from over 50 species to under 20) Plot modified from Aguirre and Riding, (2005). Data on Dasycladacean algae from Deloffre and Grainier, 1992; Grainer and Deloffre, 1993, 1994; and Bucur, 1999. Paleotemperature data from Veizer et al., (2000) derived from delta O18 from marine shells. Temperature trends are running means at 10 myr time-steps using temporal windows of 20 myr (solid line) and 50 myr (dotted line).

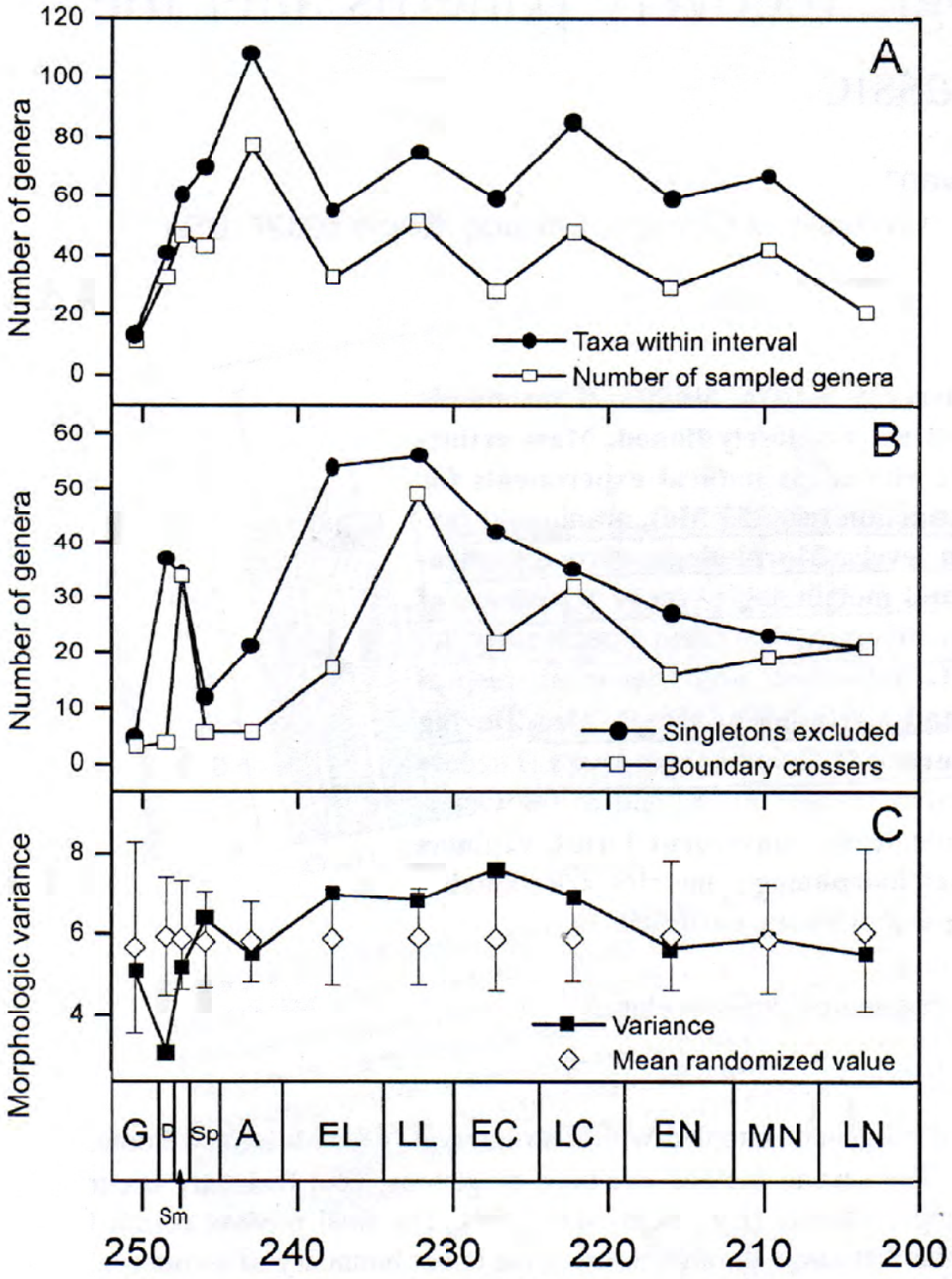

Figure 6. 8. Plots of ammonoid taxonomic data for the Triassic. In plots A &B, clear trends in decreases in number of genera can be observed. The decrease biodiversity may reflect overall weakening of the biotic community through time. From McGowan, (2004).

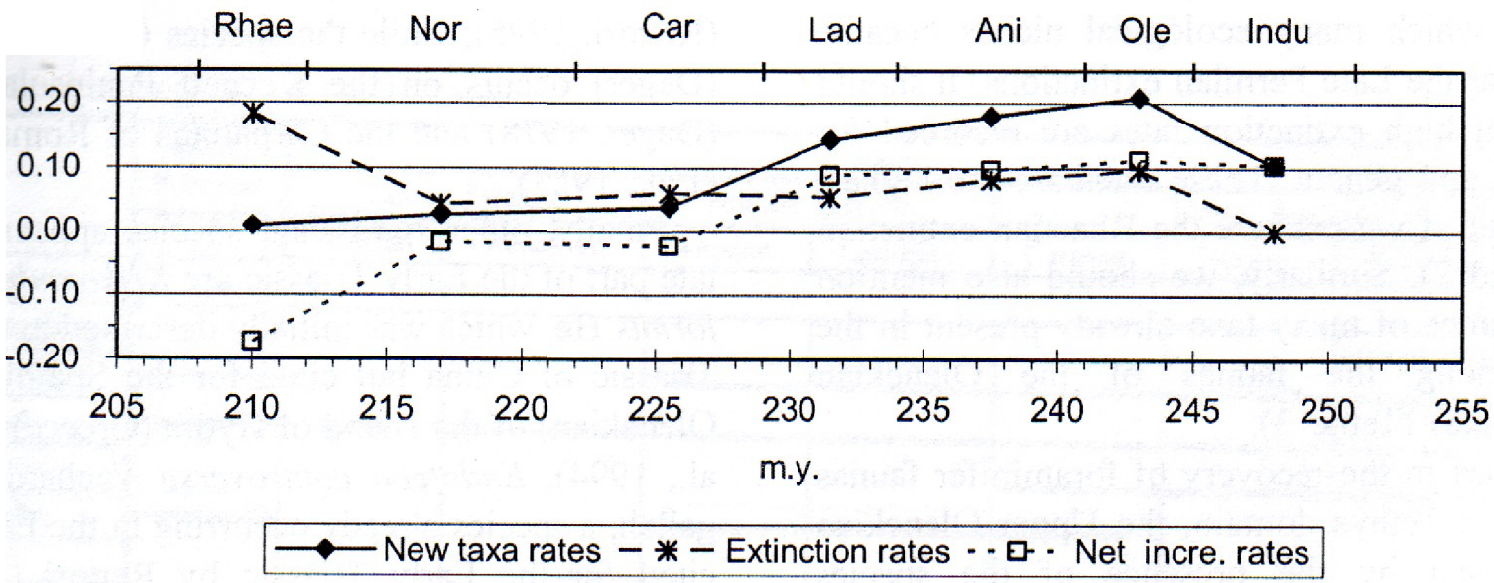

Figure 6. 9. Speciation rates of Triassic Tethyan foraminiferal fauna, showing general decrease in rates of new taxa through the Triassic, as well as a peak in extinction rates at the end of the Triassic. From Marquez (2005).

	Hopkins Group/ Goldhammer et al., (1987)	Heidelberg Group/ Zuhlke et al., (2003)	Kent et al., 2004 Emmerich et al., 2005
Cycle Periodicity	19-23 kyr	4.2 kyr	0.9 - 1.97 kyr
Amplitude	ca. 2 meters	Not defined	Not defined
Megacycle Periodicity	100 kyr	18.1 - 21.5 kyr	Not defined
Amplitude	ca. 1 meter	Not defined	Not defined
3rd Order Periodicity	10 myr	Not defined	Not defined
Amplitude	ca. 60 meters	Not defined	Not defined
Subsidence	passive margin: 0.05 m/kyr	LPF = 0.65 m/kyr	LPF = 0.78 m/kyr
		LCF = 0.27 m/kyr	LCF = 0.62 m/kyr
		MTF = 0.14 m/kyr	MTF = 0.34 m/kyr
		UCF = 0.19 m/kyr	UCF = 0.45 m/kyr
		UTF = 0.185 m/kyr	UTF = 0.43 m/kyr
Sedimentation Rates	0.05 - 0.10 m/kyr	0.65 - 0.70 m/kyr	0.78 - 0.85 m/kyr
Diagenetic Cap/ Caliche Rates	1-2 cm/kyr modern = 2-4 cm/kyr	Not defined	Not defined
Tepee Rates	Not stated, but is consistent with modern rates: Antiform buckling 4 cm/kyr cement fill 0.2-0.4 cm/kyr	Not defined	Not defined

Table 6. 1. Rates of sea level oscillation, subsidence, sedimentation, and diagenesis for the Latemar platform interior as defined per research group. Subsidence rates have been calculated per facies group in some instances. LPF = Lower Platform Facies; LCF = Lower Cyclic Facies; MTF = Middle Tepee Facies; UCF = Upper Cyclic Facies; UTF = UpperTepee Facies. Diagenetic cap / tepee formation rates are not defined by the Heidelberg group or by the Kent / Emmerich studies, but require rates of caliche formation of ca. 25. cm/kyr; rates of antiform bucking of 0.4-4.0 m/kyr and cement fill rates of 0.2-0.4 m/kyr.

Anisian/Ladinian Latemar Platform	***Ladinian/Carnian Sella Massif***	***Norian Dolomia Principale***
Goldhammer et al., (1987) 0.05 - 0.10 m/kyr	Keim and Schlager (2001) 0.6 m/kyr vertical 1.6 m/kyr progradation	This study, with DP = 750 m 0.058 m/kyr (ICS Norian)* 0.035 m/kyr (Long Norian)*
Zuehlke et al., (2003) 0.65 - 0.70 m/kyr		
Emmerich et al., (2005) 0.78 - 0.85 m/kyr		

** These values are accumulation rates*

Table 6. 2. Vertical Sedimentation Rates Through Triassic Time, The Dolomites, N. Italy

Study	Cycle Type	Cycle Period
Roth and Reijmer, 2005	Oxygen isotope excursions in a 30 m-long core from the leeward margin of the Great Bahama Bank related to aragonite content	Multi-millennial
		1.725 kyr
		0.54 kyr
Niggemann et al., 2003	Oxygen isotope excursions in 61-cm stalagmite	ca. 1.450 kyr
Bond et al., 1993, 1997, 2001	Oxygen isotope excursions & Ice-rafted sediment cycles	1.5 kyr DO Cycle 5-6 kyr Bond Cycle
Munk et al., 2001	Tidal forcing - Milennial Scale	1.795 kyr
van de Plassche et al., 1998	Mean high water marks from Hammock River marsh, Clinton, Connecticut, USA	Century-scale

Table 6. 3a. Compilation of dated modern and recent cyclic processes and behaviors with milennial periodicities.

Study	Locality	Depositional Cycle Type	Age of Most Recent S.U. Succession
Strasser and Samankassou, 2003	Florida Bay Bahamas Bermuda	Variable. Shoaling, tidal flat, and subtidal facies successions.	Variable, oldest 5630 bp youngest 680 bp
Gischler, 2003	Belize platforms	Variable. Reefal, shoaling, and subtidal facies successions.	4.5 kyr
Chappell, 2002	Huon Peninsula, Papua New Guinea	Coral Terraces	6-7 kyr
Parkinson 1989	Southwest coast of Florida	T-R cycle, capped by red mangrove peat	ca. 7 kyr
Tudhope 1989	Davies Reef, central Great Barrier Reef complex	Shallowing-up from: gravel lag; bioturbated muddy sand; shoal or exposure cap	Mid-cycle sediments dated at ca. 3 kyr. Actual cycle must be older
Logan et al., 1969	Shark Bay, Western Australia	Shallowing-up from: grainstone; skel. m/w; laminite cap	ca. 5 kyr
Taft et al., 1968	New Providence Platform, Bahamas	Coarsening-up from mud; Skel. P/G; Grapestone GS	6.7 kyr

Table 6. 3b. Compilation of dates of modern carbonate shallowing-upward facies successions. Most have not yet filled accommodation, and none of these examples exhibit stacking of shallowing-upward facies successions.

References

Adams, J.E., and Frenzel, H.N., 1950, Capitan barrier reef, Texas and New Mexico: Journal of Geology, v. 58, is. 4, p. 289-312.

Aguirre, J., and Riding, R., 2005, Dasycladacean algal biodiversity compared with global variations in temperature and sea level over the past 350 myr: PALAIOS, vol. 20, p. 581-588.

Allmendinger, R.W., 2002, Stereonet v. 6.3.3 for Mac OS X

Aigner, T., 1982, Event-stratification in nummulite accumulations and in shell beds from the Eocene of Egypt, *in* Cyclic and event stratification; symposium. Einsele, G., ed., Tuebingen, Federal Republic of Germany, April 25-27, 1980. p. 248-262.

Anderson, R.Y. and Kirkland, D.W., 1966, Intrrabasin varve correlation, Geological Society of America Bulletin, Vo. 77, pp. 241-256.

Alsharhan, A.S., and Kendall, C.G.St.C., 2003, Holocene coastal carbonates and evaporites of the southern Arabian Gulf and their ancient analogues: Earth-Science Reviews, v. 61, p. 191-243.

Assereto, R., 1973, The Permian-Triassic boundary in the Southern Alps (Italy): Memoir of the Canadian Society of Petroleum Geologists, is. 2, The Permian and Triassic systems and their mutual boundary, p.176-199

Assereto, R., and Folk, R.L., 1976, Brick-like texture and radial rays in Triassic pisolites of Lombardy, Italy: a clue to distinguish ancient aragonitic pisolites: Sedimentary Geology, v. 16, p. 205-222.

Assereto, R., and Folk, R.L., 1980, Diagenetic fabrics of aragonite, calcite, and dolomite in an ancient peritidal-spelian environment: Triassic Calcare Rosso, Lombardia, Italy: Journal of Sedimentary Petroology, v. 50, no. 2, p. 371-394.

Assereto, R., and Kendall, C.G. St.G., 1971, Megapolygons in Ladinian limestones of Triassic of Southern Alps: evidence of deformation by penecontemporaneous desiccation and cementation: Journal of Sedimentary Petrology, v. 4, no. 3 p. 715-723.

Assereto, R., and Kendall, C.G. St.G., 1977, Nature, origin and classification of peritidal tepee structures and related breccias: Sedimentology, v. 24, p. 153-210.

Atkins, P., and de Paula, J., 2002, Physical Chemistry: W.H. Freeman and Co, New York, NY, 1140 p.

Avanzini, M., 2002. Tavola 26 III - Fondo, Note Illustrative. Provincia Autonoma di Trento, Servizio Geologico, pp., 159, Trento (Italy).

Bellanca, A., Masetti, D., Neri, R., and Venezia, F., 1999, Geochemical and sedimentological evidence of productivity cycles recorded in Toarcian black shales from the Belluno Basin, Southern Alps, northern Italy: Journal of Sedimentary Research, v. 69, is. 2, p. 466-476.

Bendat, J.S. and Piersol, A.G., 1986, Random Data, 2nd Edition, John Wiley and Sons, New York, 566 pp.

Benton, M.J., 1995, Diversification and extinction in the history of life: Science, vol. 268, p. 52-58.

Bernoulli, D., 1980, Ancient continantal margins of the Tethyan ocean: Notes from the Geological Institute, The University of Basel, Switzerland, p. 1-19

Bernoulli, D., and Lemoine, M., 1980, Birth and early evolution of the Tethys: the overall situation: Memorie Bureau de Recherches Geologiques et Minieres, no. 115, p. 168-179.

Bertotti, G., Picotti, V., Bernoulli, D., and Castellarin, A., 1993, From rifting to drifting: tectonic evolution of the South-Alpine upper crust from the Triassic to the Early Cretaceous: Sedimentary Geology, Vol. 86, pp. 53-76.

Bertotti, G., Seward, D., Wijbrans, J., ter Voorde, M., and Hurford, A.J., 1999, Crustal therman regime prior to, during, and after rifting: A geochronological and modeling study of the Mesozoic South Alpine rifted margin: Tectonics, v. 18, no. 2, p. 185-200.

Black, M., 1933, The algal sediments of Andros Island, Bahamas, Royal Society of London Philosophical Transactions, series B, v. 122, p. 165-191.

Blendinger, W., 2004, Sea level changes versus hydrothermal diagenesis: Origin of Triassic carbonate platform cycles in the Dolomites, Italy, Sedimentary Geology, v. 169, pp. 21-28.

Blendinger, W., 2005a, Sea level changes versus hydrothermal diagenesis: Origin of Triassic carbonate platform cycles in the Dolomites, Italy: Reply, 178, 141-144.

Blendinger, W., 2005b, Sea level changes versus hydrothermal diagenesis: Origin of Triassic carbonate platform cycles in the Dolomites, Italy: Reply, 178, 151-153.

Bloom, A.L., Broecker, W.S., Chappell, J.M.A., Matthews, R.K., and Mesolella, K.J., 1974, Quaternary sea level fluctuations on a tectonic coast: Quaternary Research, v. 4, p. 185-205.

Bloomfield, Peter 1976, *Fourier Analysis of Time Series*, John Wiley and Sons.

Bond, G., Kromer, B., Beer, J., Muscheler, R., Evans, M.N., Showers, W., Hoffman, S., Lotti-Bond, R., Hajdas, I., and Bonani, G., 2001, Persistent solar influence on North Atlantic climate during the Holocene: Science, v. 294, p. 2130-2136.

Bond, G., Showers, W., Cheseby, M., Lotti, R., Almasi, P., deMenocal, P., Priore, P., Cullen, H., Hajdas, I., and Bonani, G., 1997, A Pervasive millennial-scale cycle in North Atlantic Holocene and glacial climates: Science, v. 278, p. 1257-1266.

Bosellini, A., 1984, Progradation geometries of carbonate platforms: examples from the Triassic of the Dolomites (Northern Italy): Sedimentology, vol. 31, p. 1-24.

Bosellini, A., 1991, Geology of the Dolomites: An introduction: Dolomieu Conference on carbonate platforms and dolomitization. Ortisei, 43 p.

Bosellini, A., and Hsü, K.J., 1973, Mediterranean plate tectonics and Triassic paleogeography: Nature, v. 244, p. 144-146.

Bosellini, A., and Hardie, L.A., 1988, Facies e cicli della Dolomia Principale delle Alpi Venete: Memorie della Societa Geologica Italiana, v. 30, p. 245-266.

Bown, P.R., and Lord, A.R., 1990, The occurrence of calcareous nannofossils in the Triassic-Jurassic boundary interval: Cahiers de l'Universite de Lyon, Serie Scientifique, v. 3, p. 127-136.

Brack, P., and Rieber, H., 1993, Towards a better definition of the Anisian/Ladinian boundary: new biostratigraphic data and correlations of boundary sections from the Southern Alps, Eclogae Geologicae Helvetiae, Vol. 86, pp. 415-527.

Brack, P., Mundil, R., Oberli, F., Meier, M., and Reiber, H., 1996, Biostratigraphic and radiometric age data question the Milankovitch characteristics of the Latemar cycles (Southern Alps, Italy), Geology Boulder, v. 24, is. 4, p. 371-375.

Brack, P., and Muttoni, G., 2000, High-resolution magnetostratigraphic and lithostratigraphic correlations in Middle-Triassic pelagic carbonates from the Dolomites (Southern Alps, Italy). Palaeogeography, Paleaoclimatology, and Palaeoceanography, vol. 161, pp. 361-380.

Broecker, W.S., Thurber, D.L., Goddard, J., Ku, T., Matthews, R.K., Mesolella, K.J., 1968, Milankovitch hypothesis supported by precise dating of coral reefs and deep sea sediments: Science, v. 159, no. 3812, p. 297-300.

Carulli, G.B., Cozzi, A., Longo Salvador, G., Ponton, M., and Podda, F., Evidence of synsedimentary tectonic activity during the Norian-Lias (Carnian Prealps, northern Italy): Memorie della Societa Geologica Italiana v. 53, p. 403-415.

Chappell, J., 2002, Sea level changes forced ice breakouts in the last glacial cycle: new results from coral terraces: Quaternary Science Reviews, v. 21, p. 1229-1240.

Chappell, J. and Shackleton, N.J., 1986, Oxygen isotopes and sea level. Nature, 324, 137-140

Cozzi, A., Hinnov, L.A., and Hardie, L.A., 2005, Orbitally forced Lofer cycles in the Dachstein Limestone of the Julian Alps (northeastern Italy): Geology, v. 33, is. 10, p.789-792.

Cozzi, A., 2000, Synsedimentary tensional features in the Upper Triassic shallow-water platform carbonates of the Carnian Prealps (northern Italy) and their importance as paleostress indicators. Basin Research, Vol. 12, pp. 133-146.

Cozzi, A., 2002, Facies Patterns of a Tectonically-Controlled Upper Triassic Platform-Slope Carbonate Depositional System (Carnian Prealpls, Northeastern Italy): Facies, v. 47, p. 151-178.

Davies, G.R., 1970, Algal laminated sediments, Gladstone embayment, Shark Bay, Western Australia. American Association of Petroleum Geologists Memoir 13, p. 169-205.

Dean, W.E., and Anderson, R.Y., 1974, Application of some correlation coefficient techniques to time-series analysis, Mathematical Geology, Vol. 6, pp. 59-75.

Demicco R.V., and Hardie, L.A., 1994, Sedimentary structures and early diagenetic features of shallow marine carbonate deposits: SEPM Atlas Series No. 1, 265 p.

Dewey, J.F., Pitman, W.C., Ryan, W.B., Bonnin, J., 1973, Plate tectonics and the evolution of the Alpine System: Geological Society of America Bulletin, v. 84, p. 3137-3180.

Doglioni C., 1987, Tectonics of the Dolomites (Southern Alps, Northern Italy): Journal of Structural Geology, v. 9, no. 2, p.181-193.

Doglioni C., 1988, Examples of strike-slip tectonics on platform-basin margins: Tectonophysics, v. 156, p. 293-302.

Doglioni, C., 1992, Relationships between Mesozoic extensional tectonics, stratigraphy, and Alpine inversion in the Southern Alps: Eclogae Geolgica Helvetica, v. 85, no. 1, p. 105-126.

Dunham., R.J., 1969, Vadose pisolite in the Capitan reef (Permian), New Mexico and Texas: Special Publication – Society of Economic Petrologists and Minerologists, v. 14, p. 182-191.

Dunn, P.A., 1991, Cyclic stratigraphy and early diagenesis: an example from the Triassic Latemar platform, northern Italy: unpublished Ph.D. dissertation, Johns Hopkins University, Baltimore, Maryland, 836 pp.

Egenhoff, S.O., Peterhänsel, A., Bechstädt, T., Zühlke, R., and Grötsch, J., 1999, Facies architecture of an isolated carbonate platform: tracing the cycles of the Latemar (Middle Triassic, northern Italy), Sedimentology, v. 46, pp. 893-912.

Einsele, G., Ricken, W., and Seilacher, A. (eds.), 1991, Cycle and Events in Stratigraphy: New York: Springer-Verlag

Ekart, D.D., Cerling, T.E., Montanez, I.P., and Tabor, N.J., 1999, A 400 million year carbon isotope record of pedogenic carbonate: implications for paleoatmospheric carbon dioxide: American Journal of Science, v. 299, p. 805-827.

Emmerich, A., Glasmacher, U.A., Bauer, F., Bechstädt, T., and Zühlke, R., 2005, Meso-/Cenozoic basin and carbonate platform development in the SW-Dolomites unraveled by basin modeling and apatite FT analysis: Rosengarten and Latemar (Northern Italy): Sedimentary Geology, vol. 175, is. 1-4, p.415-438.

Enos, P., and Perkins, R.D., 1979, Evolution of Florida Bay from island stratigraphy. Geological Society of America Bulletin, Vol. 90, pp. 59-83.

Evamy, B.D., 1973. The precipitation of aragonite and its alteration to calcite on the Trucial Coast of the Persian Gulf *in* Purser, B.M., ed., The Persian Gulf. Berlin, Springer-Verlag, p. 329-342.

Fantoni, R., and Scotti, P., 2003, Thermal record of the Mesozoic extensional tectonics in the Southern Alps: Atti Ticinensi di Scienze della Terra, no. 9, p. 96-101.

Favre, P., and Stampfli, G.M., 1992, From rifting to passive margin: The examples of the Red Sea, Central Atlantic, and Alpine Tethys: Tectonophysics, v. 215, p. 69-97.

Fischer, A.G., 1964, The Lofer Cyclothems of the Alpine Triassic: Kansas Geological Society Bulletin, v. 169, p.107-149.

Folk, R.L., 2005, Nannobacteria and the formation of framboidal pyrite: Textural evidence: Journal of Earth System Science, v. 114, no. 3, p. 369-374.

Forkner, R.M., Hinnov., L.A., Goldhammer., R.K., and Hardie, L.A., 2007 On the allocyclic interpretation of the 'Latemar cycles' (M. Triassic, The Dolomites, Italy) and implications for high-frequency cyclostratigraphic forcing. *Accepted for Publication,* GSA Special Publication in Honor of the Career of R.N. Ginsburg.

Furin, S., Preto, N., Crowley, J.L., Bowring, S.A., Rigo, M., Roghi, G., and Gianolla, P., 2006, A new U-Pb age constraint on the Upper Triassic duration from southern Italy: Geophysical Research Abstracts, v. 8, p. 3610.

Gaetani, M., Fois, E., Jadoul, F. and Nicora, A., 1981, Nature and evolution of Middle Triassic carbonate buildups in the Dolomites (Italy), Vol. 44, p. 25-57.

Ginsburg, R.N., 1971, Landward movement of carbonate mud: New model for regressive cycles in carbonates (abs.): American Association of Petroleum Geologists Bulletin, v. 55, p. 340.

Ginsburg, R.N., Hardie, L.A., Bricker, O.P., Garrett, P., Wanless, H.R., 1977, Exposure Index: A quantitative approach to defining position within the tidal zone. *in* Hardie, L.A., *ed*., Sedimentation on the Modern Carbonate Tidal Flats of Northwest Andros Island, Bahamas. The Johns Hopkins University Studies in Geology, no. 22., p. 7-11.

Gischler, E., 2003, Holocene lagoonal development in the isolated carbonate platforms off Belize: Sedimentary Geology, v. 159, p. 113-132.

Goldhammer, R.K., 2003, Cyclic Sedimentation, *in* Middleton, G.V., ed., Encyclopedia of Sediments and Sedimentary Rocks, Springer-Verlag, Netherlands p. 173-185.

Goldhammer, R.K., Dunn, P.A., and Hardie, L.A., 1987, High-frequency glacio-eustatic sea level oscillations with Milankovitch characteristics recorded in Middle Triassic platform carbonates in Northern Italy: American Journal of Science, v. 287, p. 853-892.

Goldhammer, R.K., Dunn, P.A., and Hardie, L.A., 1990, Depositional cycles, composite sea level changes, cycle stacking patterns, and the hierarchy of stratigraphic forcing: Examples from the Alpine Triassic platform carbonates: Geological Society of America Bulletin, v. 102 p. 535-562.

Goldhammer, R.K., and Harris, M.T., 1989, Eustatic controls on the stratigraphy and geometry of the Latemar buildup (Middle Triassic), the Dolomites of northern Italy, SEPM Special Publication 44, pp. 232-338.

Goldhammer, R.K., and Kaufman, J., 1995, Astronomical climatic cycles, Pleistocene glacio-eustasy, and the origin of Pleistocene platform cycles in Florida: Exxon Production Research Company Advanced Carbonates Field Report

Grabau, A.W., 1913, Principles of Stratigraphy: New York: Seiler and Co.

Gradstein, F.M., Ogg, J.G., and Smith, A.G., Agterberg, F.P., Bleeker, W., Cooper, R.A., Davydov, V., Gibbard, P., Hinnov, L.A., House, M.R., Lourens, L., Luterbacher, H.P., McArthur, J., Melchin, M.J., Robb, L.J., Shergold, J., Villeneuve, M., Wardlaw, B.R., Ali, J., Brinkhuis, H., Hilgen, F.J., Hooker, J., Howarth, R.J., Knoll, A.H., Laskar, J., Monechi, S., Plumb, K.A., Powell, J., Raffi, I., Röhl, U., Sadler, P., Sanfilippo, A., Schmitz, B., Shackleton, N.J., Shields, G.A., Strauss, H., Van Dam, J., van Kolfschoten, T., Veizer, J., and Wilson, D., 2004. A Geologic Time Scale 2004. Cambridge University Press, 589 p.

Grotzinger, J.P., 1986 Cyclicity and paleoenvironmental dynamics, Rocknest platform, northwest Canada: Geological Society of America Bulletin, v. 97, p. 1208-1231.

Haas, J. 1994, Lofer cycles of the Upper Triassic Dachstein platform in the Transdanubian mid-Mountains, Hungary, in De Boer, P.I. and Smith, D.L., eds., Orbital Forcing and Cyclic Sequences, IAS Special Publication 19, p. 303-322.

Haas, J., 2004, Characteristics of peritidal facies and evidences for subaerial exposures in Dachstein-type cyclic platform carbonates in the Transdanubian Range, Hungary, Facies, 50, p. 263-286.

Hallam, A., and Goodfellow, W.D., 1990, Facies and geochemical evidence bearing on the end-Triassic disappearance of the Alpine reef ecosystem: Historical Biology, v. 4, 131-138.

Hallam, A., and Wignall, P.B., 1997, Mass extinctions and their aftermath: Oxford University Press, Oxford, UK, 320 p.

Handford, C.R., Kendall, A.C., Prezbindowski, D.R., Dunham, J.B., and Logan, B.W., 1984, Salina-margin tepees, pisoliths, and aragonite cements, Lake MacLeod, Western Australia; Their significance in interpreting ancient analogs, Geology, v. 12, p. 523-527.

Hardie, L.A., and Ginsburg., R.N., 1977, Layering: The origin and environmental significance of lamination and thin bedding. *In* Hardie, L.A., *ed*., Sedimentation on the Modern Carbonate Tidal Flats of Northwest Andros Island, Bahamas. The Johns Hopkins University Studies in Geology, no. 22. p. 50-123.

Hardie, L.A., and Shinn, E.A., 1986, Carbonate depositional environments, modern and ancient, 3, Tidal Flats: Colorado School of Mines Quarterly, v. 81, p. 1-74.

Harris, M.T., 1996, The carbonate factory of the Middle Triassic buildups in the Dolomites, Italy: A quantitative analysis – Comment, Sedimentology, v. 43, 401-402.

Hinnov, L.A., 2000, New perspectives on orbitally forced stratigraphy: Annual Review of Earth and Planetary Sciences, v. 28, p. 419-475.

Hinnov, L.A. and Goldhammer, R.K., 1991, Spectral analysis of the Middle Triassic Latemar Limestone: Journal of Sedimentary Petrology, v. 61, p. 1173-1193.

Hinnov, L.A. and Preto, N., 2003, Analyzing the depositional signal of the Latemar Limestone (Dolomites, Italy): a multiple working hypothesis approach. in Brack, P., Schlager, W. and Stefani., M., eds., Abstract Volume, Triassic Geochronology and Cyclostratigraphy - a Field Symposium, St.Christina/Italy, September 11-13, p. 10.

Holland, S.M., Meyer, D.L., and Miller, A.I. (2000), High-resolution correlation in apparently monotonous rocks: Upper Ordovician Kope Formation, Cincinnati Arch, Palaios, Vol. 15, p. 73-80.

Hsü, K.J., and Bernoulli, D., 1978, Genesis of the Tethys and the Mediterranean: DSDP, Vol. 42, pp. 943-949.

Huynh, T.T., and Poulsen, C.J., 2005, Rising atmospheric CO_2 as a possible trigger for the end-Triassic mass extinction: Palaeogeography, Palaeoclimatology, Palaeoecology, v. 217, p. 223-242.

Imbrie, J., Hays, J.D., Martinson, D.G., McIntyre, A., Mix, A.C., Morley, J.J., Pisias, N.G., Prell, W.L., and Shackelton, N.J., 1984, The orbital theory of Pleistocene climate: support from a revised chronology of the marine $\delta^{18}O$ record, *in* Berger, A., Imbrie, J., Hays, J., and Kukla, G., and Saltzman, B., eds., Milankovitch and climate. Boston, Massachusetts, Reidel, p. 269-306.

Jacobs, D.K., and Sahagian, D.L., 1993, Climate-induced fluctuations in sea level during non-glacial times, Nature, vol. 361, p. 710-712.

Jadoul, F.; Berra, F.; and Frisia, S., 1992, Stratigraphic and paleogeographic evolution of a carbonate platform in an extensional tectonic regime: the example of the Dolomia Principale in Lombardy (Italy): Ri. It. Paleont. Strat., Vol. 98, No.1, pp. 29-44.

James, N.P., 1984, Shallowing-upward sequences in carbonates: *In* Walker, R.G., (ed.), Facies Models. Geoscience Canada Reprint Series 1, p. 213-228.

Kendall, G. St.C. and Schlager, W.,1981, Carbonates and relative changes in sea level: Marine Geology, v. 44, p 181-212.

Kent, D.V., Muttoni, G., and Brack, P., 2004, Magnetostratigraphic conformation of a much faster tempo for sea level change for the Middle Triassic Latemar platform carbonates: Earth and Planetary Science Letters, v. 228, p. 369-377.

Kerans, C.,1995, Use of one- and two-dimensional cycle analysis in establishing high-frequency sequence frameworks. *In* Read, J.F., Kerans, C., and Weber, L.J., (eds.), Milankovitch sea level changes, cycles, and reservoirs on carbonate platforms in greenhouse and icehouse worlds. SEPM Short Course Notes, no. 35, p. 1-20.

Klebelsberg R., von., 1935, Geologie von Tirol. Borntraeger, Berlin, 872 pp.

Koerschner III, W.F., and Read, J.F., 1989, Field and modeling studies of Cambrian carbonate cycles, Virginia Appalachians: Journal of Sedimentary Petrology, Vol. 59, p. 654-687.

Lambeck, K., Yokoyama, Y. & Purcell, T. 2002. Into and out of the Last Glacial Maximum: sea level change during Oxygen Isotope Stages 3 and 2.: Quaternary Science Reviews v. 21, p. 343-360.

Laskar, J., 1990, The chaotic motion of the solar system: A numerical estimate of the chaotic zones: Icarus, v. 88, p. 266-291.

Laubscher, H., and Bernoulli, D., 1978, Mediterranean and Tethys, *in* Nainn, A.E.M., Kanes, W.H., and Stehli, F.G., (eds.), The ocean basins and margins, 4A: New York, Plenum Press, p. 1-28.

Lemoine, M., and Trumpy, R., 1987, Pre-oceanic rifting in the Alps: Tectonophysics, v. 133, p. 305-320.

Logan, B.W., Read, J.F., and Davies, G.R., 1969, History of carbonate sedimentation, Quaternary epoch, Shark Bay, Western Australia: *in* American Association of Petroleum Geologists – Memoir 13, p. 38-84.

Lourens, L.J, and Hilgen, F.J., 1997, Long-periodic variations in the Earth's obliquity and their relation to third-order eustatic cycles and late Neogene glaciation: Quaternary International, v. 40, p. 43-52.

Lucia, F.J., 1968, Recent sediments and diagenesis of Bonaire, Netherlands Antilles. Journal of Geology, v. 78, p. 352-362.

Matthews, R.K., and Frohlich, C., 1994, Orbital forcing of glacioeustasy and its implications for petroleum exploration and production: AAPG Annual meeting abstracts, v. 4, p. 61-62.

Manfrin S., Mietto P., and Preto N., 2005, Ammonoid biostratigraphy of the Middle Triassic Latemar platform (Dolomites, Italy) and its correlation with Nevada and Canada. Geobios, v. 38, is. 4, p. 477-504.

Maurer, F., Hinnov, L.A., and Schlager, W., 2004, Statistical time-series analysis and sedimentological tuning of bedded rhythms in a Triassic basinal succession (Southern Alps, Italy): SEPM Special Publication no. 81, p. 83-99.

McGowan, A.J., 2004, Ammonoid taxonomic and morphologic recovery patterns after the Permian-Triassic: Geology, v. 32, no. 8, p. 665-668.

Miall, A.D., 1984, Principles of Sedimentart Basin Analysis, 2nd edition, New York: Springer-Verlag, 1990.

Middleton, G.V., 1973, Johannes Walther's Law of the Correlation of Facies: Geological Society of America Bulletin, 1973, v. 84, is. 3, p.. 979-987.

Mundil, R., T., Brack, P., Meier, M., Reiber, H., and Oberli, F., 1996, High resolution U-Pb dating of Middle Triassic volcaniclastics; time-scale calibration and verification of tuning parameters for carbonate Sedimentation, Earth and Planetary Science Letters, v. 141, is. 1-4, p. 137-151.

Mundil, R., Zühlke, R., Bechstadt, T., Brack, P., Egenhoff, S., Meier, M., Oberli, F., Peterhänsel, A., and Rieber, H., 2003, Cyclicities in Triassic Platform Carbonates: synchronizing radio-isotopic and orbital clock: Terra Nova, v. 15/2, p. 81-87.

Munk, W., Dzieciuch, M., and Jayne, S., 2002, Millennial climate variability: Is there a tidal connection?: Journal of Climate, v. 15. p.370-385.

Niggemann, S., Mangini, A., Mudelsee, M., Richter, D.K., and Wuth, G., 2003, Sub-Milankovitch climatic cycles in Holocene stalagmites from Sauerland, Germany, Earth and Planetary Science Letters, v. 216, is. 4, p. 539-547.

Ogilvie Gordon, M.M., 1927, Das Groedener- Fassa- und Enneberggebiet in den Suedtiroler Dolomiten. I und II Teil, pp. 376, III Teil, pp. 89, Geol. Bundesanstalt, Wien

Paillard, D., L. Labeyrie and P. Yiou, 1996, Macintosh program performs time-series analysis, Eos Trans. AGU, Vol. 77, p. 379. An electronic supplement of this reference is available at: http://www.agu.org/eos_elec/96097e.html

Parkinson, R.W., 1989, Decelerating Holocene sea level rise and its influence on southwest Florida coastal evolution: A transgressive/regressive stratigraphy: Journal of Sedimentary Petrology, v. 59, no. 6, p. 960-972.

Peltier, W.R., 2001, On eustatic sea level history: Last glacial maximum to Holocene: Quaternary Science Reviews, v. 21, p. 377-396.

Peterhänsel, A. and Egenhoff, S.O., 2005, Sea level changes versus hydrothermal diagenesis: Origin of Triassic carbonate platorm cycles in the Dolomites, Italy: Discussion, Sedimentary Geology, 178, p. 145-149.

Piros O., Preto N., 2003, A tentative correlation of dasycladacean biozones with ammonoid standard zones in the Anisian-Ladinian Latemar succession, Italy. Triassic Geochronology and Cyclostratigraphy field symposium, September 11-13, 2003, St. Christina, Italy

Preto, N., Hinnov, L.A., Hardie, L.A., and De Zanche, V., 2001, Middle Triassic orbital signature recorded in the shallow-marine Latemar carbonate buildup (Dolomites, Italy), Geology, v. 29 no. 12, p. 1123-1126.

Preto, N., and Hinnov, L.A., (2003), Unravelling the origin of carbonate platform cyclothems in the Upper Triassic Dürrenstein Fm. (Dolomites, Italy), Journal of Sedimentary Research, 73(5), p. 774-789.

Preto, N., Hinnov, L.A., De Zanche, V., Mietto P., and Hardie, L.A.., 2004, The Milankovitch interpretation of the Latemar platform cycles (Dolomites, Italy): implications for geochronology, biostratigraphy, and middle Triassic carbonate accumulation, SEPM Special Publication No. 81, pp. 167-182.

Preto, N., Hinnov, L.A., Hardie, L.A., and Harris M.T. (2005), Sea level changes versus hydrothermal diagenesis: origin of Triassic carbonate platform cycles in the Dolomites, Italy - Discussion, Sedimentary Geology, 178, p. 135-139.

Prosser, G., and Selli, L., 1991, Thrusts of the Mezzocorona-Mendola Pass area (Southern Alps, Italy): Structural analysis and kinematic reconstruction: Bolletino della Societa Geologica Italiana, v. 110, p. 805-821.

Rankey, E.C., and Morgan, J., Quantified rates of geomorphic change on a modern carbonate tidal flat, Bahamas: Geology, v. 30, no. 7, p. 583-586.

Read, J.F., and Goldhammer, R.K., 1988, Use of Fischer plots to determine third-order sea level curves in Ordivician peritidal carbonates, Appalachians: Geology, v. 16, no. 10, p.895-899.

Read, J.F. and Sriram, S., 1990, A computer program for generation of Fischer plots: Compass, 66, 73-78.

Read, J.F., 1995 Overview of carbonate platform sequences, cycle stratigraphy, and reservoirs in greenhouse and icehouse worlds. *In* Read, J.F., Kerans, C., and Weber, L.J., (eds.), Milankovitch sea level changes, cycles, and reservoirs on carbonate platforms in greenhouse and icehouse worlds: SEPM Short Course Notes, no. 35, p. 1-102.

Richthofen F. vonc., 1874, Ueber Mendola- und Schlern Dolomite. Zeitschr. Deutsch. Geol. Gesell., Berlin, 26, p. 225-256

Robbin, D.M., and J.J. Stipp, J.J., 1974, Depositional rate of laminated soilstone crusts, Florida Keys, Journal of Sedimentary Petrology, v. 49. p. 175-180.

Roth, S., and Reijmer, J.J.G., 2005, Holocene millennial to centennial carbonate cyclicity recorded in slope sediments of the Great Bahama Bank and its climatic implications, Sedimentology, v. 52, is. 1, p. 161-181.

Sander, B., 1951, Contributions to the study of depositional fabrics; rhythmically deposited Triassic limestones and dolomites. *English translation by Eleanora Bliss* Knopf, 160 p.

Scandone, P., 1975, Triassic seaways and the Jurassic Tethys ocean in the central Mediterranean area: Nature, v. 256, p. 117-118.

Schlager, W., 1981, The paradox of drowned reefs and carbonate platforms, Geological Society of America Bulletin, vol. 92, p. 197-211.

Schlager, W., 1999, Scaling of sedimentation rates and drowning of reefs and carbonate platforms: Geology, v. 27, no. 2, p. 183-186.

Schulz, M., and Schaefer-Neth, C., 1997, Translating Milankovitch climate forcing into eustatic fluctuations via thermal deep water expansion: a conceptual link.: Terra Nova, v. 9, no. 5, p. 228-232.

Schwarzacher, W., 1975, Sedimentation Models and Quantitative Stratigraphy: New York, Elsevier, 382 p.

Schwarzacher, W., 1993, Cyclostratigraphy and the Milankovitch theory, Developments in Sedimentology, v. 52, 225 p.

Schwarzacher, W., 1998, Bed thickness measurements and the cyclostratigraphy of the Latemar Limestone, 15th International Sedimentological Congress of the IAS, 12-17 April, Alicante, Spain, p. 707.

Schwarzacher, W., 2005, The stratification and cyclicity of the Dachstein Limestone in Lofer, Leogang and Steinernes Meer (Northern Calcareous Alps, Austria), Sedimentary Geology, v. 181, is. 1-2, p. 93-106

Sepkoski, J.J., 1996, Patterns of Phanerozoic extinction: a perspective from global databases. *In* Walliser, O.H., ed., Global Events and Event Stratigraphy, Springer-Verlag, New York, p. 35-51.

Shinn, E.A., 1986, Modern Carbonate Tidal Flats: Their Diagnostic Features., in Hardie, L.A., and Shinn, E.A., Carbonate Depositional Environments, Modern and Ancient: Colorado School of Mines Quarterly, v. 81, No. 1, p. 7-33.

Sloss, L.L., 1963, Sequences in the cratonic interior of North America: Geological Society of America Bulletin, v. 74, is. 2, p. 93-113.

Steno, Nichlaus, 1669, De Solido Intra Solidium Naturaliter Contento Dissertationis Prodromus

Strasser, A., Hillgärtner, H., Hug, W., and Pittet, B., 2000, Third-order depositional sequences reflecting Milankovitch cyclicity. Terra Nova, Vol. 12, p. 303-311.

Strasser, A., and Samankassou, E., 2003, Carbonate sedimentation rates today and in the past: Holocene of Florida Bay, Bahamas, and Bermuda vs. Upper Jurassic and Lower Cretaceous of the Jura Mountains (Switzerland and France): Geologica Croatica, v. 56, no. 1, p. 1-18.

Suess, E., 1888 Das Anilitz der Erder, Volume 2. *English translation by Sollas*, 1906 Oxford: Clarendon Press, p. 1-254.

Taft, W.H., 1968, Lithification of modern marine carbonate sediments at Yellow Bank, Bahamas, Bulletin of Marine Science, v. 18, is. 4, p.762-828

Taylor, J.K., 1990, Statistical Techniques for Data Analysis, Lewis Publishers, Inc., Chelsea, Michigan, 200 p.

Thompson, D.J., 1982, Spectrum estimation and harmonic analysis, IEEE Proceedings, v. 70, p. 1055-1096.

Thomson, D.J., and Chave, A.S., 1991, Chapter 2: Jackknifed error estimates for spectra, coherences and transfer function, in, Haykin, S.S., ed., Advances in Spectrum Analysis and Array Processing, Prentice-Hall, New York, p. 58-113.

Thompson, W.G., and Goldstein, S.L., 2005, Open-system coral ages reveal persistent suborbital sea level changes, Science, Vol. 308, pp. 401-404.

Tudhope, A.W., 1989, Shallowing-upwards sedimentation in a coral reef lagoon, Great Barrier Reef of Australia: Journal of Sedimentary Petrology, v. 59, no. 6, p. 1036-1051.

Vail, P.R., Mitchum jr., R.M., Thompson III, S., 1977, Seismic stratigraphy and global changes of sea level, part 4: Global cycles of relative changes of sea level: *in* Payton, C.E., ed., Seismic Stratigraphy – Applications to Hydrocarbon Exploration: American Association of Petroleum Geologists Memoir 36, p.83-97.

Van de Plassche, O., van der Borg, K., and de Jong, A.F.M., 1998, Sea level-climate correlation during the past 1400 yr: Geology, v. 26, no. 4, p. 319-322.

Van Hilten D., 1960, Geology and Permian paleomagnetism of the Val di Non area. Geologica Ultraiectina, 5, p. 1-95, Utrecht

Vecsei, A, 2004, Carbonate production on isolated banks since 20 k.a. BP, climatic implications: Palaeogeography, Palaeoclimatology, Palaeoecology, V. 214, Is. 1-2, p. 3-10

Veizer, J., Godderis, Y., and Francois, L.M., 2000, Evidence for decoupling of atmospheric CO_2 and global climate during the Phanerozoic eon: Nature London, v. 408, is. 6813, p. 698-701.

Venzo, G.A., and Fuganti, A., 1965, Il Trias della Mendola (Trentino – Alto Adige): Studi Trentini di Scienze Naturali, Sez. A, Vol. XLII, N. 1, p. 55-86.

Walker, R.G., and James, N.P., (eds.), 1990, Facies Models: Response to sea level change: Geological Association of Canada, 317 p.

Wanless, H.R., Tyrrell, K.M., Tedesco, L.P., and Dravis, J.J., 1988, Tidal-flat sedimentation from hurricane Kate, Caicos Platform, British West Indies: Journal of Sedimentary Petrology, v. 58, no. 4, p. 724-738.

Wilkin, R.T., and Barnes, H.L., 1997, Formation processes of framboidal pyrite: Geochimica et Cosmochimica Acta, v. 61, is. 2, p. 323-339.

Wilkin, R.T., and Barnes, H.L., 1997, Pyrite formation in an anoxic estuarine basin: American Journal of Science, v. 297, is. 6, p. 620-650.

Wilson, J.T., 1966, Did the Atlantic close and then re-open?: Nature, v. 211, is. 5050, p. 676-681.

Wilson, J.L., 1975, Carbonate facies in geologic history, New York: Springer-Verlag.

Winterer, E.L., and Bosellini, 1981, Subsidence and sedimentation on Jurassic passive continental margin, Southern Alps, Italy: AAPG Bulletin, v. 65, is. 3, p. 394-421

Wright, V.P., 1992, Speculations on the controls on cyclic peritidal carbonates: Ice-house versus greenhouse eustatic controls. Sedimentary Geology, v. 76, p. 1-5.

Yang, W., and Lehrmann, D., 2003, Milankovitch climatic signals in Lower Triassic (Olenekian) peritidal carbonate successions, Nanpanjiang Basin, South China, Palaeogeography, Palaeoclimatology, Palaeoecology, v. 201, is. 3-4, p. 283-306.

Zapfe, H., 1957, Das Meer der alpinen Trias; seine Organismenwelt und seine Ablagerungen, Universum Horn Österreich, v. 7, p. 193-201.

Zühlke, R., 2004, Integrated cyclostratigraphy of a model Mesozoic carbonate platform - the Latemar (Middle Triassic, Italy). in D´Argenio, B., Fischer, A., Premoli Silva, I. and Weissert, H., eds., Multidisciplinary Approach to Cyclostratigraphy: Society for Sedimentary Geology, Special Publication.

Zühlke, R., Bechstädt, T., and Mundil, R., 2003, Sub-Milankovitch and Milankovitch forcing on a model Mesozoic carbonate platform – the Latemar (Middle Triassic, Italy): Terra Nova, v. 15, no. 2, p. 69-80.

Vita

Robert Murchison Forkner was born on November 23, 1977, the son of Mary Emma Forkner and Larry Elbridge Forkner. Robert (Rob) graduated from Bartlett High School, Anchorage, Alaska in 1996 where he worked as an intern at the Alaska Volcano Observatory during his senior year. Rob earned his Bachelor of Science from Baylor University in Waco, Texas in 2000, and his Master of Science from Baylor University in 2002. Rob came to the University of Texas at Austin in the summer of 2002 to work with Dr. Robert K. Goldhammer on the Triassic cyclic carbonates of the Dolomite Alps in Northern Italy. Subsequent to Dr. Goldhammer's untimely passing in 2003, Rob's work passed to the supervision of Dr. Mark Cloos. During his time as a graduate student, Rob served as a teaching assistant for six semesters in introductory geology, one semester in undergraduate sedimentary rocks, and one semester in graduate carbonate facies and diagenesis courses. Rob also served as assistant instructor for 4 semesters for the undergraduate sedimentary rocks course at the University of Texas (GEO 416M), teaching the carbonates portion of the course along side Dr. Gary Kocurek and Dr. Earle McBride, who taught the clastics portion. Rob served an internship at the ExxonMobil Upstream Research Company during the summer of 2005. Rob has attended eight national and international geologic meetings (e.g., GSA, AAPG, IGC) and has presented either a poster or a talk at each of the conferences he has attended. At the time of the printing of this dissertation, chapter two has been accepted for publication

by GSA for inclusion in a special publication dedicated to the career of Dr. Robert Ginsburg. Rob is also an avid and well-known traditional Irish musician, and has both taught and played music at festivals around the country and the world. Rob also owns and operates his own drum making company, Metloef Irish Drums, which produces some of the best instruments in the world today.

Permanent address: 840 Sunrise Trail,
Spring Branch, TX 78070

This dissertation was typed by Robert M. Forkner.

A

Section: Ala

Formation: Dolomia Principale

Measured by: R.M. Forkner

B

Section: Forcella Averau

Formation: Dolomia Principale

Measured by: R.M. Forkner

C

Section: Tofana di Rozes

Formation: Dolomia Principale

Measured by: R.M. Forkner

D

Section: Tofana di Mezzo

Formation: Dolomia Principale

Measured by: R.M. Forkner

E

Section: Pelmo

Formation: Dolomia Principale

Measured by: R.M. Forkner

F

Forc. Lavaredo Section

Section: Forcella Lavaredo/ Cima Ovest

Formation: Raibl/ Dolomia Principale

Measured by: R.M. Forkner

Grain types and sedimentary structures
Whispy algal seams
Gastropods
Megalodonts
Mixed Bioclasts
Bivalves
Peloids
Burrows/Bioturbation
Erosional Debris
Rounded Debris

Shallower
Karst / Cement Disrup.
Cryptomicrobial Lam.
Fenestral Lam.
Fenestral W/P
Breccia
Wispy Laminated W/P
Skeletal W/P
Peloidal M/W
Massive Mudstone
Shale

Deeper

60 km

6 km

1 km

15 km absolute
7 km west to east

30 km absolute
13 km west to east

Grades laterally into amalgamated lopee

Ala section from upper Dolomia Principale. Does not correlate lithostratigraphically to other sections.

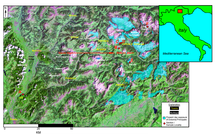


Study Area
Dolomia Principale Outcrop
Dolomia Principale Subsurface
Raibl Group
Cortina d'Ampezzo
Misurina
Auronzo di Cadore
Lago di Misurina
Tre Cime di Lavaredo
Monte Cristallo
Cima Ovest
Forcella Lavaredo
Monte Pelmo
Forcella Averau
Monte Averau
Tofana di Rozes
Tofana di Mezzo
Monte Tofana
Passo Falzarego
Cinque Torri
Lago di Braies
Lago di Dobbiaco
Dobbiaco
Monte Paterno
Monte Piana
Monte Elmo
Monte Rudo
Monte Specie
Monte Cavallino
Monte Cavallo
Monte Cristallino
Monte Cristallo